MINISTERIO DE DEFENSA

REAL INSTITUTO Y OBSERVATORIO DE LA ARMADA
EN SAN FERNANDO

BOLETIN ROA
No. 5/2005

14th INTERNATIONAL LASER RANGING WORKSHOP: PROCEEDINGS

JUNE / 2004

MINISTERIO DE DEFENSA

REAL INSTITUTO Y OBSERVATORIO DE LA ARMADA
EN SAN FERNANDO

BOLETIN ROA
No. 5/2005

14th INTERNATIONAL LASER RANGING WORKSHOP:

PROCEEDINGS

Edita:

MINISTERIO
DE DEFENSA

SECRETARIA
GENERAL
TECNICA

Imprime: Real Instituto y Observatorio de la Armada
San Fernando (Cádiz). Octubre 2005
Depósito Legal: CA 469-78
ISSN 1131-5040
NIPO 076-05-167-X

Edited by:

Jorge Garate,
Jose Martin Davila,
Carey Noll
and Michael Pearlman

Foreword

The 14th International Workshop on Laser Ranging was held in San Fernando, Cadiz, Spain, on June 7 through 11, 2004. This event is organized every two years by the International Laser Ranging Service (ILRS), with the support of the laser ranging community. This year the workshop was sponsored by the Spanish Naval Observatory (Real Instituto y Observatorio de la Armada), to celebrate the 250th aniversary of its foundation. There were about 150 people, from 25 countries, participating in the meeting, which included oral presentations, posters and discussions on science related to laser tracking as well as operational issues, hardware and software developments, and data analysis procedures. Last day of the meeting was dedicated to the ILRS annual plenary meeting.

San Fernando Naval Observatoy would like to acknowledge to all the institutions involved in the workshop organization and funding: *Ministerio de Defensa*,(Spanish Secretary of Defence) former *Ministerio de Ciencia y Tecnologia*, (Spanish Secretary of Science and Technology), Spanish Navy, Cadiz County Council, and San Fernando Town Hall. The workshop was parcially funded by the Spanish *Ministerio de Educacion y Ciencia* (Spanish Secretary of Education and Science) through the *Accion Complementaria* ESP2004-20483-E

We would like also to acknowledge the Local Organizing Committee, as well as the Scientific Committee. They got to organize a fruitfull and succesfull meeting. Of course we would like to acknowledge to all the participants because with their works they have contributed to the high scientific quality of the workshop.

This volume contains the proceedings of the workshop. It has been prepared at the San Fernando Naval Observatory, and it has been published at the Spanish Navy *Centro de Ayudas a la Enseñanza*, in Madrid

CN Juan Carlos Coma Samartin
San Fernando Naval Observatory Director

TABLE OF CONTENTS

NEW APPLICATIONS

ATMOSPHERIC CORRECTION AND MULTIWAVELENGTH RANGING

SYSTEM CALIBRATION TECHNIQUES

ENGINEERING AND Q/C ANALYSIS

ADVANCED SYSTEMS AND TECHNIQUES

OPERATIONAL ISSUES

WORKSHOP SUMMARY

The Fourteenth International Workshop on Laser Ranging continued in the tradition of providing a venue for technologists and analysts to meet and relate the current status of laser ranging from data acquisition through data analysis and interpretation. The workshop was organized into 11 sessions held during the week of June 7 - 11, 2004. The Workshop was opened with welcoming addresses and some historical overview. The participants were then treated to a briefing on the history of the Real Instituto y Observatorio de la Armada (ROA) which is celebrating its 250th anniversary.

The first day activities, which focused on scientific achievements, applications and future requirements, included an introduction to the new "Global Geodetic Observing System" project which is being organized under the International Association of Geodesy (IAG) to integrate space geodetic techniques as well as terrestrial observations into a single coordinated entity to support long-term, precise monitoring of the geodetic observables. The intent is to provide observations of the three fundamental geodetic observables, the Earth's shape, gravity field and rotational motion to maintain a stable, accurate and global reference frame for science and applications. A number of ILRS Analysis and Combination Centers reported on the state of their SLR and LLR derived output products including weekly solutions with subcm station position accuracy, geocenter variations at mm-sensitivity, and temporal variations in the low degree/order terms of the gravitational field. SLR observations of EOP continue to improve and SLR observations continue to play an important role in the development of static and time-varying gravity field models. Poster sessions included status on several current missions, the upgrade status of several SLR stations, SLR as a calibration tool for other techniques, and seasonal environmental signals at laser ranging sites.

In lunar laser ranging, the LLR systems at OCA is being upgraded with new technologies that will include ranging to low Earth orbiting satellites and strategies for finding Lunakhod 1. Efforts are underway to introduce LLR at Mt. Stromlo and work continues on APOLLO at Apache Point with an eye toward operations in 2005. Several papers were given on lunar data analysis and lunar science and analysis.

Under new applications CNES proposed the T2L2 laser time transfer experiment on the Myriade Microsatellite as a means to achieve psec timing. A plan for global laser communications using a network of modified SLR2000 systems was discussed as a means for gigabyte data collection from space vehicles. There were also three talks on planetary laser altimetry missions including Bepi-Colombo Mercury Mission and Mars Orbiting Laser Altimeter (MOLA).

In the session on atmospheric correction and multi-wavelength ranging the Shanghai Observatory reported using dual wavelength Raman ranging to LEO satellites. The Yunnan Observatory presented the results of an adaptive optics experiment to improve the LLR link budget with tip-tilt mirror pointing corrections using lunar surface features. The Graz station presented results using its new 2 KHz laser on ground and spaceborne targets for studies on turbulence and its influence on ranging. A poster presentation on atmospheric refraction modeling indicated that it might be helpful to improve both the spatial sampling resolution of atmospheric data and the spectral sampling resolution of refractivity measurements for a better understanding of the group velocity as applied to SLR.

Several groups are working on new calibration techniques. Tests at Mt. Stromlo with five spatially distributed calibration targets give uncertainties of a few mm, indicating that systems that rely on single targets may be doing even worse. We probably should stress a multi-target approach. Short target calibration tests at the Herstmonceux station also indicated that

multiple targets should be considered if we want to reach mm accuracies. Stability tests at Matera were reported to give LAGEOS full rate data RMS of 5mm and a long term station ranging stability at the mm level. Reports were given on PICO EVENT Timer, which can now handle repetition rates up to 2KHz, and the new Riga A031ET Event Timer, which showed that linearity and stability is within a few ps and that this may be an inexpensive alternative to other higher priced units. A presentation was also given on a small electronic device which uses the time difference between the compensated and uncompensated output of the C-Spad to determine return signal strength.

Under engineering and Q/C analysis a study on numerical noise introduced by data fitting procedures concluded that errors as large as one mm could be introduced in normal point data and three mm in single shot data. A study on interpolation effects indicated that predictions should be integrated at step sizes much smaller than the normal point bin size and that interpolation should be done in x/y/z rather than azimuth/elevation/range. The first version of the Engineering Data File system is working in Riga. The system is being implemented in Potsdam, Graz and Wettzell.

Several groups reported on their QC analysis of network data. In particular, the prediction time bias detection and monitoring system at Herstmonceux is operational, providing rapidturnaround information to the community.

Several groups reported the implementing of automation and remote control features at their ranging stations. A remote control demonstration via the internet and cell phone of tracking at the Zimmerwald station was very impressive. The new remote control systems for the operation of the GUTS station through dedicated communications lines from the Tsukuba Space Center was also demonstrated. Presentations were also given on the mathematical analysis required to completely define the effects of the telescope and transceiver optics on the SLR2000 laser transmit and receive pulses and on the new Consolidated Laser Ranging Prediction Format, which provides a single format for SLR, LLR and transponder predictions.

Several new satellites with retroreflectors have been launched, are planned for launch in the next few years, or are being proposed. Some are trying novel approaches to reducing the spread of the return signal. ETS-8 to be launched in geostationary orbit in 2006 will have a return signal strength equal to approximately 1% of that from LAGEOS. The design for the Shenzhou-4, the first Chinese reflector satellite in space was discussed. A report was given on the experience with three different array concepts: Reflector satellite with a distributed array, LARETS spherical satellites with small recessed corner cubes, and Meteor-3M satellite with a Luneberg sphere. Several talks were also given on analytic orbit design tools for future missions and non-gravitational force modeling for LAGEOS. Some impressive tests were reported with the Graz 2 KHz laser that singled out individual cube corners on satellites.

Studies continue on satellite signatures and satellite induced range biases that can corrupt the estimation of geodetic observables. Tests have been conducted at several stations to quantify center-of-mass offset over the operating range of signal strengths. Tests will be formulated by which stations can characterize these effects over their dynamic range of operation.

In the technology session there was a presentation on the Graz 2 KHz laser ranging system which is now fully operational with 10 ps, 400 microjoule pulses at 532nm. Hundreds of thousands of returns per LAGEOS pass are quite common. Work continues on the SLR2000, with results from early satellite passes looking quite promising. The GUTS station reported that remote-controlled operations began in early 2004 with tracking on LEO to GEO satellites. The Mt. Stromlo station is being rebuilt quickly with enhanced systems, more automated expert software, and projected lunar capability. Two-telescopes with 1 m and 1.8 m apertures and a kW-class laser with adaptive optics are also being built at Mt Stromlo for

space debris tracking, laser ablations, and other research programs. A new two-color KHz SLR system being built in Wettzell should be ready for ranging in 2006.

Under technology for the future, presentations were given on a new concept for a compact, totally passive multipass amplifier for a laser transmitter, and new detectors for the eyesafe region of 1500 nm.

In the session on operational issues, several papers were given on network response to the weekend scheduling and funding reductions, progress on resurrecting and improving the station data report card, and the new data structure being adopted by the data centers. Reports were given on the status of the Real Time Station Status Exchange, which a number of stations have already incorporated into their operations.

In addition to updates on many of the current satellite missions on the ILRS roster, reports were also given on the new Korean Research Center (Satrac) and a new solar research and engineering test bed satellite with retroreflectors that is being considered for launch by the Koreans in the 2005-7 timeframe, and a French drag free microsatellite being considered for launch as a test of the Equivalence Principle in 2006.

ROA hosted a reception and a tour to the SLR station and the Observatorio library and museum on Tuesday evening. The tour also included the FTLRS which was collocated at the site.

The participants of the workshop express their sincere appreciation to the ROA for its hospitality in hosting the Fourteenth International Workshop on Laser Ranging.

The Fifteenth Workshop will be held hosted by Geoscience Australia and EOS in Canberra in October 2006.

Michael Pearlman, Program Committee.

Welcome Note

Werner Gurtner
International Laser Ranging Service ILRS
Chairman of the Governing Board

Dear representatives of the various Spanish authorities,

dear colleagues of the Local Organizing Committee,

ladies and gentlemen, dear friends.

First of all I would like to congratulate the San Fernando observatory for the 250 anniversary and I wish you all the best for the next 250 years.

The International Laser Ranging Service is very pleased to have been offered the opportunity to hold the 14 bi-annual Laser Ranging Workshop in this beautiful part of a beautiful country. Mike Pearlman, the director of the ILRS Central Bureau, will certainly take the opportunity to look back right to the very beginning of a successful story and to let the previous years pass before your eyes or rather ears. He is especially competent for such review as one of the two colleagues who attended all 13 previous workshops so far!

Let me, instead, say a few words to the challenges our service faces at present and in the near future.

ILRS is one of four space geodetic services under the umbrella of the International Association of Geodesy.

The rocket-like raise and success of the International GPS Service brought and still brings a lot of pressure to the two older Services and techniques, the laser ranging and the very long baseline interferometry. More and more, however, the recognition surfaces that a combination of the various space techniques, by properly taking into account the individual strengths (and weaknesses of course), generates more scientific benefit than each individual one could ever do. This recognition can already be found with many scientists all around the world, and especially in the International Association of Geodesy with its new program, the Global Geodetic Observing System GGOS. Unfortunately we cannot say the same for those areas where many of us have to recruit their resources for the operation, the maintenance, and further development of our techniques and services.

The bulky and expensive part of all space geodetic services are their tracking networks: The 30 VLBI radio telescopes, the 40 Laser ranging stations, the 50 Doris stations and the two hundred GPS receivers. The only justification of their existence is the quality and quantity of their data and their usefulness for the scientific, technical, or even social applications.

Unfortunately many organizations funding components of the tracking network are NOT in the same time on the receiving end of this data refinement system and have, therefore, difficulties in raising the necessary funds. The justification of the network is not the mere existence of the network. The justification must continuously be provided and fed back by the users of the data: Certainly an area of improvement

It is equally unfortunate and unsatisfying that many and important users of the network data do take the existence of the networks for granted. Space missions supported or even rescued by laser ranging usually do not include any costs for the generation of the ranging data into their budget, an issue we might have to address in the very next future.

The workshop here in San Fernando will mainly address other issues: Issues that are in the direct responsibility of our service and technique, namely the continuous effort to improve the quality and quantity of our data and of our own direct analysis products, and to also improve the efficient and timely operation of all components and the network as a whole. We will also have to address completely new issues, e.g., how we are going to track satellites with onboard equipment that might be damaged by our laser beams under certain conditions.

The large number of presentations on the agenda promises a very interesting and fruitful week here in San Fernando. I would like to thank the local organizing committee as well as the program committee for the numerous preparations of the previous months and weeks. I am sure they will lead to an equally successful workshop as all the previous ones .

Thank you very much.

ROA: 250 YEARS OF SCIENTIFIC ACTIVITIES

Dr. Rafael Boloix, CN Director.

The origin of the Royal Naval Institute and Observatory in San Fernando, which is the oldest astronomical observatory in Spain, has its beginnings in the 18th Century. In 1751, Captain Jorge Juan of the Company of Midshipmen proposed to the Marquis de la Ensenada, the idea of building an observatory in the Castle of the Villa in Cádiz, which was the Headquarters of the Academy of Midshipmen. This was built with the intention of providing future Naval Officers with through Knowledge of Astronomy, the science that was so necessary for navigation.

From the date of 1753, the Royal Naval Observatory of Cadiz went on to earn deserved prestige in the context of European Astronomy thanks to the important development of work for personages such as Luis Godin or Vicente Tofiño and to the technical support of famous expeditions.

In 1798, the Royal Naval Observatory was transferred to the "Isla de León" in San Fernando, where it was constructed according to the plans of the Marquis of Ureña; this magnificent building has functioned until the present time. Starting in 1804, the organic dependency of the Academy of Midshipmen disappears and thus begins the scientific work of the institution into the new century, marked for well-known personages such as José Sánchez Cerquero or Cecilio Pujazón who worked in order to consolidate the function of the Observatory to its original astronomical work, added important missions to the Navy and to Spanish Science; such as the calculation of ephemeris and the publication of the Nautical Almanac, the Course of Superior Studies, the Warehouse of Chronometers and Instruments of the Navy and meteorological, seismic and magnetic observations. Nowadays the scientific activity is divided in four Departments:

- **DEPARTMENT OF EPHEMERIS:**

It is the mission of this Department to accomplish the theoretical studies and calculations of the astronomical ephemeris following the international rules of publishing in the most adequate form to their nautical and geodetic applications.

At present, the Department publishes annually the "Efemérides Astronómicas" to be used for astronomers, the "Nautical Almanac" in original and reduced version, both dedicated to the naval and air navigator and the "Astronomical Phenomena" including information concerning to eclipses, sunrise and sunset, etc.

- **DEPARTMENT OF ASTRONOMY:**

This Department develops their work within the field of the Astronomy of Position. Their fundamental mission is to determinate positions of celestial bodies and other magnitudes related to astronomy.

The Royal Naval Observatory participates with the Observatories of Greenwich and Copenhagen in the work of observation and investigation of the Danish Meridian Circle, whose installation on the Island of La Palma (Canary Islands) allows for the understanding of stellar catalogs of great extension and precision. The Department also uses a Meridian Circle Grubb-Parsons, the fundamental instrument of the Astronomy of Position, that, slightly modified and automated, studies the celestial sphere in coordination with the Meridian Circle of the Canary Island. The chosen place for their technical and environmental condition, is the Felix Aguilar Observatory of the University of San Juan (Argentina). Furthermore, the

Astrolabe Danjon directed to work observating of the Sun after conducting important modifications and the Gautier Astrograph incorporating a CDD camera to measure astrometric positions, has opened new possibilities of its utilization in the field of Astrometry and in the field of education.

- **DEPARTMENT OF TIME:**

The mission of this Department is to keep of time scales in use with the highest precision and accuracy, and to disseminate them in the most convenient way for the different scientific necessities such as navigation and national industry.

The installation is composed by an ensemble of ten Cesium Beam clocks, frequency and time primary standards, and two Rubidium, secondary frequency standards. With the readings of all of them, a Time Scale named Universal Time Coordinate with the Royal Naval Observatory, (Shortly UTC (ROA)), is generated and permanently contrasted through the Time Section of Bureau des Poids et Measures (BIPM), being its differences with the Universal Time Coordinate periodically published.

The Royal Naval Observatory in San Fernando actively participates in the intercomparison of its time scale with other time laboratories in the world and it also collaborates in determining the International Atomic Time with the inclusion of all its clocks.

The Calibration Service is allocated inside this Department with the responsibility of checking time equipments to be used in the Navy. The Laboratory of this service is integrated in the national enterprise of calibration frame and it is able to issue certifications, as National Time Standard Laboratory, on the calibrations performed to the time and frequency standards of the secondary laboratories of the quality control chain in the Spanish industry.

- **DEPARTMENT OF GEOPHYSICS:**

Concern to this Department all the subjects related with geophysics and geodesy, developing the investigation in the fields of Geomagnetism, Seismology and Satellites. It includes the Geophysical Observatory of the Navy.

For the maintenance of cooperation initiated in 1891 with the International Association of Geomagnetism, the geomagnetic installation has been moved to the Barrio de Jarana in Puerto Real, in order to avoid environmental noise.

The study of seismology has been another of the traditional fields of this Department since 1898. The equipment available includes: a Short Period seismic net, with 9 stations located in different points of the South West of Andalusia; a three components Long Period Station, located into the tunnels of the Observatory and a Broad Band seismic network, with 5 stations deployed along the South of Spain and North of Africa Region.

The Department service related to Geodesy, is called the Satellite Service, and includes the specialized observation of artificial satellites, which the Observatory incorporates from its beginnings in 1958. The service is using a 3rd generation Laser Station, installed in the dome of the main building of the Observatory, and also is working a permanent tracking GPS network. The geodetic GPS equipments belonging to the service make feasible to collaborate with different institutions in national and international campaigns.

Also belonging to this Department, is the Meteorological Station of the Observatory which is collaborating in this field with the National Meteorological Net.

This Department is responsible also for the participation in Geophysics and Geodesy

campaigns, by own initiative or by invitation of other institutions. The participation in diverse Antarctic campaigns, surveys of Seismic Profiles, marine geomagnetic surveys, etc.

- **THE LIBRARY**

The library, inseparable from the scientific chore of the Observatory and of the educational tasks of the School of Superior Studies of the Navy, has at the present time, more than, 30,000 volumes. The specialization of their bibliographic and the important collection of periodic publications transforms it into one of the most interesting scientific libraries in Spain. The old bibliographic material of the library (15^{th} to the 18^{th} Century) is composed of works by a very special group for the history of science. In addition, the Library has an important collection of cartographic material (17^{th} to 20^{th} Century) and historic documentation about the institution from 1768 to 1940.

- **EDUCATIONAL ACTIVITY**

The School of Superior Studies in Science Mathematical Physics:

Founded in 1856, it has as its mission to give to groups of Officers of the Navy, a Physical/Mathematical Sciences Superior education which allows them, to form a faculty nucleus qualifying in Physical Sciences/Mathematics for the Higher School of learning of the Navy and in general positions, that require a special scientific preparation with a current knowledge of the evolution of the Sciences.

The Teaching is organized in two cycles: Basic and Specialization.

In order to complete the fundamental mission of the School, the Basic Cycle, with a duration of three years, is planned so that this course, increases the level so scientific preparation of Managers and Officials selected for a posterior specialization in the University and National or foreign Scientific Centres.

The Cycle of Specialization in Astronomy and Geophysics, with a duration of two years, is mainly dedicated to the preparation for the investigation and the education of the scientific personnel of the Royal Institute and Observatory of the Navy.

IAG's GLOBAL GEODETIC OBSERVING SYSTEM (GGOS) IN ITS INITIAL PHASE

Hermann Drewes(1), Christoph Reigber (2)
(1) Deutsches Geodätisches Forschungsinstitut (DGFI), München, Germany
(2) GeoForschungsZentrum (GFZ), Potsdam, Germany

Introduction

The Global Geodetic Observing System (GGOS) was installed during the XXIII General Assembly of the International Union of Geodesy and Geophysics (IUGG) in Sapporo, Japan, July 2003, as the first and presently only Project of the International Association of Geodesy (IAG). IAG's Projects are, according to its bylaws, of broad scope and of highest interest for the entire field of geodesy. They serve as the flagship of the Association for a long period (decade or longer).

The initial phase of GGOS was set up directly after the Sapporo 2003 meeting by nominating the Project Board. The first meeting of the GGOS Project Board took place before the IAG EC Meeting at the EGU General Assembly, Nice, April 24, 2004. During this meeting the objectives were revised and the first structure was installed nominating initial chairpersons.

The Vision of GGOS

The vision of GGOS as IAG's flagship was discussed by the "Committee for the Realization of the New IAG Structure" during the years 2002-2003 and defined by the GGOS Planning Group. It may be highlighted as follows:

- GGOS integrates different geodetic techniques, different models, different approaches in order to achieve better long-term consistency, reliability and understanding of geodetic, geodynamic and global change processes.
- GGOS provides the scientific and infrastructure basis for all global change research in Earth sciences. In the frame of GGOS the Earth system is viewed as a whole by including the solid Earth as well as the fluid components, the static and the time-varying gravity.
- GGOS is geodesy's contribution to Earth sciences and the bridge to the other disciplines; it asserts the position of geodesy in geosciences.

The Mission of GGOS

Following these basic ideas, the mission of GGOS may be seen twofold, the coordination within geodesy and the representation of geodesy in public. The internal matters are summarized by the tasks

- to collect, archive and ensure accessibility of geodetic observations and models;
- to ensure the robustness of the three fields of geodesy: geometry and kinematics, orientation and rotation, and gravity field of the Earth;
- to identify geodetic products and to establish the requirements concerning its accuracy, time resolution, and consistency;
- to stimulate close cooperation between IAG services, to identify service gaps and develop strategies to close them.

If we look at the present situation in geodesy we may find some significant deficiencies with respect to the listed tasks. The robustness of the three fields of geodesy is not sufficiently exhausted due to some inconsistencies in the used models and provided products in the different areas. The requirements concerning accuracy and time resolution should be similar for all parameters. However, while we get 10^{-9} for the geometric parameters (e.g., surface coordinates) we are far off this level in gravimetric parameters (geoid, gravity anomalies). Gaps in geodetic services are, e.g., a unified global height reference system (global vertical datum), vertical deformation models (tectonic, isostatic, loading, ...), time dependent sea level models from (satellite altimetry), free availability of terrestrial gravity data. A close cooperation of services is needed to use identical standards, models and parameters, to generate compatible products, and to coordinate common research fields of mutual interest.

The representation of geodesy in public means in particular

- to promote and improve the visibility of geodetic research;
- to achieve maximum benefit for the scientific community and for society in general.

It is obvious that geodesy is not well-known in society although geodetic products (surface coordinates, Earth orientation parameters, gravity potential) are used in surveying, cadastre, engineering, global spatial data infrastructure, rural and urban development, space-travel, navigation etc. We have to let people know that it's geodesy that provides the basis for these applications. We must publish more in popular literature, not only in scientific journals.

To achieve more visibility and influence we have to exchange data and information with geosciences and other sciences in an easily understandable way, and provide policy makers and publicists with the necessary information for their decisions and reports. This part of geodesy has widely been neglected in the past.

The objectives of GGOS

The specified objectives of GGOS may be derived from the tasks mentioned in its mission:

- GGOS aims at maintaining the stability of time series of geometric and gravimetric ***reference frames***;
- GGOS ensures the consistency between the different geodetic ***standards*** used in the geo-scientific community;
- GGOS aims at improving the geodetic ***models*** at the level required by the observations;
- GGOS focuses on all aspects to ensure the consistency of geometric and gravimetric ***products***;
- GGOS shall be established as an official partner in the United Nations' ***Integrated Global Observing Strategy, IGOS***,
- GGOS shall represent IAG in the inter-governmental ad hoc ***Group on Earth Observations, GEO.***

Table 1 gives some examples to demonstrate the necessity of looking seriously after the consistency of standards, models and reference frames in geodetic products. We have several options to define and to realize the parameters. As a matter of fact, there is no complete homogeneity in the use of these parameters. The origin, orientation and scale of reference frames is defined differently in geometric and gravimetric applications, and they are not

always consistent. E.g., the models for reducing the effects of Earth tides are not identical in geometric and gravimetric products. While the permanent effect of Sun and Moon is normally included in gravity data and models, it is reduced in geometric parameters (e.g., coordinates). This means, that the basic formula h = H + N (ellipsoidal height = orthometric height + geoid height) is not fulfilled if we take h, H from geometric and N from gravimetric results.

Table 1: Examples for inconsistencies in geodetic standards, models, products.

	Geometric parameters	*Gravimetric parameters*
Definition of origin ... of orientation ... of scale	centre of network: X_0, Y_0, Z_0 rotation axis: X_P, Y_P, DUT c	centre of mass: C_{10}, C_{11}, S_{11} axis of inertia: C_{12}, S_{12} GM
Models for tides ... for deformation	tide free geometric only	zero tide dynamic
Product reference ... update	ITRF, GRS80 regularly	variable episodic

The Scientific Rationale of GGOS

The Global Geodetic Observing System shall have the *central theme* "Global deformation and mass exchange processes in the System Earth" which includes all the activities of GGOS in the future:

- The study of all global patterns of tectonic deformation;
- Investigations on global patterns of all types of height changes;
- Deformation due to mass transfer between solid Earth, atmosphere, and hydrosphere including ice, of geodynamic as well as of anthropogenic origin;
- Quantification of angular momentum exchange and mass transfer.

The list is not meant to be final and will be further developed.

Geodesy is capable of providing information on the mass exchange between all elements (components) of the Earth's system by observing
- deformation of the solid Earth (geometry and kinematics) by precise positioning,
- water circulation in oceans, ice covers, atmosphere, solid Earth by satellite radar and laser altimetry, atmospheric sounding, gravity),
- mass exchange between the atmosphere, the hydrosphere and the biosphere via the angular momentum by observing variations of Earth rotation and the gravity field.

Recent Activities of GGOS

The activities of GGOS within the geodetic community is done continuously by interaction closely with the IAG Services. There are twelve services which are cooperating more and more intensively in order to overcome inconsistencies in standards, models and parameters as well as to close gaps in service products. While the geometric services (International Earth Rotation and Reference Systems Service, IERS; International GPS Service, IGS; International Laser Ranging Service, ILRS; International VLBI Service, IVS; International DORIS Service,

IDS) are working together very closely, there may be some improvement of cooperation within the gravimetric services (International Gravity Field Service, IGFS; International Gravimetric Bureau, BGI; International Geoid Service, IGeS; International Centre for Earth Tides, ICET) and between both.

With respect to the representation of geodesy in international bodies, GGOS started some important activities during the last two years. It submitted a concept note for a "Dynamic Theme" within United nations' Integrated Global Observing Strategy (IGOS) and was encouraged to develop a proposal for a new theme following the IGOS-P regulations and coordinate the proposal preparation with the geohazard theme, the ocean theme and the water cycle theme.

IAG has become a participating organization in the intergovernmental ad-hoc Group on Earth Observations (GEO) and nominated the GGOS Chair Christoph Reigber as its representative to the GEO plenary. GGOS participated in the development of a 10-year implementation plan for a Global Earth Observing System of Systems (GEOSS) by working with ten members in the five corresponding subgroups.

Some regional activities were also started to support GGOS:

- In the USA the Project "Inter-Service Data Integration for Geodetic Operations" (INDIGO) will enable improved performance, accuracy, and efficiency in support of NASA's Earth science and inter-national user community by developing and providing uniform access to heterogeneous space geodetic data systems;
- The EU project on "Geodetic And Geohazard Observing Systems (GAGOS)" of the European Partners in GGOS (EPIGGOS) has the main goal to identify necessary adaptations of the existing infrastructure (including data management) and new deployments for the assessment of in-situ capabilities in Earth observation systems.

Conclusion

There are two principal aspects in the mission of GGOS:

1. "Internally" to guarantee the reliability of geodetic products by ensuring the consistency of standards, parameters, models and reference systems used in the three fields of geodesy: Earth geometry, Earth orientation, and Earth gravity field.
2. "Externally" **t**o promote and improve the visibility of geodetic research and results, to represent geodesy in international bodies, and to achieve maximum benefit for the scientific community and for society in general.

A MULTI-YEAR SLR SOLUTION

H. Mueller, D. Angermann, B. Meisel
Deutsches Geodaetisches Forschungsinstitut (DGFI), Muenchen.
E-mail: mueller@dgfi.badw.de, Fax : +49-89-230311240

Abstract

The global Satellite Laser Ranging (SLR) network is fundamental for the realization of the origin (centre of mass) and scale of the terrestrial reference frame. Hence a continuous evolution and improvement of the SLR station coordinates is necessary. Based on SLR tracking data to LAGEOS-1 in the period from January 1981 until May 2004 and LAGEOS-2 in the period from October 1992 until May 2004, a new set of SLR tracking station coordinates and velocities was computed. The basis for the computations were weekly single satellite arcs, which were accumulated to the final solution. Since periodic signals and episodic effects influence the estimation of station positions and velocities we focused on the determination of these non-linear effects in the weekly position time series. Additionally we solved for low degree spherical harmonic coefficients of the Earths gravity field. This paper presents some results from the homogeneously reprocessed twenty-years SLR solution from January 1985 until November 2004.

Introduction and motivation

SLR data to LAGEOS-1 and LAGEOS-2 are a fundamental basis for the establishment and maintenance of a precise terrestrial reference frame. The latest models (e.g. IERS Conventions 2003, McCarthy and Petit, 2004) allow a more precise modelling of the orbital errors. Therefore we have reprocessed all LAGEOS tracking data back to 1981 using the latest version of the DGFI developed software package DOGS (DGFI orbit and geodetic parameter estimation software). More information on the DOGS software is available from http://ilrsac.dgfi.badw.de/dogs/index.html. On the basis of weekly arcs we processed a first solution using 5 years of data (January 1999 – May 2004) to test the new models and to get better estimates for the new SLR tracking stations, which was presented at the ILRS Workshop in San Fernando. Meanwhile we have included data since 1984 (the data before 1984 are significantly less precise, see figure 4) and we have computed a multi-year solution from January 1985 until November 2004. The extended time span significantly improves the velocity estimations for the SLR stations.

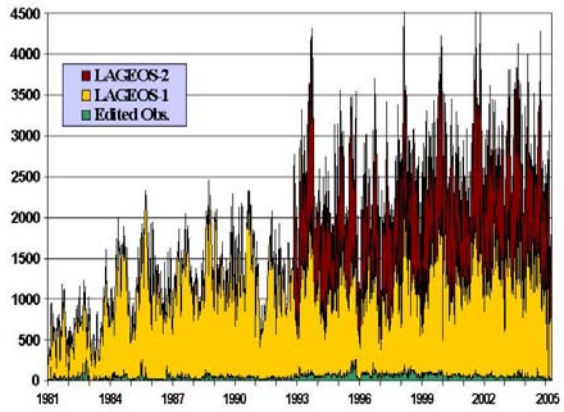

Figure 1: Number of normal points

A major goal of the reprocessing is to compute a consistent multi-year solution, which can serve as reference for various issues, such as the bias estimation for the tracking stations, the operational weekly computations and combinations of SLR solutions within the ILRS, the weekly inter-technique combination in the framework of the IERS Combination Pilot Project,

and for the computation of a refined terrestrial reference frame (see Angermann et al., 2004, Meisel et al., 2004). It is well-known, that the ITRF2000 does not include the newer SLR tracking stations, and furthermore for some stations the ITRF2000 position and velocity estimations are unreliable.

Data processing

We started the processing on the basis of weekly single satellite arcs using models and standards according mostly to the IERS Conventions 2003. We included all SLR data available, also those of stations with poor tracking quality to get a complete SLR network solution. The number of used normal points varies around 1000 to 1500 per satellite and arc from 1985 over the whole period with some fluctuations (see figure 1). Some peeks indicating intensive tracking campaigns can be identified. These weekly arcs were used to detect outliers and biases. During the processing of the weekly arcs we solved for:

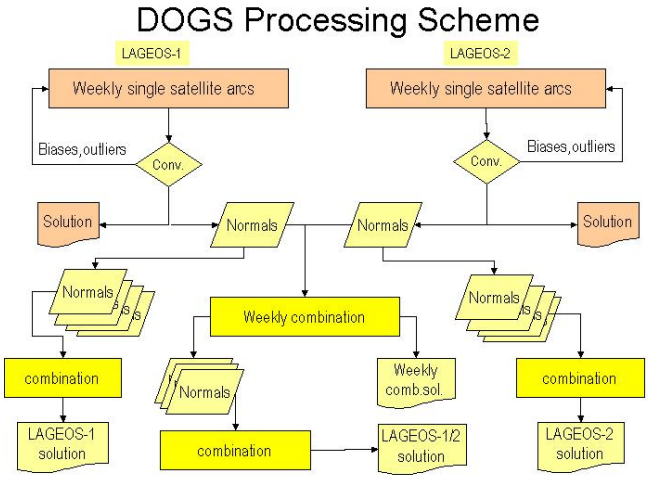

Figure 2: Processing of DGFI SLR solutions

- 6 orbital elements
- 1 revolution dependent parameter (cross and along track)
- 3 empirical along track parameters
- 3 solar radiation pressure parameters
- daily earth orientation parameters
- station coordinates
- potential coefficient J2
- significant pass dependent range and time biases.

The computation of the weekly single arcs was done with the DOGS-OC (orbit computation) module, the processing scheme is outlined in figure 2. The number of biases (either range or time biases) per week is shown in figure 3. In most cases there are only between 5 and 10 biases, with a few weeks containing more than 25. Nearly all biases are not from the core stations. We produced time series of station coordinates to verify the stability of the weekly solutions and to identify non-linear effects (e.g. peridoic signals and discontinuities). Thereby we eliminated stations with less than 10 weeks of tracking and some outliers in the time series. In a final step the weekly normal equations were accumulated to a multi-year solution containing station coordinates and velocities using the DOGS-CS (combination and solution) module. For quality control we computed independent LAGEOS-1 and LAGEOS-2 solutions and a combined solution as the final result, which was compared to the single satellite solutions.

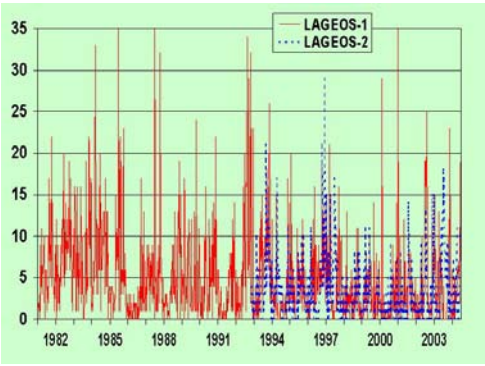

Figure 3: Number of weekly biases

Results

Figure 4 shows the r.m.s. fit of the weekly arcs over the entire data time span. During the first years (1981-1984) the tracking precision improved rapidly. Until 1993 the accuracy level was about 2-3 cm. Since the launch of LAGEOS-2 the 1 cm level was nearly reached, but for some weeks the accuracy was degraded probably due to tracking problems of some stations. Since about 2000 all stations have reached a high tracking performance, so the weekly r.m.s. is below 1 cm for both satellites.

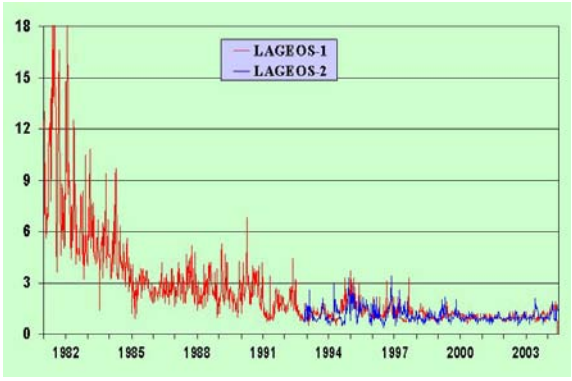

Figure 4: Weekly r.m.s. fit

As a result of the reprocessing two time series for the geopotential coefficient J_2 were generated. Figure 5 shows the weekly estimated J_2 values (relative to J_2 = 0.0010826) independent for LAGEOS-1 and LAGEOS-2. The higher scatter before 1985 can clearly be seen, which is in accordance with the worse orbit precision (see figure 4). In general there is a good agreement between the estimates of both satellites. However, the higher noise after 2000 for LAGEOS-1 and the discontinuity in the year 2000 is not yet clear and subject of further investigations.

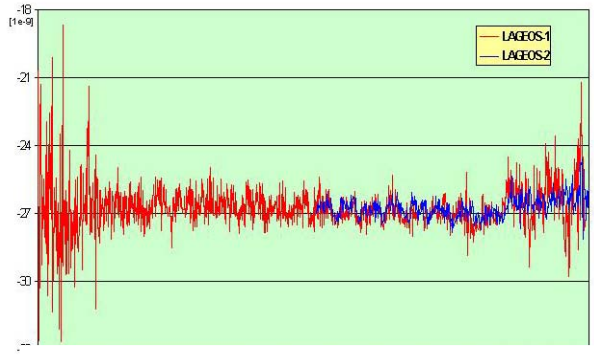

Figure 5: J2 values relative to 1.0826e-03

The time series of station coordinates proved the high stability of the weekly solutions. As an example the time series for Yarragadee, Australia, a station with long tracking history is shown (see figure 6). Each weekly solution has been transformed to the combined SLR solution, using 7 parameter similarity transformation. The offsets in X- Y- and Z-direction are a measure for the stability of the underlying reference frame. The results reflect common (global) variations of the network origin of the weekly SLR solutions w.r.t. the multi-year solution, and are sensitive to the network geometry and to changes of the selected stations used for the transformations. Figure 7 shows the translation parameters for the weekly arcs compared to the combined solution over the whole period.

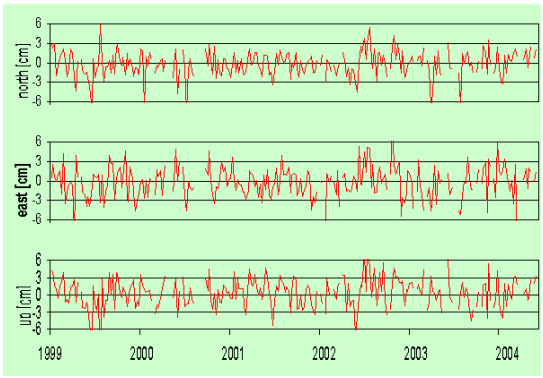

Figure 6: Time series of Yarragadee

Finally the SLR solution was compared with ITRF2000 (Altamimi et al., 2002; Boucher et al., 2004). As an example figure 8 shows the station velocities of both TRF realizations in Europe and parts of Asia. For most of the stations there is a quite good agreement. However there are

some stations with large discrepancies. The Riyad station for example has an improved velocity estimation in this SLR solution, ITRF2000 has only a few weeks of observations.
More results of the combined solution as well as the weekly SLR solutions since 2004, as part of the ILRS analysis working group project, are available from DGFI-Homepage at http://ilrsac.dgfi.badw.de.

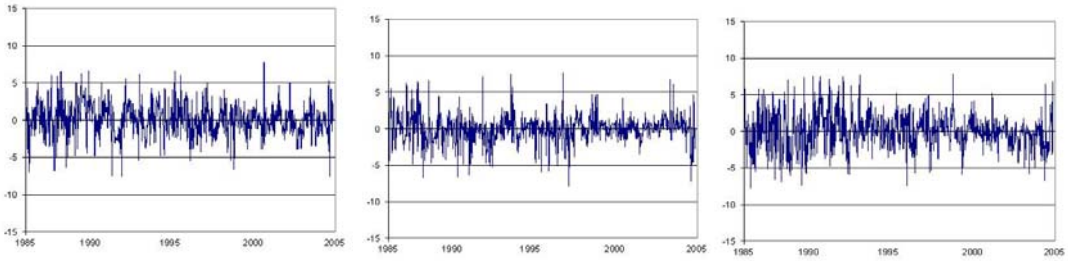

Figure 7: Transformation parameters in x, y and z of the weekly solutions in centimetre

Conclusion and Outlook

This homogeneously reprocessed twenty-years SLR solution includes station positions and velocities of nearly all SLR stations operating since 1984. It serves as a fundamental basis for various scientific issues and in particular for the realization of a refined terrestrial reference frame. Only 1 to 2 per cent of the over all tracking data were edited, see figure 1, which proves the quality of the used models. Using weekly arcs as basis for multi-year solutions helps to detect data problems and outliers and allows to identify periodical signals and discontinuities in the station positions, which are not properly considered (modeled) in recent realizations of the terrestrial reference frame, such as the ITRF2000.

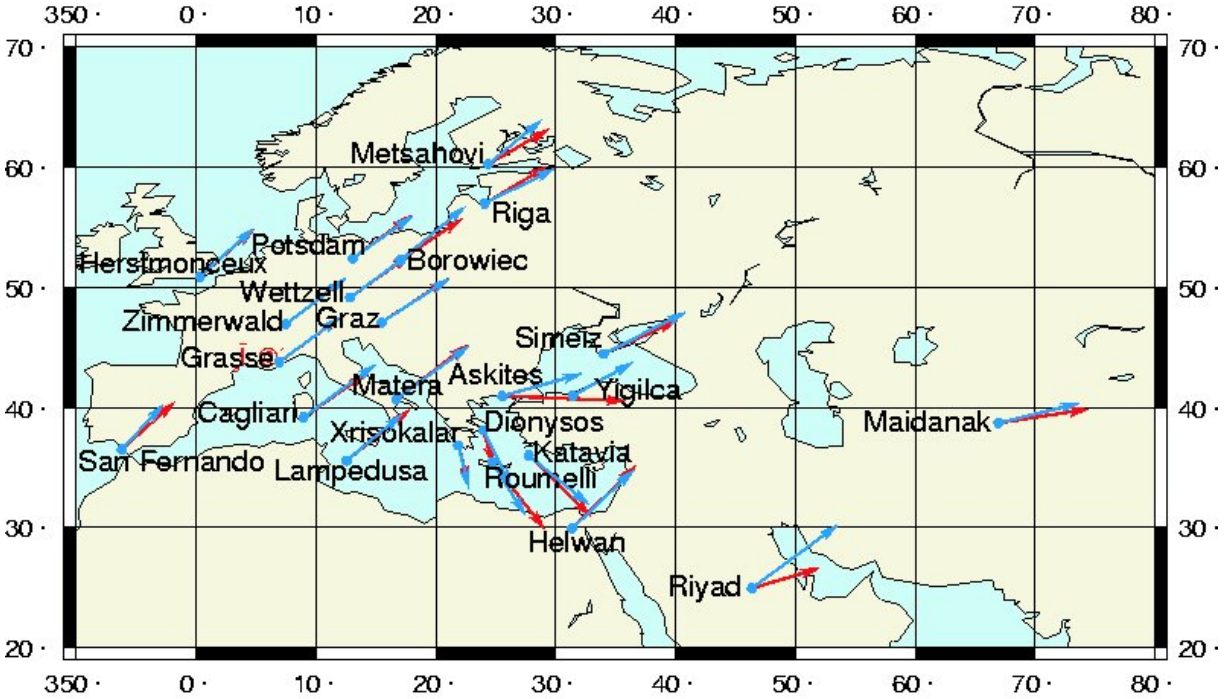

Figure 8: Some station velocities in Europe and parts of Asia (DGFI blue, ITRF2000 red)

We will also add the years 1981 to 1984 to this solution to get better velocities for those stations observing only in the early 80's and we will include ETALON1/2 and recent LAGEOS1/2 tracking data. In response to the call for submission of input data for a new ITRF2004 solution, which has been released by the end of the year 2004, we have provided weekly SLR solutions from January 1993 until the recent week containing station positions and daily Earth orientation parameters according to the guidelines from the ILRS/AWG.

References

Altamimi, Z., P. Sillard, C. Boucher: ITRF2000: A new release of the International Terrestrial Reference Frame for earth science applications, J. Geophys. Res. 107 (B7), 2214, doi: 10.1029/2001JB000561, 2002.

Angermann, D., H. Müller, M. Gerstl: Geocenter variations derived from SLR data to LAGEOS 1 and 2. In: Adam, J., K.-P. Schwarz (Eds.), Vistas for Geodesy in the New Millinium,. IAG Symposia, Springer, Vol. 125, pp. 30-35, 2002.

Angermann, D., H. Drewes, M. Krügel, B. Meisel, M. Gerstl, R. Kelm, H. Müller, W. Seemüller, V. Tesmer: ITRS Combination Center at DGFI: A terrestrial reference frame realization 2003. Deutsche Geodätische Kommission, Reihe B, Heft Nr. 313, 2004.

Angermann, D., H. Drewes, M. Gerstl, R. Kelm, M. Krügel, B. Meisel: ITRF combination - Status and recommendations for the future. In: Sanso, F. (Eds.): A Window on the Future of Geodesy. IAG Symposia, Vol. 128, Springer, 2005a.

Boucher, C., Altamimi, Z. Sillard, P., Feissel-Vernier, M. The ITRF2000. IERS Technical Note No. 31, Verlag des Bundesamtes für Kartographie und Geodäsie, Frankfurt am Main, 2004.

McCarthy, D.D., G. Petit: IERS Conventions (2003). IERS Technical Note 32, Verlag des Bundesamtes für Kartographie und Geodäsie, Frankfurt a.M., 2004.

Meisel, B., D. Angermann, M. Krügel, H. Drewes, M. Gerstl, R. Kelm, H. Müller, V. Tesmer: Refined approaches for terrestrial reference frame computations, submitted to Adv. Space Res., 2004.

Rothacher, M.: Towards a Rigorous Combination of Space Geodetic Techniques, Proceedings of the IERS Workshop on Combination Research and Global Geophysical Fluids, IERS Technical Note 30, 7-18, Bundesamt für Kartographie und Geodäsie, Frankfurt a. M., 2003.

PROCESSING 18.6 YEARS OF LAGEOS DATA

J-M Lemoine (1), R Biancale (1), G Bourda (2)
(1) GRGS/CNES, Toulouse.
(2) GRGS/SYRTE, Paris Observatory
jean-michel.lemoine@cnes.fr

Abstract

18.6 years of good quality Lageos data are now available and can give us at last some refined value of the lunar node tide (Ω_l) as well as a better estimation of the secular drift of the dynamical flattening C_{20}.
Lageos data from 1985 until 2004, merged with Lageos2 data from 1993, were used to compute the time variations of the degree 2 coefficients of the Earth's gravitational potential. This was done with recent orbit standards, taking into account the latest developments on geopotential model from the GRACE gravity mission.
Several characteristic periods appear in the C_{20} spectrum which can be correlated mainly with tidal effects. But some inter-annual variations still remain, probably due to water mass displacement in the oceans as well as on the continents.

SLR CONTRIBUTIONS IN THE ESTABLISHMENT OF THE TERRESTRIAL REFERENCE FRAME

E. C. Pavlis
JCET/UMBC and NASA Goddard, Maryland, USA
epavlis@JCET.umbc.edu/Fax: +1-410-455-5868

Abstract

The origin of the Terrestrial Reference System (TRS) is realized through the adopted coordinates of its defining set of positions and velocities at epoch, constituting the conventional Terrestrial Reference Frame (TRF). Since over two decades now, these coordinates are determined through space geodetic techniques, in terms of absolute or relative positions of the sites and their linear motions. The continuous redistribution of mass within the Earth system causes concomitant changes in the Stokes' coefficients describing the terrestrial gravity field. Seasonal changes in these coefficients have been closely correlated with mass transfer in the atmosphere, hydrosphere and the oceans. The new gravity-mapping missions, CHAMP and GRACE, and to a lesser extent the future mission GOCE, address these temporal changes from the gravimetric point of view. For the very low degree and order terms, there is also a geometric effect that manifests itself in ways that affect the origin and orientation relationship between the instantaneous and the mean reference frame. Satellite laser ranging (SLR) data to LAGEOS 1 and 2 contributed in this effort the most accurate results yet, demonstrating millimeter level accuracy for weekly averages. Other techniques, like GPS and DORIS, have also contributed and continue to improve their results with better modeling and more uniformly distributed (spatially and temporally) tracking data. We present our operational methodology and results from our latest analysis of several years of LAGEOS 1/2 and ETALON 1/2 SLR data, assess their accuracy and compare them to results from the various other techniques. A comparison of the SLR-derived trajectory of the "geocenter" with respect to the TRF, reveals a strong correlation with the recent geophysical events. The interpretation and comparison will benefit significantly from the future availability of geophysical series at higher temporal resolution and with more accurate content.

Introduction

Satellite Laser Ranging (SLR) has been for decades a primary tool in the establishment and maintenance of the Terrestrial Reference Frame (TRF) and monitoring of Earth's Orientation Parameters (EOP), in addition to being an extremely simple, precise and failsafe tracking technique. In this brief review of the contributions of SLR in the development of the TRF, we present the results for ITRF2000 [Altamimi et al., 2001], where SLR defines directly the origin and in part (50%) the scale of the TRF, as well as some indirect contributions, such as the observation of geophysical signals, improvement of models, theoretical validations, etc., which also help develop a better TRF.

Advances in technology require concomitant advances in science and vice versa. SLR has followed this principle for decades now, from the early (few-meter quality) systems to the latest (few-millimeter quality), highly automated and reduced size systems. At the same time, as scientists interpreted the higher quality results from SLR, the more interested they became and demanded even better quality data in order to reveal details that were possibly hidden in the higher level noise of the older systems. The technique reached maturity by the end of the '80s, however, it immediately entered a period of evolution which led to a wealth of major scientific contributions in several areas of terrestrial geophysics during the '90s: [Smith et al.,

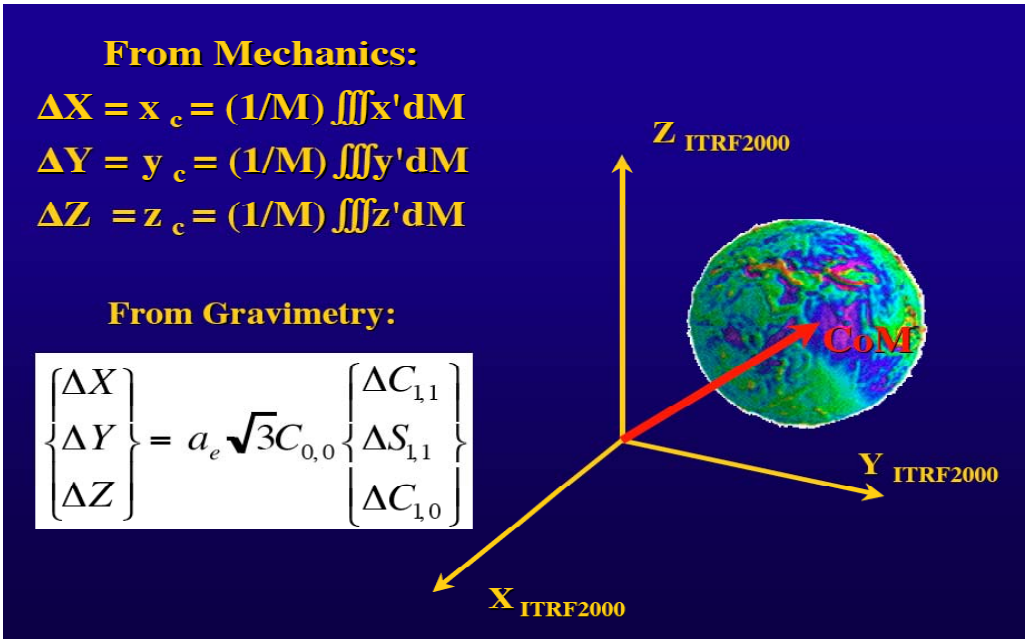

Figure 1. Center-of-mass (geocenter) definition and its relationship to gravity.

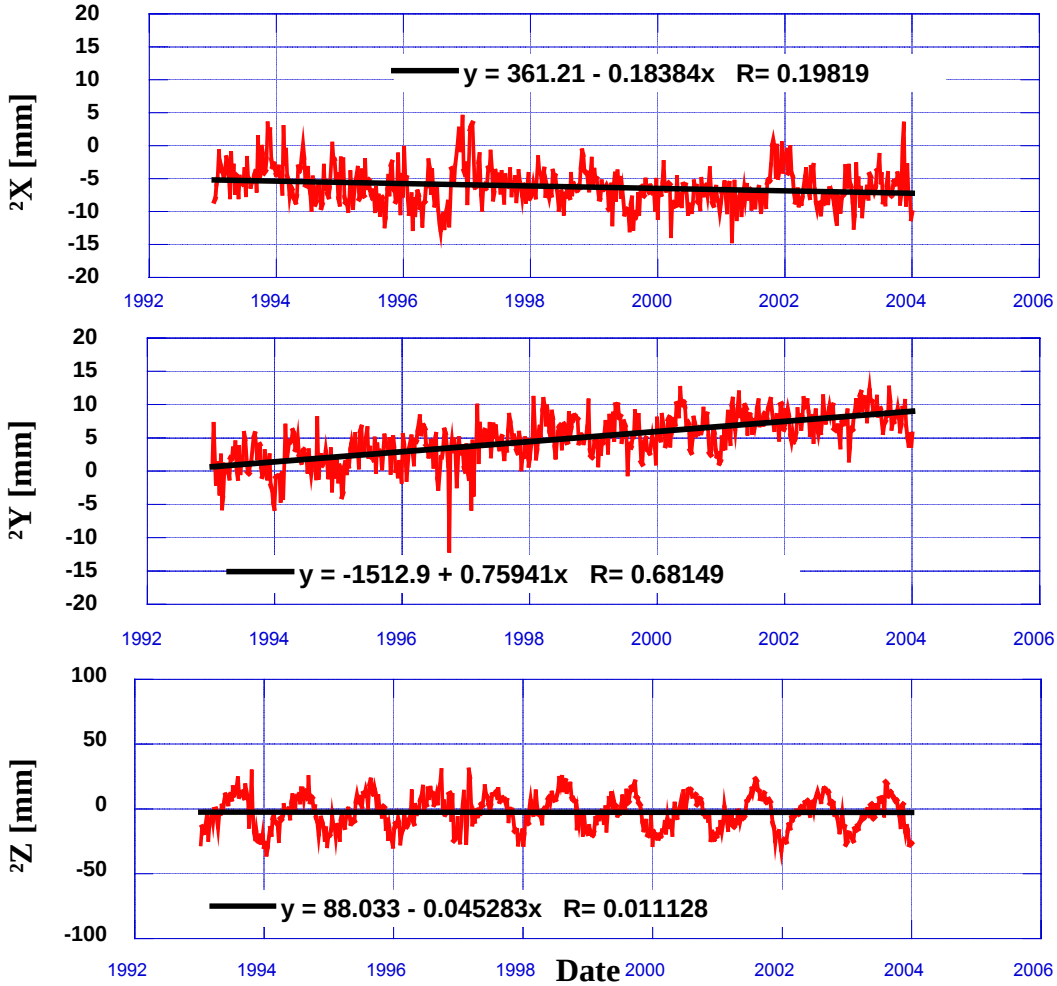

Figure 2. Center-of-mass (geocenter) variations at weekly intervals, SSC (JCET) L 2004.

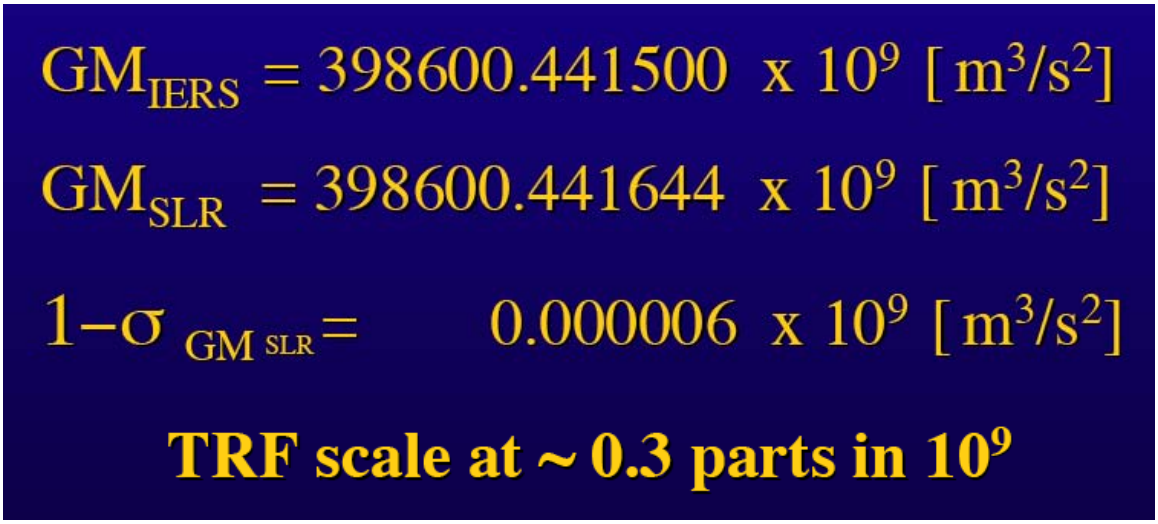

Figure 3. Scale of the TRF from 11 years of weekly SLR arcs, SSC (JCET) L 2004.

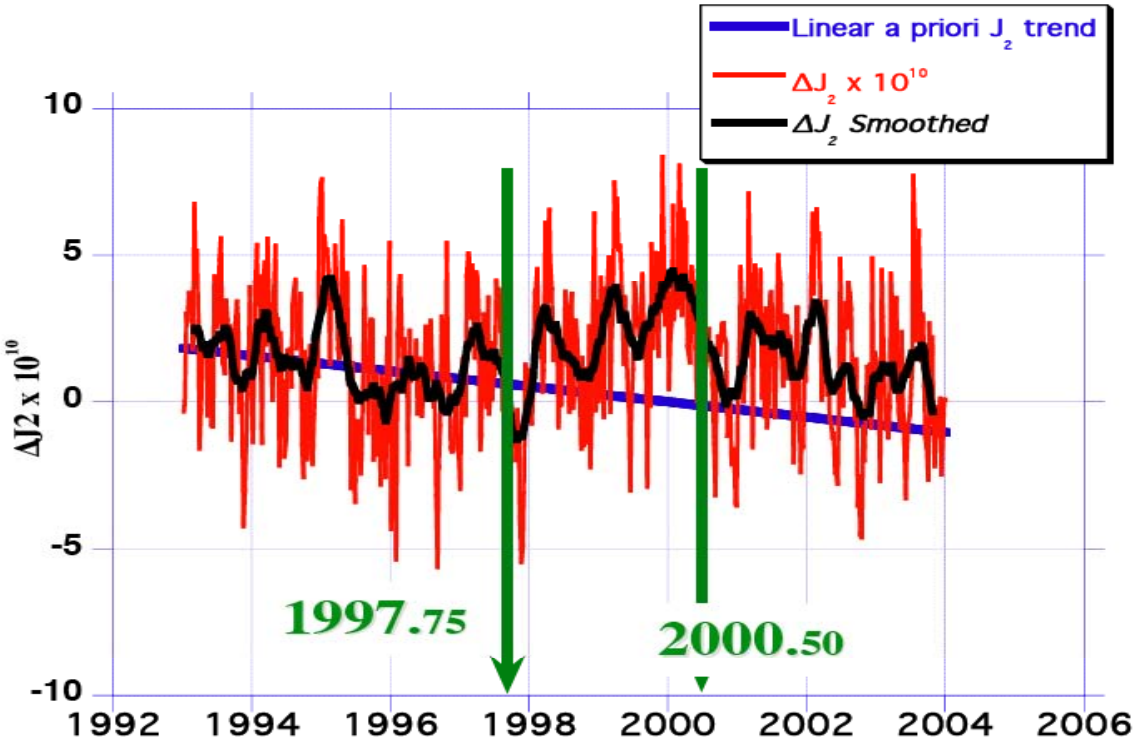

Figure 4. J_2 variation from eleven years of weekly SLR arcs, SSC (JCET) L 2004.

1990, 1994; Marsh et al., 1988, 1990; Degnan and Pavlis, 1994; Nerem et al., 1994; Pavlis, 1994; Lemoine et al., 1997].

The design and manufacturing of smaller, more efficient, autonomously operated, yet more accurate systems, ushered us into the new millennium [Degnan, 2001; Nicolas et al., 2001]. This transformation was followed by a change in the scientific applications of the SLR technique. With newer technologies (e.g. GPS) taking on the crustal deformation and tectonic motion problem at a global scale, SLR has refocused on the areas where it contributes in an unique way and with the greatest impact for science: the definition of the TRF origin (Figure 1) and its temporal variations ("geocenter motion", Figure 2), the scale of the TRF (Figure 3),

the precise determination of the long wavelength portion of the static and temporally varying part of the gravitational field of Earth (Figures 4-6), precise orbit determination (POD), the validation of radiometrically-determined orbits, the calibration of altimetric systems, exploitation of two-wavelength ranging for refraction modelling, tests of fundamental physics, interplanetary experiments, target characterization, orbital debris tracking, and several other areas.

In the following, we will highlight some of the recent achievements in the areas that are closely related to the development and maintenance of the TRF.

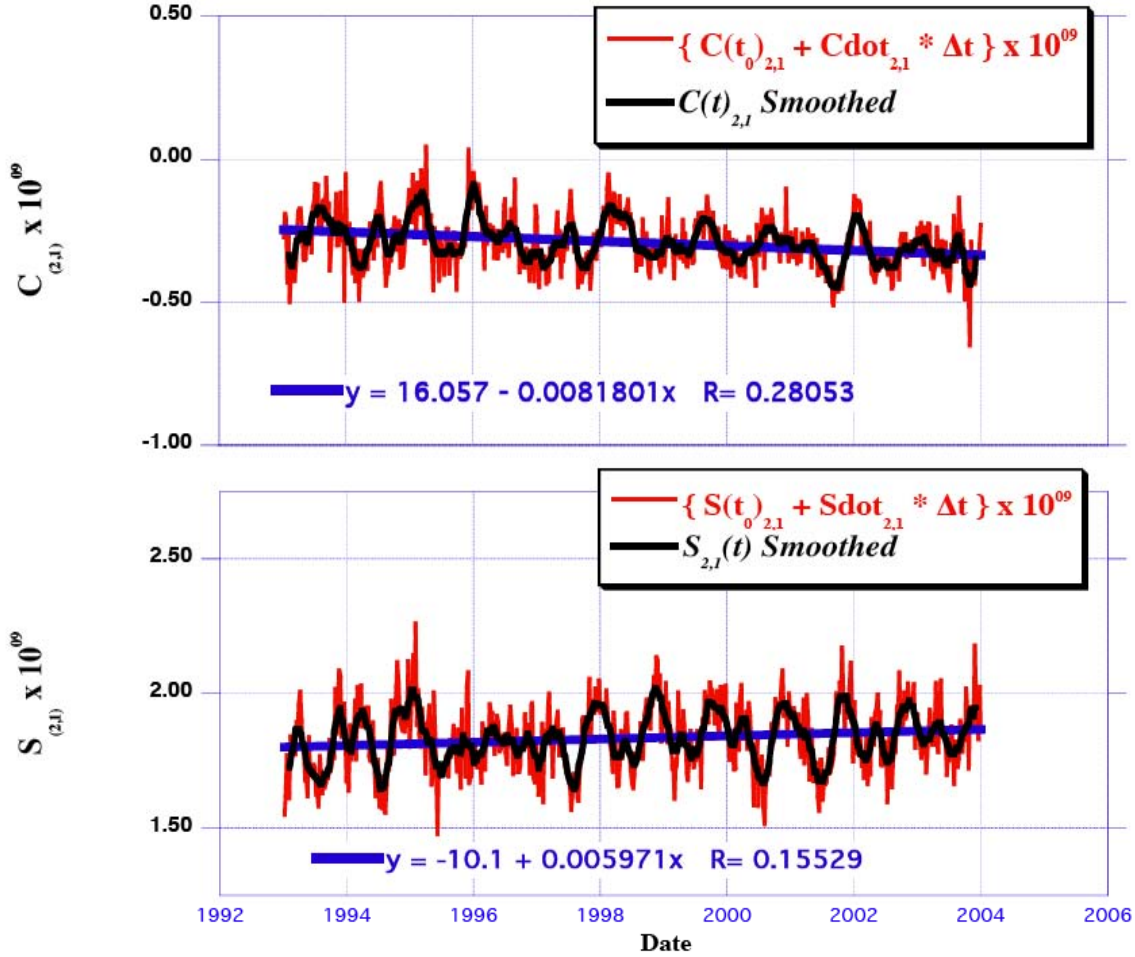

Figure 5. Axis of figure excitation from eleven years of weekly SLR arcs, SSC (JCET) L 2004.

SLR and the Terrestrial Reference Frame

The origin of the Terrestrial Reference System is realized through the adopted coordinates of its defining set of positions and velocities at epoch, constituting the conventional Terrestrial Reference Frame. Since many decades now, these coordinates are determined through space geodetic techniques, in terms of absolute or relative positions of the sites and their linear motions. In the early years (‘60s) the use of optical tracking resulted in the first “global” networks and the establishment of crude (static) versions of the TRF with meter-level quality. These techniques were soon (‘70s) followed by Doppler tracking with an order of magnitude improvement, only to be all displaced in the ‘80s by the early SLR and VLBI (Very Long Baseline Ineterferometry) systems that supported such groundbreaking international efforts as the two MERIT campaigns [Wilkins, 1981; Mueller, 1981] that launched the International

Earth Rotation Service (IERS) which took over from the astrometry-based Bureau International de l'Heure (BIH). Satellite tracking techniques use dynamics to define the origin and scale of the tracking station network since satellites "fall" naturally towards the center of mass of the central body (focus of the orbit) and the size their orbit is governed by the mass of that central body. This connection of the orbital dynamics with the properties of the central body led to the historical proposal for the use of artificial satellite dynamics for geodetic applications [Veis, 1960]. Today, the state of the art TRF is the International Terrestrial Reference Frame 2000—ITRF2000, [Altamimi et al., 2002]. An international and multi-technique effort is underway though to update this realization with a new one in early 2005, to be called ITRF2004.

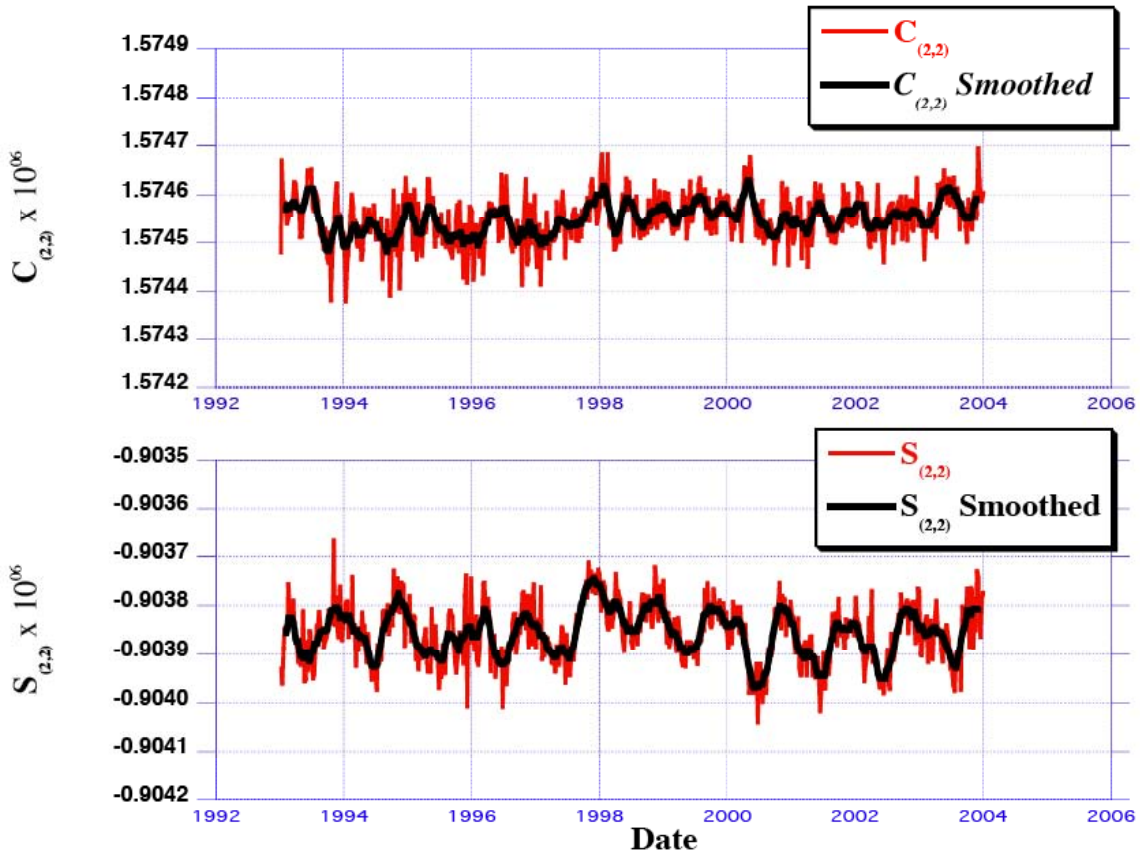

Figure 6. Dynamical equatorial flattening variation from eleven years of weekly SLR arcs, SSC (JCET) L 2004.

For the first decades of space geodesy, the terrestrial system, apart from the well known tidal variations, was viewed as a static one. Even in these early days though, it soon became apparent that if not the entire system, some of its parameters were changing in time, and the reasons were quickly traced to geophysical processes [Yoder et al., 1983]. This was followed by theoretical studies predicting farther changes due to the redistribution of masses within the individual components of system Earth: atmosphere, oceans and solid Earth. This continuous redistribution of mass causes concomitant changes in the Stokes' coefficients describing the terrestrial gravity field. This opened up an entirely new research area, temporal gravitational variations (TGV), and with it, it provided the missing link between space geodesy and climate change. This was fortuitous, since by this time the fortunes of the "big" and older space geodetic techniques (SLR and VLBI) were taken for the worse, with cutbacks and program reductions at national and international level. At the same time, it was widely

realized that since the "change" in climate change meant temporal change, the problems could not be properly addressed without a good handle on temporally changing gravitational signals with respect to a stable, well defined and very accurate reference frame. TGV thus became a new focus for the application of SLR to new problems and at the same time, a renewed role for SLR in the development of the TRF underlying the observed changes. This relationship was quickly identified as a "Catch-22", since to observe the changing world one needs a near-perfect TRF, which however is directly affected by these changes! Clearly only an iterative approach could give any results in practice.

We are thus in the early stages of this process, whereby the increased knowledge of System Earth allowed us to improve our definition of the TRF, which in turn allowed us to observe System Earth in a better way, learn even more about it, to be used to derive an improved TRF, and so on and so forth. Seasonal changes for example in the long wavelength harmonic coefficients of the gravitational potential have been closely correlated with mass transfer in the atmosphere, hydrosphere and the oceans, from independent observations of these Earth System components with other techniques and different space missions. The recently launched gravity-mapping missions, CHAMP and GRACE, and to a lesser extent the future mission GOCE, address these temporal changes directly from the gravimetric point of view. For the very low degree and order terms though, there is also a geometric effect that manifests itself in ways that affect the origin and orientation relationship between the instantaneous and the mean (over very long time periods) reference frame. This is one of the "couplings" between satellite dynamics and geophysics and geokinematics of Earth. SLR data contributed in this effort the most accurate results yet, demonstrating early enough millimeter level accuracy for short-term averages for these quantities [Pavlis, 1999, 2002]. Other satellite techniques, like GPS and DORIS, also contribute to the definition of these quantities, however, due to the nature of these techniques, their contribution is limited in accuracy. As these techniques continue to improve their results though, with better modeling and more uniformly distributed (spatially and temporally) tracking data, it is possible that they can become significant contributors in future TRF realizations. SLR can determine a "SLR-realization" of the TRF at present on a weekly basis with accuracy at the centimetre level. These weekly series are "stacked" over time, and subsequently, combined with the contributions from other space techniques, they produce the new, global TRF. This is the proposed process to be followed in the development of the new TRF realization "ITRF2004", sometime in 2005.

ITRF2000: The state-of-the-art in TRFs

The present state-of-the-art realization of the TRF is ITRF2000, as we already pointed out earlier. Here we will discuss the role of SLR contributions in its development and success. It should be pointed out that ITRF2000 was the first TRF that was developed based on a plan laid out ahead of its development and sanctioned by all techniques and analysis groups that eventually contributed to it. This was catalytic in that it engaged all analysis centers at all steps and through its evaluation over a couple of years and several dedicated meetings and workshops. During this process the value of organizing the Services for all geodetic techniques was recognized and this successful planning was used as the blueprint for the development of ITRF2004, with the individual contributions being channelled via the appropriate Services, thus ensuring uniformity, reliability and compatibility of the contributions.

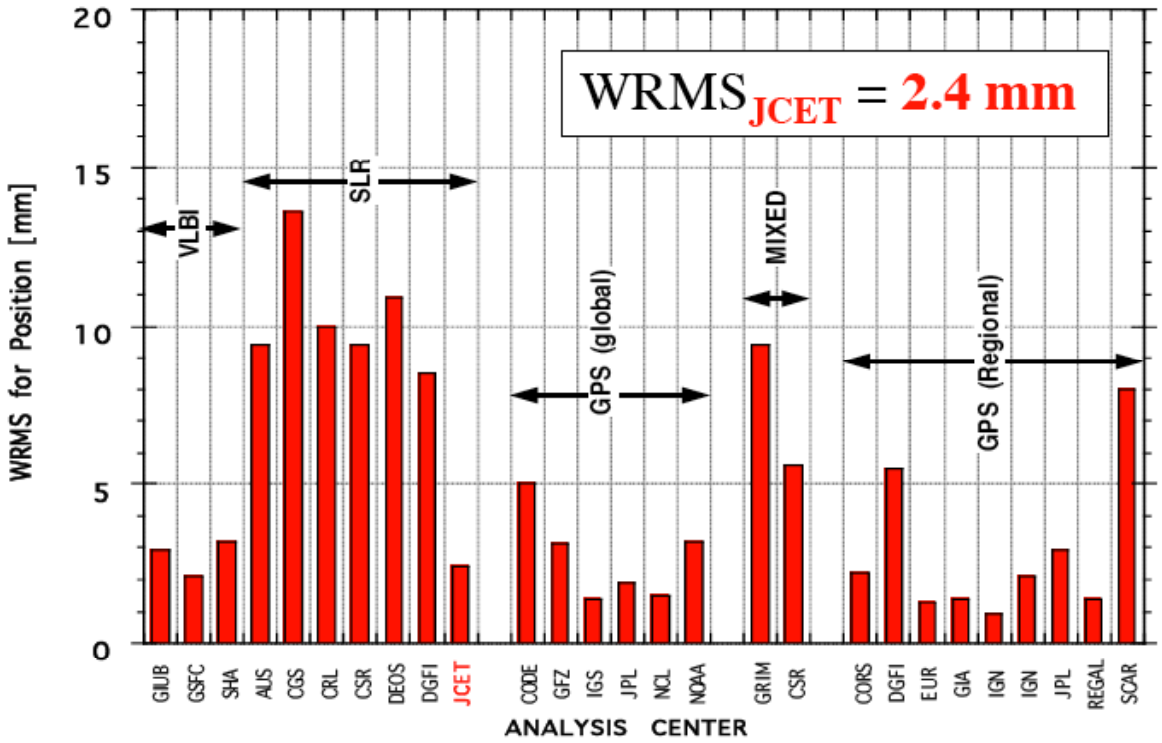

Figure 7. WRMS for positional components of individual ITRF2000 contributions.

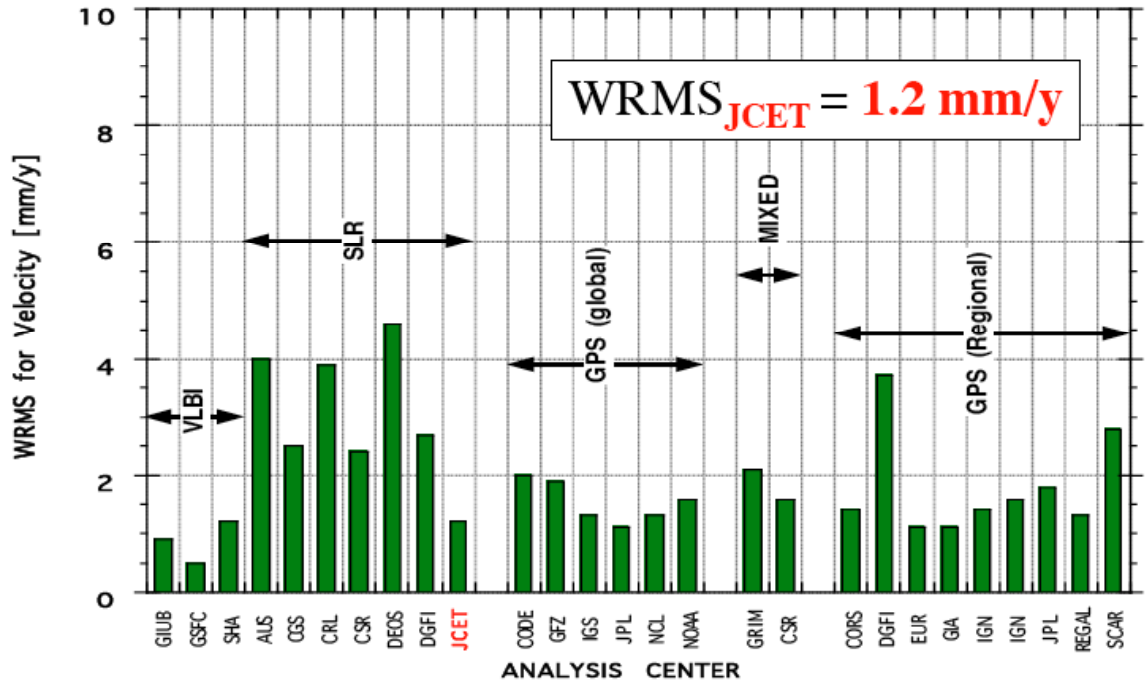

Figure 8. WRMS for velocity components of individual ITRF2000 contributions.

Figures 7 and 8 show for each of the individual contributions to ITRF2000 the level of agreement with the final product, in terms of position and velocity vectors for the common stations. They also display the corresponding quantities for the other individually

contributing techniques, as well as in combination. The superior global coverage of the GPS network and the excellent geometric sky-coverage due to multiple simultaneous targets compared to SLR, results in a far more consistent precision across various individual contributions and better agreement with ITRF2000. The marked difference between the majority of the SLR contributions and that of JCET is due to three factors. This contribution is restricted to the period 1993-2000, it allowed for the estimation of geocenter offsets on a weekly basis, and station biases were adjusted where needed due to irregularities in station performance. It is thus obvious, that with a careful approach in the analysis of the existing SLR data, the contribution to a TRF realization can be even in the relative sense, as comparable or even more significant, as any GPS contribution: Position $WRMS_{JCET}$ = 2.4 mm vs. six GPS contribution average $WRMS_{GPS6}$ = 2.8 mm and Velocity $WRMS_{JCET}$ = 1.2 mm/y vs. $WRMS_{GPS6}$ = 1.6 mm/y. This is in addition to the unique and undisputable contribution of SLR in the definition of the origin, and the equally shared definition of the TRF scale along with VLBI.

One of the unique advantages of SLR as a technique is its long history and presence, as it has a more or less global network in operation since the early '70s. This allows us to produce a uniform continuous Earth Orientation Parameter (EOP) series with a five-day resolution in the early years and a daily resolution after 1983 or so. The pole trajectory from SLR is shown in Figure 9, while in Figure 10, we plot the variations in the Length of Day (LOD), "draped" on a the integrated LOD which with the aid of benchmark values of UT1 from VLBI, provides the reference surface on which LOD is plotted.

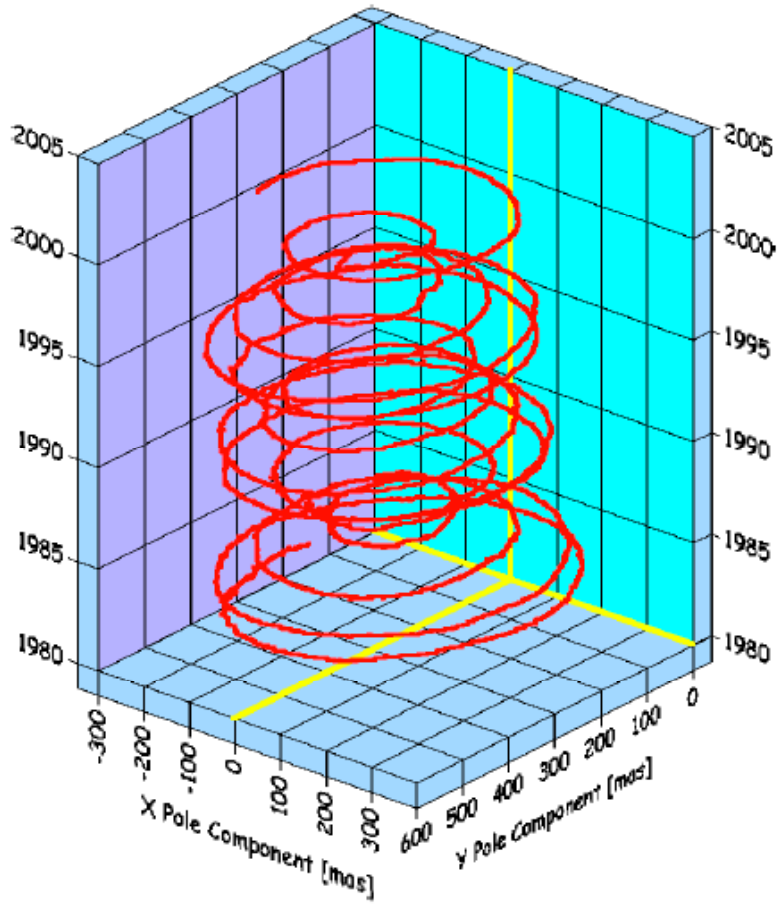

Figure 9. The trajectory of Earth's instantaneous rotational axis 1983-2002.

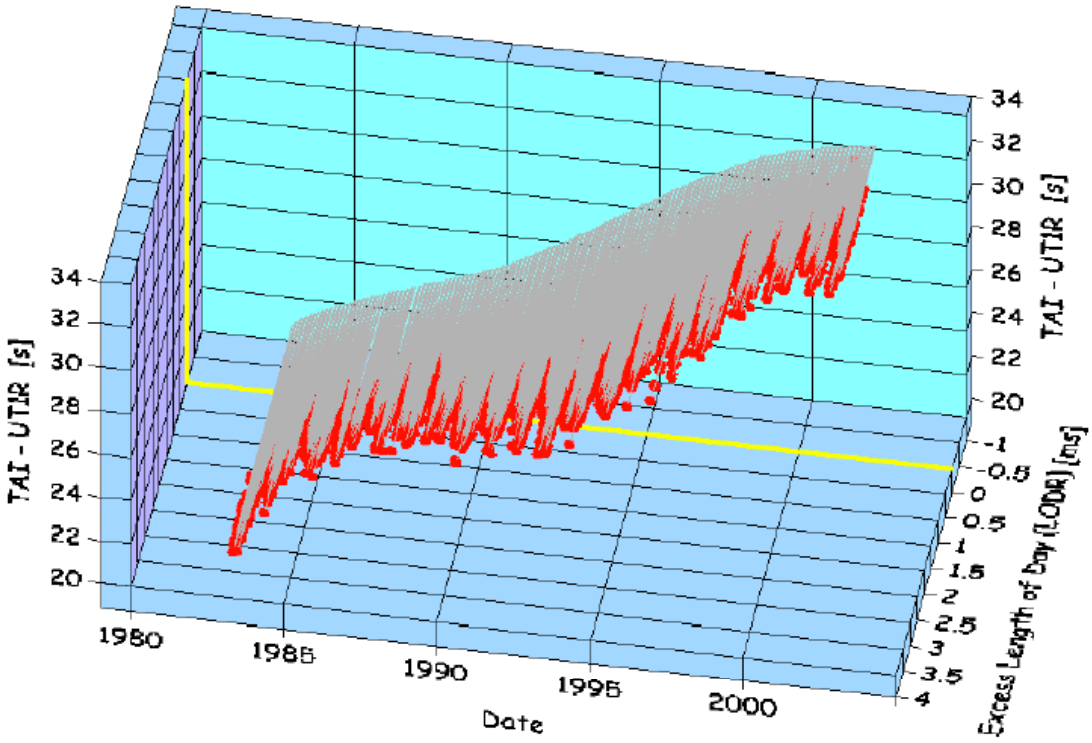

Figure 10. Excess Length of Day (LOD) and integrated UT1 difference with respect to TAI (using VLBI absolute UT1 values as control).

The value of these long in time and high in quality EOP series is in that they provide a check on the orientation of the TRF through the decades. By developing a very accurate TRF at present from (primarily) recent tracking data, we can (using these series) extend its use in analyzing older space geodetic data, collected at a time that the TRF was not available with such great accuracy and we can re-estimate the coordinates of older tracking stations that have since sized to exist, or derive other geophysical parameters of interest (e.g. long-wavelength gravitational coefficients and their temporal variations).

Geophysical Signals from SLR

SLR's direct contribution in the development of the TRF was already mentioned in the introduction and detailed in the previous sections. Here we will give some examples of how through the observation of temporal changes in the long-wavelength gravitational harmonics, it also provides an independent means of detecting geophysical signals and thus contributes in the Global Earth Observation System and in Global Climate Change studies.

We have already seen how the dynamics of the precise LAGEOS orbits are capable of delivering weekly observations of the variation in the location of the geocenter with respect to the center of figure realized by the tracking stations network (Fig. 2). One immediate observation from Figure 2 reveals that although the dominant signals are the annual and possibly a semi-annual harmonic along with high frequency "noise", there are at times significant departures persistent over time from this seemingly periodic behavior. This is very prominent in two cases, during the 1996-1997 and the 2002-2003 periods.

Both of these anomalies happen to be during periods of strong El Niño events [McPhaden, 2004]. Since the phenomenon is primarily equatorial in nature, we investigated the trajectory of the center of mass on the equatorial plane (Figure 11). We notice that while the chaotic motion is confined within a 3 mm radius circle around the mean position, there are periods with systematic excursions from this area of confinement. Generating the trajectory over annual periods we were able to correlate these excursions with the periods of the two El Niño events. They also happen in general longitudinal directions that coincide with the transport of water masses during these events (Indonesia and Polynesia). The magnitude and direction of the shift is consistent with the expected water mass change based on the oceanographic observations of the total sea-surface height changes (Figure 12 for the 2002-2003 case), and the assumption that the real mass change corresponds to about 10-15% of the total observed sea-surface height variation, the remainder majority change being the effect of thermal expansion.

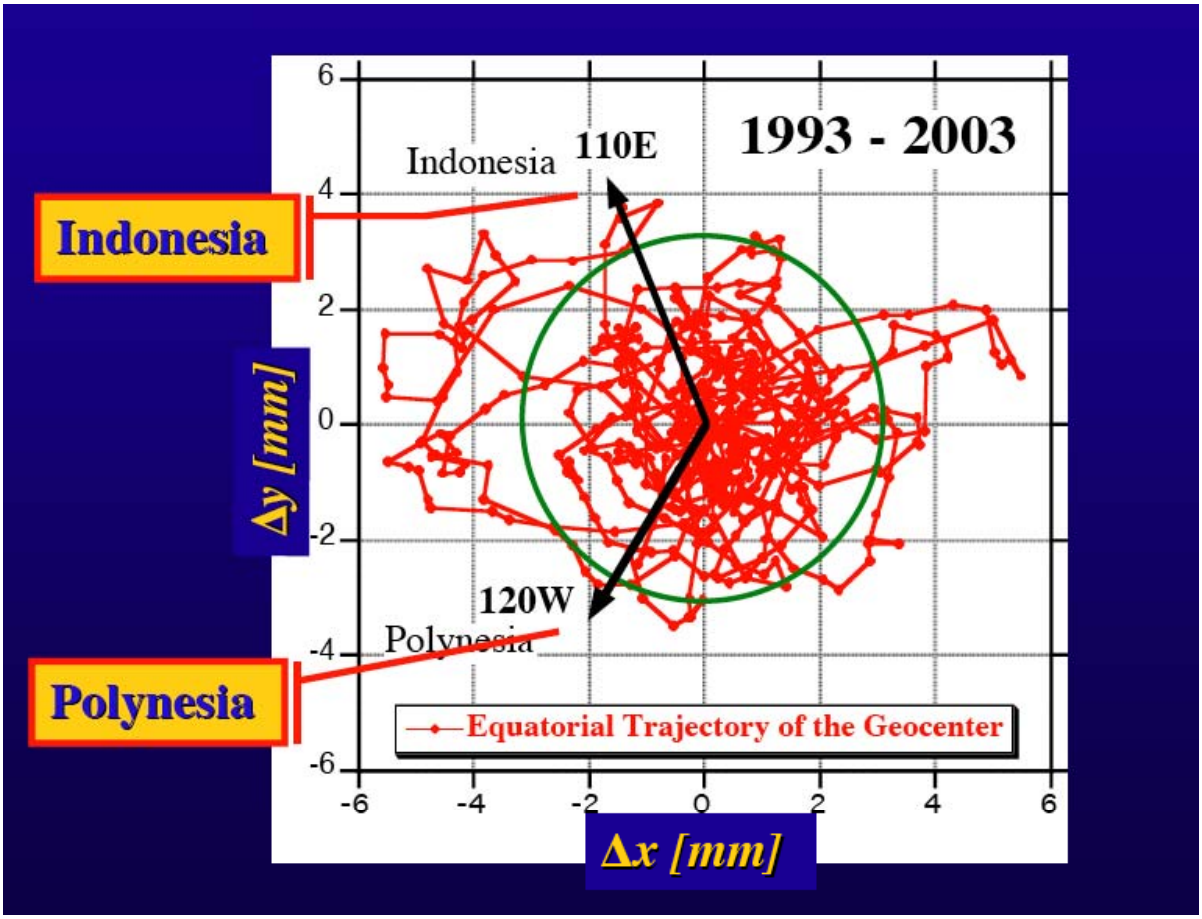

Figure 11. Trajectory of the center of mass projected on the equatorial plane, for the period 1993-2003. The 3 mm radius circle marks an area within which the motion is confined for most of the time. The two excursions between longitude 110E and 120W (and the anti-diametric ones) are correlated in time with the two El Niño events of 1996-97 and 2002-03.

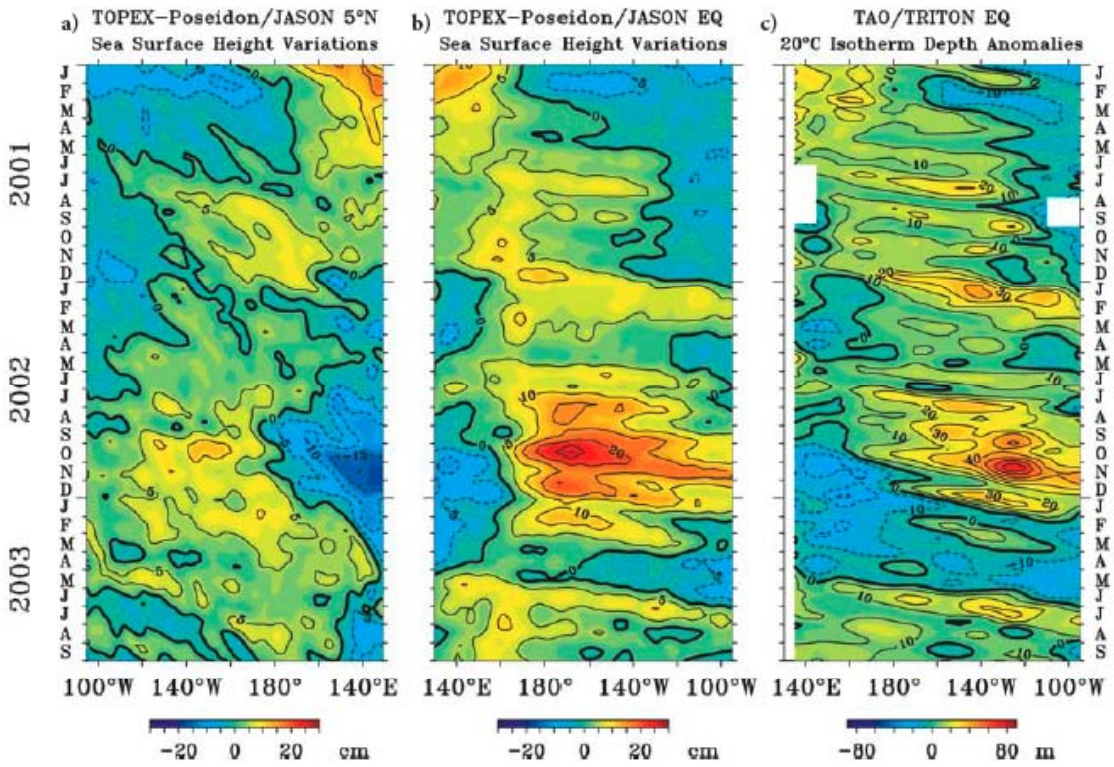

Figure 12. Ten-day anomalies of sea level from a 1° lat/long analysis of TOPEX/Poseidon and Jason altimeter data along (a) 5°N and (b) averaged between 2°N–2°S. Panel (c) shows 5-day 20°C isotherm depth anomalies averaged between 2°N–2°S. Anomalies are relative to climatologies based on data from 1993– 2001, (see original reference for a detailed discussion: Fig. 4, page 683, from [McPhaden, 2004]).

Modeling improvements in the analysis of SLR data

Despite the wealth of interesting and valuable phenomena that SLR currently observes, recent advances in our understanding of the Earth System and the interactions between its components, mandate that we constantly update and improve our modeling and analysis of SLR data, even when the accuracy of the raw data themselves does not change. The expected changes in the level at which we can "fit" the observations with the improved models are nowhere near those that we witnessed a decade ago, but today, with the stringent scientific requirements to resolve geophysical signals at the millimetre and 0.1 mm/y level, changes in our products at that level are very significant and contribute directly in achieving the ultimate goal. Furthermore, since this goal is not a SLR-only affair, we must harmonize our standards, analysis principles and line of products to those commonly accepted by all the other Space Geodetic Services, and sanctioned by the ultimate customer they all serve: the International Earth Rotation and Reference Systems Service (IERS). IERS has recently adopted a new set of Conventions and Standards in 2003, [McCarthy and Petit, 2004]. This new set of models, standards and analysis principles is now being implemented in the main software packages that are used in the analysis of SLR observations. In addition to the new standards, there have also been independently taken initiatives by each technique to improve technique-specific models, whose quality is still far from satisfactory. One such model in the case of SLR is the one that describes the atmospheric delay due to signal propagation through the atmosphere. For decades SLR has relied on a model that was developed in the early '70s, [Marini and Murray, 1973], tuned primarily to the most common laser wavelength used by the systems of the time. Today there is new knowledge about the atmosphere, and new laser systems that

operate in a wide range of wavelengths from 355 to 1064 nm and beyond. There is also increased need to separate measurement biases from errors in the atmospheric delay and possible vertical motion at the tracking sites, all of which dictated that we revisit this model and develop a new one that would be applicable today. Here, we will give some examples of the application of these innovations in the SLR data modelling and analysis, for cases that we have already obtained initial results.

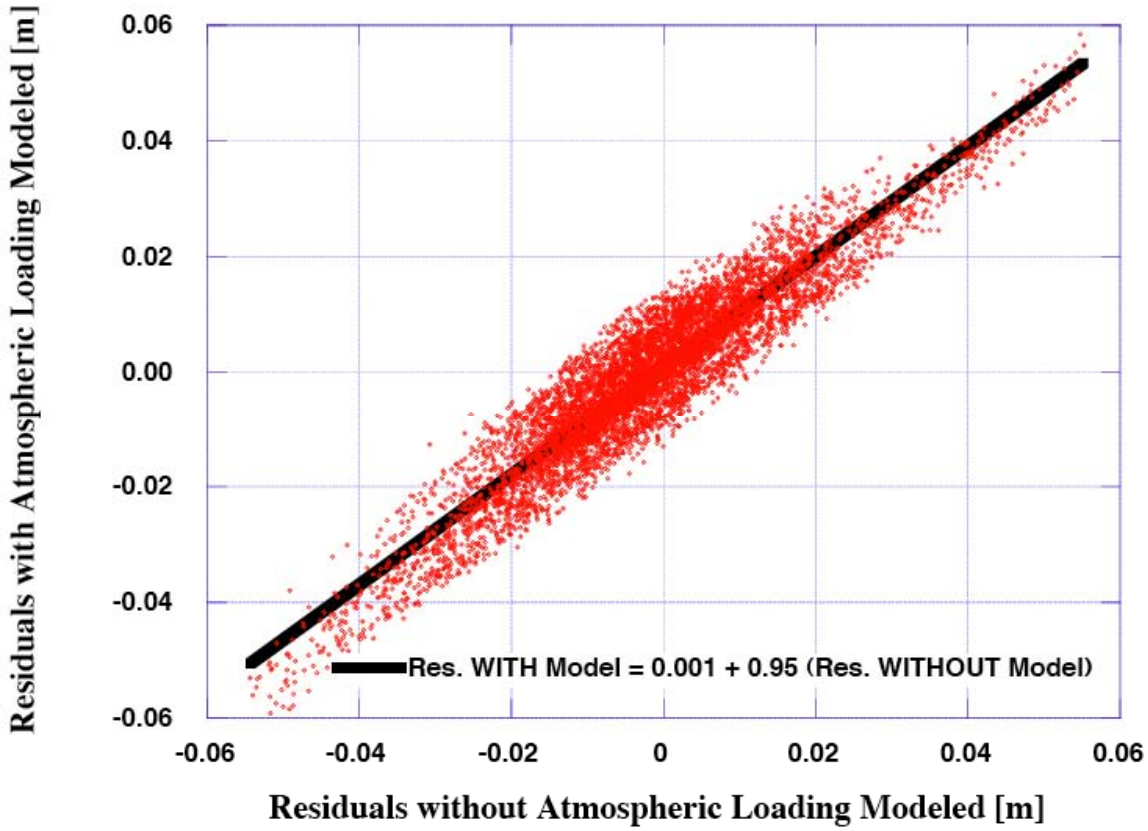

Figure 13. Regression plot of SLR range residuals analyzed in two different modes: the standard mode (x-axis), and the case when atmospheric loading at the tracking sites is modeled. The loading is obtained from NCEP 6-hour global fields [Petrov and Boy, 2004].

One of the topics that has seen a lot of attention and progress lately is the interaction of the components of the Earth System and in particular, their temporal spectrum. Missions such as CHAMP and GRACE were launched to address some specific questions associated with these topics and as a result, we already have a good insight in some areas. As a result of atmospheric circulation and consequent pressure changes at the tracking stations, the crust is regionally loaded with variable loads which in turn cause changes in what we call "station height" over a wide temporal spectrum. This was already recognized for some time, but it is only recently that access to global data sets of these loading effects became widely and routinely available to the analysts at *http://gemini.gsfc.nasa.gov/aplo*, [Petrov and Boy, 2004]. Although inclusion of atmospheric loading will likely have a bigger impact in the analysis of SLR data at the longer wavelengths by removal of such strong signals as the annual and seasonal, the benefits can be seen already when we examine a 28-day LAGEOS arc that is analyzed with the inclusion of these temporal changes. Figure 13 shows the regression of the range observation residuals to two, otherwise identical models, one of which includes the atmospheric loading signal, and one that does not. Apart from an insignificant (0.1 mm) bias, the residuals with the loading modeled are 5% smaller than those that do not.

When a long record of SLR data is analyzed with atmospheric loading included, what we expect to see is a much less noisy behavior in the recovered station heights, with a substantially systematic-free variation, and similar improvements in the recovered scale-related parameters of the TRF (i.e. $GM_{\oplus}$). Another model component that is also associated with "geophysical fluids" circulation is the effect (attraction) of their variable mass on the satellite itself.

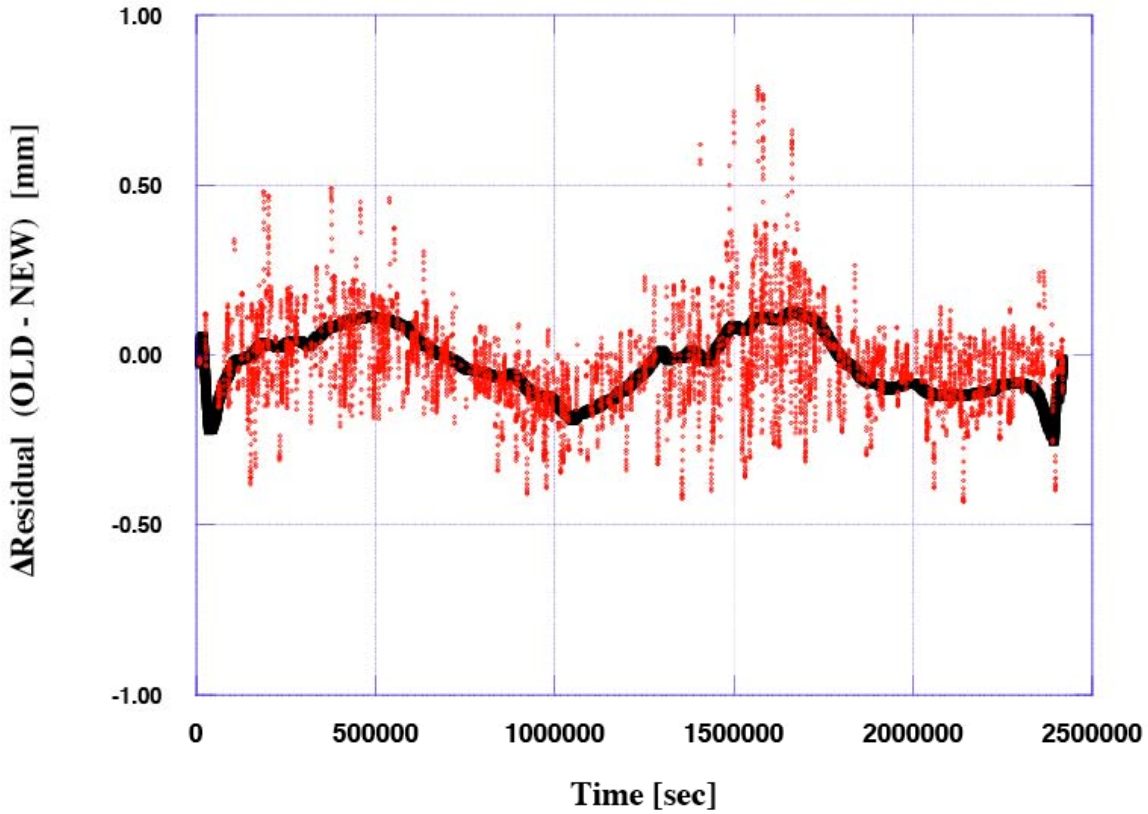

Figure 14. Differences of SLR range residuals analyzed in two different modes: using the IERS Conventions 1992(?) model for tidal motions at the tracking sites, and the case where the IERS Conventions 2003 model is used.

This is not included in the analysis shown in the above figure, GRACE however is already observing this at monthly intervals and can provide the appropriate information. Furthermore, the same process that produces the loading signal of the atmosphere produces in parallel the required changes of the gravitational harmonics at the same 6-hourly intervals. It is thus possible now to include this effect in our future analyses, and because these variations are available for all years for which SLR data exist, we can even retroactively improve our analyses adding further value to the older data. The magnitude of the effect is rapidly diminishing with altitude of course, so this improvement is far more important for the low altitude missions than for satellites like LAGEOS.

The adoption of the new IERS Conventions and Standards improves the modeling of the tidal variations in the station coordinates, with the height being the primary beneficiary again, as in the case of atmospheric loading. Figure 14 shows an example for a 28-day arc fit with LAGEOS data, of the effect this change has on range observation residuals when we move from the old model to the new. Again, we stress that the change in itself is not dramatic, ±0.5 mm, but if we compare it to signals of global change that we are after today (0.1 mm/y), it is

very significant, and it can easily introduce systematic variations which can be misinterpreted.

Improving the geophysical modelling is not the only area where significant advances were achieved over the past, in some cases based in part or entirely on SLR observations. We have also progressed in our ability to understand and better model the behavior of the targets themselves, and thus improve the quality of the orbits we derive on the basis of our observations. Considering that these orbits act as the quasi-inertial frame with respect to which we monitor the terrestrial frame and its evolution, along with a myriad of geophysical signals, it is an easy conclusion that these improved orbits, can only result in further improvements in the development and monitoring of the TRF.

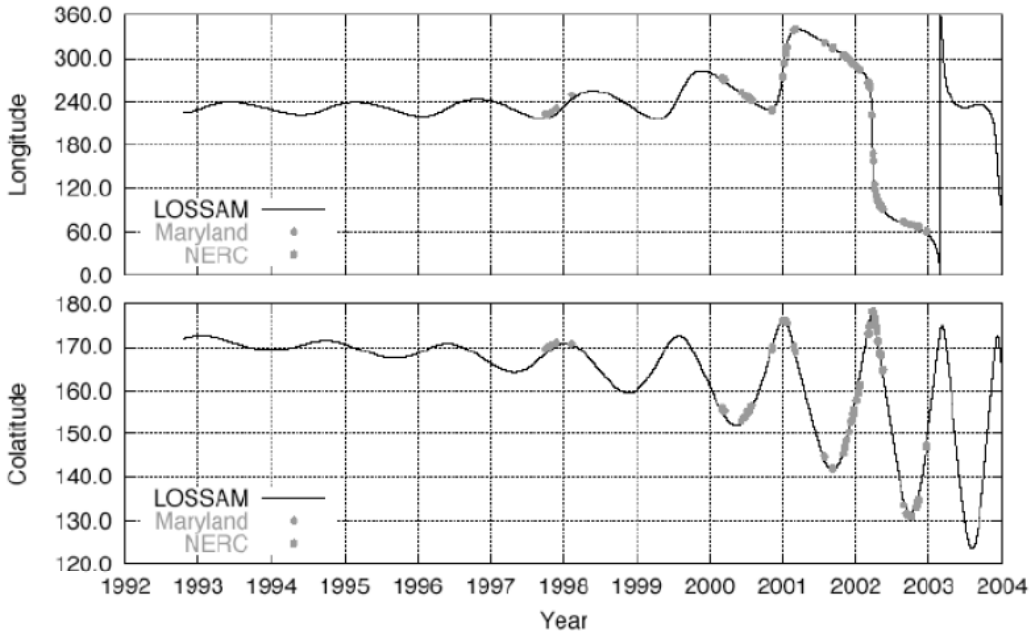

Figure 15. Spin-axis evolution for LAGEOS and LAGEOS 2 [Andrés et al., 2004].

With the LAGEOS satellites being the primary targets in this effort, the majority of investigators also focus on improving these particular targets' orbital models. A recent significant improvement in this area is the development of a better model for the evolution of the spin-axis orientation for the two LAGEOS [Andrés et al., 2004]. This improvement was partially enabled by improved SLR observations and analysis, and in part from the existence of optical observations from various locations on Earth. These improved models are now used in the analysis of LAGEOS SLR observations and their inclusion resulted in the reduction of the magnitude of *ad hoc* accelerations, previously used in our models to account for phenomena that are not entirely understood yet [Lucchesi et al., 2004].

One common problem for all space techniques is the propagation of the transmitted and received signals through space, and primarily, through the atmosphere and ionosphere. Laser (optical) signals are impervious to ionospheric effects, they are however sensitive to atmospheric signal retardation. The hydrostatic zenith delay due to the atmosphere is of the order of 2.5 m, while the non-hydrostatic part, due to the water vapor in the troposphere, is about 10% of the hydrostatic. The effects of both delays are amplified greatly as we move away from zenith towards low elevations. The quality of the modeled effect is dominated

here by the so-called "mapping function" (MF), which maps the predicted zenith delay (ZD) to the true elevation that the observation is taken.

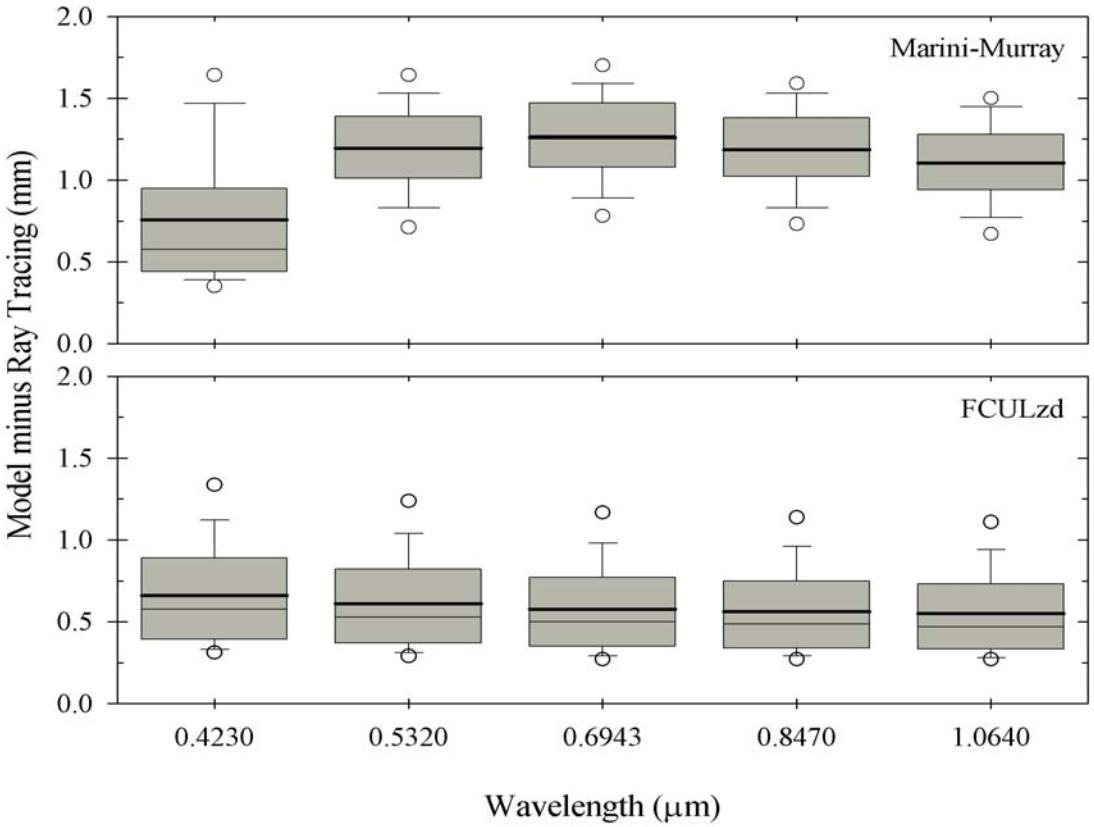

Figure 16. Validation statistics for the Mendes-Pavlis (MP) and the Marini-Murray (MM) models in the 423-1064 nm band. Box-and-whisker plots using the RMS values obtained at each individual radiosonde station used in the validation. The statistical quantities represented are the median and the mean (thinner and thicker lines inside the boxes, respectively), the 25th and 75th percentiles (vertical box limits), the 10th and 90th percentiles (whiskers), and the 5th and 95th percentiles (open circles), from [Mendes and Pavlis, 2004].

Traditionally SLR observations were taken above the 20° degree elevation for safety reasons. With the installation of radars at most tracking sites, it is now possible to range at very low elevations, as low as the surrounding orography and nearby obstructions permit. Collecting observations at low elevations allows for a better separation of measurement biases and station height local variations. This is therefore a very important reason to pursue the low elevation data. The traditional atmospheric refraction model used since the early days of SLR is that of Marini and Murray (MM), published in 1973, as we already mentioned earlier. The model provides high quality atmospheric delay estimates above 10° elevation, in a fashion that the ZD and the mapped ZD are all computed in a single step. The model was also tuned to a single wavelength, with quickly degrading performance as one moved away from that wavelength. While atmospheric modeling for radiometric techniques as GPS, VLBI and

DORIS, where the effects are much larger and variable, was making quick progress with a multitude of improved MF and ZD models, SLR kept using the very successful MM model since its performance was deemed adequate. In recent years however, we not only found a need for low elevation observations, a number of new systems initiated operations at two-colors, in hopes to use them for a direct estimation of the atmospheric delay [Degnan, 1993]. Suddenly, we were presented with the task to analyze data at wavelengths that ranged from 355 nm all the way 1064 nm. Furthermore, the performance of the MFs had to be improved and the atmospheric corrections had to be computed on the basis of standards recommended and adopted by the International Association of Geodesy (IAG) [Int. Union of Geodesy and Geophysics (IUGG), 1999], not in existence during the development of the MM model.

This presented a new challenge, and following the adoption of the IAG resolution, ILRS established a Refraction Study Group to address these issues. Several of its members in collaboration over years, initially developed a new and improved MF valid down to 3° elevations [Mendes et al., 2002], and later, a new, unbiased ZD model, applicable with the same performance over the entire spectrum of SLR wavelengths of interest [Mendes and Pavlis, 2004]. Figure 16 summarizes the statistics of the validation of the new ZD model across the 423-1064 nm band. Results for 355 nm were excluded from the graph for clarity, since MM under-predicts the delay at this wavelength by a whopping 7 mm.

With the MF and the ZD models improved, one final area in media propagation modeling that had not received any attention since the early days of NASA's Crustal Dynamics Project was that of the effect of horizontal gradients in the atmosphere. Again, the radiometric techniques, because of the order of magnitude increased sensitivity in these effects, had made strides in this area over the past decades, and they are now routinely including this modeling in their analyses [MacMillan and Ma, 1997].

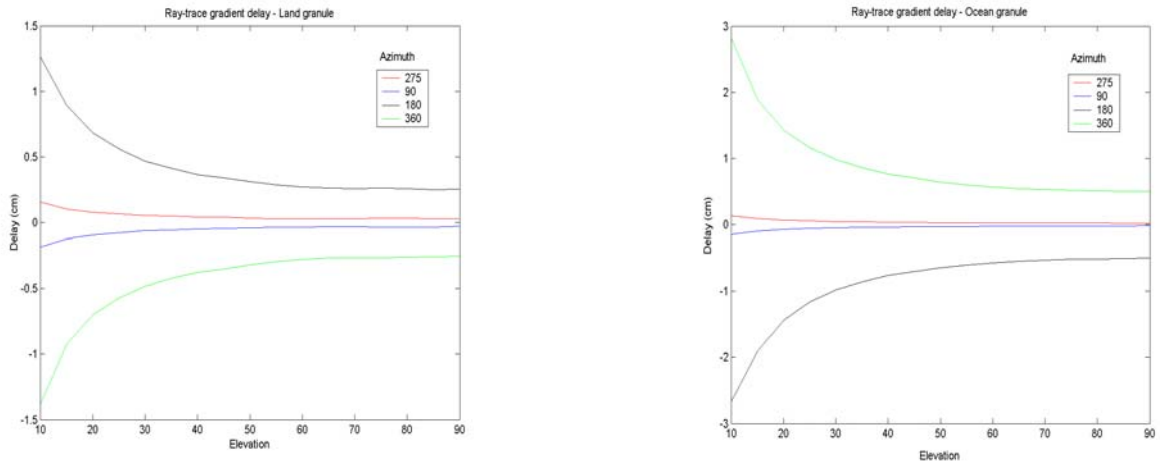

(a) **(b)**

Figure 17. Predicted atmospheric delay (cm) due to horizontal gradients: (a) over a land area and (b) over an ocean area. Based on the AIRS ray-tracing method at four cardinal azimuths and at all elevations, on a specific date.

It was therefore time for the SLR community to address this source of error, determine how serious it is, and following that, develop the appropriate modeling. This effort is now underway with the aid of near-real-time globally available remote sensing data for the atmosphere from space missions, primarily from the AIRS system on NASA's AQUA

platform (for more details see [Hulley et al., this proceedings]). The initial results from [*ibid.*] indicate that horizontal gradients are not nearly a problem for SLR as they are for radiometric techniques (Figure 17), a result that was already theoretically expected. On the other hand, the effect of the gradients can be limiting accuracy of the SLR products in the case of the most stringent requirements, and in cases where SLR sites are located at the coast with large bodies of water on one side, it may even introduce systematic, seasonal errors. The comforting result from this study is that existing models can be extended and applied to SLR wavelengths with great success, so that even in the absence of regional observations of the atmosphere in the surroundings of a tracking site, we can apply the effect of horizontal gradients on the basis of analytical models and with input from the meteorological data collected at the site, at least adequately enough for most applications. The investigation though continues and we look forward to first results by about a year from now.

Summary

The establishment of the Terrestrial Reference Frame is a collective effort of many research institutions and all of the space geodetic techniques. Although many of the techniques share strengths and weaknesses, each technique has a unique and irreplaceable role in this effort. Satellite Laser Ranging, one of the very first precise space geodetic techniques to contribute to this effort, uniquely defines the origin of the TRF and its temporal variations, and in part its scale and its variable orientation. As the development of the TRF over time improved, so did our ability to analyze SLR data, thereby contributing higher quality products for subsequent realizations. This presentation gave some examples of SLR contributions in the past (ITRF2000), and discussed with examples, the improvements in the analysis and modeling of SLR observations as we embark in the development of a new realization of the TRF (ITRF2004). These few examples show clearly that the usual tag-war between science and technology is alive and well, and guarantees that our knowledge about Earth and its environment will continuously improve, as long as we continue to invest in these efforts.

References

Altamimi, Z., D. Angermann, D. Argus, G. Blewitt, C. Boucher, B. Chao, H. Drewes, R. Eanes, M. Feissel, R. Ferland, T. Herring, B. Holt, J. Johannson, K. Larson, C. Ma, J. Manning, C. Meertens, A. Nothnagel, Pavlis, E. C., G. Petit, J. Ray, J. Ries, H.-G. Scherneck, P. Sillard, and M. Watkins, "The Terrestrial Reference Frame and the Dynamic Earth", *EOS*, *Transactions, AGU, 82(85), pp. 273, 278-279,* 2001.

Altamimi, Z., Sillard P, Boucher C, ITRF2000: A new release of the International Terrestrial Reference Frame for Earth science applications, *J. Geophys. Res.*, 107 B02214, 2002.

Andrés, J. I., R. Noomen, G. Bianco, D. G. Currie, and T. Otsubo, Spin axis behavior of the LAGEOS satellites, *J. Geophys. Res.*, 109, B06403, doi:10.1029/2003JB002692, 2004.

Degnan, J. "Millimeter Accuracy Satellite Laser Ranging: A Review", in Contributions of Space Geodesy to Geodynamics: Earth Dynamics, *Geodynamics 25*, D. E. Smith and D. L. Turcotte (eds.), pp. 133-162, American Geophysical Union, 1993.

Degnan J. J., "Unified approach to photon-counting microlaser rangers, transponders, and altimeters", *Surv. Geophys.* 22, 6, pp. 431-447, 2001.

Degnan, J. J. and E. C. Pavlis, "Laser Ranging to GPS Satellites with Centimeter Accuracy", *GPS World*, September 1994.

Hulley, G., Pavlis, E. C., V. Mendes, and D. E. Pavlis, “Multiwavelength refraction modeling improvements for SLR observations”, these proceedings, 2004.

International Union of Geodesy and Geophysics (IUGG), Resolution 3 of the International Association of Geodesy, in Comptes Rendus of the XXII General Assembly, pp. 110–111, Birmingham, UK, 1999.

Lemoine, F.G., D.E. Smith, L. Kunz, R. Smith, E. C. Pavlis, N.K. Pavlis, S.M. Klosko, D.S. Chinn, M.H. Torrence, R.G. Williamson, C.M. Cox, K.E. Rachlin, Y.M. Wang, S.C. Kenyon, R. Salman, R. Trimmer, R.H. Rapp, and R.S. Nerem, "The Development of the NASA GSFC and NIMA Joint Geopotential Model", Proc. of IAG Symposium 117: *"Gravity, Geoid and Marine Geodesy "*, Tokyo, Japan, Sept. 30 -Oct. 4, 1996, pp. 461-469, Springer-Verlag, Berlin, 1997.

Lucchesi, D. M., I. Ciufolini, J. I. Andrés, E. C. Pavlis, R. Peron, R. Noomen, D. G. Currie, “LAGEOS II perigee rate and eccentricity vector excitations residuals and the Yarkovsky–Schach effect”, *Planetary and Space Science*, 52 (2004) 699-710, DOI:10.1016/j.pss.2004.01.007, Elsevier Science B.V., Amsterdam, The Netherlands, 2004.

MacMillan, D.S. and C. Ma, “Atmospheric gradients and the VLBI terrestrial and celestial reference frames” J. Geophys. Re., Vol. 24, No.4, pp. 453-456, 1997.

Marini, J. W., and C. W. Murray, “Correction of laser range tracking data for atmospheric refraction at elevations above 10 degrees”, NASA Tech. Memo., NASA-TM-X-70555, 60 pp., 1973.

Marsh, J. G., F. J. Lerch, B. H. Putney, D. C. Christodoulidis, D. E. Smith, T. L. Felsentreger, B. V. Sanchez, S. M. Klosko, E. C. Pavlis, T. V. Martin, J. W. Robbins, R. G. Williamson, O. L. Colombo, D. D. Rowlands, W. F. Eddy, N. L. Chandler, K. E. Rachlin, G. B. Patel, S. Bhati and D. S. Chinn, “A New Gravitational Model for the Earth from Satellite Tracking Data: GEM-T1”, *J. of Geophys. Res.*, 93, pp. 6169-6215, June 1988.

Marsh, J. G., F. J. Lerch, B. H. Putney, T. L. Felsentreger, B. V. Sanchez, S. M. Klosko, G. B. Patel, J. W. Robbins, R. G. Williamson, T. L. Engelis, W. F. Eddy, N. L. Chandler, D. S. Chinn, S. Kapoor, K. E. Rachlin, L. E. Braatz and E. C. Pavlis “The GEM-T2 Gravitational Model”, *J. of Geophys. Res.*, 95, pp. 22,043-22,071, December 1990.

McCarthy, D. D. and G. Petit, IERS Conventions (2003), IERS Technical Note (32), pp. 127, Verlag des Bundesamts für Kartographie und Geodäsie, Frankfurt am Main, 2004.

McPhaden, M. J., Evolution of the 2002–2003 El Niño, *Bull. Am. Meteorol. Soc.*, 85, 677–695, 2004.

Mendes, V. B., G. Prates, E. C. Pavlis, D. E. Pavlis, and R. B. Langley, “Improved mapping functions for atmospheric refraction correction in SLR”, Geophys. Res. Lett., 29(10), 1414, doi:10.1029/2001GL014394, 2002.

Mendes, V. and E. C. Pavlis "High-Accuracy Zenith Delay Prediction at Optical Wavelengths", Geophysical Res. Lett., 31, L14602, doi:10.1029/2004GL020308, 2004.

Mueller, I.I., "Reference Coordinate Systems for Earth Dynamics: A Preview", Reference Coordinate Systems for Earth Dynamics, pp. 1-22, 1981.

Nerem, R.S., Lerch, F.J., Marshall, J.A., Pavlis, E.C., Putney, B.H., Chan, J.C., Klosko, S.M., Luthcke, S.B., Patel, G.B., Pavlis, N.K., Williamson, R.G., Tapley, B.D., Eanes, R.J., Ries, J.C., Schutz, B.E., Shum, C.K., Watkins, M.M., Rapp, R.H., Biancale, R., and

Nouel, F., "Gravity Model Development for TOPEX/POSEIDON: Joint Gravity Models 1 and 2", *J. of Geophys. Res.*, 99, C12, 1994.

Nicolas, J., Pierron, F., and Samain, E., et al, "Centimeter accuracy for the French Transportable Laser Ranging Station (FTLRS) through sub-system controls", *Surv. Geophys.* 22 (6): 449-464, 2001.

Pavlis, E. C., "High Resolution Earth Orientation Parameters From LAGEOS SLR Data Analysis at GSFC", in *IERS Technical Note16*, Observatoire de Paris, 1994.

Pavlis, E. C. "Fortnightly Resolution Geocenter Series: A Combined Analysis of LAGEOS 1 and 2 SLR Data (1993-96)", in *IERS Technical Note 25*, Observatoire de Paris, April 1999.

Pavlis, E. C. Dynamical Determination of Origin and Scale in the Earth System from Satellite Laser Ranging, in *Vistas for Geodesy in the New Millennium*, proceedings of the 2001 International Association of Geodesy Scientific Assembly, Budapest, Hungary, September 2-7, 2001, J. Adam and K.-P. Schwarz (eds.), Springer-Verlag, New York, pp. 36-41, 2002.

Petrov, L. and J.-P. Boy, Study of the atmospheric pressure loading signal in VLBI observations, *J. of Geophys. Res.*, 10.1029/2003JB002500, 109, No. B03405, 2004.

Smith, D. E., R. Kolenkiewicz, P. J. Dunn, J. W. Robbins, M. H. Torrence, S. M. Klosko, R. G. Williamson, E. C. Pavlis, N. B. Douglas, and S. K. Fricke, "Tectonic Motion and Deformation From Satellite Laser Ranging to LAGEOS", *J. of Geophys. Res.*, 95, pp. 22,013-22,041, 1990.

Smith, D.E., Kolenkiewicz, R., Nerem, R.S., Dunn, P.J., Torrence, M.H., Robbins, J.W., Klosko, S.M., Williamson, R.G., and Pavlis, E.C., "Contemporary global horizontal crustal motion", *Geophys. J. Int.*, 119, pp.511-520, 1994.

Veis, G., "Geodetic Use of Artificial Satellites", Smithsonian Contributions to Astrophysics, 3(9), pp.95-161, 1960.

Wilkins, G.A., "A Note on the Origin, Objectives and Programme of Project MERIT", Reference Coordinate Systems for Earth Dynamics, pp. 275-276, 1981.

Yoder, C. F., Williams, J. G., Dickey, J. O., Schutz, B. E., Eanes, R. J., and Tapley, B. D., "Secular Variation of Earth's Gravitational Harmonic J_2 Coefficient from LAGEOS and Nontidal Acceleration of Earth Rotation", Nature, V.303, pp. 757-762, 1983.

LONG TERM MONITORING OF GEOPHYSICAL PARAMETERS USING SLR

V.Luceri (1), C.Sciarretta(1), G.Bianco(2)
(1) Telespazio S.p.A. , Centro di Geodesia Spaziale, Matera, Italy
(2) Agenzia Spaziale Italiana, Centro di Geodesia Spaziale, Matera, Italy
cinzia.luceri@asi.it / Fax: +39-0835-377226

Abstract

The SLR observation dataset, similarly to the other space geodetic techniques, is a valuable source of data for measuring fundamental geophysical parameters and their temporal variations with respect to different time scales. As an example, the distinctive sensitivity of the SLR technique to global parameters as the origin and scale of the Terrestrial Reference Frame profits from the remarkable length of its observations dataset, allowing the stable and accurate retrieval of those parameters, turning into a reliable maintenance of the TRF.

The most recent and updated ASI/CGS analyses of Lageos-I and Lageos-II data cover two decades and provide time series of daily Earth Rotation Parameters (EOP) and Length Of Day (LOD), weekly geocenter offsets with respect to the TRF, weekly J_2 estimates, station coordinates and velocities together with orbital parameters, biases, and other technique-based nuisance parameters. The complex interrelation among all the parameters allows the crosschecking and helps in detecting real geophysical signals from the parameters time series.

Some of the results coming out from the solutions are shown, with particular emphasis to the terrestrial reference frame monitoring. Comparisons are made with the standard IERS references.

Introduction

SLR observations from Lageos-I and Lageos-II are the fundamental database of most geodetic analyses and essential for the establishment of terrestrial reference frames. The upcoming of state-of-the-art models makes necessary to re-analyze the whole dataset from time to time to retrieve homogeneous time series of geophysical parameters. The reprocessing can be accomplished thanks to the relatively small amount of computer time needed to process several years of data, almost negligible if compared, for example, to the time needed for GPS data analysis.

In the latest geodetic solutions computed at the ASI/CGS the worldwide laser tracking dataset, from January 1985 to December 2003, has been processed by means of the GeodynII/Solve software developed at the NASA Goddard Space Flight Center. Besides the long term monitoring of the consistency of the TRF, by means of 'classical' geodetic parameters (i.e. site coordinates/velocities and EOPs), the added value of these ASI/CGS solutions is the retrieval of the TRF origin offsets, i.e. the geocenter time series.

Data processing

All the normal points collected from the worldwide network in the period 1985-2003 are analysed in 15-day arcs when using Lageos-I data only and 7-day arcs when using Lageos-I and Lageos II, so that the amount of data in each arc is roughly homogeneous over the entire period (Figure 1).

Arc data reduction is performed separately for each satellite and, in this phase, the complete orbit and force model is defined together with the analysis approach (i.e. arc length, type of estimated parameters) but only the arc dependent parameters are estimated, namely those related to the orbit (i.e. state vectors and non-gravitational forces) and to the observations (i.e. measurement bias). The arc solution adopts the most recent models:

ITRF2000 as *a priori* site coordinates and velocities, IERS EOPC04 for *a priori* EOP values, EGM96 geopotential (up to degree 70), GOT99.2 ocean tides model, ocean loading from Scherneck and GOT99.2 tides, taking into account the secular drift and the influence of the dynamical pole on C21 and S21 coefficients, all the major planets perturbations as well as the relativistic effects.

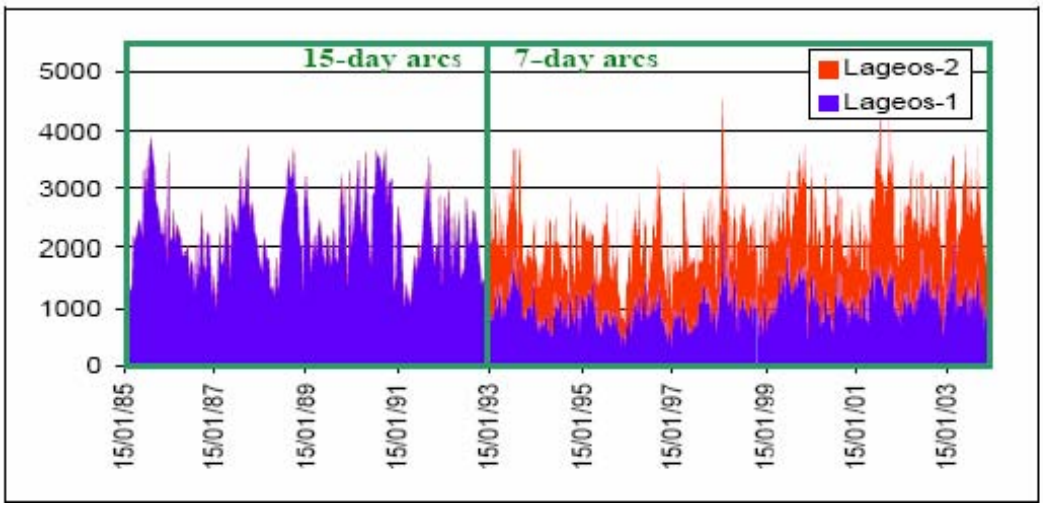

Figure 1. Dataset

A measure of the differences, on average, between the calculated ranges and the observed ones is shown in Figure 2 (series labelled Lageos-1 and Lageos-2) through the weighted root mean square of the residuals (wrms) . The time series of the arc wrms reflect both the precision of our orbital fit and the improvement of the laser tracking systems: values around 4 cm. at the beginning of the analysed period, lower down to less than 2 cm.

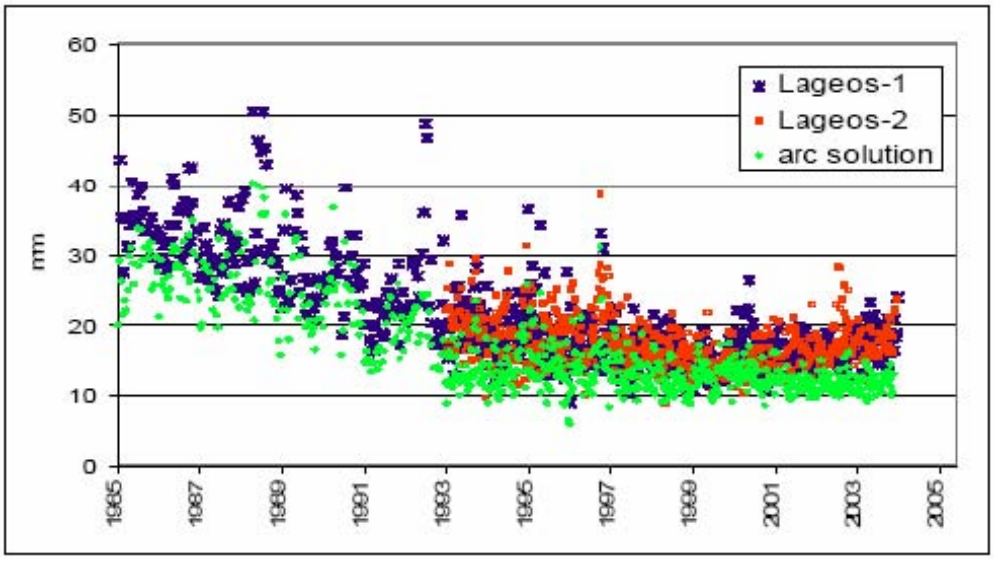

Figure 2. Weighted root mean square of the satellite residuals

The normal equations built in the arc data reduction are then combined and inverted to estimate the so-called 'global' parameters (site coordinates, EOPs, geocenter offsets etc.) and update the arc dependent parameters. Two strategies can be adopted to combine the equations over the two decades: a *long arc solution* or a *short arc solution* strategy *(*fortnightly/weekly solutions).

Long arc solution

This analysis approach provides a unique final solution from the inversion of the combination of all the arc normal matrices, in which all the global parameters are solved in a least squares

sense and provided with their full covariance matrix: fortnightly or weekly C_{10}, C_{11}, S_{11} (immediately related to the geocenter offsets), 3-D site coordinates and velocities, 3-day (until 1992) and daily (from 1993 on) EOP (X,Y,UT1R-UTC) and LOD.

The realization of the reference frame is constrained to ITRF2000 by fixing to those values the position and velocities of two sites, Greenbelt (7105) and Herstmonceux (7840). The tight realization of a unique terrestrial reference frame, constrained throughout the solution, permits the estimation of the center of mass offsets. The global wrms of the coordinate residuals, measuring the robustness of the chosen TRF realization, is 18 mm.

Short arc solutions

This approach provides a time series of solutions, one for each arc from the combination of Lageos-I and II, in which only the parameters (and their covariance matrix) relevant to that arc are present. For each arc, the site coordinates and EOP/LOD are estimated and the arc dependent parameters updated. The reference frame is loosely constrained to ITRF2000 site by setting a value of 1 meter as *a priori* constraint to the site coordinates and EOPs. The geocenter offsets are not retrieved as directly estimated parameters but they are obtained in a geometric way by a 7-parameter Helmert transformation, projecting each solution into ITRF2000. The time series of the residual wrms is shown in Figure 2, labelled as 'arc solution'.

Results

A geodetic solution covering so many years gives a tremendous amount of information and sets the basis for further and deeper investigations. The results shown in this paper are the immediate output of the analysis and are mainly given in terms of time series of geophysical parameters.

A discussion of the main analysis results relevant to the long term monitoring of the TRF, including the geocenter motion, is reported in the following. In addition, the global resultsrelevant to the time variations of the low-degree geopotential coefficients are reported, with a few hints on the satellite accelerations, estimated in the ASI/CGS solutions as empirical parameters, to make evident some still unmodeled effects acting on the satellites and influencing the accuracy of the estimated geophysical parameters.

- *Monitoring of TRF classic parameters: Site Coordinates/velocities and Earth Orientation Parameters*

The 1985-2003 ASI/CGS solution realizes the terrestrial reference frame in different ways, according to the different analysis strategy.

The *long arc solution* provides a unique estimate of coordinates at a certain date and an associate linear velocity field, adopting as constraints the ITRF2000 *a priori* values for two sites (Greenbelt, Herstmonceux). This is a logical but arbitrary realization of the TRF as ITRF2000. The robustness of this realization can be measured by a complete 14-parameter Helmert transformation, whose estimated values are reported in Table 1.

Short arc solutions provide a time series of coordinates for the global SLR sites polyhedron, loosely constrained in reference frames different from arc to arc. This approach prevents network deformation, allowing the retrieval of homogeneous time series of geophysical parameters after 7-parameter Helmert transformations to ITRF2000, one for each solution. A drawback of the method is that the network considered in the weekly (or fortnightly) solutions can be very small, thus adding a non-negligible uncertainty in a transformed parameter.

Table 1. Transformation parameters to ITRF2000

HELMERT PARAMETERS [mm, mas, mm/yr, mas/yr)]							
	Tx	Ty	Tz	Scale	Rx	Ry	Rz
Val:	6.1	-6.6	-3.8	2.8E-011	-0.28	-0.17	-0.021
Sig:	0.5	0.61	0.65	8.9E-011	0.029	0.023	0.017
	Txdot	Tydot	Tzdot	Scldot	Rxdot	Rydot	Rzdot
Val:	0.24	-0.04	0.27	-1.4E-010	0.008	0.009	-0.013
Sig:	0.09	0.10	0.13	1.6E-011	0.007	0.004	0.003

The SLR Earth Orientation Parameters endorsed by the ILRS are the X-pole, Y-pole and LOD and they are estimated both in the *long arc* and *short arc solutions*. UT1R-UTC is also estimated but, due to the high correlation with the node of the satellites, it is not a reliable parameter measured with satellite techniques. The estimation of the X and Y component of the pole rate degrades the quality of the SLR solutions and removable constraints have been applied. The plot on the left of Figure 3 shows the residuals of time series obtained from the long arc solutions: the differences with the combined IERS series EOPC04 are computed in the ITRF2000 reference frame. The mean errors for the X and Y pole components are ~0.1 mas, slightly higher in the case of the *short arc solutions*, and 0.03 ms for LOD.

The comparison with EOPC04 makes evident the existence of biases and drifts: 0.023mas/yr and 0.036 mas/yr in X and Y respectively (see right plot in Figure 3). Since the estimated EOP are, by construction, in the ITRF2000 frame, the linear trends are most probably due to an inconsistency between ITRF2000 and the EOPC04 series. The values of the bias in 2004 are confirmed by the SLR weekly combined solutions delivered to the ILRS.

A preliminary spectral analysis was performed on the LOD residuals with respect to EOPC04 and significant signals were found with periods of 14 days, 148 days and 1 year.

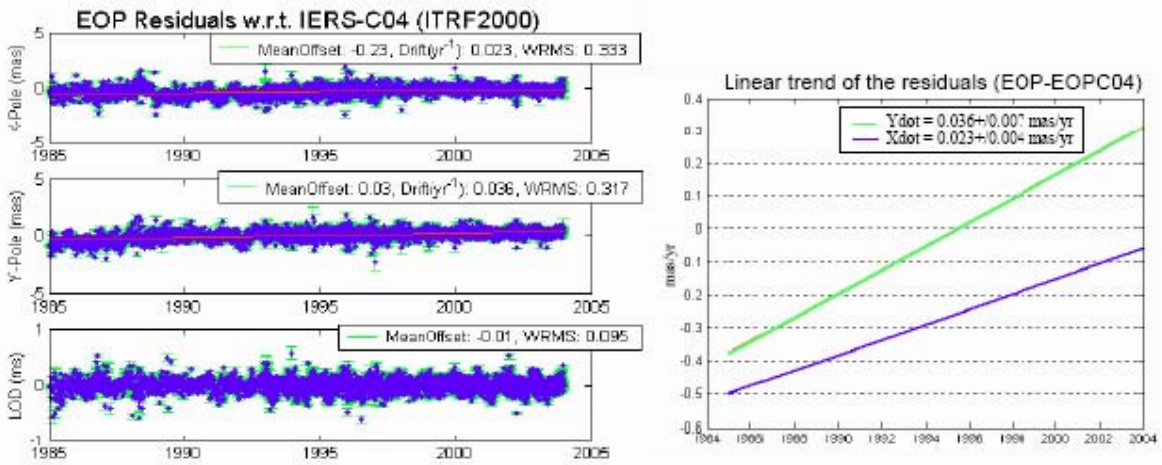

Figure 3. EOP residuals and drifts with respect to EOPC04

- *Monitoring the TRF origin offsets: Geocenter motion*

The ITRF models, ITRF2000 and previous ones, assume that the origin of the global geodetic network is placed in the Earth center of mass. In parallel, the geopotential models, framed in the current ITRF at epoch, assume the earth center of mass, on average, in the center of the geodetic network (i.e. zero values for degree 1 geopotential coefficients).

Despite these assumptions, satellite tracking data, SLR being the most accurate in this respect, have provided evidence that the Earth center of mass is continuously changing its position relative to a crust fixed reference frame. This translation motion is generally known as "geocenter motion". Two different methods, already experienced during the IERS Analysis Campaign to Investigate Motions of the Geocenter [Devoti et al, 1999], have been applied in the ASI/CGS solution to retrieve the geocenter time series: a direct estimation of the degree one geopotential harmonics in the *long arc solution* and a computation of Cartesian coordinate offsets from ITRF using the time series of *short arc solutions*. In both cases we will obtain time series of estimated Cartesian translations, one estimate every 15 days until 1992 (Lageos-I only) and every week from 1993 on (Lageos-I and II). The first approach, from now on the "dynamic method", provides estimates of the C_{10}, C_{11}, S_{11} geopotential coefficients related to a global translation of the terrestrial reference frame as follows:

$$Tx = \alpha \cdot \overline{C}_{11} \cdot \sqrt{3}$$
$$Ty = \alpha \cdot \overline{S}_{11} \cdot \sqrt{3}$$
$$Tz = \alpha \cdot \overline{C}_{10} \cdot \sqrt{3}$$

where α is the mean equatorial terrestrial radius, the geopotential coefficients are normalized, the geocenter vector (Tx, Ty, Tz) defined from the ITRF origin to the Earth center of mass.

The second way of estimating the geocenter motion is through the time series of *short arc solutions*, from now on "geometric method". Each TRF realized by the SLR stations in a loose solution places naturally its origin in the center of mass of the Earth: its Cartesian coordinate offsets from a conventional origin describe the geocenter location. The adopted conventional frame is the ITRF2000 and the translations in the 3 directions have been computed by Zuheir Altamimi (Institut Geographique National, ENSG/LAREG).

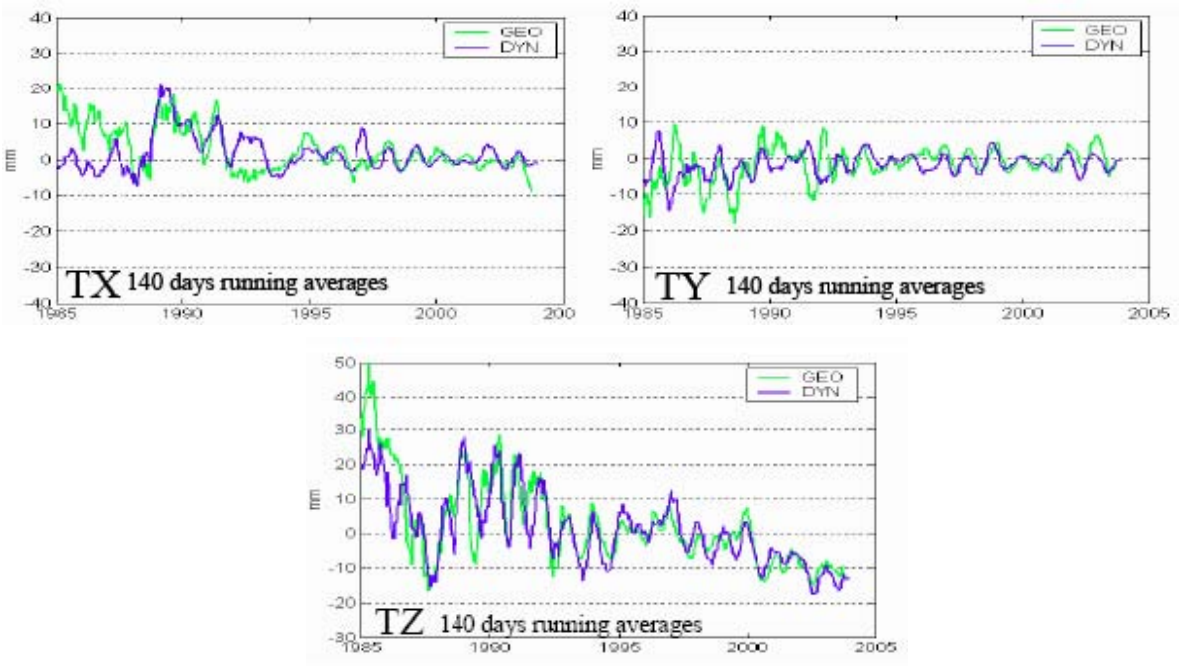

Figure 4. The geocenter motion

Both methods provide offsets with mean sigmas at the millimeter level, higher in the Tz component, more scattered in the geometric case. The three plots, above and aside, show the 140 days running average built on the dynamic and geometric translation series. The agreement is quite satisfactory with a few exceptions above all in the period preceding the

inclusion of Lageos-II data (1993). The position change in the XY plane is roughly confined in ±10 mm, with no significant drift; it is worthwhile to put in evidence the bump larger than 1 cm in the years from 1989 to 1992. It is recovered using both methods but no explanation is found at the moment: further investigation is needed.

The variation in the Z component is larger, almost double, and a linear drift of -1.3 mm/yr is present. Also in this case further investigation should be directed to understand if this is a real center of mass drift or an indirect effect (i.e. due to the network).n annual signal is clearly visible in all the translations.

- *Long term monitoring of low degree geopotential coefficients: the fundamental contribution by the SLR technique*

Ongoing mass redistribution over the Earth induces changes in the low degrees coefficients of the gravity field, changes that can be monitored by SLR back to decades. The uniqueness of the technique lies in its capability to provide the low degree zonal rates of the geopotential useful to constrain the rheology of the mantle and the lithospheric thickness.

Multi-satellite solutions are generally used and the satellite constellation is chosen to exploit the sensitivity of the various satellite to the different zonal degrees.

The latest gravity solution at the ASI/CGS is computed analysing the data from 4 satellites: Lageos-I, Lageos-II, Starlette and Stella. The overall strategy is similar to the long arc solution outlined in this paper and it is detailed in Devoti et al. [2000].

The most relevant result, the J2 time series, is shown in Figure 5. The zonal secular drift has been estimated together with a seasonal signal (amplitude and phase) using a non-linear least squares method.

In the rate estimation process the J2 frequency dependent tidal correction has been applied following the IERS96 conventions.

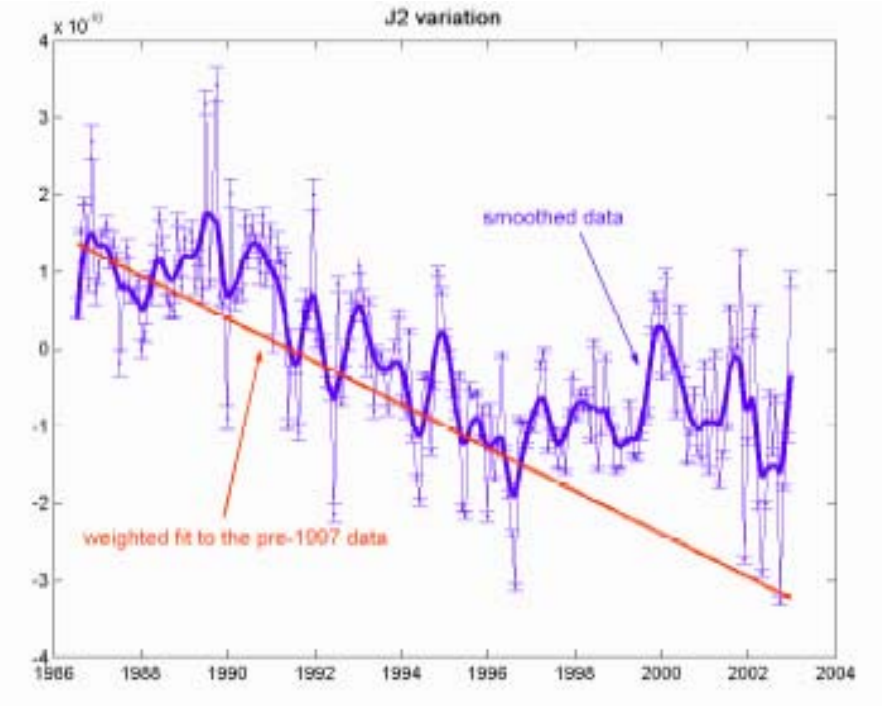

Figure 5. The J2 time series

Another deviation from the negative linearity is present from 1989 to 1991, even if less evident than the one discussed. A new gravity solution is now under construction, with more satellites and covering a longer time span.

- A critical issue: unmodeled satellite accelerations

The residual unmodeled perturbations on the satellite orbits due to the non-gravitational forces are absorbed by the estimation of empirical accelerations in the along-track (constant and once-per-revolution) and cross-track directions (once-per revolution). The accurate modelling of non-gravitational forces is important in trying to separate the gravity response of the geodetic satellites. Although the theories were widely discussed during the 90's, the observed residual forces were never fully explained by the proposed models for the involved forces (i.e. charged and neutral particles, thermal drag).

The along-track accelerations shown in Figure 6 are obtained from the *long arc solution*. It's interesting to note the different patterns in subsequent time spans which can indicate a change in the satellite state occurred in two specific years and precisely: 1989 and 1997. A similar situation doesn't occur when looking at the Lageos-II accelerations. Also in this case, the estimates provide material for further investigations.

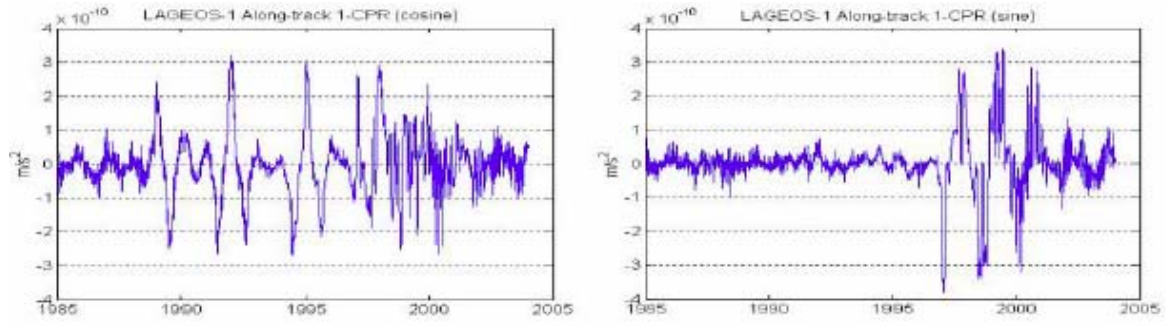

Figure 6. Lageos-I along-track once-per-rev accelerations

Summary

The contribution of SLR data analysis to the long term monitoring of geophysical parameters is of key importance for its capability to profit of a two decadal acquisition dataset. Besides, the sensitivity of the SLR technique to the Earth center of mass makes this technique a unique tool to detect the geocenter motion at various time scales.

The ASI/CGS SLR global solutions exploit these capabilities; the choice to simultaneously follow two different strategies permits to check the implemented methods by comparing the equivalent parameters and gives a feeling of the weakness and strength of the two approaches.

As an example, in one case the reference frame is well established but you can only estimate linear velocities, in the other, a time series of coordinates is obtained but the problem of managing different reference frames must be faced. The latest trend in the worldwide analysis community goes toward the short arc solution approach to monitor some geophysical parameters in quasi-real-time but this tendency has to be complemented with the global view given by a long arc solution.

Acknowledgment

The authors would like to thank:

- Zuheir Altamimi (IGN) for his work on the "geometrical geocenter" retrieval from the time series of short-arc solutions.
- Roberto Devoti (INGV) for his helpful contribution on the low degree gravity field recovery.

References

Cox CM and Chao, BF. *Detection of a Large-Scale Mass Redistribution in the Terrestrial System Since 1998*, Science, 297, 5582, 831-833, 2002.

Devoti R, Fermi M, Sciarretta C, Luceri V, Pacione R, Rutigliano P, Vespe F, *CGS geocenter timeseries from SLR and GPS data, in Ray*, J.R. (ed.)*, IERS Technical Note 25,* Paris Observatory, pp. 39–46, 1999.

Devoti R, Luceri V, Sciarretta C, et al., *The SLR secular gravity variations and their impact on the inference of mantle rheology and lithospheric thickness*, Geophys. Res. Lett., (5): 855-858 MAR 1 2001

Dickey JO, Marcus SL, de Viron O, and I. Fukumori, 2002. *Recent Earth oblateness variations: Unraveling climate and postglacial rebound effects*, Science, 298, 1975-1977.

COMBINATION OF SPACE GEODESY TECHNIQUES FOR MONITORING THE KINEMATICS OF THE EARTH

D. Coulot (1-2), P. Berio (2), R. Biancale (3), J.-M. Lemoine (3), S. Loyer (4), L. Soudarin (5), A.-M. Gontier (6), P. Exertier (2), Z. Altamimi (1), N. Capitaine (6) and D. Gambis (6)

(1) IGN/ENSG/LAREG, 6 et 8 av. B. Pascal, F-77455 Marne la Vallée
(2) OCA/site de Grasse, av. N. Copernic, F-06130 Grasse
(3) CNES/OMP, 14 Av. E. Belin, F-31400 Toulouse
(4) NOVELTIS, 2 Av. de l'Europe, F-31520 Ramonville-Saint-Agne
(5) CLS, 8 et 10 rue Hermès, F-31526 Ramonville-Saint-Agne
(6) Observatoire de Paris/SYRTE, 61 Av. de l'Observatoire, F-75014 Paris
david.coulot@obs-azur.fr /+33-04-93-40-53-84/Fax:+33-04-93-40-53-33

Abstract

In the framework of activities of the International Earth Rotation and Reference Systems Service (IERS) Combination Research Centres (CRC), the french Groupe de Recherche en Géodésie Spatiale (GRGS) studies the benefit of combining four geodetic techniques (SLR, VLBI, GPS and DORIS) at the measurement level in order to obtain a global and consistent solution for Earth Orientation Parameters (EOPs): polar motion x_p and y_p, universal time UT and celestial pole offsets in longitude and obliquity d and d with a six-hour sampling, as well as weekly station positions. A one-year test period (the year 2002) has been chosen to prove the power of such a combination moreover worked out in a homogeneous global terrestrial reference frame. All techniques were processed with the same computational framework (GINS/DYNAMO) so with the same a priori models and a priori values for parameters. The optimal relative weights between each geodetic technique were obtained with an optimal variance component estimation method. The aim of this paper is to describe the processing and the precision level of each individual technique for EOPs, to show how we handled with the combination of techniques and to discuss some results.

Introduction

The International Earth Rotation and Reference Systems Service (IERS) is an interdisciplinary service responsible for the definition, the production and the maintenance of the International Terrestrial and Celestial Reference Frames (ITRF and ICRF) and Earth Orientation Parameters (EOPs). This service also provides users with conventions (physical constants and models) which should especially be used by the IERS analysis centres to derive the IERS products. Concerning Earth orientation, IERS provides daily EOPs since 1962 (time series *EOPC04*, for example). These series are derived from VLBI measurements and spatial geodetic measurements (such as SLR, GPS and DORIS). VLBI provides absolute but sparse reference for the determination of the universal time and the celestial pole offsets. The geodetic techniques provide the short-period variations of these quantities and provide the polar coordinates as well. The production of EOP time series consists in combining solutions of each individual technique which have been computed by different IERS analysis centres. The inaccuracies of such a combination come from (i) the heterogeneity of the reference frames in which individual EOP solutions have been derived and (ii) the diversity of the softwares (algorithms, constants and models) developed and used by IERS analysis centres. Furthermore, the different products of IERS (ITRF, ICRF and EOPs) are still computed independently and it can cause inconsistencies between them. Even if inaccuracy due to (ii)

should be reduced thanks to the IERS conventions, subtle differences may still lead to systematic effects. In order to fully cancel these sources of inaccuracy and these inconsistencies, we combine VLBI, SLR, GPS and DORIS techniques at the measurement level in order to obtain a global and consistent solution for EOPs (polar coordinates, universal time and celestial pole offsets with a six-hour sampling), as well as weekly station positions. All techniques are processed with the same softwares (GINS/DYNAMO), so with the same fundamental constants, the same physical models and the same *a priori* values for parameters of interest. EOPs and Terrestrial Reference Frames (TRFs) are computed together during the same processing in order to avoid for inconsistencies between them. The processing and the main results for EOPs are presented in this paper. After having described the method of the global combination carried out at the measurement level (Sect. 2), we analyse and discuss the results (Sect. 3).

Method of combination

The test period chosen for the combination is the year 2002. More precisely, this period begins on December 30, 2001 (Julian Date 2 452 273,5) and ends on January 01, 2003 (Julian Date 2 452 643,5). The GINS software provides the sensitivity of measurements with respect to parameters of interest, through weekly normal matrices per technique. In our case, these parameters are EOPs and positions of GPS, SLR, DORIS and VLBI stations. Each week, normal matrices of the four techniques are used to obtain a "four-technique" normal matrix. This processing is carried out in two steps. In the first step, the four matrices are used to compute the relative weights between techniques with an optimal variance component estimation method [Sahin and Sellers 1992]. These four relative weights are used in the second step to gather the four individual normal matrices in a global weekly normal matrix taking into account the quality of each technique. The weekly normal system so obtained can not be solved for without any additional information on parameters (EOPs every six hours and station positions every week). We so give these supplementary informations as constraints on parameters ("continuity constraints" on EOPs acting as a filter and minimum constraints for station positions [Sillard and Boucher 2001]) which allow us to invert the normal system and to obtain the final solutions. The EOP offsets are computed with respect to the IERS time series *EOPC04* [EOP PC] corrected with the diurnal and sub-diurnal model of [Ray et al. 1994]. The station position offsets are computed with respect to ITRF2000 positions [Altamimi et al. 2002] corrected with models of IERS conventions [Mc Carthy 1996].

Results for EOPs

There is no absolute method to evaluate the quality of EOP time series. Usually, the quality assessment of time series is done through comparisons with other series and/or with theoretical models. In our case, we choose to compare the one-day and six-hour sampling combined time series with each individual series through the RMS of the estimated offsets (Table 1). The dx_p, dy_p and dUT series with a six-hour sampling are also analysed in the frequency domain (Figure 1).

The RMS of the individual series are in good agreement with those usually obtained by the IERS analysis data centres. The C_{1D} series present a RMS of 0.1mas for the pole coordinate offsets in agreement with the GPS series whereas the RMS of dUT is strongly reduced. This shows that our combination process takes advantage of the characteristics of each technique. So the dUT series seem to be mainly influenced by the VLBI technique which is known as the best one for this parameter, even if the RMS for UT of the combined series is more than two

Table 1. Root Mean Squares of the individual and combined EOP time series. Units are mas for x_p and y_p and ms for UT. The names C_{1D} and C_{6H} correspond respectively to the combined series with a one-day and a six-hour sampling.

Technique	**dx_p**	**dy_p**	**dUT**	**Technique**	**dx_p**	**dy_p**	**dUT**
GPS	0,107	0,101	0,0175	SLR	0,182	0,180	0,0198
DORIS	0,650	0,552	0,153	VLBI	0,150	0,230	0,0056
C_{1D}	0,108	0,106	0,0131	C_{6H}	0,423	0,423	0,0177

times greater than those of the VLBI series. This is probably explained by the different kind of constraints applied for the VLBI series. Indeed the VLBI technique can not give a continuous daily sampling for EOPs. For this reason, we use constraints to zero for EOPs and not continuity constrains as for other techniques or combinations.

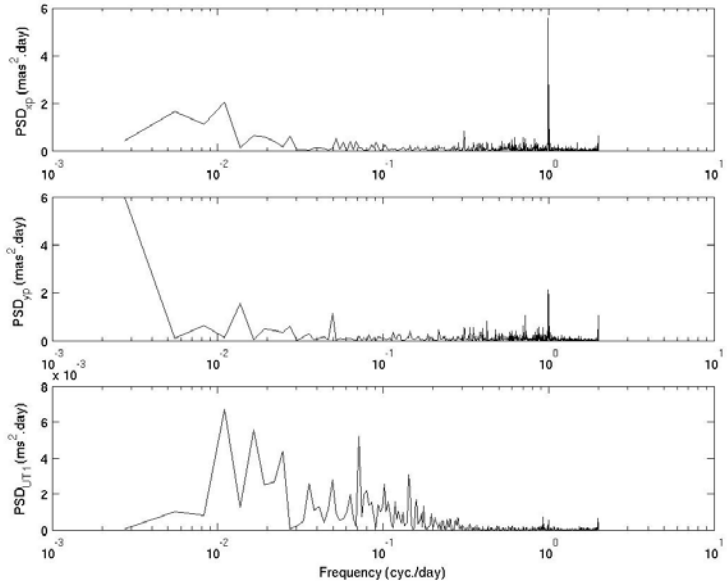

Figure 1. Power Spectral Densities (PSDs) of the x_p, y_p and UT offsets

As shown on Figure 1, the pole coordinate offset time series present an harmonic with a frequency of 1 cycle/day. This diurnal term in polar motion is retrograde and has an amplitude of 140 as. It is probably associated with orbit computation deficiencies (correlation between a daily retrograde polar motion and the right ascensions of the ascending nodes and the inclinations [Hefty et al. 2000]). Besides the three PSDs present low frequency harmonics. Their associated periods are mainly multiples of one week. The week is the characteristic period of our combination process since EOPs are estimated week per week. Therefore these low frequency harmonics seem to be mainly due to our processing method and to have no physical sense in terms of Earth rotation.

Conclusions

The analysis of the combined series of EOPs with a six-hour sampling shows that our method of combination at the measurement level is working. Furthermore this method provides a global and consistent solution of EOPs and station positions simultaneously with a satisfactory sampling. This kind of computation seems to be the future for Reference System realization and maintenance.

References

Altamimi, Z., Sillard, P. and C. Boucher, *Journal of Geophysical Research*, 107, B10, 2214, 2002.
EOP Product Center website, http://hpiers.obspm.fr/eop-pc/
Hefty, J., Rothacher, M., Springer, T. et al., *Journal of Geodesy*, 74, 479, 2000.
Mc Carthy, D. D., *IERS Conventions*, IERS Technical Note 21, 1996.
Ray, R. D., Steinberg, D. J., Chao, B. F. et al., *Science*, 264, 830, 1994.
Sahin, M., Cross, P. A. and P. C. Sellers, *Bulletin Géodésique*, 66, 284, 1992.
Sillard, P. and C. Boucher, *Journal of Geodesy*, 75, 63, 2001.

INTERANNUAL AND ANNUAL VARIATIONS IN THE GEOPOTENTIAL OBSERVED USING SLR

C.M. Cox(1,2), B. F. Chao(2), and A. Au(1,2)
(1) Raytheon Information Solutions, Landover, Maryland, USA
(2) Space Geodesy Branch, NASA Goddard Space Flight Center

Abstract

Recent Satellite Laser Ranging derived long wavelength gravity time series analysis has focused to a large extent on the effects of the recent large changes in the Earth's zonals, particularly J_2, and the potential causes, or the long-term secular rates. However, it is also possible to estimate the shorter wavelength coefficients, including non-zonals, over monthly time scales, and to connect these with known geophysical signals. For example, the results of Cox and Chao [2002] showed that the recovered J_3 time series shows remarkable agreement with NCEP-derived estimates of atmospheric gravity variations. Likewise, the non-zonal degree-2 terms showed reasonable correlation with atmospheric signals, as well as climatic effects such as El Niño Southern Oscillation. While the formal uncertainty of these terms is significantly higher than that for J_2, it is clear that there is useful signal to be extracted. Consequently, the SLR time series has been reprocessed to improve the time variable gravity field recovery, with the intent of recovering complete fields through maximum spherical harmonic degree 4. Initial comparisons of the average annual signals with the GRACE monthly fields shows a promising agreement over the continents, The recovered gravity rate map also is in general agreement with expectations of post-glacial rebound, depending on the period considered. We will present recent updates on the J_2 evolution, as well the interannual and annual variations of the gravity field, complete through degree 4, and geophysical and climatic connections.

Introduction

The long time history of satellite laser ranging (SLR) provides an absolutely unique data set of observations for the analysis of geophysical changes. Analysis of SLR tracking has yielded precise determination of the temporal variation in the low-degree spherical-harmonic components of Earth's gravity field, beginning with the initial observations of J_2 change made by observing Lageos-1 orbital node accelerations [*Yoder et al*., 1983; *Rubincam*, 1984]. Those earliest results demonstrated the ability to observe large-scale terrestrial change using SLR. More recent studies have extended the knowledge to higher degree zonals [e.g. *Gegout and Cazenave*, 1993; *Cheng et al*., 1997; *Cox et al.*, 2003], and examined the annual signals in the low-degree geopotential, the non-tidal part of which is dominated by climatological signals. Overall, SLR data have played a key role in understanding changes in the solid Earth at millennial and decadal time scales, as well as providing insight into climatological variations over annual time-scales.

Analysis of the J_2 signal

Figure 1 shows the complete J_2 data series. With the exception of the additional data, it is similar to Figure 1 of *Cox and Chao* [2002]. Processing and development of the series is described in *Cox et al.* [2003]. The 1998 J_2nomaly is evident as the hump after that period. It is also characterized by a change in the amplitude and nature of the seasonal cycle. The anomaly appears to start earlier than 1998, however, that portion of the departure from the long-term trend is the result of atmospheric mass variation. This is shown in Figure 2, which compares the J_2 series after removal of the pre-1998 slope and annual signals, with that based

on NCEP-derived atmospheric mass signal. After sometime in 2001, it appears as if the anomaly has changed slope, returning to something closer to the expected signal, however, it has not recovered to the original path that the pre-1998 slope would predict.

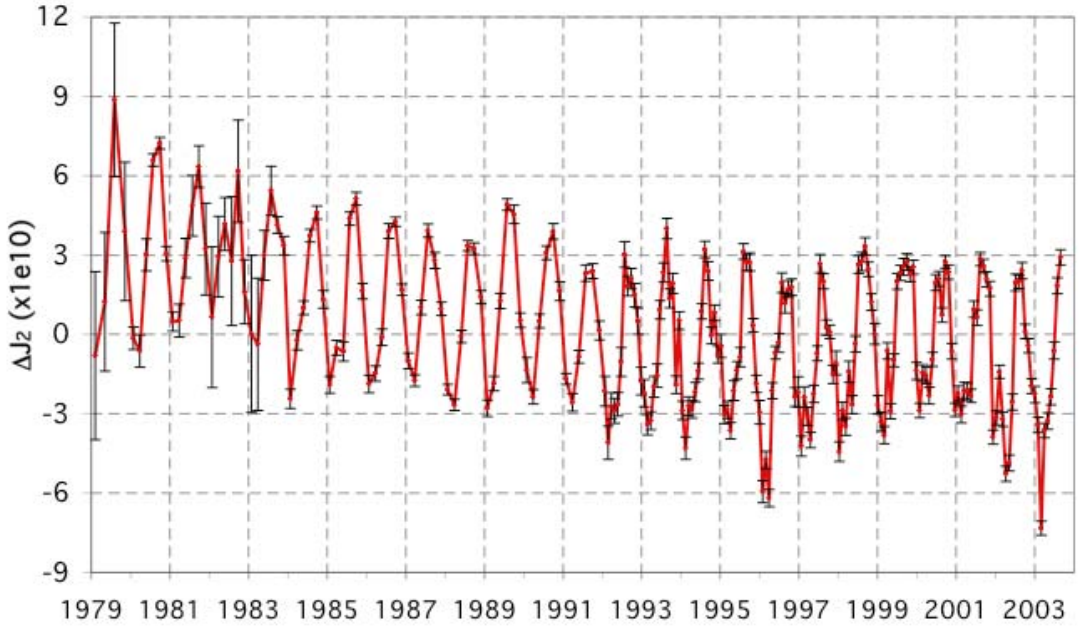

Figure 1. Observed ΔJ_2, including the atmospheric signal. Error bars are the observed J_2 uncertainties.

In addition to the J_2 zonal, time series for J_3 was also estimated. The J_3 zonal, which describes north-south mass distribution, does not show any significant anomalies corresponding to the timing of the J_2 anomaly. Provided this result is accurate, it implies that whatever is causing the J_2anomaly is largely symmetric around the Equator.

The cause of the anomaly has not been positively identified, however, it has been associated with oceanic [*Chao et al.* 2003] and possible glacier mass changes [*Dickey et al*., 2002]. The timing of the J_2 anomaly onset corresponds to the last big El Niño event, raising the possibility of an oceanographic connection. If the TOPEX/Poseidon (T/P) sea surface height (SSH) data is treated as being entirely caused by mass redistribution, the implied change in J_2 is consistent with the SLR results, if not a close match. EOF/PC (Empirical Orthogonal Function/Principal Component) analysis of the sea surface temperature (SST) and T/P SSH for the extratropic Pacific regions show an abrupt change around 1998. A breakdown of the SSH analysis for each region (not shown) indicates that the Northern pacific is the dominant contributor. The SST mode corresponds to the Pacific Decadal Oscillation (PDO), which is correlated at some level with the observed J_2data [*Cazenave and Nerem*, 2002]. Figure 3 shows the J_2 series compared with the SST-derived PDO Index. The correlation implies a connection with that ocean mode.

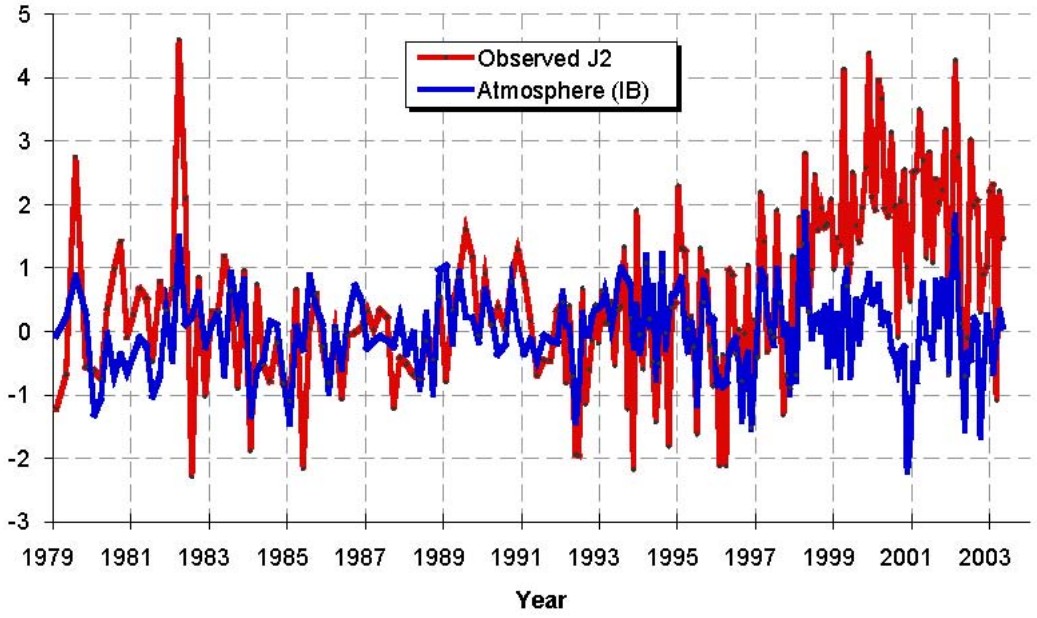

Figure 2. Observed ΔJ_2, after removal of pre-1998 slope and annual signals, compared with the corresponding atmospheric time series.

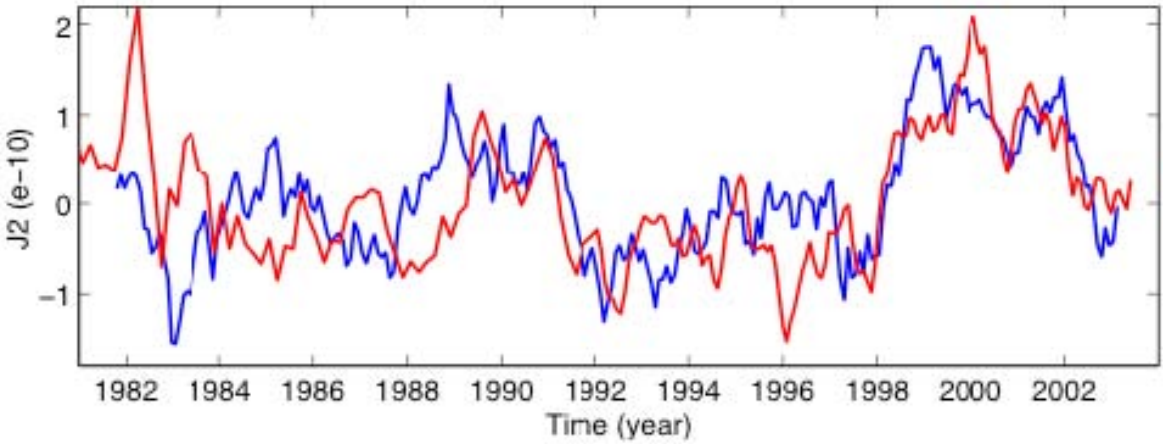

Figure 3. Non-seasonal ΔJ_2 (red curve) and the Pacific Decadal Oscillation (PDO, blue curve). The pre-1998 slope was removed from the ΔJ_2 series, as well as all annual signals. The PDO Index time series has been shifted to the right by five months.

Figure 4 shows a comparison of the atmosphere corrected J_2 series, after removal of the background (pre-1998) slope, with the cumulative totals from hydrology, the ocean, and sub-polar glaciers. The curve shown in green is the NCEP-derived soil hydrology. It shows some similarities, including the pre-anomaly dip, and a rise during the anomaly, but at most explains 20% of the anomaly. The blue curve shows the combination of the hydrology signal with the results from the assimilation mode output of the ECCO consortium ocean model [*Stammer, et al*., 1999] as run by JPL (run KF047A). The ocean may explain another 20% of the anomaly. The results of *Cox and Chao* [2002] dismissed sub-polar glaciers as a primary cause of the anomaly based on the estimated mass flux data then available for the period up through 1998. *Dickey et al.* [2002] pointed out scenarios where the glacier contribution could be a possible major contributor (in addition to the oceans) based on three extrapolations of the glacier data. The black curve in figure 3 shows the total of the hydrology, ocean, and sub-polar glacier data using updates to the observations complete through 2001 [*Dyurgerov*,

2005]. The sub-polar glaciers may contribute another 20% to the total. Overall, the three geophysical signals only explain no more than half of the 1998 J_2 anomaly.

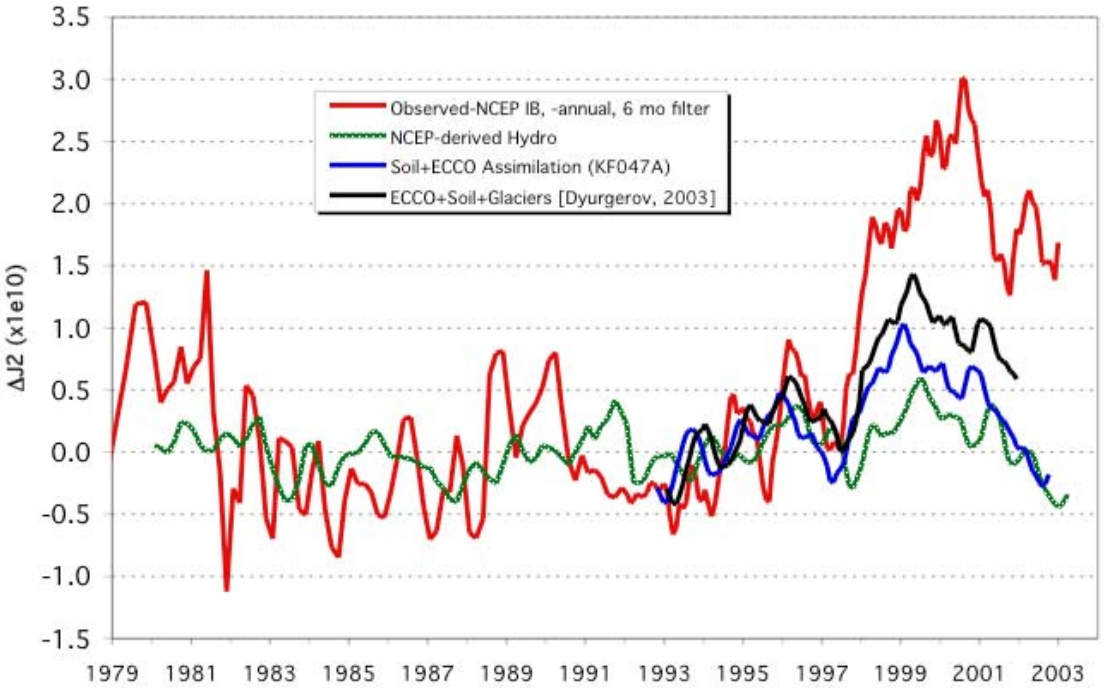

Figure 4. Non-seasonal atmosphere-corrected ΔJ_2, and the modeled contributions of hydrology, the oceans (ECCO Assimilation run KF047A), and estimated mass changes in the sub-polar glaciers.

The insufficiency of the hydrology, ocean, and glacier variations to explain the J_2 anomaly should not be unexpected. These represent only three potential contributors, and for that matter the models used to represent them are not complete. Greenland and Antarctica, which are not included in the glacier statistics, may have contributing roles. In addition the polar seas, which are not modeled in ECCO, and the actual hydrological signal including aquifers may have contributions. Furthermore, the oceanic global circulation models tend to underestimate the true variabilities.

All of the signals investigated to explain the J_2anomaly have regional components that are non-zonal in nature, which may be useful for positive identification of the contributors to the J_2 anomaly. Comparison of the geophysical models with an appropriate observed gravity time series will allow identification of the known contributors to the interannual variations, as well as identify gaps in our knowledge of global mass transport. The earlier results of *Cox and Chao* [2002] were primarily designed to recover zonal signals -- while there is some non–zonal signal of interest in the available series [*Cox et al.*, 2003], the longitudinal signals have been suppressed for the most part.

Revised Processing

In an effort to recover a complete time-variable gravity time series, a new series has been prepared that is complete through spherical harmonic degree 4 from 1976 through 2004. The series was estimated at 60-day intervals prior to 1993, and nominally 30-day (actually 3 T/P cycles) after that point. This series used SLR tracking of Lageos-1, Lageos-2, Starlette, Ajisai, Stella, Westpac, and limited amounts of SLR and DORIS tracking of T/P. The ITRF2000

reference frame was used with the latest NASA GSFC pre-GRACE gravity field model - pgs7751q2 – which was a development of EGM96 [*Lemoine et al*., 1998]. The solid Earth tides are modeled in the same fashion as EGM96. Monthly atmospheric time-variable gravity complete through spherical harmonic degree 5, and with respect to the mean for 2000-2001, were made based on the NCEP monthly pressure fields, and the assumption of an inverse barometer (IB) response over the oceans. The GOT99 ocean tide model [*Ray*, 1999] was used in a "Demos number" representation [*Christoldoulidis et al*., 1988] with equilibrium values for Sa and Ssa C_{20} tides, and zero for the other harmonics of those tides. The tide model was complete through degree 10 for the following constituents: 2N2, 2Q1, Ae2, J1, L2, M1, Oo1, Phi1, Pi1, Psi1, R2, and T2. A number of the constituents were modeled to degree 20: K1, K2, M2, N2, O1, P1, Q1, S2. The 18.6-year and 9.3-year ocean tide C_{20} amplitudes were set to the values estimated in a comprehensive solution using data from 1979 through 1997 [*Cox et al.,* 2002]. Rates and annuals for the $C_{2...4,0}$ zonals derived from the earlier processing were used in the data reductions and gravity solutions, then restored in the post processing.

Interannual signals

The revised C_{20} time series is shown in Figure 5. The signal is generally commensurate with the previous J_2 ($=-\sqrt{5}\ C_{2,0}$) time series, although there is a new feature in the 1984-1986 period, which also appears in C_{40} series (Figure 6). There is some correlation with the C_{40} signal suspected in this case (overall correlation between the two series only 0.4). Post-1998 both the C_{20} and C_{40} series show significant anomalies. In this case correlation between the two series is not suspected, due to more satellites being present in the solution, and the fact that if it is spatially driven correlation in both the 1984 period and the post-1998 period, the correlation should have a consistent sign.

Because of concerns over possible correlations, the average geoid height by latitude band was computed, looking at the equatorial region (|lat|<30°), mid latitudes (30°< |lat| < 60°) and polar regions (60°<|lat|). The results are shown in Figure 7. As the figure shows, the mid-latitude geoid has remained fairly constant over the entire period. However, around 1996 to 1998, the polar geoid started to drop, whereas the equatorial geoid rose. This is indicative of a mass transport from the high latitudes to the low latitudes of large proportion, as it must overcome post-glacial rebound (see next section) to result in such a drop in the polar geoid [*Cox and Chao*, 2002].

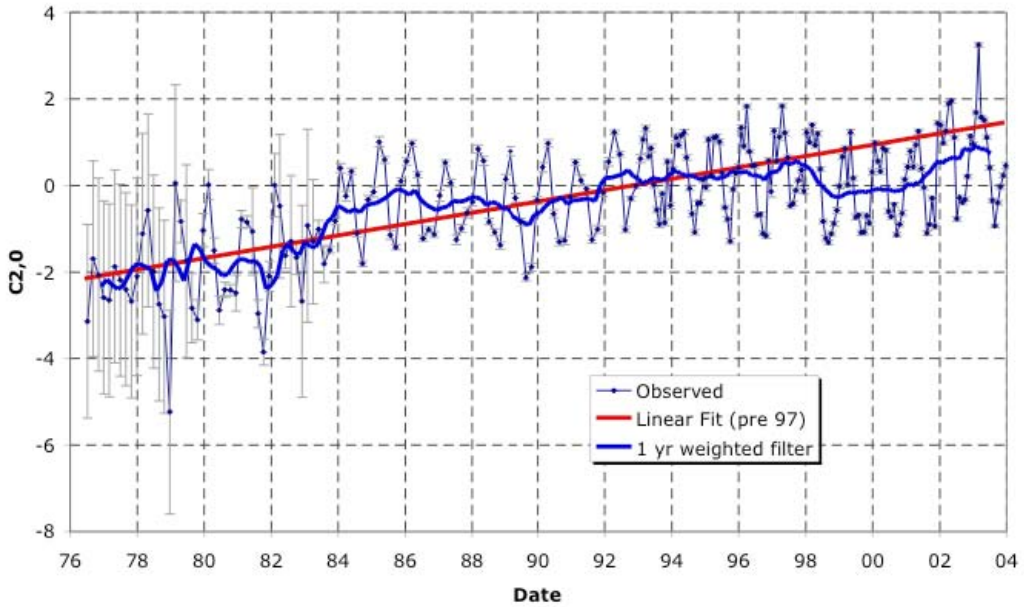

Figure 5. C_{20} from revised processing. Units are $1x10^{-10}$

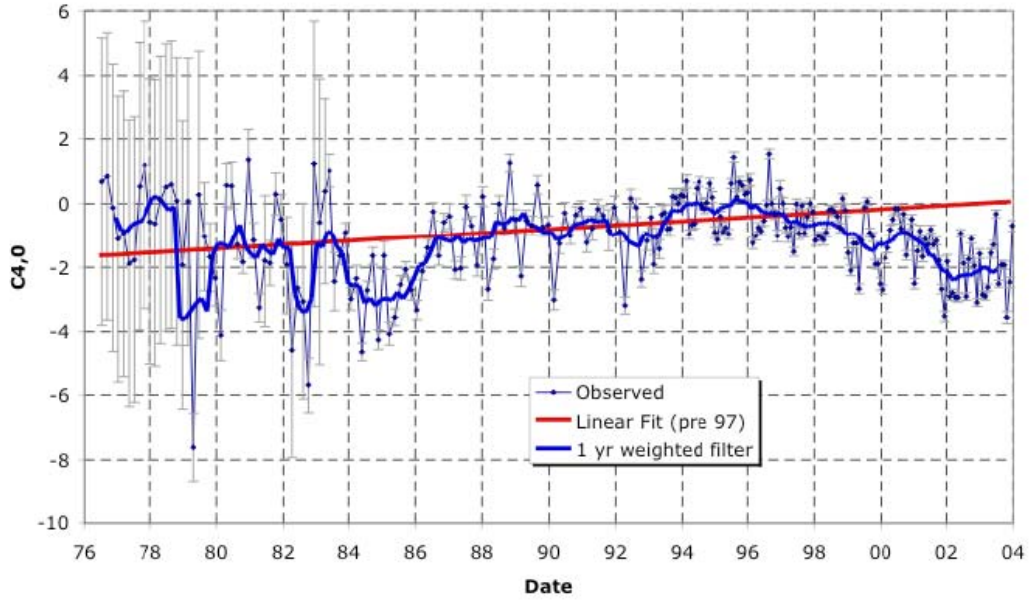

Figure 6. C_{40} from revised processing. Units are $1x10^{-10}$

The non-zonal terms of the gravity also show significant changes. Figure 8 shows the time series for the S_{33} term, which is dependent only on longitude. This spherical harmonic coefficient shows some of the larger signals. Significant variation is seen in the 1986-1992 period, but this period is determined with only three satellites (Starlette, Ajisai, and Lageos1), so it could be satellite related. After 1993 there are several more spacecraft involved and the variations are smaller. However, after 2000 there are substantial departures that are of the magnitude seen with the zonals.

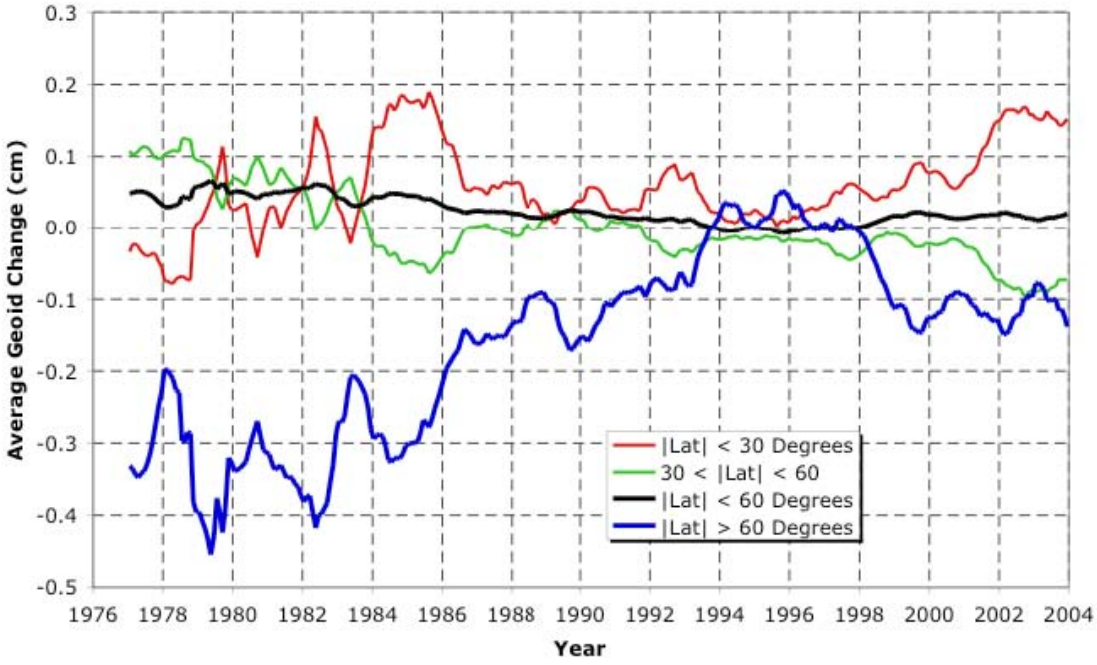

Figure 7. Zonal changes in the geoid over the equatorial (|lat|<30°), mid latitude (30°< |lat| < 60°) and polar regions (60°<|lat|). An annual filter has been applied to the data.

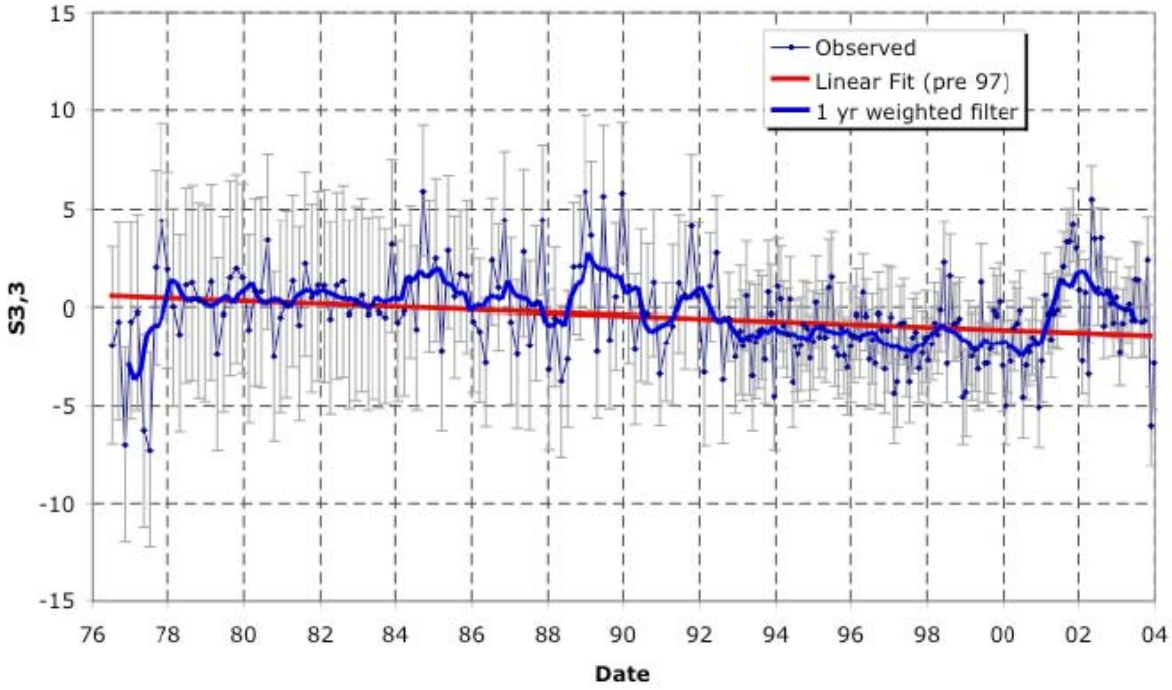

Figure 8. S_{33} from revised processing. Units are $1x10^{-10}$

Geoid Rates

As discussed earlier, SLR has been used to assess zonal changes in the gravity field, but it has not been used to directly assess the changes in the complete geoid. Preliminary geoid rates complete through degree 4 have been computed from the time series, and are shown in the map Figure 9 for the 1980-1997 period. The rates shown are with respect to the IERS2000 definition for the C/S_{21} rates. For this computation, the post-930101 SLR solution data was effectively weighted at 2x the earlier data. For the period 1980-1997 there are large increases in the Greenland/North America and Antarctic regions (~0.5 mm/yr). For comparison, Figure 10 shows the corresponding geoid rate amp through degree 4 due to the mantle post-glacial rebound (PGR), computed by Erik Ivins (see http://bowie.gsfc.nasa.gov/ggfc/mantle.htm), based on an ICE-3G ice loading history model and a lower mantle viscosity of $2x10^{21}$ Pa s. As that model shows, the principle features at the 5000 km spatial scale of the SLR results is confined to the Hudson Bay area and Greenland in the northern hemisphere, and a fairly uniform, and larger, change over the south pole. There are some features at the lower latitudes, but they are much smaller, relative to the polar changes, than those seen in the SLR results. For the full period over 1980-2002 the observed geoid change is reduced by 50% (Figure 11). Of note is the relative scale of the changes over Greenland and Antarctica, with Greenland dominating, which is reversed from that expected based on PGR. Either present-day mass loss in Antarctica, or less likely, mass accumulation in Greenland could explain this feature.

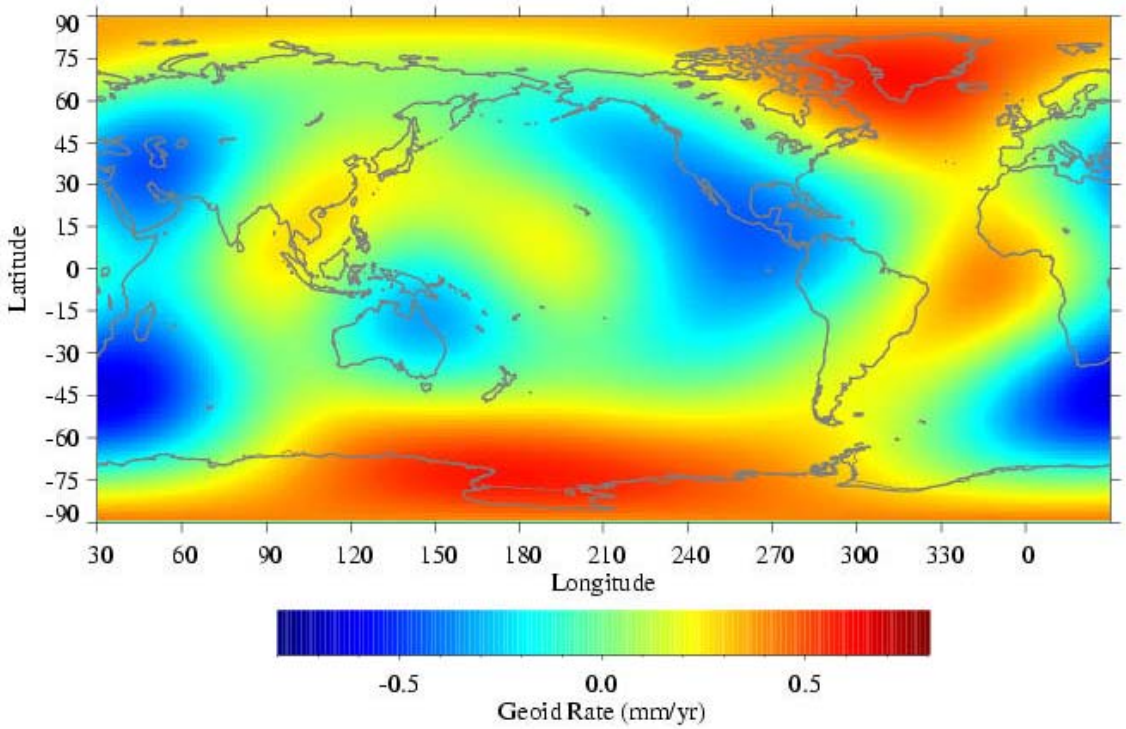

Figure 9. Mean geoid rate map in mm/yr derived from SLR tracking from 1980 through 1997. shown with respect to the IERS definition for the C/S_{21} rates.

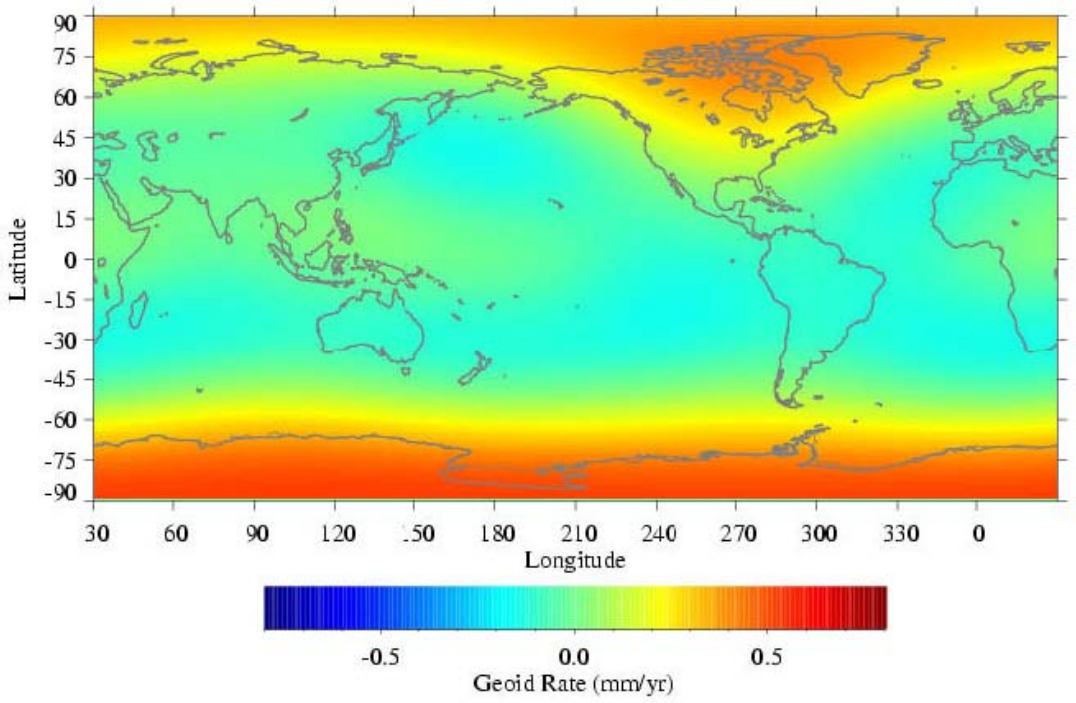

Figure 10. Mean geoid rate map for PGR in mm/yr through degree 4, predicted based on an ICE-3G ice loading history model and a lower mantle viscosity of $2x10^{21}$ Pa s (courtesy of Erik Ivins).

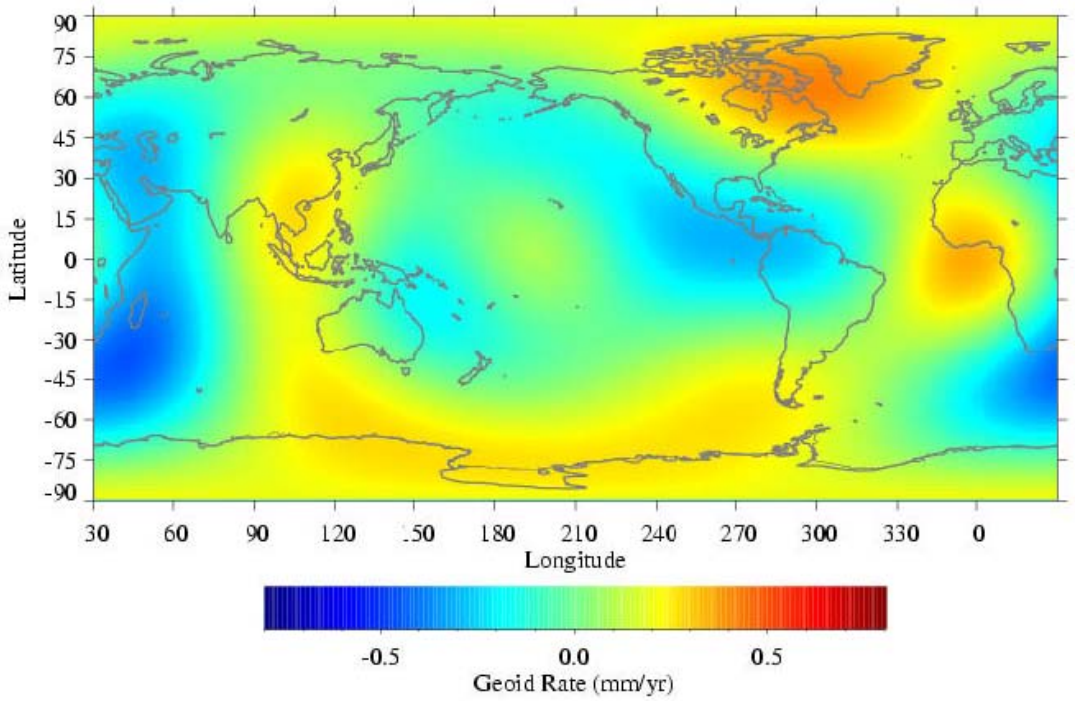

Figure 11. Same as Figure 9, but for the period 1980 through 2002.

The comparatively large changes sensed by SLR in the low latitude regions are commensurate with the T/P observed sea-level change shown in Figure 12 [Figure 3 from *Anderson et al*., 2002]. Both show prominent increases in the western Pacific and a drop in the eastern Pacific, as well as a general increase in the Atlantic. The implication is that the sea level changes represent actual mass transport, and that the changes in sea level are not the sole result of steric effects by themselves.

More detailed analysis is required, including: error assessment, consideration of steric effects for the ocean data comparisons, and comparison with hydrological changes over land in order to make a more thorough assessment of the mass transport budgets. Nonetheless, the results shown here, although preliminary and qualitative in nature demonstrate that SLR may have merit in looking at climate induced mass transport at the decadal scales.

Annual and Semi-Annual Signals

In contrast to the large differences between the SLR and GRACE time-variable gravity fields, similar seasonal (annual and semi-annual) variations are present in both. Figure 13 shows the monthly sequence maps, complete through degree 4, expressed as the equivalent water height [e.g., *Chao*, 2005]. The SLR seasonal terms were derived from the 5-year period 1998-2002. The nineteen GRACE (UT/CSR) monthly solutions were fit with mean, linear, annual, and semi-annual terms, and only the annual and semi-annual terms plotted.

There are some significant differences in the make up of the fields. First, the treatment of the ocean correction is different. The SLR series only considers the IB response to the atmosphere, whereas the GRACE products are corrected for both pressure and wind driven changes in the ocean mass distribution based on a barotropic ocean model [*Tapley et al*., 2004]. The C_{20} annual and semi-annual terms from both data sets were used in generating the maps, however a large rate was removed from the GRACE data. Also, in an attempt to match the nature of the $C_{odd,0}$ term estimated in the SLR results, the C_{30} and C_{50} GRACE terms were

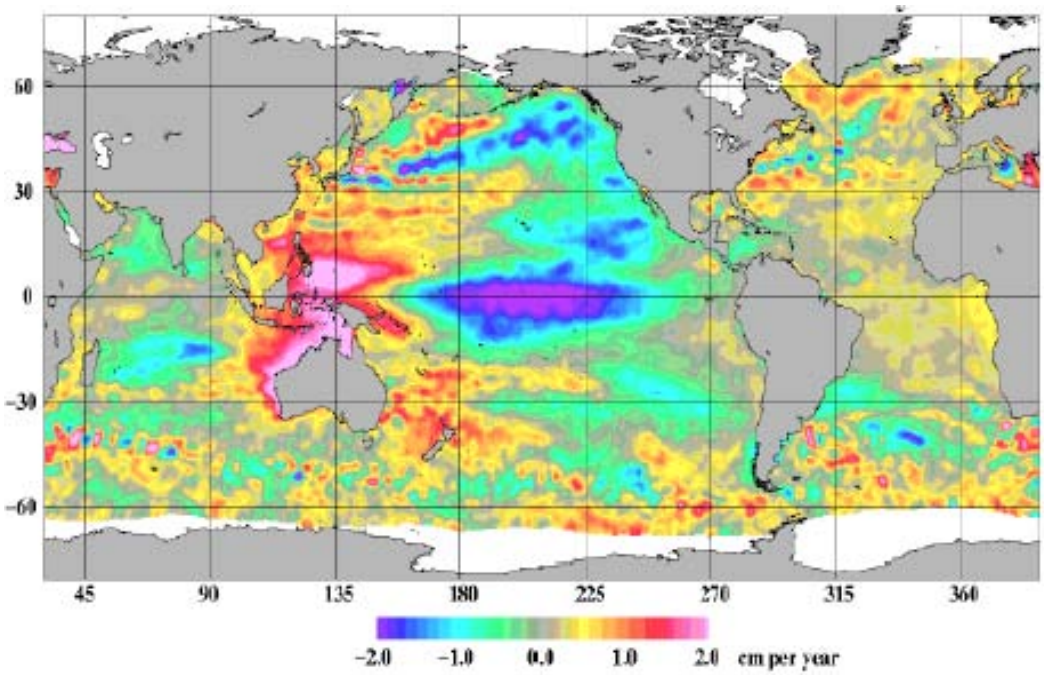

Figure 12. Sea Level trend from T/P for the period from September 1992, through February 2000. From figure 3 in *Anderson et al*., [2002].

used. Finally, the selected time periods differ, making the comparison valid only in terms of the "average" signal, and then only in the case where climate variability does not cause changes in the amplitude, and possibly phase, of the variations. There is some indication of this in the long C_{20} time series (not shown).

Despite the differences in the make up of the solutions, the seasonal signals have fairly good agreement over land. The seasonal cycle over the Amazon (peaking in April/May) is captured by both SLR and GRACE datasets. There are similar structures and evolutions over Africa and Europe as highs and lows move from East Africa to Northwest Africa to the North Atlantic then to Europe, and east into Asia. Also, the monsoons in India, peaking in July/August, then progressing east and north along the Asian coast, are evident in both sets of results. The SLR results do show more power over the oceans, which is expected since only the IB (not the wind-driven) ocean correction was applied. Likewise, there are differences in the polar latitudes, possibly caused by the differences between $C_{odd,0}$ from SLR and $C_{30} + C_{50}$ from GRACE.

Conclusions

A large anomaly in C_{20} (or J_2) began sometime around 1998, and has persisted until the present time. Sometime in 2001, the slope changed again. The C_{20} signal has returned about 50% of the way to the long-term trend dictated by PGR. Consequently, the deviation may be interannual in nature, and therefore does not necessarily represent a departure from the long-term trend. Overall the signal is well correlated with the pacific decadal oscillation, however the available ocean data does not explain the mass anomaly. The oceans, continental hydrology, and sub-polar mountain glaciers may each explain ~20% of the anomaly.

The revised processing, intended to recover complete gravity fields, has resulted in more signal in the C_{30} and C_{40} series. While there is some concern over their separability, the sum of the zonal terms $C_{2..4,0}$ terms indicates the possibility of a rapid drop in the geoid over the polar regions. There is a corresponding rise in the geoid in the lower latitudes, but as of yet ascertaining where the presumed ice mass went (ocean or land) is not possible.

The observed geoid rates are similar to the PRG predictions. The signal in the northern regions is larger compared to the Antarctic regions than the PGR models predict. Is the excess related to present-day mass loss? There are also differences in the Equatorial regions, with more rise being observed in the Atlantic than is predicted by the PGR models. The rise is in general qualitative agreement with the observed sea level trend.

There is reasonable agreement between the annual and semi-annual time-variable gravity signals derived from 5 years of SLR observations, and the 19 monthly solutions available from the GRACE Mission at spatial scales of ~5000 km. However, there are significant differences in the mean fields and individual spherical-harmonic terms estimated at monthly timescales.

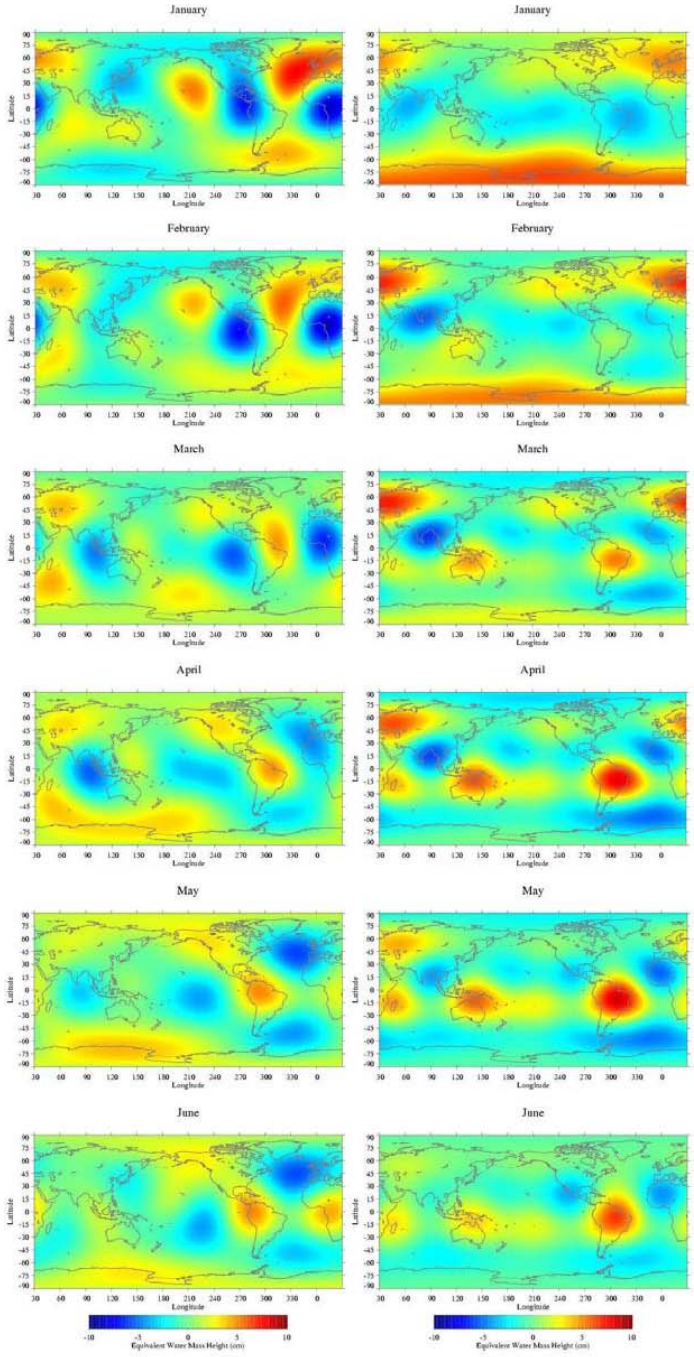

Figure 13a. Seasonal (annual plus semi-annual) time-variable gravity field expressed in terms of equivalent water height, January (top) through June (bottom). The SLR/DORIS results are shown on the left and the GRACE on the right. The color scale range is ±10 cm.

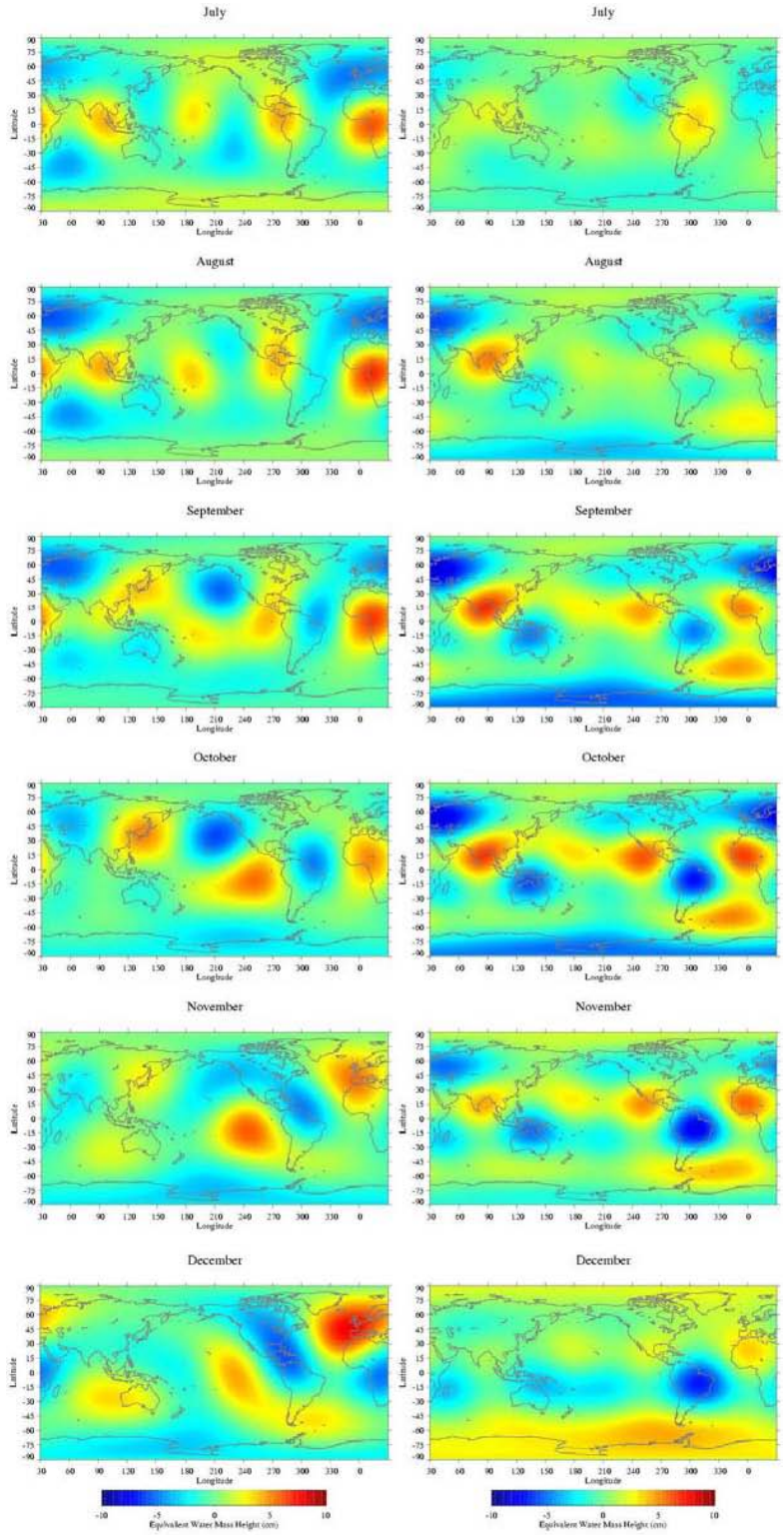

Figure 13b. Seasonal (annual plus semi-annual) time-variable gravity field expressed in terms of equivalent water height, July (top) through January (bottom). The SLR/DORIS results are shown on the left and the GRACE on the right. The color scale range is ±10 cm.

References

Anderson, O.B., P. Knudson, and B. Beckley, Monitoring Sea Level and Sea Surface Temperature Trends from ERS Satellites, *Phys and Chem of the Earth*, 27, Nos 32-34, 1413-1418, 2002.

Cazenave, A., and R.S. Nerem, Redistributing the Earth's Mass, 297, 783, August 2, 2002.
Chao, B. F., On inversion for mass distribution from global (time-variable) gravity field, in press, *J. Geodynamics*, 2005.
Cheng, M.K., C.K. Shum, B.D. Tapley, Determination of long-term changes in the Earth's gravity field, *J. Geophys Res,* **102**, 22377, 1997.
Christoldoulidis, D.C., D.E. Smith, R.G. Williamson, and S.M. Klosko, "Observed Tidal Braking in the Earth/Moon/Sun System," *J. Geophys. Res*., 93, B6, 6216-6236, 1988.
Cox, C.M., and B.F. Chao, Detection of a Large-Scale Mass Redistribution in the Terrestrial System Since 1998, Science, 297, 831, August 2, 2002.
Cox, C.M., A. Au, J.-P. Boy, and B.F. Chao, Time-Variable Gravity: Using Satellite-Laser-Ranging as a Tool for Observing Long-Term Changes in the Earth System, Proceedings of the 13th International Workshop on Laser Ranging, R. Noomen, S. Klosko, C. Noll, and M. Pearlman, eds., October, 2003.
Dickey, J. O., S. Marcus, O. de Viron, I. Fukumori, Recent Earth oblateness variations: Unraveling climate and postglacial rebound effects, *Science 298*, 1975-1977, 2002.
Dyurgerov, Mark. Glacier Mass Balance and Regime: Data of Measurements and Analysis. INSTAAR Occasional Paper No. 55, ed. M. Meier and R. Armstrong. Boulder, CO: Institute of Arctic and Alpine Research, University of Colorado. Distributed by National Snow and Ice Data Center, Boulder, CO. 2002, updated 2005.
Gegout, P. and A. Cazenave, Temporal Variations of the Earth's Gravity Field for 1985-1989 from Lageos, *Geophys J Intl*, 114, 347-359, 1993.
Lemoine, F.G., Kenyon, S.C., Factor, J.K., Trimmer, R.G., Pavlis, N.K., Chinn, D.S., Cox, C.M., Klosko, S.M., Luthcke, S.B., Torrence, M.H., Wang, Y.M., Williamson, R.G., Pavlis, E.C., Rapp, R.H., and Olson, T.R., The Development of the Joint NASA GSFC and the National Imagery and Mapping Agency (NIMA) Geopotential Model EGM96, NASA TR 206861, 1998.
Ray, R.D., A global ocean tide model from Topex/Poseidon altimetry: GOT99.2, NASA Tech. Memo. 209478, Goddard Space Flight Center, 58 pp., 1999.
Rubincam, D.P., Postglacial Rebound Observed by Lageos and the Effective Viscosity of the Lower Mantle, *J. Geophys Res,* 89, 1077-1087, 1984.
Stammer, D. et al., The consortium for estimating the circulation and climate of the ocean (ECCO) -- Science goals and task plan, The ECCO Consortium, Report No.1, November 1999.
Tapley, B. D., S. Bettadpur, J. C. Ries, P. F. Thompson, and M. M. Watkins, GRACE measurements of mass variability in the Earth system, *Science, 305*, 503-505, 2004.
Yoder, C.F., J.G. Williams, J.O.Dickey, B.E. Schutz, R.J. Eanes, B.D. Tapley, Secular Variation of earth's gravitational harmonic J_2 coefficient from Lageos2 and non-tidal acceleration of earth rotation, *Nature*, 303 (5920): 757-762 (1983).

ATMOSPHERIC "BLUE SKY" EFFECTS ON SLR STATION COORDINATES

Toshimichi Otsubo (1), Toshihiro Kubo-oka (1), Tadahiro Gotoh (2), Ryuichi Ichikawa (1)
(1)Kashima Space Research Center, National Institute of Information and Communications Technology. 893-1 Hirai, Kashima 314-8501 Japan otsubo@nict.go.jp
(2)Koganei Headquaters, National Institute of Information and Communications Technology 4-2-1 Nukuikita, Koganei, Tokyo 184-8795 Japan

Abstract

Satellite laser ranging (SLR) station coordinates are found to be dependent on local atmospheric pressure through a precise 5-year orbit analysis of LAGEOS-I and LAGEOS-II satellites. The loading coefficients of the station heights are estimated to be mostly around -0.3 to -0.5 mm/hPa. This result indicates that the site displacement due to the atmospheric pressure loading effect is detected for the first time by the SLR technique. Furthermore, due to its weather restriction, a -0.4 to -1.3 mm offset is theoretically predicted in the height of SLR stations when it is compared to all-weather microwave-based geodetic techniques like GPS and VLBI.

Introduction

Earth's crust is deformed by the load of atmospheric mass, as well as other factors, such as solid earth tides, ocean loading, and snow loading. The displacement due to the atmospheric pressure loading is typically 10 to 20 mm peak-to-peak, mainly in the vertical component, at hardly predictable frequencies from a day or so (distribution variation of atmospheric pressure) to a year (seasonal distribution variation).

Rabbel and Zschau [1985] applied the Green's function convolution to the idealized atmospheric load distribution, and derived a simplified form to approximate the vertical variation of the station coordinates Δu (in mm):

$$\Delta u = -0\ 35\ \Delta p - 0.55\Delta p_\ell \qquad (1)$$

where Δp is the pressure variation at the surface point in hPa, and Δp_ℓ is the long-wavelength (circular 2000-km region) averaging pressure variation in hPa ignoring the variation of the ocean area. Note that the first term contributes more than the second term as Δp changes more than Δp_ℓ.

The effect was already seen in Global Positioning System (GPS) and Very Long Baseline Interferometry (VLBI) data [van Dam and Herring, 1994; MacMillan and Gipson, 1994; van Dam et al., 1994]. Compared to these microwave-based geodetic techniques, satellite laser ranging (SLR) observation has an advantage in accurate model of propagation delay, which must result in accurate determination of a vertical component of station coordinates. Variation of a vertical component due to atmospheric loading effect has been researched for a couple of decades, and the amount of deformation is typically 1 cm peak-to-peak or less. On the other hand, unlike GPS and VLBI, SLR observation data volume is, in general, not sufficient to derive the station coordinates at a high time resolution like a daily interval. Analysis Working Group of International Laser Ranging Serive (ILRS) has recently started generating weekly solutions, but most of the atmospheric pressure change is averaged out for a week's time span. Therefore, we cannot use such 'preformed' station coordinates to detect the signal of the atmospheric pressure loading from SLR observation data.

Signal of atmospheric pressure loading in SLR data

Our attempt to detect the atmospheric pressure loading in SLR data is basically described as:

$$\Delta u = \alpha \Delta p = \alpha (p - p_0) \qquad (2)$$

where α is the station-dependent loading coefficient to be adjusted, and p is the local atmospheric pressure at the observation epoch and p_0 is the average atmospheric pressure at the site.

Instead of using daily 'preformed' station coordinates, the estimation procedure of the α coefficient is implemented in the orbit analysis software 'concerto' that has been developed in NICT, and the coefficient is solved for simultaneously with other parameters such as satellite orbits, station coordinates, etc.

We used the five-year (Jan 1999 to Dec 2003) SLR data to LAGEOS-1 and LAGEOS-2 satellites. The atmospheric pressure p is taken from the SLR normal point data, and the average pressure p_0 was just a simple five-year average of observed atmospheric pressure. We estimated the orbits (six elements, constant along-track acceleration and once-per-rev along-track acceleration) every 5 days, and station coordinates, range biases every year. The α coefficients were, at the same time, solved for every year for the 12 stations which has been produced consistent quantity and quality. This procedure was performed for LAGEOS-1 and independently for LAGEOS-2. After all, we therefore obtained ten α solutions per site.

Figure 1 shows the five-year estimates of the α coefficients for Graz (Austria; 7839) and Herstmonceux (UK; 7840). They are constantly negative throughout the period, which means the station heights get lower when the atmospheric pressure is high. The averages were -0.43 mm/hPa for Graz and -0.29 mm/hPa, which are close to the values -0.47 mm/hPa and -0.33 mm/hPa respectively referred in IERS Conventions [IERS, 2003]. This analysis also reveals the station height of Herstmonceux is less sensitive to atmospheric pressure change than Graz. This is probably because the station is more surrounded by oceans which partly absorb the variation of atmospheric pressure. The peak-to-peak ranges of atmospheric pressure are about 40 hPa at these two sites, so the peak-to-peak height changes due to atmospheric pressure loading amount to 12 mm (Herstmonceux) to 19 mm (Graz).

Such stable results, however, cannot be seen for some stations. Figure 2 shows the estimates for McDonald (USA; 7080) and Monument Peak (USA; 7110). They scatter much more than Figure 1, and the average values -0.82 mm/hPa and -0.01 mm/hPa are more deviated from the IERS values -0.47 mm/hPa and -0.40 mm/hPa respectively, despite of the data quality being as good as the previous two stations. We found that the variation range of atmospheric pressure is narrow at these sites - only 3hPa rms. Therefore the height change itself is smaller, which is considered to have resulted in the poor estimates of the loading coefficients α.

A numerical summary of the 12 stations are listed in Table 1. Except for three stations, McDonald, Monument Peak and Hartebeesthoek, where the atmospheric pressure changes less, the loading coefficients are estimated around -0.3 to -0.5 mm/hPa.

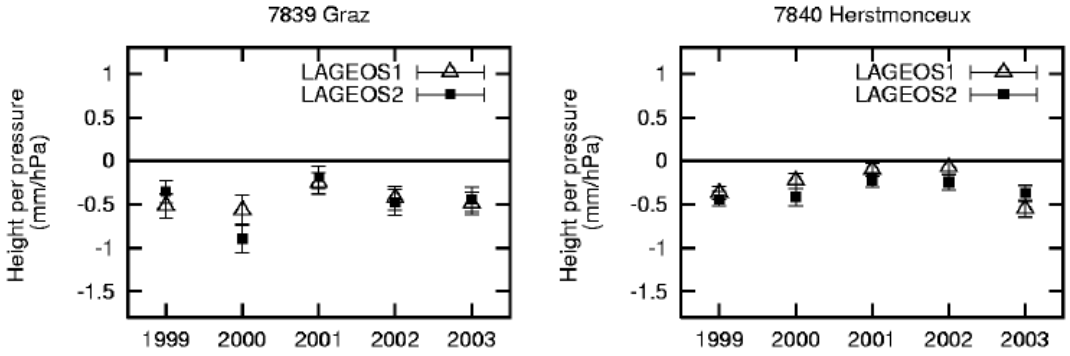

Figure 1. Estimated loading coefficients α (well estimated case). The average values are -0.43 mm/hPa for Graz and -0.29 mm/hPa for Herstmonceux.

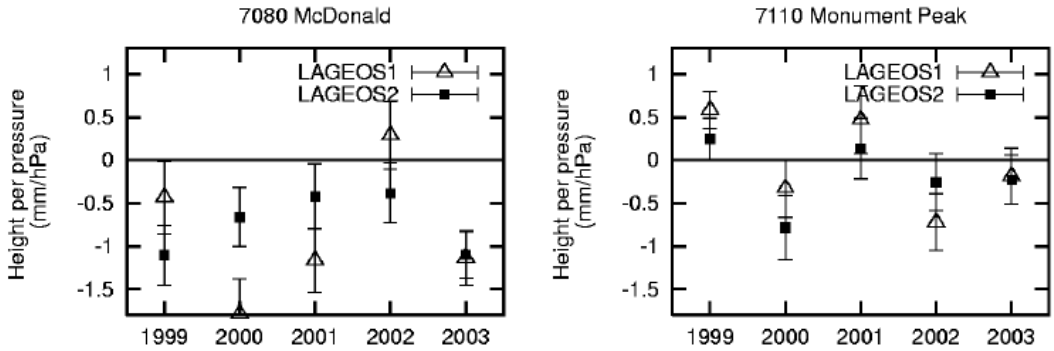

Figure 2. Estimated loading coefficients α (poor estimated case). The average values are -0.82 mm/hPa for McDonald and -0.01 mm/hPa for Monument Peak.

Table 1. Estimated loading coefficients α for 12 SLR stations.

Station (ID)	estimated (mm/hPa)	Pres. (hPa)	Rms IERS (mm/hPa)
McDonald (7080), USA	-0.82 +/- 0.16	3.4	-0.47
Yarragadee (7090), Australia	-0.36 +/- 0.10	5.3	-0.42
Greenbelt (7105), USA	-0.37 +/- 0.07	6.5	-0.36
Monument Peak (7110), USA	-0.01 +/- 0.14	2.9	-0.40
Changchun (7237), China	-0.73 +/- 0.22	8.0	
Hartebeesthoek (7501), S. Africa	-0.10 +/- 0.42	3.2	-0.57
Zimmerwald (7810), Switzerland	-0.48 +/- 0.11	5.0	-0.41
Grasse (7835), France	-0.38 +/- 0.09	5.6	-0.34
Graz (7839), Austria	-0.43 +/- 0.05	6.3	-0.47
Herstmonceux (7840), UK	-0.29 +/- 0.04	8.9	-0.33
Mt. Stromlo (7849), Australia	-0.33 +/- 0.07	6.1	-0.37
Wettzell (8834), Germany	-0.49 +/- 0.15	5.7	-0.44

All from 1999-2003 data, except Hartebeesthoek (2000-2003) and Mt. Stromlo (1999-2002).

Blue Sky Offset

Multiple space geodetic techniques can currently define the scale of a terrestrial reference frame. In the analysis of the most recent International Terrestrial Reference Frame (=ITRF2000 [Altamimi, 2002]), the agreement between analysis centres was more or less within ± 1 ppb, equivalent to ± 6 mm for the radius of the Earth.

The SLR data can be obtained only when a sky is clear, whereas other microwave-based techniques such as VLBI and GPS can be operational under any sky conditions. Considering the fact that the atmospheric pressure is generally high under a blue or starry sky, the 'mean' station coordinate for SLR is expected to be biased—lower than the all-weather techniques.

In order to assess the blue-sky height offset, the difference between the blue-sky mean and all-time mean of atmospheric pressure is required. This is possible for just six SLR stations where the collocated GPS facility has constantly recorded the meteorological data. We here define that the all-time mean is just a plain average of IGS meteorological time series and the blue-sky mean is an average of ones at the SLR (LAGEOS-1 and LAGEOS-2) time stamp. Processing the 3 to 5 years' data, the differences were:

McDonald	+0.8 hPa
Greenbelt	+1.0 hPa
Zimmerwald	+1.9 hPa
Graz	+1.6 hPa
Herstmonceux	+3.3 hPa
Wettzell	+2.6 hPa

The blue-sky pressure means are found to be indeed higher than the all-time pressure means. Multiplying these by the α coefficients in Table 1, we obtain the blue-sky height offset:

McDonald	-0.7 mm
Greenbelt	-0.4 mm
Zimmerwald	-0.9 mm
Graz	-0.7 mm
Herstmonceux	-1.0 mm
Wettzell	-1.3 mm

Such small height offsets are not sensitive by the current level of multi-technique comparison/combination, but they should be seen in the future with a further enhancement of observation/analysis accuracy in SLR and other techniques.

Conclusions

Our orbit analysis of recent five-year SLR data detected the site displacement due to atmospheric pressure loading, and it amounts up to 2 cm peak-to-peak. When one compares/combines the terrestrial reference solutions from multiple geodetic techniques at 1 mm accuracy, particular care should be taken for the site-dependent blue sky height offset. The other way is that all analysts should use a theoretically calculated displacement table (e.g. Petrov's website [Petrov, 2003]).

References

Altamimi, Z., P. Sillard, and C. Boucher, ITRF2000: A new release of the International Terrestrial Reference Frame for earth science applications, *J. Geophys. Res*., 107(B10), 2214, doi:10.1029/2001JB000561, 2002.

McCarthy, D. D., and G. Petit, IERS Conventions (2003), *IERS Technical Note 32, International Earth Rotation and Reference Systems Service,* 2003 (in print).

MacMillan, D. S., and J. M. Gipson, Atmospheric pressure loading parameters from very long baseline interferometry observations, *J. Geophys. Res*., 99(B9), 18081-18087, 1994.

Petrov, L., and J. P. Boy, Study of the atmospheric pressure loading signal in VLBI observations, submitted to *J. Geophys. Res*., 2003.

Rabbel, W., and J. Zschau, Static deformation and gravity changes at the earth's surface due to atmospheric loading, *J. Geophys*., 56, 81-99, 1985.

van Dam, T. M., and T. A. Herring, Detection of atmospheric pressure loading using very long baseline interferometry measurements, *J. Geophys. Res*., 99(B3), 4505-4517, 1994.

van Dam, T. M., G. Blewitt, and M. B. Heflin, Atmospheric pressure loading effects on Global Positioning System coordinate deformations, *J. Geophys. Res*., 99(B12), 23939-23950, 1994.

FTLRS support to the GAVDOS project : tracking and positioning

P. Berio (1), P. Exertier (1), F. Pierron (1), J. Weick (1), D. Coulot (1,2), O. Laurain (1), P. Bonnefond (1) and Ftlrs Laser Staff.

(1) Observatoire de la Côte d'Azur, GEMINI/UMR6203-CNRS, Av N. Copernic, 06130 Grasse, France.

(2) IGN, ENSG/LAREG, 6 et 8 Avenue Blaise Pascal, Cité Descartes, Champs-sur-Marne, 77455 Marne-la-Vallée cedex 2, France.

Abstract

In 2002, the FTLRS system performed a very successful six months campaign in Corsica for the altimeter calibration (CAL/VAL) of the JASON-1 satellite. The results have been presented on last laser workshop in Washington. After a short period of maintenance, this mobile station was again engaged in 2003 in the framework of the European GAVDOS project. The primary objective of this project is the establishment of an absolute sea level monitoring and altimeter calibration facility on the isle of GAVDOS, south of the island of Crete, Greece. The GAVDOS project will determine consistently and reliably (1) the altimeter biases and drifts for each satellite altimetric missions (TOPEX/Poseidon, JASON1, ENVISAT,…) and (2) the bias among different missions. It will also determine the mean sea level and the earth's tectonic deformation field in the region of Crete.

The FTLRS was set up in Crete (from April to October 2003 with a two month stop in July and August to avoid too warm days) in order to provide accurate data for altimeter calibrations, orbit validations and accurate positioning.
In this talk, we will present the observational balance sheet of the FTLRS Crete campaign and the positioning results obtained with a combination of LAGEOS -1, -2, STELLA, and STARLETTE observations. This solution will be compared to a GPS one.

Introduction

GAVDOS is a research project supported by the European community. Its primary objective is the establishment of an absolute sea level monitoring and altimeter calibration facility on the isle of Gavdos, south of the island of Crete, Greece. It will determine consistently and reliably (1) the altimeter biases and drifts for each of these missions and (2) the bias among different missions. It will also determine the mean sea level and the earth's tectonic deformation field in the region of Crete, Greece.

The FTLRS system is one of the instruments deployed for this project. It was set up on the Chania University site in Crete, in the north of the Gavdos Isle. The FTLRS is a highly mobile Satellite Laser Ranging (SLR) system dedicated to the tracking of geodetic satellites equipped with retroreflectors. This instrument was developed by the Observatoire de la Côte d'Azur (OCA) and the Centre National d'Etudes Spatiales (CNES) in collaboration with the Institut National des Sciences de l'Univers (INSU) and the Institut Géographique National (IGN) (Nicolas et al., 2000). The capabilities of this laser ranging system have been greatly enhanced between 1997 and 2001 to meet the 1 cm accuracy level required by the new altimetry missions, and to track the LAGEOS -1 and –2 satellites. In 2002, the FTLRS system performed a very successful six months campaign in Corsica for the altimeter calibration (CAL/VAL) of the JASON-1 satellite (Bonnefond et al., 2003).

The SLR technique is the major contributor to the altimeter calibration : (i) SLR data of the whole network are used to derive ultra precise orbit of altimeter satellites (in combination with DORIS and GPS data) and (ii) FTLRS conducts comparative laser distance measurements between the facility and satellite radar altimeters. The altimeter calibration could be derived from the FTLRS distance measurements only if the FTLRS position is known with a sub-centimetric accuracy.

The purpose of this paper is to present the observational balance sheet of this FTLRS campaign and to explain the method we used to determine the coordinates of the FTLRS. The positioning results obtained from FTLRS data will be compaired to a positioning realized from GPS data only.

FTLRS technical and operational issues:

Ftlrs specifications:
–Total weight : 350 kg
–Electrical power : 5 KVA
–Laser: Yag frequency doubled 10hz /20 mj
–telescope = 13 cm (emission/reception)
–Time = GPS steered rubidium
–LEO satellites to Lageos
–Time to setup : 48 h

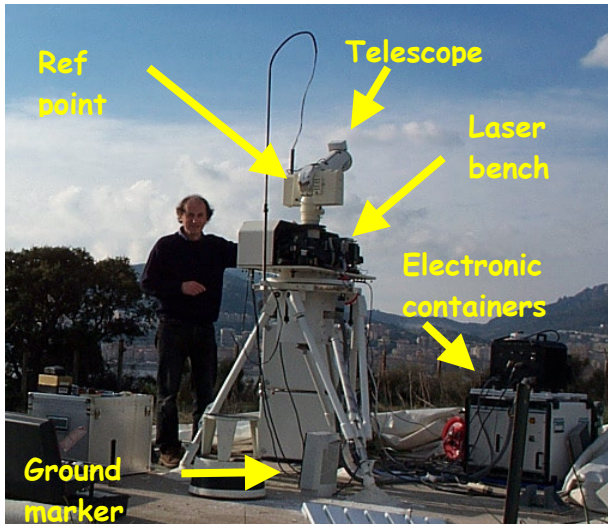

Typical setup of the station (Corsica 2002 for Jason1 calibration)

Previous campaign : Corsica in 2002 for Jason calibration

Ftlrs system, after many technical upgrades became really operational with this campaign in 2002 after a three month collocation phase in Grasse observatory with both the fixed slr system and lunar station.
This 6 months campaign in Ajaccio was devoted to positioning and to calibrate Jason1/Topex altimeter.

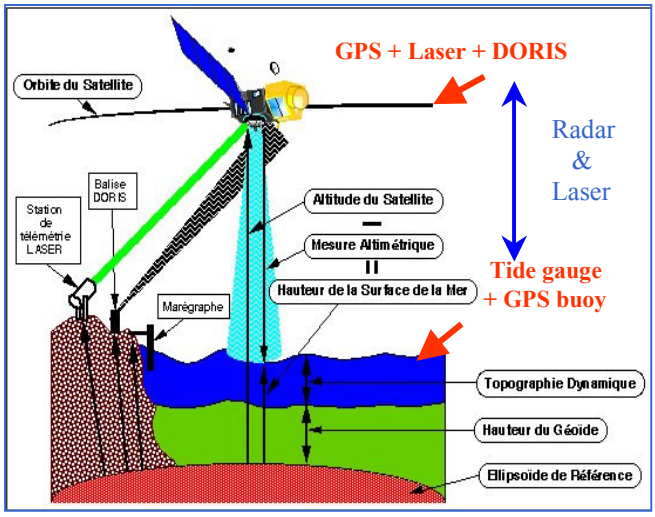

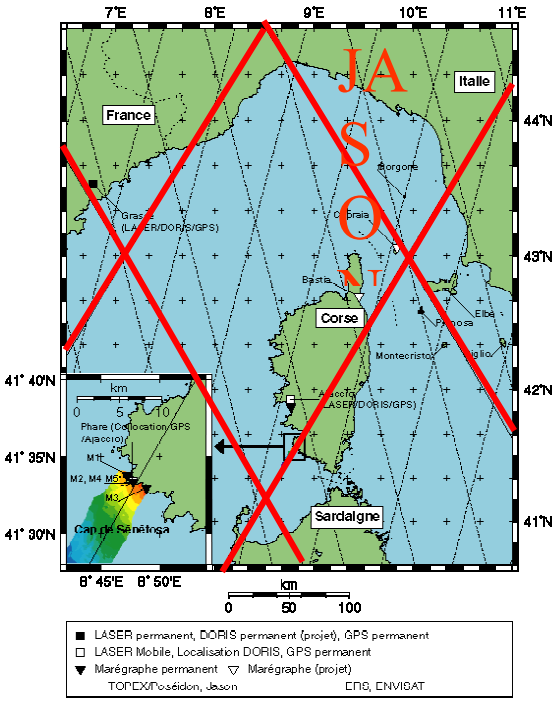

- JASON-1 absolute calibration and orbit validation (CAL/VAL) in tandem mission with TOPEX/Poseidon
- Precise positioning
- Altimeter calibration = precisely compare : altimeter data - satellite altitude above sea level

Gavdos campaign (April to October 2003) :

In the framework of an European and multi-agencies project, we have set up a semi-permanent site in Crete (Technical University of Chania) with the lowest possible installation and monitoring costs. The ultra mobile FTLRS system (French Transportable Laser Ranging Station, weight 300 kg), has been deployed here during the period from March to November 2003.

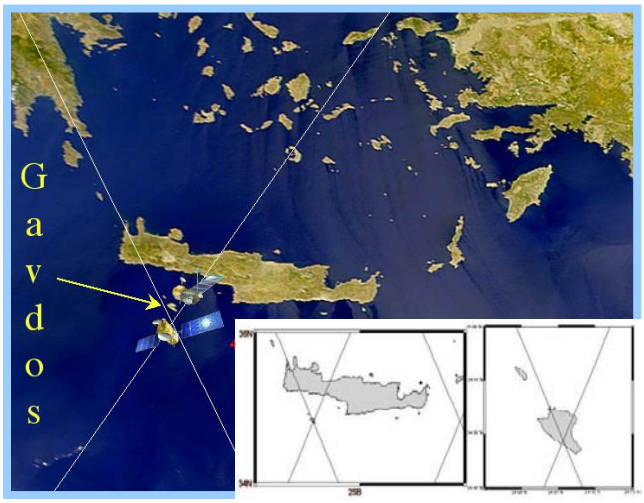

FTLRS system tracked satellite passes during 6 months roughly, in particular both ascending and descending JASON-1 passes which over flight the Gavdos island.

Our team in Chania (2 peoples during 6 months) contributed to observe and to permanently realize adjustments and maintenance of optics, laser, telescope, etc.

The results

This campaigns has been done in very good conditions thanks to the Technical University of Crete staff supplying supports when needed for infrastructure, power and internet lines during theses 6 months.

Observations gathered more than 1400 passes including lageos and with high priorities on Jason1 and Topex.. The accuracy of the positioning finally obtained in solutions were at some millimeter levels.

Data treatment have been achieved at OCA-CERGA and are described in this paper.

- Accurate positioning and short arcs
- Cal/val processing for Jason1/Topex above Gavdos island calibration point.
- GPS treatment and comparison

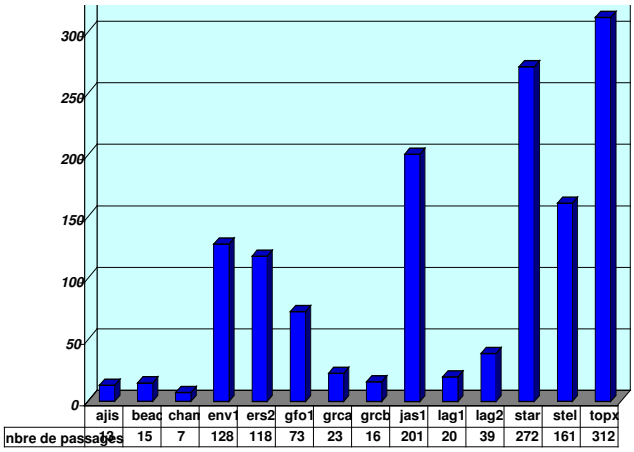

Laser positioning method

The methodology, based on a geometrical approach, first consisted in computing the orbits as accurately as possible (for the lower altitudes especially). Then, we established the normal matrices for estimating the station geocentric coordinate updates and a range bias value through a least-squares fit.

The orbit restitution process has been performed with the GINS software (GRGS, Toulouse) from a selected subset of SLR stations, apart from the FTLRS. Actually, we considered a kind of "core stations" almost well distributed on the Earth and with high criteria concerning the quality and the quantity of their data. We computed 5-day and 9-day arcs, respectively for STARLETTE and STELLA, and for LAGEOS-1 and -2 satellites, over the 6 months of the campaign. We used in each case the same following dynamical models and reference frame: the GRIM5-S2 Earth gravity field model (Biancale et al., 2000}, the FES99 ocean tides model (Lefevre et al., 2002}, the DTM atmospheric density model (Berger et al., 1998) for STARLETTE and STELLA only, and the ITRF2000 solution. Results, in terms of orbit precisions are (mean RMS over the whole campaign) : RMS_{LA1} = 1.05 cm, RMS_{LA2} = 0.82 cm, RMS_{STA} = 1.98 cm, RMS_{STE} = 2.17 cm.

The FTLRS coordinates are estimated by comparing the FTLRS measurements to the computed orbits. The model fitted to the FTLRS range measurements was the following:

$$D = \sqrt{\sum_{i=1}^{3} \left[X_{i,0} + \Delta X_i + X_{i,pt} + X_{i,et} - X_{i,sat} \right]^2} + B \quad (1)$$

where $X_{i,0}$ are the initial mean coordinates, $X_{i,pt}$ and $X_{i,et}$ are the corrections of the polar and Earth tides following the IERS 96 conventions (Mac Carthy, 1996}, $X_{i,sat}$ are the satellite coordinates expressed in the terrestrial reference frame, B is the FTLRS range bias, and ΔX_i are the updates in the terrestrial reference frame. These updates were estimated in a spherical

frame: East, North, and Up (λ, ϕ, and h, respectively). The estimation of ΔX_i and B required to solve the following linear system:

$$\left(A^T \Sigma A\right) X = A^T \Sigma Y \quad (2)$$

where A and Σ are the design and the weight matrices, and X and Y are the parameter and the observation vectors, respectively. We used the JCET solution as initial mean coordinates of the FTLRS (see Table 2).

Range biases were key parameters, when analyzing SLR data. Indeed, the vertical component of station coordinates was strongly correlated to this systematic error present in the SLR measurements (correlation of 0.9 to 1, typically). In addition, it was also strongly correlated to the radial component of the local orbit error. Using a geometrical approach, the difficulty so consisted in separating these different parameters from themselves at the level of 1-2 mm. Naturally, low elevation measurements and simultaneous SLR tracking observations from a regional network (short-arcs) were fundamental to reduce the correlations between range bias, vertical positioning, and radial orbit error. We have also developped specific data processing strategies for reducing the correlation between range bias and vertical component. The first one consisted in estimating one range bias per satellite. This was fully justified since the four geodetic satellites had different signatures. The second one consisted in estimating the range bias per satellite over the whole campaign whereas the coordinates updates are estimated each week. In such a way, the range bias was temporally decorelated from the vertical updates.

Laser positioning results

Table 1showed the FTLRS positioning and range bias values obtained. The multi-satellite solution has been obtained with two different methods. The first one (typed 1) consisted in estimating mean coordinate updates and a range bias value per satellite over the whole campaign. As a consequence of estimating two constant and correlated parameters at the same time, we obtained a too high correlation coefficient C (0.93) between the vertical component and the range bias values. The second method (typed 2) so consisted in estimating weekly solutions for the coordinate updates whereas the range bias values were still estimated over the whole campaign. The weekly solutions are then averaged to obtain the mean FTLRS pcoordinates over the whole campaign. This allowed to decrease C to 0.57, which can be considered as a limit, and also to decrease the standard error of h.

	dϕ (cm)	dλ (cm)	dh (cm)	B_{LA1}	B_{LA2}	B_{STA}	B_{STE}
Method 1	-0.59±0.1	0.25±0.1	0.03±0.3	-1.97±0.4	-2.06±0.3	-2.24±0.2	-2.83±0.2
Method 2	-0.58±0.3	0.16±0.3	1.25±0.3	-0.96±0.2	-0.97±0.2	-1.57±0.1	-2.02±0.1
GPS proc.	-0.58±0.1	0.48±0.1	1.13±0.3				

Table 1 : Results of the FTLRS positionning . The method 1 and 2 correspond to the laser processing.

GPS positioning

The GAMIT software has been used (with IGS precise orbits), as in the JCET solution (E. Pavlis, June, 1, 2004). Observations have been made over two periods :

- March 12th –15th and 20th – 24th 2003 (9 days)

- January 28th – February 9th 2004 (13 days)

We estimated the FTLRS updates with respect to the JCET solution for each day of observations. The results are presented in figure 1. Then, GPS coordinates have been corrected from estimated plates motions and brought back to the laser measurements average date (July 16th 2003). Results are presented in Table 1.

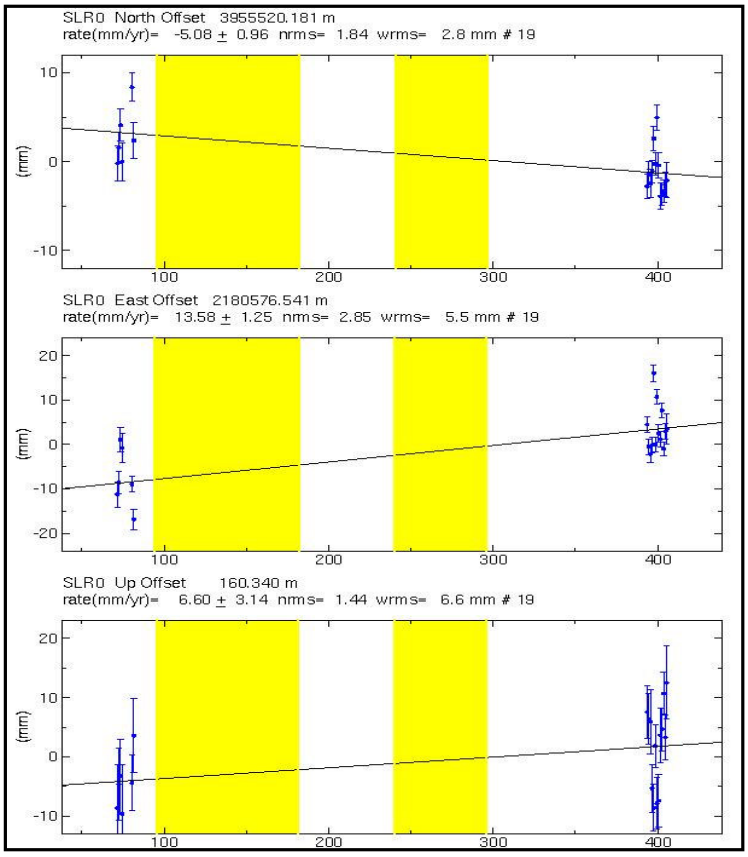

Fig : Results of the GPS processing. Each point represented a daily updates with respect to the JCET solution. The yellow areas represented the observation dates of the FTLRS.

Discussion

Considering the laser processing, our final solution was those obtained by applying method 2. Our choice is motivated by the weak coorelation between range bias and the vertical component. However, two remarks could be done considering the range bias values. The expected bias of the FTLRS was about 5mm. This value has been determined during the Corsica campaign in 2002 (Exertier et al., 2004). The value of 10mm found for this campaign could be explained by the fact that:

- the local tie of the calibration target was determined within 10mm
- the accuracy of chronometer on short time flight was not better than 5mm.

Considering the relative high value estimated for the STELLA bias, several tests have been realized. These tests consisted in a geometrical computing of STELLA's orbits with the short-arc technique from at least 3 European laser tracking station, observing at the same time a satellite pass. With 17 computed short arcs, we showed that permanent and radial orbit error of STELLA orbit existed and was at a level of 10 mm. It certainly explained the greater value obtained for the STELLA bias (of –2.02 cm) relative to LAGEOS ones.

The GPS and Laser results were in very good agreement (see Table 1). The difference between both solutions were lower than 5mm. Finally, The coordinates of the FTLRS in the IRTF2000 reference frame was:

	X (m)	Y(m)	Z(m)
JCET solution	4744552.5533	2119414.5451	3686245.1363
Laser solution	4744552.5636	2119414.5525	3686245.1388
GPS solution	4744552.5614	2119414.5550	3686245.1381

Table 2 : Coordinates of the FTLRS.

Conclusion

After a very succesfull campaign in Corsica for the altimeter calibration of the JASON-1 satellite, the FTLRS confirmed and validated its performances. Moreover, the success of this campaign in Crete has been obtained in the context of a European joined project.

The method of estimating the FTLRS coordinates has been used succesfully. In particular, this method allowed to decorrelate the range bias values and the vertical component of the coordinates. The accuracy of our solution was at the millimeter level and has been validated from a GPS solution.

PRECISION ORBIT DETERMINATION OF LOW ALTITUDE LUNAR SPACECRAFT WITH LASER SYSTEMS

David E. Smith (1), Maria T. Zuber (2,1)
(1) Laboratory for Terrestrial Physics, NASA Goddard Space Flight Center.
(2) Dept of Earth, Atmospheric and Planetary Science, MIT.
dsmith@tharsis.gsfc.nasa.gov Fax: 301-614-6015

Abstract

The need for high accuracy positioning of spacecraft in orbit about the Moon is becoming more important as many nations consider going to the Moon for both exploration and science. Particularly challenging is the control and knowledge of spacecraft position on the farside of the moon where spacecraft are unobservable from the surface of the Earth. Although, spacecraft are routinely out of view of Earth when behind any planet or body it is unique that we are never able to see and study the farside of Earth's moon from the Earth's surface. This is particularly difficult for the positioning of low altitude spacecraft that are very sensitive to even small gravity anomalies of unknown location and magnitude on the lunar farside. Of course, a variety of 2-spacecraft gravity missions could reduce the problem of unknown gravity and if suitably placed could also act as a communications relay. In the long term the establishment of a farside communications spacecraft system will probably be the solution to this problem for most spacecraft. For scientific spacecraft in low altitude orbits requiring very precise spacecraft location this may not be adequate.

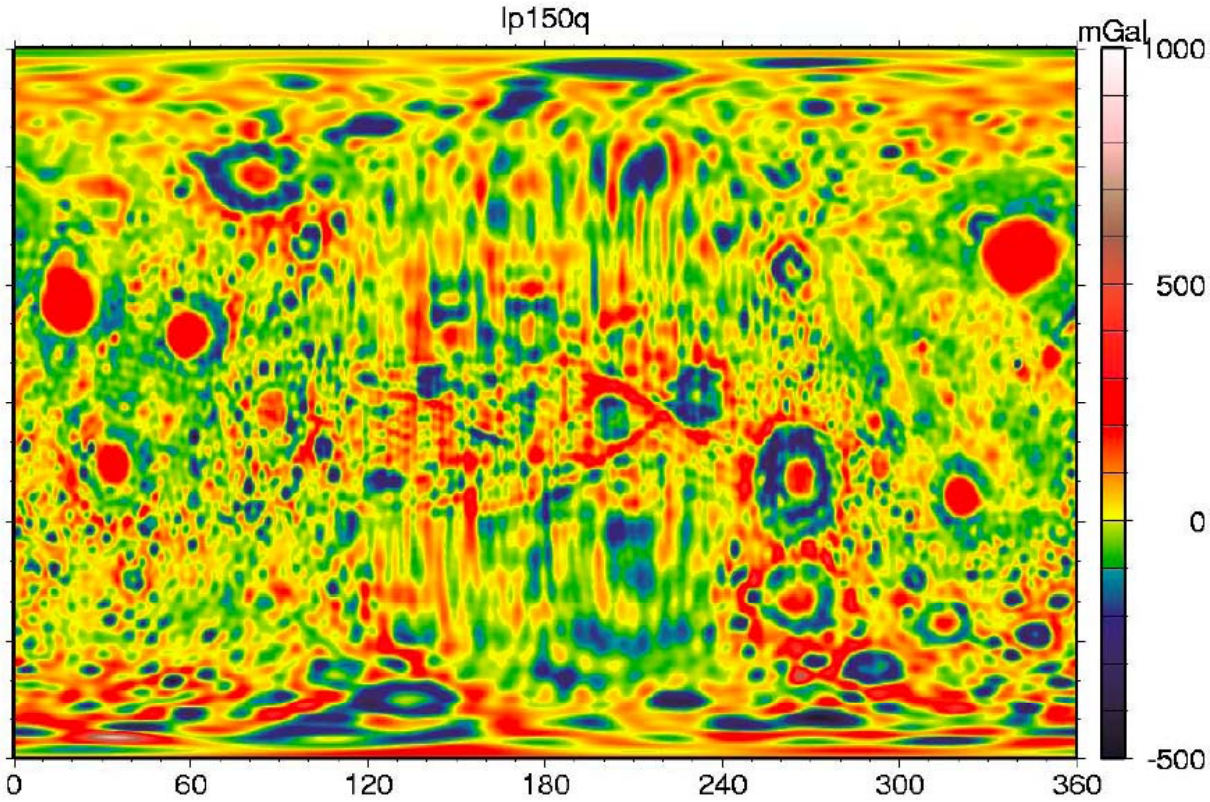

Figure 1. The gravity field of the Moon (Konopliv, 2001)

This issue reveals itself in fig 1, a map of the gravity anomaly field of the Moon derived from Clementine and prospector tracking data. The farside of the Moon is between longitudes 90 through 270 and the figure shows clear linear striping along the ground track of the spacecraft over these longitudes. In comparison the nearside shows no such linear patterns.

One solution to improving the gravity field of the Moon is Earth-based laser tracking of a lunar satellite in conjunction with a high quality laser altimeter. Laser tracking of a lunar satellite via an optical transponder system can provide sub-centimeter level range accuracy at several kilohertz rate, equivalent to a velocity of a few tens of microns/s every 10 seconds. In addition, laser altimetry can be used to assist in the orbit determination by the introduction of altimeter cross-over measurements into the orbit determination process. This technique has been used successfully with Earth altimeter satellites over the ocean areas but has also been used successfully at Mars with the Mars Orbiter Laser Altimeter (MOLA) in the determination of the orbit of Mars Global Surveyor. But the altimeter can also be used to help determine the gravity field. Altimeter data obtained at two distinct altitudes over a region is sensitive to the higher degree and order gravity coefficients that affect the lower spacecraft more than the higher altitude spacecraft. Thus, from the analysis of the altimetry for the surface topography it is possible to extract gravity information for the region; and with global coverage it is possible to obtain global solutions suitable for precision orbit determination. Thus, for the Moon, one method of improving our knowledge of the farside gravity is to analyze a combination of nearside tracking data and nearside and farside altimetry data acquired at different orbital altitudes. With this approach we believe it is possible to obtain 10 cm radial and 5 to 10 meter horizontal accuracy orbits over the entire Moon.

SOLAR-SYSTEM DYNAMICS AND TESTS OF GENERAL RELATIVITY WITH PLANETARY LASER RANGING

J. F. Chandler (1), M. R. Pearlman (1), R. D. Reasenberg (1), J. J. Degnan (2)
(1) SAO, Harvard-Smithsonian Center for Astrophysics.
(2) Sigma Space Corporation
jchandler@cfa.harvard.edu

Abstract

The solar system is the classical laboratory for testing the laws of gravity. Many of the most important tests of general relativity have been made using solar-system bodies. These include tests based on the advance of the perihelion of Mercury, the deflection of starlight passing near the Sun, the Shapiro time delay to the Viking landers, the frequency shift of signals to the Cassini spacecraft, and the (lack of) violation of the equivalence principle manifest by the motion of the Moon (Nordtvedt effect). Planetary Laser Ranging (PLR) promises to open up a new era of tests by yielding a major advance in the measurement of the distance between Earth and a planet. We present the results of a series of covariance studies that include the massive SAO set of solar-system data augmented by PLR pseudo-data under a variety of assumptions. In particular, we consider PLR to Mars and its contribution to a time-delay test, to the measurement of the relativistic advance of planetary perihelia, and to the bound on the time-variation of the strength of the gravitational interaction (G), as measured in a system of units defined by atomic processes (e.g., using atomic time). We find a time-delay test approaching a part in 10^7 in a multi-year experiment.

I. Introduction

Planetary laser ranging (PLR) offers three types of scientific output: solar-system dynamics, tests of general relativity, and studies of the target planet. Any solar-system object with a solid surface and a transparent atmosphere would be a suitable platform for a PLR system, but some objects are more accessible than others. There would of course be considerable interest in improved ranging to Mercury for all three categories of science, but we recognize that an easier target might be a better place to start. In this paper, we consider the case of a single PLR system on Mars although we note advantages in placing two or more systems to help in separating individual effects that would fall within reach of the dramatically improved sensitivity of PLR.

In this section, we describe some of the scientific uses of PLR to set the stage for a more detailed discussion of some of them. Since this is a preliminary survey, we allow for different levels of accuracy for the ranging normal points: we assume the single-day measurement uncertainties would be between 1 mm and 100 mm.

Solar System Dynamics. A precise measure of the Earth-Mars distance, measured between their centers of mass and taken over an extended period, would support the better determination of numerous parameters of the solar-system model. Among these would be the orbital elements of both Earth and Mars, several planetary masses, the masses of many asteroids, and, indirectly, the orbital elements of some of the outer planets (Jupiter, Saturn, and possibly Uranus). These model improvements would be of interest, not only for their own sakes, but also as a necessary step toward testing general relativity.

Relativity Tests. The Shapiro time delay has been measured by the Viking Mission to 1 part in 10^3 (Reasenberg et al. 1979) based on ranging to the landers with a few meters of uncertainty. The solar corona corrupted the most valuable data, forcing the experiment to rely

on data less sensitive to the effect. Note that the same relativistic space-time curvature which gives rise to the Shapiro delay also produces related effects for electromagnetic signals passing near a massive body, such as the frequency shift related to a changing impact parameter and the deflection. For example, the deflection of radio waves has been measured to 2 parts in 10^4 (Shapiro et al. 2004) using very-long-baseline interferometry. Also, the delay rate or frequency shift has been measured by the Cassini Mission to 1 part in 10^5 (Bertotti et al. 2003).

With PLR, there could be an improvement of at least two orders of magnitude beyond the Cassini result. This is sufficient to see the term proportional to the square of the solar mass, a spectacular qualitative improvement, with possible implications for discriminating among theories. To achieve such accuracy in the delay test, data would be needed over an extended period, not just during a short span around superior conjunction (when the effect is at a maximum). As noted above, the solar-system model as a whole needs to be improved concurrently with the relativity test. We present the results of sensitivity studies of the delay test in section II.

One hears about the relativistic advance of the perihelion of Mercury (nominally 43 seconds of arc per century) because it is large and historically important in the confirmation of general relativity. The effect for Mars is smaller by a factor of about 14 (measured in distance per unit time), and the lower eccentricity of the orbit (9.3% vs. 20.5%) makes the effect correspondingly more difficult to observe. However, the measurements of Mercury have been limited to planetary radar with an uncertainty typically around 100 m, and corrupted by still larger topography. The range of topographic relief on a terrestrial planet is on the order of 10 km, and, although the large-scale variations can be modeled and removed after observing the planet through many apparitions, there are local features of up to about 1 km that can be removed only by the use of the rare "closure points" where the same spot on the surface is observed at widely separated times. Even the closure points provide only partial cancellation of topographic noise because of the imperfect overlap and evolving radar technology that yields different footprints at different epochs.

In contrast, repeated ranging measurements to a fixed point on the surface require only the planetocentric position of the point in question and a model of planet rotation for reducing the measured distances to center-of-mass distances. For sufficiently precise data, the former might need to be time-dependent and the latter, very detailed. For Mars, the Viking and Pathfinder landers provided ranging uncertainties of 5-10 m, about two orders of magnitude better than Mercury radar, but mm-level PLR measurements of Mars would be over five orders of magnitude better than Mercury radar, and the perihelion advance would, in principle, be measured better by more than three orders of magnitude. Nonetheless, the time span of Mercury radar data is measured in decades, encompassing many perihelia. Obtaining a comparable time span for PLR may be difficult. Our sensitivity studies have shown that even five years of PLR measurements for Mars would just barely begin to separate out the perihelion advance from the other observable effects that can mask it. Note that a secular effect, like the perihelion advance, bestows a particular advantage upon long-term observations because the expected signature grows with time.

There has long been a question of the possibility that the strength of the gravitational interaction (G), as measured in a system of units defined by atomic processes (e.g., using atomic time), may be varying. It was discussed by Dirac (1937) in connection with the Large Numbers Hypothesis, but it has many modern incarnations, including those in string theory. The effect of $\dot{G}$, as it is known, is to advance a planet along its orbit by an extra distance that grows quadratically with time. For the Earth-Mars distance, the observations go back decades, but the extreme accuracy of PLR data could allow a significant improvement in the

uncertainty of the $\dot{G}$ estimate based on a few years of data taking. We examine this effect in more detail in section II.

If, as expected, Mars is a "proper rotator," then its rotation period (after accounting for geophysical effects) is constant in proper time. Because the Mars orbit is eccentric (9.3%), the rotation period (as measured in the barycentric frame) will change by about 1 part in 10^9 over a Martian year. This was nearly detectable with Viking data. It would be well observed with PLR data and would be the first observation of the proper rotation of a planet. The principal challenge would be to separate the relativistic effect from the seasonal effects due to mass and angular-momentum transfers between planet and atmosphere. Fortunately, proper rotation has already been observed in binary pulsars (Smarr and Blandford 1976). Thus, we are free to assume proper rotation in the case of Mars and to use the observations to study the Mars geophysical effects.

Studies of Mars. At the mm level, a wide array of Mars-specific physical effects will be manifest in the data. A detailed analysis of such effects is beyond the scope of this paper, but we mention some of them here for background. Variations in rotation rate (UT) will be due to the deposit and release of atmospheric material at the poles as well as global wind patterns. Similarly, there will be wobble terms due to related processes. These atmospheric effects fall under the heading of *weather* and thus will vary at all time scales. Solid body tides should be visible, and it may be possible to model the elastic properties of the body. By looking at the precession and nutation of Mars, it should be possible to bound or measure the non-elastic (i.e., liquid) behavior of the core. Through the reflex motion of Mars around the Mars-satellite center of mass, we might obtain a measure of the masses of Phobos and Deimos, the two satellites of Mars. These masses might also be determined through the Mars nutation they induce. Finally, we note that separating the numerous effects would require the use of more than one PLR system on the surface of Mars. Further, the separation of the myriad effects, many of which have well defined temporal signatures, would require an extended observing period. In return for this effort, we would learn about many aspects of the planet.

II. Design of Sensitivity Studies

In this section, we discuss a series of studies designed to illustrate the results that might be obtained with a PLR transponder on Mars. In order to provide some realism, these studies combined our current solar-system data set with the hypothetical PLR data in a simultaneous covariance analysis. Table 1 shows a summary of the parameters in our model of the solar system. Since the 1548-parameter model already includes the orientation of Mars (necessary for the Viking and Pathfinder lander range data), we need only three additional parameters (coordinates of the PLR transponder) to handle the hypothetical PLR data. The parameters shown in the table relate to dynamical and physical properties of the observed bodies, and are thus of some intrinsic interest, but the present analysis focuses on others (shown in Table 3) that characterize possible violations of general relativity.

Although one can infer the existence, and even the dynamical properties, of other planets through their perturbations of the orbits of Mars and the Earth as seen via precise Earth-Mars ranging, the real task at hand is to characterize the scientific gains due to PLR in the context of knowledge already available. Thus, our current data set provides the backdrop for studying the uses of PLR. Table 2 shows the types and numbers of the solar-system data used in our studies. For the purposes of this study, we are not assuming any additional data of these types will be acquired. We believe this assumption does not significantly affect our conclusions.

Table 1. Solar-System Analysis Model

Parameter Type	Number
Masses	19
Asteroid class densities	5
Moon mass distribution	9
Sun mass distribution	1
Orbital elements	43
Earth-Moon tides	3
Earth orientation	364
Moon orientation	6
Mars orientation	9
Interplanetary plasma density	1
Station coordinates	33
Target coordinates (Moon)	12
Target coordinates (Mars)	9
Mercury topography	566
Venus topography	444
Measurement biases	24

Table 2. Supporting Data Sets

Type	Number	Range Uncertainty	Time Span
Mariner 9 normal points	185	30 m - 300 m	1971-1972
Viking lander delays	1280	2 m - 20 m	1976-1982
Pathfinder delays	90	10 m - 20 m	1997-1997
Outer planet normal points	6	3 km - 50 km	1973-1979
Mercury radar delays	8054	30 m - 150 m	1969-1997
Venus radar delays	5674	20 m - 750 m	1969-1982
LLR normal points	13538	3 cm - 30 cm	1969-2001

The goals of these studies include an exploration of the dependence of scientific output on three factors: the accuracy of the ranging data (assumed to be from 1 to 100 mm), the longevity of the transponder, and the Sun avoidance angle. The first of these would give a simple scale factor were we not using a fixed set of other data (Table 2) to condition the analysis. The second factor, experiment duration, is likewise complicated by the other data; in their absence, the results would show a power-law dependence on duration. The third factor, Sun avoidance, is crucial to the time delay experiment, since the effect is sharply peaked at superior conjunction, when both the ground-based telescope and the PLR transponder must point nearly at the Sun. Figure 1 shows the time dependence of the Shapiro delay through two superior conjunctions of Mars. In Section IV, we discuss some of the issues in setting the Sun avoidance angle. In this context, we note that duration is not the only

important timing consideration, since a one-year mission in 2004 or 2006 would cover a superior conjunction, while a one-year mission in 2005 or 2007 would not. In nearly all of the studies, we began the observations on 2004 Mar 18, six months before the imminent superior conjunction.

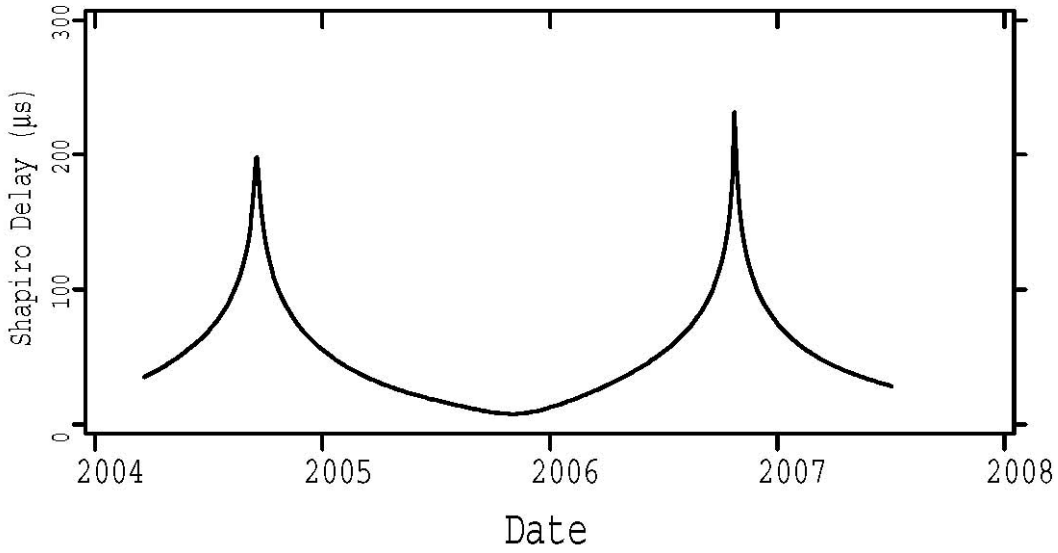

Figure 1: Contribution of the Shapiro effect to the Earth-Mars-Earth delay

Each covariance study was done in the same manner. We assumed a PLR transponder near, but not on, the Mars equator (specifically, at 11° N and 99° W). The longitude does not matter, and the latitude scarcely matters because we took dummy data as if both Mars and the Earth were transparent. Also, we assumed only one observatory taking data (the McDonald Laser Ranging Station). The normal observing schedule was one observation every four days, but we assumed a special effort would be made near superior conjunction, with daily observations during the month centered on each superior conjunction (the first being 2004 Sep 15). This schedule was subject to the Sun avoidance criterion, but all allowed observations on the schedule were assumed to be made successfully and with the same measurement uncertainty between the designated start and stop dates. Each study was performed three times, once with each of the three chosen round-trip range uncertainties: 1 mm, 10 mm, and 100 mm. We also covered a broad range of duration (up to 5 years) and Sun avoidance angle (0.5 to 15°). In this study, we defined the avoidance angle as the minimum angle between the limb of the Sun and the target, as seen from one of the observing stations. For simplicity, we applied the Sun avoidance criterion only to the Earth observatory. (At superior conjunction, the relative Mars-Sun-Earth distances are always about the same, and the Earth-based criterion therefore maps into a consistent, though different, Mars-based criterion.) It is important to note that the Sun-Earth angle as seen on Mars near conjunction is about 2/3 of the Sun-Mars angle as seen on Earth, and therefore the Sun avoidance is inherently a more difficult problem for the PLR transponder than for the Earth observatory.

III. Results of Sensitivity Studies

Figures 2-4 display the results of our studies. They show the dependence of scientific output on the three design variables: measurement uncertainty, experiment duration, and Sun avoidance criterion. In broad outline, the first two variables behave in much the same way for all of the tests. At short duration, the predictions of our existing solar-system model are

extrapolations because we are not assuming any extension of our existing data set. Thus, the PLR data cannot contribute at full strength to the relativity tests at first. However, when the geometry becomes favorable, the parameter uncertainties associated with the three levels of measurement uncertainty separate and gradually approach saturation, where the PLR contribution dominates the test, and the sensitivity simply scales with measurement uncertainty.

As can be seen in Figure 2, the time delay test rapidly approaches saturation after the first superior conjunction (six months into the experiment). In contrast, the $\dot{G}$ test shown in Figure 3 is nowhere near saturation even after five years. The perihelion test (not shown) is comparable to the $\dot{G}$ test, in terms of both the maximum improvement (about a factor of ten) over the five-year duration and the spread (about a factor of three) between 1 mm and 100 mm results. It is clear that the payoff for the time-delay test is optimum as long as the experiment covers at least one conjunction and a sufficient time before or after to refine the solar-system model. On the other hand, the $\dot{G}$ and perihelion tests benefit from a PLR experiment that lasts as long as possible. This contrasting behavior stems from the difference between stationary and secular effects. Despite this contrast, we compare the payoffs for all three tests after a uniform two years in Table 3.

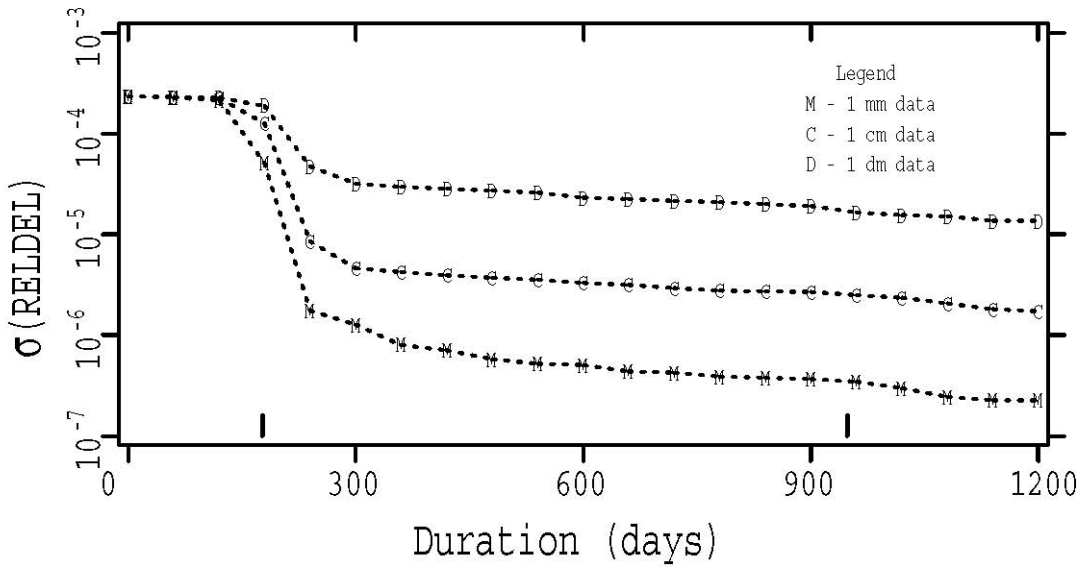

Figure 2: Dependence on duration of the time-delay test, using 5° Sun avoidance. The dramatic reduction in σ(RELDEL) about six months corresponds to the first superior conjunction (marked). The reduction at the similarly marked second superior conjunction is the expected √2 change.

Table 3. Scientific payoffs after two years with 15° Sun avoidance. Payoff is here defined as the ratio of starting standard error to final standard error of the stated parameter. RELDEL and RELFCT are model coefficients for the time delay and the relativistic motion (including perihelion advance), respectively.

	Measurement Uncertainty		
Test	**100 mm**	**10 mm**	**1 mm**
$\dot{G}$	**1.6**	**2.4**	**3.0**
RELDEL	**2.4**	**10.2**	**48.6**
RELFCT	**2.7**	**6.5**	**8.7**

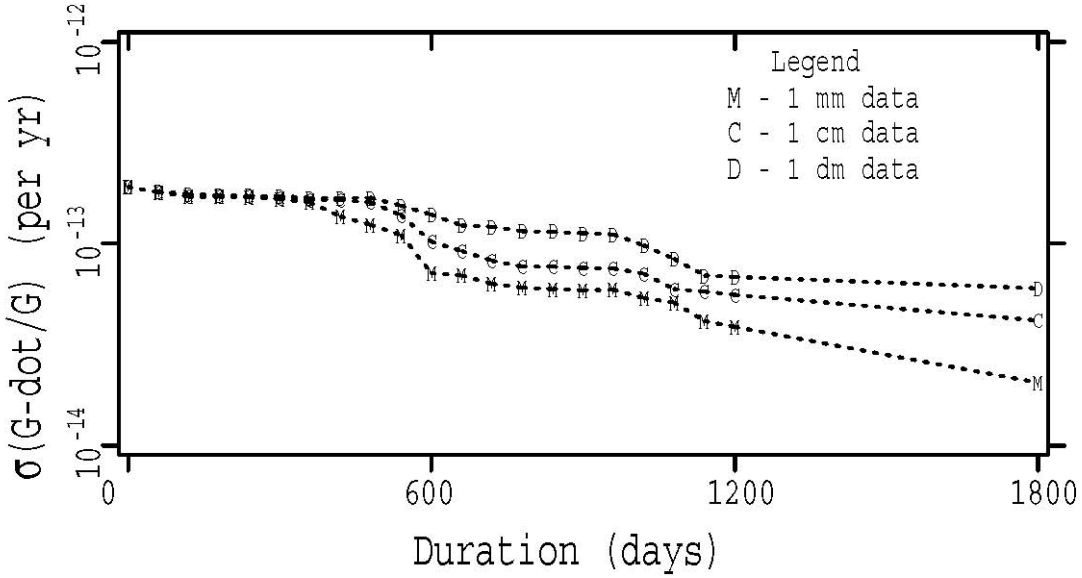

Figure 3: Dependence on duration of the Ġ test, using 5° Sun avoidance.

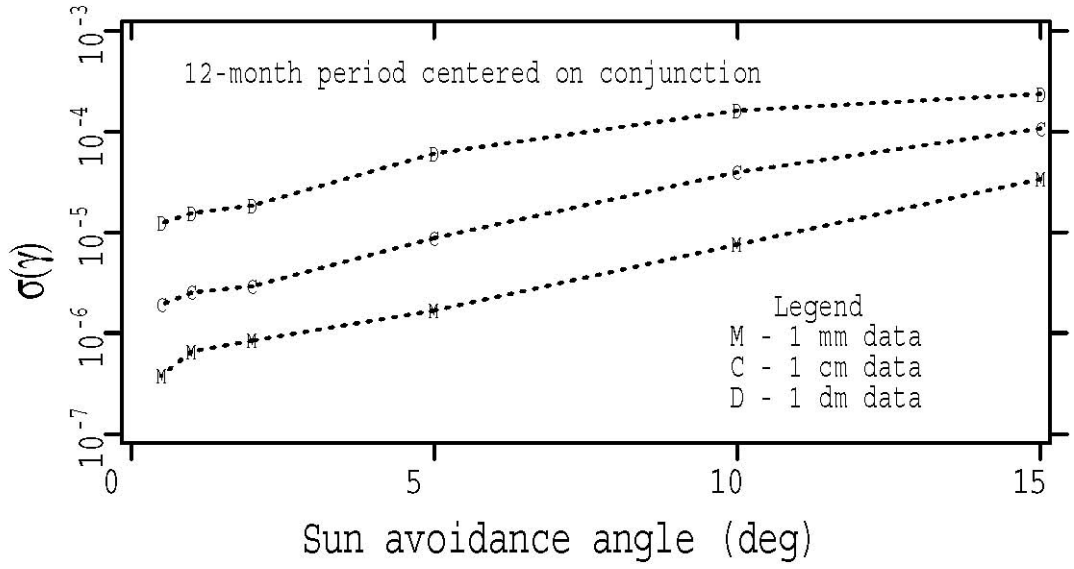

Figure 4: Dependence of the time-delay test on Sun avoidance, using 12 months of data. The closest approach in this apparition (2004) is 0.75°. For avoidance angles of 5° or more, the entire month around conjunction is blocked.

Figure 4 shows the dependence on Sun avoidance angle of the sensitivity of the time-delay test in a one-year experiment. For angles of 5° or more, the entire one-month period of daily observations is disallowed. Other factors, such as the orbital eccentricity, contribute to the complexity of detail in the figure. The striking result is that the test can be strengthened by as much as two orders of magnitude for 1 mm data by narrowing the Sun avoidance angle from 15° to 0.75°. This contrast provides the motivation for observing as close to the Sun as possible. As expected, there is little dependence on avoidance angle in the other tests.

IV. Working Close to the Sun

Measurement of the Shapiro delay requires operation of the transponder over propagation paths which pass very close to the solar disk. For such observations, one must be concerned about possible optical damage to the detector, excessive solar heating of the instrument, and excessive background noise due to solar scattering within the instrument that might obscure the transponder signal. Accurate navigation and attitude information plus Sun avoidance hardware/software are clearly baseline requirements for such a mission.

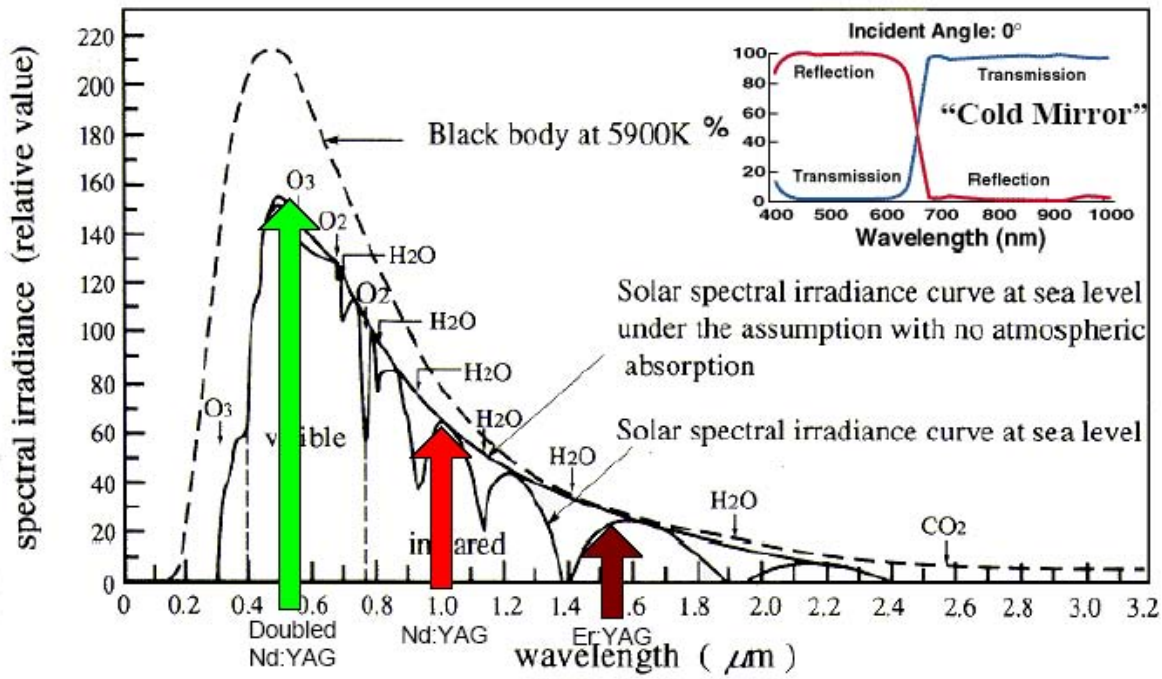

Figure 5: Exo-Atmospheric solar spectral irradiance (dashed curve) and at sea level with and without atmospheric absorbers. Also shown are three popular visible and near-IR laser wavelengths for which short pulse microchip lasers exist – Doubled Nd:YAG (532 nm), Nd:YAG (1064 nm), and Er:YAG (1550 nm). The inset shows the typical transmission and reflection properties of a "cold mirror" suitable for a laser with $\lambda > 700$ nm.

One approach to minimize the solar problem is to operate at a laser wavelength with good atmospheric transmission and well off the peak of the solar spectrum. Figure 5 displays several items pertinent to this issue:

- The exo-atmospheric solar spectral irradiance approximates that of a black body at 5900 K and has significant output in the UV, visible, and near infrared
- The solar irradiance at sea level due to atmospheric scattering alone
- The solar irradiance at sea level including atmospheric absorbers
- Colored arrows indicating three popular laser wavelengths in the visible and near IR for which short pulse (< 1 ns) microchip lasers and/or high speed detectors exist – Doubled Nd:YAG (532 nm), Nd:YAG (1064 nm), and Er:YAG (1550 nm).

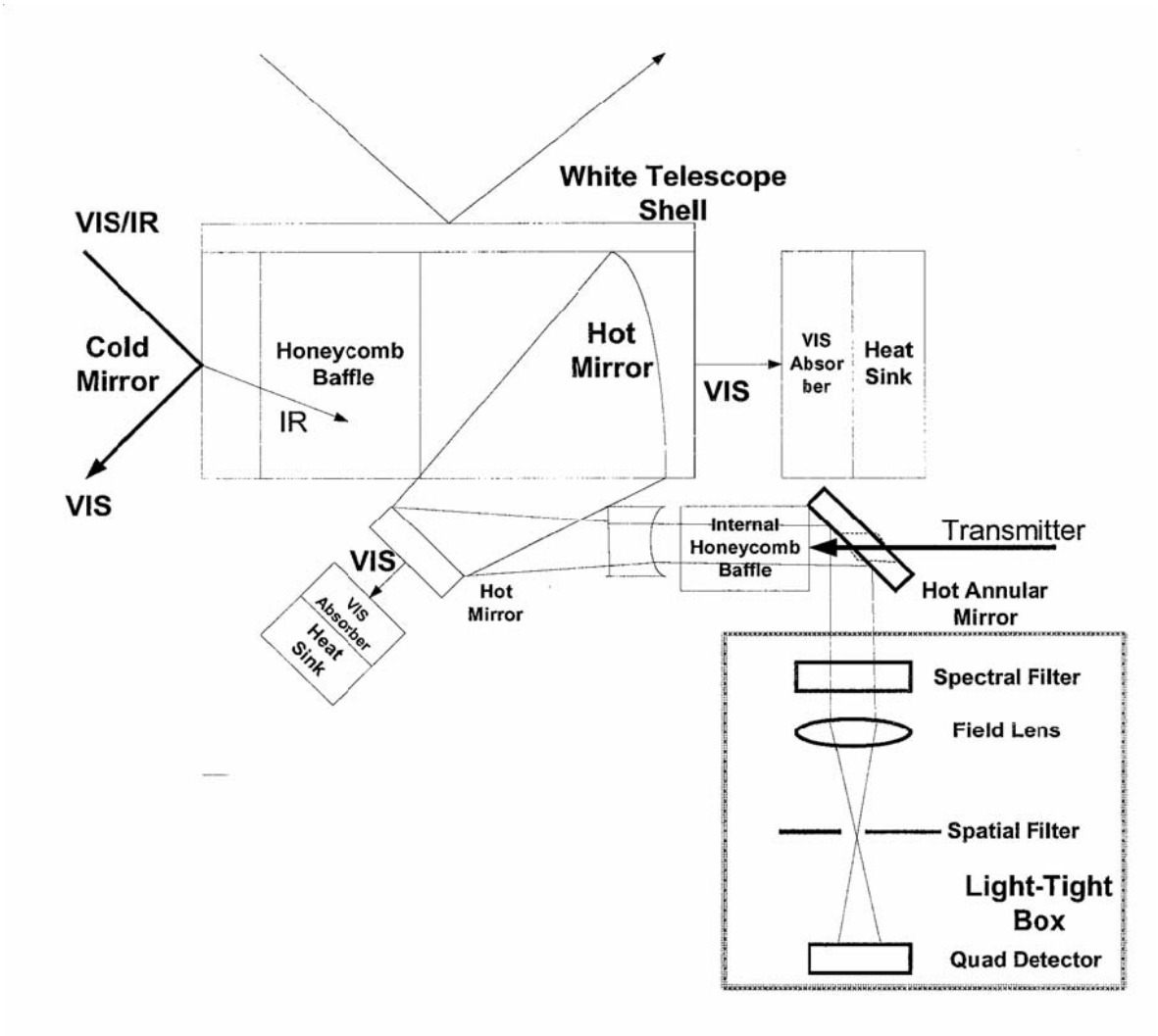

Figure 6: Conceptual design of a transponder for operating along sight lines close to the Sun. In the light-tight box (camera), the detector is placed beyond the focus at the spatial filter to allow the pointing error to be measured (and corrected) over an extended range.

Ideally, one would like to operate the near-Sun transponder well into the infrared where the solar spectral irradiance is greatly diminished and intermittent regions of high atmospheric transmission exist. Unfortunately, the availability of compact, moderate energy, short pulse lasers and/or fast, low noise, high quantum efficiency detectors is problematic beyond 1550 nm. Failing this "ideal" situation, one would at least like to be able to reflect most or all solar irradiance from telescope surfaces and entrance window as in Figure 6. The majority of the solar radiation entering from the upper left-hand corner of the figure is reflected from the outer white shell of the instrument and from the cold mirror entrance window to the telescope. Cold mirrors reflect the shorter, visible wavelengths while transmitting the longer, infrared wavelengths. Their analog, "hot mirrors", do the opposite. In both cases, the center wavelength separating the regions of reflection and transmission can be tailored to the application by modifying the optical coatings. The inset to Figure 5 also shows the transmission and reflection properties of a typical "cold mirror".

The near infrared solar radiation transmitted by the "cold mirror" entrance window encounters a blackened honeycomb baffle. This second optical barrier defines how closely in angle the transponder can operate to the Sun. In Figure 7, δ_{max} is the acceptance half angle, D is the nominal diameter of the circle which circumscribes the hexagon, and L is the length of the honeycomb tube. To operate within 2º of the Sun, we require that $D/L \leq 0.04$. For near-Sun operation, the interior surface of the honeycomb must be specially treated so that it does not show strong specular reflection at incidence angles approaching 90°.

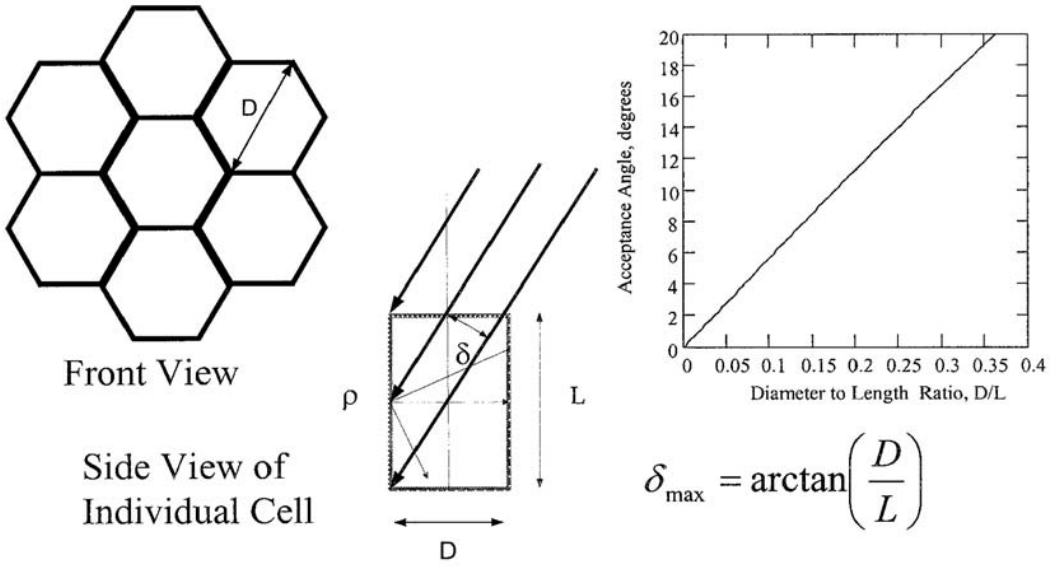

Figure 7: Effect of honeycomb baffle on acceptance half angle for solar radiation.

After being transmitted through the honeycomb baffle, the residual near-IR solar radiation encounters a "hot mirror" primary and a hot mirror fold flat, each of which further filters out the residual short wavelength radiation and transmits it to an absorber, which is thermally coupled to a radiative panel viewing deep space or some other heat dissipation device. After being recollimated by a negative lens and passed through a second (optional) internal honeycomb grid, the transponder signal from the opposite terminal (and any background noise) is reflected by an annular mirror into a light tight receiver box which contains a narrow band spectral filter, a field lens and spatial pinhole, and a quadrant photon-counting detector. The latter outputs an "incoming photon event" to be time-tagged and recorded by the onboard event timer. The photon times of arrival are transmitted back to Earth and combined with similar data at the Earth station to compute a precise time series of Earth-to-spacecraft range and clock offset (Degnan 2002). The timer also records the quadrant that detected the incoming photon, and any imbalance in the quadrant count after many events is used to provide an error signal to the onboard pointing system (Degnan and McGarry 1997).

An interplanetary laser communication system is already being developed for missions to Mars and other targets. The present design includes a Nd:YAG laser at 1064 nm and a requirement of operation at Sun-Earth-target angles as small as 3° (Boroson et al 2004).

V. Conclusions

PLR to Mars offers significant potential for improving tests of gravity. These improvements can be realized incrementally, provided that the transponder functions for at least six months, but lifetimes of five years or more would be useful, especially for the tests of secular effects.

For measuring the Shapiro delay, it is important for the instruments (both transponder and ground-based telescope) to work as near as possible to the solar limb, but other tests can be performed at much larger Sun avoidance angles. It would be very useful to conduct similar studies with Mercury and with multiple transponders.

References

Bertotti, B., Iess, L., and Tortora, P., "A test of general relativity using radio links with the Cassini spacecraft," Nature, 425, pp. 374-376, 2003.

Boroson, D. M., Biswas, A., and Edwards, B. L., "MLCD: Overview of NASA's Mars Laser Communications Demonstration System," SPIE Vol 5338, Free-Space Laser Communications Technologies XVI, pp. 16-49, Bellingham, WA, 2004.

Degnan, J. J., "Asynchronous Laser Transponders for Precise Interplanetary Ranging and Time Transfer", Journal of Geodynamics (Special Issue on Laser Altimetry), pp. 551-594, November, 2002.

Degnan, John J. and Jan McGarry, "SLR2000: Eyesafe and autonomous satellite laser ranging at kilohertz rates", SPIE Vol 3218, Laser Radar Ranging and Atmospheric Lidar Techniques, pp. 63-77, London, UK, Sept. 24-26, 1997.

Dirac, P. A. M., Nature, 139, p. 323, 1937.

Reasenberg, R. D., Shapiro, I. I., MacNeil, P. E., Goldstein, R. B., Breidenthal, J. C., Brenkle, J. P., Cain, D. L., Kaufman, T. M., Komarek, T. A., and Zygielbaum, A. I., "Viking relativity experiment - Verification of signal retardation by solar gravity," Astrophys J (Lett), 234, pp. L219-L221, 1979.

Shapiro, S. S., Davis, J. L., Lebach, D. E., and Gregory, J. S., "Measurement of the solar gravitational deflection of radio waves using geodetic Very-Long-Baseline Interferometry data, 1979-1999," Phys Rev Lett, 92, p. 121101, 2004.

Smarr, L. L., and Blandford, R., "The binary pulsar: Physical processes, possible companions, and evolutionary histories," Astrophys J, 207, pp. 574-588, 1976.

SAN FERNANDO NAVAL OBSERVATORY: 250 YEARS WORKING IN ASTROMETRY AND GEOPHYSICS (1753-2003)

F. J. González, A. Pazos, J. Gárate
Real Instituto y Observatorio de la Armada, 11110 San Fernando. Cadiz SPAIN
biblio@roa.es

Abstract

San Fernando Naval Observatory is an ancient institution, founded in 1753 in Cádiz. It was the first Observatory deployed in Spain. The beginnings were devoted to research on positional astronomy and related fields, as Celestial Mechanics, in order to issue Nautical Almanac, and Astronomical Ephemeris. But soon the researching interest was extended in different ways, as Geophysics, Geodesy or Time Keeping and Dissemination. The researching in Spain on several Geophysical branches (Seismology, Geomagnetism, Meteorology) started here. The Observatory was also the first Spanish Institution hosting a satellite tracking device: The Baker-Nun Camera delivered by the Smithsonian Institution. It is also remarkable that the observatory has got the responsibility for Time Keeping in Spain. In this paper, we point out the main features, in order to show a general view of the history of this ancient but living Observatory

Introduction

We would like to show the historical evolution of the main duties developed at the San Fernando Naval Observatory since 1753, when it was founded, until now. It is the oldest astronomical observatory in Spain. Its origin is directly related to the Navy and the Science reactivation enforcement made bye the illustrated governments during the 18th century. Jorge Juan was a naval officer and scientist who developed the idea of the installation of an astronomical observatory in a tower at the *Castillo de la Villa* in Cadiz, where the Naval Academy was placed. He was the director of the Naval Academy, and he tried to promote learning and practice Astronomy among the future naval officers.

A brief historical summary

In 1753 first instrumentation was mounted at Real Observatorio de Cdiz (Royal Cadiz Observatory), how it was called in the beginning. However, there were needed some years before the Observatory astronomical works gained some scientific notoriety. Vicente Tofio was the Naval Academy Director who organized the first systematic astronomic observation plan (1773-1776). After that, and with the aid of the King Carlos III government impelling scientific activities, Cadiz Observatory became a truth astronomical academy for the new generation of sailor scientists. They got scientific education needed to organize and participate in the expeditions developed at the end of the 18th century.

In 1798 the Observatory was moved from its original place at the *Castillo de la Villa* in Cadiz to a new building made at Torre Alta Hill in Isla de León, which was the name for San Fernando until 1814. In such a way the former *Real Observatorio de Cádiz*, changed its name for *Real Observatorio de la Isla de León*. So, the observatory came to

the 19th century with new installations and also with the first director who had no relationship with the Naval Academy. The observatory was becoming to reborn as an independent institution.

Along the 19th century, and once the crisis of the beginning of the century was overcome, the observatory was adding new missions to its astronomical duties, besides the yearly issue of the Nautical Almanac. First of all some scientific works were undertaken, as organizing, realizing and publishing meteo, magnetics and seismic observations, as well as the Observatory participation in the international project known as Photographic Sky Map. Moreover new duties were assumed, because the Naval Nature of the Observatory: Instrumentation and Timing Devices Store, Mathematics and Physics Naval High School, Magnetic Needles Center, and Coastal Meteo Service.

San Fernando Naval Observatory today

At present, two hundred and fifty years after its foundation in Cadiz, San Fernando Naval Observatory organizes its duties in four scientific departments. Astronomy Department main mission is due to astrometry, i.e. to determine positions of celestial bodies. The observatory has got its own astrometric instrument, a Grubb-Parsons Meridian Circle. In 1996 it was moved to the University of San Juan (Argentina) facilities at *Estación de Altura Carlos Ulrrico Cesco*. Furthermore, the observatory participates in the observation works made at La Palma Island by using the University of Copenhaguen Carlsberg Meridian Circle.

The Ephemeris Department is also directly related to the Astronomy. Its main duty is to determine astronomical ephemeris, since 1791, at Cadiz, besides to disseminate this information among sailors, astronomers and geodesists. Other missions of this department are to perform theoretical studies related to Celestial Mechanics, and to report on astronomic phenomena, such as sunrise and sunset time, moonrise and moonset time, lunar phases or eclipses.

Geodesy and Geophysics are the duties of the Geophysical Department. It was born in mid nineteenth century. This department counts on the Naval Geophysical Observatory. It is the responsible unit for performing and yearly publishing meteo, geomagnetic and seismic observations. There is also a third generation satellite laser tracking station, and a set of GPS permanent receivers at the Alboran Sea Region.

Time Department was created in 1971, from the Time Service which belonged to the Astronomy Department until then. The task of this department is to keep time scales in use with the maximum precision and accuracy, and to disseminate this information in the most efficient way not only to the sailors necessities, but also to the scientific community and the national industry as well. It counts on a set of Cesium Atomic Clocks to keep the Universal Time Coordinate (UTC) scale at ROA, and to determine the Official Time in Spain.

On the other hand, San Fernando Naval Observatory develops a teaching activity which started with the so called Greatest Studies Courses given during the 18th century, in

order to improve the illustrated naval officers scientific knowledge. At present teaching duties are still given at the Physics and Mathematics Naval High School, to prepare naval officers to teach those subjects at the different Naval Schools.

Historical and cultural heritage accumulated at the institution is composed of the Ancient Instrument Collection, the Historical Archive and the Library. San Fernando Observatory has needed a lot of instrumentation to develop its activities along two hundred and fifty years working. The Historical Archive watches over administrative and scientific documentation generated at the departments since their very beginnings. At last, but not least, bibliographic funds kept at the Library are composed of a very interesting collection of books and scientific periodic publications.

References:

(1) Lafuente, A.; Sellés, M. *El Observatorio de Cádiz (1753-1831)* (Madrid, 1988).
(2) González; F.J.: *El Observatorio de San Fernando (1831-1924)* (Madrid, 1992).
(3) González; F.J.:*El Observatorio de San Fernando en el siglo XX* (Madrid, 2004).

THE PASAGE PROJECT:
ASTROMETRIC POSITIONING OF GEOESTATIONARY SATELLITES

T. López Moratalla (1), C. Abad (2), F. Belizón (1), J.C. Coma (1), F.J. Montojo (1), J.L. Muiños (1), J. Palacio (1) and M. Vallejo (1)
(1) Real Instituto y Observatorio de la Armada, San Fernando (Spain) teodoro@roa.es
(2) Centro de Investigaciones de Astronomía (CIDA), Mérida (Venezuela)

Abstract

To have precise ephemerides of geosynchronous satellites available at any time is of great importance for satellite's station keeping routines, both for planning maneuvers and for checking the results of these maneuvers.
The major goal of this project is to use earth-based astrometric observations both for obtaining precise ephemeris of geosynchronous satellites, and for orbit determination of these satellites. This use will be a new and important application of earth-based astrometry, and will require the development of the necessary techniques and algorithms for processing the observations.
Topocentric equatorial coordinates of the satellite can be obtained with one single telescope, and a sufficient number of observations can be used for orbit determination purposes. The Gautier astrographic telescope of the Real Instituto y Observatorio de la Armada (ROA), if provided with an appropriate CCD camera, will be an adequate device for doing the task. The improvement of the telescope's performances by using CCD techniques will suppose the recovery of this instrument, obsolete at present.
A better ephemeris determination can be achieved by means of astrometric observations taken from several telescopes. Observations with the Schmidt camera of Centro de Investigación de Astronomía (CIDA) in Merida (Venezuela) will be available from the beginning of the project. In the mid term, the ROA's Baker-Nun camera will also be available at Observatory Fabra II, in the Catalan Pirinee. Processing astrometric observations from these three telescopes will provide high accurate satellite positions.
The geographic positions of San Fernando, in Spain, and Mérida, in Venezuela, are ideal locations for performing astrometric observations of many different geosynchronous satellites, among which we can find the Hispasat satellites.
A redundant check on the ephemeris precision can be supported by using "two way" synchronizing techniques. Range measures can be obtained with this procedure, and at present range measurement of INTELSAT 903 are routine operations in ROA. In fact, both techniques could be mutually validated.

Supported by Spanish Goverment, “Dirección General de Investigación” (# AYA2004-03298)

DETERMINATIONS OF THE SITE POSITION AT THE SLR TRACKING STATION (7824) AT SAN FERNANDO, SPAIN.

I. Vigo-Aguiar (1), J.M. Ferrándiz (1), J. Gárate (2), J. Martín Dávila (2), M. Quijano (2), C. Belza (2), D. García (1).

(1) Dpt. Applied Mathematics, EPS. University of Alicante, E-03080- Alicante, Spain

(2) Real Instituto y Observatorio de la Armada. 11110- San Fernando. Cádiz, Spain.

Abstract

In recent years the San Fernando 7824 SLR station has been under an improvement process. This work reports on efforts that have been made in the determination of the site position. A series of solutions (UA98, UA98-UP, UA00) for the station position is obtained reducing the root-mean-square (RMS) values of the station and improving its contribution to the determination of satellite orbits, and plate motions for related geodetic studies.

The most recent solution, UA00, lowers RMSs for the station between 1.0 and 2.4 cm. for LAGEOS POD and between 2.5 and 4.9 cm. for T/P POD, reaching the standards of the best stations of the SLR network and significatively improving the ITRF00 solution for San Fernando site.

Introduction

The Royal Observatory of the Spanish Navy (ROA) at San Fernando is strategically located near the Strait of Gibraltar, by the boundary between the Eurasia and African tectonic plates. A satellite laser ranging (SLR) station, a Global Positioning System (GPS) station and a set of atomic clocks are co-located at this site. While routinely contributing to laser ranging to several satellites as well as the international time service, the San Fernando SLR station is engaged in an improvement process in hardware and software.

The ROA at San Fernando and the University of Alicante collaborate in a joint research project, which aims at improving the Spanish capabilities with regard to the tracking of geodetic satellites and the analysis of the data. Special attention has been paid to the SLR tracking station at San Fernando, after instrument upgrade to meet present precision standards, as well as the requirements for enhanced computation of crustal motions and other local and regional applications in Geodesy and Geodynamics.

Figure 1: Geographic situation of the ROA .

In the last years, a complete overhaul of 7824 SLR Station electronics and its optics have enabled routine tracking of LAGEOS at over 400 successful LAGEOS night passes per year,

while at the same time doubled the number of successful night passes for lower orbit satellites. Improved determinations of the site position have been obtained by analyzing precise laser ranging data to LAGEOS satellite, that together with LAGEOS II have been the mainstay in station positions and velocities for solutions of IERS in the past. After the upgrade process that the San Fernando SLR station has been under, past determinations of the station coordinates with respect to ITRF97 had RMSs values as large as 18 centimeters, hindering a definitive contribution to the determination of satellite orbits, and plate motions for related geodetic studies. Currently, a series of solutions has been obtained in all cases fitting 3 months data from LAGEOS I in 10-day arcs, using normal points from the global SLR tracking network. The present solution, UA00, lowers RMSs for the station between 1.0 and 2.4 cm. for LAGEOS POD and between 2.5 and 4.9 cm. for T/P POD, reaching the standards of the best stations of the SLR network.

Station Position Determination

In all cases the solutions have been obtained fitting data from LAGEOS in 10-day arcs, using normal points from the global SLR tracking network. The data have been provided by NASA´s CDDIS and processed using the NASA/GSFC software for POD and geophysical and geodynamical parameters adjustment GEODYN/SOLVE II.

The procedure followed is common to the different solutions. The 10-day arcs were combined to derive a set of station positions and station velocities, including the 7824 San Fernando station relative to certain other fiducial stations such as the 7110 Monument Peak as a reference to check the procedure evolution. Earth Orientation Parameters were estimated as independent values of time and polar motion at daily intervals. The IERS standards were followed except for the adoption of the EGM96 gravity field with expanded ocean tidal terms and a value of GM = 398600.4415 km^3/s^2.

A first solution, named UA98, was computed fitting data between March and June 1998. For this solution the CSR93 coordinates were used for San Fernando site as apriori. Once all adjustments were made combining the ten 10-day arcs, UA98 lowered RMSs below 3cm. Within the process of improving the quality of the SLR measurements, the replacement of the old dome for a new one provided a change in the SLR site position in April 1999. We applied the correction for the new position, 35 cm higher, on the former leading to UA98-UP solution.

We applied the same procedure for fitting data between September and December 1999, using as apriori value for San Fernando site the UA98-UP solution, and applying ocean loading and measurement bias adjustments -although the latter were almost negligible (in the order of a few millimeters). The resulting solution that we called UA00 is shown in Table 1 together with the corresponding solution of the ITRF 2000. In the ITRF2000 the old SLR system (until April 1999) is refereed as S004 and the SLR Fixed system, the one we include here for comparison, is refereed as S007. A comparison of the ITRF 2000 solution (for the S007 system) with the alternative solutions for SANF 7824 it is shown in Table 2. In particular we consider: the CSR93 solution, our apriori station position, the UA98 introduced above, the ITRF97 which is the first ITRF solution that includes SANF 7824 station that was computed before the new position of the laser reason why gives a large difference in the vertical, the UA98-UP corrected for new position of the laser 35 cm. higher, and the current solution UA00.

Table 1: Current solutions for San Fernando 7824 SLR station

	X /Vx	Y /Vy	Z / Vz
	(m/m s^{-1})		
UA00	5105473.9947	-555110.7739	3769892.8067
	-.237661D-09	.646437D-09	.415114D-09
ITRF00	5105473.975	-555110.726	3769892.801
	-. 294901D-09	.431253D-09	.351978D-09

Tabla 2: Comparison of solutions for SANF 7824 to the ITRF00 solution

	ΔX (m)	ΔY (m)	ΔZ (m)	ΔHeight (m)
CSR93	-0.2122	-0.0988	-0.3970	-0.4010
UA98	-0.2133	-0.0397	-0.2527	-0.3220
ITRF97	-0.2280	0.0290	-0.1880	-0.2960
UA98-UP	0.0667	-0.0660	-0.0444	0.0282
UA00	0.0197	-0.0479	0.0057	0.0233

Table 3 shows how RMSs for the station have been lowered, reaching the standards of the best stations of the SLR network. To validate the solution, and bearing in mind that our solution has been obtained fitting LAGEOS data, we have computed the TOPEX orbit provi-

Tabla 3: Comparison of solutions for SANF 7824 to the ITRF00 solution

All solutions have been obtained with SANF 7824 data withheld (downweighted)		TOPEX DATA			LAGEOS DATA		
		ARC1 991025	ARC2 991123	ARC3 991203	ARC1 991025	ARC2 991123	ARC3 991203
ITRF97	7824 STATION RMS	0.2203	0.1294	01813	0.2562	0.2062	0.2156
	POD RMS (2W RNG)	0.0601	0.0372	0.0435	0.0620	0.0415	0.0606
UA98-UP	7824 STATION RMS	0.0690	0.0490	0.0533	0.0367	0.0461	0.0340
	POD RMS (2W RNG)	0.0339	0.0318	0.0355	0.0560	0.0409	0.0508
UA00	7824 STATION RMS	0.0497	0.0253	0.0405	0.0165	0.0101	0.0246
	POD RMS (2W RNG)	0.0319	0.311	0.0351	0.0498	0.0333	0.0365
ITRF00	7824 STATION RMS				0.0542	0.0436	0.0566
	POD RMS (2W RNG)				0.0548	0.0333	0.0397

ding the position to the 7824 station of this series of solutions. For each solution we show in table 3 the POD RMS and the San Fernando 7824 station RMS. The present solution UA00, provide San Fernando station position which yields RMSs between 1 and 4 cm. for LAGEOS

POD and between 2.5 and 4.9 cm. for T/P POD. The large RMSs obtained for the 7824 station with the ITRF97 solution are not surprising bearing in mind it does not take into account the new position after the change of the dome in April 99, and the processed data is posterior. In all cases the UA00 and the ITRF00 solutions provide the lowest RMSs. UA00 reduces notably the station RMS, while for the POD lowers the RMSs with respect to the ITRF00 in the order of a few millimeters.

It is expected that further analysis of the data will yield further and better adjustments of the station position. Currently, we are in the process of analyzing additional data while combining LAGEOS I and II.

Acknowledgments

The research is mainly supported by the Spanish Space Research Program funded by CICYT (Projects no. ESP2001-4533-PE & ESP2001-4514-PE) and the Spanish Navy. We would like to thank all people at the Space Geodesy Branch of NASA/GSFC for facilitating carrying out this work, in particular D. Rowlands who has provided invaluable technical supports in data analysis concerning precise determination of orbits and related geodetic parameters, R. Ray for providing us with the ocean loading values for the San Fernando site, and D. Chinn for made available and helped with the processing of the T/P data.

References

Altamimi Z., P. Sillard, and C. Boucher, ITRF2000: A new release of the International Terrestrial Reference Frame for earth science applications, J. Geophys. Res., 107(B10), 2214, doi:10.1029/2001JB000561,2002.

Boucher C., Z. Altamimi, P. Sillard (eds.): Results and Analysis of the ITRF96, IERS Technical Notes No. 24.

Boucher C., Z. Altamimi, P. Sillard (eds.): The 1997 International Terrestrial Reference Frame (ITRF97) IERS Technical Notes No. 27

Boucher C., Z. Altamimi, P. Sillard, and M. Feissel-Vernier: The ITRF2000, 2004 (In print, available online http://www.iers.org/iers/publications/tn/tn31/) IERS Technical Notes No. 31

McCarthy D.D. (ed.): IERS Conventions (1996), (available online http://maia.usno.navy.mil/conventions.html) IERS Technical Notes No. 21

Lemoine, F. G., S. C. Kenyon, J. K. Factor, R.G. Trimmer, N. K. Pavlis, D. S. Chinn, C. M. Cox, S. M. Klosko, S. B. Luthcke, M. H. Torrence, Y. M. Wang, R. G. Williamson, E. C. Pavlis, R. H. Rapp and T. R. Olson. The Development of the Joint NASA GSFC and NIMA Geopotential Model EGM96, NASA Goddard Space Flight Center, Greenbelt, Maryland, 20771 USA (http://cddis.gsfc.nasa.gov/926/egm96/nasatm.html),

FTLRS POSITIONING FOR THE EU/NASA ALTIMETER CALIBRATION PROJECT GAVDOS

E. C. Pavlis (1) and S. P. Mertikas (2)
(1)Joint Center for Earth Systems Technology, UMBC & NASA Goddard, epavlis@JCET.umbc.edu/Fax: +1-410-455-5868,
(2)Tech. Univ. of Crete, Chania, Greece

Abstract

The Eastern Mediterranean area is one of great interest for its intense tectonic activity as well as for its regional oceanography. Recent observations convincingly demonstrated the importance of the area for regional meteorological and climatologic changes. GPS monitors tectonics, while tide gauges record the variations in Mean Sea Level (MSL). Monitoring tide gauge locations with continuous GPS on the other hand, will remove the uncertainties introduced by local tectonics, that contaminate the observed sea level variations. Such a global tide gauge network with long historical records is already used to calibrate satellite altimeters (e.g. on TOPEX/POSEIDON, GFO, JASON-1, ENVISAT, etc.), at present, a common IOC-GLOSS-IGS effort --TIGA. Crete hosts two of the oldest tide gauges in the regional network, at Souda Bay and Heraklion. We recently completed the instrumentation of a third, state-of-the-art MSL monitoring facility in southwestern Crete, on the isle of Gavdos, the southernmost European parcel of land. Our project –GAVDOS, further expands the regional tide gauge network to the south, and contributes to TIGA and MedGLOSS. This presentation focuses on the altimeter calibration aspect of the facility, in particular, its application to the JASON-1 mission. Another component of the project is the repeated occupation of the older tide gauges at Souda Bay and Heraklion, and their tie to the new facility. The Gavdos facility is situated under a ground-track crossing point of the original T/P and present JASON-1 orbits, allowing two calibration observations per cycle. It is an ideal site if the tectonic motions are monitored precisely and continuously. The facility hosts in addition to the two tide gauges, multiple GPS receivers, a DORIS beacon for positioning and orbit control, a transponder for direct calibration and it is visited periodically by Water Vapor Radiometers and solar spectrometers. At frequent intervals we also deploy GPS-laden buoys and conduct airborne surveys with gravimeters and laser profiling lidars for a high resolution and increased accuracy of the geoid and an independent observation of the local Sea Surface Topography (SST). The French Transportable Laser Ranging System (FTLRS) completed recently a co-location campaign at the Chania, Crete base site, which has a long GPS record since 1997. The FTLRS occupation provides us with an absolute SLR-derived position in the ITRF2000 frame, the ability to compare with the GPS-derived position, and improved orbit control over the site during the campaign. This will ensure the best possible and most reliable results from the project. We will present our latest estimates of the FTLRS position and the GPS-derived velocity vectors for the site, and other relevant results.

Introduction

Seal level change has become one of the hottest research topics in the past decade. The advent of remote sensing techniques from space (altimetry) provides frequent synoptic pictures of the state of Earth's oceans at regular interval. The TOPEX/POSEIDON mission was the first to do this in a very precise and routine fashion since mid-1992. This was followed by Jason-1, launched in time to allow for a comfortable overlap of the two missions. Since any instrument is characterized by systematic and random errors usually different from any other instrument even of the same type, it is prudent, and absolutely necessary in a case as this, to verify that past, current and future altimeter instruments, all measure sea level using the same "yard-

stick", the same standard. This is ensured by calibration of the instruments before launch as well as while in space. It is also a matter of continuous monitoring of instrument performance, since electronic and mechanical systems age with time, and they do not necessarily perform equally throughout their lifetime [Mitchum, 1998]. Satellite Laser Ranging (SLR) was initially used to measure precisely the distance to the satellite when over-flying a laser site, to compare with the observed altimeter radar range. As altimeters became more precise though and science requirements more stringent, the primary role was taken by a global network of tide gauges, and the role of SLR has become that of a provider of a locally ultra-precise orbit. SLR is also used to determine the position of the experiment site in the same reference frame as it is used in computing the satellite orbits, ITRF2000 [Altamimi et al., 2002].

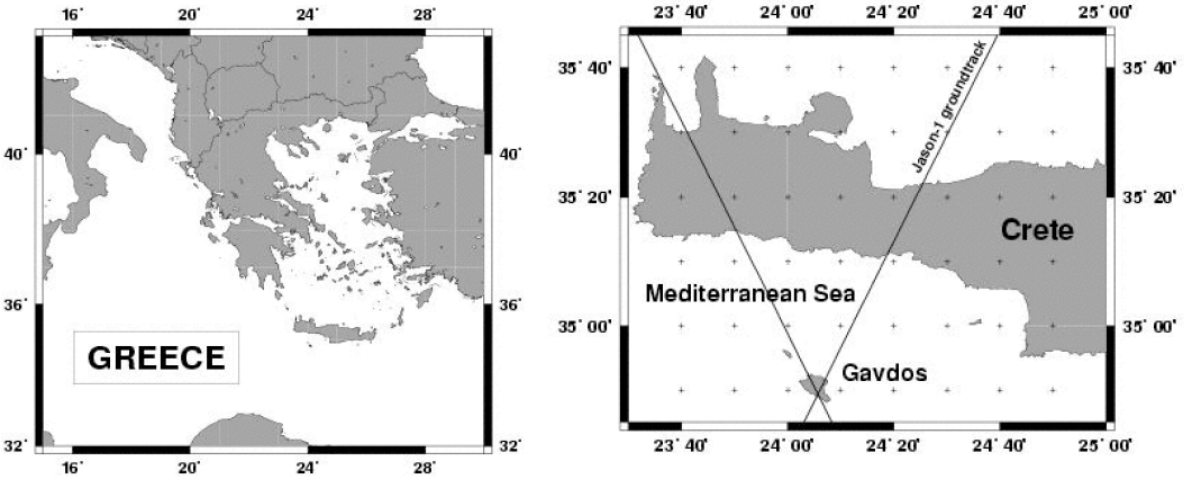

Figure 1. The location of the island of Gavdos, south of Crete and the Jason-1 ground-tracks.

The GAVDOS project goals are the absolute calibration of altimeter missions and in particular, of the TOPEX/POSEIDON (T/P) and Jason-1 systems, and the continuous monitoring of these instruments for bias drifts or other temporal changes. Naturally, the continuous tide gauge and positioning of the tide gauge with GPS, provides also an independent measurement of local/regional sea level, in an area void of other such observations (Figure 1). Due to a fortuitous coincidence the Jason-1 groundtracks cross exactly over the tiny island of Gavdos south of Crete, Greece. This makes it a perfect regional calibration site, due to its small expanse, open sea location, small tides, fairly well known local geophysics and proximity to mainland. JCET in collaboration with the Tech. University of Crete at Chania (TUC), and several other European institutes, submitted a proposal to establish an altimeter calibration and sea level monitoring site on Gavdos. The project was funded jointly by the European Union (EU), the National Aeronautics and Space Administration (NASA), and the Swiss Federal Government, and enjoys the participation of many institutes from Europe, and JCET group from the USA [Pavlis et al., 2004].

Figure 2 illustrates the various sites that comprise the regional network and gives a brief description for the function of each of them. For a more detailed description of the project and its initial results, consult [*ibid.*]. This contribution will focus on the discussion of the deployment of the French Transportable Laser Ranging System (FTLRS—Figure 3), the positioning results from the six-month 2003-deployment at OCC, and a comparison to results obtained with GPS over the same time-period [Nicolas et al., 2001]. In addition to these, we will discuss in detail the pre- and post- campaign local surveys of the FTLRS deployment pad and calibration target, using precise GPS techniques.

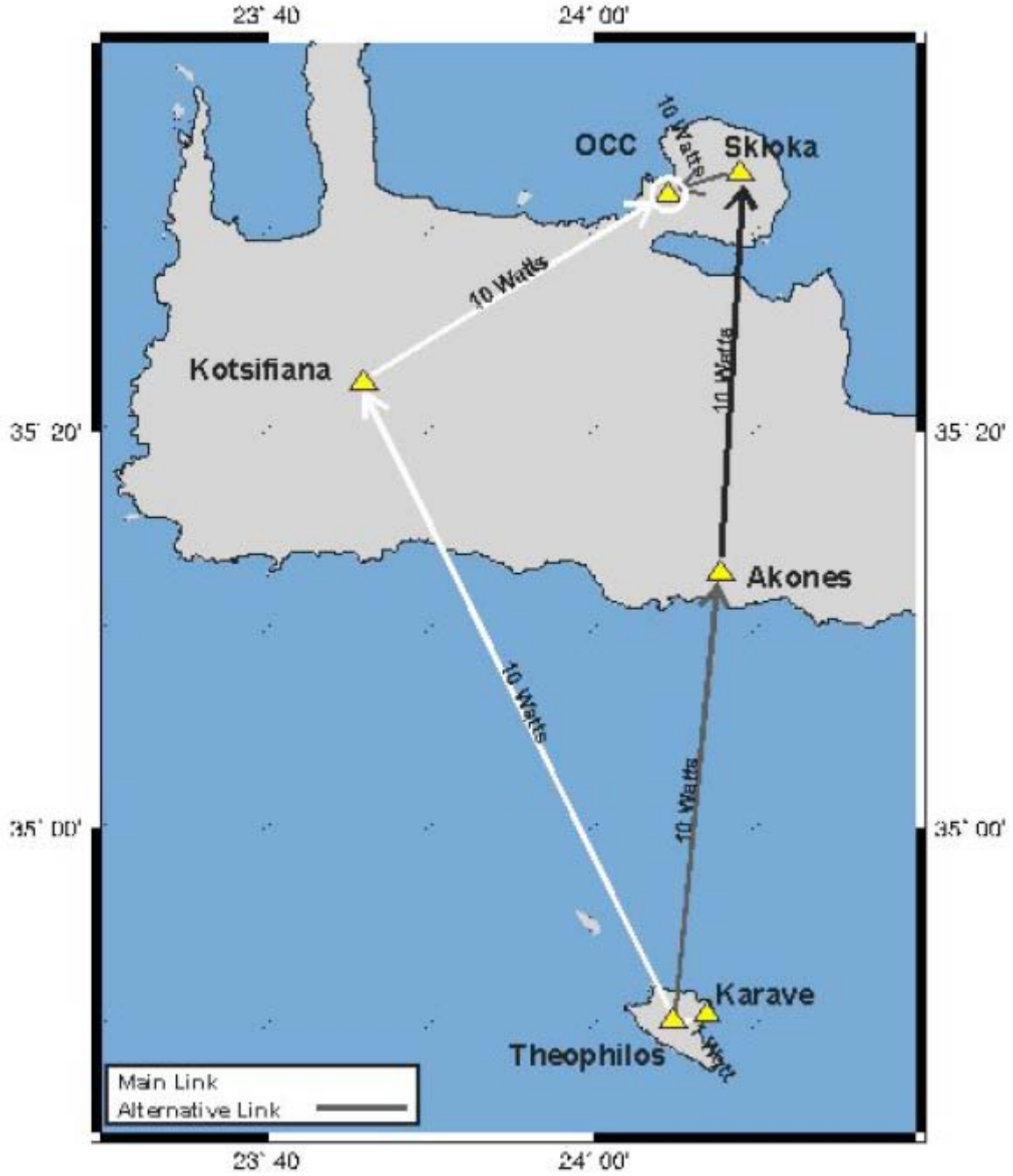

Figure 2. The regional GAVDOS network of sites: (a) OCC, the Operations Control center at the TUC campus, (b) the Karave tide gauge and GPS site on Gavdos, and (c) the Theofilos control and communications site on Gavdos, with the back-up GPS and DORIS beacon. The lines between sites indicate the possible communications links (and power) between the various sites for data access and instrument control operations.

SLR Positioning at OCC

Reference frame consistency, especially in the vertical, is of primary importance for an altimeter calibration and sea level monitoring project. Local orbital improvement over the calibration site, is also highly recommended during these experiments. Since the Gavdos site is fairly far away from permanent SLR tracking sites (Matera, Italy and Graz, Austria are the closest two), we opted to include a short-term campaign with a transportable system visiting the oldest site of the GAVDOS network, the OCC at TUC. This established a SLR collocation

with one of the GPS network sites that has the longest observational record. The deployment of FTLRS at TUC (Figure 4) lasted from March to October 2003, with data primarily collected during two periods, April-June and Sept.-October, avoiding the high temperature mid-summer months. The data, promptly submitted to the ILRS data centers, were analysed by various Analysis Centers, including OCA/CERGA and JCET/NASA. The system tracked a number of SLR target satellites, with emphasis placed on the two altimeter-carrying missions, T/P and Jason-1. The distribution of the acquired passes and Normal Point (NP) data is shown in Figure 5.

Figure 3. FTLRS deployment at the TUC campus, the ranging system on the pad.

For precise positioning of the system, two different approaches were used by OCA and JCET, both leading to essentially the same results, given the differences in the amount and distribution of the data used. JCET used the LAGEOS and LAGEOS 2 tracking exclusively, while OCA supplemented that data with data from lower altitude targets, such as Starlette and Stella.

At JCET we used a dynamic technique and data taken only on the two geodetic targets, LAGEOS 1 and 2, [Pavlis, 2002, 2003]. Separate solutions were done for the small data set of Spring 2003, as well as the entire set of data, using a fixed velocity vector relative to stable Europe, derived from many years of GPS observations at TUC1: 35.7 mm/yr at an azimuth of 226° [Pavlis, et al., 2002]. The position of FTLRS was determined in a quasi-ITRF2000 frame, realized by constraining the rest of the SLR sites' positions and velocities to their ITRF2000 values.

At OCA, the technique of SLR data reduction was based on their short-arc methodology with end-arc-overlaps [Bonnefond et al., 1995], using data taken on the two LAGEOS spacecraft (s/c) and additionally, on the low altitude geodetic satellites Starlette and Stella. The OCA

Figure 4. FTLRS at the TUC campus, the system and the facility as seen from OCC.

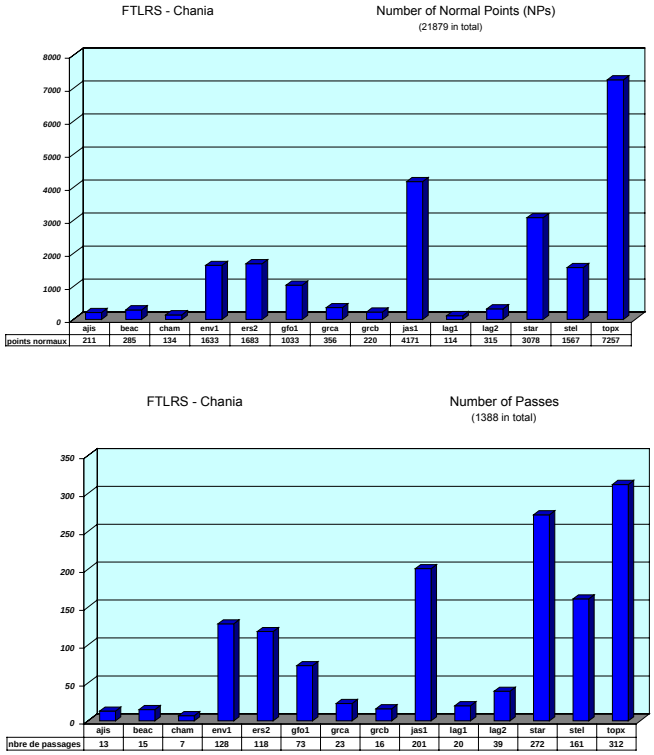

Figure 5. FTLRS-acquired SLR data during 2003: normal point data (top) and number of passes (bottom), at TUC, Chania, Crete, Greece.

analysis allowed for the estimation of measurement biases for each target satellite, assuming the biases stable over the entire campaign, with a strategy that minimized the correlation

between the height component and the estimated biases. The JCET analysis made no use of low altitude satellites and since JCET's preliminary analysis did not indicate the existence of biases, we did not allow for such parameters in the final solution. The bias recovered from the OCA analysis is at the level of 10 mm, as opposed to an expected level of about 5 mm. The Cartesian positions from SLR, along with those obtained by GPS, are shown in Table 1 for both, the JCET and the OCA analyses. The results are in excellent agreement within techniques as well as across techniques, with only exception the Z-component values between the JCET and OCA SLR solutions and the corresponding GPS estimates.

Table 1. FTLRS Position vector derived from SLR and GPS data

Site and Epoch	X [m]	Y [m]	Z [m]
SLR0 1st part 1997.0 *(JCET SLR)*	4744552.665 ±0.021	2119414.416 ±0.022	3686245.086 ±0.019
SLR0 all data 1997.0 *(JCET SLR)*	4744552.665 ±0.006	2119414.426 ±0.006	3686245.095 ±0.006
SLR0 all data 2003.7 *(JCET SLR)*	4744552.558 ±0.006	2119414.553 ±0.006	3686245.158 ±0.006
SLR0 2003.7 *(JCET GPS)*	4744552.558 ±0.005	2119414.553 ±0.005	3686245.135 ±0.008
SLR0 4 S/C 2003.7 *(OCA SLR)*	4744552.564 ±0.006	2119414.553 ±0.006	3686245.139 ±0.006
SLR0 2003.7 *(OCA GPS)*	4744552.561 ±0.005	2119414.555 ±0.005	3686245.138 ±0.008

The discrepancy with GPS of some 20 mm may be due to the fact that the GPS values are simply averaged between the daily estimates from pre- and post-deployment solutions, while for the JCET SLR reductions, the GPS-derived velocity vector was used in the analysis. OCA also averaged their position estimates over the campaign period, making no use of an underlying velocity vector as JCET did. It should also be noted that both, JCET and OCA, used the same GPS processing software, the GAMIT suite, [King and Bock, 2000]. These issues are being investigated, as the SLR data taken on the other targets during the campaign are analysed and alternative estimates at JCET, allowing for biases are explored.

Local Surveys

The reference marker on the concrete pad that was built at the Chania campus of TUC for the FTLRS deployment, was surveyed with GPS prior to the deployment in early 2003, and a couple of months after the cease of operations, in early 2004. The setup of the GPS instruments and antennae was different on different days in 2003, and this is indicated in Figures 6 and 7. A single setup was used in 2004.

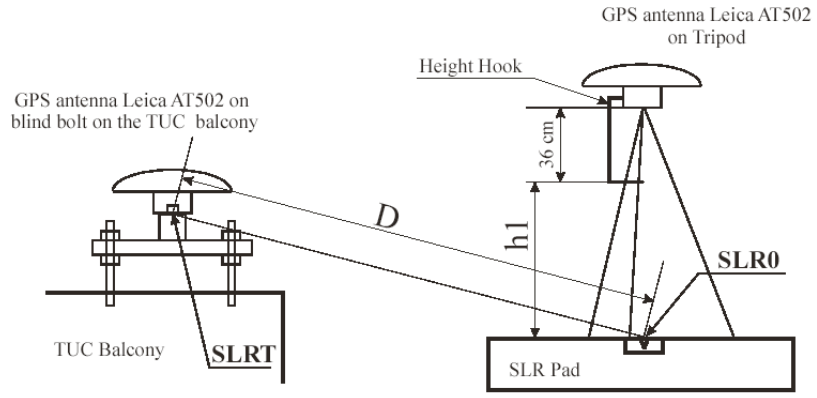

Figure 6. Local survey setup of GPS instruments and antennae on DOY 71-74, 2003.

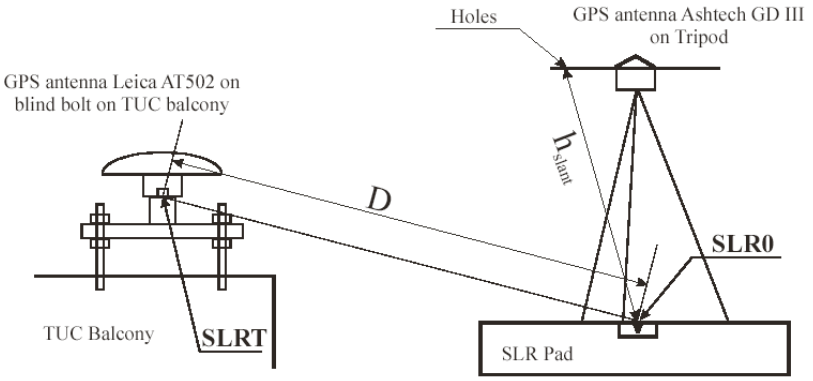

Figure 7. Local survey setup of GPS instruments and antennae on DOY 80-81, 2003.

The results from 2003 are slightly noisier and they are sparser compared to those from 2004. The changes indicated in each coordinate are consistent with changes expected due to tectonic activity in the area. The SLR calibration target was surveyed only in 2003.

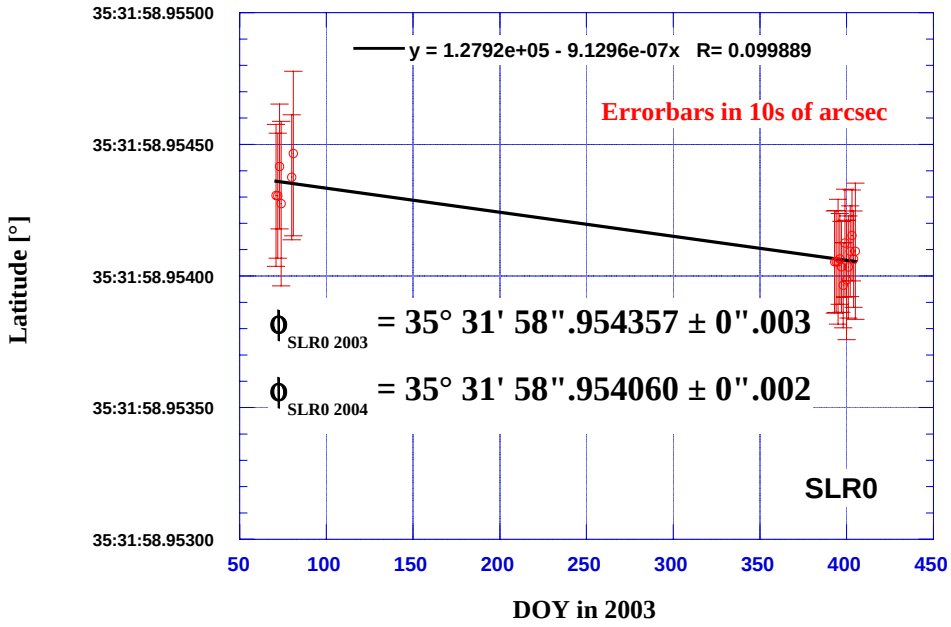

Figure 8. GPS-derived latitude estimates of the SLR marker "SLR0", in 2003 and 2004.

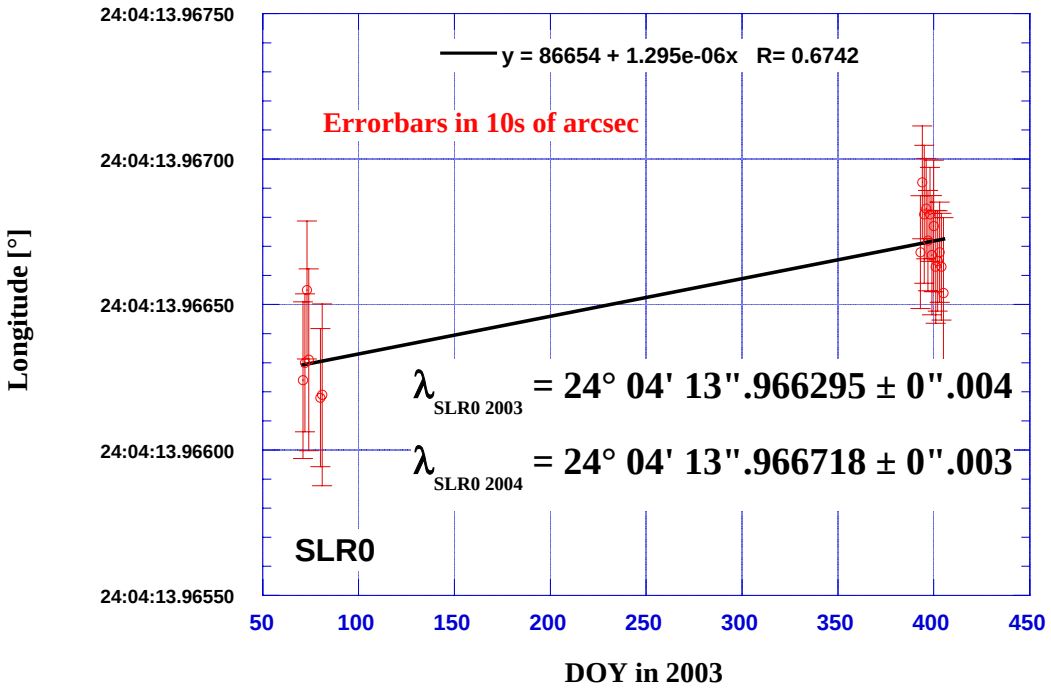

Figure 9. GPS-derived longitude estimates of the SLR marker "SLR0", in 2003 and 2004.

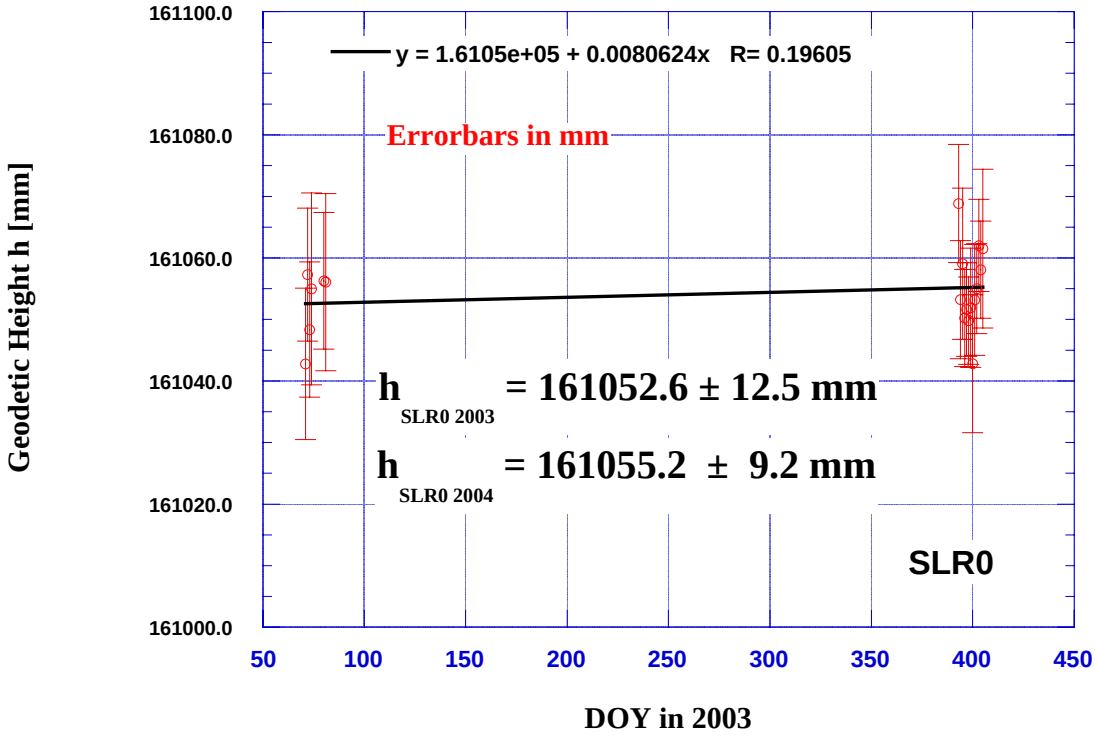

Figure 10. GPS-derived height estimates of the SLR marker "SLR0", in 2003 and 2004.

Figures 8 through 10 show the results of the two surveys of the SLR marker, SLR0, in 2003 and 2004. Figures 11 through 13 show the 2003 survey results for the SLR calibration target.

The results for the calibration target indicate some systematic change over the four days of observations, however, the magnitude of these changes is at the two millimeters per day level and they are well within the accuracy range for such surveys.

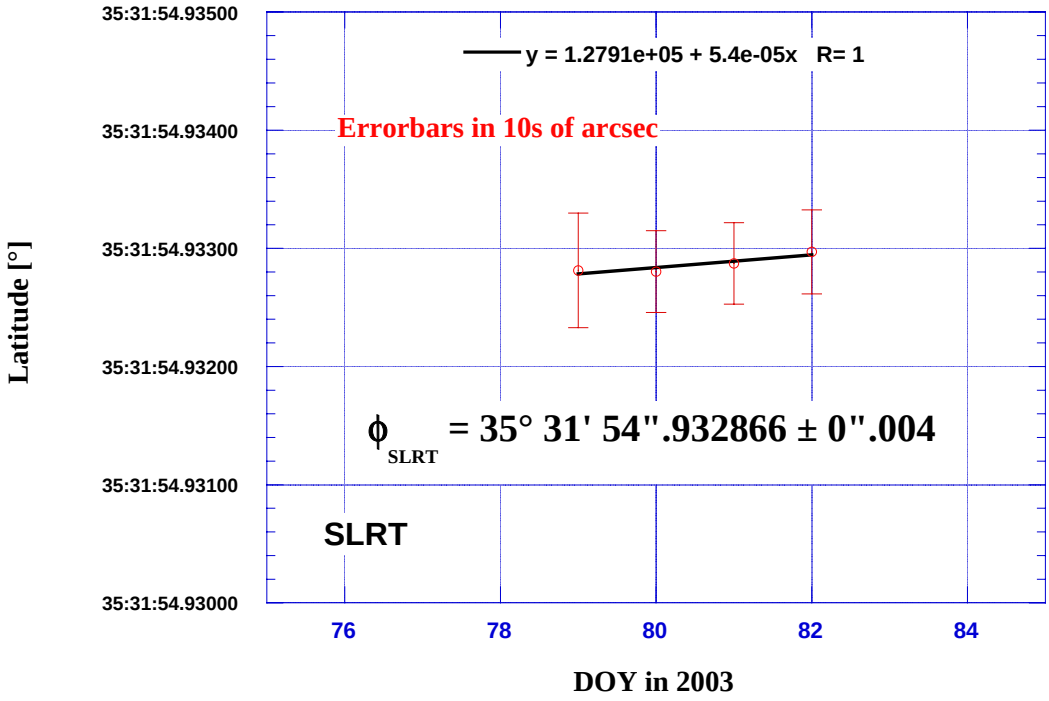

Figure 11. GPS-derived latitude estimates of the SLR calibration target "SLRT".

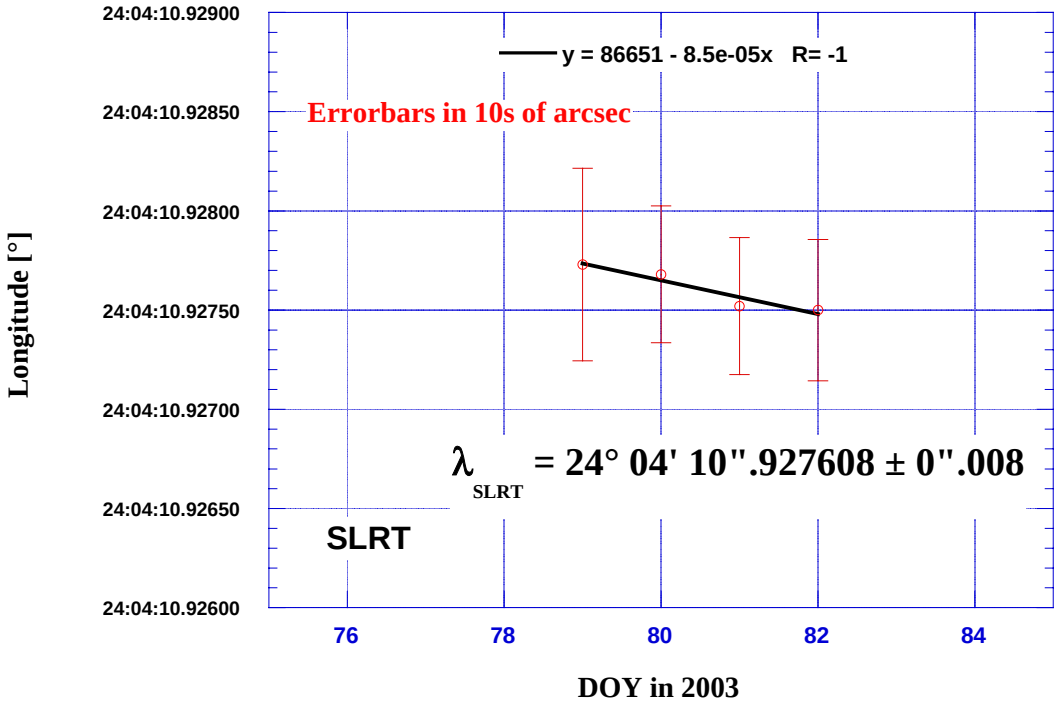

Figure 12. GPS-derived longitude estimates of the SLR calibration target "SLRT".

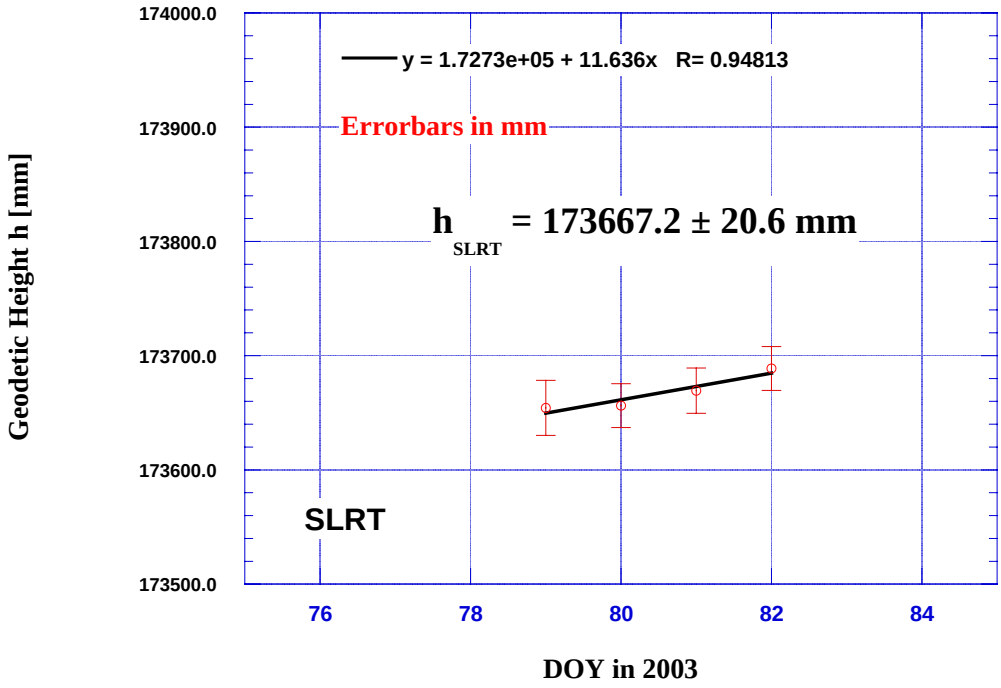

Figure 13. GPS-derived height estimates of the SLR calibration target "SLRT".

Figure 14. The Theofilos control site, with the GPS and DORIS (insert) pillars.

The spread of the height estimates for the calibration target (Figure 13) are slightly more disturbing, not so much for their size, in that sense they are consistent with the height estimates for SLR0 during the same period (cf. Figure 10, 2003 results), but rather for the very systematic nature of the change. This seems to be more related to the fact that the target was placed at the corner of a three-story building. It will be interesting to compare these results with average daily temperatures over these four days.

The regional network data of the continuously operating GPS receivers have been consistently analyzed with GAMIT and with the establishment of an ITRF2000-consistent absolute position at OCC/TUC, we can now propagate these absolute coordinates throughout the network. In the next step we plan to generate a similar absolute position based on the DORIS data from the Theofilos site (Figure 14), and compare these coordinates to those obtained from the GPS and SLR combination.

Summary

We discussed the recent deployment of the French Transportable Laser Ranging System at Chania, Crete, Greece, in the realm of the GAVDOS altimeter calibration and sea level monitoring project. The SLR data provide an absolute, ITRF2000-consistent position for one of the older project sites, with the longest GPS record. We can now propagate the absolute position of OCC/TUC to all sites linked to it via the continuously operating GPS network. This campaign has demonstrated that with the proper planning, mobile SLR systems can provide solid positioning support in a very short time for such projects. The success of this effort convinced us to plan to repeat the campaign in the future in order to control any long-term changes in the tectonic behavior of the region, and to further improve the quality with which the absolute locations of the regional network are known.

References

Altamimi, Z., Sillard P, Boucher C, "ITRF2000: A new release of the International Terrestrial Reference Frame for Earth science applications", *J. Geophys. Res.*, 107 B02214, 2002.

Bonnefond, P., P. Exertier, P. Schaeffer, S. Bruinsma, and F. Barlier, "Satellite altimetry from a short-arc orbit technique: Applications to the Mediterranean", *J. Geophys. Res.* 100(C12):25365-25382, 1995.

King, R. W. and Y. Bock, "Documentation for the GAMIT GPS analysis software, Release 10", Department of Earth, Atmospheric, and Planetary Sciences, Massachusetts Institute of Technology and Scripps Institution of Oceanography, University of California, San Diego, Cambridge, MA, 2000.

Mitchum, G.T. "Monitoring the stability of satellite altimeters with tide gauges", *J. of Atmos. and Oceanic Tech., 15, 721-730*, 1998.

Nicolas, J., Pierron, F., and Samain, E., et al, "Centimeter accuracy for the French Transportable Laser Ranging Station (FTLRS) through sub-system controls", *Surv. Geophys.* 22 (6): 449-464, 2001.

Pavlis, E. C., "Dynamical Determination of Origin and Scale in the Earth System from Satellite Laser Ranging", *Vistas for Geodesy in the New Millennium, Proceedings of the 2001 International Association of Geodesy Scientific Assembly*, J. Adam and K.-P. Schwarz eds., Springer-Verlag, New York, pp. 36-41, 2002.

Pavlis, E. C., "Monitoring the origin of the TRF with space geodetic techniques", *Proceedings of the 13th International Laser Ranging Workshop*, S. Klosko, C. Noll and M. Pearlman eds. NASA CP 2003-212248, NASA Goddard, pp. 113-120, 2003.

Pavlis, E. C. and THE GAVDOS TEAM, "Absolute sea level monitoring and altimeter calibration at Gavdos, Crete, Greece," Geophysical Res. Abstracts (CD), 3, Abstract EGS02-A-03480, EGS, Nice, France, April 2002.

Pavlis, E. C., S. P. Mertikas and the GAVDOS Team, "The GAVDOS Mean Sea Level and Altimeter Calibration Facility: Results for Jason-1", 3rd Jason special issue, *Mar. Geod., (27), 3-4,* DOI:10.1080/01490410490902106, pp. 631-655, 2004.

LASER RANGING AS A PRECISE TOOL TO EVALUATE GNSS ORBITAL SOLUTIONS.

Graham M Appleby (1), Toshimichi Otsubo (2)
(1) Natural Environment Research Council Space Geodesy Facility, Herstmonceux, Hailsham, East Sussex, BN27 1RN, U.K. (gapp@nerc.ac.uk).
(2) National Institute of Information and Communications Technology, Kashima Space Research Center, 893-1 Hirai, Kashima 314-8501 Japan. (otsubo@nict.go.jp).

Introduction

In this paper from our poster presentation we bring up to date our use of precise laser range observations to carry out independent checks on the accuracy of published orbits of a subset of the GPS and GLONASS navigational satellites. Range measurements obtained by the ILRS tracking network to two GPS satellites and several of the GLONASS satellites are compared in two ways with precise orbits computed by the IGS; by direct comparison between SLR measurements and equivalent ranges computed from the microwave orbits, and by comparison of SLR-based orbits to the microwave orbits. Our previous work, which is outlined here, has shown that in such comparisons it is necessary to understand both the potential for systematic range ambiguity induced by the laser reflector arrays and the need for accurate on-satellite positions of the array phase centres. For the GLONASS and GPS satellites these parameters are now accurately known for the several different types of array currently in orbit, and the SLR results provide an accurate assessment of the radial quality of the IGS orbits, which is currently at a level of about 10 cm rms. Particularly for the GLONASS satellites, this quality has improved in recent months, but the well-known radial offset of a few cm remains between the laser measurements and the ranges computed from the radiometric orbits for the two GPS satellites. We further look forward to using similar techniques on the pilot satellites of the EU GALILEO navigational system, due for launch during 2005.

GLONASS Reflector Arrays

Early satellites in the GLONASS constellation carried very large (1m × 1m) reflector arrays, giving a good link budget but presenting a new challenge for precise interpretation of range data. For the GPS and new GLONASS satellites, the arrays are small and systematic effects much reduced, at the expense of a strong link budget. Laser range measurements to these flat arrays can cause attitude-dependent offsets from the centres of the array, the magnitude of which depends both on the physical size of the array and upon the characteristics of the laser ranging station. In outline, a station working at high levels of return energy will on average measure the distance from the station to some region near the closest, outer edge of the array, since it is reflections from this region that return first and are thus more likely to be detected. A station working at energies close to single photons, on the other hand, will on average measure the distance to the centre of the array since single photons are equally likely to come from any part of the array.

These effects are now fairly well understood and, as expected, depend upon the characteristics of the tracking station (Otsubo *et al,* 2001). They may be detected through precise orbit determination, where in addition to solving for orbital force-model parameters, we also solve for the 'effective size' of the reflector array, as determined by each tracking station. More details and results are given in Otsubo *et al,* 2001 and Appleby and Otsubo, 2003.

Using SLR data to monitor radiometric orbits

Two methods can be employed to use SLR data for an independent check on the quality of GNSS orbits; we can either compute independent orbits using SLR data alone and compare them with radiometric orbits, or compare laser ranges directly with satellite-station distances derived from microwave orbits.

For the GLONASS satellites, sufficient SLR data usually exists to compute SLR-only orbits and compare them point-by-point with radiometric orbits. However, for the two GPS satellites, often there are too few laser measurements for this approach. We now discuss in more detail both these approaches.

- **SLR-orbit comparisons**

  7-day orbital arcs are fitted to SLR data from the global ILRS network by adjustment of a standard set of parameters, including 1-per-revolution terms to remove un-modeled non-gravitational perturbations. Post-fit residual rms values are typically about 5 cm. From the fitted orbit, 15-minute geocentric rectangular ephemerides are computed, referred, through the assumed locations of the SLR stations, to the ITRF2000 system. Daily IGS orbits for the GPS and GLONASS satellites are available in the same reference frame from the CDDIS public ftp site. From these ephemerides we compute 15-minute coordinate differences and map them onto in- and out-of-plane directions, taking velocities from the SLR-only orbits.

  The results in general imply that the rms of along- and across-track differences are at a level of about 50 cm, with radial differences of between 10 and 20 cm rms, the GLONASS results being somewhat poorer than those of GPS.

- **Direct comparison**

  Orbital comparisons of course contain error contributions from both the SLR and radiometric orbital solutions. However, a comparison of precise SLR normal points with station-satellite distances determined from the radiometric orbit will be close to a direct measure of orbit radial error, since at a level of better than10 mm the laser ranges may be assumed to be 'true'. Using a modified version of our SLR orbit determination software SATAN we have computed range differences between each SLR normal-point observation and the corresponding distance to the centre of the reflector array as deduced from the IGS orbits. These differences (o-c) may then be used as measures of the radial error in the IGS orbit.

  This process has been carried out for the GLONASS satellites GL80, GL84, GL86 and GL87, when available during the period 2000 July to 2003 April (GL80 ceased operational service in February 2002) and for the GPS satellites GPS35 and GPS36 for the period 1999 January to 2003 April.

  - **GLONASS Results**

    We find that long-term systematic radial bias in the radiometric orbits is very variable for GLONASS. Present are annual periodic, 60 cm level radial biases in the results for all the GLONASS satellites up to mid 2002. However, a marked improvement in radial orbit quality is evident from 2002 June onwards for all these satellites,

suggesting that improvements have been made thereafter in IGS operational orbit determination. It is considered likely that those improvements have been to solar radiation modelling, the most difficult force to model accurately. The improvement in orbital quality as detected using laser measurements is illustrated in the results for GLONASS-84, shown in Figure 1, for the period 2001 February to 2003 April. The large amplitude excursions in the O-C values occur approximately at semi-annual periods, suggesting a lack of accuracy in solar radiation modelling. From 2002 June, when this problem appears to have been solved, the radial accuracy of the IGS orbit approaches 8 cm rms. Shown in more detail in Figure 2 are the O-C values for the final four months of our analysis. Besides the much improved radial precision revealed by these results, interesting is the overall mean O-C value, which at approximately –5 cm, is close to those values determined previously in our work with GPS35 and 36, and as discussed below.

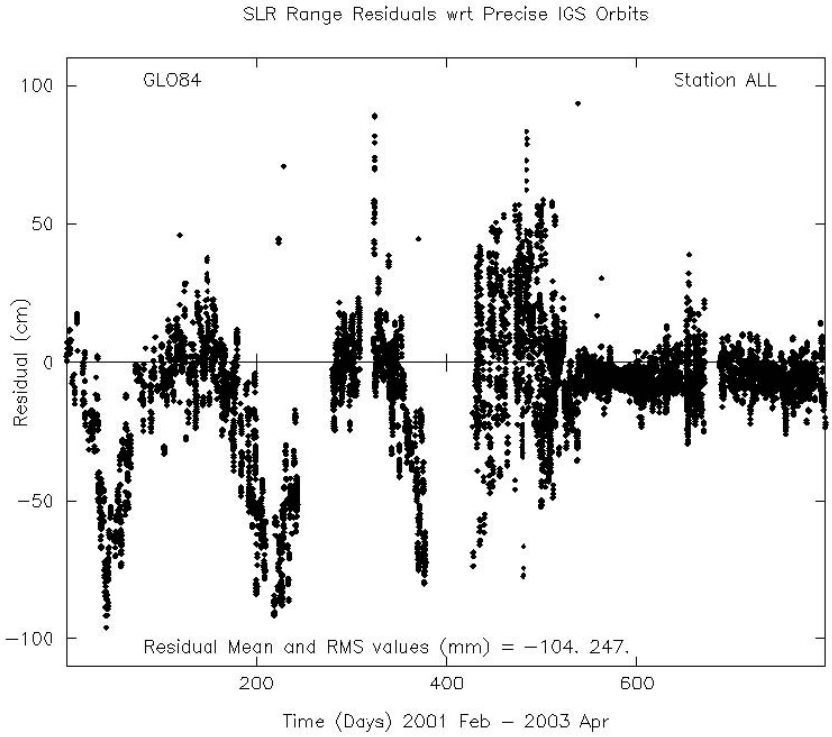

Figure1. Time series of GLONASS-84 O-C values for 2001 February - 2003 April.

➢ GPS Results

The results of comparison of laser range measurements to GPS35 and 36 are now considered. As discussed above, previous studies (e.g. Ineichen *et al*, 2001, Appleby and Otsubo, 2003) reveal a persistent ~5cm radial bias in the IGS orbits; the orbits are 'too big' when checked using SLR data. Such an offset may be attributable to unidentified errors in the assumed locations of the phase centres of the microwave antennae, which to some degree corrupt the orbital determination, or it is also possible that the adopted locations of the GPS laser retro-reflector arrays are incorrect. Shown in Figure 3 are our O-C values for GPS 36 for the period 1999 January to 2003 April. The values are much less scattered and systematic than those shown for GLONASS 84, due no doubt to better orbital monitoring and better global tracking coverage by IGS GPS receivers.

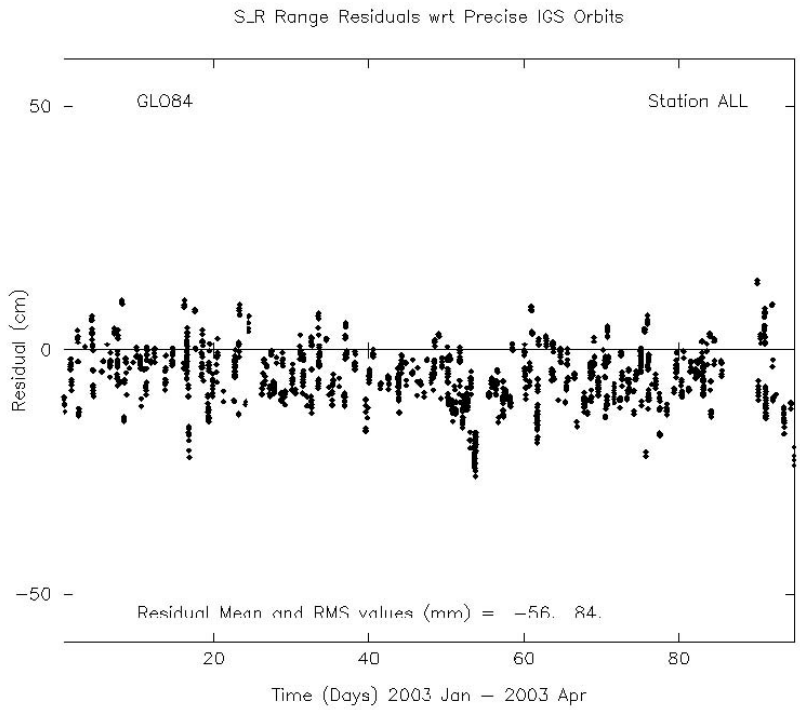

Figure 2. Time series of GLONASS-84 O-C values for 2003 January - April.

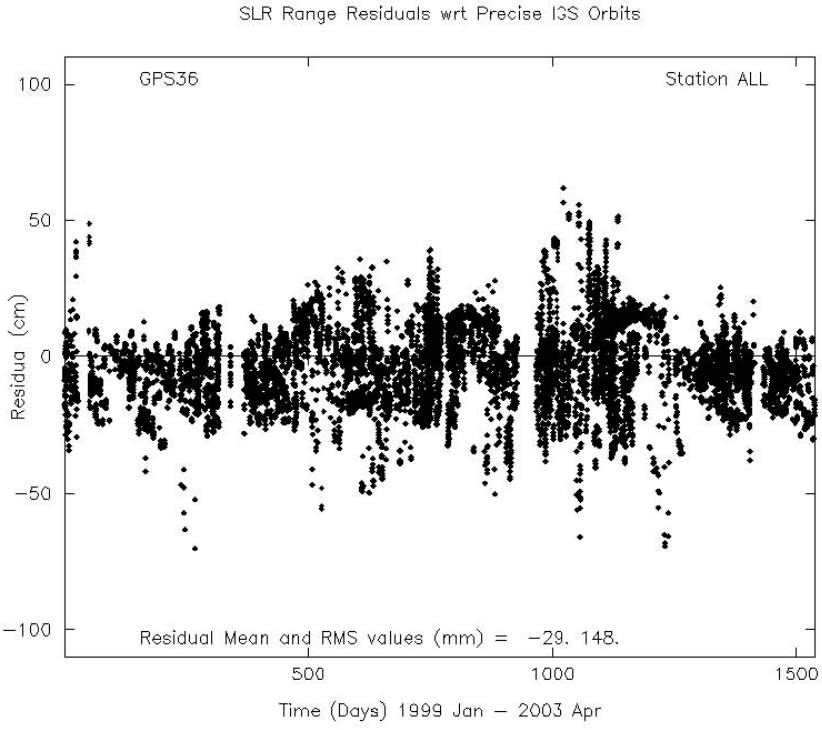

Figure 3. Time series of GPS-36 O-C values for 1999 January - 2003 April.

However, we find that care must be taken in interpreting the data. Our SLR – IGS orbital comparisons suggest that along- and across-track errors in either orbit are at a level of at least

50 cm rms. Simple geometric considerations imply that significant contamination from this error source will occur in any determination of radial bias in the IGS orbits using direct comparison with SLR, unless only near-zenith measurements are used. For instance, at a zenith distance of 10º, contamination of any true radial error is at a level of nearly 5% of the along- or across-track error; for an average zenith distance of 40º, the effect is 16%. The plots below, Figure 4, illustrates this, where we show the O-C results for laser ranges made within 2º of the local zenith. These results do represent good determinations of the true mean radial errors in the IGS orbits, namely -6.6 ±0.7 cm for GPS35 and –3.1 ±0.4 cm for GPS36.

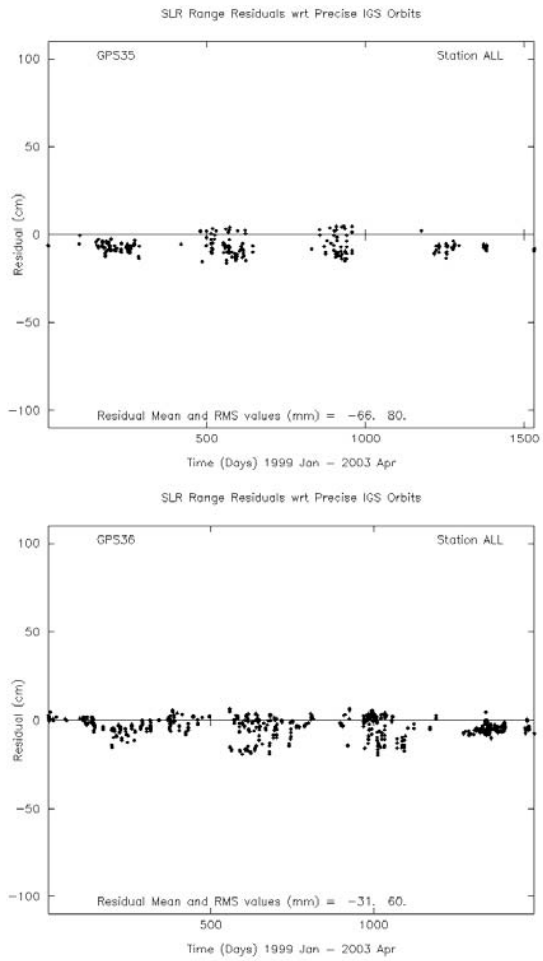

Figure 4. Time series of high elevation GPS-35 and 36 O-C values for 1999 January - 2003 April.

Conclusions

Since mid 2002, IGS GPS and GLONASS orbital solutions appear to be of similar accuracy, with radial rms precision better than 10 cm. A persistent ~5 cm radial bias exists in the GPS orbits which may be attributable to unidentified errors in the assumed locations of the phase centres of the microwave antennae; such errors could lead to bias during precise orbit determination. It is also possible of course that the assumed locations of the GPS laser arrays are incorrect. However, our discovery in the GLONASS 84 results of a similar mean radial error of approximately –5 cm leads us to surmise that if the GPS results are indicative of a scale problem for the whole GPS constellation, then that scale 'error' may have been imposed on the GLONASS orbits also.

Acknowledgement

The results presented here depend upon the observations and products of two of the Services of the International Association of Geodesy, namely the ILRS (http://ilrs.gsfc.nasa.gov) and IGS (http://igs.gsfc.nasa.gov). The support of all elements of these Services is gratefully acknowledged.

References

Appleby GM & Otsubo T *Evaluation of Potential systematic Bias in GNSS Orbital Solutions. In, Proc. 13th Int. Workshop on Laser Ranging*, Washington, DC, NASA/CP-2003-212248, October 2003

Otsubo T, Appleby GM, Gibbs P *GLONASS laser ranging accuracy with satellite signature effect.* Surveys in Geophysics 22 (6): 509-516 2001

Ineichen D, Springer T, Beutler G. *Combined processing of the IGS and the IGEX network* J. Geodesy 75 (11): 575-586 Nov. 2001

Seasonal effects on Laser, GPS and Absolute Gravimetry vertical positioning at the OCA-CERGA geodetic station, Grasse (FRANCE)

***Nicolas J.*[1], *Nocquet J.-M.*[2], *Van Camp M.*[3], *Boy J.P.*[4], *Hinderer J.*[5], *Amalvict M.*[4], *Gegout P.*[4], *Calais E.*[6], *and Walch J.-J.*[7]**

[1]ESGT-Laboratoire de Géodésie et Géomatique (L2G),ESGT, 1, Bd Pythagore, Le Mans, F-72000 France – [2]Department of Earth Sciences University of Oxford, Parks Road, Oxford, OX1 3PR, UK – [3]Royal Observatory of Belgium (ROB), Avenue Circulaire 3, B-1180 Brussels – [4]EOST/IPGS, 5 rue René Descartes, F-67084 Strasbourg Cedex, France – [5]NASA Goddard Space Flight Center, Greenbelt Maryland 20771, USA – [6]Dept. of Earth & Atmospheric Sciences, Purdue University, West Lafayette, IN 47907-1397, USA – [7]Observatoire de la Côte d'Azur (OCA), GEMINI, Avenue Copernic F-06130 Grasse, France

Contact: joelle.nicolas@esgt.cnam.fr

Introduction

Grasse observatory

- Grasse fundamental geodetic station
- Several techniques operating continuously and offering long time series
- Located in the Southern Western Alps on an ~ 1270 m high karstic plateau

Objectives

- Monitoring the vertical displacements of the Grasse fundamental geodetic observatory
- Comparing the time series of 3 independent geodetic techniques
  - –Satellite Laser Ranging (SLR)
  - –GPS
  - –Absolute Gravimetry (A.G.)
- Comparing the observations with geodynamical models of the different loading effects to better understand the annual signal
- 6-year time series spanning 1998-2003

Data

5 years of SLR time series

- LAGEOS-1 and -2 satellite monthly combined solution
- ITRF2000, GRIM5-S1 gravity field, IERS96 standards, no loading effect
- Mean 1-σ standard deviation of the vertical component: 3 mm

6 years of GPS time series

- Weekly CODE (Centre for Orbit Determination in Europe) position solutions expressed in ITRF2000 with CATREF software (*Altamimi et al. 2002*)
- IERS96 standards, correction for ocean tides (*Scherneck model, 1991*), no atmospheric loading correction
- Standard deviation on the vertical component : 4 mm

14 A.G. campaigns

- FG5 accuracy 1-2 µGal
- Corrections for earth tides, ocean loading, polar motion, and local atmosphere effects (- 0.3 µGal / hPa due to loading and to mass attraction)

Results

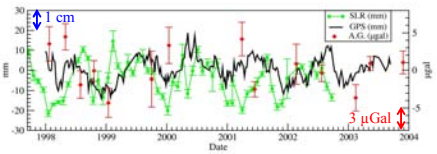

- Both SLR and GPS time series of the vertical component show a **significant annual signal**
- Non linear least squares algorithm to search for periodical signal :
  - – Amplitude : 5.5 mm (GPS) – 6.1 mm (SLR)
  - – Phase : maximum near July
- A.G. time series shows a more complex signal
  - – Annual term: 1.7 µGal (8.5 mm)
  - – Second principal term: 204-day period, 2.6 µGal (13 mm)
- BUT lack of data could mask an annual signal
- No secular gravity variation higher than ~ 0.7 µGal/yr at the 2-σ level
- If we take a -0.2 µGal/mm gradient to convert gravity variations into vertical deformation, A.G. signal amplitude larger than GPS and SLR signal
- Discrepancy should be due to contribution to gravity measurements of local ground water mass variations in the karst

Acknowledgements

We are grateful to the OCA laser team for their help during the measurements and to F. Barlier, P. Exertier, F. Mignard. We thank the GPS team for supporting the experiment. We thank Eric Calais who provided us the GPS results of the REGAL network. Finally, we thank M. Llubes (CNES) for providing us the time series of ocean loading.

Discussion

Impact of Newtonian effect

- A.G. measurement = deformation + Newtonian effect
- Initially, conversion of the A.G. measurements in vertical displacements with a ratio of – 0.2 µGal/mm But gradient time variable, for instance because of the water mass redistribution on the Earth surface
- Conversion of gravity into vertical displacement when loading effects is dangerous

➔ NO conversion in this study

- The A.G. variations (up to 8.8 µGal) would be explained by a cylindrical ground water table located at 800 m deep with either:
  - – 5 m level variation for a 1 km radius cylinder and 10% porosity
  - – 5 m level variation for a 5 km radius cylinder and 5% porosity
  - – 2.5 m level variation for a 5 km radius cylinder and 10% porosity
- But not enough information on the ground water table (deep, size…) located under the observatory to conclude (underground structures with permeable and impermeable layers not well known in this area)

Impact of GPS data processing

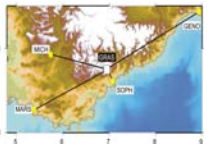

- Influence of the GPS time series computation strategy, and in particular the ZTD (Zenithal Tropospheric Delay) estimation
- Example: Comparison between 2 data processing strategies
  - –RGP (French permanent GPS network)
  - –REGAL (Regional permanent network in the Western Alps)
- Baseline between Marseille and Grasse (137 km)
- Estimation of annual term magnitude
  - –REGAL: 1.5 mm
  - –RGP: 2.5 mm
  - –Shift in phase: 2.5 months

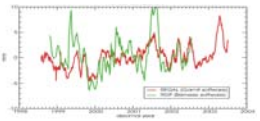

➔ Influence of the strategy can be of the order of 1 mm in estimating the annual signal amplitude

Local or regional effect ?

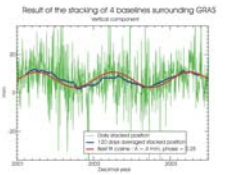

- Analysis of baselines between Grasse and surrounding permanent GPS sites from REGAL network
- If local effect: consistent signal for all the baselines
- If regional effect: random signal on the short baselines (noise)
- We stacked the time series of 4 baselines from REGAL solutions
- Stacked series clearly shows an annual signal with magnitude of 4 mm It corresponds to an annual signal of ~ 1 mm at Grasse (< 2 mm)

➔ 5-6 mm observed annual signal = 1 mm local + 4-5 mm regional

➔ The main part of the observed signal = regional loading effects

Loading models

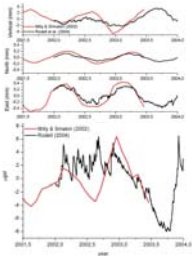

- Atmospheric loading model in vertical displacement from the ECMWF data
- Tidal oceanic loading in displacement and in gravity from the FES99 model
- Hydrological models in displacement and in gravity from (*Milly & Shmakin, 2002)* and (*Rodell et al., 2004)*: seasonal cycle difference of ~ 10-20%)

Observation and model comparison

- Atmospheric loading : 1-2.5 mm
- Ocean loading (tidal and non tidal effects) : 1 mm
- Hydrological loading : 2-3 mm
- Correlation between GPS and (atmosphere + hydrology) = 0.32

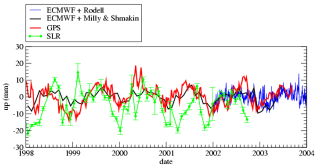

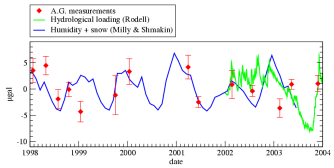

Conclusion and prospects

- Amplitude of the signal at magnitude close to the accuracy of each individual technique
- Main part of the annual signal explained (regional loading)
- A.G. = absolute, not dependent on any reference system = very good instrument to constraint the long term stability of the observatory
- Necessity of continuous gravity measurements on the Calern OCA observatory to monitor the variation and extract the local signal linked to the karst
- Comparison with local hydrological measurements (water catchment at Bramafan spring)
- Comparison with other SLR time series (shorter time sampling, new ILRS AWG results) in different sites where independent geodetic technique time series are available

EARTH ORIENTATION PARAMETERS FROM SATELLITE LASER RANGING

E. C. Pavlis
JCET/UMBC and NASA Goddard, Maryland, USA
epavlis@JCET.umbc.edu/Fax: +1-410-455-5868

Abstract

We present the new re-analysis of Satellite Laser Ranging (SLR) data to LAGEOS 1/2 and ETALON 1/2 for the definition of the Terrestrial Reference Frame (TRF) and its crust-fixed orientation (Earth Orientation Parameters –EOP). The TRF plays an important role in the multi-technique monitoring of temporal variations in the gravitational field and its very low degree and order components. This area is becoming extremely important with the launch of recent and future geopotential mapping missions for the referencing and calibration of the data and products from these missions. Satellite laser ranging (SLR) has for a long time monitored the continuous redistribution of mass within the Earth system through concomitant changes in the Stokes coefficients of the terrestrial gravity field. Seasonal changes in these coefficients have also been closely correlated with mass transfer in the atmosphere and oceans. The hydrological cycle contributions however are the most difficult to measure accurately so far. This latest analysis of the 1993-present SLR data set from SLR data for the International Earth Rotation Service (IERS) TRF (ITRF) development includes the weekly monitoring of such compound changes in the low degree and order harmonics. Along with the static parameters of the TRF we have determined a time series of variations of its origin with respect to the center of mass of the Earth system (geocenter) and the orientation parameters (pole coordinates and length of day) of the TRF, at daily intervals. The data were obtained by the ILRS global tracking network and they were reduced using NASA Goddard's GEODYN/SOLVE II software, resulting in a final RMS error of ~8 mm – close to the data noise level. We will discuss our solution, compare it to EOP series inferred from other techniques, and examine their spectrum.

Introduction

The analysis of Satellite Laser Ranging (SLR) data to LAGEOS, LAGEOS 2 and in recent years, the two ETALON satellites results in a SLR-based realization of the Terrestrial Reference Frame (TRF), complete, with a consistent series of Earth's Orientation Parameters (EOP) at daily intervals. We present here the new re-analysis of this data for the definition of the TRF and its crust-fixed orientation. This analysis of the 1993-present SLR data set for the International Earth Rotation and Reference Systems Service (IERS) TRF (ITRF), includes the weekly monitoring of weekly changes in the low degree and order harmonics (up to degree two). Along with the static parameters of the TRF we determine a time series of variations of its origin with respect to the center of mass of the Earth system (geocenter) and the orientation parameters (pole coordinates and length of day) of the TRF, at daily intervals. The data were obtained by the ILRS global tracking network and they were reduced using NASA Goddard's GEODYN and SOLVE II software, resulting in a final RMS error of ~8 mm – close to the data noise level. For a detailed discussion of the products from this analysis, see [Pavlis, these proceedings; and Pavlis, 2002]. In the following sections we will discuss our EOP results, compare them to EOP series inferred from other techniques, and examine their spectrum.

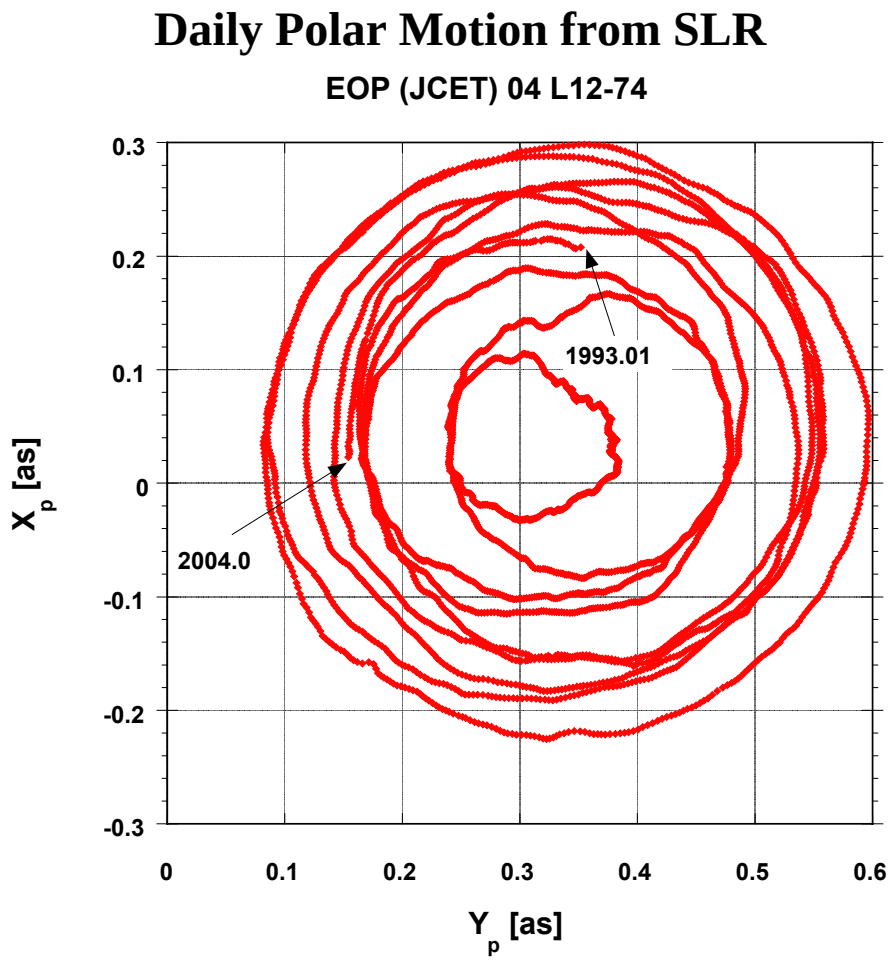

Figure 1. The daily resolution path of the pole from 1993 to 2004, EOP (JCET) L 2004.

The JCET/GSFC 2004 Solution

JCET/GSFC contributes weekly to the newly established ILRS Combination Project, for a SLR-technique optimally combined product, to be generated and submitted to the IERS. Since many years now, JCET has generated these weekly solutions for station positions EOP and long-wavelength gravitational harmonics, and generated annually a multi-year TRF realization on the basis of these weekly normal equations.

The weekly updates of the annual solution are generated by sequential addition of the normal equations generated from the last weekly solution, and they are subsequently solved using minimal constraints that assure the solution is aligned in a fixed manner with the chosen TRF definition, in this case ITRF2000 [Altamimi et al., 2002]. This approach has the advantage of being referenced to the same datum throughout the time, as opposed to the approach involving the estimation of the EOP from a single, stand-alone weekly set of equations, in a datum-free mode. The EOP that we produce out of our analysis exhibit datum continuity and are free from biases, trends, etc. from one week to the next. The “polhode”, the trajectory of the instantaneous rotational axis projected on the equatorial plane is shown in Figure 1.

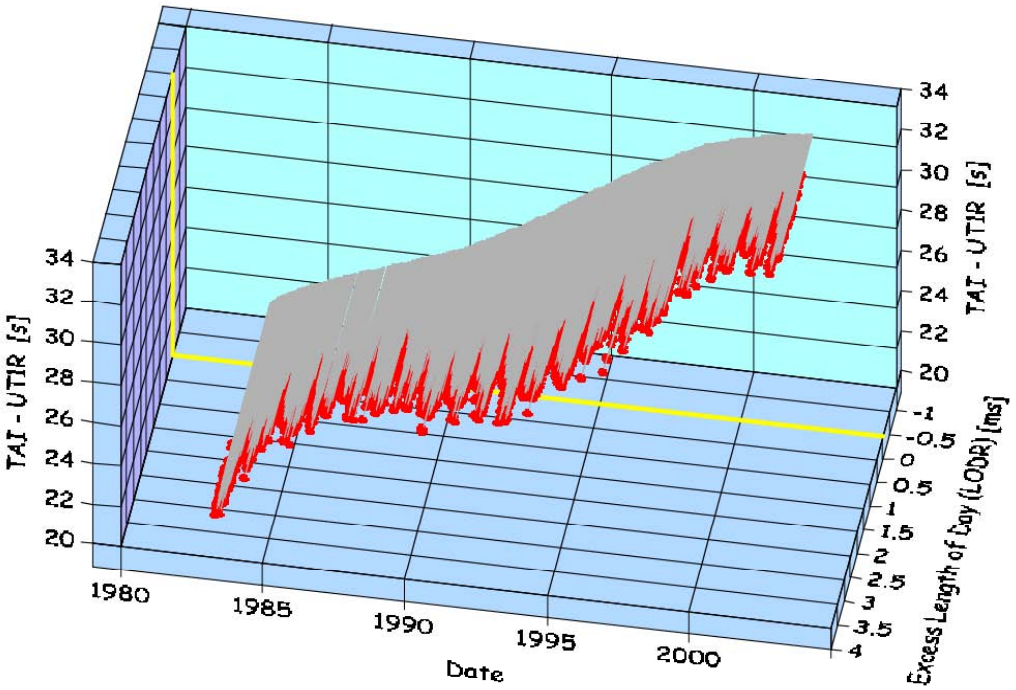

Figure 2. LOD variations at daily intervals, and integrated effect, EOP (JCET) L 2004.

Along with polar motion, satellite techniques are sensitive in variations in the orientation of Earth under the "quasi-inertial" frame realized by the dynamics of the orbit. Thus, although we are not sensitive to Earth Rotation in the absolute sense (UT1), we can observe its derivative, the Excess Length of Day (LOD). To do this we adopt an initial orientation based on Very Long Baseline Interferometry (VLBI), which is sensitive and does observe UT1 directly. By integration of the SLR-derived LOD, we can thus produce a UT1-like series also,

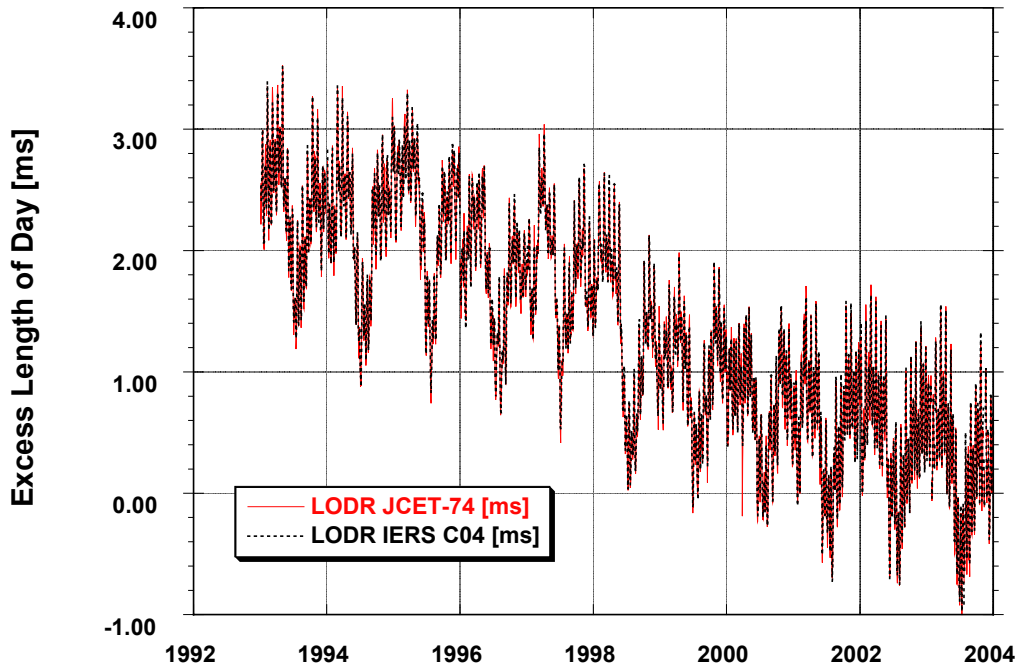

Figure 3. LOD from EOP (JCET) L 2004 and the a priori series, IERS C04.

although it should be recognized that it is not an independent product, since the long-wavelength evolution of these series is governed by the VLBI benchmark values adopted

every week. Figure 2 shows the surface produced by plotting the difference of these series from TAI (Int. Atomic Time) versus time (grey surface), and on that, the variations in LOD (red dots) at daily intervals. For a clearer picture of LOD that reveals the seasonal and decadal variations, you can see Figure 3.

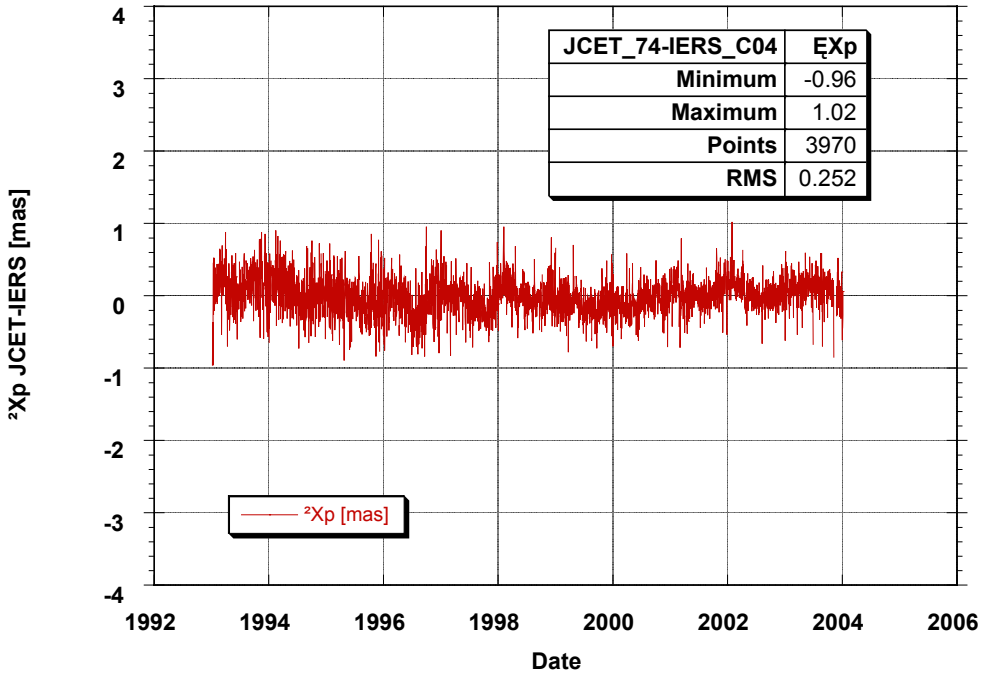

Figure 4. X-pole daily differences between IERS C04 and EOP (JCET) L 2004.

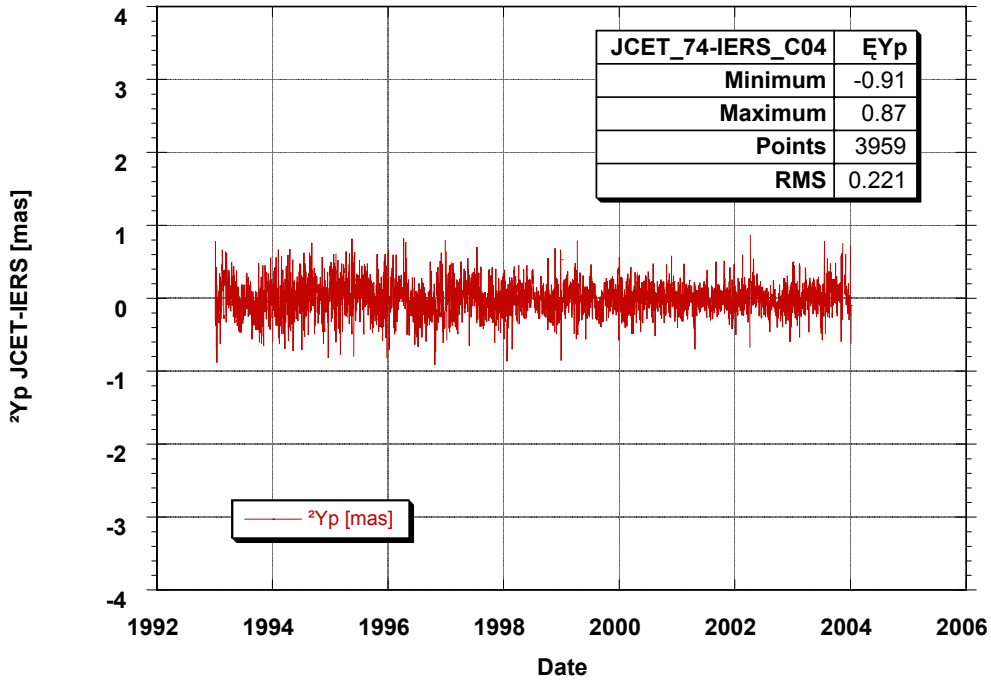

Figure 5. Y-pole daily differences between IERS C04 and EOP (JCET) L 2004.

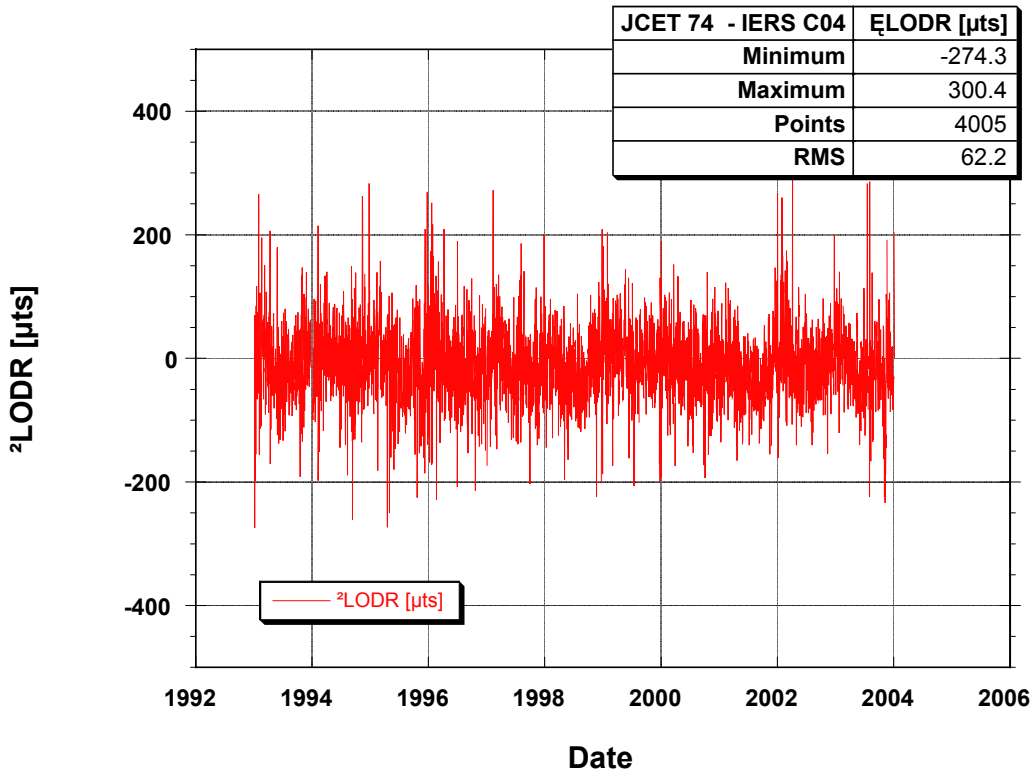

Figure 6. LOD daily differences between IERS C04 and EOP (JCET) L 2004.

The datum on which IERS C04 is based is different from that of ITRF2000, and that manifests itself as a bias and trend when comparing EOP series derived with ITRF2000 as the underlying TRF, versus the IERS C04 series. Once these biases and trends are removed though, the differences of the two series can be used to gauge the quality of the SLR products, since IERS C04 is heavily dependent on GPS and to a lesser extent, VLBI input. The time series of the differences in polar motion and LOD are displayed in Figures 4 through 6. It should be noted that the majority of the observed noise originates in the SLR series, as IERS C04 is a smooth series, albeit only very mildly so.

The EOP differences and associated statistics are based on an editing process that removed all points whose differences are larger than 4σ of the population. This is an insignificant percentage of the total and these outliers are primarily due to poor tracking on certain days, especially near the end-of-year period and Christmas. The results indicate that the accuracy of the SLR-derived Polar Motion is of the order of 0.25 mas and the LOD is at the 62 µs level. These are about 2-3 times higher than the internal precision of the results, and are primarily due to poor distribution of the tracking data, network asymmetries (north-south and east-west hemispheric distribution of tracking sites), and to a lesser extent, geophysical signals, primarily originating in the atmosphere, that are not yet modeled in our analysis.

Operational Series

For operational purposes, EOP users require a series that is precisely and consistently referenced to the currently adopted TRF, presently ITRF2000. JCET generates a parallel series along with the one discussed above, which is based on a TRF with all its sites fixed to the ITRF2000 positions. These series differs insignificantly from the nominal series, however

it tracks very closely the rapid service series from NEOS, the primary user of such operational solutions (http://maia.usno.navy.mil/).

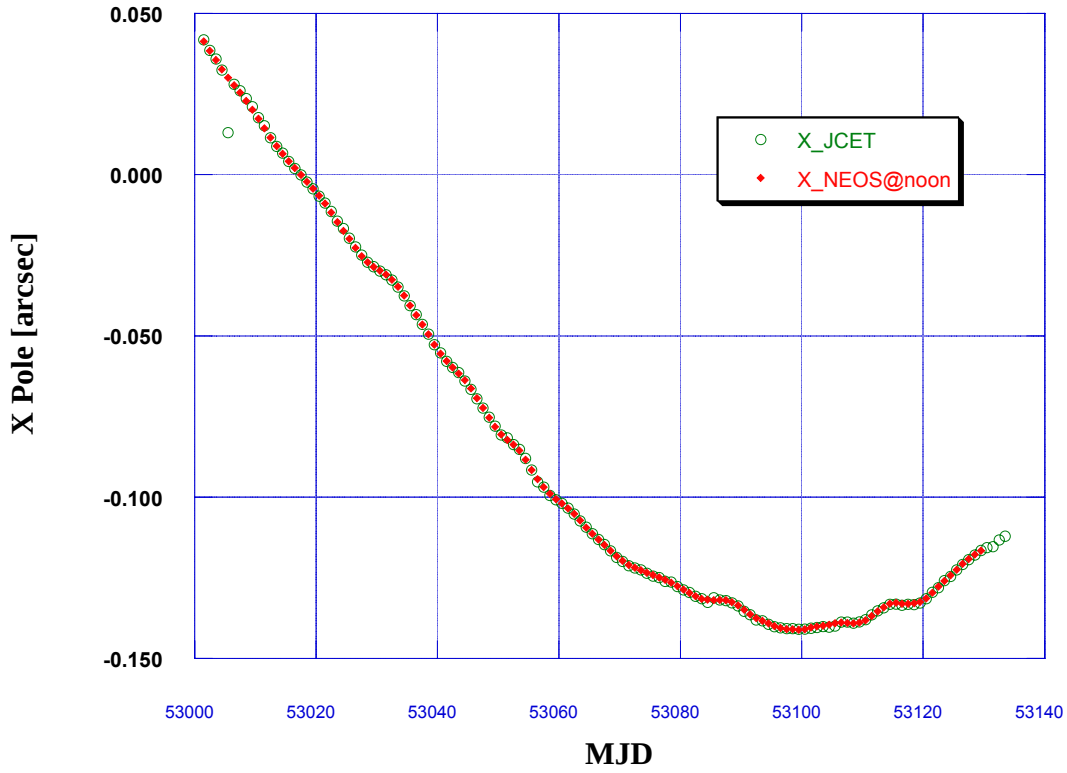

Figure 7. Comparison of X-pole from EOP (JCET) L 2004 and NEOS.

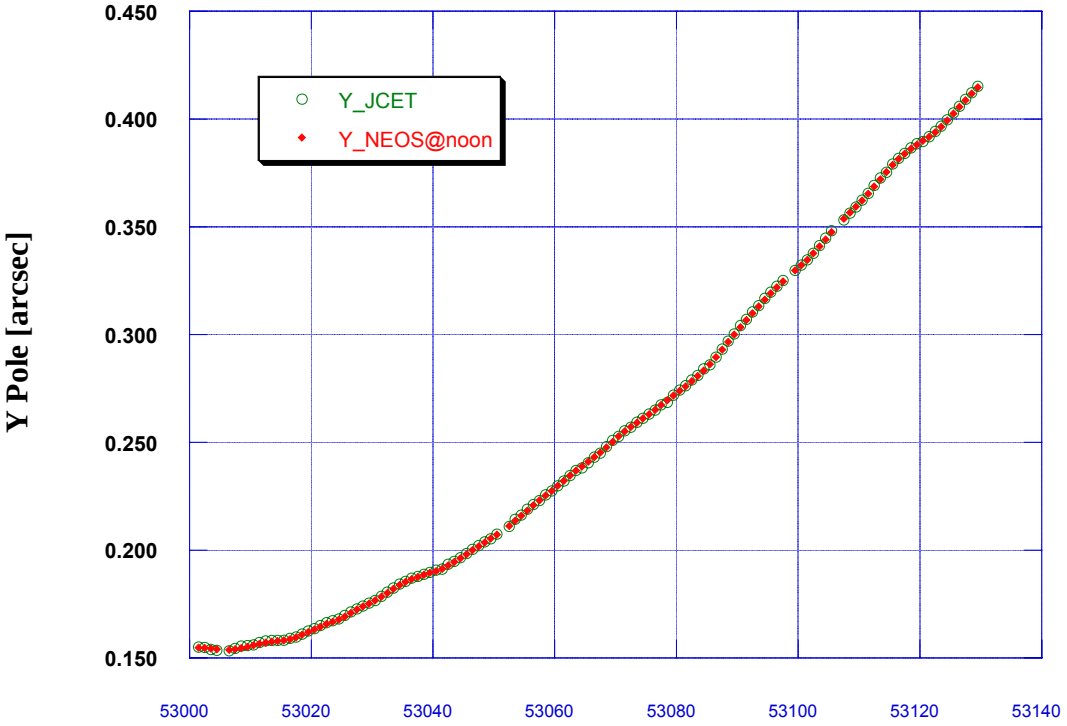

Figure 8. Comparison of Y-pole from EOP (JCET) L 2004 and NEOS.

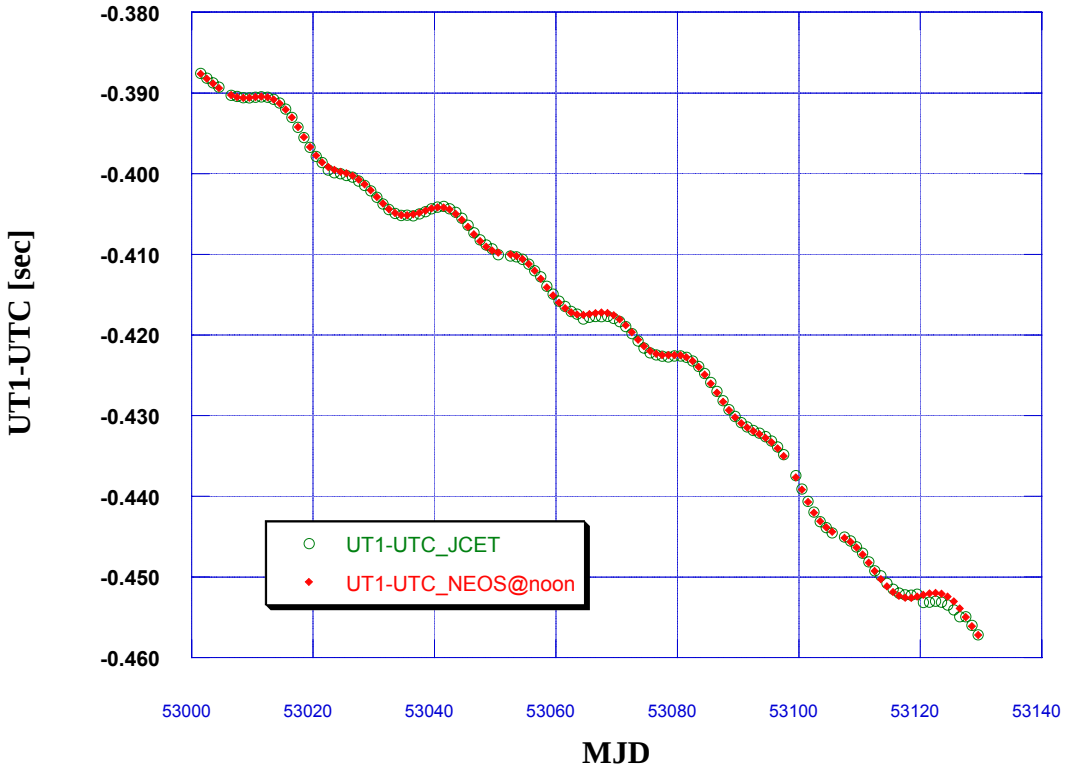

Figure 9. Comparison of UT1-UTC from EOP (JCET) L 2004 and NEOS series.

Figures 7 through 9 display a comparison of the strictly ITRF2000-based JCET/GSFC EOP series with the operational rapid service NEOS series. It is obvious that the two series are describing the same phenomenon in the long-and intermediate wavelength band, although there are events and shorter period variations that are not common to both. Because of the operational nature, the SLR results will sometimes show variable quality due to lack of tracking on certain days, station drop-outs, weather problems, etc. This can be alleviated in the future with a more uniformly distributed network, a greater availability of suitable targets (as opposed to only two LAGEOS), and improved, automated design of future systems.

Summary

The maintenance of the Terrestrial Reference Frame requires that we continuously monitor its evolution, and in particular its orientation with respect to inertial space, as well as with respect to the crust on which our tracking stations are located. Satellite Laser Ranging is one of the very first precise space geodetic techniques to contribute to this effort. In addition to contributing to the definition and the development of the TRF, it delivers in a routine fashion over many decades now, the daily motion of the pole and the daily variations in the Length of Day. In this presentation we examined one series of SLR contributions of EOP and compared them to those published by IERS, in their definitive IERS C04 series. We conclude from these comparisons, that the accuracy of SLR polar motion series is in the order of 0.25 mas, while the LOD series is accurate at the 60 μs level, both for daily resolution. Long, uniform quality series as those obtained from SLR, help extend the applicability of the current TRF in the past, and allow us to analyze data that were taken many decades ago, once again, with better models and better station positions, not available at the time of the data collection. This is the last SLR series produced on the basis of the old IERS Conventions 1996, the upcoming

analysis uses the newly adopted IERS Standards and Conventions 2003 [McCarthy and Petit, 2004], which will be the basis for future TRF development and EOP reference.

References

Altamimi, Z., Sillard P, Boucher C, ITRF2000: A new release of the International Terrestrial Reference Frame for Earth science applications, *J. Geophys. Res.*, 107 B02214, 2002.

McCarthy, D. D. and G. Petit, IERS Conventions (2003), IERS Technical Note (32), pp. 127, Verlag des Bundesamts für Kartographie und Geodäsie, Frankfurt am Main, 2004.

Pavlis, E. C., "High Resolution Earth Orientation Parameters From LAGEOS SLR Data Analysis at GSFC", in *IERS Technical Note16*, Observatoire de Paris, 1994.

Pavlis, E. C. Dynamical Determination of Origin and Scale in the Earth System from Satellite Laser Ranging, in *Vistas for Geodesy in the New Millennium*, proceedings of the 2001 International Association of Geodesy Scientific Assembly, Budapest, Hungary, September 2-7, 2001, J. Adam and K.-P. Schwarz (eds.), Springer-Verlag, New York, pp. 36-41, 2002.

TIME SERIES OF SATELLITE LASER RANGING STATION POSITIONS

D. Coulot (1-2), P. Berio (2), P. Exertier (2) and O. Laurain (2)
(1) IGN/ENSG/LAREG, 6 et 8 av. B. Pascal, F-77455 Marne la Vallée
(2) OCA/site de Grasse, av. N. Copernic, F-06130 Grasse
david.coulot@obs-azur.fr /+33-04-93-40-53-84/Fax:+33-04-93-40-53-33

Abstract

The International Terrestrial Reference System is the current positioning reference for all geodetic computations. Its computation is evolving through the use of time series of terrestrial station positions together with time series of Earth Orientation Parameters. As a first step, we study here a processing strategy to determine position time series by the Satellite Laser Ranging technique (ranging measurements -from the international tracking network- and precise orbit determination for LAGEOS satellites). We show that, owing to improvements in orbit computation, physical signals clearly appear in the position time series determined in a free network approach.

Introduction

The underlying of physical phenomena by experiments implies the use of measurements. The computation of a model based on these measurements requires to link them to a given reference. It is always the case in geodesy, science with a great amount of data. Therefore, terrestrial reference systems are of great importance. The International Terrestrial Reference System (ITRS) is the current positioning reference for all geodetic calculations. The computation of its representation (the International Terrestrial Reference Frame - ITRF) is evolving. Indeed, it will no more be based on single sets of coordinates and velocities of terrestrial stations but station position and Earth Orientation Parameter (EOP) time series. These time series are in better agreement with geodynamical phenomena and allow the computation in the same process of the terrestrial reference frame and the EOPs. In this context, to participate in the pilot project of the International Laser Ranging Service (ILRS) and to provide the International Earth Rotation and Reference System Service (IERS) with a French solution, we study a processing strategy to determine position time series by the Satellite Laser Ranging (SLR) technique. These time series should also allow us to underline and study geodynamical phenomena such as oceanic and atmospheric loading effects. In practice, the SLR technique limits inevitably the sampling of such time series (inability to track several satellites at the same time and no tracking with bad meteorological conditions). On the other hand, with its present sub-centimetric precision, this technique should be able to explain variations of station positions under the centimetric level. Therefore, to analyse accurately the geodynamical phenomena acting on the station movements and to participate in the ITRF calculation, our aim is to obtain time series with a reasonable sampling (ten days typically) and an accuracy better than 5 mm.

Processing Strategy

A geometrical approach

The method of computation of SLR station position time series typically used is a geometrical one (see [Nicolas 2001] and [Coulot et al 2002]). This method uses the two geodetic satellites LAGEOS-1 and LAGEOS-2. These two satellites are of great interest in SLR. Indeed, due to their high altitude (about 6000 km), they are less sensitive to Earth's gravity field and to non

gravitational forces. So they represent the most stable targets for SLR positioning. In a first step, orbital arcs of ten days are computed for both satellites. The ten-day length is a good compromise between a good distribution of SLR measurements with time and space and a good quality of the orbits. The average of mean weighted residuals of these computed arcs is about 2 cm for both satellites. In a second step, SLR measurements are used with orbital arcs to compute SLR station position offsets in a least-squares adjustment process. We assume that these offsets are constant over ten days to keep a reasonable distribution of the two LAGEOS measurements which are so cumulated. These offsets are given with respect to the position of the station given in ITRF2000 [Atamimi et al. 2002] corrected for Earth tides and the polar tide according to IERS96 conventions[McCarthy 1996]. The least-square residuals ("measurement minus model") of such adjustment are shown on Figure 1. We can clearly see a signal remaining in the residuals for one satellite pass. The model used for computation is not satisfactory and position offsets must be inaccurate. Indeed, there are two sources of inaccuracy on these offsets: the residual orbital errors and the mismodelling of the crustal movements.

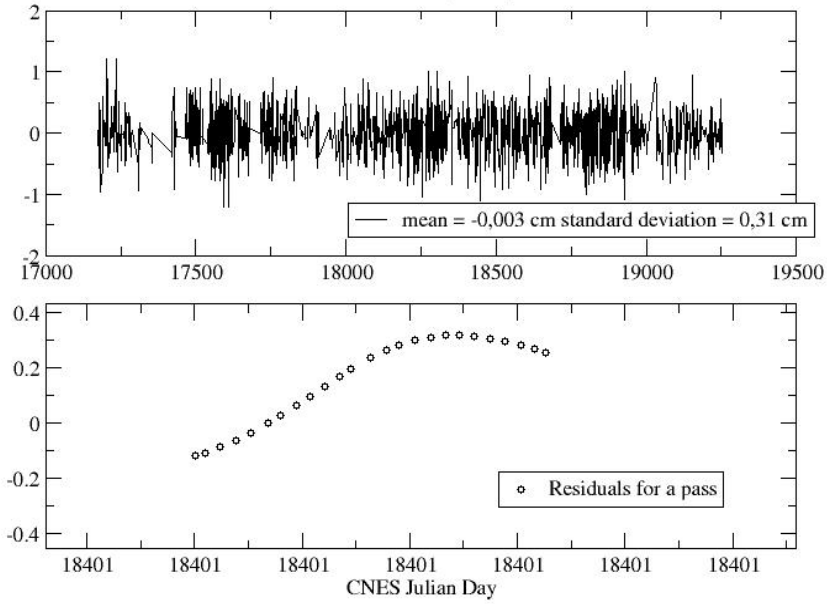

Figure 1. Least-square residuals for LAGEOS-1. Station 7835 (Grasse). The unit is cm.

Although they are of great quality, the orbital arcs are not perfect: physical models used for numerical integrations have limits and the SLR global tracking network is deficient in the southern hemisphere. Our simulations show that these residual orbital errors can induce inaccuracies at the centimetre level. The model used for station position variations (ten-day constant offsets) implies to suppose that phenomena like atmospheric loading can be averaged on ten days. Furthermore, with this constant model, we suppose that computed offsets represent the means of geodynamical signals on ten days. Our simulations show that it is not necessarily the case. Indeed signals are averaged not only temporally speaking but through the design matrix too. This averaging by the design matrix (matrix of partial derivatives of the measurements with respect to station position offsets) can induce inaccuracies at the level of few millimetres.

Improvements

To obtain position time series with an accuracy better than 5 mm, we have to reduce the impact of orbital errors and to use a satisfactoring model for station position variations.

Regarding orbital errors, the approach used is semi-dynamical. Hill's theory gives a physical model for orbital errors (periodical and constant functions in acceleration) [Crétaux et al. 1994]. By integrating second-order differential equations for satellite motion, we can obtain an empirical error function for the spatial position of the satellite. Using this empirical model, we can adjust orbital errors with station positions. But doing this gives rise to strong correlations between the various parameters estimated in the least-square process. To avoid for this, we first compute the orbital errors alone for each satellite using a minimal network. Then, orbital errors and station positions are computed together for this minimal network, orbital errors being constrained to their previous values. Finally, the orbital errors updated are fixed and position time series are computed for the whole SLR network. Figure 2 shows such time series for stations located in the USA.

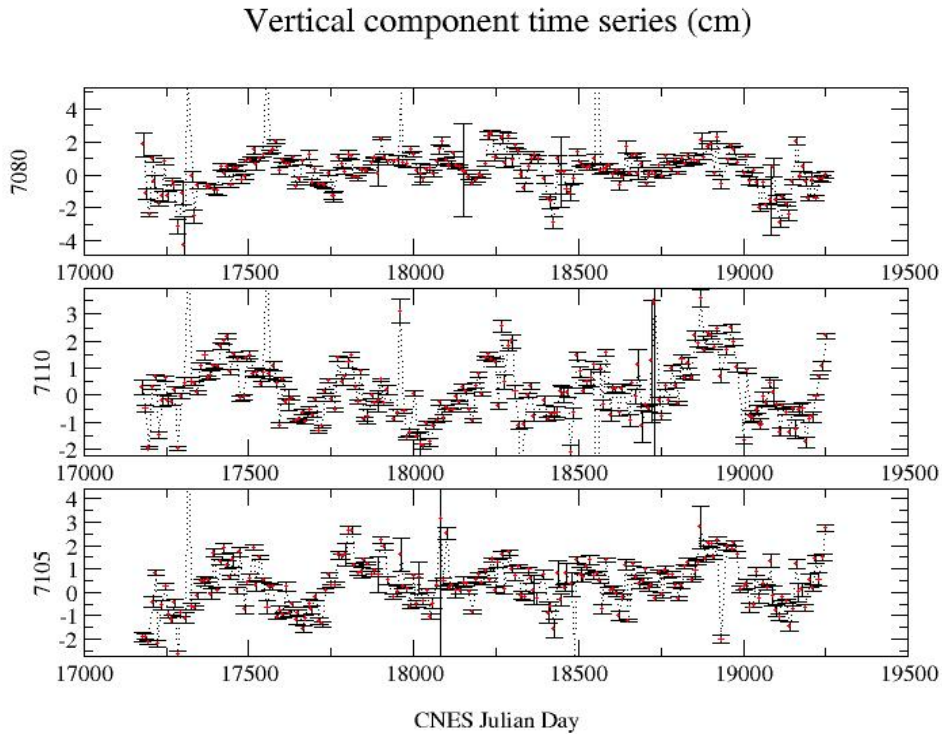

Figure 2. Vertical component time series. 7080: Mc Donald, 7110: Monument Peak and 7105: Greenbelt.

These time series still correspond to constant offsets over ten days. They clearly show periodical variations certainly linked to geodynamical phenomena such as loading effects. To better represent these physical signals and to reduce the average through the design matrix, we test alternative series such as periodical models or decompositions in wavelet basis. Range biases are also sources of inaccuracies on estimated station vertical components. To avoid for the great correlation (99%) between these biases and the vertical components, we use a method to “temporally decorrelate” these quantities. Indeed, biases are estimated over a month or more and station positions are still computed with a ten-day sampling. Moreover we estimate not one bias but a range bias per satellite. Doing this, correlations between biases and vertical components are not greater than 50%.

Conclusion and prospects

Our semi-dynamical method allows us to compute SLR station position time series with an accuracy of about 5 mm. We think that alternative models for station positions will allow us

to reach a better accuracy and, furthermore, to give a better representation of geodynamical phenomena we are interested for. Another way to obtain this is to reduce the sampling of time series. We could so determine station positions by combining measurements on several satellites like LAGEOS-1 and -2 (“classical approach”) and STELLA and STARLETTE (low geodetic satellites: altitude of about 800 km). The new challenge will then consist in reducing the orbital errors for STELLA and STARLETTE, which are greater than for both LAGEOS.

References

Altamimi, Z., Sillard, P. and C. Boucher, *Journal of Geophysical Research*, 107, B10, 2210-2214, 2002.

Coulot, D., Nicolas, J. and P. Exertier , *Bulletin d'Information de l'IGN*, 73, B14, 2002.

Crétaux, J.-F., Nouël, F., Valorge, C. and P. Jannière, *Manuscripta Geodetica*, 19, 135-156, 1994.

Mc Carthy, D.D., *IERS Conventions*, IERS technical note 21, 1996.

Nicolas, J., *La Station Laser Ultra Mobile. De l'obtention d'une exactitude centimétrique des mesures à des applications en océanographie et géodésie spatiales*, thèse de doctorat, 2000.

PROPOSED INTERNATIONAL INSTITUTE FOR SPACE GEODESY AND EARTH OBSERVATION (IISGEO)

L.Combrinck (1), A. Combrink (1), D Carter (2), M Pearlman (3), P. J. Shelus (4), J.Györgyey-Ries (4), R.R Ricklefs (4), J. R.Wiant (4), R Eanes (4), W. Gurtner (5), K. Nordtvedt (6), E. Samain (7), B.Engen (8), W Schlueter (9).

(1) Hartebeesthoek Radio Astronomy Observatory.
(2) NASA GSFC.
(3) Harvard-Smithsonian Center for Astrophysics.
(4) University of Texas at Austin.
(5) University of Berne.
(6) Northwest Analysis.
(7) OCA-CERGA.
(8) Geodetic Institute, Norwegian Mapping Authority.
(9) Fundamental Station Wetzell. ludwig@hartrao.ac.za /Fax: +27-12-3260756 /Tel: +27-12-3260742

Abstract

This proposal tables the transformation of the HartRAO Space Geodesy Programme into a joint HartRAO/SAAO/NASA/OTHER_PARTNERS international facility, dubbed the International Institute for Space Geodesy and Earth Observation (IISGEO). We propose that the main observing site of IISGEO be located at a suitable location (possibly Lesotho or the Sutherland site of SAAO in the Northern Cape). Equipment at HartRAO which in the future will become redundant due to old technology and inferior specifications will be phased out without losing valuable scientific collocation advantages. IISGEO will be a node of the proposed Global Geodetic Observing System (GGOS) and will have a large capacity building component, locally and regionally, with the production of high quality PhDs as target. Due to its multi-disciplinary nature, space geodesy is ideally suited for a diversity of projects which crosses the floor between astronomy, navigation, mathematics, geophysics, geology, orbital dynamics and space exploration. The development of IISGEO will aid in global earth stewardship and will be an important component of South Africa's contribution to the Global Earth Observation System of Systems.

Introduction

HartRAO currently has three main divisions: radio astronomy, space geodesy and science awareness. The space geodesy programme was a progeny of radio astronomy, as there is much synergy between geodetic Very Long Baseline Interferometry (VLBI) and radio astronomy techniques. The Space Geodesy Programme developed considerably during the last few years. With the addition of Satellite Laser Ranging (SLR) and Global Positioning System (GPS) to HartRAO, the facility has become one of only five fiducial geodetic sites in the world. Projects operate within the standards and guidelines of internationally recognised bodies, such as the International Association of Geodesy (IAG), International Astronomical Union (IAU) and their related services and commissions. The scenery of space geodesy is changing however as the need has been identified to improve the geometrical distribution of fundamental stations and to improve the accuracy and sampling rates of instrumentation. The location of space geodesy equipment at HartRAO is partially a spin-off from the NASA deep space tracking programme, the consequent CSIR establishment of radio astronomy utilising the tracking antenna, and the efforts from the space geodesy programme to collocate GPS and SLR with the telescope.

The HartRAO site was never "selected" in terms of scientific requirements in a way to optimize output based on astronomical seeing and cloud coverage criteria, so is not optimally located for scientific output, especially considering SLR or LLR. The future of space geodesy globally, is in the development and installation of dedicated geodetic VLBI antennas, (VLBI2010 project), KHz satellite laser ranging (SLR2000), denser GPS networks (AFREF) and the dissemination of data in near real-time. This concept is termed GGOS, an acronym for Global Geodetic Observing System, which is the first and only project of the newly restructured International Association of Geodesy (IAG).

Basically GGOS views the Earth system holistically by including the solid Earth, the fluid components and static and time-varying gravity field in its products. This concept combines different techniques, models, and approaches in order to achieve a better understanding of geodetic, geophysical and geodynamical processes. GGOS will provide the scientific and infrastructural basis for all geodetic global change research. This IAG Project commenced with the definition phase in 2003 and is based on the IAG Services. VLBI 2010 will operate at S, X and Ka bands. The present HartRAO telescope cannot operate efficiently at Ka band (32 GHz). VLBI2010 requires dedicated, 24 hour geodetic measurements monitoring earth rotation to find sub-diurnal rotational variations on the micro-arcsecond level as well as dedicated equipment to monitor Total Electron Content of the ionosphere, maintenance and expansion of the ICRF etc. Currently only 15 % of the HartRAO telescope is allocated to space geodesy which is a fraction of what is required. Opportunities for obtaining VLBI2010 radio telescopes could be had by collaboration with SKA/NASA DSN technology and projects.

Air pollution, proximity of large cities and industrial areas impose severe restrictions on HartRAO as a facility to expand and improve its activities in SLR and to develop LLR capability. Considering the suitability of the current SAAO Sutherland Observatory for optical astronomical observations, the existing infrastructure and synergistical benefits which can be had, it makes sense to locate the proposed International Institute for Space Geodesy and Earth Observation (IISGEO), which will be South Africa's component of GGOS, at the Sutherland site of the South African Astronomical Observatory (SAAO) site.

The sister of the Hobby Ebberly telescope (HET,) named SALT (Southern African Large Telescope), has just been built on the SAAO site. Other sites have been considered, such as a high elevation site located in Lesotho (elevation 3400 m), but logistical problems will be problematic and expensive.

SLR/LLR

HartRAO supports the ILRS through operating MOBLAS6 as part of the NASA SLR network. A host of scientific disciplines are being investigated using these data. NASA has agreed to provide an SLR2000 unit for the new station which will eventually phase out MOBLAS6. A new LLR station (and the only one in the southern hemisphere) will be developed in collaboration with Observatory Cote D'Azur (OCA, France), McDonald Observatory (NASA, USA), Fundamental Station Wetzell (BKG, Germany) and other partners. Discussions are in progress to move the OCA 1 meter SLR telescope to South Africa, in collaboration with OCA and CNES, where it will be refurbished and converted to a SLR/LLR unit, to be located at Sutherland. Co-authors of this proposal has shown interest and support for the development of IISGEO and a southernhemisphere Lunar Laser Ranging system.

Site Selection at Sutherland

The SAAO Sutherland site was considered during an evaluation of possible locations for a future geodesy site which would be suitable for SLR, LLR and VLBI. Collocation benefits already exist. We established an IGS GPS station during 1997 on the site. GFZ (Potsdam) has installed a superconducting gravimeter as part of their Geodynamics Observatory. An appropriate location was found which is shielded from the possible adverse effects of microwave radiation from the on-site housing (criteria for VLBI) and which will shield the optical telescopes from any direct laser emission from the SLR or LLR facilities. This site is located towards the south of the main hill where the optical telescopes are located. From within this small valley, a relatively open sky is available, with a 12 degree elevation cut-off towards the north and 11 degree cut-off towards the south. The east and west have low horizon cut-offs. This site is suitable in many respects and it would be very suitable to use as a location for IISGEO.

Figure 1 provides a near birds-eye viewpoint of the proposed site. As it is envisaged that a complete geodetic station will be built here, the whole area within the photo will be required to house SLR, LLR and VLBI instrumentation plus necessary short term accommodation, control room and laboratory facilities. The relatively dry air at Sutherland will be advantageous to SLR and LLR as well as VLBI due to reduced absorption of light and radio waves. In addition the characterisation of parameters such as Love numbers to enable accurate modeling of earth-tide movements at Sutherland will be possible using the GFZ Superconducting Gravimeter data. This will facilitate the removal of vertical movement of the site as a diurnal effect during observations. Earthtide causes the surface at Sutherland to move up and down with and amplitude of about 35 cm.

Management Structure

We propose a management structure for IISGEO which will consist of a board made up of representatives of its major stakeholders. This should include NASA, other foreign partners, the NRF and university representatives.

Site Features

Several features of the SAAO Sutherland location make it a preferred site:

- Collocation with existing GPS, SG and wideband seismometer
- Accessibility is excellent as it is flanked by an existing tar road
- Water and power tap-off point only 1.5 km away
- Low horizon, no topographical barriers with elevation higher than 15 degrees
- Astronomical seeing is approximately one arc-second
- Secluded valley shields site from radio frequency interference
- Mirror re-aluminising facility on-site
- Collocation with a major international optical obseratory

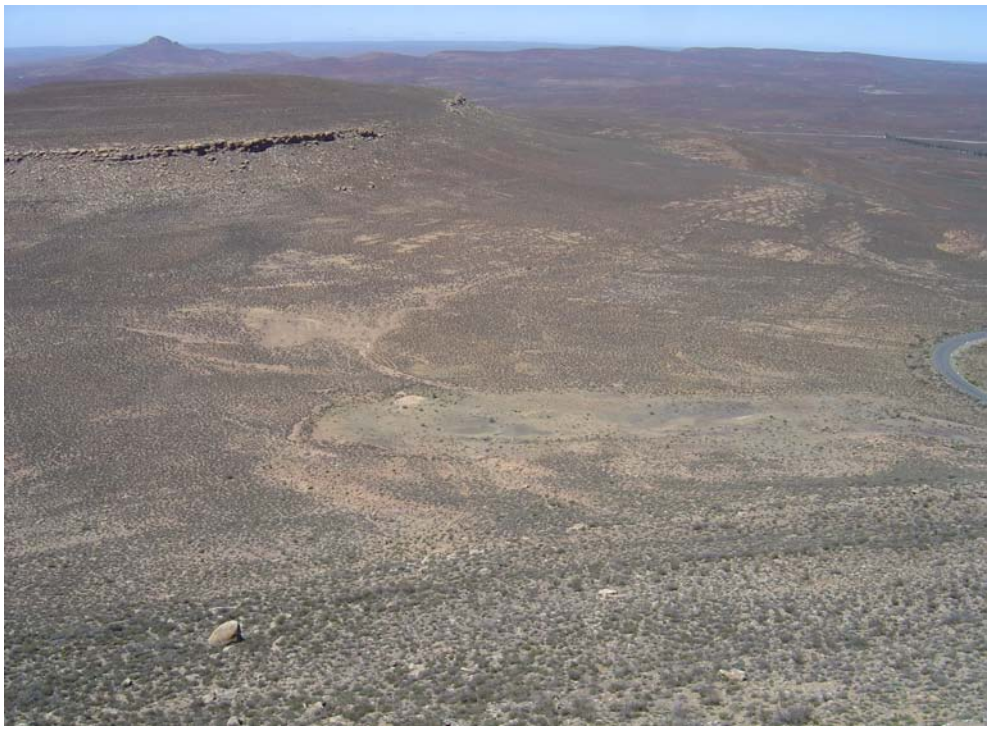

Figure 1. View of the proposed site for IISGEO observatory as seen from the southern side of the SAAO main observing hill. The tar road leading up towards the SAAO site is visible on the right-hand centre. Access to the IISGEO site is directly off this road.

Summary and Conclusión

IISGEO will be an investment in the future of Space Geodesy and will ensure continued participation in the global networks of VLBI, SLR and GPS from the southern part of Africa.

MEO THE FUTURE OF THE FRENCH LUNAR LASER RANGING STATION

E. Samain, G.Aridon, R. Dalla, P. Exertier, J. F. Mangin, G. Martinot Lagarde, J.L.Oneto, J.Paris, F. Pierron, J.M. Torre
Observatoire de la Côte d'Azur, 2130 route de l'observatoire, 06460 Caussols, France
Etienne.samain@osazur.fr

Abstract

It has been decided to enlarge the capability of the French Lunar Laser Ranging (LLR) station and to initiate a new research and development program, in addition to the actual program on the Moon. The LLR station is renamed MeO, for Metrology and Optics. Data acquisitions on low altitude satellites, that were performed until now by the French SLR station, will be done in the next future by MeO exclusively. The new research and development activity on laser ranging will include: new kind of laser modulation, filtering, detection, multicolors, Doppler, adaptive optics and also research on laser ranging in the solar system (ASTROD, TIPO). In order to achieve all these objectives, many developments are in preparation:

Telescope: high speed motorisation, high accuracy pointing,
Dome: new guiding device,
Building: focus laboratory, offices,
Optics: optical benches for experimental research, optical path,
Operational telemetry: lasers, high speed laser commutation, photodetection,
Software.

Introduction

The French laser ranging capacity is based on 3 laser tracking stations:

Lunar Laser Ranging (LLR) for the Moon and high altitude satellites,
Satellite Laser Ranging (SLR) for low altitude satellites,
Transportable Laser Ranging System (FTLRS) for mobile campaigns.

Since the beginning of the year 2004, a new organization has been set up that will permit to initiate a new research and development activity, in addition to the actual program on the Moon and on satellites. The CERGA department was restructured and a new name was given: Gemini. It has been decided to centralize our work on both LLR and FTLRS stations and to stop, in the next future, SLR definitively. LLR station which was built at the end of the seventies, to track exclusively the Moon, will be transformed to be able to track targets from low altitude satellites up to future interplanetary spacecrafts. Because the station will become more versatile, it will loose its LLR denomination and will be renamed MeO: Metrology and Optics.

Stations developments

• Optics

The station is based on a Ritchey Chretien telescope having a diameter of 1.5 m connected to a Nd:YAG laser at 10 Hz (figure 1).

Until now, the same telescope was used for the laser emission (laser located in a fix laboratory), and the detection and the video (units on a Nasmyth table in the dome of the telescope). The optical commutation was performed by a 2 rotating mirrors at 10 Hz, one for the emission and the reception, and the other one for the commutation between the video and the reception. All the fold mirrors was treated for both 532 and 1064 nm and the telescope was treated with a classical metalization.

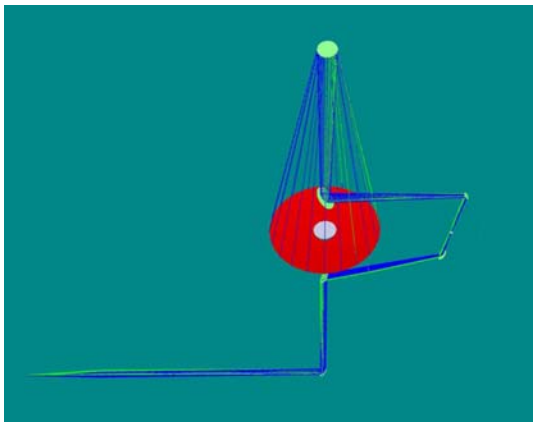

Figure 1. Ritchey Chretien telescope and fold mirrors.

In the new design :

- Optical path for both emission and reception will be common in order to minimize the pointing differences between the beams. The detection module is put together with the laser on a common optical bench. The field of view allowed by the geometry is 300 arcsec. This imply large fold mirrors having a diameter of 200 mm.
- The optical flux coming from the telescope will be distributed through 5 different optical benches with the capability to dispatch the flux simultaneously on 2 different benches.
- The laser commutation will be well suited for low altitude satellites, that is to say capable of switching in less than 1 ms.
- The spectral bandwith for both emission and reception will be in the range 400-1100 nm.

The principle of the new laser commutation is shown on figure 2. It uses an active retarder plate based on liquid crystal. This allow to switch beams having diameter as large as 100 mm. The separation between the input and the output is performed by 2 polarizer beam splitters. A retarder plate (with a circle arrow on the figure) is inserted between these 2 polarizers. It is controlled by an active signal synchronized with the laser. This plate is not active during the laser shoot so that the laser beam (horizontaly polarized) went through the system without any

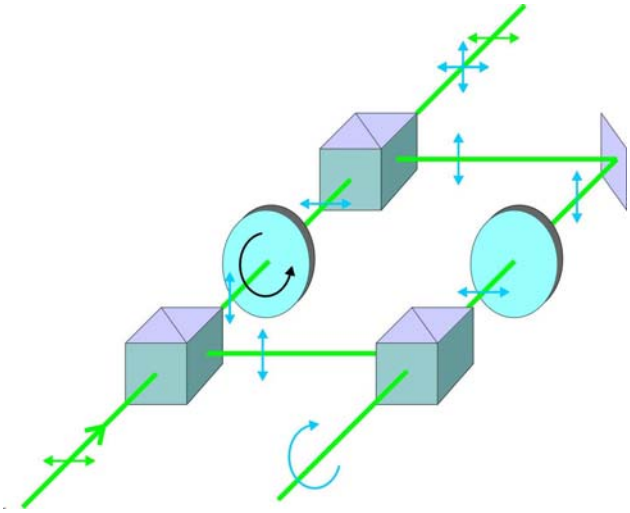

Figure 2 Laser commutation based on liquid crystal retarder plate.

modification.The return beam, which is depolarized by the target, is split into 2 distinct polarizations by the output polarizer. The vertical polarization is directly sent into the

reception path while the horizontal one is actively transformed in vertical polarization by the retarder plate and mixed with the first direct vertical polarization by a third polarizer. At the end, both vertical and horizontal polarizations are recovered even if the target destroys the polarization figure. Some damage threshold tests have been done on a 10 mm retarder plate. The limit has been mesured at 30 mJ/cm² @ 200 ps. It is due to the temperature elevation of the liquid and should be solved in the next future with a suitable radiator.

All the mirrors, expect the primary mirror, will be treated by some broadband dieletric coatings made by Sagem. The damage threshold is 10 J/cm² @ 10 ns and the mean value of the reflection factor is greater than 98 % (figure 3). This coating has been already used by the Bern University.

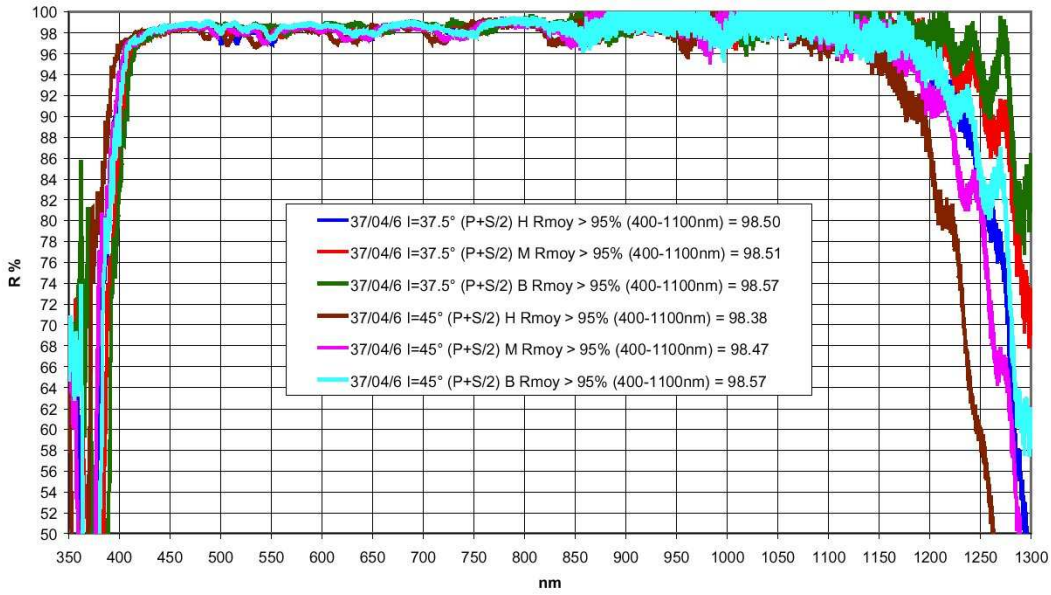

Figure 3 : Broadband dielectric coatings (Sagem, France).

• Laser

The laser will be implemented on a large optical bench together with the photodetection system. It will include 3 ND:Yag cavities, one to produce laser pulses at 20 ps and 50 mJ, the second one for 200 ps and 300 mJ and third one for 2 ns and 1 J. The amplification system will be common for these 3 cavities. It will include a regenerative amplifier that will be able to produce coherent pulse trains.

• Telescope

The mechanical part of the telescope is presented in figure 4. Both the azimuthal and elevation rotations, performed until now with endless screws and tooghed wheels, will be replaced by a direct drive system. It will allow to improve the pointing accuracy of the telescope and to increase the speed limit. The cumulated pointing error of the actual system is better than 0.5 arcsec integrated over 1000s (figure 5).

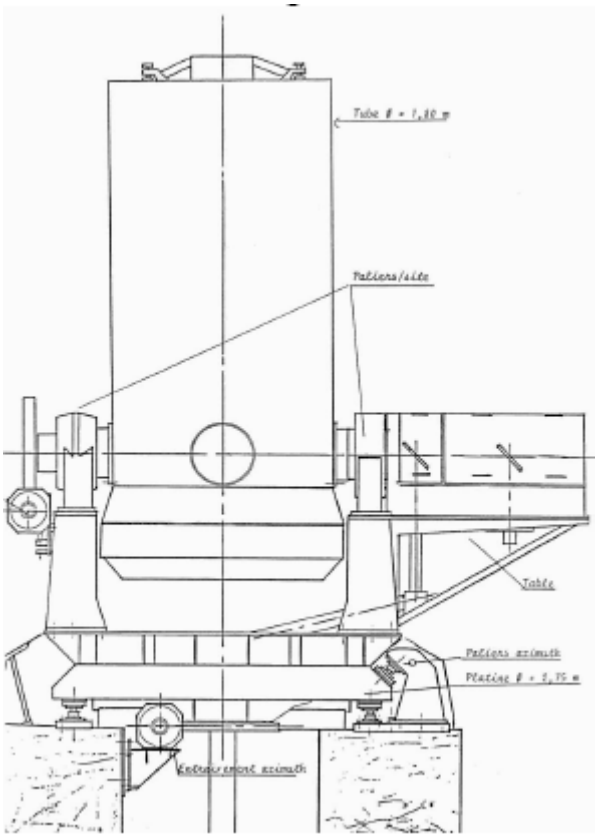

Figure 4 : Telescope

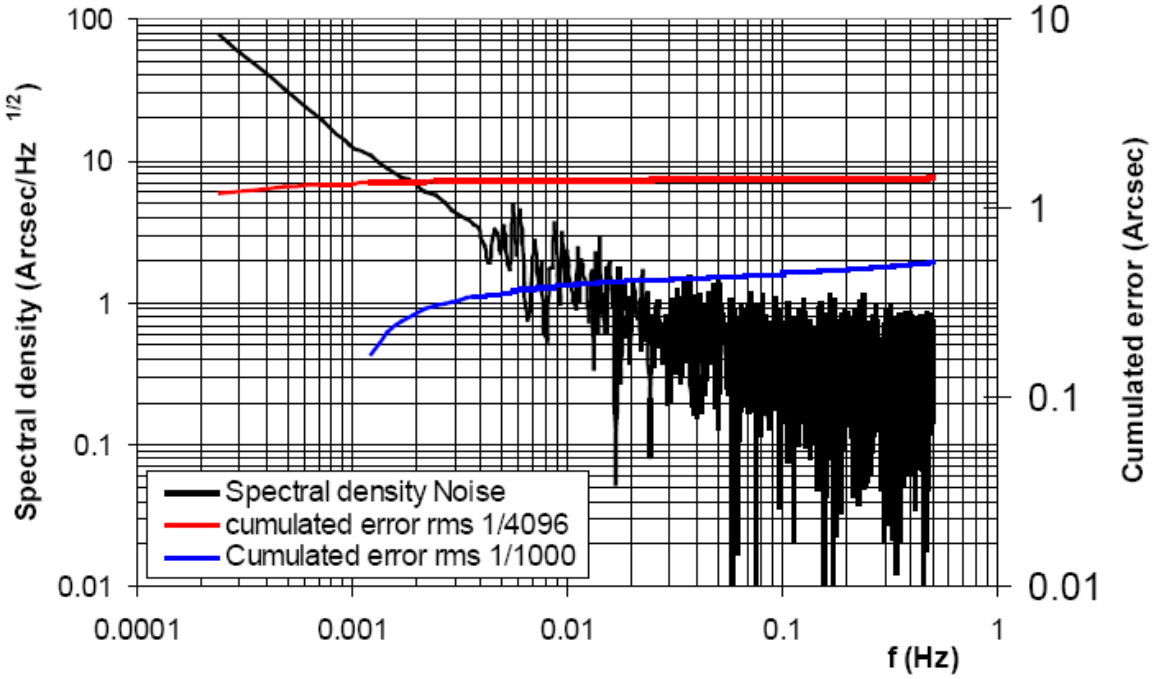

Figure 5 : Spectral density of pointing and cumulated error in arcsec rms.

• Software

The software synoptic is shown on figure 6. It will be based on a Win32 client/server architecture. The station will be piloted by a central machine linked through ethernet conections to instrumental machines

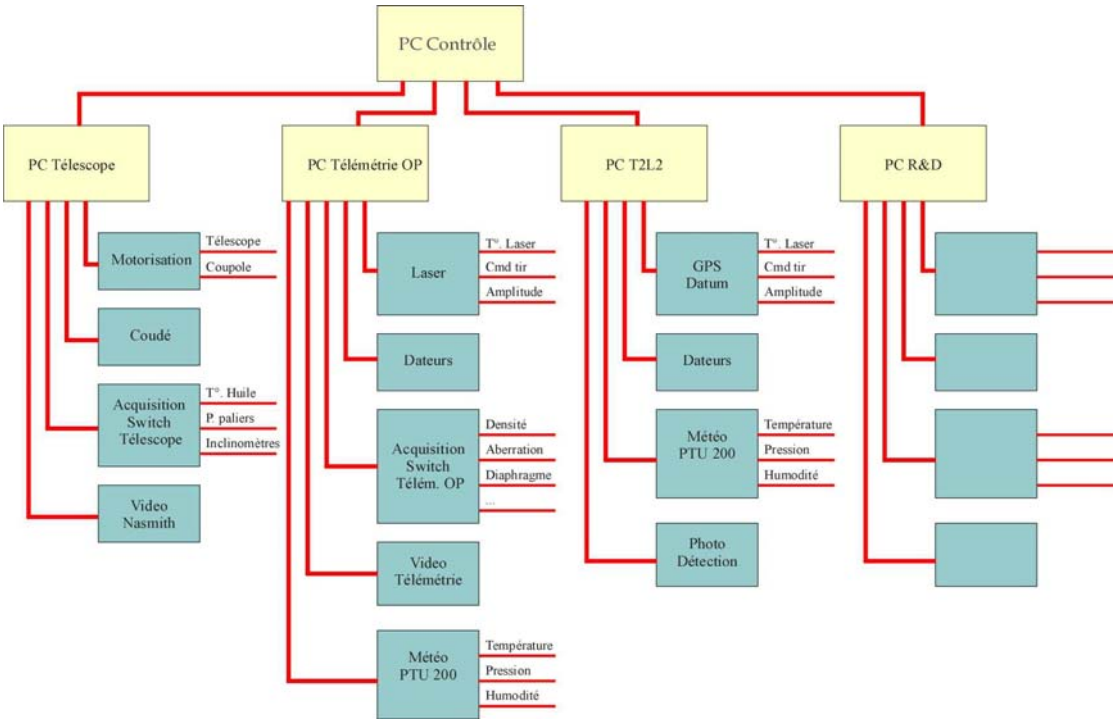

Figure 6 Synoptic of the MeO station software.

Conclusion and prospective

All these developments are crucial for the future to be able to track both low and high altitude satellites and also to have the capability to integrate new research and development projects on the station. In the medium term, laser ranging in France will be done by the FTLRS station for low altitude satellites and mobile campaigns, and by the MeO station for all targets and specially the moon. Our future research and development program will include :

Coherent modulation,
Femtosecond lasers Streak camera multicolor laser ranging,
Multiphotons detection,
Cw laser and low noise video for target research,
Time transfer by Laser Link (T2L2).

Even if this program represents a large amount of work, tracking satellites and tracking the moon will remain the most important task for our station.

MEO IMPROVEMENTS FOR LUNOKHOD1 TRACKING.

J. M. Torre, M. Furia, J.F.Mangin, E. Samain.
Observatoire de la Côte d'Azur, avenue Copernic, F06130Grasse. jeanmarie.torre@obsazur.fr

Introduction

The LLR experiment has started when ApolloXI disposed retroreflectors in 1969[1]. Since this date, five targets have been set down on the Moon. Three by American missions (ApolloXI, XIV, XV) and two by Soviet missions (LUNA17, LUNA21). The targets of LUNA missions are installed on rovers (Lunokhod1 and 2). One of these targets, put down by LUNA17 mission, is not used at the present time.
The goal of the MeO improvements is to be in the best conditions to try to acquire data on Lunokhod1 retroreflectors[2].

Lunokhod1 target constitution

This target is made by fourteen triangular retroreflectors (length side:10.6 cm). Its size is 44 cm by 19 cm. These retroreflectors have been optimised for 694.3 nm (ruby laser), nevertheless the efficiency increases by 8% at 532 nm. These retroreflectors are efficient for 0 to 25 degrees beam incidence angle. The sides of the corner cube are covered by silver for best efficiency. The drawback of the silver coating is the deformation of the corner cube when the temperature increases.

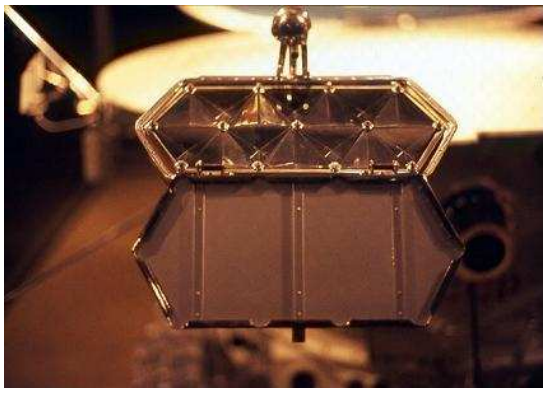

The following table gives the sensitivity tothe sun light.

i sun	Night	90°	85°	71°	42°	23°
η	0.82	0.74	0.44	0.16	0.09	0.045

In conclusion, this target lost half of the efficiency twelve hours after the sunrise[3].

Previous campaigns

The first echoes have been obtained in December 1970 at the Pic du Midi Observatory (France) [4]. After this date, the Lunokhod1 vehicle moved to another place. Since this date, no return have been obtained. From Soviet Union, few returns have been obtained in 1974, but not enough to be used for research. In 1975 and 1998, some attempts have been done at Mac Donald observatory (Texas, USA) and Grasse LLR station (France) without any good result.

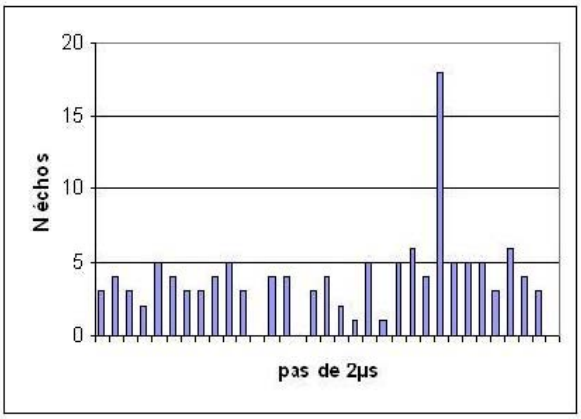

Tracking constraints

- Reflector coordinates

The tracking difficulties are due to the bad knowledge of the reflector positioning. In 1998, Jim Williams provided a set of coordinates, probably with a large uncertainty. In the end of 2003, Jim Williams furnished a new coordinates set, based on a possible identification of the site of the Lunokhod1 rover by Prof. P.J. Stooke (University of Western Ontario in Canada). The uncertainty estimates are 1000m for longitude and 600 m for latitude. The total range uncertainty is about 4 microseconds with 45 nanoseconds/hour range rate.

- Goodtime ranging

The best ranging period is when the Moon is high in the sky (lowest crossing atmosphere thickness), and when the reflector is in to the night (highest efficiency and low noise).

This favourable period begins in January and finish in June. The observations are done over six days, from four days after the new Moon to two days after the quarter.

MEO improvements

- Detection improvements

The main difficulty is due to the bad knowledge of the distance. In fact, even if the position is not well known, the spot size of the laser beam on the Moon having six kilometres, the pointing is not too difficult. On the other hand, a kilometre uncertainty on the distance, make you activate during few microseconds the SPAD. To be in these conditions, we have had to remove the used SPAD (SSO AD230) and to adapt a new one (K14) less noisy.

- Laser improvements

On the other Moon targets, we use a QUANTEL laser with 150mJ pulse in 300 picoseconds. Due to the lower range rate prediction, the echo detection is done by an histogram. As we

have seen before, the range rate prediction of Lunokhod1 could reach 0.75 nanoseconds/minute. In ten minutes, if we want to detect echoes with an histogram like for the other targets, we need to have five nanosecond histogram step and height microseconds width. With such a large rate, the accuracy is not very good. Instead of using SLR software to increase the accuracy by time bias corrections, we choose to increase the efficiency by changing the laser.

Our BMI laser has been adjusted to emit 0.65 Joules in 7 nanoseconds pulse at 10 times per second rate. In this case the efficiency is four times higher than with the QUANTEL laser.

- Conclusions

With the new SPAD, the station is slightly less efficient, but we are able torange with 8μs gate. The new laser is four times more powerful.

Scientific interests

Like it has been written by Jim Williams, this reflector should be good for:

- Physical librations:
  - Northsouth spreadincreases of 36%
  - Eastwest spreadincreases of 20%
- Tides displacement
- New accurate location on the Moon

2004 Campaign

The attempts have been made during three Lunar days from March to the end of May. Only six nights by Lunar day are good for the observations.

The following table gives the results.

On the first line you have the quality of the sky and on the second line the number of echoes on ApolloXV corresponding to this quality.

On the three following lines you see the number of nights lost when the sky was cloudy, or the number of attempts when it was possible torange.

We have done an attempt on Lunokhod1 only if it was preceded by goodresults on ApolloXV. Each attempt is ten minutes ranging time.

Sky quality		Very clear	Clear	Hazy	Cloudy
AXV echoes		N > 50	50 > N > 10	N < 10	0
Nights or attempts	March	0	8 attempts	9 attempts	3 nights
	April	0	0	5 attempts	3 nights
	May	0	0	0	6 nights

Conclusions

We began the campaign too late, in March.

We have only installed the nanosecond laser in April.

We have not yet had good weather. It should be better to begin in December or in January, when the weather in the evening is often better than in spring.

We will try again next year with new improvements, except if there are results in the two new and performing Lunar Laser Ranging stations in Matera (Italy) or Apache Point Observatory (USA).

References

1. P. L. Bender, D. G. Currie, R. H. Dicke, D. H. Eckhardt, J. E. Faller, W. M. Kaula, J. D. Mulholland, H. H. Plotkin, S. K. Poultney, E. C. Silverberg, D. T. Wilkinson, J. G. Williams, C. O. Alley, "The Lunar Laser Ranging Experiment", Science, 182, 229238, (1973).

2. G. I. Petrov, "Investigation of the Moon with the Lunokhod 1 space vehicle", Space Research, XII, 112, (1972).

3. M. Fournet "Le réflecteur laser de Lunokhod", Space Research, XII, 261277, (1972).

4. A.Orzag, J. Röch, O. Calame, "La station de télémétrie de l'observatoire du Pic du Midi et l'acquisition des cataphotes français de Luna 17", Space Research, XII, 205210, (1972).

LUNAR RANGING FROM MOUNT STROMLO

B. Greene, C. Smith, Y. Gao, J. Cotter, C. Moore, J. Luck, I. Ritchie
EOS Space Systems Pty Limited
bengreene@compuserve.com, Ph +61 2 6298 8010, Fx +61 2 6299 6575

The Mount Stromlo SLR system is co-located with the EOS space Research Centre [SRC] which has extremely powerful laser tracking capabilities.
The SLR normally operates with 0.5W of laser power, but in recent months the system has been coupled to an available 50W laser and LLR sessions have been programmed from late May by EOS, using EOS research funds.
The LLR link should be acceptable with 50W laser power, since the SLR telescope has 100cm high-quality optics and 5 microradian absolute pointing. The accuracy of the experimental configuration will be at the 10 cm level, but this can be later upgraded once target links have been established.
The initial objective of this experiment is to determine [update] the relative responsiveness of various lunar targets, and establish operational parameters for a long-term lunar capability using millimetre-accurate systems.
The operational configuration of this system, and any initial results will be presented.

LUNAR LASER RANGING SCIENCE

James G. Williams, Dale H. Boggs, Slava G. Turyshev, and J. Todd Ratcliff
Jet Propulsion Laboratory, California Institute of Technology, Pasadena, CA, 91109, USA.
James.G.Williams@jpl.nasa.gov, Dale.H.Boggs@jpl.nasa.gov,
Slava.G.Turyshev@jpl.nasa.gov, J.Todd.Ratcliff@jpl.nasa.gov.

Abstract

Analysis of Lunar Laser Ranging (LLR) data provides science results: gravitational physics and ephemeris information from the orbit, lunar science from rotation and solid-body tides, and Earth science.
Science from the orbit. *Sensitive tests of gravitational physics include the equivalence principle, limits on the time variation of the gravitational constant G, and geodetic precession. The equivalence principle test is used for an accurate determination of the Parametrized Post-Newtonian Parameter β. Lunar ephemerides are a product of the LLR analysis used by current and future spacecraft missions. The analysis is sensitive to astronomical parameters such as orbit, masses and obliquity. The dissipation-caused semimajor axis rate is 37.9 mm/yr and the associated acceleration in orbital longitude is -25.7 "/cent^2, dominated by tides on Earth with a 1% lunar contribution.*
Lunar science. *Lunar rotational variation has sensitivity to interior structure, physical properties, and energy dissipation. The second-degree lunar Love numbers are detected; k2 has an accuracy of 11%. Lunar tidal dissipation is strong and its Q has a weak dependence on tidal frequency. A fluid core of about 20% the Moon's radius is indicated by the dissipation data. Evidence for the oblateness of the lunar fluid-core/solid-mantle boundary is getting stronger. This would be independent evidence for a fluid lunar core. Moon-centered coordinates of four retroreflectors are determined.*
Earth science. *Station positions and motion, Earth rotation variations, nutation, and precession are determined from analyses.*
Future. *Extending the data span and improving range accuracy will yield improved and new scientific results. Adding either new retroreflectors or precise active transponders on the Moon would improve the accuracy of the science results.*

Introduction

A 13th Workshop paper gave a review of lunar science and gravitational physics results plus an extensive comparison of the dynamical and analysis experiences for the Moon and Earth (Williams and Dickey, 2003). This present paper updates JPL lunar science and gravitational physics results and discusses future Lunar Laser Ranging (LLR). For recent results from the Paris Observatory analysis center see Chapront, Chapront-Touzé, and Francou (2002).

Lunar science update

LLR is important for understanding the properties of the Moon. Early LLR data were important for determining gravitational harmonics and moment differences and discovering free librations and strong rotational energy dissipation. Now the accurate data of recent years permits the Moon's interior properties to be investigated.

Tides on the Moon

The elastic response of the Moon to tidal forces is characterized by Love numbers. The second-degree tides are strongest and these tidal displacements are sensitive to the second-degree Love numbers $h2$ and $l2$ while the rotation is sensitive to the potential Love number $k2$. The amplitudes of the two largest monthly terms are both about 9 cm. In practice, LLR

solutions are more sensitive to $k2$. A solution, with data from 1970 to 2003, gives $k2 = 0.0227 \pm 0.0025$ and $h2 = 0.039 \pm 0.010$ (Williams, Boggs, and Ratcliff, 2004). $l2$ was fixed at a model value of 0.011. For comparison, there is an orbiting spacecraft determination of the lunar Love number $k2 = 0.026 \pm 0.003$ determined from tidal variation of the gravity field (Konopliv et al., 2001).

Accurate Love numbers are valuable because they give information on the elastic properties of the lunar interior. For comparison with the solution results, model calculations have been made for lunar Love numbers. Love number calculations start with an interior model (Kuskov and Kronrod, 1998) which is compatible with seismic P- and S-wave speeds deduced from Apollo seismometry. There is little seismic information below 1100 km and the seismic speeds have to be extrapolated into the deeper regions above the core. The 350 km radius of the fluid iron core was adjusted to match the LLR-determined $k2$ and small adjustments were made to the densities to satisfy mass and moment constraints. In addition to matching the above $k2 = 0.0227$, the model calculations give $h2 = 0.0397$ and $l2 = 0.0106$.

The LLR solutions are also sensitive to tidal dissipation (Williams et al., 2001). In general, the specific dissipation Q depends on frequency. In the above solutions, the whole-Moon monthly tidal Q is found to be 33±4. For $k2 = 0.0227$ the power-law expression for tidal Q as a function of tidal period is determined to be $33(\text{Period}/27.212\text{d})^{0.05}$ so the Q increases from 33 at a month to 38 at one year. At tidal frequencies the Moon exhibits strong dissipation.

A molten lunar core

Evidence for a distinct lunar core comes from the moment of inertia (Konopliv et al., 1998), the induced dipole moment (Hood et al., 1999), and Lunar Laser Ranging. LLR analyses indicate that the core is fluid and the detection of this molten core is a major accomplishment of the LLR effort. This is a small dense core, presumably iron rich with elements such as sulfur which lower the melting point.

In addition to strong tidal dissipation, the lunar rotation also displays a strong source of dissipation which is compatible with a fluid core (Williams et al., 2001). This source of dissipation arises from the fluid motion with respect to the solid mantle at a fluid-core/solid-mantle boundary (CMB). With the aid of Yoder's (1995) turbulent boundary layer theory these dissipation results give a 1-σ upper limit for radius of 352 km for a pure Fe core or 374 km for a fluid Fe-FeS eutectic (Williams et al., 2001). Upper limits are used because any topography on the CMB or the presence of an inner core would tend to decrease the inferred radius. More recent solutions find a somewhat stronger fluid core dissipation torque.

The detection of the oblateness of the fluid-core/solid-mantle boundary would be independent evidence for the existence of a liquid core. Fluid flow along an oblate boundary exerts torques on both the fluid and the overlying solid Moon. In recent years rotation evidence for an oblate boundary has been strengthening (Williams, Boggs, and Ratcliff, 2004). In the solutions core oblateness and $k2$ anticorrelate resulting in a smaller $k2$ value than previous spherical core solutions gave. The core oblateness is expected to be the next major LLR lunar science result.

The internal structure and material properties of the Moon must be deduced from external evidence and the deepest regions are the most elusive. In order to determine the variety of permissible interior structures and properties, a large number of models have been generated which satisfy, within measurement uncertainties, four lunar quantities: the mean density, the moment of inertia's measure of mass concentration toward the center, the $k2$ elastic response to solid-body tides, and tidal dissipation Q (Khan et al., 2004). Typically, the central regions of the acceptable models have a higher density core which can take several forms such as completely solid, completely fluid, and a solid inner core within a fluid outer core.

Learning whether the Moon has a small solid core inside a liquid outer core is a future possibility. There should be signatures in the rotation data if that is the case, but they could be small.

Positions on the Moon

A return to the Moon with robotic and manned spacecraft is now projected. This presents an opportunity for new retroreflectors and optical transponders to go to the Moon. The LLR retroreflectors have the most accurately known positions on the Moon. A small number of accurate positions on the Moon are serving as control points for lunar geodesy (Davies, Colvin, and Meyer, 1987; Davies et al., 1994; Davies and Colvin, 2000) and it is hoped that future missions enable this network of accurate control points to be expanded.

Gravitational physics motivation

Einstein's general theory of relativity has proved remarkably successful. Nonetheless, this is a time for improved tests of gravity. In physics there is an expectation that a theory of gravity can be found which is compatible with the quantum theories of the stronger forces. Among the most promising extensions of relativistic gravity beyond general relativity are the scalar-tensor theories. These theories can give small violations of the equivalence principle as well as a time-varying gravitational "constant", two quantities that LLR determines well.

Different aspects of metric theories of gravity are described with Parametrized Post-Newtonian (PPN) β and γ parameters. These PPN parameters have a unit value for general relativity, but a deviation from unity at levels of 10^{-5} to 10^{-7} has been predicted by Damour and Nordtvedt (1993) and Damour, Piazza, and Veneziano (2002).

The great stability of the lunar orbit allows LLR to use the orbital motion to make accurate tests of gravitational physics. A discussion follows of LLR tests of the equivalence principle, the implication for PPN β, and variation of the gravitational constant. The following new LLR solution results used LLR data through April 2004 (Williams, Turyshev, and Boggs, 2004).

Equivalence principle

The equivalence principle is a foundation of Einstein's theory of gravity. The LLR analysis tests the equivalence principle by examining whether the Moon and Earth accelerate alike in the Sun's field. Nordtvedt (1968, 1970) gave theoretical analyses of the effects of a violation of the principle of equivalence. For the Earth and Moon accelerated by the Sun, if the equivalence principle is violated the lunar orbit will be displaced along the Earth-Sun line, producing a range signature having a 29.53-day period.

The LLR test of the equivalence principle shows that the Earth and Moon are accelerated alike by the Sun's gravity with Δacceleration/acceleration of $(-1.0\pm1.4)\times10^{-13}$. This solution corresponds to a (2.8±4.1) mm cos D signature in the lunar distance.

A violation of the equivalence principle might depend on composition or the strength of the gravitational attraction within a finite body (gravitational self energy). The former was tested in the laboratory by Adelberger (2001) with an uncertainty similar to the LLR result. The latter requires large bodies such as the Moon or planets and it depends on PPN β and γ. Combining the LLR result, the laboratory composition result, and the recent Cassini time delay test of γ (Bertotti, Iess, and Tortora, 2003), one derives $\beta - 1 = (1.2\pm1.1)\times10^{-4}$. This is the strongest limit on PPN β to date and is not significantly different from the unit value of general relativity.

Does the gravitational constant vary?

Einstein's general theory of relativity does not predict a variable gravitational constant G, but some other theories of gravity do. A changing G would alter the scale and periods of the

orbits of the Moon and planets. LLR is sensitive to $\dot{G}/G$ at the 1 AU scale of the annual orbit about the Sun (Williams et al., 1996). No variation of the gravitational constant is discernible, with $\dot{G}/G = (4\pm9)\times10^{-13}$ /yr. This is the most accurate result published to date. The uncertainty corresponds to 1.2% of the inverse age of the universe. The scale of the solar system does not share the cosmological expansion. The sensitivity of changing G depends on the square of the LLR time span so significant improvements are expected when future data accumulate.

Geodetic precession

The geodetic precession of 19 mas/yr is a relativistic effect from the annual motion of the Earth-Moon system around the Sun. From the precession of the lunar orbit, LLR has provided the only accurate determination of the geodetic precession to date. The latest LLR result is Kgp = –0.0019±0.0064, where the quantity Kgp gives the relative deviation of the geodetic precession from the general relativity value, so the uncertainty corresponds to 0.12 mas/yr. Correlation is high with the lunar Love number $k2$ and the core oblateness.

Two objectives of the Gravity Probe B mission are to make accurate measurements of the Lense-Thirring effect and the geodetic precession using very precise gyroscopes. For the Moon, the Lense-Thirring effect, a gravitomagnetic frame dragging by a spinning body, causes a very small precession rate which is too small for current measurement. LLR is sensitive to the orbital counterpart of the gravitomagnetic effect. If GPB fulfills its objectives it will produce a more accurate geodetic precession test than LLR.

Other relativistic gravity

There is not a broadly agreed upon theory of relativistic gravity to replace Einstein's general theory of relativity. Consequently, many alternatives have been proposed and there will be more in the future. To be realistic any of these theories must be compatible with the tests of relativity that are provided by LLR and planetary ranging. We can expect that LLR will continue to play an important role in winnowing out some of these theories.

Dark matter and dark energy are among the more exotic aspects of modern astronomy. The mysterious dark matter is known from its gravitational pull and it is more abundant than normal matter. A search for a dark matter equivalence principle effect has been reported by Nordtvedt, Müller, and Soffel (1995) and a test for a preferred frame effect has been done by Müller, Nordtvedt, and Vokrouhlicky (1996). Dark energy, which causes the expansion of the universe to accelerate, is another surprising discovery.

Lunar ephemeris

Analysis of the LLR data is used to generate the lunar ephemeris which, in combination with the planetary ephemerides, is used to navigate interplanetary spacecraft. The lunar and planetary ephemeris is available at http://ssd.jpl.nasa.gov/. The lunar rotation, the physical libration, is also part of the ephemeris files. An accurate lunar ephemeris is critical for future missions to the Moon and the physical librations are critical to landing on the Moon, navigation on the Moon, and observations from the Moon.

Modeling

To analyze LLR data with a lengthening span and high accuracy, the data analysis models and programs must be improved. Standish and Williams (2003) describe the lunar and planetary numerical integrator used to generate past ephemerides. Many small modeling improvements

would benefit analyses of current and future data; an overview is given by Williams, Turyshev, and Murphy (2004). A new set of changes to the integration program has been started.

Current interests and future possibilities

LLR results related to the Moon's interior are of current interest. These include the Love numbers, tidal dissipation Q vs frequency, core dissipation, and core oblateness. Core oblateness effects now appear to be significant. In the future it may be possible to learn whether the Moon has a small solid core inside a liquid outer core. There should be signatures in the rotation data if that is the case, but they could be small. The 75 yr lunar pole wobble may be related to effects at the core/mantle interface (Yoder, 1981). High accuracy tracking might detect stimulation events for this free mode.

Studies of gravitational physics look for perturbations of the orbit of the Moon and small relativistic effects in the time of flight to and from the Moon. Currently, the most important contributions of LLR to gravitational physics are the equivalence principle test and the rate of change of the gravitational constant G. In addition, LLR has sensitivity to geodetic precession and other effects of general relativity, and other future tests are expected.

LLR contributes to geophysics and geodesy with Earth rotation, tidal acceleration, precession and nutation results. Still, the existence of only two active stations is a limitation. If LLR is to increase its impact in Earth sciences then more stations, with wide distribution, are needed.

Looking toward the future, the analysis depends on high-quality data and improved range accuracy helps all results. Lengthening data span strongly helps long-time-scale effects like station motion, Earth precession, 18.6 yr nutation, tidal acceleration, orbital inclination, node, and precessions, the search for changing G, and lunar core dissipation and free librations. New retroreflectors on the Moon would most strongly help the lunar science, but would also benefit other areas. The return to the Moon with robotic and manned spacecraft increases the importance of LLR contributions to science, ephemerides, and positions on the Moon while offering the opportunity for additional passive retroreflectors and active optical transponders.

Acknowledgments

We acknowledge and thank the staffs of the Observatoire de la Côte d'Azur, Haleakala, and University of Texas McDonald ranging stations. The research described in this paper was carried out at the Jet Propulsion Laboratory of the California Institute of Technology, under a contract with the National Aeronautics and Space Administration.

References

Adelberger, E. G., New Tests of Einstein's Equivalence Principle and Newton's inverse-square law, *Classical and Quantum Gravity*, *18*, 2397-2405, 2001.

Bertotti, B., L. Iess, and P. Tortora, A test of general relativity using radio links with the Cassini spacecraft, *Nature*, *425*, 374-376, 2003.

Chapront, J., M. Chapront-Touzé, and G. Francou, A new determination of lunar orbital parameters, precession constant and tidal acceleration from LLR measurements, *Astron. Astrophys.*, *387*, 700-709, 2002.

Damour, T., and K. Nordtvedt, Tensor-scalar cosmological models and their relaxation toward general relativity, *Phys. Rev. D*, *48*, 3436-3450, 1993.

Damour, T., F. Piazza, and G. Veneziano, Violations of the equivalence principle in a dilaton-runaway scenario, *Phys. Rev. D*, *66*, 046007, 1-15, 2002. hep-th/0205111.

Davies, M. E., T. R. Colvin and D. L. Meyer, A unified lunar control network: The near side, *J. Geophys. Res.*, *92*, 14177-14184, 1987.

Davies, M. E., T. R. Colvin, D. L. Meyer, and S. Nelson, The unified lunar control network: 1994 version, *J. Geophys. Res.*, *99*, 23211-23214, 1994.

Davies, M. E., and T. R. Colvin, Lunar coordinates in the regions of the Apollo landers, *J. Geophys. Res.*, *105*, 20277-20280, 2000.

Hood, L. L., D. L. Mitchell, R. P. Lin, M. H. Acuna, and A. B. Binder, Initial measurements of the lunar induced magnetic dipole moment using Lunar Prospector magnetometer data, *Geophys. Res. Lett.*, *26*, 2327-2330, 1999.

Khan, A., K. Mosegaard, J. G. Williams, and P. Lognonne, Does the Moon possess a molten core? Probing the deep lunar interior using results from LLR and Lunar Prospector, *J. Geophys. Res.*, *109* (E9), 10.1029/2004JE002294, 1-25, 2004.

Konopliv, A. S., A. B. Binder, L. L. Hood, A. B. Kucinskas, W. L. Sjogren, and J. G. Williams, Improved gravity field of the Moon from Lunar Prospector, *Science*, *281*, 14761480, 1998.

Konopliv, A. S., S. W. Asmar, E. Carranza, W. L. Sjogren, and D. N. Yuan, Recent gravity models as a result of the lunar prospector mission, *Icarus*, *150*, 1-18, 2001.

Kuskov, O. L., and V. A. Kronrod, Constitution of the Moon 5. Constraints on composition, density, temperature, and radius of a core, *Phys. Earth and Planetary Interiors, 107*, 285-386, 1998.

Müller, J., K. Nordtvedt, Jr., and D. Vokrouhlicky, Improved constraint on the α1 PPN parameter from lunar motion, *Phys. Rev. D*, *54*, R5927-R5930, 1996.

Nordtvedt, K., Jr., Testing relativity with laser ranging to the Moon, *Phys. Rev.*, *170*, 1186-1187, 1968.

Nordtvedt, K., Jr., Solar system Eotvos Experiments, *Icarus*, *12*, 91-100, 1970.

Nordtvedt, K. L., J. Müller, and M. Soffel, Cosmic Acceleration of the Earth and Moon by Dark-Matter, *Astron. Astrophys.*, *293*, L73-L74, 1995.

Standish, E. M., and J. G. Williams, Orbital Ephemerides of the Sun, Moon, and Planets, Chapter 8 of the *Explanatory Supplement to the American Ephemeris and Nautical Almanac*, in press, 2003.

Williams, J. G., X X Newhall, and J. O. Dickey, Relativity parameters determined from lunar laser ranging, *Phys. Rev. D*, *53*, 6730-6739, 1996.

Williams, J. G., D. H. Boggs, C. F. Yoder, J. T. Ratcliff, and J. O. Dickey, Lunar rotational dissipation in solid body and molten core, *J. Geophys. Res.*, *106*, 27933-27968, 2001.

Williams, J. G., and J. O. Dickey, Lunar Geophysics, Geodesy, and Dynamics, *13th International Workshop on Laser Ranging*, October 7-11, 2002, Washington, D. C., eds. R. Noomen, S. Klosko, C. Noll, and M. Pearlman, NASA/CP-2003-212248, pp. 75-86,2003. http://cddisa.gsfc.nasa.gov/lw13/lw_proceedings.html

Williams, J. G., S. G. Turyshev, and T. W. Murphy, Jr., Improving LLR Tests of Gravitational Theory, *International Journal of Modern Physics D*, *V13* (No. 3), 567-582, 2004. http://www.worldscinet.com/ijmpd/13/1303/S0218271804004682.html

Williams, J. G., D. H. Boggs, and J. T. Ratcliff, Lunar Core and Tides, abstract #1398 of the *Lunar and Planetary Science Conference XXXV*, March 15-19, 2004.

Williams, J. G., S. G. Turyshev, and D. H. Boggs, Progress in lunar laser ranging tests of relativistic gravity, submitted to *Phys. Rev. Lett.*, 2004.

Yoder, C. F., The free librations of a dissipative Moon, *Philos. Trans. R. Soc. London Ser. A, 303*, 327-338, 1981.

Yoder, C. F., Venus' free obliquity, *Icarus*, *117*, 250-286, 1995.

CONSOLIDATED LASER RANGING PREDICTION FORMAT: FIELD TESTS

R. Ricklefs
Center for Space Research, The University of Texas at Austin ricklefs@csr.utexas.edu /Fax: 1-512-471-3570

Abstract

The new International Laser Ranging Service (ILRS) consolidated ranging target prediction format has been developed by the ILRS Prediction Formats Study Group to provide a single format to encompass traditional artificial satellite and lunar ranging targets as well as proposed transponder targets on or around the moon and other planets. The primary benefit will be to allow any ranging station convenient access to ranging any of these target categories. In addition, the new format is designed so that predictions will not be subject to the inaccuracies inherent in tuning to a specific gravitational or drag model as found in the current IRV format.

While details of a few extensions to the format remain to be worked out, the core lunar and satellite components of the format are stable and have been subjected to a pilot study at the McDonald Laser Ranging Stations (MLRS). A discussion of the sources for the new predictions is presented, as is an analysis of the results of the ranging tests. Plans for future tests and implementation are also discussed.

Introduction

The Consolidated Prediction Format (CPF) provides a method of ranging to disparate targets using one format. [1] This allows cross-technique ranging attempts. A lunaronly station can then easily try to range a satellite or transponders target. An SLRonly station can perform feasibility tests on the moon. When a new deep-space satellite is launched, there are 40 stations around the world that should be able to track and possibly range to it.

Some additional advantages of the new format are that it does not rely on on-site gravity model, tuning, or separate drag and time bias functions. It is a tabular format containing un-tuned state vectors at time intervals appropriate to the target. The state vectors are typically in true body fixed system of date.

Purpose of Field Tests

Field tests have begun for the purpose of demonstrating the new format. The tests are necessary to verify that nothing has been forgotten, either in the data fields or in the overall concepts. The tests also give an opportunity to assess the performance of the predictions in some of the various configurations – low and high earth satellites as well as lunar reflectors, and, eventually, transponders.

There will inevitably be some bottlenecks, confusion, and mis-steps in producing and handling the predictions. Tests with a small number of stations will allow these to be identified and corrected before the entire network is involved.

A side-effect of the tests will be the building of infrastructure for network implementation. As various prediction centers and stations come into the tests, the distribution network will be put into place and shaken out.

MLRS Field Tests

To begin field testing, MLRS has taken a multi-faceted approach. To track satellite targets, HTSI Tuned Inter-range Vectors (TIVs) [2] are numerically integrated to produce one-minute

state vectors which are then converted into the new format. This provides an easy way to start testing, using existing data products and provides a way to check out real-time point angles and ranges against existing software and predictions. The NERC Space Geodetic Facility (NSGF) tabular predictions are also being evaluated for use in the tests. For lunar ranging, the JPL DE-403 ephemeris is used as a basis for predictions produced in the new format.

Changes to the MLRS data acquisition software permit both old and new formats to be used, for quick switching during tests. This also minimizes maintaining nearlyduplicate versions of the code during the period prior to full switch-over to the new format.

Satellite and lunar normalpoint software does not currently use the new tabular format, due to development time constraints. The plan is to find time within the next few months to modify the normalpoint code so that it can use either the new or old format.

There have been no transponder tests, although Mars Global Surveyor predictions have been produced in the new format and verified to reproduce the original ephemeris to about 10 meters with the sample interpolation code. Hopefully, when Mercury Messenger returns in mid-2005, a number of stations will be able to track it using the new format.

Results

Preliminary code modifications are in place at MLRS, and predictions are available for internal tests. Data has been acquired on 4 satellite passes using the HTSI-derived predictions described above. At this time, the NSGF predicts are being evaluated. A couple of problems are delaying lunar tests, but those do not constitute major difficulties.

Conclusion

The fields tests are just starting at MLRS, and the results are encouraging, with passes being successfully tracked with the new format. LLR tracking with the new format should be tested soon. As time progresses, we expect more sources of predictions and more stations taking part in the tests.

Acknowledgements

Members of the ILRS Prediction Format Study Group have been involved in various phases of the field tests. To name 2, David Rowlands of Goddard Space Flight Center has provided Mars Global Surveyor predictions, and Graham Appleby of NSGF has provided satellite predictions in the CPF. We also wish to acknowledge funding for this project from NASA Contract NAS5-01096, NASA Grant NAG5-11464, and NSF Grant AST-0204127.

References

1. R. Ricklefs, “Consolidated Laser Ranging Prediction Format”, Proceedings of the Thirteenth International Workshop On Laser Ranging, Washington, D.C., October 2002.
2. “SLR IRV Format”: http://ilrs.gsfc.nasa.gov/products_formats_procedures/predictions/tirv_format.html.

APOLLO: MEETING THE MILLIMETER GOAL

T. W. Murphy, Jr.(1), J. D. Strasburg (2), C. W. Stubbs (3), E. G. Adelberger (4), L. Tom(3), A. E. Orin(1), E. L. Michelsen(1), J. Battat(3), C. D. Hoyle(4), E. Swanson(4), E. Williams(1)
(1)UC San Diego, 9500 Gilman Dr. 0424, La Jolla, CA 920930424.
(2)Pacific Northwest National Labs, P.O. Box 999, Richland, WA 99352.
(3)Harvard University, 60 Garden St., Cambridge, MA 02138.
(4)Box 351560, University of Washington, Seattle, WA 918951560.

Abstract

As APOLLO (the Apache Point Lunar Laserranging Operation) progresses toward initial operation, we continue to explore ways in which our apparatus may introduce biases in our measurement. In this way, we can develop instrumentation and methodologies to remove or diminish these systematic bias sources. In this paper, we present a detailed study of the time behavior of our avalanche photodiode array devices. Most notably, we observed the dependence of avalanche report time as a function of spatial position of the illumination spot on the detector. If unchecked, the differing illumination pattern of the internal corner cube versus the lunar return would introduce a bias of roughly 100 ps (15 mm one-way). We discuss our implementation of an optical solution to the problem involving ground glass to match these illumination patterns. We also discuss the issue of thermal variations, and our strategy to minimize the impact of these on our differential timing scheme. The project status is summarized at the end.

Introduction

Since its undertaking, Lunar Laser Ranging (LLR) has performed the most precise tests of a number of gravitational phenomena, LLR has set the most stringent limits yet on the strong equivalence principle, the time rate of change of Newton's gravitational constant, geodetic precession, gravitomagnetism, and departures from the $1/r^2$ gravitational force law [1, 2, 3, 4, 5]. As we continue to grapple with the inherent incompatibility between general relativity and quantum mechanics, precision tests of basic gravitational phenomenology become increasingly important. The fact that the universe appears to be accelerating in its expansion indicates that we may not yet fully understand largescale gravity. Perhaps this is an indication of new physics such as the presence of a scalar field modification to general relativity. Such scalar fields generically violate the equivalence principle, and also tend to introduce secular changes in the fundamental constants of nature [6].

Table 1: APOLLO Random Error Budget Per Photon

Random Error Source	Time Uncertainty (ps)	Range Error (mm)
Retroreflector Array Orientation	100–300	15–45
APD Illumination	60	9
APD Intrinsic	< 50	< 7
Laser Pulse Width	45	6.5
Timing Electronics	20	3
GPSdisciplined Clock	7	1
Total Random Uncertainty	136–314	20–47

Multiphoton Lunar Ranging

The Apache Point Observatory Lunar Laser-ranging Operation (APOLLO) [7] is a new effort in lunar ranging that aims to achieve onemillimeter range precision—representing an order-of-magnitude improvement over other LLR efforts. Corresponding to about 7 ps of round-trip range delay, this puts stringent demands on the detection and timing of photons. The range determined from a single photon has much more uncertainty than one-millimeter, so that we must average many photon detections to arrive at the requisite precision. Table 1 lists the various sources of random uncertainty per photon. Our largest source of random error is the orientation of the retroreflector array, which changes as a function of lunar libration. The array can be tilted by as much as 10º, so that photons reflecting off of the nearest edge report a smaller range thatn photons that reflect off of the far edge. This effect can translate to roughly 950 ps of peak-to-peak range uncertainty for the largest reflector array. When the reflector array is oriented nearly perpendicular to the line of sight (about 15% of the time), we are most limited by the avalanche spreading phenomenon.

A full avalanche current is established once the entire active area of the detector element is participating in the avalanche. This state is attained most expediently if the avalanche begins in the center of the element and propagates outward from there. On the other extreme, if an avalanche begins at one edge, it could take roughly twice as long to establish full current. The rest of the random error budget includes things such as the effects of the finite laser pulse width, other temporal uncertainties in the APD detectors, timing electronics jitter, and timebase jitter.

All together, onemillimeter range precision demands that we acquire enough data points such that $\sigma final$ = 1 mm = $\sigma photon/\sqrt{N}$, where N is the number of photons collected, each with intrinsic uncertainty $\sigma photon$. In the case of $\sigma photon$ = 50 mm, one needs 2500 photons to achieve the requisite reduction in random uncertainty. By comparison, the currently operating LLR stations build normal points out of typically 10–100 photons. Realistic attempts to quantify the range signal from the 3.5 m telescope at the Apache Point Observatory (in southern New Mexico at an altitude of 2800 m) result in predictions of several photons per pulse. Taking one photon per pulse as a baseline, at 20 Hz pulse repetition rate we would expect to net 1200 photons per minute, so that our millimeter goal may be realized on a timescale of a few minutes. Previous publications document the photon signal expectations in greater detail [8, 9].

Two aspects of this multi-photon-per-pulse regime deserve special mention. The first is that the detector only responds to the first photon to trigger an avalanche. In order to avoid biasing the range measurement to shorter values, multiple detector elements must be available to collect photons. Because of this, we are using an array detector [10], discussed below. The second point is that even at a photon rate 100 times lower than calculated expectations, we will detect roughly one photon per second. This rate is high enough to allow realtime system optimization in regard to telescope pointing, transmitter/receiver pointing offset (for velocity aberration), beam divergence and telescope focus. The two dimensional detector array facilitates the pointing corrections. The net result is that it should be possible to “steer” onto a return rate close to expectations, even starting at a rate two orders-of-magnitude lower.

The APOLLO detector is a 4×4 array of avalanche photodiode (APD) elements: each is 30μm in diameter, separated by 100 μm (Figure 1—this spacing limits crosstalk). Thus 16 “buckets” are placed in the receiver stream, and sized such that the “pixels” oversample the seeing-limited spot

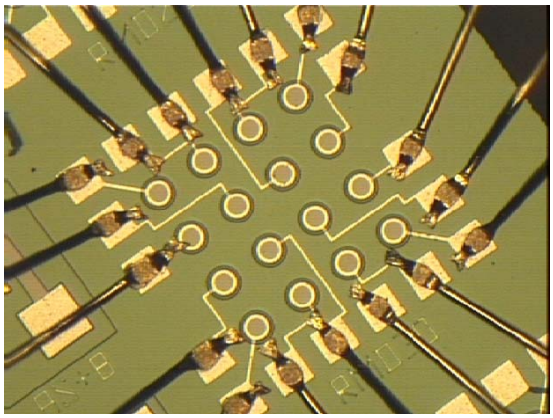

Figure 1: Lincoln Labs APD array: 30 μm active areas on 100 μm centers. The array provides multiple detectors to accommodate a multiphoton return, and also allows closed-loop signal tracking.

size from the lunar array. The spacing between elements results in a low fill-factor, so that we use a micro-lens array in front of the detector to recover nearly 100% fillfactor. The lenslet array is itself located at a reimaged telescope focus. In this way, each lens, or "pixel" represents a spatial position on the sky—in our case about 0.35 arcseconds on a side. The detector array is then located roughly one focal-length away from the lenslets, so that a pupil image is formed within the confines of the 30 μm detector element (Figure 2). By tracking the average hit rate for each APD element, an illumination pattern is built up, and we can tell if the lunar return is centered on the array. The formation of a pupil image on the APD element means that in effect an image of the primary mirror is formed there. Returned lunar photons strike the telescope entrance aperture (primary mirror) in random locations, so that the APD element is roughly uniformly illuminated (except for the central obstruction from the secondary mirror).

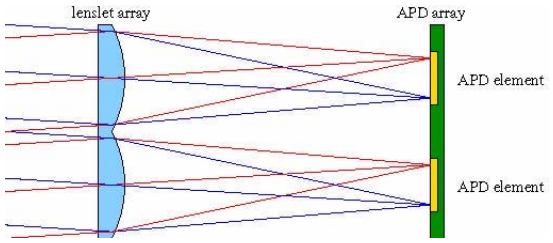

Figure 2: The microlens—or lenslet array—concentrates incoming light onto the individual APD elements. The lenslet itself is located at a telescope focus. The rays in the figure are colorcoded to indicate origin of location on the primary mirror. An image of the primary is formed on each APD element.

The spread in location of the incident photon within the APD element translates to a timing uncertainty, discussed in Section 3. One dangerous aspect of this spread regards the fiducial corner cube. A corner cube is located in the exit aperture of the telescope to catch light leaving the primary mirror enroute to the moon. Photons returned from this corner cube are detected in a way that is identical to the lunar retroreflector returns—identical in terms of optical path, signal level, detection, and timing. The corner cube thus provides a time fiducial for the outgoing pulse. The danger is that the corner cube does *not* spread photons uniformly across the telescope aperture (and thus the detector element), but rather in a wellconfined spot. This has the effect of biasing the differential measurement since the average time-to-

avalanche may differ between lunar and fiducial photons. It is for this reason that we have studied this problem in detail.

Avalanche Initiation Location

When a photon impinges on an avalanche photodiode, it penetrates some distance before creating an electron-hole pair in the semiconductor. For silicon, the characteristic penetration depth at a wavelength of 532 nm is about 1.0 μm. The penetration depth varies from photon to photon, leading to a spread in the initial depth of the electron-hole pair. An electric field drives the electron toward the p-n junction and multiplication region. At a saturation velocity of about 105 m/s, (0.1 μm/ps), the variable penetration depth translates to roughly 10 ps of

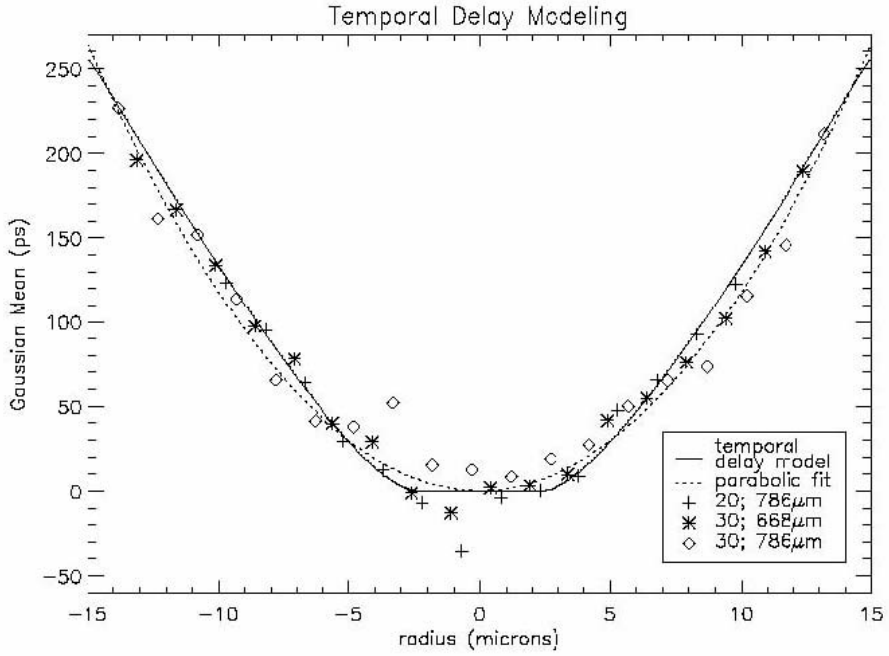

Figure 3: Spatial scans of avalanche initiation delay for two different devices at two different wavelengths. A crude parabolic fit is plotted, as well as a model based on linear spread of the avalanche front.

variability in when an electron reaches the multiplication region. At this point, a microplasma of avalanching electronhole pairs spreads across the disk-shaped multiplication region. It may be assumed that the front of this plasma propagates across the silicon at a uniform speed—presumably not much slower than the thermal speed of an electron in silicon (1.2×10^5 m/s). In this model, an avalanche initiated in the center of the detector element reaches saturation current (the whole disk in avalanche) sooner than an avalanche initiated at the edge of the element. Variation my be expected to be $>$ 150 ps for a 30 μm element.

We have observed this effect in our APD elements, by illuminating the detector with a pulsed laser spot a few microns across, and measuring report time while scanning this spot across the spatial extent of the array. For this study, we used a shortpulse laser diode with a pulsewidth of 40 ps and a wavelength of 786 nm. The shift in avalanche report time is tracked as a function of spatial position, producing data like that presented in Figure 3. Both the 20 μm and 30 μm devices follow the same rules, showing a delay that evolves quadratically as a function of position away from the center. Models that allow the microplasma front to grow linearly until it hits an edge of the element, and an avalanche trigger at some fraction of the

saturation current (current is assumed to be proportional to area) produce results consistent with the data in Figure 3, whose simplified form is approximately $1.2r^2$ ps, where r is the distance from the element center, in microns. We can fit this model to the data with a single parameter, corresponding to the speed of the microplasma front. In doing so, we infer a speed of 3.5×10^4 m/s, or roughly 1/3 the electron thermal velocity.

This microplasma development phenomenon means that any specific illumination pattern on the APD element will have an associated delay, but also a spread in the report times. Any small spot or thin, centered annulus will have little spread, but the intended illumination for APOLLO (most of the active area) will result in a spread of about 65 ps, and a delay of 115 ps compared to a centrally-initiated avalanche.

Though the random uncertainty arising from the illumination pattern is unwelcome, a more serious problem exists in the potential bias introduced in our "differential" measurement scheme. The placement of a corner cube in the exit aperture of the telescope allows a near real-time comparison to the lunar return sharing the same optical path, detectors, and timing system. Only the signal level is different, and this is adjusted to roughly match the lunar signal via a battery of attenuators on rotating glass disks. The statement that the two returns follow the same optical path is, however, not strictly true. The fiducial photons only strike a small part of the primary mirror. Because this mirror is imaged onto the APD array elements, the fiducial photons then hit each detector in one small spot. Therefore, the avalanche initiation delay from the fiducial corner cube will not in general match the average delay experienced by the lunar photons. If left uncorrected, this would amount to a range bias of the order of 100 ps, or about 15 mm.

Eliminating the Avalanche Initiation Bias

The range bias resulting from the different illumination of lunar and fiducial photons on the detector is not in itself a cause for concern if it is static. This bias would be systematic in the data analysis, and could be fit out. However, it is difficult to guarantee that the corner cube return always hits the same spot on the detector, as even slight optical tweaks could affect this. For instance, if the corner cube is located near the edge of the primary mirror, the fiducial photons would strike the outer edge of the APD element, where the slope in the delay curve is large (r^2 dependence: Figure 3). For our system, a motion of one micron near the edge of the detector would result in a delay difference of about 40 ps. A variable range delay of even one sixth of this would negatively impact our goal of long-term millimeter range precision. We require a solution to this problem that is robust against changes in optical alignment.

By intermittently placing a ground glass diffuser into the optical beam at the time of laser fire, we can effectively spread the fiducial photons from the corner cube into a distribution that mimics the lunar return. This works properly only in certain locations within the optical beam. The diffuser randomizes angle (15º FWHM Gaussian is typical), and this has the effect of mimicking the lunar photons only at a focal plane (Figure 4). The resulting nearly-uniform illumination at the detector reduces our bias between lunar and fiducial events to 3 ps, which can easily be estimated and removed at the sub-picosecond level.

Because the diffuser is located at a focus, the illumination pattern at the diffuser is small—and this is an advantage, because the diffuser must be switched in and out at the repetition rate of the laser. The switching requirement isn't essential, but one otherwise looses flux in the lunar return by the action of diffusion (much of the light no longer finds the detector).

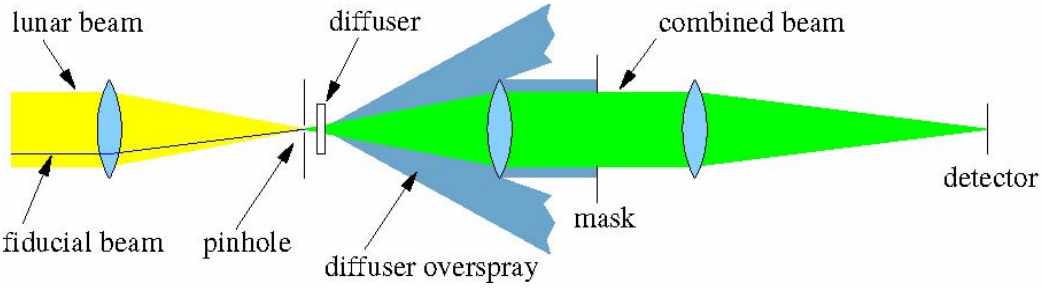

Figure 4: Schematic of diffuser location within the receiver. Within the collimated input beam, the fiducial occupies a very small part of the crosssection—corresponding to the area the corner cube covers on the primary mirror. After the diffuser and mask, the lunar and fiducial photons have identical optical paths.

The APOLLO optical system employs a spatial filter for background reduction, with an aperture of 3 arcseconds (400 μm). This is an ideal location for the diffuser, which we have implemented as a rotating disk with one quadrant ground into a diffuser. A mask located downstream of the spatial filter in a section of collimated beam ensures that the lunar and fiducial illumination patterns are identical on the detector even in the presence of optical misalignment. The detector and mask form conjugate image planes.

We have chosen to use a single-quadrant diffuser rotating at half the laser repetition rate rather than a half-covered disk rotating at full speed. This results in every *other* fiducial return passing through the diffuser. The fiducial returns then alternate between biased-but-sharp and unbiased-but-blurry. In this way, it is possible to recover the full time-precision associated with the laser pulse width, the APD intrinsic jitter, and the timing electronics jitter without intentionally introducing the rather large timing spread associated with the avalanche initiation variability. Thus this non-diffused fiducial serves as a diagnostic of the temporal quality of our laser pulse, detector, electronics, etc. At the same time, every other shot is spread out across the APD element in such a way as to mimic the delay associated with the spread-out lunar photons. By comparing the two, we can directly monitor the bias, and apply this bias correction to the sharp pulse, thus preserving the best that both have to offer. Ultimately, we will use only the sharp (un-diffused), but bias-corrected fiducial returns. Because the avalanche initiation spread dominates the error budget, using only half of the fiducial photons in this way is more than compensated by the sharpness of the un-diffused pulse.

Physical Implementation

The quadrant opposite the diffuser has a coating for attenuation (approximately 1 O.D.) to balance the signal loss associated with the light diffusely scattered outside of the detector's active area. In this way, differential biases associated with signal level (e.g., first-photon bias) is avoided. Our quadrant diffuser disk is mounted on a rotating shaft along with two other quadrant attenuators— each clear in the two lunar quadrants and attenuating in the two fiducial quadrants. One of the two attenuator disks is a fixed value, while the other disk is an angularly variable attenuator spanning 1.5 optical densities. By tuning the phase of the quadrant diffuser/attenuator assembly, one may adjust the overall attenuation of the fiducial path. Given 16 available detectors, a 10% hit rate corresponds to roughly two fiducial photons per shot. At this level, the firstphoton bias is small, and may be reasonably corrected. Most of the attenuation along the fiducial path is generated at the transmit/receive switch, where the dielectric coatings on the front and back of the rotating disk result in about 10^{-6} transmission.

The quadrant diffuser/attenuator assembly contributes another ~ 4 orders-of-magnitude of fiducial attenuation.

Thermal Effects

The differential measurement scheme employed by APOLLO in essence measures the distance between a fiducial corner cube located near the telescope secondary mirror and the corner cube array on the moon. The same exact optical path (with the exception of a few optical coatings) is used for both, as well as the same detection/timing scheme. By making the two measurements as identical as possible, we are largely insensitive to intermediate- or long-term drifts. As long as the system is stable over the ~ 2.5 sec of roundtrip travel, the differential approach is valid.

One of the most worrisome potential failures of the differential measurement scheme is the time-to-digital converter that APOLLO uses for its highresolution time measurement. The TDC measures the time between an ECL pulse generated from a detected photon (the START) and a second ECL pulse (STOP) generated based on the 50 MHz time reference. The Phillips Scientific model 7186 TDC measures a 100 ns range to 25 ps resolution, with a typical RMS uncertainty of 13 ps. The reported bin number (12-bit digital time) for a given Δt is a roughly linear function, NTDC = $a + b\Delta t$, with "offset," a, and "gain," b. Both the offset and gain are known to vary with temperature. From Figure 5, it is seen that the TDC "gain" varies by approximately 160 parts per million per degree Celsius. This becomes important if the phasing of the lunar and fiducial signals with respect to the 50 MHz clock are different, so that the Δt values are mismatched. If these time offsets from the 50 MHz reference could be made to be the same, there would be no need to understand the parameters a and b, as these would perfectly cancel in the differential measurement. If the Δt values differ by T nanoseconds, then the temperature-induced variations will amount to $\Delta b/b \times T$. If T is allowed to be half of the TDC's range, or 50 ns, then a 5 ps bias requirement restricts gain variations to $\Delta b/b < 10^{-4}$, implying a thermal stability (or knowledge) of about 0.5ºC.

We can significantly reduce this burden by arranging to use the same range of the TDC for both lunar and fiducial measurements. On a shot-by-shot basis, it is impossible to control where either the lunar or fiducial photons land with respect to the 50 MHz frequency standard, since the laser fire time and the lunar distance are asynchronous with this clock. But we *can* control *which* clock pulse is used as the STOP for any event. Thus each photon signal can be maintained within a 20 ns range. Moreover, the two ranges can be made to exactly overlap, so that the TDC measurements are on average the same for both signals. If we control the average TDC position of the two signals relative to each other to 1 ns, our 5 ps bias requirement now implies an acceptable temperature range of 25ºC. Maintaining the relative position of the two signals to 1ns is not very challenging, given that we will accumulate enough data to determine the relative positions within a few seconds, and the lunar range estimate varies by far less than this (typically < 100 ps) over the anticipated hour timescale of lunar ranging operation.

Though the forced overlap in TDCspace reduces the systematic thermal influence, we will supplement our knowledge with temperature measurements at several key locations within the TDC unit. We will also conduct a TDC calibration every few minutes wherein a series of START/STOP pairs separated by integral multiples of 20.00ns (derived from frequency standard) are sent to the TDC to determine the gain, offset, and loworder nonlinearity of each of the 16 TDC channels. This process takes only five seconds at 1000 START/STOP pairs per pair separation. Thus we can perform this routine frequently.

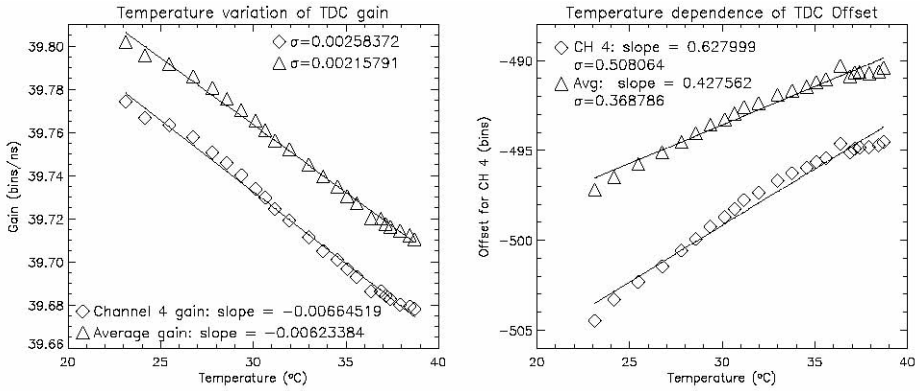

Figure 5: TDC gain and offset as a function of temperature. Plots are shown for an individual channel, as well as for the average of all 16. The slope of 0.0064 bins/ns per Cº translates to 160 ppm per Cº.

Project Status

APOLLO expects to be operational before the close of 2005. At present (Jan 2005), the laser is mounted on the telescope and housed in an insulating enclosure. Two other insulated enclosures have also been constructed to house the electronics, power supplies, computer, and chillers. Much effort has gone into thermal considerations—not only for temperature control/stability, but also to limit the heat flux into the dome to less than 50 W at all times. Most of the optical train for the receiver is built and tested. The APD array has been thoroughly tested and the final set of electronics is in fabrication. The central detection--timing system is well-established, and turning out ~ 20 ps performance. Among the major tasks that remain before initial operation are: establishing the umbilicals cabling/tubing from the static structures to the laser enclosure on the moving telescope; fabricating the remaining optical mounts; installing a microlens array onto the APD array; and developing the user interface software. We anticipate initial lasing in July 2005, and science operation in the following fall.

References

[1] Williams, J. G., Turyshev, S. G., & Boggs, D. H., "Progress in Lunar Laser Ranging Tests of Gravity," *Phys. Rev. Lett.*, **93**, 261101, (2004)

[2] Williams, J. G., Boggs, D. H., Dickey, J. O., & Folkner, W. M., "Lunar Tests of the Gravitational Physics," *Proceedings of the Ninth Marcel Grossman Meeting*, Rome, Italy, June 2000, World Scientific Publications, R. Jantzen, ed., (2001)

[3] Nordtvedt, K., "Lunar Laser Ranging—A Comprehensive Probe of PostNewtonian Gravity," arXiv:grqc/0301024

[4] Anderson, J. D., & Williams, J. G., "LongRange Tests of the Equivalence Principle," *Class. Quantum Grav.*, **18**, 2447, (2001)

[5] Williams, J. G., Newhall, X. X., & Dickey, J. O., "Relativity parameters determined from lunar laser ranging," *Physical Review D*, **53**, 6730, (1996)

[6] Damour, T., & Nordtvedt, K., "Tensorscalar cosmological models and their relaxation toward general relativity," *Phys. Rev. D*, **48**, 3436, (1993)

[7] Murphy, T. W., Strasburg, J. D., Stubbs, C. W., Adelberger, E. G., Angle, J., Nordtvedt, K., Williams, J. G., Dickey, J. O., & Gillespie, B., "The Apache Point Observatory Lunar Laserranging Operation (APOLLO)," *Proceedings of the 12*th *International Workshop on Laser Ranging*, (2000)

[8] Murphy, T. W., Adelberger, E. G., Strasburg, J. D., & Stubbs, C. W., "APOLLO: Multiplexed Lunar Laser Ranging," *Proceedings of the 13*th *International Workshop on Laser Ranging*, (2002)

[9] Murphy, T. W., Adelberger, E. G., Strasburg, J. D., Stubbs, C. W., & Nordtvedt, K., "Testing gravity via nextgeneration lunar laserranging," *Nuclear Physics B*, **134**, 155, (2004)

[10] Strasburg, J. D., Murphy, T. W., Stubbs, C. W., Adelberger, E. G., Miller, D. W., & Angle, J., "Lunar Laser Ranging Using Avalanche Photodiode (APD) Arrays," *Proceedings of the SPIE: Astronomical Instrumentation*, **4836**, 387, (2002).

THE PERFORMANCE OF CHANGCHUN SLR STATION

Chengzhi Liu, You Zhao, Cunbo Fan, Xingwei Han, Xinghua Zhang, Jianyong Shi, Haitao Zhang
National Astronomical Observatories/ Changchun Observatory, Chinese Academy of Sciences, Jing Yue Tan Xi Shan, Changchun 130117, China
Lcz868@126.com/Fax:+86-431-4513550

Abstract

This paper introduces the performance and observation summary of the SLR system at Changchun Observatory, Chinese Academy of Sciences. The performance of the SLR system has been greatly improved since August 1997. The single shot precision reaches 1-2 cm from 5-7 cm and the normal point precision reaches 4-7 mm. The long term stability is better than 1cm.[1][2] The amount of observation has been increased from about 1000 passes to more than 4000 passes.

Technical Improvement

1. Laser System. An active-passive mode-locked Nd:YAG laser is used to generate a 532 nm harmonic with 200 ps width optical pulses. They have energy of 100 mj per pulse and 1,2,4,5,8 and 10 pulses repetition rate per second. The laser firing is controlled by real-time tracking software, typically 4 and 8 pps repetition rate adopted. In recent years, we improve the laser room's environment and apply the high precision power and some new pieces for laser system, so the stability and reliability of laser system have been greatly improved, and now it can completely satisfy the routine observation.

2. Controlling System. All of the operations in Changchun SLR system are completely controlled by a Pentium 586 industrial computer. There is a controlling card in it. Its main functions include laser firing, rang gate controlling, telescope real-time tracking, data gathering and recording.

3. Receiving System. The C-SPAD with time walk compensation circuit and the temperature control shell was adopted as photo-electronic detector instead of the old photo-multiplier tube. The features of C-SPAD are high quantum efficiency, small time walk, automatic compensation and low working voltage. So it decreases the system ranging bias caused by the variation of return signal amplitude and has larger dynamic range. It has been shown in the test that the timing error of the C-SPAD is 43ps, so better observation accuracy can be obtained [3][4].

4. Timing System. HP58503A GPS time frequency receiver supplies 10MHz signal and the second pulse that is synchronized to GPS time to the control system and receiving system. The tracking software is improved to synchronize time automatically every pass so as to reduce time walk and enhance the stability of time system.

5. Servo System and Encoder Electronics. A new servo system for the mount was built. As some microprocessors substitute for the old relays, the stability becomes better. The servo system adopts IGBT, its tracking ability for low orbit satellite boost up, and the tracking error for high orbit satellite is apparently diminished [5]. The new encoder electronics uses a circuit with 23 bit (0.155″resolution), and the output signal becomes better. Also, the output signal of encoder is less affected by the intensity variation of encoder light. So the encoder is more stable.

6. Satellite Prediction and Pre-processing Software. The new prediction software for satellites was introduced, and the accuracy of prediction for position and range of satellite is improved.

The prediction accuracy of range for low orbit satellite reaches 20m and is better for LAGEOS. The accurate position prediction can increase the return rate from satellite. The accurate ranging prediction is in favor of narrowing ranging gate and reducing interference of background noise. The data pre-processing software picks up the useful data from large numbers of the raw observation data and generates normal point data for precise determination of orbit and other applications [6][7]. In addition, sometimes the laser produces two pulses at one firing, which might cause ranging bias for this pass. We compiled special software for dealing with two pulses, and the availability of observation data has been increased.

7. Terrestrial Ranging. The terrestrial ranging is adopted to calibrate the system delay. We have three short distance ground targets and a long distance ground target that is often used. The corn cube reflector of long distance ground target is installed on a side of a mountain building. One way distance is 1268.6215m. The laser energy is controlled and smaller receiving aperture is adopted during terrestrial ranging in order to simulate the actual target satellite ranging and protect the detector.

Summary and Conclusion

In recent years, the data quality of the Changchun SLR Station has been greatly improved and the data volume has been doubled. In 2003, we got total 4463 passes. Table 1 shows the data volume and quality of Changchun Station during January 1, 2003 through December 31, 2003. The long and short term stability has also been upgraded. The long-term stability reaches 1 cm or better and the short term stability reaches 2 cm. Table 2 shows the orbital analysis results of Changchun Station from CSR, MCC, Delft and CRL [8]. In a word, Changchun Station has become an important station in the international SLR Network. Now Changchun Observatory is developing the daylight tracking capability, research on data analysis and applications. More high quality data and some application results will be obtained.

Table 1. Data Volume and Quality (January 1, 2003 through December 31, 2003).

Data Volume									**Data Quality**		
LEO Total	LAGEOS Totals	High Tot	Total passes	LEO NP Total	LAGEOS NP Total	High NP Total	Total NP	Minutes of Track	Cal. RMS	ERS RMS	LAG RMS
3578	493	392	4463	54595	4930	2694	62219	40056	11.5	12.7	13.9

Table 2. Orbital Analysis Results of Changchun Station

Quarry	NP RMS	Short Term (mm)	Long Term (mm)	% of good LAGEOS NP
CSR	6.8	18.8	7.2	97.6
MCC	4.9	13.0	17.4	81.2
Delft	7.4	18.8	6.0	100.0
CRL	6.5	22.1	5.4	100.0

References

[1] Liu Chengzhi, Zhao You, Fan Cunbo etc. Performance and observation summary of Changchun Satellite Laser Ranging Station, *Chinese Science Bulletin*, 2002, **47** (13):1070─1072.

[2] Zhao You, Zhang Junrong, Fan Cunbo et al., Improvement of range precision and stability of satellite laser ranging system in Changchun Station, *Acta Electronica Sinica* (in Chinese), 1999, **27**(11): 110.

[3] Prochazka, I., Hamal, K., SPAD detectors for ranging with sub-millimeter bias, Proceedings of 10th International Workshop on Laser Ranging Instrumentation (eds. Yang Fumin, Chen Wanzhen), Shanghai: Shanghai Astronomical Observatory, 1996, 287—292.

[4] Kirchner, G., Koidl, F., Prochazka, I., et al., SPAD time walk compensation and return energy dependent ranging, Proceedings of 11th International Workshop on Laser Ranging Instrumentation (eds. Schluter, W., Schreiber, U., Dassing, R.), Frankfurt: Verlag des Bundesamtes für Kartographie und Geodasie, 1998, 521—525.

[5] Yang Fumin, Xiao Zhikun, Chen Wanzhen et al., Design and observations of the satellite laser ranging system for daylight tracking at Shanghai Observatory, *Science in China*, Ser. A, 1999, **42**(2): 198.

[6] Tan Detong, Zhang Zongping, Zhang Jianhua, The observation software of SLR station in Shanghai Astronomical Observatory, Observation and Research of Satellite (in Chinese), 1996, 1: 37.

[7] Zhang Zongping, Yang Fumin, The progress in satellite laser ranging, *Progress in Astronomy* (in Chinese), 2001, **19**(2): 283.

[8] Carey Noll. SLR Global Performance Report Card, Period - January 1, 2003 through December 31, 2003.

PROGRESS FOR DAYLIGHT TRACKING IN CHANGCHUN SLR SYSTEM

You Zhao, Cunbo Fan, Xinwei Han, Chengzhi Liu, Xinhua Zhang, Jianyong Shi
National Astronomical Observatories/Changchun Observatory, CAS, Changchun Jing Yue Tan, Changchun 130117, China
youzhao@public.cc.jl.cn, ccslr@public.cc.jl.cn/Fax: +86-431- 4513550,4511337

Abstract

In this paper, first it briefly summaries the Changchun SLR data quality and quantity from data analysis centers: single shot rms, NP rms, long and short—term stability, data percentage and its rank in ILRS after the system improvement. Second it introduces the problems and difficulties facing this system for daylight tracking—mount model, the separation of emitting and receiving parts of the telescope, control range gate, installing narrower filter. Third it presents some work which were done in the system for daylight tracking: system stability improvement, laser stability improvement, mount model adoption, control system, etc. From these analysis and work which have been done, daylight tracking in Changchun SLR system will be possible in the near future.

Upgrade history

In 1998, a upgrade of SLR system in Changchun took place. A new C-SPAD detector with high quantum efficiency, low work voltage, low jitter and time walk compensated, and Met3 meteorological sensor were installed. More accurate meteorological data can be obtained and to be used to correct the data. Also three near ground targets were set up to be used to compare the old ground target. A PCS was used to collocate to find the system time bias and range bias(1,2,3). After that, during the following years, the system was kept in a good condition by taking following ways:

1. Changing new Laser power supply to keep and improve the Laser stability
2. Keeping to change and maintain Laser rod and other laser accessories in good condition
3. Improving the computer control system to make it more convenient and easy to use and to check the system
4. Paying more attention to maintain system, several technicians to check and adjust the system regularly
5. Checking other parts in regular time(4,5).

The Data quantity and quality during the year from Jan-2003 to Dec-2003 in following figure1 (6):

Data quantity:

- Whole 2003 year: 4696 passes
- Ranked No.9 of 40 stations in the global SLR

Data quality:

- Single shot precision: 1cm (Fourth quarter of 2003)
- NP rms: <1cm
- System long and short-term stability: < 2cm (year of 2003)
- Data percentage: >95%

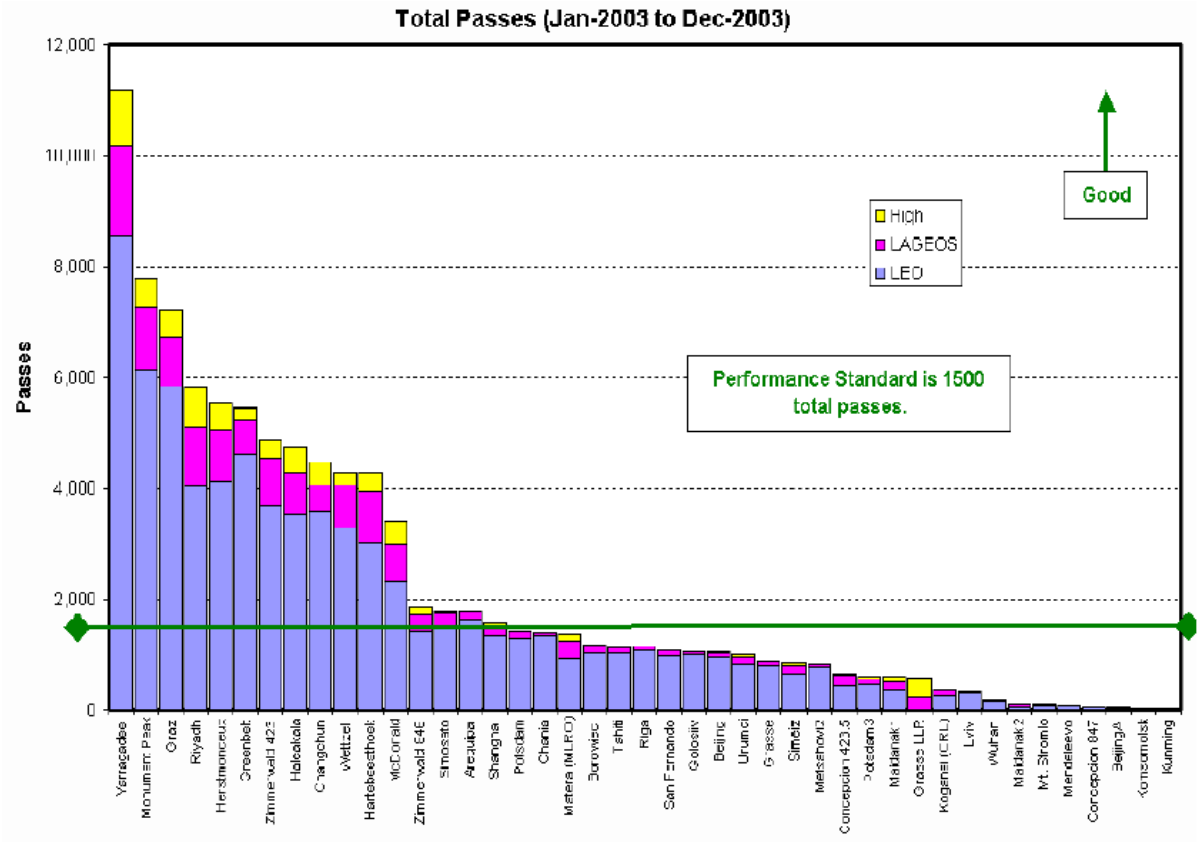

Figure 1. Total passes from Jan-2003 to Dec-2003

Daylight tracking for Changchun SLR

The daylight tracking is necessary and the tendency of SLR in the future. Many stations in the world can take the daylight observations. Because this is necessary and also there are many advantages, such as increasing the number of passes and number of observations, finding systematic errors in products easily, having shorter gaps in orbit coverage, etc. Following is figure 2 to show ILRS stations which can track daylight or not. Compared to above figure 1 and following figure 2, we find that the passes Changchun station got rank about 9 during last year, but no daylight tracking passes. This is a pity and also a loss for such an important station, and its contribution to ILRS and global is limited. The problems or difficulties for Changchun daylight tracking are:

- Bad pointing of the telescope
- Mount model problem for the telescope
- Separation of emitting and receiving parts of the telescope
- Generating control range gate narrower
- Installing narrower filter in the telescope
- Detector on the front of telescope(7,8).

Work done

Even there are so many difficulties, we still have done some work to try to fulfill daylight tracking, such as system stability improvement, laser stability improvement, mount model adoption, control system, etc. In order to improve the system stability, a new control system has been adopted, including an industrial control computer, data collecting board and counter

card for timing and range gate. Control and data preprocessing software are also updated so that all work can be done automatically. For laser stability, the room is air conditioned. The

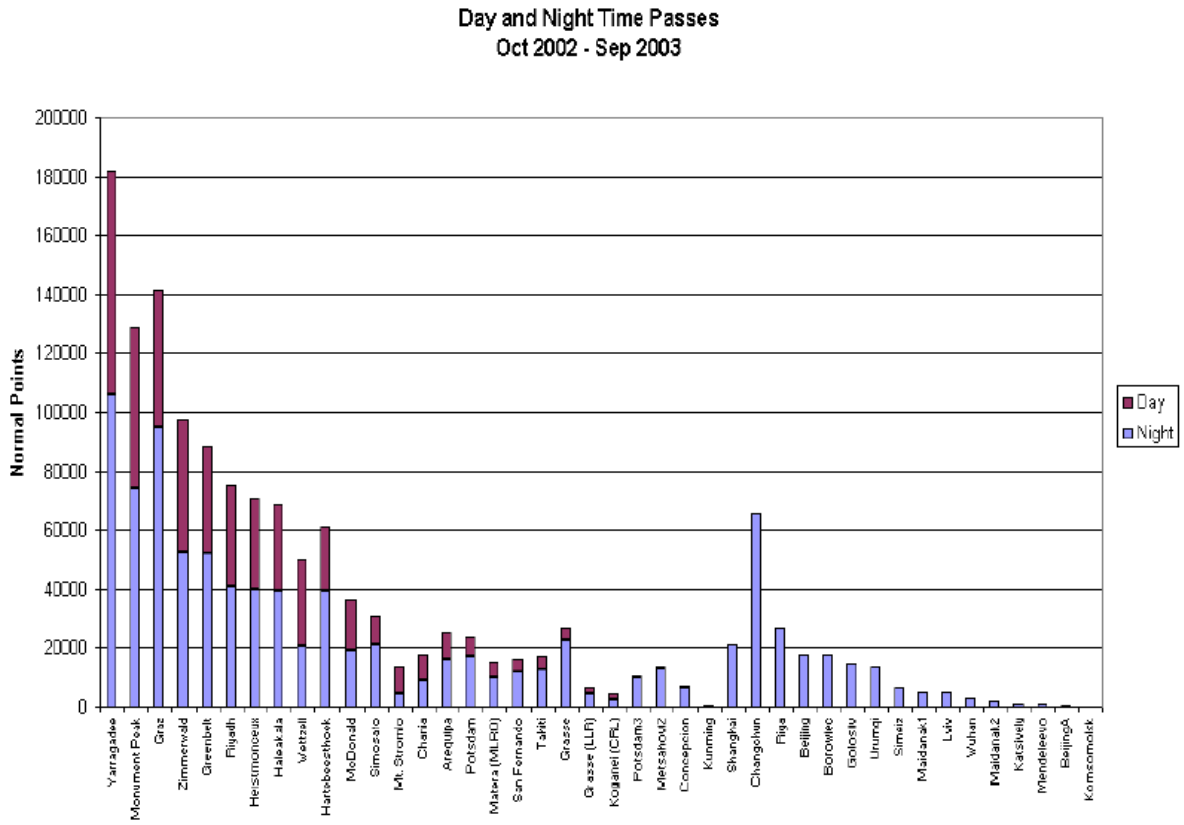

Figure 2. Day and night passes

cooling system is also improved for its liable working, including some system protections. In order to improve the pointing accuracy, mount model correction is also adopted in the satellite prediction. A spherical harmonics pointing model was built by using astronomical observation at our telescope system .It is proved that the pointing model is an effective correction to the system error. This makes the pointing bias become very small in most position. But the result is not good enough for daylight observation. More efforts must be made in the near future.

References

1. Zhao You, Zhang Jun-Rong, Cui Dou-Xing. The improvement of Changchun satellite laser ranging system, in Optical Remote Sensing of the Atmosphere and Clouds, Jinxue Wang, Beiying Wu, Editors, Proceedings of SPIE Vol. 3501, Beijing, 1998 (453—460).

2. Zhao You. Upgrade of Changchun SLR System. Proceedings of 11th International Workshop on Laser Ranging, Deggendorf, Germany, Sep. 1998 (188—196).

3. Zhao You, Kunimori H., Hamal K., Prochazka I. PCS in Changchun Station Proceedings of 11th International Workshop on Laser Ranging, Deggendorf, Germany, Sep. 1998 (174-180).

4. Liu Chengzhi, Zhao You, Fan Cunbo, Cui Douxing, Han Xingwei, Yang Fumin. Performance and observation summary of Changchun Satellite Laser Ranging Station. Chinese Science Bulletin. Vol 47 No 13. July 2002 (1070—1072).

5. You Zhao, Cunbo Fan, Chengzhi Liu, Xinwei Han, Jianyong Shi, Xinhua Zhang, Haitao Zhang. System Stability Improvement of Changchun SLR. Proceedings of 13th International Workshop on Laser Ranging. Oct. of 2002, USA

6. ILRS publications SLR Station Performance Report Card 2003, on the internet

7. Yang Fumin, Xiao Zhikun, Chen Wanzhen, et al. Design and Observations of the Satellite Laser Ranging System for Daylight Tracking at Shanghai Observatory, Science in China Series A_Vol.42, No.2, 1999. (198—206)

8. Werner Gurtner, Ulrich Schreiber. Daylight Tracking. ILRS Technical Workshop, Kötzting, Germany, October 28 - 31, 2003

NEW DRIVE AND SERVO-CONTROL SYSTEM OF KUNMING SLR STATION

Zheng Xiangming, Jiang Chongguo, Xiong Yaoheng, Zhang Yuncheng, Li Zhulian, Wang Hanping, Fu Honglin,
Yunnan Observatory, National Astronomical Observatories,
Chinese Academy of Sciences. R.P.China
xiongyh@public.km.yn.cn, FAX: 86-871-3920154

Abstract

A new project is now being carried on for Kunming SLR station at Yunnan Observatory: to upgrade drive and servo-control system of 1.2m telescope. The aim of the project is to improve the LEO satellite tracking capability. We will report the progresses and initial results of this project.

SAN FERNANDO SLR STATUS AND FUTURE OBJECTIVES.

Jorge Garate, Jose Martin Davila, Manuel Quijano, Carmelo Belza.
Real Instituto y Observatorio de la Armada en San Fernando.
jgarate@roa.es

Abstract

San Fernando SLR station is involved in a process of constant evolution. In the frame of the Spanish Government researching projects support, the station is being prepared to be able to extend to three tracking shifts, by using CSPAD not only during nightime but also during daylight. Some problems have to be overcome before we get this jump, i e. a more accurate control of the horizontal movement of the tellescope and a system to control the ray beam offset during daylight.

As soon as the station meet this goal, we will move to the next objective: the tracking of the highest satellites, ETALON, GLONASS, GPS and the coming GALILEO constellation.

Refurbishment of the SLR facilities

During the spring of 2003, a lot of work were developed in order to improve the quality of the SLR station facilities. Besides the refurbishment of the control hall, a new air-conditioned temperature controlled room was built. Air conditioning equipments were improved in order to keep the temperature for the essential systems as stable as possible. A new rack containig timing devices and control system was installed into the new room. The laser bank is also located there. Laser bank cover was replaced for a new one, more accesible and more easy to manage than the old one, as one can see in fig.1.

Figure 1: San Fernando laser bank: old vs new aspect.

Calibration system

The external calibration target is still mounted on the top of a building located a distance of about 1.5 kilometer from the telescope. Although it is no longer used to make calibrations during the trackings, we use it to periodically check the laser beam divergence, shooting over it with very low energy. To calibrate the system during the tracking sessions we use two optical squares that we have mounted into the dome very close to the telescope, as shown in figure 2. Mirrors and a diffusers are the main components of these squares. Figure 3 is showing the calibration process principle. The short distance from the transmitting telescope and the receiving system tries to ensure we are avoiding tropospheric uncertainties.

Figure 2: Calibration squares mounted into the telescope dome

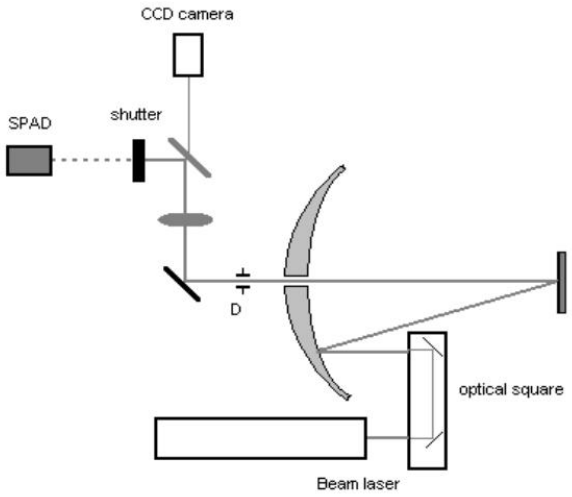

Figure 3: Calibration principles

Receiving System

The receiving device attached to the telescope allows us to choose between a C-SPAD and a Photomultiplier to be used as detector. We only use C-SPAD during nightime operations, while the photomultiplier is selected as diurnal detector. Different ray paths originate different calibration values depending on which elements is used. We are in the way of eliminate the photo, to improve the single shot rms during daylight tracking.

Control System

The system is controlled by a computer with a Pentium 4 processor, using MSDOS operative system yet. One of the objectives in the near future is to split the work in two different computers. One of them will be devoted exclusively to control the movement of the system in a more smooth and suitable way. Software to control the telescope movement has been written already. The other computer will control the rest of the parameters of the observation. But both of them will be connected through the local network. A migration to a more modern operative system is mandatory. We are considering Linux as a suitable option.

Timing System.

The new rack located at the air controlled room contains up to three SR620i time counters. One of them was calibrated during the EUROLAS Workshop 2003 held at Herstmonceaux Castle. Another one belongs to Graz SLR station. We have to acknowledge Graz SLR staff for their support, by borrowing us the equipment. The idea of using three timing devices is to make comparisons among them, trying to keep the timing system as accurate as possible. On the other hand the syncronization is performed by using a 10Hz signal from the Cesium atomic clocks located at the Observatory Time Department.

Figure 4: Timing devices in the control rack before and after the station refurbishment.

Summary

Data quality and quantity of San Fernando SLR Station is improving in a smooth but continuous way. A strong effort has been made to modernize the station, by recognizing those elements which would need to be improved, and by fixing problems encountered. In this way we expect that in the very near future San Fernando SLR station will be able to track LAGEOS during daylight as well as during the night, and with a high quality standards in the trackings. Next step will be tracking high satellites. But it will be mandatory to improve the quality of the pointing. Servo control of azimuthal and height motor need to be studied and improved.

Acknowledgments

Financial support for the technical improvements has been got from the Spanish Government through the researching project ESP 2001-4514-PE. We have also get a strong support by the Spanish Navy, in order to improve the quality of the station facilities.

TRANSFORMATION OF THE BAKER-NUNN CAMERA OF SAN FERNANDO

FJ. Montojo (1), J. Núñez (2,3), J.L. Muiños (1), M. Merino(3), O. Fors (2,3), F. Belizón (1), M. Vallejo (1), J.M. Codina (2).
(1) Real Instituto y Observatorio de la Armada en San Fernando
(2) Observatori Fabra. Real Academia de Ciencias y Artes de Barcelona
(3) Departamento de Astronomia y Meteorologia. Universidad de Barcelona
fjmontojo@roa.es

Abstract

We present the transformation of a Baker-Nunn Camera (BNC) for remote and robotic use with a large format CCD, and its transfer to a new site located in Catalan Pyrenees. This project is a collaboration between the Fabra Observatory (Real Academia de Ciencias y Artes de Barcelona) and the Real Observatorio de la Armada de San Fernando (ROA). Once refurbished, the 50cm f/1 camera will have a useful FOV of 5ºx5º and will be controlled via Internet. This is not a restoration of an old astronomical facility but a completely innovative refiguring of the instrument. We will modify both its mechanics and optics and will set up a new unique facility in Catalonia operating in real robotic and remote mode. Once the BNC will be operating, our scientific project considers two kinds of observing programs: a systematic observing program (QDDS) and selective observing programs. The Quick Daily Sky Survey will operate by means of TDI (Time Delay Integration) CCD observation. It will be able to cover almost the entire northern sky in 4 or 5 nights up to V=20 producing up to 25 Gb/night of data. The other specific observing programs include the discovery and tracking of solar system objects (NEOs, PHAs, main belt asteroids, comets and TNOs), the detection of extra-solar planets, the detection of novae and supernovae, the quick localization of counterparts of GRBs, the detection of dangerous space debris and, in general, any program that could benefit of the large FOV and quick reaction of the camera.

Introduction

The Automatic Wide Field Telescope (AWFT) project (Núñez et al., 2002) is a San Fernando-Fabra collaboration to enable a Baker-Nunn camera for remote and robotic CCD use. The original Baker-Nunn cameras (BNC) were f/1, 50cm aperture modified Schmidt telescopes originally created by Smithsonian Institution (Henize, 1957) to photographically observe artificial satellites. The superb optical design of the camera achieved a fast response (f/1) yielding out extraordinary useful field of view (FOV) of 5ºx30º with a spot size inferior to 20 microns throughout the field. This turned BNC into an extraordinary instrument in spite of its manually altazimutal movement and the use of curved 55cm cinemascope film as detector. One of the BNCs was installed at the Real Instituto de la Armada de San Fernando (ROA) during the 60s. Once the photographic observation of satellites was relegated, the camera was donated to ROA, where it has been maintained inactive but in excellent state of conservation. In order to transform this BNC to a proper remote and robotic use with a large format CCD, an extensive optical and mechanical transformation project must be performed. It will operate as a quick reaction full robotic and stand alone facility observing in remote real time mode in order to follow the most appropriate scientific programs. The experience of the ROA in the automatization of the Meridian Circles of La Palma (CAMC) and San Fernando (CMASF) operating from Argentina (Muiños et al., 2001) will guarantee the right performing of all the refurbishment stages. Besides, the nearly centenary experience of Fabra Observatory in high quality astrometic observations and the experience with the recent restoration and modernization of its own facilities ensure the right development of the project and the best scientific use of the transformed-BNC.

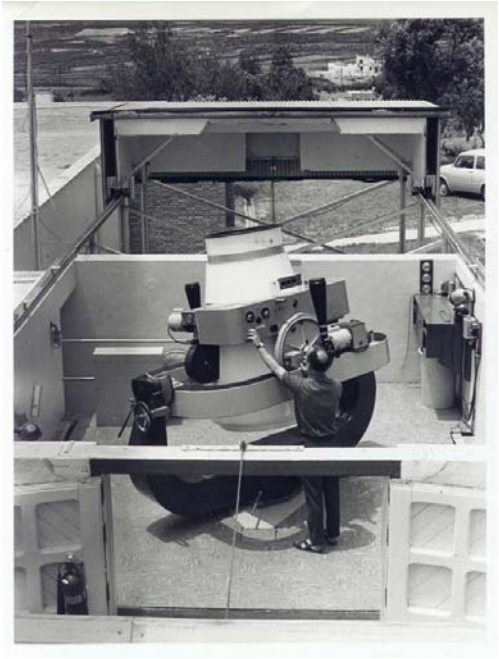

Figure 1. Baker-Nunn at ROA when it was still on active service.

Refurbishment project.

Through a simple optical modification for adapting the camera for the use with CCD, we will achieve an useful FOV of 5ºx5º. This provides us with a unique instrument to perform precise systematic observations of large sky areas in a reduced amount of time and to a relatively high limiting magnitude. Moreover, the camera and all other instruments involved in the observatory will be modified for operating as a totally automatic robotic and remote facility controlled via Internet. The refurbishment project consists in the following phases:

- Mechanical modification and remote telescope control.

  Conversion of original mount to equatorial, installation of new servo drive for RA and DEC axes, positional absolute encoders, multi-axe closed-loop controller and a GPS card must be implemented. These modifications are now being held at the military facilities in San Fernando.

- Optical modification

  CCD adaptation implementing a 4kx4k-9□m front-illuminated CCD with optional filters will be held. To maximize the useful FOV maintaining the low magnitude of aberrations we should modify certain optical parameters and add a field flattener 3 element corrector. A new precise optical design is currently being studied to achieve the best performance.

- Software adaptation for telescope control system.

  Adaptation and/or creation of software appropriate for our specific instrument and operating mode for both telescope working and observatory control. Own telescope movement, guidance and pointing software is available to be adapted to the new requirements in San Fernando. Dome, weather station and other observatory parts controlled by software are chosen to work with known available TCS.

- Building and observatory elements transformation.

  Remodeling of the building, including dome, weather station and microwave telemetry and data link system installation at the chosen site can be done only at summer time because of high mountain climate.

Nowadays, there are two similar projects involving BNCs transformations. One of them, the Australian Automated Patrol Telescope project (Carter et al.), has already accomplished successfully those objectives. The other, held at the Rothney Observatory (Canada) is currently in the late stages of refurbishment project.

Figure 2. Mechanical transformation of the Baker-Nunn camera is being held in San Fernando, where they have consolidated experience with astronomic instruments.

Scientific project

For such a fast response high FOV instrument we must consider two different kind of observing programs to be developed. First, an ingenious survey capable of optimize the BNC performance which has been chosen to be the Quick Daily Sky survey (QDSS). And besides, other specific observational programs of diverse nature related to different areas of astronomical and astrophysical interest.

Nevertheless, this division may not be always so clear since some specific programs could take advantage of the QDSS mode not only using its resulting data, but also enabling several real time data processing tasks and other possible interactions such as programmed automatic launch alarm systems.

- Quick Daily Sky Survey (QDSS)

The systematic observing program would operate by means of TDI (Time Delay Integration) CCD observation. This scanning technique consists in covering sky areas following celestial meridians towards the pole while the CCD charge is transferred at the same rate that the telescope is slewed. With the planned modified BNC FOV, would be allowed to cover daily up to 25% of the sky between declinations -30<d<+70 up to more than V=20 mag. Given the aperture of the BNC, a integration time of 2 minutes, the scale, and considering a CCD detector with moderate-high quantum efficiency (70%) offered by a typical commercial CCD

camera, we estimate the limiting magnitude of the QDSS of at least V=20 mag. In this range there are many astronomical and astrophysical fields of research that could benefit from the obtained data.

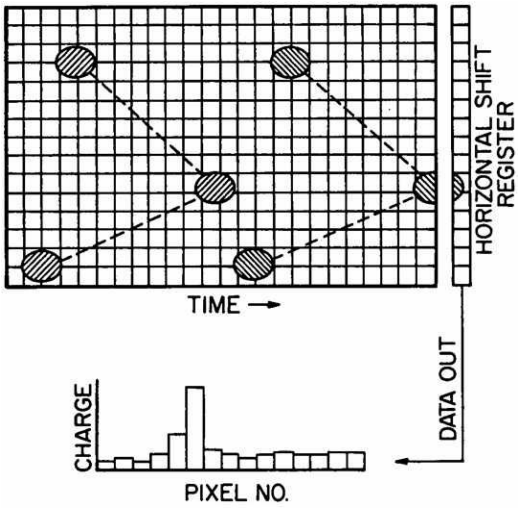

Figure 3. Diagram of TDI operating mode. Once the CCD is oriented in N-S direction, the telescope moves covering sky areas following celestial meridians towards the pole while CCD charge is transferred at the same rate. TDI allows a wide coverage of declination with an improved magnitude limit (it depends on the readout rate chosen) with an easy synchrony to work.

- Specific observing programs

Apart from the systematic programs as QDSS, BNC will be able to operate specific programs of diverse nature. Extraordinary large FOV and quick reaction in remoterobotic mode enables modified BNC to work in observational programs such as:

- Discovering and tracking of NEOs, PHAs, MBOs, comets, KBOs and TNOs. A complete census of these objects is demanding for accurate calibration of Earth-collision probabilities (NEOs, PHAs) and of present models of solar system origin, composition and evolution (MBOs, comets, KBOs, TNOs). Observation and tracking of comets and asteroids has been developed at Fabra and San Fernando Observatories for more than a century. BNC technical specifications will be ideal to enforce this activity since the extraordinary large
- FOV besides the ability of working within a wide range of temporal resolution will greatly increase the probability of detection and discovery.
- Detection of extrasolar planets. Photometric transit technique applied over a large FOV is likely to bring positive detections since it greatly increases the number of measured stars and, consequently, the probability of spotting transit
- Detection and monitoring of optical transient events such as gamma ray bursts (GRBs), supernovae (SNs) and novae. Again, the BNC large FOV combined with its planned fast slewing response will permit to point the GRB afterglow few tens of seconds after satellite alarm has been given.
- General and temporal high-resolution CCD photometry in scanning mode. The use of the filters added to the modified BNC during scanning modes (both QDSS and non-QDSS scanning) will permit to cover large areas of sky within a wide range of time resolution in selected wavelength range.

- Discovery and tracking of space debris (0.1m-1m). A complete orbit catalog and tracking of these objects is demanding, since they can put in danger current or future space missions.

Data flow and processing

BNC operations will generate a large amount of data to be transmitted, processed and archived. The proper flow, processing, analysis, archiving and retrieval of such huge amount of data will be another challenge of this project. For instance, only QDSS data would produce up to 12 Gb/night. Managing of this amount of data for real time remote operations require a fast data flow. In our project, it will be trough microwave technology from the high mountain top site chosen to the Catalan universities fast speed network. Specifically, the processing and following use of the data would go through the following steps:

1. Immediate and in situ processing. Basic image handling, automatic search for minor bodies (NEOs, MBOs, TNOs,..), supernovae (SNs), novae, gamma-ray bursts (GRBs), extrasolar planets… or programmed automatic launch alarm systems.
2. Short term processing. Includes not only data transfer, storing and archiving and the usual knowledge discovery through traditional data processing, but also other more sophisticated digital processing techniques of reconstruction, fusion,…
3. Mid and long term processing. Besides the storage of raw data, all the developed data should be passing through an efficient image compression system and be available in some kind of permanent archiving with access from some international astronomical databases coordinated group.

Site

In order to take advantage of the BNC specifications, this should be moved to a site with very good astronomical conditions. The definitive site is still under study but probably it will be at Catalan Pyrenees.

Conclusions

Automatic Wide Field Telescope (AWFT) has been presented and described as the project of transformation a BNC into a fast high FOV remote and robotic CCD standalone facility operated through internet, its placement at a new location and the following use of the instrument for scientific purposes. Finally, we must remark that this project does not have a character of restoration of an old facility to equip it with the new instrumentation, but it consists in a completely innovative refiguring of the instrument for achieving such special specifications for a successful developing of the relevant scientific tasks described.

Acknowledgements

Partial funding provided by grants AyA2001-3092, AyA2001-4114-E and AyA2002-11251-E from the Spanish Ministry of Science and Technology.

References

Carter B.D., Ashley M.C.B., Sun Y.S. and Storey J.W.V. (1992) "Redesigning a Baker-Nunn Camera for CCD Imaging" *Proc. ASA* **10** (1) 1992.

Desmond King Hele (1966) "Observing Earth Satellites" pg. 82

Henize K.G. (1957) "The Baker-Nunn Satellite-Tracking Camera" *Sky and Telescope*, **16** nº3, 108-111

Muiños, J.L., Belizón, F., Vallejo, M. Mallamaci, C.C. and Pérez, J.A, 2001, "El Círculo Medidiano Automático de San Fernando en San Juan", in *First Latin America Meeting on Astrometry*, ed. C.López et al., in press.

Núñez, J., Muiños, J.L., Fors, O., Belizón, F., Vallejo, M., Codina, J.M., 2002, "Transformation of the camera Baker-Nunn of San Fernando: quick CCD survey" in *Highlights of Spanish Astrophysics III*, eds. J.Gallego et al., in press.

MODERNIZATION OF THE BOROWIEC SLR SYSTEM

J. Bartoszak, S. Schillak
Space Research Centre of the Polish Academy of Sciences
Astrogeodynamic Observatory, Borowiec
sch@cbk.poznan.pl / Fax: +48-61-8170-219

Abstract

The poster presents the process of quality improvement of the satellite laser ranging system in Borowiec performed in the period 2002-2003. The following new devices were installed: time interval counter STANFORD SR620, fast start photodiode and Constant Fraction Discriminator TENNELEC TC-454 in start and stop channels. The realization consists several steps; installation and examination of a new counter, correction of the amplitude and shape of laser pulse by means of the fast photodiode, regulation of discriminator delay and levels for start and stop channels. All these works were finished in May 2003. The single shot precision and normal point precision was improved from 30 mm to 18 mm and from 7 mm to 4 mm respectively. Two centimeters systematic deviation of STANFORD time interval counter was eliminated. The better stability of the system delay vs amplitude of stop signal was observed. The accuracy of the Borowiec SLR data obtained from the results of the several orbital centers confirmed the improvement of the quality of the satellite laser ranging system in Borowiec.

Introduction

The paper presents the process of improvement the quality of the Borowiec SLR data performed in the period 2002-2003. The electronic system hitherto in used based on old Time Interval Counter PS-500 with accuracy 80 ps, Maximum Likelihood Timing Discriminator B6 and avalanche photodiode for start pulse introduced single shot precision on the level of 3 cm. Installation of the new devices allowed for near two times reduction of standard deviation of the satellite measurements.

The modernization of the Borowiec SLR system included in 2002 and 2003 the following tests and new devices:

- comparison tests of Borowiec Time Intervals Counters STANFORD SR620-A and SR620-B in Herstmonceux - 1-13 March 2002
- Time Interval Counter PS-500 replaced by STANFORD SR620-A - 7 May 2002 installation of neutral filters wheel - 25 October 2002

- Time Interval Counter STANFORD SR620-A replaced by STANFORD SR620-B - 15 November 2002
- installation a new fast photodiode in start channel - 19 November 2002
- discriminator TENNELEC TC-454 in start channel - 19 November 2002
- discriminator B6 replaced by discriminator TENNELEC TC-454 in stop channel - 29 March 2003
- installation of spatial filter - 18 May 2003

The system after modernization is presented in Figure 1.

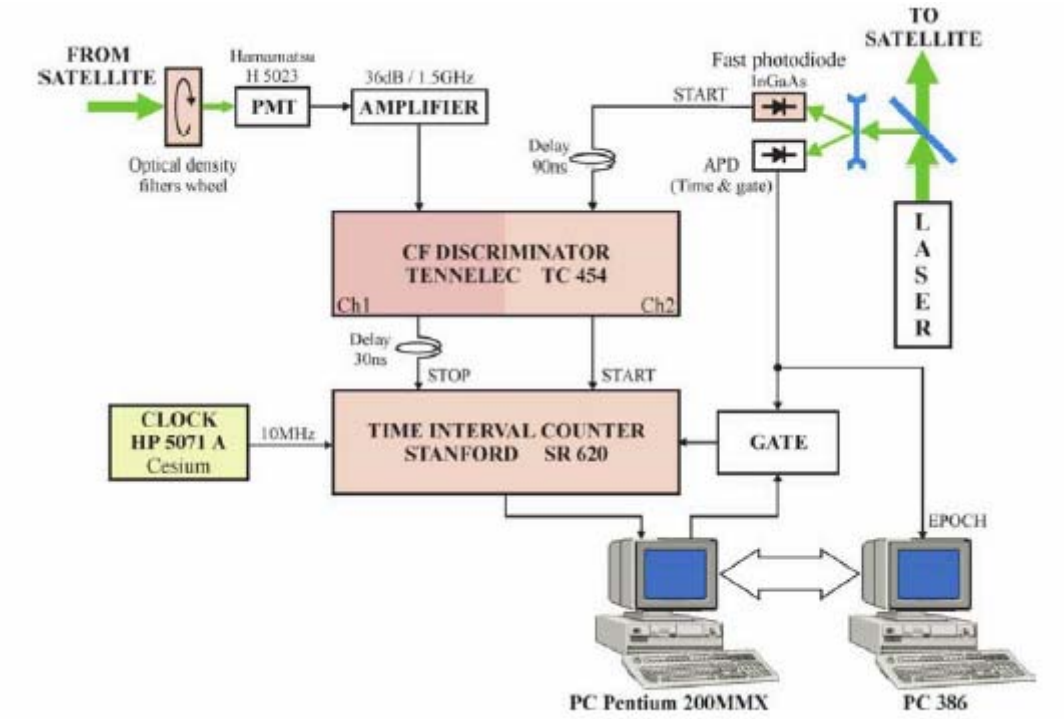

Figure 1. The scheme of the Borowiec SLR system.

Table 1. Comparison of the time intervals counters PS-500 and STANFORD SR620

	PERIOD	ORBITAL RMS (mm)	RANGE BIAS (mm)	PRECISION (mm)
PS-500	1998.05.01- 1998.05.18	30	-22	6
STANFORD	1998.05.19- 1998.06.10	53	-48	10
PS-500	1998.06.11- 1998.06.30	28	-27	5
PS-500	2002.01.01- 2002.04.11	28	-5	9
STANFORD	2002.05.17- 2002.11.30	48	-38	6
STANFORD	2002.12.01- 2003.02.28	28	-18	4

Time Interval Counter

The experiments performed with time interval counter STANFORD SR-620 in 1998 show about 2 cm systematic shift in comparison to the counter PS-500 (Table 1). The tests performed for both Borowiec STANFORD counters in Herstmonceux in March 2002 didn't confirm of this shift (Fig. 2). The maximum systematic deviations for both counters for the distance to LAGEOS were on the same several picoseconds level (Gibbs et al., 2002). The STANFORD SR620 was used in the Borowiec SLR system from May 2002. The two centimeters systematic shift was confirmed again (Table 1). The testing experiments revealed that the reason was a mistake in counter gating. The mistake was eliminated in December 2002.

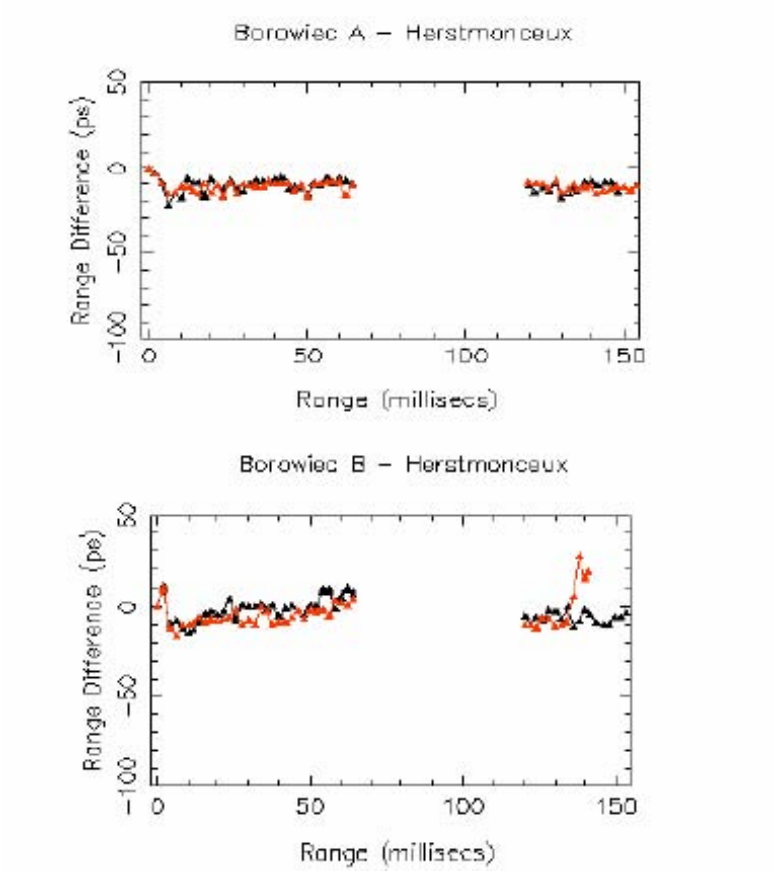

Figure 2. Comparison tests between Herstmonceux STANFORD SR620 timer and Borowiec SR620 timers (A and B) – two series of measurements (black and red), (Gibbs, Herstmonceux 11-13 March 2002)

Start photodiode and discriminator

The second step in upgrading of the Borowiec SLR electronics was installation of the fast start photodiode and Constant Fraction Discriminator TENNELEC TC-454. The start pulse from new photodiode is presented in figure 3, the old start signal from avalanche photodiode is used now as start pulse for epoch registration and gate generator (left pulse in down part of figure 3). The use of time interval counter STANFORD SR620 and fast photodiode open possibility for installation of CF discriminator TENNELEC TC-454, first in start channel and then in stop channel after regulations of the levels and delay for achievement the best parameters of discriminator. The photo of new electronic system is presented in figure 4.

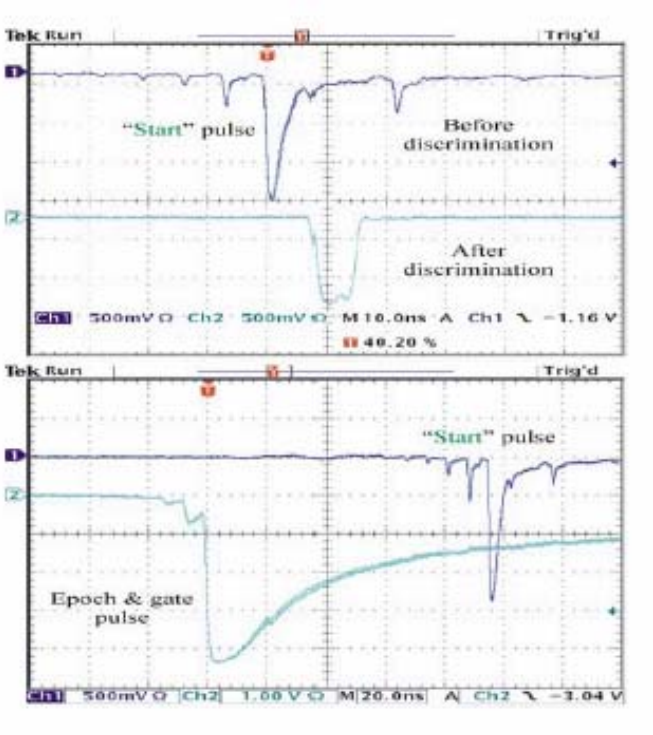

Figure 3. Start and epoch-gate pulses

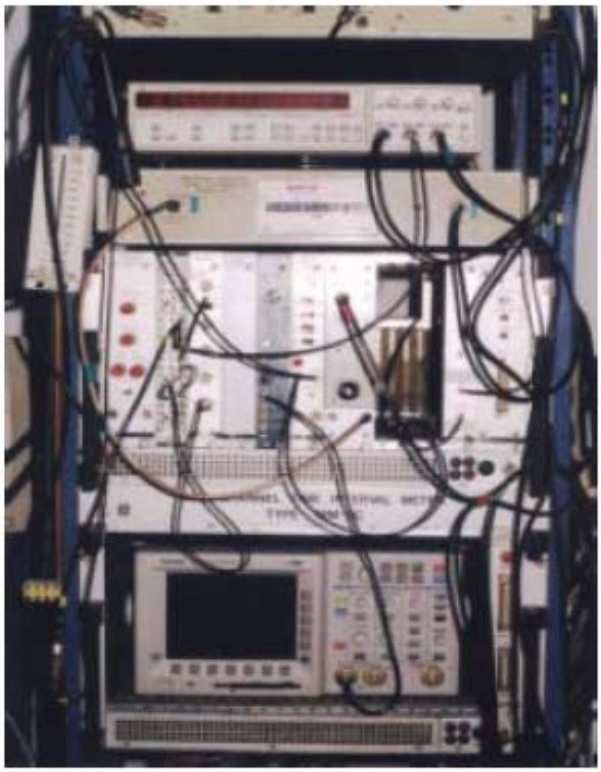

Figure 4. Measuring system: Time Interval Counter **STANFORD SR620**
Amplifier **HAMAMATSU C5594**
CF Discriminator **TENNELEC TC454**
Oscilloscope **TEKTRONIX 3052B**

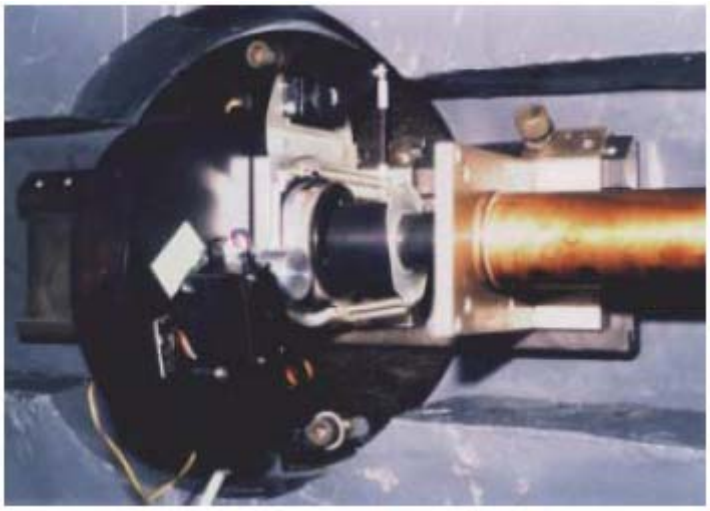

Figure 5. Photomultiplier HAMAMATSU H5023 with filters wheel, diaphragm and green filter

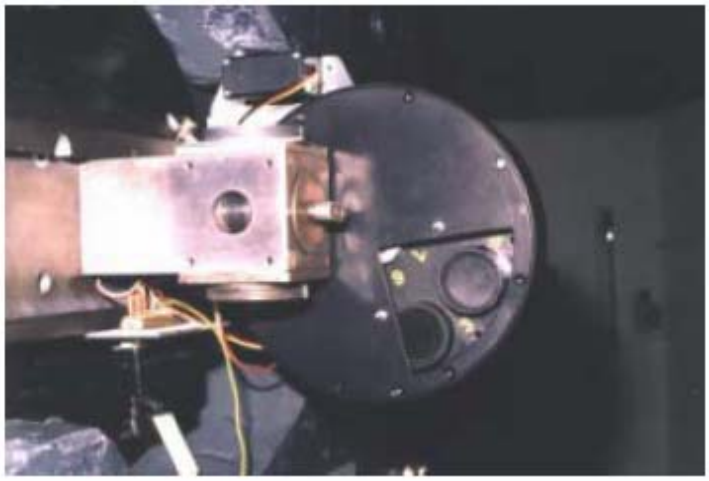

Figure 6. Filters wheel

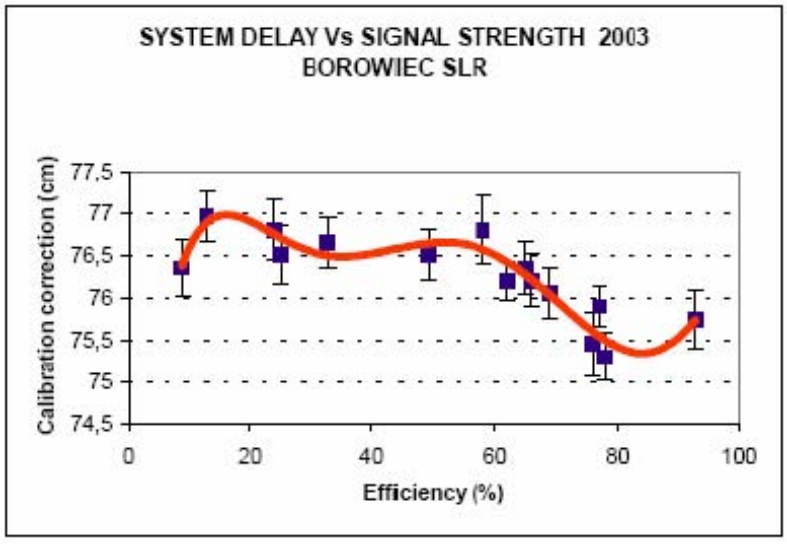

Figure 7. System delay vs signal strength

Table 2. Effect of the Borowiec SLR system modernization

	Before (mm)	**After (mm)**
Single shot standard deviation	30	18
Normal points standard deviation	7	4
Overall system accuracy	18	10

Conclusions

As the effect of modernization of the Borowiec SLR system is near two times better precision and accuracy of measurements (Table 2). The precision is presented on the ILRS web page http://ilrs.gsfc.nasa.gov/stations/sitelist/charts/BORL_LAGEOS_RMS.gif

The jump of RMS in March 2003 is visible. The accuracy of the Borowiec SLR data obtained from results of the four orbital centers in the form of short term stability on the level of 10 mm confirmed the improvement of the quality of the satellite laser ranging system in Borowiec http://ilrs.gsfc.nasa.gov/docs/2003q2_short.gif .

The next step needed to enhance the accuracy of the Borowiec SLR to a level below 1cm is the implementation of a microchannel photomultiplier (MCP) and an event timer ensuring a precision below 10 ps. Improvement of the pointing accuracy of the telescope is important for an increase in the tracking efficiency to more than 100 points per a normal point, high satellites tracking, in future Galileo, and daylight observations. This improvement would demand a substantial modernization of the telescope, which is planned in the next few years.

Acknowledgements

The authors wish to thank Philip Gibbs and staff of Herstmonceux SLR station for tests of the Borowiec time interval counters. This work has been supported by the Polish Committee for Scientific Research within grant no. 9T12E02419 (July 2000 to June 2003).

References

Gibbs P., Koidl F., Kirchner G. (2002). *Range Comparison Results for Various EUROLAS SLR Timers*, Proc. 13th International Workshop on Laser Ranging, Washington, 7-11.10.2002.

TIMER ACCURACY ESTIMATION FOR THE FRENCH TRANSPORTABLE LASER RANGING STATION (FTLRS)

Monique Pierron D.Feraudy, M.Furia, F.Pierron and FTLRS staff.
OCA-GEMINI Avenue N.Copernic - 06130 Grasse - France monique.pierron@obs-azur.fr

Abstract

Timer accuracy estimation is fundamental to reduce station bias. This study is evaluation and modelling of FTLRS Stanford chronometer for different time intervals (linearity), and in time evolution (long-lasting effect).

FTLRS in San Fernando (Spain) June2004

Method.

To evaluate our timing system accuracy, we use two timing systems and compare results of each. We dispose of

- Two Dassaut Timers as the reference, and
- The FTLRS Stanford chronometer (temperature controlled).

As shown on Figure 1, the context is identical and these measures are done on the same events which are echo or noise.

- The laser pulse is distributed to one Dassaut timer, and is the start signal for Stanford counter.

- The return pulse is detected with a SPAD and distributed, via a SPAD Signal Discriminator Card, to the second Dassaut Timer and the Stanford Counter stop signal.

The important item is to note that these measurements are achieved without mutual perturbation.

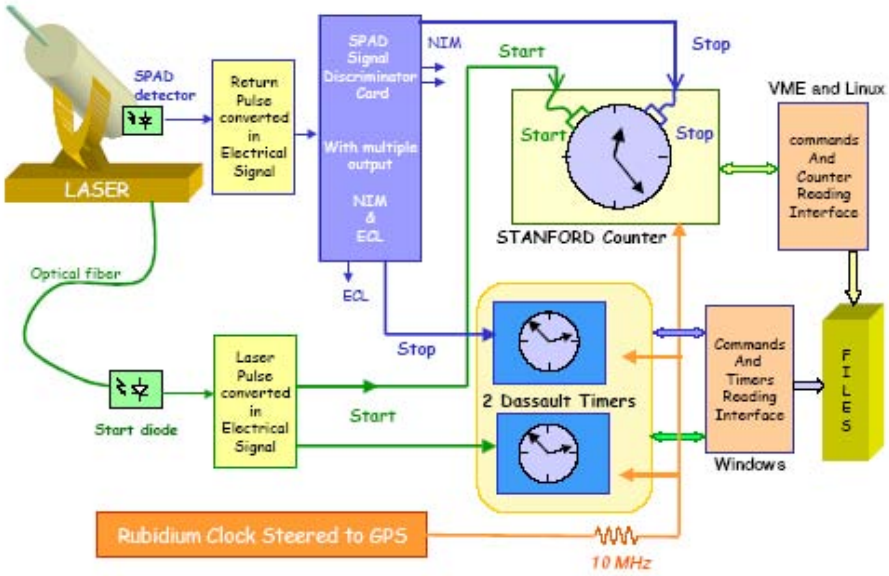

Data acquisition achieved by normal or simulation trac-king software (VME real time and Linux system).

- For FTLRS system with Stanford, the dating is absolute
- For Dassault timers, the dating is relative

Figure 1: Hardware configuration

Dating storage.

The two dating system's results are saved on files. For the same event, FTLRS timing system (including Stanford chronometer) save absolute date, but Dassaut timers timing system save relative dates. To determine which record in each file correspond to the same event (we have just to determine the first correspondence), we have compared on each file the difference between two consecutive laser pulse date, and this method was very efficient.

First result: time stability evaluation

We evaluated the stability of Stanford counter by tracking during one or two hours different targets, from very near (some meters) to 10 000km.

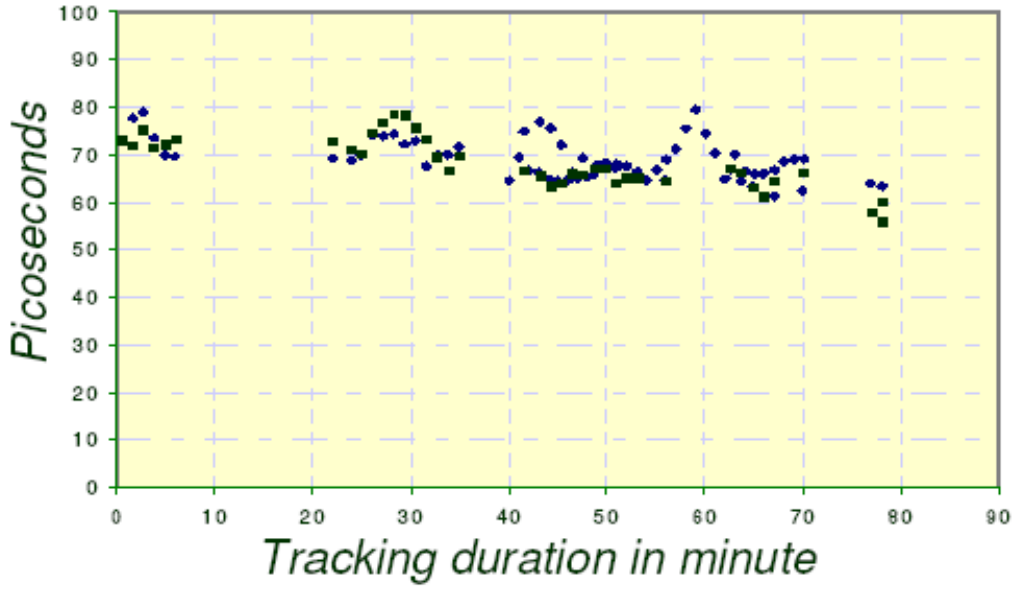

Figure 2: Timing systems difference, LONG-LASTING EFFECT

As shown on Figure 2 (Y_axis is difference between the 2 timing systems), stability is satisfactory, and not range depending at 10 ps level.

Results for internal calibration: from 15ns to 55ns

For this test, and to obtain different roundtrip times, we changed the size of an optical cable; The 2 timing systems difference (in picoseconds) evaluation is on Figure 3. When roundtrip time is less than 33 nanoseconds, this timing difference seems unpredictable: look at Figure 3 After 34 ns, results are repetitive but complementary measurements are to achieve if we want use it as internal calibration

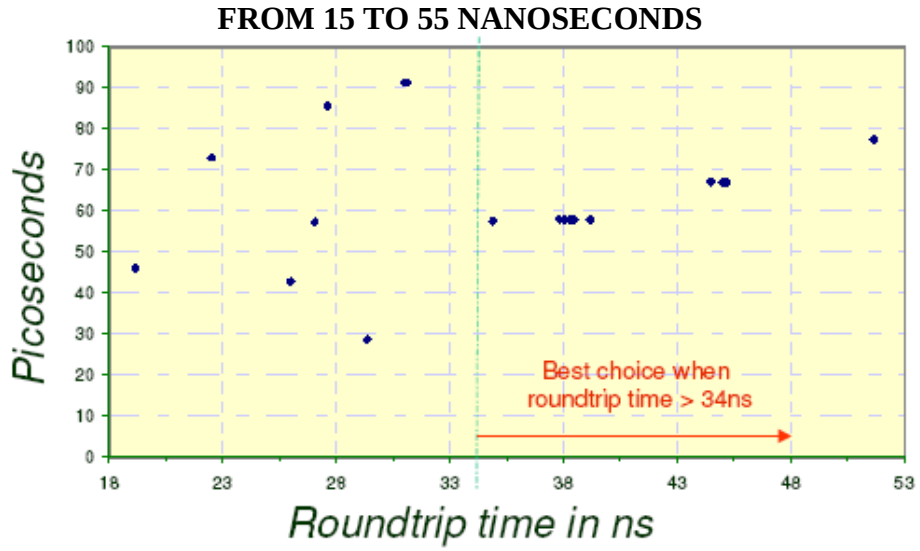

Figure 3: timing systems difference close INTERNAL calibration

Results for target from 100 meters to 1 km:

At different days, we did a lot of measures and observe always the same behaviour of curve. So, range near external calibration is easy to model. The best result is done when target is between 100 to 500 meters as shown on Figure 4

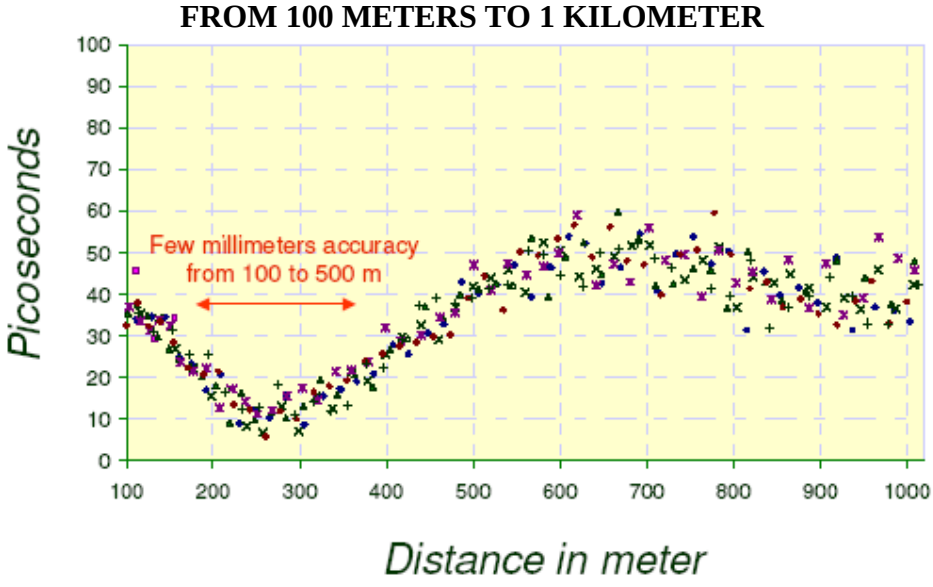

Figure 4: timing systems difference close EXTERNAL calibration

Results for satellite tracking range

For satellite tracking range, the difference between the 2 timing systems is less than 25 picoseconds. On Figure 5 we link all the results. The difference between satellite and external calibration is between 30 and 60 picoseconds. This can explain a part of data range bias during Crete campaign (from the analysis, we had about 40 ps).

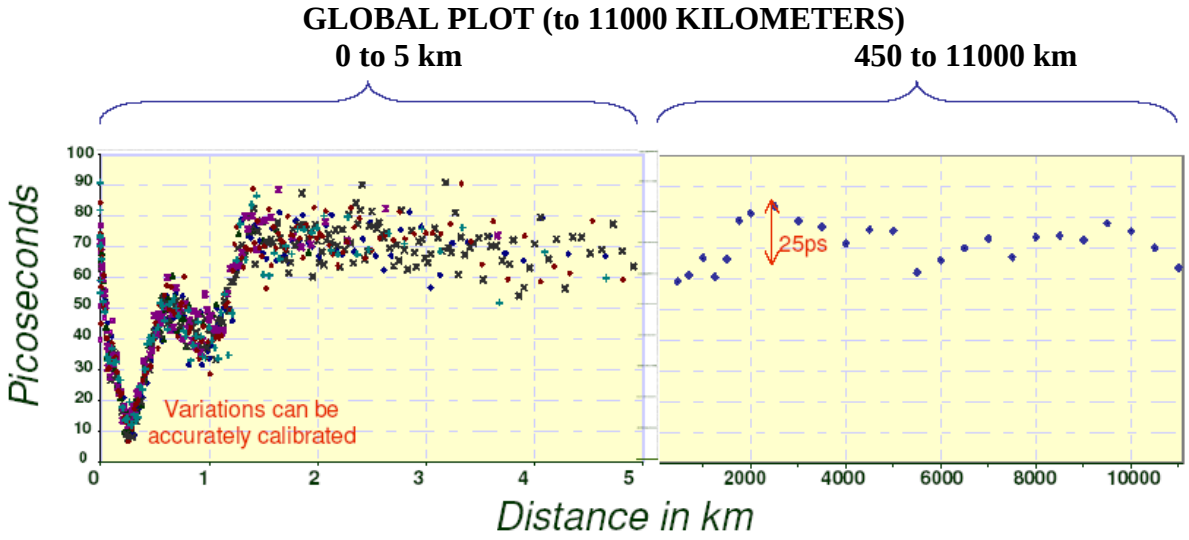

Figure 5: global result for calibration and satellite ranging

Conclusion

It is very important to model chronometry behaviour at different ranges, and to process the calibration value accordingly.

- Stanford Chronometer can achieve few millimetres accuracy during satellites tracking (from 400 to 10 000km).
- Range near external calibration is easy to model; the correction to achieve for this external calibration can be tuned to 30/60 ps depending on the target's range.
- Values near internal calibration range are more difficult to evaluate, except when the roundtrip time is longer than 34 ns. The difference between external and internal calibrations is about 50 ps (7.5mm).

THE PERFORMANCE AND OBSERVATION OF MOBILE SYSTEM TROS-I IN CHINA

Guo Tangyong, Tan Yechun, Li Cuixia, He Shihua, Li Xin, Wei Yinzhen
Institute of Seismology,China Earthquake Administration, Wuhan 430071.
whslr@public.wh.hb.cn /FAX:+86-27-87863471

Abstract

The TROS-I (Transportable Ranging Observation System) is the new generation mobile SLR (Satellite Laser Ranging) system in China. The TROS-I was set up and began to track satellite in 2000. Since its outset of test operation, a lot of field observations were made successfully in Urumqi and Lhasa, western China and the observations filled up gap of SLR tracking in Asia. A series of field experiments has showed that the single shot precision of the system is about 1 to 3cm and about 10mm for the normal point. The largest ranging distance is 20,000km. The mobile system has achieved outstanding performance and extended remarkably the coverage of the existing SLR network from the eastern China to the western part. The ongoing and incoming observations by TROS-I will enhance greatly the ability of SLR in crustal movement monitoring in China. and contribute to precise orbit determination of scientific satellite missions. For instance, the Chinese satellites and other low orbit satellite such as GRACE and Champ.

The Current tectonic activities in China are intensive, evident by widespread deformation of various patterns and frequent strong earthquakes. At present, the application of GPS(Global Position System) measurements to tectonics have been remarkably increased in China and a great deal of advances on monitoring present crustal deformation has been made in the past decade[1]. SLR is also served as useful tool to addressing tectonic study, for instance, with a contribution to monitoring crustal movement by, verifying GPS-derived velocity field and maintaining the reference frame on a scale of continent. However, SLR capability is limited greatly by few stations and uneven configuration of the existing SLR network, majority of which are located in the eastern China. A mobile SLR system costs nearly as much and performs as outstandingly as a fixed system. Moreover, the mobile system has a great flexibility to set up sites on the request , therefore enhancing the ability in monitoring crustal movement and tracking various satellite missions for precise orbit determination It is logical step to develop a mobile system in China for strengthening the network configuration of the fixed SLR stations

In 1999, ISCEA(Institute of Seismology, China Earthquake Administration) offered a mobile SLR system-CTLRS for Xi'an institute of surveying and mapping[2,3].However, CTLRS didn't enter into a routine operation stage mobile for some reasons since then. In 2000, sponsored by the national scientific project CMONOC(Crustal Movement Observation Network Of China)[4], ISCEA developed a new generation mobile SLR system TROS-I[5]on a basis of the forerunner. A lot of upgrade were made in optical, timing and tracking subsystems. TROS-I started the first experimental observation at Beijing, Oct. 2000. It is proved that ranging precision of the TROS-I is 1-2cm for single shot, at a distance up to 20,000km and

environment temperature for operation in the field is –20ºC~+45ºC. The whole performance reaches or exceeds the specifications proposed by designers. TROS-I has already been a standard station of IRLS network (International Ranging Laser Service), and has joined, as one of few mobile systems, in ILRS organization. We have acquired much high-quality data in Urumqi and Lhasa, China. Here we present the technical performance and the observation status of the TROS-I system.

Table 1. The summary of satellites and passes for four sites

Satellite	**Beijing 7343 51 days**	**Urumqi 73558401 44 days**	**Lhasa 7356 150 days**	**Urumqi 73558402 173 days**	**Total** Passes
LAGEOS-1,2	42	44	120	138	344
GPS35,36				6	6
GRACE-A,B				48	48
ENVISAT				55	55
GLONASS	44	2	14	27	87
ETALON	13	1	9	20	43
ERS-2	17	16	2	74	109
GFO	15	3	5	75	98
CHAMP	8	1	0	15	24
TOPEX,JASON	53	10	27	233	323
BE-C	43	2	10	82	137
AJISAI	60	0	32	133	225
STARLETT	22	0	7	107	136
STELLA	23	3	14	6	46
WESTPAC	4	3	0		7
Passes	344	85	244	1019	1688

References

[1] Wang Q , Zhang P-Z, J.T. Freymueller, et al . 2001, Present-day crustal deformation in China constrained by Global Positioning System measurements, *Science,* **294**, 5542, 74-577.

[2] Xia Zhizhong,Cai Qingfu,Ye Wenwei,Guo Tangyong,Wang Linhua, "A Transportable Laser Ranging System in China (CTLRS)", *Proceedings of the 10th International Workshop on Laser Ranging Instrumentation,* Shanghai, 1996, 160-166

[3] GuoTangyong,Wang Linhua, Cai Qingfu,etc,1997,Transportable Laser Ranging Observation *System Devolepment, diastrophism and seism,***18**(supplement):66-72.

[4] Niu Zhijun.Ma Zongjin,Chen Xinlian,etc.2002.Crustal Movement Observation Network of China(CMONOC).*Journal of Geodesy and Geodynamics*.**22**(3):88-93.

[5] Guo Tangyong, CMONOC Transportable SLR System, *Proceedings of 11th International Workshop on Laser Ranging,* Deggendorf, Germany, 1988, :121-125

THE MOUNT STROMLO SATELLITE LASER RANGING (SLR) SYSTEM LOCAL TIE CONNECTIONS BEFORE AND AFTER THE 2003 DESTRUCTIVE CANBERRA FIRES

J. Dawson (1), G. Johnston (1), S. Naebkhil (1), R. Govind (1) and J. Luck (2)
(1) Geoscience Earth Monitoring, Geoscience Australia, Canberra, Australia.
(2) Electro Optic Systems Pty Limited, Queanbeyan, Australia.
John.Dawson@ga.gov.au Tel: +61 2 6249 9028

Abstract

The integrity and strengths of multi-technique terrestrial reference frames such as ITRF2000 depend on the precisely measured and expressed local tie connection between space geodetic observing systems at co-located observatories. The destructive Canberra fires of January 2003 completely destroyed the Mount Stromlo Satellite Laser Ranging observatory including the SLR, DORIS, GLONASS and GPS instruments located at the site. Fortunately, Geoscience Australia has routinely performed classical terrestrial surveys at Mount Stromlo, including surveys in 1999, 2002 and 2003 (post-fire). These surveys have included the determination of the SLR invariant point or IVP. Using existing undamaged survey pillars a consistent stable terrestrial network has been used to compute the relationship between the pre and post fire local tie connections. This relationship includes the millimetre level accurate connections and their associated variance covariance matrix and provides an unbroken contribution of the Mount Stromlo observatory to future terrestrial reference frames and other scientific outputs. Observational and analysis techniques are reviewed and results are given.

Introduction

The Mount Stromlo Satellite Laser Ranging (SLR) observatory is located in the Australian Capital Territory (ACT), see Figure 1. In this analysis the ground survey observations from the 1999, 2002 and 2003 surveys are subject to a combined analysis.

Local Tie Methodology

The Mount Stromlo local tie survey observation and analysis follows the routine procedure used at Geoscience Australia, it is outlined here for completeness:

- The calibration of all geodetic instrumentation including: total station instruments; levelling staffs; fixed height mounts; and reflectors (targets);
- The observation of a vertical geodetic network by application of geodetic levelling (in our case specifically EDM-Height traversing) to all survey marks in the vicinity of the observatory;
- The observation of a horizontal geodetic network by application of terrestrial geodetic observations, including angles and distances to all survey marks in the vicinity of the observatory;
- The observation of a Global Positioning System (GPS) network on suitable survey marks in the vicinity of the observatory (these marks are included in the geodetic levelling);
- The observation of targets located on the observing system (Satellite Laser Ranging instrumentation) during rotational motion about each of its independent axes. This includes zenith angle observations to a staff on a levelled survey mark in the vicinity for precise height of instrument determination;

- The reduction of terrestrial geodetic observations, including the correction of observations for instrument and target bias, set reduction and atmospheric effects, and includes the height of instrument determination from observations to a staff;
- Classical geodetic least squares (minimum constraint) adjustment of all terrestrial geodetic observations, including deflection of the vertical and geoid corrections (derived from the Australian national gravimetric geoid, (Johnston and Featherstone, 1998)). This results in terrestrial-only coordinate estimates and their associated variance-covariance matrix (in a local system) of the geodetic network and targets located on the SLR instrumentation;
- Invariant Point (IVP) modelling and estimation, includes the estimation of IVP, the axes of rotation and associated system parameters such as axis orthogonality and the offset of the axes; Includes readjustment of terrestrial-only network;
- Analysis of GPS observations. This results in GPS-only coordinate estimates and associated geocentric variance-covariance matrix;
- Transformation (translation and rotation only) of the readjusted terrestrial network and computed IVP coordinate variance-covariance matrix into a global reference frame including a geocentric variance-covariance matrix (estimated and *a priori*); The previous GPS analysis is used as the global reference frame realisation; and the
- Reduction of the complete solution to stations of primary interest (i.e. those with DOMES numbers) and output of a SINEX format solution file including all *a priori* constraints.

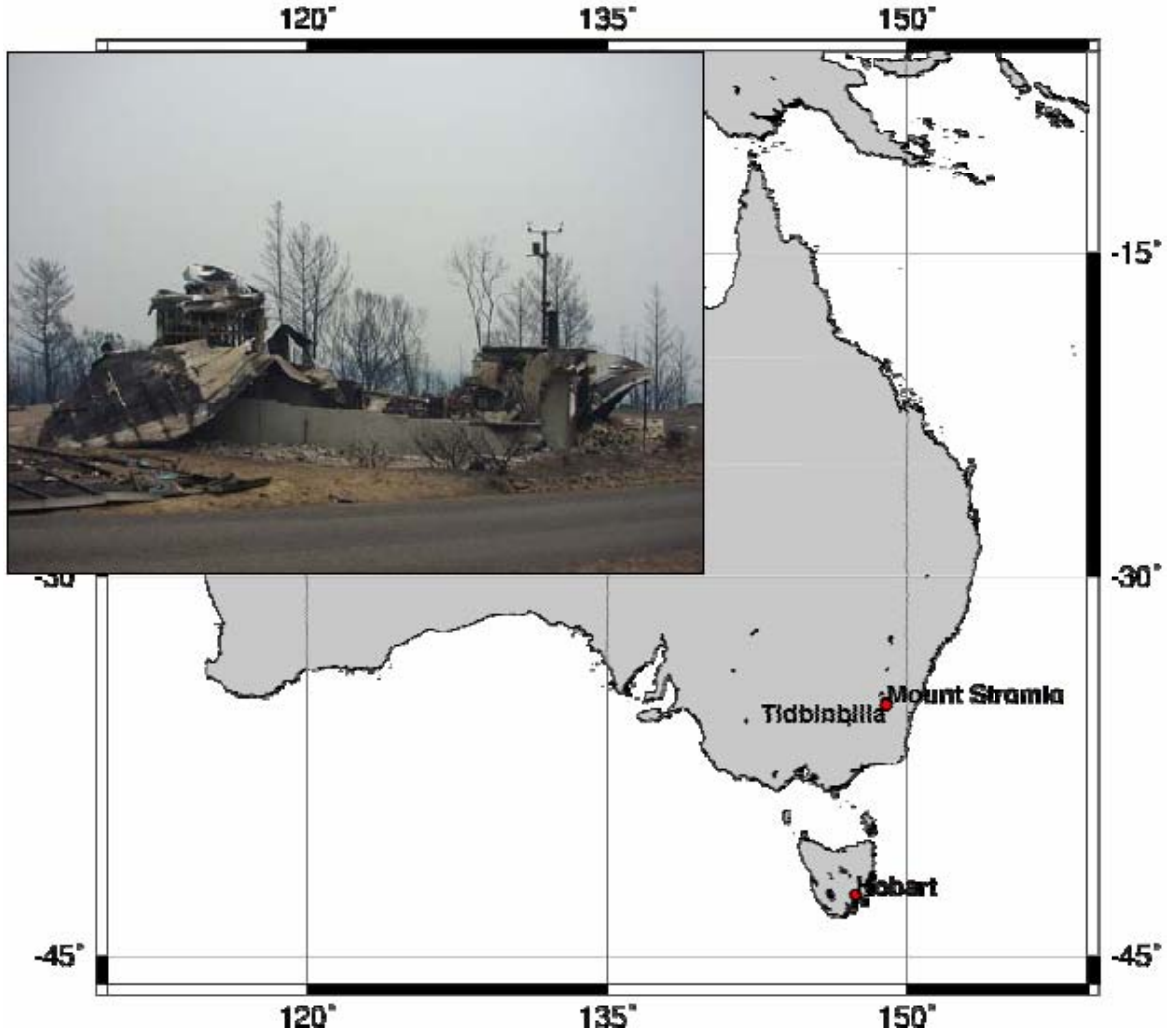

Figure 1. Location of the Mount Stromlo Satellite Laser Ranging (SLR) Observatory. The co-located observatory includes SLR, GPS, DORIS and GLONASS systems; Inset: Mount Stromlo Satellite Laser Ranging station post-fire.

Terrestrial and Global Positioning System (GPS) Observations

Terrestrial observations generally consisted of five sets of observations at each standpoint, see Figure 2. A set consists of a round of face left observations, followed by the reverse round of face right observations. Slope distances and zenith angles were recorded for each observation as well. Atmospheric corrections were not applied in the instrument, but later applied to distances in post processing using conventional correction formulae and local meteorological observations. The heights of instrument were observed using the technique described in Rueger and Brunner (1981), which routinely returns values for height of instrument accurate to 0.1mm. The technique relies on the height difference between the ground marks being determined from levelling observations. Levelling was carried out using an EDM-height traversing technique. It comprises height difference observations to a prism mounted on a fixed-height prism pole, which is braced by a bi-pole and placed over the survey mark. Differential heighting can then be achieved. This technique minimises thermal expansion effects and refraction caused by thermal flux since the lines of sight are near to parallel along the ground surface. Long term GPS continuous observations between the STRR (GPS/GLONASS) and STR1 (GPS) stations were used to align the arbitrary local system to the global system, see Figure 3.

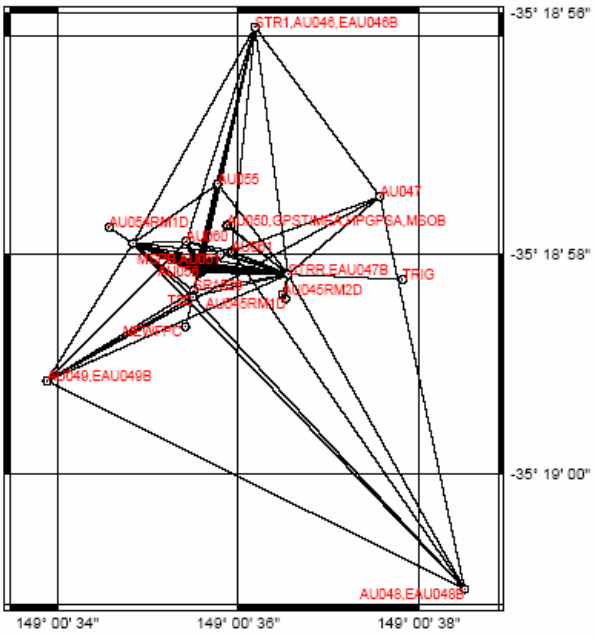

Figure 2. The Mount Stromlo (1999/2002/2003) terrestrial geodetic network. Terrestrial observations between stations are shown as inter-connecting lines. STRR is the permanent GLONASS station; STR1 is the permanent IGS GPS station.

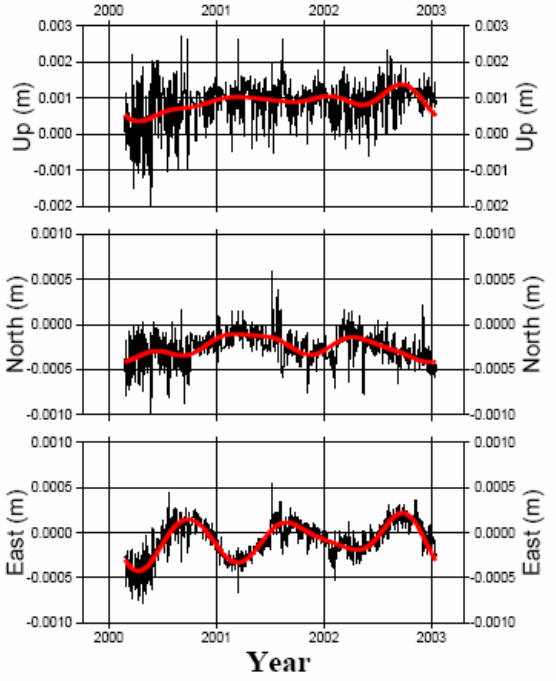

Figure 3. Mount Stromlo GPS baseline time series between STR1 and STRR. Analysis indicates inter-pillar stability at the 1mm level although a sub-millimetre annual signal remains in the baseline (at this time most likely explained by pillar motion).

Satellite Laser Ranging System Invariant Point Determination

The Mount Stromlo Satellite Laser Ranging (SLR) system reference point is invariant point or IVP and is defined as the intersection of the azimuth axis with the common perpendicular of the azimuth and elevation axes. A method based on 3-dimensional circle fitting is applied as the basis for IVP determination. Three dimensional coordinate observations to targets on the

SLR telescope during rotational sequences are used to determine the independent axes of rotation. Multiple realization of the elevation axis (i.e. observed at multiple azimuths) are observed and computed. A least squares method is used for the computation of the axes of rotation and the IVP. A target located on a rigid body, rotating about one independent axis can be fully expressed as a circle in 3-dimensional space. This circle can be described by seven parameters, namely the circle centre (3 parameters), a unit normal vector (3 parameters) perpendicular to the plane of the circle and a circle radius parameter (1 parameter). A minimum of three rotational sequences are required to enable the solution of the equation of a circle.

The method makes the following assumptions: during rotational sequence target paths scribe a perfect circular arc in 3D space; there is no deformation of targeted structure during rotational sequence; there is no axis wobble error; and the axis of interest can be rotated independently of the other axis. No assumptions of axis orthogonality, verticality/horizontality or the precise intersection of the axes are made. The indirect geometrical model includes a number of conditions, including (refer to Figure 4):

- Target paths during rotation about an independent axis scribe a perfect circle in space;
- Circle centres derived from targets observed while being rotated about the same axis are forced to lie along the same line in space;
- Normal vectors to each circle plane derived from targets observed while being rotated about the same axis are forced to be parallel;
- The orthogonality (or non-orthogonality) of the elevation axis to the azimuth axis remains constant over all realisations of the elevation axis;
- Identical targets rotated about a specific realisation of an axis will scribe 3-dimensional circles of equal radius;
- The offset distance between the elevation axis and azimuth axis remains constant over all realisations of the elevation axis;
- The distance between 3-dimensional circle centres for all realizations of the elevation axis are constant over all realisations of the elevation axis; and
    - The IVP coordinate estimates remain constant over all realisations (combinations) of the azimuth/elevation axis;
    - Because the 3-dimensional circle (described by seven parameters) includes a normal vector to the circle plane, the following constraint is also applied;
- The unit normal vector perpendicular to the circle plane is of magnitude one;

The linearized equations take the form of two sets of equations, namely conditions and constraints with added parameters

$$Av + B\Delta = f$$

$$D_1 \Delta + D_2 \Delta' = h$$

where v is the parameter vector of residuals of the input classical adjustment results, Δ is the parameter vector of the circle parameters, Δ' is the parameter vector of the parameters associated with the IVP estimates, f and h are the constant vectors associated with the evaluation of the conditions and constraints respectively and A, B, D_1 and D_2 are matrixes of

coefficients. The least squares solution is obtained from the following system of normal equations (Mikhail, 1976).

$$\begin{bmatrix} -W & A^t & 0 & 0 & 0 \\ A & 0 & B & 0 & 0 \\ 0 & B^t & 0 & D_1^t & 0 \\ 0 & 0 & D_1 & 0 & D_2 \\ 0 & 0 & 0 & D_2^t & 0 \end{bmatrix} \begin{bmatrix} v \\ k \\ \Delta \\ k_c \\ \Delta' \end{bmatrix} = \begin{bmatrix} 0 \\ f \\ 0 \\ h \\ 0 \end{bmatrix}$$

where W is the weight matrix of the input coordinates derived from the classical adjustment and k and k_c are vectors of Lagrange multipliers required to satisfy the Least Squares criteria.

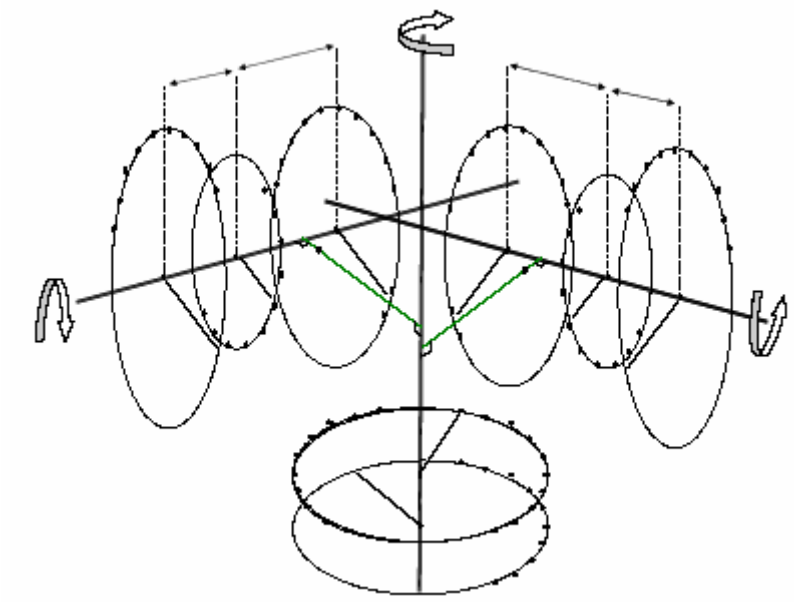

Figure 4. Mount Stromlo IVP model. Note that to simplify the diagram only two targets are shown on the azimuth axis and three targets are shown on the elevation axis.

The solution to the normal equation system is iterated as required for the non-linear condition and constraint equations. An updated estimate of the input coordinates and their variance-covariance matrix is obtained together with an estimate of the IVP coordinate, their variance-covariance matrix and the inter-relating covariance matrix.

Results

Comparisons between the multi-year combined adjustment and each individual survey were undertaken. To remove the influence of datum 3-dimensional translations and a rotation about the local vertical were performed between the combined solution and the individual solutions before comparison. The Root Mean Square (RMS) error between the combined and 1999 coordinate solutions was 0.8, 0.5 and 1.0 mm in the north, east and up components respectively, while the RMS error between combined survey and the 2002 and 2003 surveys was 0.6, 0.2 and 0.3 mm (2002) and 1.2, 0.6, 0.0 mm (2003) in the north, east and up components respectively. Thus in general there is good agreement between the 1999, 2002

and 2003 surveys. Because of this network stability the network realisations have been combined to provide a consistent multi-year local frame at the Mount Stromlo observatory.

Table 1 gives the coordinate of the old SLR invariant point relative to the new laser system. The replacement of axis bearings in the SLR system in late 2001 may account for the small differences between the 1999 determination of ***7849 50119S001*** to the 2002 determination, namely -0.8, 0.4, -0.6 mm east north up components respectively. Please note that the new SLR system was constructed in approximately the same horizontal position as the old system but approximately 0.95 metres higher.

Table 1. IVP determination coordinate relative to SLR IVP 7825 50119S003

	East (mm)	**North (mm)**	**Up (mm)**
7849 50119S001 1999 survey	5.1	-1.9	-948.6
7849 50119S001 2002 survey	5.9	-2.3	-948.0
7825 50119S003 2003 survey	0.0	0.0	0.0

The least squares solution of the SLR IVP position included; 36 targets; 5 IVP estimates (constrained together); 1284 pseudo-observations; 252 unknowns; 69 additional unknowns; 846 conditions; 76 constraints and 178 additional constraints. The resultant linear system was 2705 x 2705 with degrees of freedom 2063. IVP model (circle) fit residuals were 0.9 mm Root Mean Square Error (RMS) for the in-plane residuals and 0.7 mm for the out-of-plane residuals. The Root Mean Square Error (RMS) of the terrestrial coordinate observations to the IVP model were 1.1, 0.5 and 0.5 millimetres in the east, north and up components respectively.

Access to Results

The SINEX file corresponding to this paper is ***AUSSTRO0312GB.SNX***, and can be found at ftp://ftp.ga.gov.au/sgac/sinex/ties/. This file supersedes both the SINEX file aus00c05.snx submitted to the International Earth Rotation Service (IERS) in 1999 for the ITRF2000 computation and ***AUSSTRO0312GA.SNX*** which had incorrect time tags.

References

Johnston G. and W. E. Featherstone, AUSGEOID98: a new gravimetric geoid for Australia, *Australian Surveying and Land Information Group (AUSLIG), available online: http://www.ga.gov.au/nmd/geodesy/ausgeoid/docs/iemsgary.pdf, 1998.*

Mikhail E. M., Observations and least squares, Dun-Donnelley Publisher, New York, 1976.

Rueger, J. M. and F.K. Brunner, Practical results of EDM-Height Traversing, *The Australian Surveyor*, June, 1981, Vol. 30, No. 6., 1981.

N.E.R.C SPACE GEODESY FACILITY, HERSTMONCEUX; CURRENT STATUS AND FUTURE UPGRADES

G Appleby, D Benham, P Gibbs, C Potter, R Sherwood, V Smith, M Wilkinson, I Bayer.

Abstract

The NERC Space Geodesy Facility (SGF) at Herstmonceux, UK features a very accurate and prolific ILRS SLR system, two IGS GNSS receivers and associated environmental monitoring systems. Automatic QC processes continually monitor the quality of all the observational products, the results of which are made available daily on the SGF website. Current funded plans for system upgrade include building an event timer based upon highly accurate timing modules and integration of a KHz solid-state laser system. In the near future plans include a funded proposal to place permanently on site an absolute gravimeter to compliment the space geodesy measurements and make possible new science from the site. In this poster and paper we highlight the current diverse facilities at SGF and outline the future prospects.

Satellite Laser Ranging System

The HERL SLR system remains a very effective ILRS core station, with 8mm single-shot ranging precision to flat calibration targets. This precision decreases to 16mm for LAGEOS observations, which for the strict single-photon operational philosophy is the theoretical level of precision for the satellite. Based on knowledge of the quantum efficiency of the C-SPAD detector (~0.2) it is likely that on average only a single photon is reaching the detector provided that the return rate is less than about 15%.

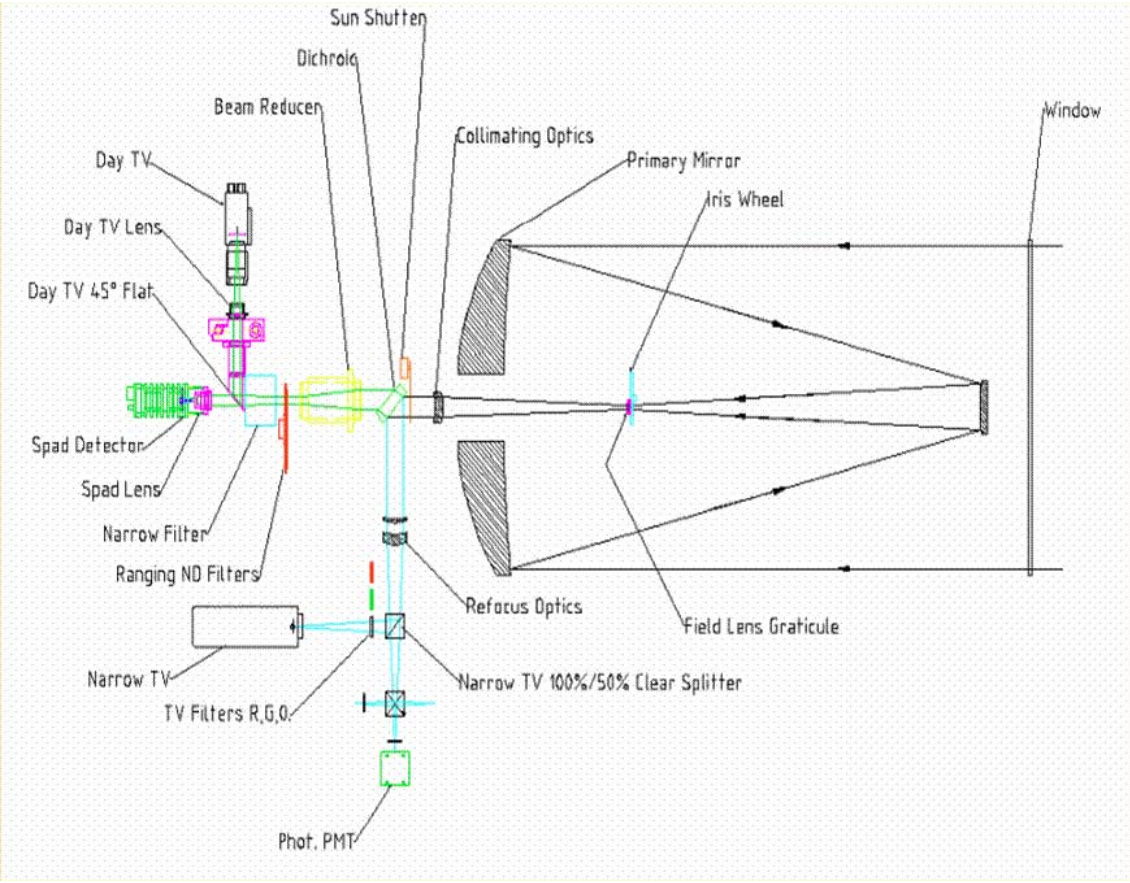

Figure 1. Optical layout of the SGF SLR system.

Returns are maintained statistically at single photon levels by automatically and rapidly determining the current true return rate throughout all calibration and satellite range operations and automatically varying the value of the neutral density filter that is placed in the optical receive path. The optical layout of the whole system is shown in Figure 1, where the neutral density wheel is seen in front of the narrow-band daylight filter.

Also seen is the narrow-field TV system for night time pointing assistance, a TV system for daytime imaging of laser backscatter and a photo-multiplier tube for high-speed photometry.

One of the problems that has been overcome for successful daytime ranging using narrow divergence, low energy laser systems is pointing error caused by heating-induced distortion of both transmit and receive optical mounting systems. The 'day TV' system shown schematically in Figure 1, in combination with a frame-grab processor, allows daytime visual monitoring of the backscattered image of the laser and of bright stars. These innovations are invaluable for fine adjustment of the directions of transmission and reception, and greatly aid daytime tracking.

Occasionally, after a manoeuvre, satellites can be difficult to acquire for laser tracking. The SGF telescope is equipped with a wide-field telescope and camera combination that is used to aid night time acquisition; a visual real-time display is provided (seen in Figure 2 picture below), along with digital frame-by-frame recording. Recently the system has been upgraded to enable detection of a field of view of nearly 2º, very useful for recovery of objects as faint as 12th magnitude.

Figure 2. Wide-field TV system, during laser ranging operations.

- **SLR system Upgrade.**

The philosophy of the SGF laser ranging program has always been to maximise the stability of the data product. This aim has been achieved, as regularly evident in the ILRS quality report cards, by continually monitoring the accuracy of each element of the system. In particular, we have made many test measurements on the detectors and counters, the results of which have been widely published and are available on our website. Results that directly impact on ranging accuracy are: (a) non-linearity of the Stanford counters used to measure

time-of-flight and (b) time-walk within the C-SPAD when ranging to extended targets at high return levels. The solutions to these issues that are in place at present are to determine and remove the counter non-linearity effects using a series of comparisons between the Stanford counters and a high-precision event timer (Gibbs, *et al*, 2003) and to keep strictly to single photon return levels (Appleby, Gibbs, *et al*, 1999), at the expense of an inevitable increase in random noise. In addition, at single photon return levels, it is possible to compute very accurate corrections to refer the laser range measurements to the centres-of-mass of the primary spherical geodetic satellites (Otsubo and Appleby, 2003).

However, better solutions that are in the advanced planning stage are to build a high-accuracy (sub-mm) event timer based on picosecond-level Thales timing modules, and to purchase a 2kHz, short-pulse laser system, that will increase both data yield and single-shot precision. The event timer is currently being built in-house from the timing modules and the laser is due to be installed in summer 2005. Of course, to carry out high-repetition laser ranging, the event timer is an essential element to deal with the multiple pulses in train to the satellite and back throughout each pass. However, we have carried out link-budget calculations based on work by Degnan (1993), which suggest that even though the single-pulse energy of the new laser will be some fifty times less than that of the current Nd-YAG system (0.4mJ *cf* 20mJ), a reasonable number of returns should be detected even if the new laser is used at low repetition rate (10-13Hz). It is likely that the first stage of the upgrade will follow this route, with high-rate ranging awaiting full implementation of the event timer.

GNSS systems.

It is an ILRS requirement that Operational Stations be co-located with IGS receivers. In fact, the IGS site HERS has been operational at Herstmonceux for some fifteen years and the site HERT (relocated HERP system) has been operational since 2002. Besides producing hourly and daily RINEX GPS and GLONASS data, the HERT system also streams navigational data directly to the Internet in support of a EUREF realtime Pilot Project. Unfortunately, during the period 1999 April to 2001 May the HERS system was performing sub-optimally, with the result that it appeared to GPS analysts that the site had jumped some 14mm east. This resulted in both lack of confidence by the community in data from HERS and a second, erroneous, entry for HERS coordinates in ITRF2000. In order to detect early any further problems with either receiver, we have developed automatic GPS QC processes that may be of interest to the ILRS community. The first is a daily sky-coverage plot, taken from the previous day's RINEX files, and is designed as a check on antennae performance. The more detailed QC processes are based on full global and HERS-HERT differential GPS solutions, using the GAMIT processing software developed at MIT, USA. Baseline solutions between the two Herstmonceux systems, which are some 100m apart, are very good checks on the quality of their data, as well as being of interest in studies of site stability. Results from all these QC solutions are updated daily on the SGF website at http://nercslr.nmt.ac.uk .

Absolute Gravimetry.

Funding from the UK Natural Environment Research Council has been secured, in a joint proposal with the UK Proudman Oceanographic Laboratory (POL), for the purchase and installation at Herstmonceux of an FG5 Absolute Gravimeter, built by Micro-G Solutions, Inc. Key to Earth-system monitoring is maintenance of a terrestrial reference system with accuracy in global scale of 1 part per billion. In order to develop such a capability within the European and global community, an initiative to establish a European Combined Geodetic Network (ECGN, Ihde, Baker, *et al*, 2003) is underway within the auspices of EUREF, a European sub-commission of the International Association of Geodesy. One of the objectives of ECGN is to establish core sites where geometric positioning (GPS/GLONASS/SLR),

physical height and gravity field components are all measured to sub-cm accuracy. Given its long record of precise space geodetic and ancillary measurements the SGF site at Herstmonceux has already been accepted as a 'station' within ECGN. Linked to the existing space geodetic techniques by precise site-ties, the absolute gravimeter will contribute absolute gravity measurements from this site of precisely known location within the international terrestrial reference frame. In addition, the site will be very valuable for side-by-side inter-comparison of the POL, and other, absolute gravimeters. This addition to the capability of the SGF site will make the SGF into one of the leaders worldwide, because of the range of different techniques that are now available. It will undoubtedly strengthen absolute gravimetry work within the UK.

Specifically, the absolute gravimeter observations will be used to determine the vertical crustal movements at Herstmonceux to better than 1 mm/year (Williams *et al*, 2001). The absolute gravimetry technique is completely independent of the space geodesy measurements and will therefore provide an important check on any systematic errors in those measurements or in their interpretation and in particular will provide information on global seasonal signals, as well as higher frequency local deformations from the seasonal to the tidal bands.

The gravimeter will be installed in the basement at Herstmonceux in autumn 2005.

Conclusion.

The Space Geodesy Facility is undergoing a major upgrade and expansion of capability. It will soon have KHz ranging capability and a very accurate epoch timing system. The inclusion of absolute gravimetry measurements on site will greatly add to the scientific value and scope of the Facility. These upgrades, however, will be carried out at no cost to the precision, accuracy or quantity of the laser ranging observations from the site, which have been made essentially un-interrupted since 1983.

References

Appleby, G.M., Gibbs, P. Sherwood, R.A. and Wood, R. Achieving and maintaining sub-cm accuracy for the Herstmonceux single-photon SLR Facility, *Laser Radar Ranging and Atmospheric Lidar Techniques II,* SPIE Vol **3865**, 52-63, 1999.

Gibbs, P, Koidl, F and Kirchner, G. Range Comparison Results for Various EUROLAS SR Timers, in *Proc. 13th International Workshop on Laser Ranging*, Washington DC, 2003.

Otsubo, T. and Appleby, G.M. System-dependent center-of-mass correction for spherical geodetic satellites, *Journal of Geophysical Research*, Vol. **10**, No. B4, 2003.

Ihde, J., Baker, T., Bruyninx, C., Francis, O., *et al*. Development of a European Combined Geodetic Network (ECGN), ECGN Working Group, IUGG General Assembly, Sapporo, Japan, 2003.

Williams, S., Baker, T. and Jeffries, G. Absolute Gravity Measurements at UK Tide Gauges, *Geophysical Research Letters*, Vol. **28**, No. 12, June 15, 2001.

Degnan, J.J., Millimeter accuracy satellite laser ranging: a review, Contributions of Space Geodesy to Geodynamics: Technology, Geodynamics Series, D.E. Smith and D.L. Turcotte (Eds.), AGU Geodynamics Series, **25**, pp. 133-162, 1993.

CURRENT STATUS OF SAN JUAN SLR STATION IN ARGENTINA

T. Wang, F. Qu, Z. Wei, N. Liu, B. Cheng and Q. Xiang(1);Y. Han and W. Liu(2)
(1) Chinese Academy of Surveying and Mapping (CASM)
(2) National Astronomical Observatories, Chinese Academy of Sciences
wangtq@casm.ac.cn /Fax:0086-10-68218654

Abstract

A new SLR station will be founded in the near future. The whole SLR systems were already developed completely and checked and accepted by the investor. Some introductions of configurations and characteristics for the systems were in the paper. Also some test results of technique parameters and some achievements of testing observations were introduced. The newest status of station constructions in Argentina and the timetables of the packing and shipment were mentioned as well as in the paper.

Introduction

The project of build a new SLR station in San Juan of Argentina is a kind of cooperation between University of San Juan, Argentina and National Astronomical Observatories (NAO), Chinese Academy of Sciences. The investor for the SLR system is Ministry of Science and Technology in China. The whole system was designed and developed by Beijing SLR station, Chinese Academy of Surveying and Mapping (CASM) in the years of 2000 to 2003. The new station building in Astronomical Observatories, University of San Juan, Argentina is nearly ready for installing the SLR systems now including the dome designed and constructed by University of San Juan, Argentina.

The horizontal mount is the most convenient constructions for telescope mounts for tracking satellite especially for low satellite, including their observations in zenith zone. The initial alt-azimuth telescope mount is just same with the one of Beijing SLR station but a lot of changes were made with it by the common work of the people in Shanghai and Beijing station and National Astronomical Observatories (NAO).

The good hardware and software of controlling and servo system were benefit from the people of Wuhan station. The precision was satisfied from the data analysis reports of Delft University.

The whole SLR systems were already developed and tested completely and checked th and accepted by the investor, Ministry of Science and Technology in China, in 12 of January, 2004.

The South America is a lack of SLR station for many years so the new San Juan station with its good weather conditions will improve the distributing of SLR station in the world. The ILRS needs such a station and the SLR technology needs such a station.

The packaging and shipment will begin before the end of this month and the SLR data of first pass in the new station in Argentina can be ahead of the end of this year if things going well

The System Configuration

Reflecting telescope: bi-axes; sender and receiver separated.
Control system: only by mouse; tracking, predictions, preprocessing…
Servo system: Bi-close-loop control for velocity and position
Laser system: Nd:YAG passive mod-locked
Receiver: C-SPAD
Counter: SR-620

TV system: ntensifier + CCD.
Timing and frequency: HP58503A GPS time and frequency receiver.
Calibration: short distance target, out-install, inside the dome.
The frame diagram of configurations for the whole system is shown as figure1.

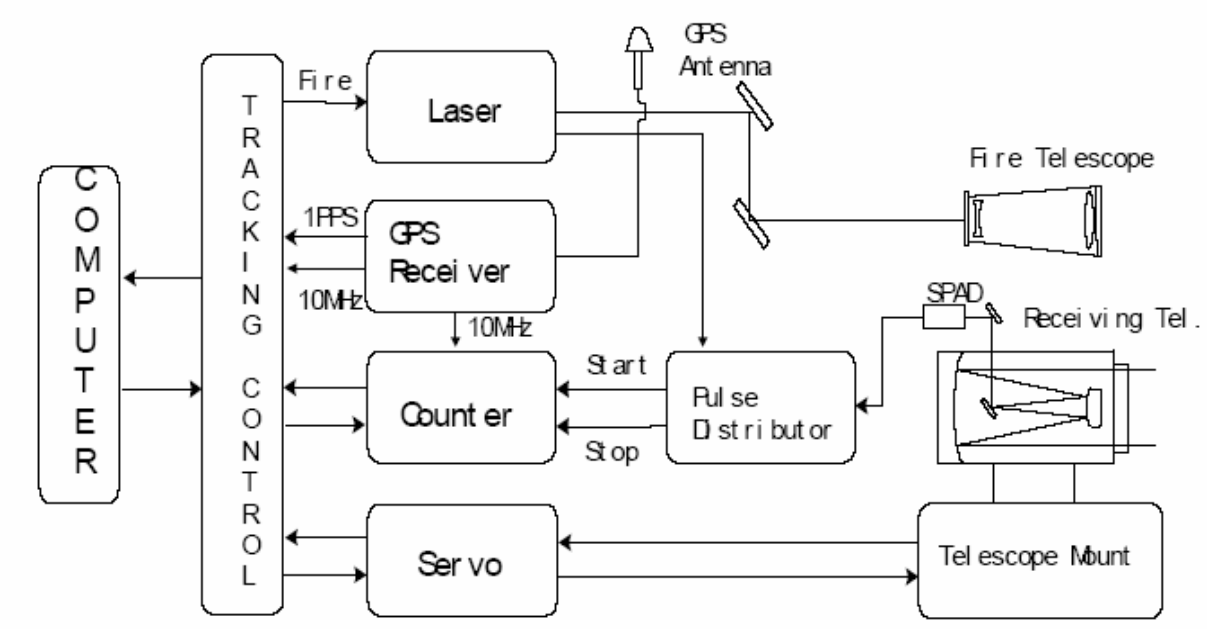

Figure 1. The frame diagram of configurations for the system.

Mechanical Construction

The alt-azimuth telescope mount has flexible mechanical construction with the possibility to dismantle it into separate components to allow packaging in several wood cases for the common container and easily airproof in order to ship the telescope with a long way to South America. It contains a foundation with azimuth plate, an azimuth frame, an elevation frame and a main telescope cylinder with main mirror container and secondary mirror mount.

A general view of the telescope mount is shown in figure 2.

Optical Receiving System

The optical receiving system has a microcrystalline glass main mirror (weight 80kg) with the diameter of 630mm and a microcrystalline glass secondary mirror with the diameter of 200mm. Also there are a spectroscope, an adjustable set of pinhole, an autocollimator and a broadband filter of 10nm in the optical receiving system. The optical receiving system is able to receive both visible light for ICCD and green laser for ranging detector without any additional adjustment due to the spectroscope.

Laser System

The computer controlled and passive mode-locked laser(Nd: YAG) firing rate up to 20Hz has the pulse width of 30ps and pulse energy of 50mj for wavelength 532nm laser. The principle diagram of the laser is shown as figure 3.

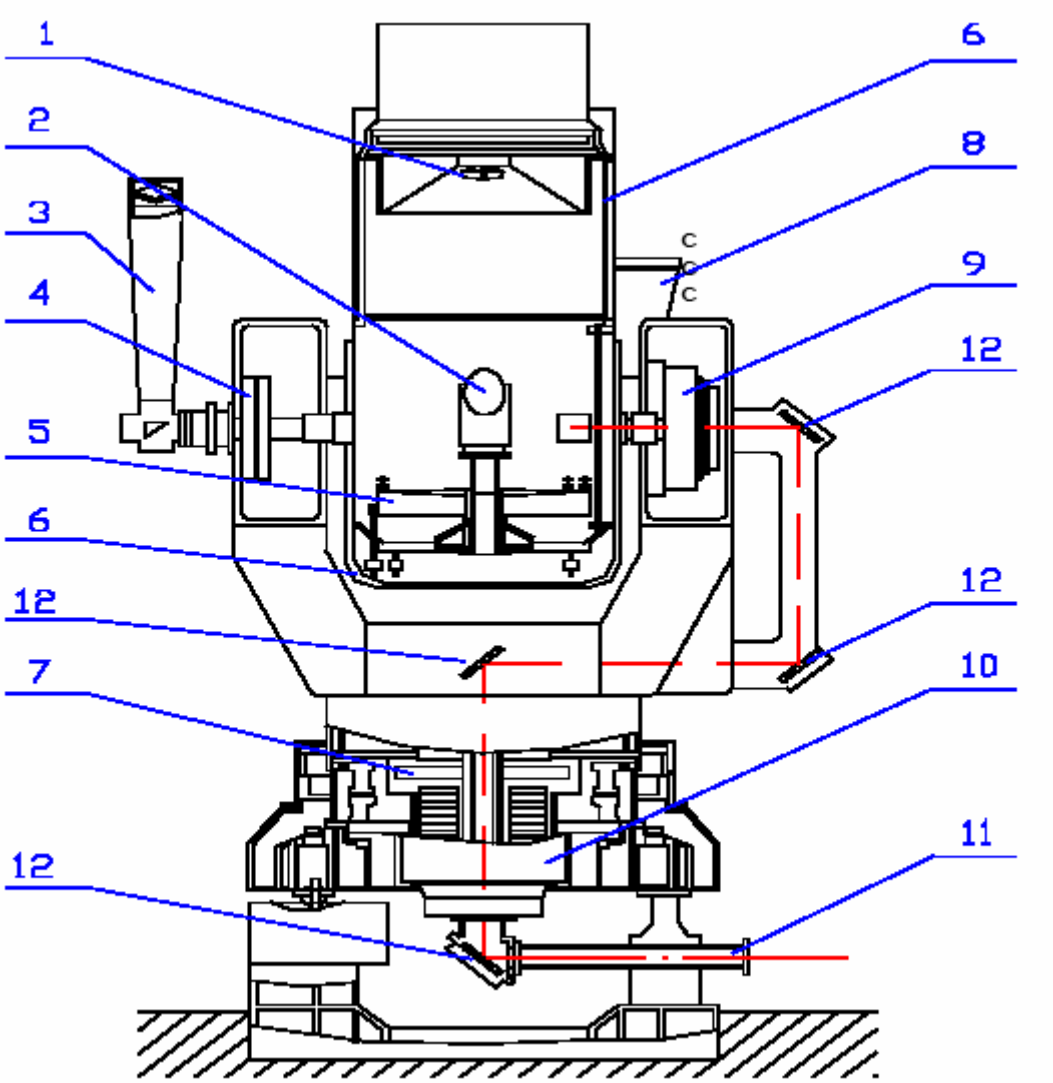

1---SecondaryMirror
2---45degree Mirror
3---Telescope for view
4---Elevation Encoder
5---Main Mirror
6---Main Telescope
7---Azimuth Encoder
8---Emitting Telescope
9---Moment Motor for Elevation
10---Moment Motor for Azimuth
11---Coude Path
12--- Coude Path Mirror

Figure 2. General view of the telescope mount

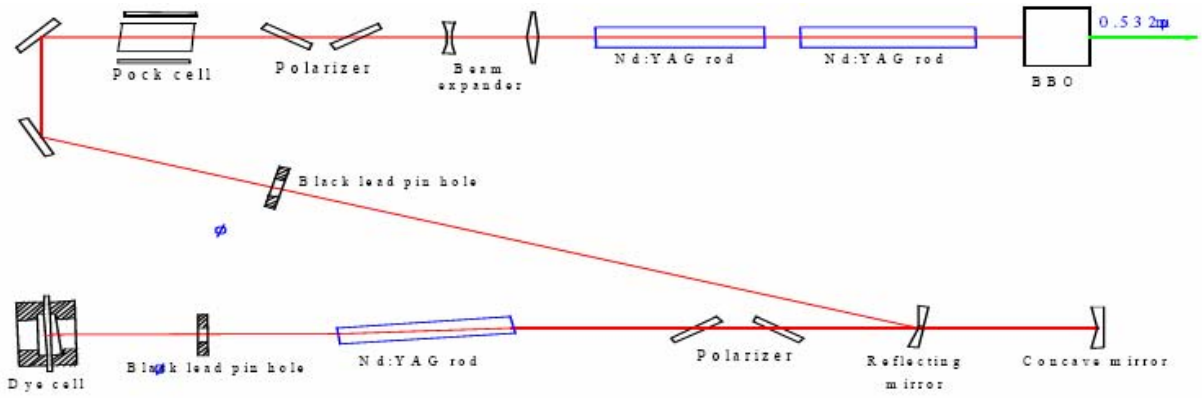

Figure 3. Principle diagram of Nd:YAG laser

Tracking Control and Servo System

A common PC computer is used for telescope control, range gate setting, laser firing and data acquisition etc. All software including satellite predictions and data pretreatment is running in windows operation system and all things can be down just by the computer mouse. The principal design for tracking control and servo system is given in figure 4.

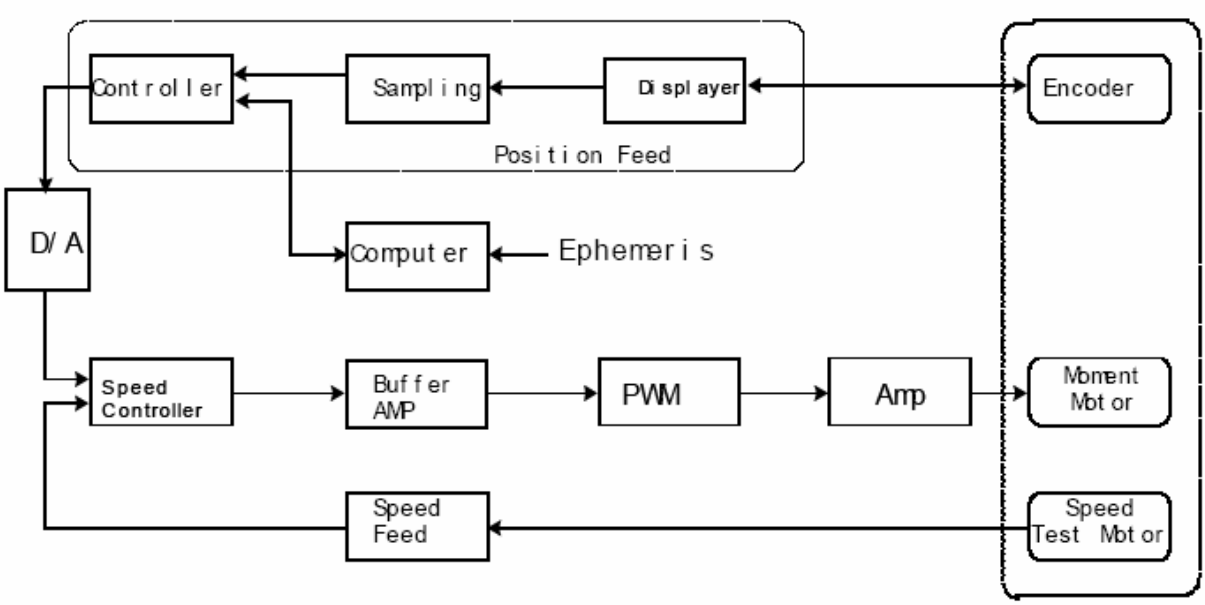

Figure 4. The frame diagram of tracking control and servo system

Test and Test Observations

For check and accept of the investors some tests and test observations were achieved since the end of 2002 to 12th of January 2004. The results of tests and test observations are show as following:

1) **Velocities and Accelerations of Tracking for the Telescope Mount.**

Working velocity:
- A. 5degree/s . E. 1degree/s

Working acceleration:
- A. 0.1degree/s/s1 E. 0.1degree/s/s

Min. velocity:
- A. 0.004 Arc second/s. E. 0.004 arc second/s

Max. velocity:
- A. 24.27 degree/s. E. 12.36 degree/s

Max. acceleration:
- A. 14.91degree/s/s. E. 15.64degree/s/s

Tracking Precision(RMS):
- A. 4.747 arc second. E. 4.857 arc second

2) **Laser System**

Wave length: 0.532μm (Base:1.064μm)
Output energy:51.0mj (1pps). 54.0mj (5pps). 54.0mj (10pps)
Energy unstable: 4%. Continuous running 40 minutes.
Pulse width: 30-50 ps
Repeat of wave form: 83%,1Hz. 88%, 5Hz.

Beam divergence: 0.41mrad (1Hz); 0.30mrad (5Hz)
Output mode: TEM-00
Beam Size of output: 9mm (1Hz); 8mm (5Hz)
Repetition: 1 to 10Hz

3) **Perpendicularity and Pointing Precision for Telescope Mount**

Perpendicularity: -2.75 Arc second
Pointing Precision:

A. 2.19 Arc second E. 2.49 Arc second

4) **Ground Target Calibration**

west cal target			short cal target		
	RMS (cm)	DT (m)		RMS (cm)	DT (m)
1	0. 8	14. 909	1	1.0	14. 912
2	0. 9	14. 909	2	0.8	14. 911
3	0. 8	14. 907	3	0.9	14. 911
4	0. 8	14. 908	4	0.8	14. 912
5	0. 9	14. 908	5	0.9	14. 910
6	0. 7	14. 907	6	1.0	14. 911
7	1.0	14. 910	7	0.9	14. 910
8	0. 8	14. 907	8	0.8	14. 910
Average	0. 84	14. 908	Average	0. 9	14. 911

5) **Satellite Ranging**

60 passes of satellite range data were obtained from the test observation period including all SLR satellite of that time and for Lageos 28 passes. The precision was very good and satisfied from the data analysis reports of Delft University. Hereinafter is a Lageos pass in 14th of August 2003. More than 8000 returns were in the pass.
Figure 5 is the tracking screen of the computer and gives a Lageos pass in semi-trains.

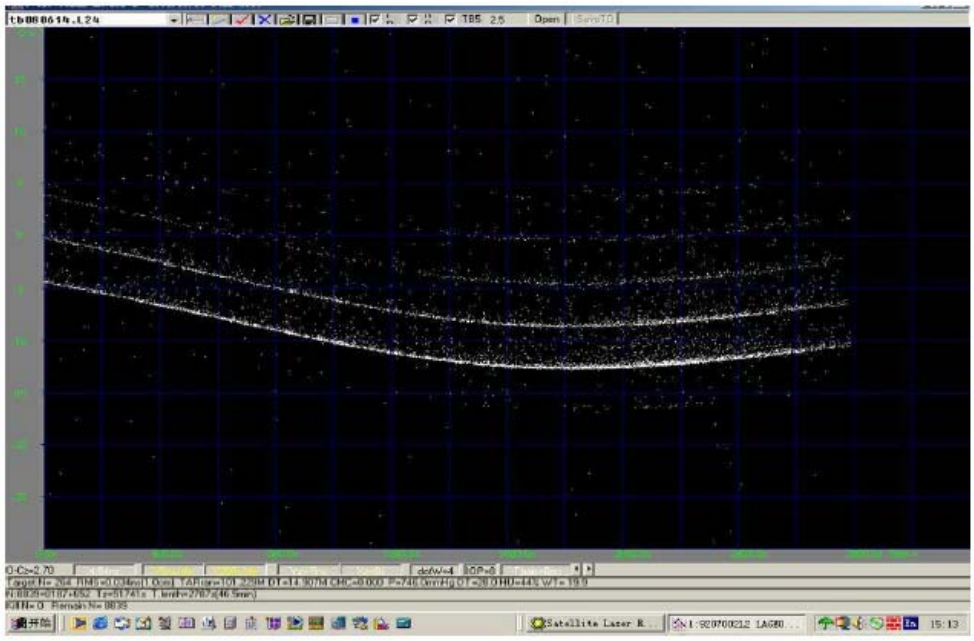

Figure 5. A typical Lageos pass in the tracking screen of the computer

6) **Star Tracking for the Mount Test**

The pointing Test

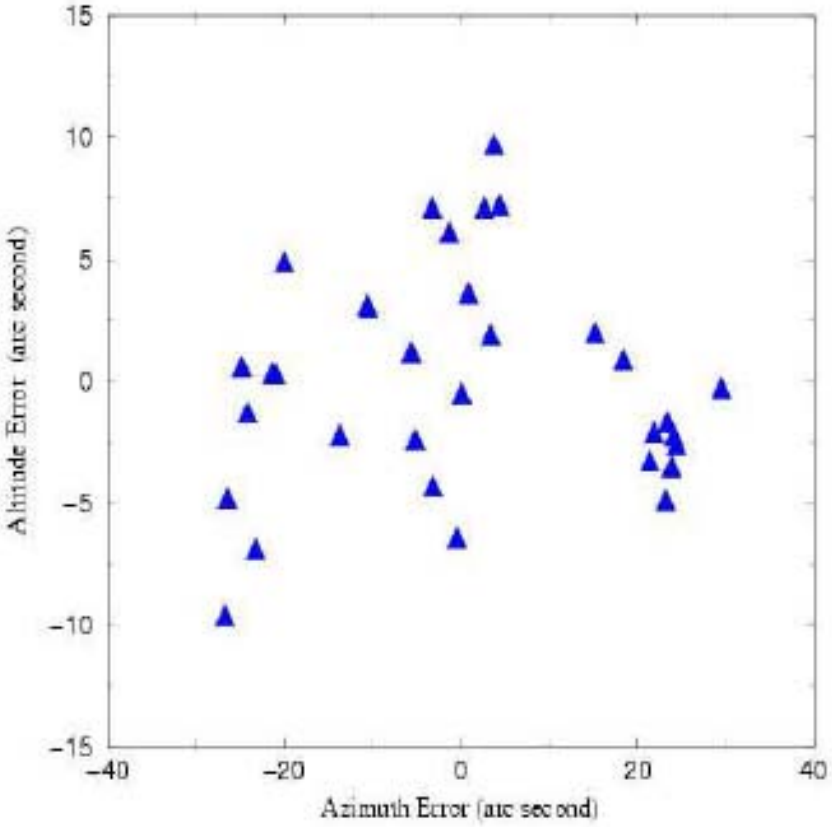

7) **Satellite Tracking for the Mount Test**

The tracking test os Satellite Lageos

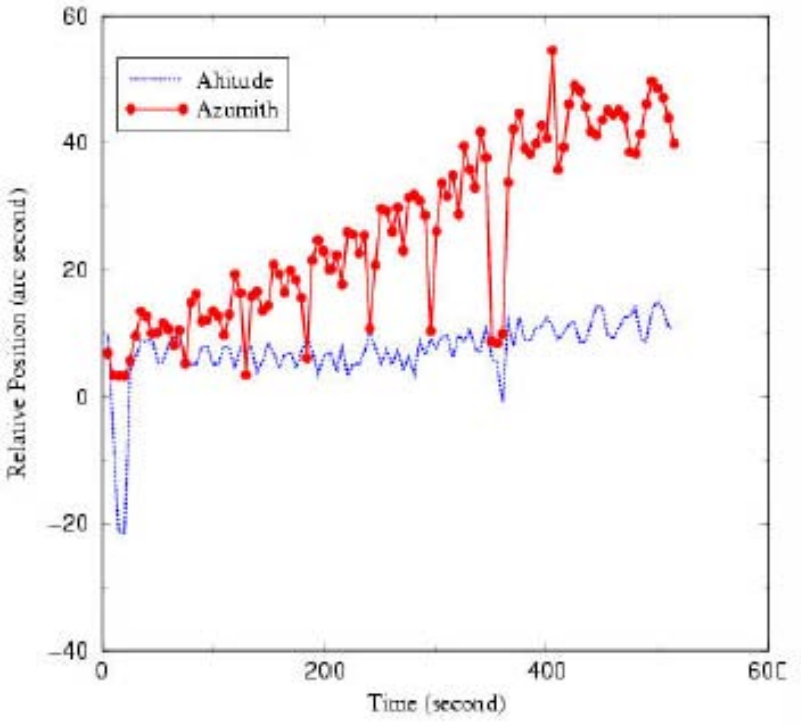

8) **The Test Observation Result from ILRS Data Analysis Center.**
Station BeijingA is the system for Argentina station.

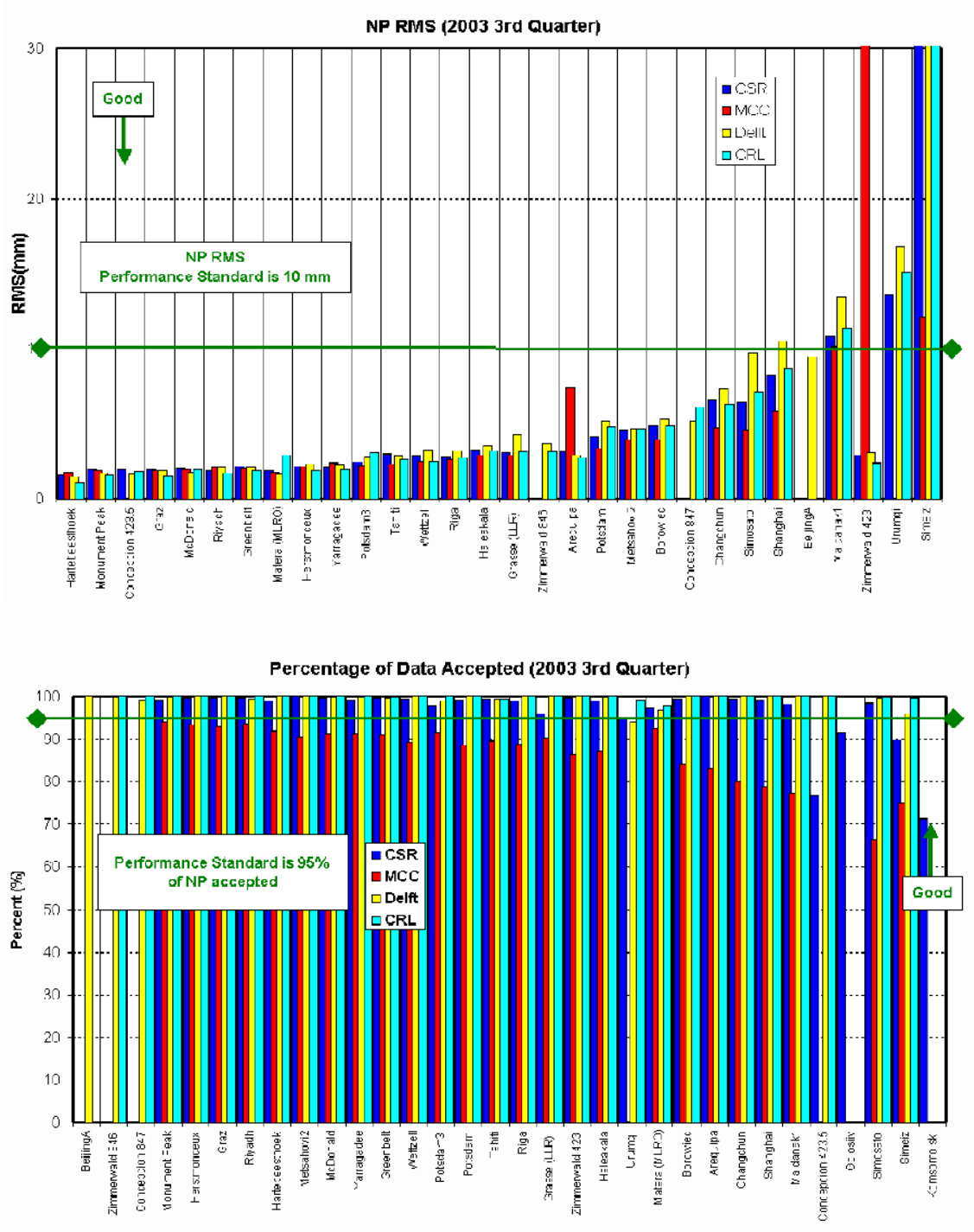

Summary

The New SLR station in San Juan of Argentina will be running soon. Now the whole system was ready to packing and shipping it to Argentina. The building for SLR purpose in University of San Juan of Argentina was nearly got through maybe in next month. The packaging and shipment will begin before the end of this month when we go back to China after the meeting ended and the SLR data of first pass in the new station in Argentina can be ahead of the end of this year if things going well. The test observations got 60 passes ranging data for nearly all SLR satellites including GPS 35 and once more than 8000 returns of one pass were obtained for Lageos.

SELF-MIXING OPTICAL DOPPLER RADIAL VELOCITY MEASUREMENTS: A PROSPECTIVE STUDY

Jean-Louis Oneto(1) Odile Calame(2)
(1)Observatoire de la Côte d'Azur / MEO / GEMINI / CNRS
oneto@obs-azur.fr / Fax: (+33)[0]4.93.40.53.33
(2)Observatoire de la Côte d'Azur / GMC / GEMINI / CNRS
Odile.Calame@obs-azur.fr / Fax: (+33)[0]4.93.40.53.33

Abstract

Optical Doppler measurements of satellite radial velocity would give complementary data to actual ranging measurements. This could help to further constraint the orbitography models. An analytical study of Doppler Effect is presented. A tentative experimental setup using continuous laser with self-mixing autodyne interferometric detection seems very promising.

Introduction

Speed measurements using Doppler were used at the dawn of artificial satellite orbitography, in radiofrequency domain. This was abandoned in favor of laser ranging techniques. While it would be useless to turn back to such methods, the conjoint use of Doppler and laser distance measurements should help to better constraint the orbitography solutions. The former Doppler used downlink techniques with stability provided by on-board atomic clocks. The radio-frequency spectrum gave the advantage of the excellent selectivity of the receivers. The use of two-way Doppler in optical spectral domain takes advantage of existing retro-reflector arrays.

Computation of the satellite motion

For illustrating our purpose, we consider the very simplified case of a satellite orbiting around the Earth, in a Keplerian motion, with a laser station on the terrestrial surface.

The used parameters are defined as following:

R: Earth radius
e: Orbit eccentricity
a,b: Semi-major and semi-minor axes
i: Orbit inclination
Ω*:* Right ascension of the ascending node of the orbit on the equator:
ω*:* Argument of perigee
L: Longitude of the laser station
φ: Latitude of the laser station
T_e*:* Sidereal period of the Earth
w_e*:* Sidereal angular speed of the Earth (2/ eπ *T)*
w_s*:* Angular speed of satellite on its orbit
t: Time

Let denote by *T* , *L* and *S* the position of center of Earth, Laser station and Satellite respectively (Figure 1). The corresponding vectors are derived from them.

The geocentric coordinates of laser station in the equatorial frame are:

$$\mathbf{TL}_{eq} = \begin{pmatrix} R \cdot \cos(L + w_e \cdot t) \cdot \cos\varphi \\ R \cdot \sin(L + w_e \cdot t) \cdot \cos\varphi \\ R \cdot \sin\varphi \end{pmatrix}$$

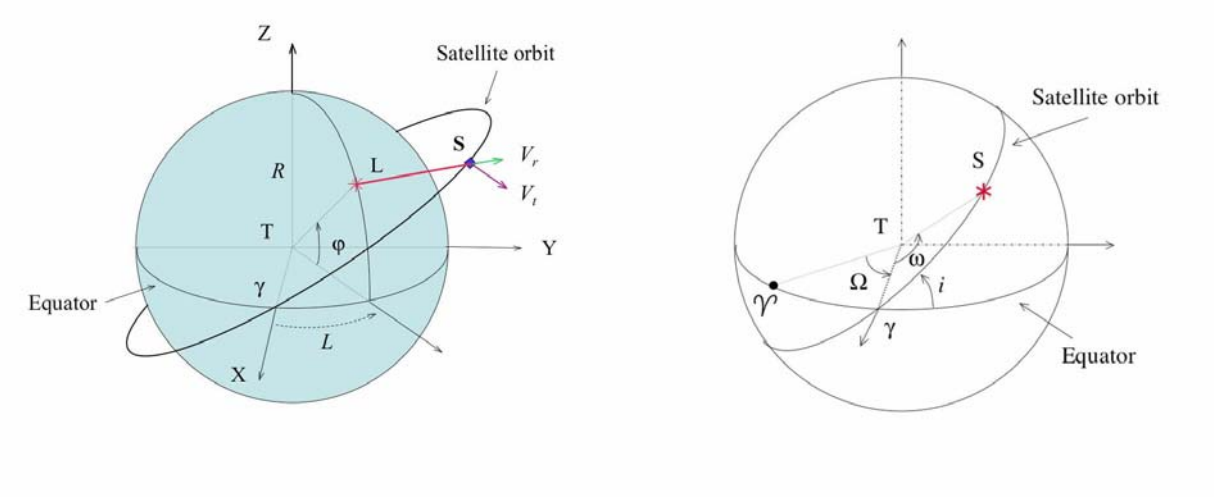

Figure 1: Notation summary

The geocentric coordinates of satellite in orbit frame are:

$$\mathbf{TS}_o = \begin{pmatrix} -a \cdot (e - \cos(w_s \cdot t)) \\ b \cdot \sin(w_s \cdot t) \\ 0 \end{pmatrix}$$

By successive rotations of the oriented angles ω, $-i$ and Ω, with respect to the corresponding Z, X and Z axes, we obtain the geocentric coordinates of satellite in the equatorial frame:

$$\mathbf{TS}_{eq} = Rot_Z(\Omega) \cdot Rot_X(-i) \cdot Rot_Z(\omega) \cdot \mathbf{TS}_0$$

(where $Rot_X(u)$designates the rotation around the X axis of an u angle) .

The development of the matrix products gives:

$$\mathbf{TS}_{eq} = \begin{pmatrix} \cos\Omega \cdot \cos\omega - \cos i \cdot \sin\Omega \cdot \sin\omega & -\cos\Omega \cdot \sin\omega - \cos i \cdot \sin\Omega \cdot \cos\omega & \sin i \cdot \sin\Omega \\ \sin\Omega \cdot \cos\omega + \cos i \cdot \cos\Omega \cdot \sin\omega & -\sin\Omega \cdot \sin\omega + \cos i \cdot \cos\Omega \cdot \cos\omega & -\sin i \cdot \cos\Omega \\ \sin i \cdot \sin\omega & \sin i \cdot \cos\omega & \cos i \end{pmatrix} \cdot \mathbf{TS}_o$$

We define a local frame by a system with the first axis X in the direction of **LS**, the two others being directly perpendicular. We calculate the two components of the speed vector of **LS** along the X axis ($\mathbf{LS}_r = V_r$) and in the normal plane ($\mathbf{LS}_t = V_t$). For that, we have to compute the derivatives of the precedent vector coordinates with respect to the time and apply the adequate rotations.

The following numerical applications and graphs use the Lageos1 elements and the Grasse SLR position as example. The dashed lines denote that the satellite is below the local horizon.

The Figure 2 illustrates the variations of these two components of the speed of satellite, in a topocentric frame.

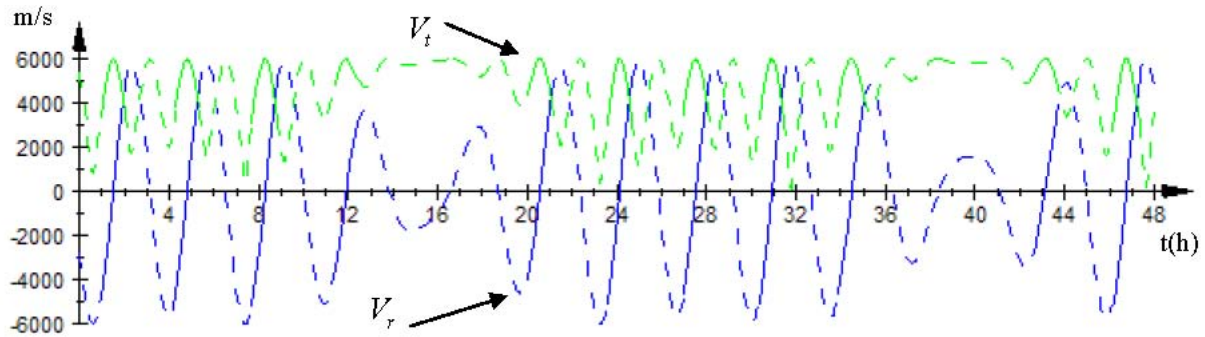

Figure 2: Speed vector components

Doppler Effect

Let define as c the speed of light and λ the wavelength. The corresponding frequency ν is the equal to c/λ. From a relativistic point of view, the Doppler effect in frequency has two components, radial ($\Delta\nu_r$) and transverse ($\Delta\nu_t$).

Let define: $\beta_r = V_r/c$ *and* $\beta_t = V_t/c$

$$\Delta\nu_r = \nu \cdot \left(\sqrt{\frac{1-\beta_r}{1+\beta_r}} - 1 \right)$$
$$\Delta\nu_t = \nu \cdot \left(\sqrt{1-\beta_t^2} - 1 \right)$$

It is to be noted that β_r and β_t are very small quantities with respect to unity, so that the developments in series give:

$$\Delta\nu_r = \nu \cdot \left(-\beta_r + \tfrac{1}{2}\beta_r^2 + O(\beta_r^3) \right)$$
$$\Delta\nu_t = \nu \cdot \left(-\tfrac{1}{2}\beta_t^2 + O(\beta_t^4) \right)$$

The classical contribution is:

$$\Delta\nu_c = \nu \cdot \left(-\frac{\beta_r}{1+\beta_r} \right)$$
$$\Delta\nu_c = \nu \cdot \left(-\beta_r + \beta_r^2 + O\left(\beta_r^3\right) \right)$$

In absolute value, the relativistic correction to the radial effect is of the same order than the transverse part.

The Figure 3 shows the three corresponding curves.

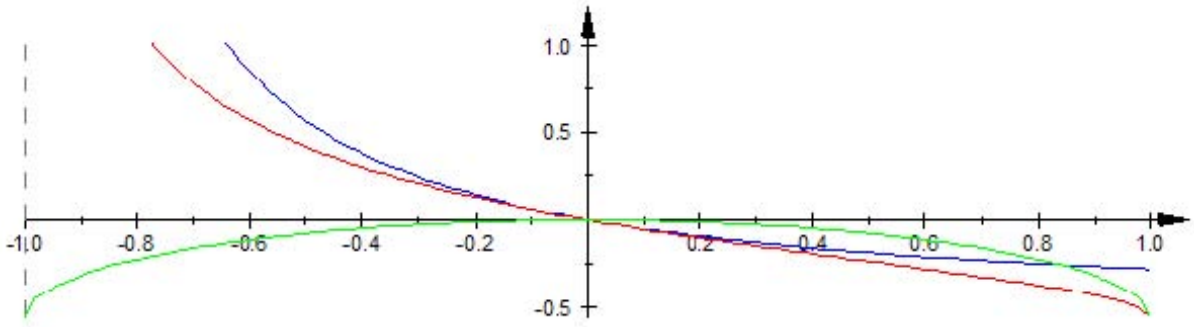

Figure 3: Doppler effects: classical radial and relativistic radial/transverse

The curves, in Figure 4 and Figure 5, show that $\Delta\nu_t$ is by several orders of magnitude smaller than $\Delta\nu_r$.

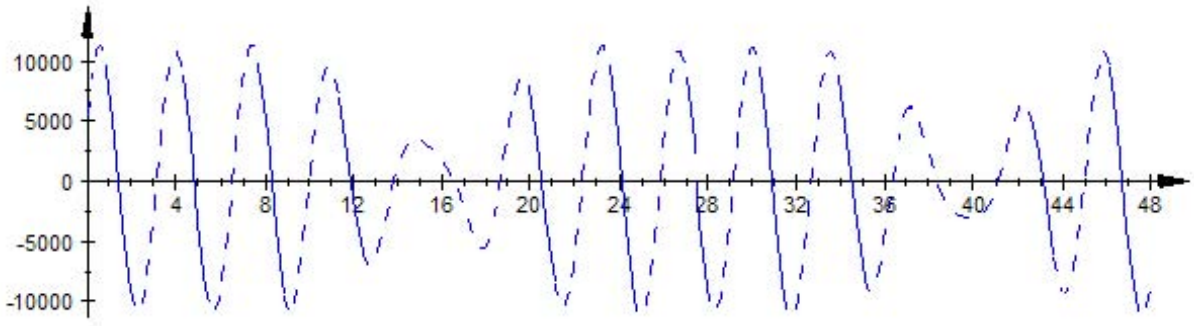

Figure 4: Relativistic Radial Doppler in Frequency

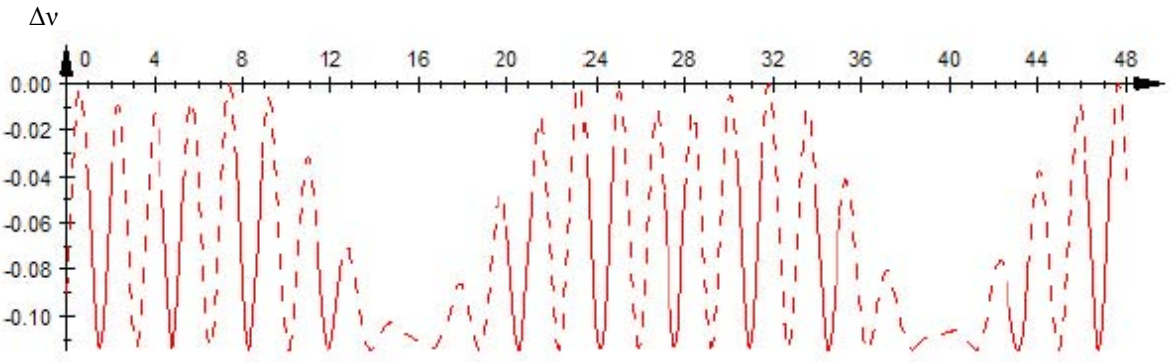

Figure 5: Relativistic Transverse Doppler in Frequency

Nevertheless, the transverse effect cannot be neglected. The physical measurement gives only access to the sum of these two effects, so that in order to retrieve the radial component alone, it is necessary to evaluate the transverse speed and compute the transverse Doppler

component. The sensitivity of this effect being very low, even a rather coarse satellite motion determination with respect to the station would be sufficient.

Discussion of detection methods for optical Doppler:

- **Direct spectroscopy:**

The radial orbital speed of a satellite (V_r) being of the order of few km/s, $\beta_r = V_r/c$ is of the order of $2 \cdot 10^{-5}$. The associated Doppler effect is of the same order of magnitude, and this leads to $\Delta\lambda \approx 635 \cdot 2 \cdot 10^{-5} \approx 0.01$ nm . In order to determine the speed with enough precision to be of any use, one needs at least a resolution of 1m/s corresponding to a wavelength resolution of 10^{-5} nm . The achievement of this goal would require a very high resolution spectroscope, very expensive and bulky.

- **Interferometry::**

The classical use of interferometry supposes that the path difference must be less than the coherence length. For an ordinary laser, the coherence length is of the order of few meters, and it reaches only a few kilometers, even for an extremely stabilized laser like those used in the Virgo experiment.

In order to obtain interferences between the local reference laser beam and the reflected signal, it would be necessary to have a coherence length greater than twice the satellite distance, i.e. near 1000 km even for the lower orbits!

This also applies to the case of the self-mixing Doppler interferometric velocimetry that is often used to check the speed of terrestrial targets.

- **Fixed delay Interferometry:**

Also known as Fringing Spectroscopy, this method was described by Jian Ge [1] and David Erskine [2], especially for extra-solar planet detection. Even in that case, they have achieved 2 m/s resolution and expect sub-m/s results, even without a sophisticated optimization.

In the present case, the source is coherent and easily accessible, the required stability is of the order of the light round trip, i.e. a less than a second, instead of several hours, months or even more. This should leads to a sub-mm/s resolution.

The detection setup (Figure 6) consists of a fixed delay interferometer followed by a low-resolution dispersion spectrometer. In our case (Figure 7), this spectrometer is useless since the laser light is highly monochromatic. This leads to the paradox of a high-resolution spectroscopic device without any dispersive element!

In this design, the delay is chosen to a convenient value: the sensitivity of the device is proportional to the delay, but if must be small enough compared to the coherence length in order to avoid a decrease of the fringe contrast.

The Doppler information is carried by Moiré fringes and must be detected by twodimensional devices.

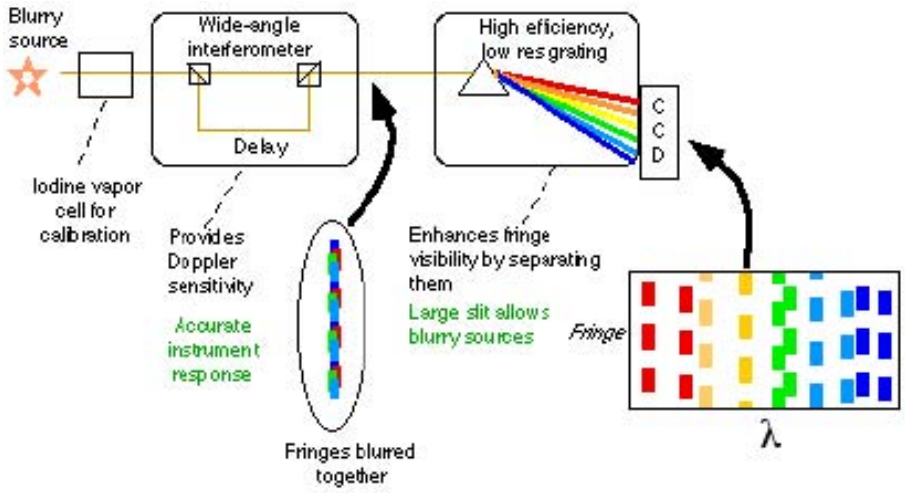

Figure 6: Fixed delay interferometer

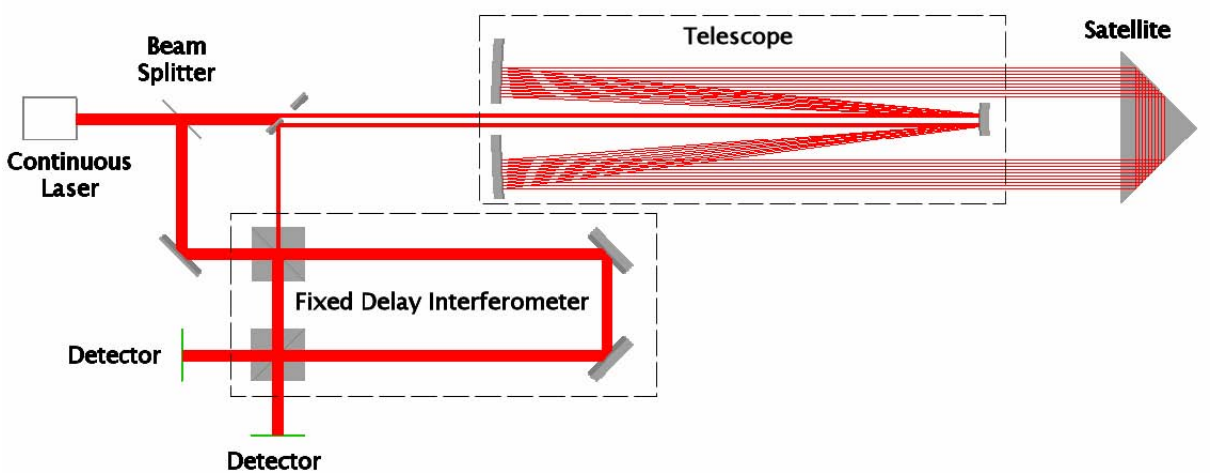

Figure 7: Fixed Delay Interferometer variant for laser

Conclusion

This kind of project may yield a complement of information in conjunction with classical telemetry. Even with distance measurements in the millimeter precision range, direct determinations of speed through Doppler techniques at comparable level, will bring independent and hence significant improvement of satellite dynamics knowledge.

References

[1] Ge, J., Fixed delay interferometry for extra-solar planet detection, ApJ. **571**, L165-L168, 2002

[2] Erskine, D., Ge, J., Basri, G., Rushford, M., Macintosh B., and Alcock, C., Doppler Planet Search with a Fringing Spectrometer, published on the Web at: http://www-phys.llnl.gov/H_Div/doppler

STATUS OF THE RUSSIAN LASER TRACKING NETWORK

M.V. Baryshnikov, V.B. Burmistrov, V.D. Shargorodsky, V.P. Vasiliev
IPIE, Russia

Abstract

Brief description is given of the laser tracking network present status, as well as of further development plans and intentions.

The Russian laser tracking network includes the following SLR stations:

Komsomolsk-on-Amur (ID1828)
Maidanak-1 (ID1864)
Maidanak-2 (ID1863)

The stations general view and their basic technical parameters are shown in Figures 1 and 2.

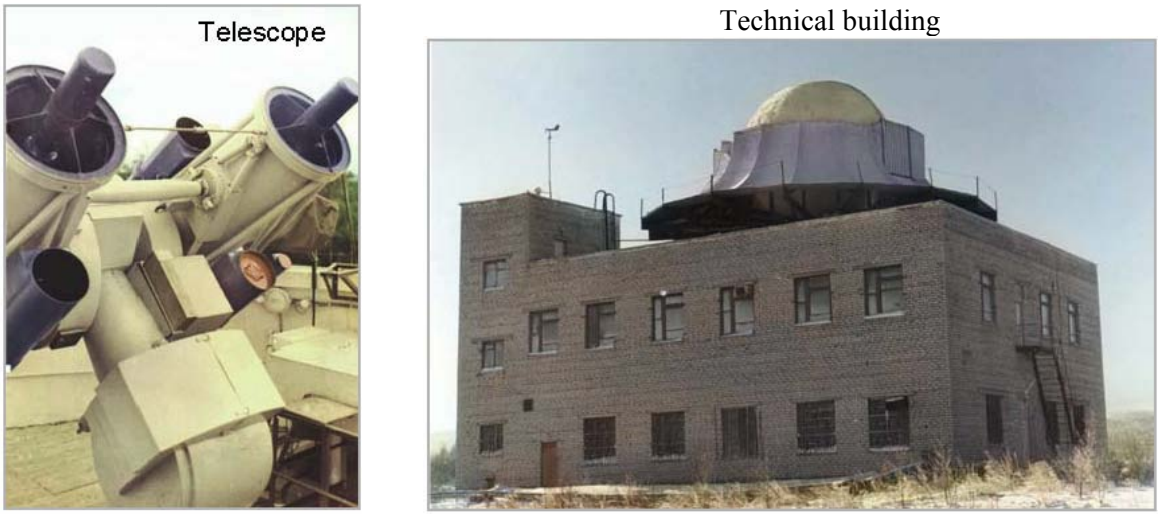

Figure 1. Laser Tracking Station near Komsomolsk-on-Amur

Upgrade completed:

- Introduction of a coude path
- New laser transmitter: $\lambda = 532$ nm, $\tau = 200$ ps, E = 40 mJ, rep. rate = 5 Hz

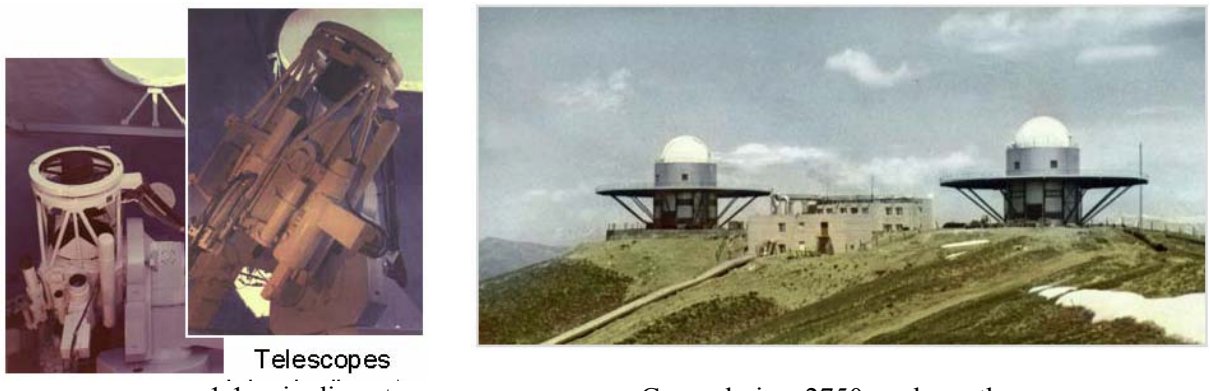

Figure 2. SLR station on top of Maidanak mountain (Usbekistan)

The station is operable since December, 2002. It operates under the Russia/Usbekistan agreement on its joint control and use.

Two more stations are operating in an experimental mode (no data are still delivered to the international data analysis centers). The stations, shown in Figures 3 and 4, are:
Shelkovo (near Moscow) (ID 1111)
Altay optical and laser tracking center (ID 1050)

Basic parameters		
Range	**Angular measurements**	**Photometry**
Orbit height: Nighttime – up to 36000 km Daytime – up to 6000 km	Visual star magnitude: 14^m – 15^m	Visual star magnitude: 12^m – 13^m
RMS NP error: 3 – 5 mm	RMS measurements error for SC: 2 arc sec	Brightness determination error: max 0.2^m

Figure 3. SLR station near Moscow. The station is in regular operation since 2003. Data delivery to ILRS will be provided after permission to participate in international programs.

Figure 4. Altay optical/laser ranging center

The main goals of laser tracking by Russian stations are:

- Estimation of the GLONASS ephemeris and frequency/time accuracy during the navigation system operation period.

- Upgrade of spacecraft motion models.
- Better precision in Earth rotation parameter determination.
- Better precision of measurements for space geodesy and Earth gravity field parameter determination.
- Angular and photometric monitoring of spacecraft in high elliptical orbits (including SC failure cases).
- Failure-case backup of microwave SC tracking systems.
- Participation in international SC laser tracking programs for geodesy and geophysics, as well as for producing catalogues of SC and space debris.

Ephemeris data are routinely used by all five stations for tracking of more than 20 satellites, including GLONASS-84, GLANASS-87, GLONASS-89, ETALON-1, ETALON-2, ERS-2, TOPEX, STARLETTE, STELLA, AJISAI, GPS-035, GPS-036, LAGEOS-1, LAGEOS-2, GFO-1, BEACON-C, JASON, LARETS, METEOR-3M and CHAMP. The observation results are processed by the MCC SLR data analysis group.

After preliminary processing and filtration with use of STARK software, normal point data are formed and delivered to the European Data Center (EDC).

In addition to routine SLR, some work has been made recently on combining SLR with other techniques. An example of this is frequency drift monitoring of GPS/GLONASS on-board oscillators.

The accumulated experience on GLONASS operation shows that the navigation field quality depends primarily on time/frequency errors caused by the on-board frequency standard instability.

Thus, currently it is important to estimate the on-board standard frequency drift and to find the corresponding time/frequency correction values.

To implement this technology, the SLR station near Moscow is additionally equipped with an H_2 – maser having a stability of $7 \cdot 10^{-15}$ per day, as well as by a high-accuracy GLONASS/GPS signal receiver (ASHTECH Z-18) and corresponding software.

Figure 6 shows the GPS time-scale drift during a month-long period.

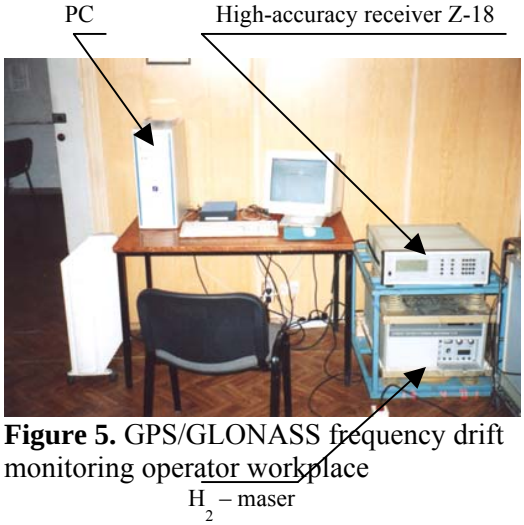

Figure 5. GPS/GLONASS frequency drift monitoring operator workplace

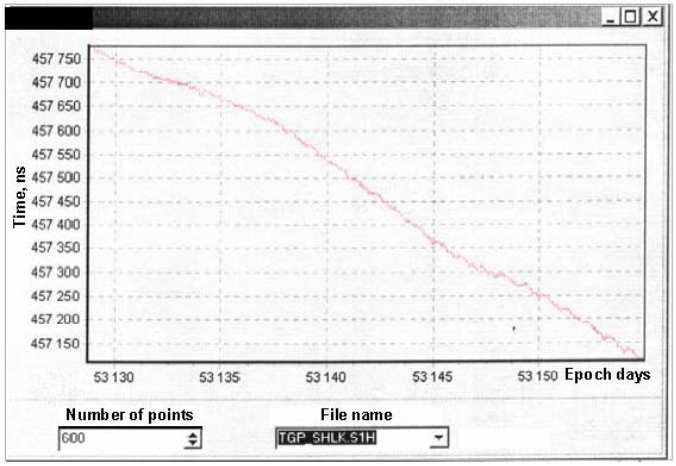

Figure 6. GPS time-scale drift 01-05-04 to 31-05-04

An important feature of Russian SLR development program is designing and manufacturing of transportable stations (Figure 7) and of miniature modular stations (Figure 8).

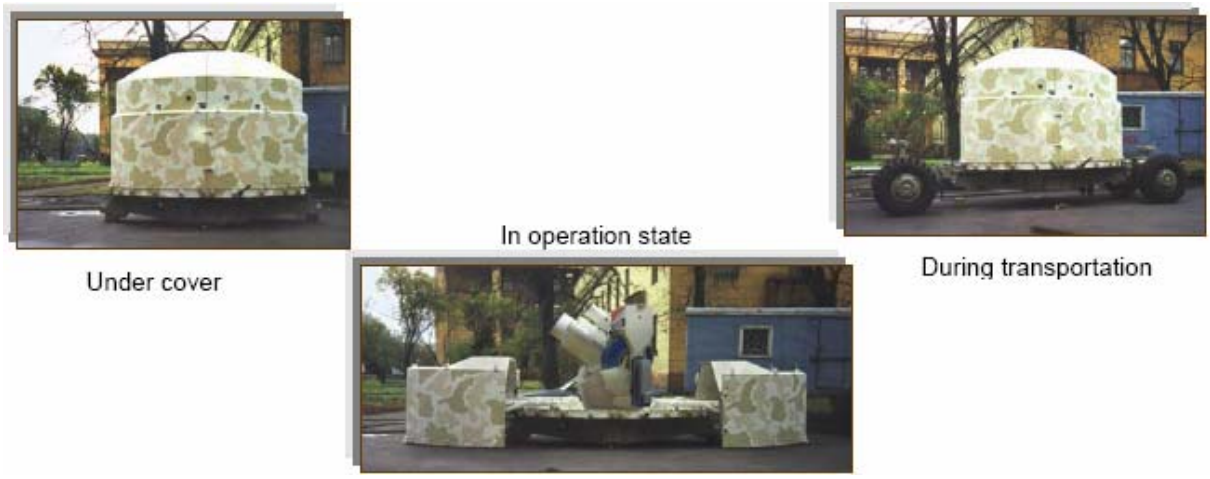

Figure 7. Transportable SLR station.
It is planned to install the station at the Baikonur launching site during 2005.

Figure 8. Miniature modular SLR station

The modular station shown in Figure 8 may be used for ranging of CCR-equipped spacecraft in orbits as high as 23000 km at nighttime and 6000 km at daytime, as well as for angular measurements of spacecraft with brightness down to 14-th star magnitude, and photometric observations. The expected ranging accuracy is about 0.4 cm, and accuracy of angular measurements – less than 2…5 arc sec (depending on spacecraft brightness and atmospheric conditions).

The modular SLR station consists of the following subsystems and major components:

- Az/El mount with cover and tracking systems (2 arc sec accuracy).
- laser transmitter with optics unit: λ = 0,532 nm, E = 2,5 mJ, Rep. rate = 300 Hz.
- Tx collimator optics.
- High-sensitivity TV system for angular measurements.
- 250-mm diameter objective.
- TV photometer.
- GLONASS / GPS-controlled time/frequency standard.

- Automatic weather station.

The miniature diode-pumped laser transmitter combines high average power (0.75 W) with short pulse duration (250 ps). A narrow-band holographic filter is used in the receiver; as a photodetector, a Hamamatsu MCP PMT is used. The TV camera (MCP image intensifier + CCD) operates in photon-counting mode and has a FOV of 1°.

The total system weight is less than 350 kg; when dissembled (during transportation), the weight of any single module is less than 50 kg. Assembling and adjustment is made by two qualified operators during a single working day. After assembling, automatic angular sensor alignment using catalogue stars takes ~30 min (at nighttime). Ranging bias determination is made by means of a built-in calibration system. Cable length allows to place the optical unit as far as 50 m from the other equipment.

It is planned to produce more than 10 such stations, starting from 2005 (one station per year).

Thus, the Russian SLR tracking network is currently in a state of extensive development. We hope that until 2010 it will comprise 12…14 stations, more or less uniformly distributed over the State territory.

CHARACTERIZATION OF THE SPACE SEGMENT FOR THE T2L2 PROJECT

Muriel Ravet(1), Etienne Samain(1), Robert Dalla(1), Patrick Aubry(2), Philippe Guillemot(2), Jean-Louis Oneto(1),Jean-Marie Torre(1), Jean-François Mangin(1), Jocelyn Paris(1).
(1) OCA 2130 Route de l'observatoire, 06460 Caussols, FRANCE
(2) CNES 18 Avenue Edouard Belin, 31401 Toulouse, FRANCE

Introduction

The T2L2 experiment allows the synchronisation of remote clocks on Earth, and the monitoring of a satellite clock, with a time stability of the order of 1 ps over 1000 s and a time accuracy better than 100 ps. The principle is based on the propagation of light pulses between the clocks to synchronise. The ground segment is a satellite laser ranging station with a special instrumentation able to time light pulses accurately as compared to the ground clock to synchronize.

T2L2 has been proposed on MicroSatellite Myriade under development at CNES. So, the study of the space optics has been conducted for a MicroSatellite having an altitude of 800 km. At this altitude, the field of view is 120?and speed aberration is in the range of 10 arcseconds.

The phase B study of the space segment was concluded at the beginning of 2004. This study permitted to design an instrument having a mass in the range of 10 kg and a power consumption of 40 W. It comprises the following elements:

A detection unit based on an avalanche photo-diode working in a Geiger mode.

A time tagging unit able to time the photo-diode output in the satellite clock time scale with a precision better than 3 ps.

A high index corner cube (100 mm diameter) having a large field of view.

Optical package description

The aim was to design a corner cube, determining its size, shape, refractive index, dihedral angle error, and its optic efficiency to satisfy the necessary field of view of 120?at an altitude of 800 km. The choice has been an unique corner cube having an high refractive index for the reflection unit and a truncated vertex for the photodetection.

To determine parameters of optics, the calculated link budget takes into account many parameters like optical power of the laser, orbit of satellite, laser station, atmospheric transmission but also the return transmission of flux which depends on reflector crosssection.

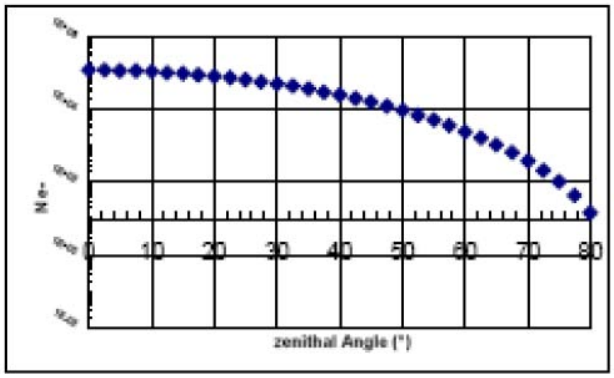

Figure1 : Link budget

The link budget is an estimation of return photons number detected on laser station as a function of zenithal angle. So, it allows to determine the specifications of this optical model. Adjusting the optic parameters to have at least 1 photon for all angles -60° ≤ θ ≤ 60º, the reflection optics must be a corner cube having a refractive index of 1.8, a diagonal of 120 mm and the back side is covered by an Aluminium protected coating because of necessary 120° field of view. Its triangular shape is important to improve the link budget for the high angle θ. The dihedral angle errors must be less than in the range of 2.

For an altitude of 800 km, speed aberration is in the range of 10 arcseconds. In order to compensate for it, a cylindrical lens has been added in front of the corner cube to get a divergence of 10 arcseconds.

The curvature radius is 1.6 km with refractive index of 1.8. The spot of diffraction is spread along the direction of the satellite speed vector. This lens serves also a window to protect the corner cube against radiation.

The detection unit is a photodiode operating in a Geiger Mode for the chronometry and a linear photo-detection to quantify the photon number and to polarize the Geiger diode.

Behind the window (*Lw*), the equipped linear detection optics with a spectral filter is fixed which improves the S/N ratio. The non-linear detection optic allows to collect and to forward a little quantity of light to the photo-detector system. The beam at the truncated vertex have 120°aperture. The vertex is truncated on few millimetres. An optical fiber is set behind the corner cube vertex. This option has been chosen to have the detection point and the reflection point at the same location. This aspect is fundamental for chronometric error budget. Moreover, this choice doesn't generate any shadows in front of the corner cube. One needs a 5 m delay line in order to compensate the linear detection transit time. An optical fiber with a large numerical aperture, a large diameter and a low time dispersion is necessary. This leads to the choice of a multimode graded index fiber. Its characteristics are numerical aperture of 0.29 so a field of views of 34° and core diameter of 100 µm. A 3 lens afocal coupling optics has been inserted between the corner cube vertex and the optical fiber in order to reduce the 120° field of view to the fiber acceptance angle. At intermediate focus, a radial density compensates the variation of the photons number on the non linear detector into contact with the photons number on the linear detector in the direction of incidence angle.

Figure 3 : Prototype
(a) front: reflector
(b) back: detection optics

Reflection optics studies

An interferometric analysis has been performed to verify the corner cube surface accuracy and quality. The reflected wavefront has a distorsion of peak-to-valley 1.28λ (rms 0.28λ) corresponding to 2" deviation or 0.7" error between 2 surfaces of corner cube.
For the 3 reflective surfaces, the surface accuracy is PV λ/6 with the test wavelength 0.632µm, or alternatively the root-mean-square surface accuracy of about λ /36 and a surface quality of about 40/20. For input face, the PV surface accuracy is λ/2 and a surface quality of about 40/20. And for the surface output (truncated vertex), the p-v surface accuracy is λ/4 and a surface quality of about 10/5.
A testing bench (fig. 4) was realized to study the corner cube polarization. The principle was to materialize a plane wave having a diameter of 140 mm in order to cover the whole diameter of the corner cube. A 1 mW laser source is used at a wavelength of 532nm with a linear polarization. So, we created an expander with an afocal system based on 2 convergent achromats.
The return beam is sent through non-polarizing cube beamsplitters on energy meter.

Figure 4: Testing bench

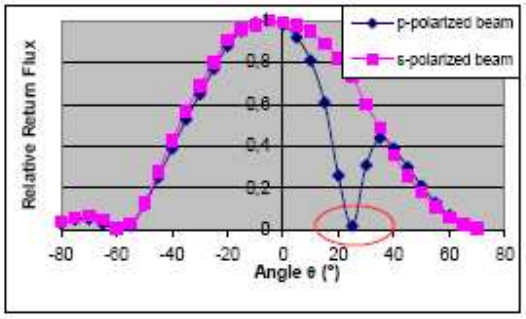

Figure 5: Polarization studies

The curve (fig.5) shows the measured polarization as a function of the angle of incidence θ. The reflectance factor is near zero for θ = 30° i.e when the angle between the internal beam (the refracted) and the normal to the rear face is 70° for a p-polarized light at wavelength of 532 nm. The problem is coming from the primary layer of the reflection coating of the corner cube which was added to improve the adherence of the metalized layer to the special high index glass.

The simulation of the coating as a function of incidence angle in the glass is consistent with the measures, and shows a zero reflectance factor for p-polarization and for an angle of 70°, as induced by the experiment. Suppressing the primary layer in the simulator, a correct curve is obtained. A study will be undertaken to find the suitable layers for avoiding this problem.

With this testing bench, we will also deduce the real link budget of this prototype. The energy meter will be replaced by a CCD and we will collect the spots of diffraction for different angle θ. Then, calculating the position of laser station in spot, we will deduce the light intensity in this point. So, we will plot the experimental estimation of return photons number as a function of incidence angle θ.

Detection optics studies

An experiment is realized to verify the variation of the flux on the detection fiber as a function of incidence angle θ.

The incident beam is represented by a green He-Ne laser coupled with an afocal system which give a 2mm collimated beam.

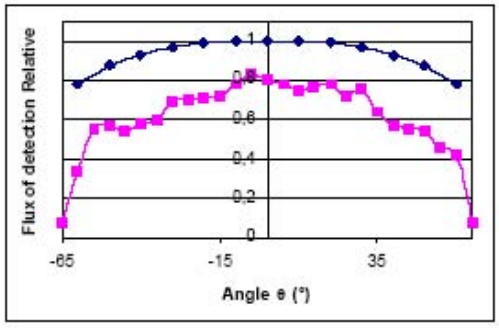

Figure 6: Variation of relative detection flux as a function of θ.

The variation of theoretical flux is given by the diamond blue curve and the square red one represents the experimental measures.
The fit between the 2 curves is relatively good, and shows that the detection system is able to work up to 60°. The beam crosses 10 optic surfaces before it reaches the detector. Every surface has a transmission factor of 98%: this gives a 0.98^{10}=0.82 in accordance with the experimental curve.
Using a streak camera, we studies the temporal deformation of laser pulse after the detection optics with and without the optical fiber. The laser source is taken on doubled Nd: YAG laser (150 mJ; 10 Hz; 40ps). We don't observe special influence of the incidence angle on the shape of pulse without fiber. Nevertheless, the fiber widening of laser pulse is of order of 2 ps/m.

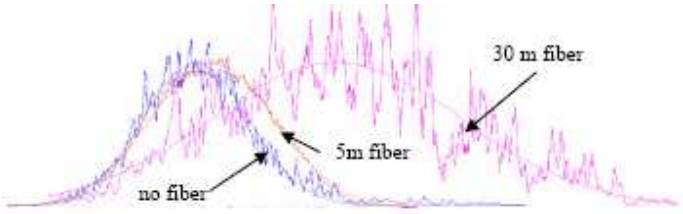

Figure 6: Influence of fiber lenght.

After have crossed the detection optics, the laser flux is sent on an avalanche photo-diode that we study.

Photodiode K14

This study is on the photo-detector K14 lent by Czech Technical University in Prague.
Because the K14 diode could be used in the space segment, we have undertaken an irradiation study of the component.

The first experiment consists to analyse the noise rate of diode during the irradiation. The sent dose corresponds to the dose if the diode K14 was in the space during 3 years.

To do that, the diode is excited with a pulse generator at 100 Hz and the noise events are recorded with a frequency meter during all the experiment. The pulse delays are firstly adjusted to get an output rate in the range of 50 Hz.

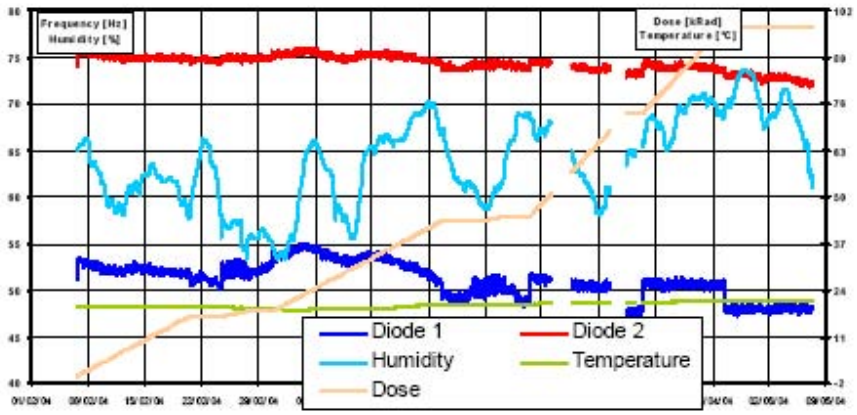

Figure 8: irradiation of the K14 diode

The source used is a cobalt 60 source which emits γ-Rays. The results are satisfactory. A small noise variation seems linked to the irradiation flux but the diode is insensitive to the accumulated irradiation because the noise is unchanged. So, after 3 months of irradiation on diode K14, it's still working !

Now, we have to measure the chronometry of the diode and to verify that there is no precision variation and that the quantum efficiency is unchanged.

Conclusion

The ground segment linked to the MéO station (the ex-Lunar laser ranging station) at Grasse and a prototype of the space segment allowed us to do a real simulation of the T2L2 time transfer.

This simulation permitted to evaluate very precisely the global performances of the link with a realistic atmospheric propagation.

TIME TRANSFER BY LASER PULSES BETWEEN GROUND STATIONS

Yang Fumin, Zhang Zhongping, Chen Wanzhen, Li Xin, Chen Juping, Wang Bin
Shanghai Astronomical Observatory, Chinese Academy of Sciences; yangfm@shao.ac.cn

1. Introduction

The first author of this paper with his colleagues at the Shanghai Observatory had carried out an experiment of time transfer by laser pulses between the headquarter of observatory and the old SLR station during 1981-1982 [1]. The distance between the two sites is 25.2 km. A Q-switched ruby laser with 15-20 ns pulse width, 3 sets of timer with resolution of 100ps, 2 sets of rubidium clock and PMTs with rise time of 2 ns were adopted for the experiment. The standard deviation of the mean of the rubidium clock differences is 1.3ns for a 120 sec interval.

After 21 years, we try to do the experiment with more accurate timing devices again. The purpose of the experiment is to verify the precision of time transfer by laser pulses and preparation for future global time transfer experiments.

2. Principle and configuration of the system

There were two stations: A and B. Station A was equipped with a SFUR mode-locked Nd:YAG laser and ranging system. Station B was equipped with a retro-reflector and a receiving optics and timing system. The principle of the experiment is shown in Fig. 1

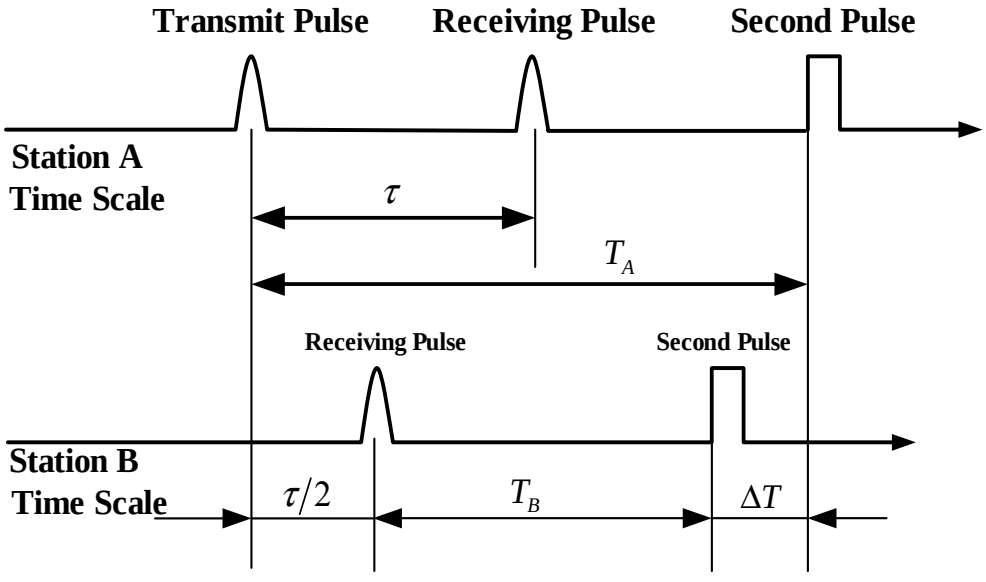

$$\Delta T = T_A - T_B - \frac{\tau}{2}$$

Fig. 1. Principle of experiment

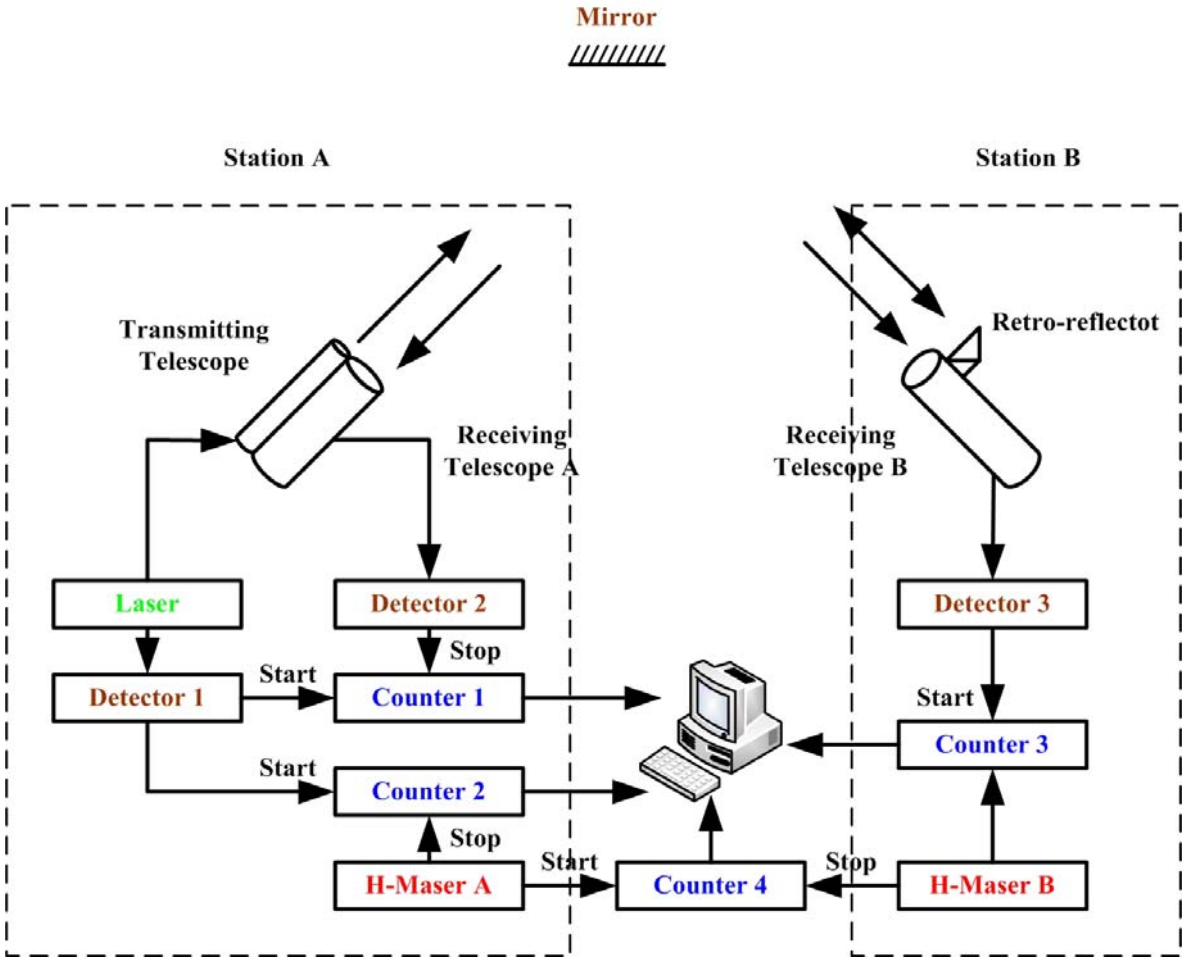

Fig. 2. Block scheme of local time transfer by laser pulses

The block scheme of the experiment is as Fig. 2

Actually, two stations (A and B) were located in a same room in the headquarter of Shanghai Observatory in the city. A 300mm diameter mirror for reflecting laser beams was set up at 250 meters away. Both stations were equipped with hydrogen masers made by the Shanghai Observatory and the two masters were directly compared with a SR-620 timer continuously.
The Characteristics of the time transfer system was as follows:

Laser:	Nd:YAG SFUR, 2mj,30ps,1-10pps
Receiver:	3 sets of Si-PIN diode Corner cubes
Mirror:	Dia 300mm
Timer:	4 sets of SR620
Clock:	2 sets of hydrogen maser
Discriminator:	TC454
Computer:	1 set for data acquirement of 4 timers

3. Experiment and result

The period of experiment was during May-June of 2003. Fig. 3 shows the hydrogen masers (right side), 4 sets of SR620 timer (left side) and computer. Fig.4 shows the station A (right table), on the table, are the SFUR laser (front), receiving telescope and PIN detectors, and the station B is at the left table and the corner cubes and the PIN detector are on it.

Fig. 3. Hydrogen masers, SR-620 timers and PC

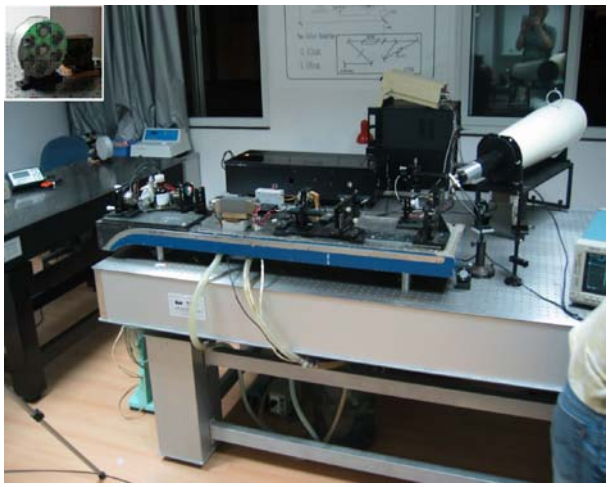

Fig.4 Station A (right table: SFUR laser, optics and detectors) and Station B (left table: corner cubes and detector)

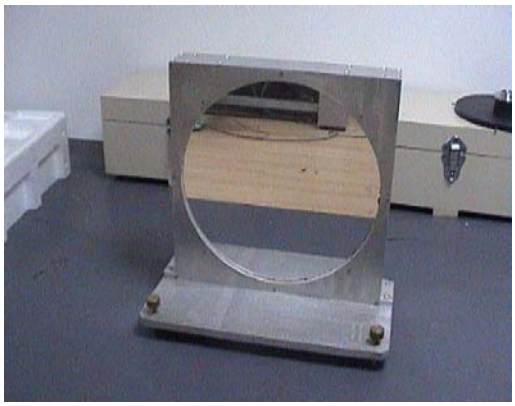

Fig. 5 The diameter 300mm reflector

The result of the experiment on June 13, 2003 is listed in Table 1, and is shown in Fig.6.

It is shown in the experiment that the Standard deviation of the mean of the clock differences determined by laser pulses is 24.1ps(rms) for a 100sec interval. The relative stability of frequency for two masers is 1.8×10^{-13} /200sec (Allen Deviation), due to without temperature control. The uncertainty of measurement for the relative frequency differences by laser link for two masers is 4×10^{-15} during 6000 sec. In Fig. 6, the Line 1 is the result of clock differences by the timer directly,

and its slope rate is 5.77×10^{-13}. the Line 2 is by the laser link, and its slope rate is 5.82×10^{-13}. The comparison result by laser link is very coincident with the direct timing method. Therefore, the clock comparison via laser pulses is feasible and reliable.

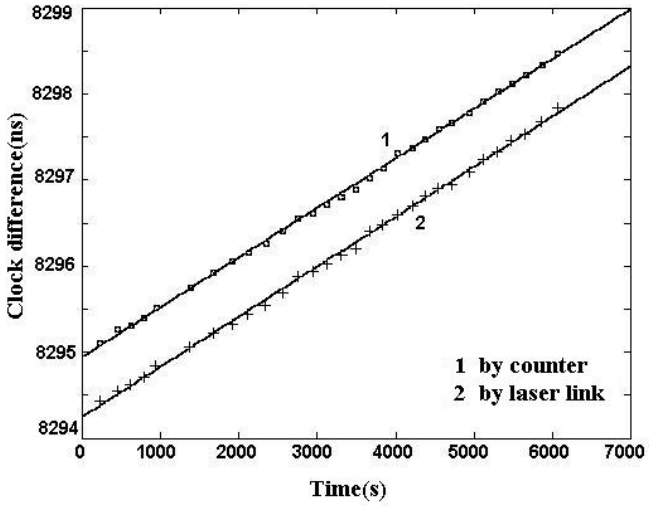

Fig. 6 Local time transfer result by laser pulses

4. FUTURE PLANS

4.1 Upgrade of Performance of Clocks

- Keep the Hydrogen masers in a special clock room, variation of temperature □±0.2ºC
- Better rise time of the second pulses of masers:□4 ns

4.2 Upgrade of Accuracy of Time Comparison

- Systematic biases measurement
  Time delays by PIN diode, discriminator, timer…
- Systematic errors analysis

4.3 SPAD application

2 sets of for better sensitivity SPAD will be adopted to replace the PIN diodes as the detectors for better sensitivity

4.4 Time comparison with high repetition rate

- 1 KHz time comparison with 1 KHz laser, and 10 ps pulse
- Clock difference measurement within one second
- Frequency difference measurement within 5-10 minutes

Reference

[1] Yang Fumin, Zhuang Qixiang, Su Jinyuan et al. Time comparison experiment via laser pulses, KEXUE TONGBAO (Science Bulletin in China), V.29, P.207, 1984.

Table 1. Result of clock differences by laser pulses

Set	Clock diff. by laser				Clock diff. by timer			Laser ranging data		
	Point	Mean (ns)	Single shot precision (ps)	Precision of mean (ps)	Mean(ns)	Single shot precision (ps)	Precision of mean (ps)	Mean(ns)	Single shot precision (ps)	Precision of mean (ps)
1	79	8294.4361	192.2	21.6	8295.1076	176.5	18.8	3410.967	62.7	6.7
2	85	8294.5456	208.7	22.6	8295.2665	195.2	20.8	3410.9641	51.2	5.6
3	64	8294.6283	191.1	20.7	8295.3145	181.3	18.7	3410.9718	65.1	7.8
4	81	8294.7095	268.7	29.9	8295.3963	248.2	25.2	3410.9478	56.9	6.6
5	68	8294.839	274.8	33.3	8295.5156	199.1	20.9	3410.9661	46.8	5.9
6	75	8295.0386	275.6	31.8	8295.7367	204.7	21.2	3410.9683	89.4	10.0
7	73	8295.2236	231.9	27.1	8295.9195	168.8	17.6	3410.9681	65.9	7.7
8	74	8295.3337	213.5	24.8	8296.0501	195.3	19.9	3410.9656	51.5	6.2
9	80	8295.4334	188.0	21.0	8296.1541	148.7	15.8	3410.9712	59.4	6.8
10	80	8295.5426	189.8	21.2	8296.2565	185.5	18.7	3410.9747	62.2	7.0
11	78	8295.6821	187.3	21.2	8296.4044	195.3	20.1	3410.9857	58.8	6.7
12	84	8295.8746	209.9	22.9	8296.5451	190.8	19.7	3410.989	52.2	5.9
13	83	8295.9377	222.2	24.4	8296.6086	178.4	18.6	3410.9913	55.9	6.3
14	81	8296.0246	202.6	22.5	8296.7145	175.8	18.5	3410.9869	58.4	6.2
15	82	8296.1201	255.9	28.3	8296.8100	194.9	20.0	3410.9638	33.2	4.1

16	79	8296.1997	249.9	28.1	8296.8903	206.8	21.2	3410.9642	60.6	7.1
17	71	8296.3962	152.7	18.1	8297.0179	151.0	15.7	3410.9535	50.0	5.9
18	78	8296.4827	235.5	26.7	8297.1384	174.1	18.2	3410.9533	56.2	6.3
19	79	8296.5954	204.4	23.0	8297.3161	133.1	14.3	3410.9443	71.7	8.0
20	82	8296.6873	167.7	18.5	8297.3709	168.3	17.4	3410.9319	48.1	5.6
21	74	8296.8184	214.6	24.9	8297.4782	208.4	21.7	3410.9338	62.8	8.0
22	83	8296.9122	245.7	27.0	8297.591	140.8	15.0	3410.9367	51.2	6.5
23	70	8296.9442	202.6	24.2	8297.666	208.6	21.2	3410.9433	63.1	7.8
24	74	8297.0934	180.4	21.0	8297.7887	162.9	17.0	3410.9164	50.1	6.4
25	84	8297.2371	205.8	22.5	8297.9168	186.4	19.3	3410.9599	64.9	7.5
26	73	8297.33	195.1	22.8	8298.0334	186.5	19.2	3410.9301	40.3	4.8
27	78	8297.4598	178.2	20.2	8298.1223	159.7	16.5	3410.943	56.1	7.1
28	73	8297.5217	208	24.3	8298.2232	177.7	18.0	3410.9406	55.5	6.8
29	85	8297.6806	238.5	25.9	8298.3354	184.4	19.7	3410.9534	58.9	7.4
30	83	8297.8418	213.9	23.5	8298.4751	176.7	19.4	3410.9652	44.8	5.6
Ave-rage			**213.5**	**24.1**		**182.1**	**19.0**		**56.8**	**6.7**

SLR2000C: AN AUTONOMOUS SATELLITE LASER RANGING AND SPACE-TO-GROUND OPTICAL COMMUNICATIONS FACILITY

John J. Degnan (1), Antonios Seas (1), Howard Donovan (2), Thomas Zagwodzki (3)
(1) Sigma Space Corporation.
(2) Honeywell Technology Solutions Inc.
(3) NASA Goddard Space Flight Center
John.Degnan@sigmaspace.com/ Fax:01-301-552-9300

Abstract

The adaptation of NASA's SLR2000 satellite laser ranging station to a dual mode ranging and optical communications terminal for space-to-ground links is discussed. The SLR2000C concept assumes multiple communications channels near 1550 nm, which allows the use of commercially available fiberoptic communications components. Preliminary link calculations suggest that the 40 cm aperture of SLR2000 would permit several Gbps downloads per channel from geosynchronous or lower Earth orbits and several tens of Mbps per channel from lunar orbit with nominal spaceborne transmitter powers on the order of a few watts. A ground network of approximately 25 SLR2000C stations coupled into a ground-based fiberoptic network would meet most of the foreseeable needs of "instantaneous" high data rate space-to-ground communications, including Earth-orbiting satellites and Deep Space missions. A simple space architecture based on four interlinked geosynchronous satellites (plus up to four additional satellites for polar coverage), would provide greater than 99% link availability and permit instantaneous transfer of data between an airborne or spaceborne remote sensing terminal and any point on the ground that is connected to the fiberoptic network. A single 10 cm diameter cube on each of the GEO satellites would provide adequate cross-section for the ranging link.

Introduction

NASA is currently field testing a prototype fifth generation Satellite Laser Ranging (SLR) system at the NASA Goddard Space Flight Center in Greenbelt, MD. Unlike past manned systems, the photon-counting SLR2000 system, illustrated in Fig. 1, is designed to be fully automated and eyesafe [Degnan et al, 2003]. The transmitter produces low energy subnanosecond pulses at high repetition rates (130 mJ @ 2 kHz = 260 mW), and the ranging receiver has single photon sensitivity. Eye safety is achieved through a combination of low pulse energies and large transmitted beam areas. Due to a unique and totally passive transmit/receive (T/R) switch design, the transmitter and receiver can simultaneously share the entire telescope aperture. Recent field experiments with the prototype have demonstrated the ability of SLR2000 to detect single photon returns from passive retroreflector arrays on satellites during both day and night tracking operations [McGarry et al, 2004]. The system has been designed to track the current constellation of retroreflector-equipped satellites at altitudes between about 300 km (LEO) and 20,000 km (GPS, GLONASS).

Recently, we investigated the possibilities for upgrading the SLR2000 system to permit high data rate laser communication downlinks and uplinks to and from Earth orbiting satellites in parallel with centimeter accuracy laser ranging operations. The marriage of the two applications is highly synergistic since the requirements for autonomous satellite laser tracking and communications overlap significantly. Specifically, the baseline SLR2000 system provides:

- Internet/modem/phone connections to support a variety of command and control functions (e.g. scheduling, updated orbital and time bias predicts, diagnostics, etc.), data transfer to a central processor, and internal instrument health and security monitors
- a “Smart” Meteorological Station which provides protection against local weather conditions (wind, precipitation, etc) and monitors ground visibility and cloud cover for efficient lasercom operations
- a GPS-disciplined Rubidium Time and Frequency Reference which yields accurate epoch times for reliable satellite acquisition as well as a stable clock reference for optical communications
- a 40 cm off-axis telescope with sufficient aperture to handle high bandwidth (2.5 Gbps per channel) optical com downlinks from Earth orbiting satellites using modest onboard laser powers (few watts at geosynchronous altitudes) but small enough to accommodate large phase front tilts due to the atmospheric effects or pointing errors in small aperture COTS lasercom detectors
- an arcsecond precision (command vs control) tracking mount augmented by automated star calibrations and a sophisticated 22 term mount model for high accuracy absolute pointing (~2 arcsec RMS over 66 stars)
- a photon-counting quadrant detector with pointing feedback capability for locking onto and maximizing both the ranging and optical com signals
- a unique transceiver design with a passive transmit/receive switch which allows the transmitter and receiver to simultaneously utilize the full telescope aperture without limiting the two-way data transfer rate and allows for improved eye safety margins and narrower transmit beams
- Communication satellites can be easily included in SLR constellation for automatic updating of orbit predictions by the central processor for rapid target acquisition

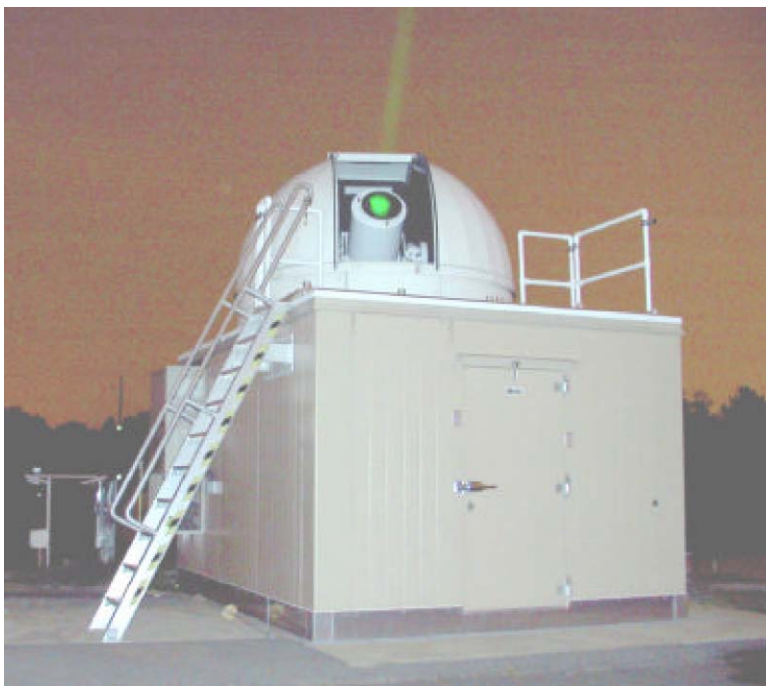

Figure 1: Prototype SLR2000 satellite laser ranging system undergoing field tests at the NASA Goddard Space Flight Center.

Laser ranging off passive retroreflectors placed on the nadir-viewing face of communications satellite also provides: (1) a highly accurate orbit which implies less search time and faster target acquisition during subsequent orbits; (2) independent verification that the satellite has been acquired by the ground station; and (3) a bright beacon at 532 nm for the spaceborne lasercom terminal to lock onto.

The conceptual design of the proposed global network of upgraded SLR2000C (C = Communications) station, which will be described in the present paper, has followed the same developmental principles as the baseline SLR2000 system, i.e. maximum use of Commercial Off The Shelf (COTS) components, long life and reliability, and simplicity of operation. In particular, the proposed design leverages heavily off near-IR lasercom components being developed by the telecom industry at wavelengths near 1550 nm. The inclusion of a 10 Gbps (4 channels at 2.5 Gbps per channel) downlink and a 10 Mbps uplink lasercom capability is expected to increase the replication cost by less than $700K, or about 30% of the baseline station cost of approximately $2M. Current applications under active investigation include a global space-to-ground optical communications network and a lunar mapping mission.

SLR2000C Technical Goals and Constrains

In considering the dual application SLR2000C system, we set the following goals for the overall lasercom space architecture and ground network:

- Dual mode SLR and two-way lasercom system with minimal interference between the two subsystems
  - Sub-cm ranging at 532 nm
  - 10 Gbps downlink and 10 Mbps uplink communications at 1550 nm
- 24/7 “instant” optical relaying of 10 Gbps data from any LEO remote sensing satellite or UAV (Point A) to any ground site (Point B) which is connected to a fiberoptic or other high speed hub. Thus, each SLR2000C site serving as a space-to-ground relay must have a direct fiberoptic or free space optical communications link to a ground communication hub.
- Reduce non-recurring engineering and replication costs by using COTS optical telecom components wherever possible
  - Adopted telecom industry components at 1550 nm
  - Large and competitive selection of transmitters, detectors, filters, splitters, etc
  - Eyesafe wavelength
  - Excellent atmospheric transmission and low solar scatter.
  - Keeps the differential replication cost between SLR2000 and SLR2000C relatively low (typically $500K to $700K depending on specific features)

In addition, we constrained operations above 20^{o} elevation for a number of reasons:

- At sufficiently low elevation angles, differential refraction effects in the atmosphere cause the lasercom and ranging beams to follow different paths thereby destroying their coalignment.
- Losses due to atmospheric transmission and scintillation become more severe
- Even though both beams meet OSHA eye safety standards, operating above 20^{o} elevation helps satisfy FAA “startle” requirements at nearby airports.

Laser Communications at 1550 nm

Fig. 2 shows a block diagram of a typical four channel lasercom receiver configured from existing COTS telecom parts. A simple dichroic mirror, inserted into the existing SLR2000 optical train, separates the ranging photons at 532 nm from the lasercom photons at 1550 nm in both transmit and receive mode. It is assumed here that each lasercom channel can carry 2.5 Gbps of downlinked data for a total of 10 Gbps as is typical in ground-based fiberoptic links, and the question that must be answered is whether or not these components can be utilized successfully in a free space optical communications link with reasonably powered space-qualified laser transmitters. When compared to a fiberoptic link, the free space atmospheric channel is significantly less benign due to scattering and turbulence effects which lead to beam attenuation, spreading, wander, and scintillation of the laser beam [Degnan, 1993]. In addition, one must consider optical losses due to imperfect pointing of both the transmitter and receiver. Preliminary link calculations suggest that a 3 W transmitter on the GEO satellite (which already exists in the laboratory) with simple OOK modulation can easily downlink a few Gbps to an SLR2000C station with bit error rates of less than 1 pps. Additional link margin can be obtained by employing more sophisticated laser modulation and/or coding schemes.

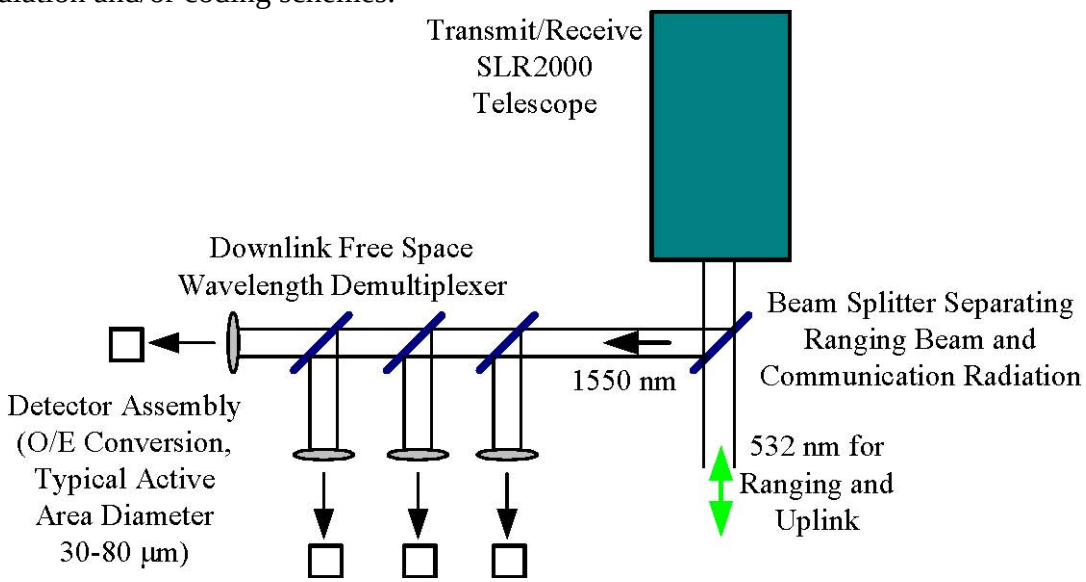

Figure 2: Block diagram of a four channel downlink each having a 2.5 Gbps capacity. The ranging/beacon and lasercom beams are separated by a simple dichroic mirror in both transmit and receive mode.

Satellite constellation architectures

Let us assume that we wish to transfer large quantities of data "instantaneously" from lasercom terminal A on an Unmanned Aerial Vehicle (UAV) or Low Earth Orbiting (LEO) satellite via one or more relay satellites and/or a direct link to an SLR2000C ground station to a Ground User Terminal B where that data will be analyzed and used. Independent of the space architecture, both the SLR2000C and Terminal B must be interconnected by either a high capacity ground fiberoptic network (as provided by commercial or military users) or a "last mile" free-space communications system between SLR-2000 and a fiberoptic hub. If an individual station has a 50% average availability (due to local weather, scheduled maintenance and repairs, etc.), the active relay satellite would require 7 ground stations in its field of View (FOV) for 99% availability of a clear link. Ten such stations in view would

provide 99.9% availability.

There are three types of space architectures routinely used for spaceborne communications: (1) Store and Forward, (2) Bent Pipe, and (3) Intersatellite Crosslinks. In a general "Store and Forward" architecture, a UAV or LEO would beam data to a relay satellite which would then store the data onboard until it could downlink it to a waiting SLR2000C ground station. Such an architecture clearly does not meet our 24/7 "instant" relaying criteria unless the ground network of SLR2000C stations was so dense that one was within view, both geometrically and optically, at all times. At lower relay satellite altitudes, the spatial correlation of weather patterns would greatly reduce the probability of an available link and or delay data delivery (high latency) even for a high concentration of ground stations.

A "Bent Pipe" architecture, in which the LEO transmits data to a clear SLR2000C site via a single intermediate relay satellite, can meet the 24/7 instant relay requirement provided there are enough ground stations and single-hop relay satellites in the constellation. The required numbers of ground stations and satellites decrease dramatically with an increase in the relay satellite altitude.

With "Intersatellite Crosslinks", one can use multiple linked relay satellites to transfer the data from Terminal A to any available SLR2000C station in the world. Thus, a global network of only 10 ground SLR2000C sites would provide 99.9% availability of a clear space-to-ground channel from any UAV or LEO location, independent of the satellite crosslink architecture. However, as in the "Bent Pipe" case, the number of required relay satellites decreases dramatically with increasing altitude of the relay constellation.

Geosynchronous Intersatellite Relay Example

It is well-known that operating at Geosynchronous (GEO) altitudes offers several distinct advantages. Fig. 3 shows the global communications coverage provided by four geosynchronous satellites with a ground station elevation cutoff of 20º. There is full coverage between latitudes of + 48º and partial coverage up to + 62º latitude, and the satellites can be positioned longitudinally to service most of the populated regions of the Earth. If necessary, full polar (and therefore global) coverage can be obtained through the addition of up to four complementary satellites in high polar or Molniya orbits. Because they are stationary with respect to a ground site, GEO satellites are relatively easy to acquire and track. Furthermore, they require no transmitter point-ahead correction or velocity aberration correction in the passive retroreflectors used for ranging. In addition, a GEO constellation requires the fewest ground sites when operating in "bent pipe" mode (~25 stations for 99% availability). As mentioned previously, with intersatellite links between GEO's, only ten ground stations would provide 99.9% availability.

On the negative side, the longer slant range to the ground from GEO altitudes reduces the signal levels for both the ranging and lasercom links for a given laser power-telescope aperture product. The lasercom signal varies as R^{-2} whereas the reflected signal strength from a given passive reflector array varies as R^{-4}.

In designing a ground network, one must clearly:

- **Choose good weather sites**
  - –Beneficial to both geodesy and lasercom
  - –Improves single station availability

- **Quasi-uniform global distribution**
  - –Weather diversity increases overall availability

–Permits global “bent pipe” operation
–Multiple stations in view for lunar and/or deep space missions that can’t benefit from satellite relays

- **Choose sites connected to or near fiber-optic based communications hubs**
  –Required for instant relay of space-to-ground data
- **Provide a sufficient number of ground stations to support the various space architectures and applications**
  –12 stations would support continuous LAGEOS tracking for geodesy and high availability (>99.9%) lasercom architectures using intersatellite links
  –25 to 30 sites would be needed to support bent-pipe GEO and lunar/deep space links

Fig. 3 shows 25 globally distributed SLR2000C sites, most of which are currently occupied by internationally manned SLR stations operated on behalf of the International Laser Ranging Service (ILRS) to support geodetic and other Earth and lunar science measurements. Since in this example 3 of the sites service the polar regions , each GEO satellite can typically view 6 meteorologically diverse ground stations on multiple continents. Fig. 4 shows the site locations relative to a global fiberoptic grid operated and maintained by MCI.

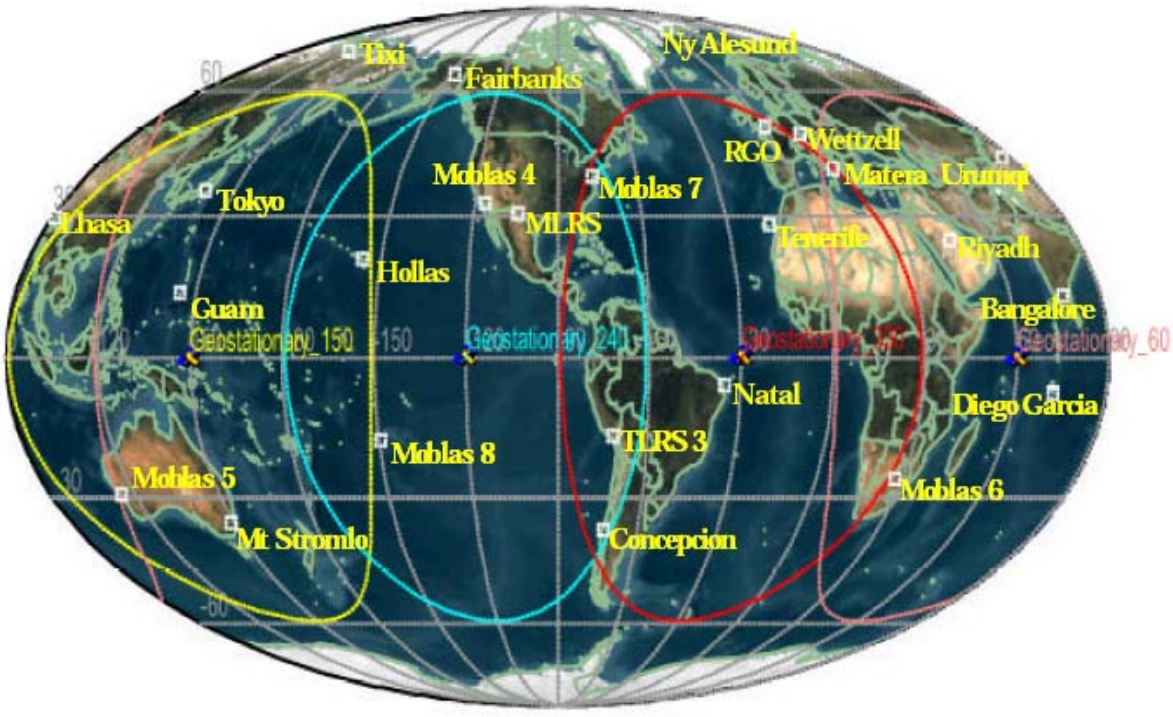

Figure 3: Global map showing geosynchronous satellite coverage for a four satellite constellation. Also shown are 25 potential SLR2000C ground sites which would largely meet the space-to-ground needs of global Earth, lunar, and deep space communications.

Figure 4: Candidate SLR2000C site locations relative to global MCI fiberoptic net.

Geo-to-Ground Terminal Acquisition Sequence

The ground-based laser ranging beam from SLR2000C provides a strong beacon which, when viewed through a narrowband (0.3 nm) spectral filter, would appear as a bright pixel in a monochromatic CCD array (256x256 or greater) viewing the entire Earth disk. The location of the pixel immediately identifies the "clear" or "active" station and negates the need for separately transmitting ground terminal information to the GEO satellite. Assuming a 15 cm diameter telescope on the GEO satellite and operation at elevation angles above 20º , between 0.03 and 0.1 nW of beacon laser power at 532 nm would be absorbed by the onboard detector, corresponding to several tens of thousands of photoelectrons generated in the detector per ranging pulse at a 2 kHz fire rate.

Since there is no significant relative motion between the GEO satellite and ground station, there is no need to "spoil" the retroreflector dihedral angles as in lower satellites to compensate for velocity aberration effects. "Spoiling" typically reduces the natural optical cross-section by 1 to 2 orders of magnitude [Degnan, 1993]. Furthermore, the Earth disk subtends an angle of only + 8.6º at the GEO terminal, well within the + 15º angular field of view (FOV) of a hollow retroreflector [Degnan, 1993]. Thus, a single unspoiled 10 cm diameter hollow cube corner mounted to the nadir face of the GEO satellite has a huge optical cross-section (almost 2 billion square meters) and can provide a steady stream of ranging data to the ground station. Link analyses suggest 20 to 220 ranging photoelectrons per second at elevation angles between 20 and 90 degrees respectively resulting from this simple and compact GEO target. Using the reflected photons from the satellite and a photon-counting quadrant detector, the SLR2000C can acquire and lock onto the satellite reflector, totally independent of the lasercom system.

The proposed acquisition sequence follows:

1. SLR2000C initiates search for GEO satellite, acquires 532 nm returns from the onboard retroreflector, and locks onto the satellite using existing ground quadrant

detector. It then informs the ground lasercom system, which is co-boresighted with the ranging system, of successful acquisition and lock. The ground lasercom goes into "ready to transmit or receive" state.

2. The onboard wide FOV CCD array with 532 nm filter constantly views the entire Earth disk (+8.5 deg) through the pointing telescope and sees the active 2 kHz SLR2000 "beacon" as a bright pixel.
3. The onboard lasercom mount controller centers the bright pixel ("Coarse" pointing correction) which in turn brings the SLR2000C ranging beam into the much narrower FOV of an onboard 532 nm quadrant detector.
4. The onboard quadrant detector locks onto the ground ranging beacon, refines the lasercom pointing ("Fine" pointing correction), and informs the onboard lasercom system of successful acquisition and lock onto the ground terminal. Space lasercom system goes into "ready to transmit or receive" state.
5. At this point, the space lasercom terminal can either begin transmitting to the ground via the downlink or receive an upload via the 10 Mbps uplink.
6. If the beacon link is broken, both terminals will lose 532 nm lock simultaneously and can stop send/receive operations until the link is re-established via steps 1 through 5.

Downlink bit error rates from Geosynchronous orbit

Figure 5 shows the results of an optical communications downlink analysis to SLR2000C from geosynchronous orbit. The analysis was done for three popular wavelengths – 532 (green), 1064 (red), and 1550 nm (brown). A spaceborne transmitter with an output of 3 W, a full beam divergence of 4 arcsec between Gaussian $1/e^2$ intensity points, simple On-Off Keying (OOK) at 2.5 Gbps, and an on-off modulation depth of 10^3 was assumed. The transmitted power for 532 nm was reduced to 1.5 W to reflect a 50% power conversion loss in the frequency doubler, but, on the positive side, the modulation depth of the original 1064 nm transmitter is squared by the same process. In addition to this "transmitter noise" due to imperfect extinction of the 0's, we assumed a worst case high noon scenario for solar scattering in the atmosphere. Detector dark counts were assumed to be negligible compared to solar scattering and were not included in the analysis. The best detector quantum efficiencies available were assumed for each wavelength. We also included the effects of the atmospheric turbulence including beam wander, spread, and scintillation. The scintillation indices used are plotted in Figure 5a and reflect both the increased atmospheric scattering at shorter wavelengths (green = 532 nm, red = 1064 nm, brown = 1550 nm) and the theoretical $[\sec(qz)]^{11/6}$ power dependence of the index on the satellite zenith angle [Andrews and Phillips, 1998]**.** The goal of one bit error per second is indicated by the dashed horizontal line in Fig. 5b Based on our atmospheric noise models, the detector threshold was varied with zenith angle to maintain a rate of false 1's below the targeted bit error rate. However, the number of false 0's (undetected 1's) increases rapidly with zenith angle beyond some wavelength dependent break point due to scintillation-induced fading. That breakpoint was 37º at 1064 nm (but the BER goal was met up to 45º) and 55º at 1550 nm. The frequency-doubled laser was never able to meet the BER goals at the reduced power level. Increasing the transmitted power by 66% to 5 W allows the 532 nm wavelength (2.5 W) to meet the BER goals down to zenith angles of about 15º and only extends the breakpoint and BER limits at 1064 and 1550 nm outward by about 7º to 52º and 62º respectively.

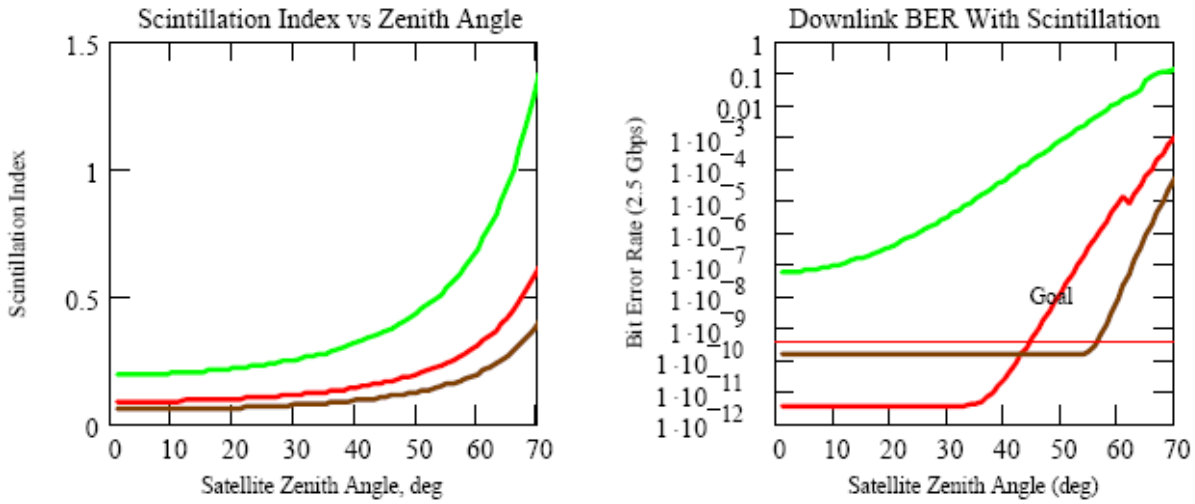

Figure 5: (a) Scintillation index used in the multiwavelength lasercom link analysis; (b) Computed daylight Bit Error Rate (BER) at 2.5 Gbps as a function of wavelength and satellite zenith angle. Goal (dashed red horizontal line) reflects one bit error per second.

Lunar and Deep Space Communications

Because the signal from a passive retroreflector target falls off as the fourth power of the range (R^{-4}), an active laser transponder would be substituted for the passive target when considering combined ranging and communications between SLR2000C and a spacecraft at lunar or interplanetary distances [Degnan, 2002]. Both the transponder and lasercom signals would now fall off as R^{-2}. Since a distant spacecraft sees half the Earth disk but is above 20 degrees elevation over only 33% of the Earth surface, we would need approximately 3 x 7 = 21 uniformly distributed stations for 99% availability or 3 x 10 = 30 stations for 99.9% availability, again assuming a mean single station availability of 50% .

Summary

We have argued that satellite laser ranging and lasercom applications are highly synergistic since most of the ground support capabilities required for an automated ground lasercom station are provided by the baseline SLR2000 design. A space-to-ground 10 Gbps downlink and 10 Mbps uplink lasercom capability can be added to SLR2000 for a differential replication cost of about $600K at an eyesafe wavelength of 1550 nm using COTS telecom parts. The 1550 nm wavelength is not only eyesafe, but the high atmospheric transmission and low scatter combined with low solar output in this spectral region greatly improves the signal to noise situation for free space laser communications.

At geosynchronous altitudes, a single 10 cm diameter, unspoiled hollow cube corner is capable of satisfying the SLR2000C ranging link and contributes no error to the range measurement. Range returns from the passive reflector provide independent verification of satellite acquisition and lock and greatly simplifies terminal acquisition for lasercom. An onboard CCD array can view the upcoming ranging beacon through a 532 nm filter for initial acquisition of the ranging beacon, in situ identification of the active ground station by its position on the Earth disk, and initial coarse pointing of the onboard lasercom terminal. Narrow FOV 532 nm quadrant detectors at both terminals can further refine the pointing at the sub-arcsecond level. For longer deep space links, active laser transponders can be substituted for passive reflectors. Both lasercom data rates and range returns will fall off as R^{-2} for a given transmitter power/receive aperture product.

A 12 station ground SLR2000C network can provide >99.9% availability for LEO to Earth communications using intersatellite relay links. A denser 25 to 30 site SLR2000C network would support both global “bent pipe” LEO to GEO to Earth communications and deep space coverage with > 99% availability. Preliminary link calculations suggest the feasibility of 10 Gbps near-Earth downlinks (4 channels @ 2.5 Gbps per channel) and a 70 Mbps downlink capacity from the Moon with achievable laser powers of a few watts per channel. It is hoped that multi-user support will increase the likelihood for funding of a substantial global network which would benefit both geodesy and global scientific space-to-ground communications.

References

Andrews, L.C. and R. L. Phillips, Laser Beam Propagation through Random Media”, SPIE optical Engineering Press, Bellingham Washington, 1998.

Degnan, J., "Millimeter Accuracy Satellite Laser Ranging: A Review", in *Contributions of Space Geodesy to Geoodynamics: Technology*, D. E. Smith and D. L. Turcotte (Eds.), AGU Geodynamics Series, Volume 25, pp. 133-162, 1993.

Degnan, J., "Asynchronous Laser Transponders for Precise Interplanetary Ranging and Time Transfer", J. Geodynamics, pp. 551-594, November, 2002.

Degnan, J., J. McGarry, T. Zagwodzki, H. Donovan, D. Patterson, C. Steggerda, A. Mallama, and J. Cheek, “NASA’s Photon-Counting SLR2000 Satellite Laser Ranging System: Progress and Applications”, Proc. AMOS 2003 Technical Conference, Maui, HA, Sept. 8-13, 2003.

McGarry, J., T. Zagwodzki, J. Degnan, P. Dunn, J. Cheek, D. Patterson, H. Donovan, A. Mann, A. Mallama, and R. Ricklefs , “Early Tracking Results from SLR2000”, these proceedings, 2004.

TECHNICAL CONCEPT OF A EUROPEAN LASER ALTIMETER FOR PLANETARY EXPLORATION

U. Schreiber(1), H. Michaelis (2), J. Oberst (2), I. Leike (3), T. Spohn (2)
(1) ForschungseinrichtungSatellitengeodäsie der TUMünchen, Fundamentalstation Wettzell, D93444Kötzting, Germany
(2) German Aerospace Center, BerlinAdlershof, Germany
(3) Physics Solutions, Hörlkofen, Germany
schreiber@wettzell.ifag.de;
Harald.Michaelis@dlr.de,
Juergen.Oberst@dlr.de,
Ines.Leike@gmx.de,
Tilman.Spohn@dlr.de

Abstract

In the past year, our team has developed an alternative concept for a high performance Laser Altimeter for Planetary Exploration (LAPE) for a Mercury mission with parameters similar to the BepiColombo Mercury Planetary Orbiter mission. The instrument must be capable to operate in a harsh thermal environment. Its mass is required to be less than 10kg and the power consumption less than 20W. In order to avoid excessive thermal loading and to keep the weight down we have chosen to study the applicability of a small receiver telescope with 15cm aperture.The key features of this alternative altimeter concept are a high repetition rate microlaser and single photon detection by gated "Geigermode" APDs. The cwoperation of the pump laser diodes of the microlaser avoids power switching and also makes bulky capacitor banks unnecessary. These features lower the operation risk and mass requirements substantially. However, due to the high shot repetition rate the data processing becomes more complex and requires special provisions for binning and averaging of the data. The basic performance of our concept has been evaluated by simulation. This paper outlines critical aspects of the altimeter design and discusses some of the simulation results.

Introduction

Laser altimeters have become useful tools for planetary exploration as has been convincingly demonstrated by e.g., the MOLA (Mars OrbitingLaser Altimeter) instrument on Mars Global Surveyor [1]. The Mercury Laser Altimeter MLA [3] has been launched on board NASA's Messenger mission in the summer of 2004. Another laser altimeter is part of the strawman payload of the ESA cornerstone mission BepiColombo which is scheduled for launch to Mercury in 2012[2]. The general concept of a laser altimeter is shown in figure 1. A solid state pulse laser (L) generates short laser pulses of approximately 1ns pulse width and transmits them via a small optical telescope. A high bandwidth optical detector such as a PIN diode records the moment of laser fire and logs it with respect to a high precision timescale. After traveling between 400 and 1600km the laser pulse hits the groundon Mercury and a proportion of around 20% is reflected[5]. When returning back to the spacecraft another optical telescope picks up the remaining light of the laser pulse and focuses it onto a highly sensitive photo detector (D). Sharp spectral and spatial filtering is applied in order to keep the noise background and the thermal load low. This moment of detection again is timed by the on board event timer and the range (d) of an individual measurement taken at the epoch of the start event is determined by evaluating the time of flight as $d=c \bullet t/2$. In order to reduce the

measured raw ranges to a meaningful altitude above ground, it is necessary to correct these raw range measurements for internal delays caused by the time of transit of the electrical signals inside the altimeter instrument. Furthermore one has to reduce the range measurement to a geometrical point of reference at the spacecraft. The difference Δt between stop and start epoch valid for the moment of laser fire t_0 is then converted to a range measurement according to:

$$h(t_0) = x(t_0) - \frac{1}{2}c(\Delta t(t_0) - d) ,$$

where $x(t_0)$ is the orbital position of the satellite, c the vacuum velocity of light and d accounts for constant internal signal delays in order to reference the range measurements to the center of mass of the satellite. The mission requirement for the precision of the altitude measurements is less than 1.5 m. A prerequisite of the altimeter operation is a good control of the satellite orientation in "Pitch" and "Roll", as well as a stable nadir telescope pointing and a precise orbit determination. The post-processing error must be substantially smaller than the measurement resolution. For this paper's discussion a sufficient knowledge of the satellites reference point is assumed.

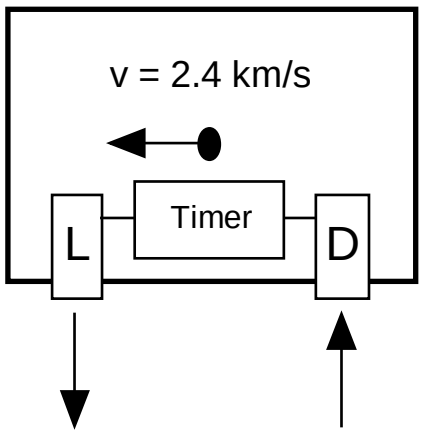

Figure 1: Schematic diagram of an altimeter on a spacecraft. Only the transmitting pulse laser (L), the detector with receive telescope (D) and control electronics including the event timer (Timer) are indicated.

Conventional altimeter concept: In previous altimeter missions in Earth and Mars orbit, such as LITE and MOLA telescopes with apertures larger than 0.5 m have been used. Together with a pulse energy of more than 20 mJ at a repetition rate of 10 Hz, this produces a comfortable link budget margin. Even under the application of detectors with moderate quantum efficiency, echoes are obtained at almost every shot. This allows to carry out measurement of the time of flight as well as to use the variations in the pulse width as a terrain slope indicator. For a mission to the innermost planet the application of a large telescope aperture is critical because of the hostile environmental conditions, in particular the excessive solar heat influx. MLA has four telescopes with 12.5cm aperture [3]. The recently proposed BepiColombo Laser Altimeter BELA foresees a telescope with 25cm aperture [4].

Alternative altimeter concept: In this paper, we report on a study of an alternative altimeter concept, which may have the potential of achieving the mission goals by going from a strict conventional multi-photon return pulse requirement to a statistical single photon detection scheme. At the same time the instrument is much more compact and the requirements for

power and weight are greatly reduced. Instead of using high power Nd:YAG pulse lasers we consider a high repetition microlaser working at a pulse repetition rate of about 20 kHz at an energy level of around 10 μJ[1]. Because of the moderate demands on the range resolution of 1.5 meter, the pulse width is not critical and may be chosen to be around 2 ns. In comparison to high power pulse lasers with low repetition rate, microlasers do not require water cooling and are much smaller and lighter than conventional Nd:YAG systems. Since the microlasers of interest are cw- pumped, there is the considerable advantage of a reduced risk of laser failure. In order to match the high repetition rate and the low energy of the transmitter, corresponding changes to the detector system are necessary. Avalanche photo diodes (APD) operated in the Geiger mode [6] reach quantum efficiences well in excess of 50% and have demonstrated their suitability for extreme sensitive single photon detection in Lunar Laser Ranging [7]. Since they are solid state devices they require less space and work under convenient operating voltages in contrast to a photomultiplier. In order to satisfy the 1.5 m range resolution requirement the altimeter is equipped with a direct counting clock operated at a frequency of 350 MHz. The time-scale in the form of a frequency reference and 1 pulse per second (pps) signal is presumably provided by the interface bus of the spacecraft and is therefore considered as given here. The noise reduction, averaging of data points and slope detection is done in the onboard unit of the altimeter in real time as the spacecraft carries out the measurements. The preprocessed data are then transmitted back to Earth. Suitable averaging and data format definitions have to ensure that the maximum data rate of 500 bps is not exceeded.

The entire alternative altimeter concept is based on a differently arranged trade-off. We avoid large apertures, high mass, and high risk of failure by utilizing higher receiver sensitivity, single photon counting and a statistical data processing approach. This is achieved through a substantially higher repetition rate of the data taking cycle. Simply speaking, we are looking at hardware of lower complexity at the expense of more sophisticated software requirements. The concept study offers interesting perspectives for future planetary missions to Mercury or beyond. Nevertheless, the full development of such an instrument is a complex undertaking. Because the schedule for the development of instruments for BepiColombo is very tight and funding is limited we have not proposed this alternative altimeter for the BepiColombo payload.

Design considerations

Before the design considerations for this alternative approach are discussed, we are summarizing important mission characteristics (see table 1):

Table 1: Laser Altimeter Operation Characteristics

Parameter	Value	Specification/Comment
Mercury Properties		
Albedo	0.2	mean value at the Laser wavelength
Distance to sun	68.5 / 104 Mio km	perihelion / aphelion
Observing conditions		
S/C Distance to surface	400 / 1500 km	periherm / apoherm

[1] Recently a compact microlaser with an extra amplifier stage capable of approximately 100μJ pulse energy was considered feasible.

S/C Speed w.r.t. Ground	2.6 / 1.35 km/s	periherm / apoherm
Operation		
Laser Spot Diameter	40 / 150 m	periherm / apoherm
Shot-to-Shot Spacing	0.16 / 0.084 m	periherm / apoherm
Single Shot Detect. Prob.	0.0188 / 0.0012	periherm / apoherm
Typical Integration Time	0.1 / 0.5	periherm / apoherm
Int. Detection Probability	0.9 / 0.2	periherm / apoherm
Maximum Data Rata	500 bps	
Heat / Solar Flux		
Solar Irradiance at Mercury Surface	14490 / 6290 W/m^2	periherm / apoherm
Planet's Black Body Surface Temperature	630 / 575 K	periherm / apoherm
VIS Flux	2.7 W	VIS flux encountering the optics *)
	0.05 W	Vis flux entering the optics *)
IR Flux	10.8 W	IR flux encountering the optics *)
	3.2 W	IR flux entering the optics *)

*) worst case: Mercury at perihelion, spacecraft at periherm

Figure 2 shows a block diagram of the altimeter design. The central function block is the orbit reference. It provides time and spacecraft position. Based on this information the microlaser is fired. The epoch of the generated laser pulse is recorded by an event timer. An afocal beam expander is used to fill the full aperture of a small (3cm diameter) coelestat.

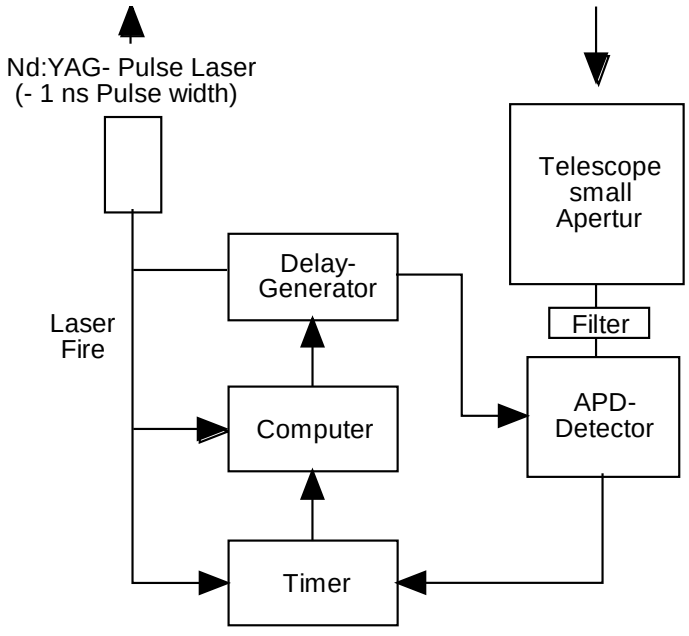

Figure 2: General block diagram of a laser altimeter

This mirror can be adjusted to compensate for velocity aberration, should this be necessary. The reflected pulse from the Mercury surface is captured by a 15 cm aperture receive telescope in Cassegrain configuration. Both telescopes are operated near the diffraction limit. A 1 or 2 nm wide spectral filter with an additional coating for solar heat flux reduction at the

front end of the receiving telescope minimizes the amount of unwanted radiation substantially and therefore reduces the heat influx. A spatial filter at the Cassegrain focus lowers the background light input and limits the receiver field of view to about 5 seconds of arc. Additional spectral filtering reduces the unwanted background light even further. Based on the precision of the orbit reference the microprocessor unit provides a range gate of 2 μs corresponding to 300 m tolerance for the range. Since the entire concept is based on the single photon detection mode, we detect far less than one photo-electron (p_e) per shot, on average $p_e \sim 0.005$. Neglecting the contribution from background light far less than one echo per gate is expected. However in the presence of background light we may well have the case of more than one photo-electron per gate. Since the detector and timing system can handle only one event per gate, we also have to consider the case of the loss of valid returns due to the detector dead-time.

For that purpose the concept is using a high repetition rate of 20 kHz and a statistical approach by binning dead-time corrected data of 2000 shots. This allows us to obtain one final measurement at 260 m intervals (periherm) and 675 m (apoherm and longer averaging), while the spot-size of the collimated laser beam on the ground is 40 m at periherm (400 km) and goes up to 150 m for an altitude of 1600 km.

Avalanche photodiodes operated in the Geiger- mode are currently the most sensitive type of detectors for photon counting applications [7]. Depending on the type of solid state diode a quantum efficiency of more than 50% can be achieved. The Geiger- mode is characterized by gating the bias voltage of a reverse operated avalanche photo-diode well above the breakdown voltage [8]. As a consequence however this results in the detection of one event per gate. A rather short gate length of around 10 μs is a practical maximum, unless cryogenic cooling is employed. In case of a high background noise level the duration of the gate must be reduced further.

Handling as much as 20 000 shots per second is a considerable demand for the timing device, which therefore must be as simple as possible. For this purpose a direct counting Epoch timer with a clock rate as high as 350 MHz, corresponding to a range resolution of 2.9 ns per clock cycle is sufficient. This is well within the range resolution requirement of 1.5 m and avoids the necessity of complicated interpolator hardware.

Simulations

Based on the above outlined severe mission constraints we have built a simulation suite in order to analyze the properties of the photon counting approach. This suite allows the investigation of the impact of variations in the parameters of various altimeter components. Figure 3 shows an example of such a simulated range measurement.

The simulation with an integration time of 0.1 s per frame is based on an orbit height of 800 km above the Mercury surface, a microlaser with 2 μJ pulse energy and a repetition rate of 16 kHz. A telescope aperture of 15 cm with a system transmission efficiency of 50% and a detector quantum efficiency of 60% was chosen. Since the signal to noise ratio (SNR) is barely exceeding a value of 2, not all averaged frames will obtain an ad hoc valid range measurement. However suitable post-processing strategies are expected to allow echo identifications at a SNR worse than this example. This possible improvement is considered as an extra option and was not taken as a baseline for the altimeter design. Because the SNR at

higher altitudes will always be very low, we have looked at the probability of detecting a return as a function of integration time. Three situations were of particular interest:

- maximum peak detection scheme
- simple range prediction based on previous return identifications
- a less conservative but still highly realistic parameter ensemble

The parameter sets for these simulation runs are summarized in table 2 and correspond to a worst case scenario with the satellite at apogee.

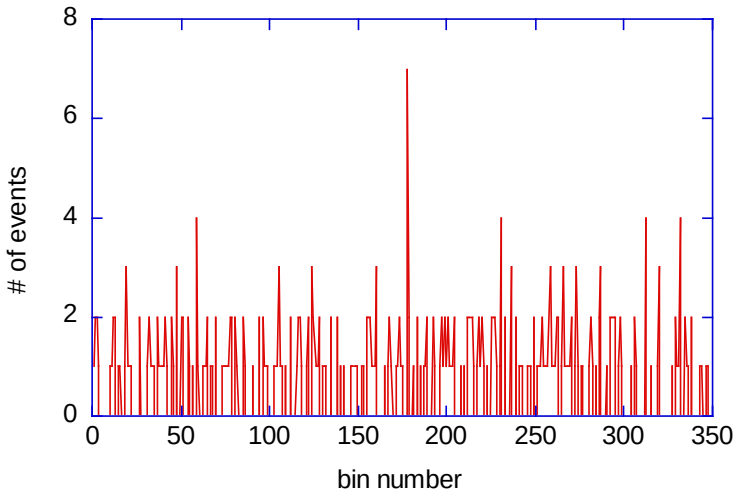

Figure 3: Example of a simulated altimeter range measurement at a distance of 800 km, obtained after 0.1 second of integration.

When applying an integration time of 2 seconds the detection probability of the very conservative parameter set Case 1 approaches 80% while it is 20% at an interval width of 0.5 seconds, which will still give a reasonable resolution for adjacent data points along the ground-track of the satellite. Case 2 assumes more laser power, a slightly higher system transmission and detector quantum efficiency, but also a wider optical bandpass filter. Apart from the laser specifications, which seem a reasonable expectation, the system parameters are still assumed to be very moderate and therefore leave room for optimization.

Table 2: Parameter list as used in the simulation based on a modified program of [9]

Parameter	Case 1	Case 2	Units
Wavelength	0.532	0.532	µm
Pulse Energy	2.0	8.0	µJ
Pulse Length	1.0	1.0	ns
Laser Beam Divergence	100.0	100.0	µrad
Telescope Aperture Size	0.15	0.15	m
Receive Optics Transmission	0.5	0.6	
Pulse Repetition Rate	16	16	kHz
Detector Noise Rate	200	200	kHz
Detector Quantum Efficiency	0.6	0.7	
Range Gate Width	1.0	1.0	µs

Clock Frequency	350	350	MHz
Filter Bandwidth	0.1	0.15	nm
Range	1600	1600	km
Mercury Albedo	0.2	0.2	
Averaging Time	0.1 – 2.0	0.1 – 0.4	s
Sun Illumination	no	no	

Without any changes to the hardware parameters of the ranging system one can improve the detection rate by including a priori information in the histogram analysis. The middle line (1) in figure 4 illustrates this for a simple case. When the maximum search in the measured histogram does not give an unambiguous result, the largest peak around the range value of the previous unambiguously identified ground echo is chosen as the most probable result.

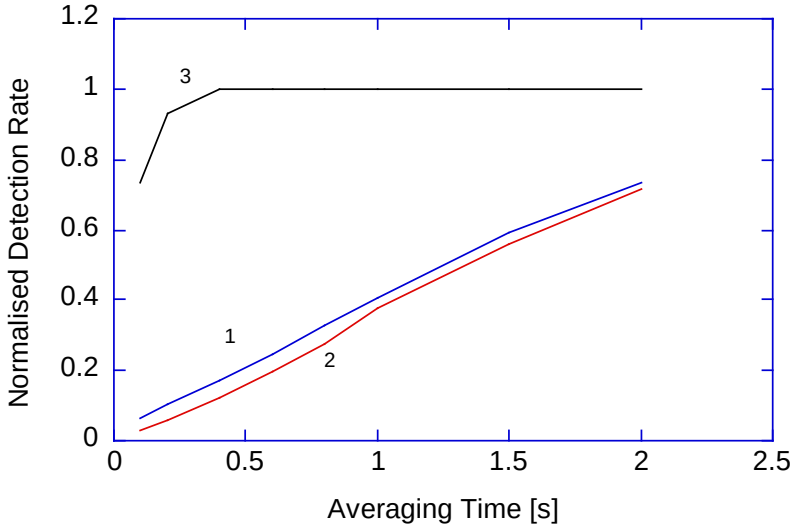

Figure 4: Normalized detection rate for the LAPE from an orbit height of 1600 km. A simple return prediction model (1) improves the return rate already noticeably over a plain range-gate evaluation (2). For the case of moderately improved parameters the detection rate improves as in curve (3).

Other more rigorous forms such as additional pulse width evaluation in the return histogram will improve the detection rate still further. This approach is based upon the assumption that the Mercury topography will spread the histogram peaks of the returns in a characteristic fashion and therefore helps to distinguish echoes from arbitrary noise events in the averaging process. In On top of that this approach provides additional information about the slope of the terrain. The drawback however is a dramatically reduced SNR when the pulse spreading becomes large.

For the poor case scenario “Case 1” in table 2 a sample dataset of the recovered ground-track is shown in figure 5. Since the averaging time has been set to 0.5 seconds, a little over 20% of the data contains identified ground returns. This corresponds to one range reading at roughly every 2.5 seconds. Since the space probe is assumed to be at apoherm the ground speed is at its minimum of approximately 1.4 km/s. A blow up of the front portion of the Mercury surface track of figure 5 is shown in figure 6. One can see that despite of all gaps a fair part of the echoes could still be recovered. At perigee the SNR is much more than one order of

magnitude better and the averaging time can be reduced substantially to values as low as 0.2 seconds.

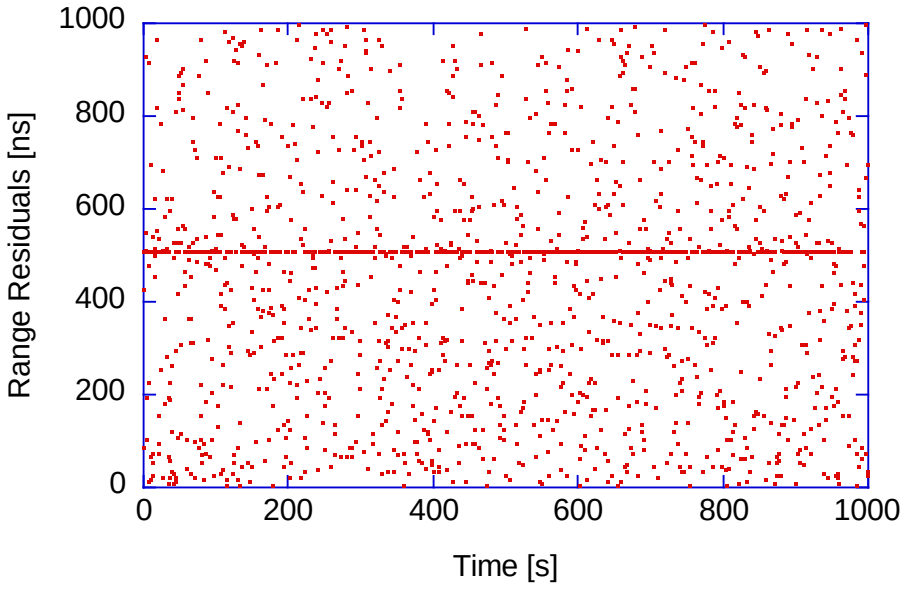

Figure 5: Simulated range residuals with a range resolution of 44 cm. The diagram shows an interval of 1000 seconds worth of data computed for a total range of 1600 km with a detection probability of around 20%.

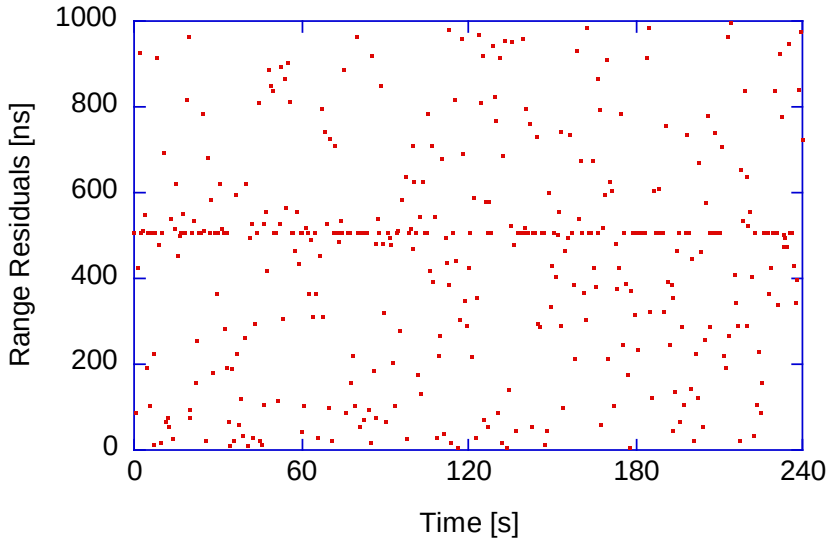

Figure 6: Blow up of the beginning of the diagram of figure 5. A section of the ground track corresponding to 4 minutes of the mission is shown.

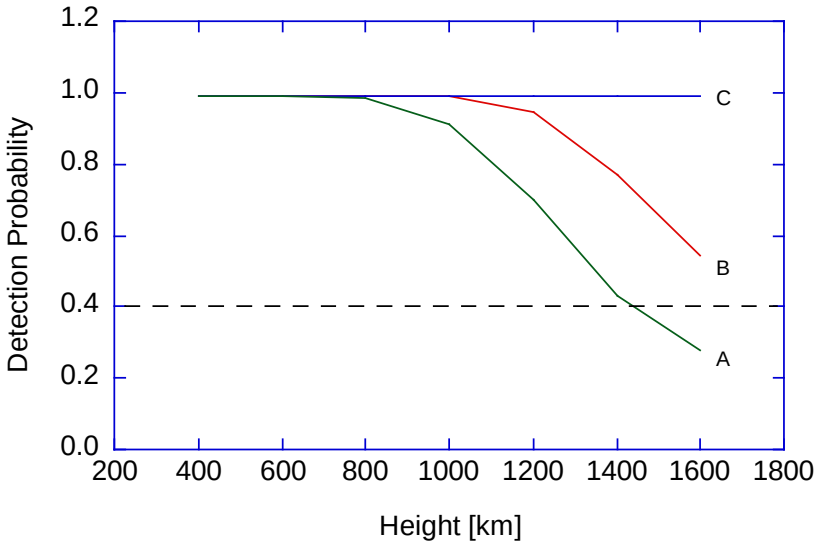

Figure 7: Detection Probability versus satellite height of one identified altimeter reading per time bin for 3 different parameter sets similar to table 2. The integration is 1 s and the laser energy was set to 2 µJ (A), 4 µJ (B) and 6 µJ (C).

Finally, it was investigated what detection probability as a function of range can be expected from a single photon counting altimeter. The laser beam energy of case 2 in table 2 was set to values of 2µJ (track A), 4 µJ (track B) and 6 µJ (track C). The corresponding integration time was 1 s for all 3 cases. Figure 7 shows that except for the last part of track A, the required detection is well in excess of 40%, which is an important mission requirement.

Conclusion

An alternative concept for a Mercury altimeter has been investigated. We have analyzed the potential of a single photon counting approach that will save mass, power, and volume. Instead of using a large and powerful pulse laser we have looked at a microlaser with a very high repetition rate. High receiver sensitivity and a statistical data evaluation technique allowed us to work in a different parameter regime of the link budget equation. Many aspects of the approach in this paper have been tested in the past in a different context, so that essentially only the high repetition rate of this altimeter concept is currently fully untested. Simulations show, that a fair number of mission requirements are well met by this concept, however there are also shortcomings and high risk aspects to be mentioned. Operations in daytime (target area illuminated by the sun) are not practical with the system parameters as used in this study. In particular a significant increase in laser power of more than a factor of 10 over the maximum values used in this work would be required to enable daylight operation. This seems feasible but is not yet demonstrated. Another issue is the reliable setting of a sufficiently wide range-gate under all mission conditions. A possible solution will increase the software complexity of this concept significantly.

Acknowledgements

This work was funded by the ESA design study “Laser Altimeter for Planetary Exploration – Definition Study” (Reference: IMTCS/HB/691/2002). We wish to thank Nicola Rando and Eamonn Murphy (ESA/ESTEC) for many thoughtful discussions during this study.

References

[1] D. Smith et al., Mars Orbiter Laser Altimeter: *Experimental Summary after the first year of global mapping of Mars*, J. Geophys. Res. Vol. 106, No. E10, 23,689-23,722, 2001.

[2] Science Advisory Group, *BepiColombo, an interdisciplinary cornerstone mission to the planet Mercury*, ESASCI (2001) 2001.

[3] R. E. Gold, S.C. Solomon, R.L. McNutt Jr., A.G. Santo, *The MESSENGER spacecraft and payload*, Proceedings, 53rd International Astronautical Congress, 10-19 October 2002, Houston, Texas, IAC-02-Q.4.1.02, 2002.

[4] K. Gunderson, N. Thomas, T. Spohn, K. Seiferlin andthe BELA team, “*A tradeoff investigation for the BepiColombo Laser Altimeter design*”, submitted to the Proceedings of the SPIE conference, 2004

[5] F. Vilas, C.R. Chapman andM.S. Matthews, eds., *Mercury*, The University of Arizona Press, 59-76, 1988

[6] U. Schreiber, W. Maier, K.H. Haufe, B. Kriegel; “*Properties of Avalanche Photo Diodes*”; Proceedings of the 9th Workshop on Laser Ranging Instrumentation, 113–120, (1994)

[7] U. Schreiber, K.H. Haufe, J.F. Mangin, J.M. Torre, C. Veillet; “*Operating the APD SP114 at the LLR Station in Grasse*“ Lidar Techniques for Remote Sensing, Chr. Werner, Editor, Proc. SPIE 2310; 25–32, (1994)

[8] A. W. Lightstone, R. J. McIntyre; *Avalanche Photodiodes for Single Photon Detection*, IEEE Trans. Electron Devices, **ED28**, 1210(1981)

[9] I. Leike, C. Werner: *Mercury altimeter simulation module* (part of the BepiColombo feasibility study)

LASER ALTIMETER FOR PLANETARY EXPLORATION

Ivan Prochazka, Karel Hamal
Czech Technical University in Prague.Brehova str. 7, 115 19 Prague 1, Czech Republic
prochazk@mbox.cesnet.cz phone +420 723 920 786, fax +420 224 922 822

Abstract

We are reporting on the research and development of a Laser Altimeter for Planetary Exploration (LAPE). It has been selected by ESA as a key-technology for future planetary missions. The device has to provide altimetry in the range of 400 to 1400 km and 1m range resolution under rough environmental conditions - Sun illumination, high background radiation under extremely limited weight and power consumption allowances. The proposed LAPE is designed to be a modular test equipment to test critical components and technologies such as the microlaser source, the photon counting detector and its electronics. In particular the signal to noise ratio under various background light conditions in the near infrared and the detector sensitivity under various cooling concepts need to be characterised. Photon counting strategies for high repetition rate data acquisition, signal processing techniques and data reduction will be investigated. This project builds on our experience acquired within the Russian altimeter missions Mars '92 and in Lidar for the NASA Mars Polar Lander '98.

Goals:

- To develop a modular test equipment: Technology Demonstrator to test critical components and technologies of the photon counting Laser Altimeter for Planetary Exploration LAPE.
- CRITICAL COMPONENTS
  - microlaser multi kHz
  - detector SPAD / ADP
  - optical filter
- CRITICAL PROCEDURES
  - energy budget link & S/ N ratio
  - data acquisition and processing
  - signal mining techniques

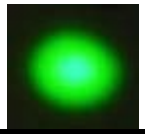

LAPE Parameters

- Altitude 400 – 1000 (1400) km
- Resolution 1 meter
- Background day and night operation on planetary orbit
- Concept photon counting multi kHz repetition rate
- Mass / Power 5 kg / 10 W
- Optics separate T / R
  - receiver reflector, 150 mm
  - transmitter refractor 30 mm

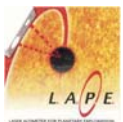

LAPE Technology Demonstrator

Philosophy

- Based on experience acquired in space projects MARS and Mars Polar Lander
- Use of off-shelf components whenever possible
- Optical apertures scaled down
  - to enable indoor and ground based tests of energy budget link
  (Difficult to test 1000 km / vacuum baseline)
- Receiver FOV and filter bandwidth scaled up
  - to enable indoor and ground based tests of the S/N ratio and signal processing techniques

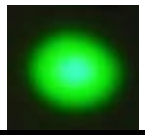

Photon Counting Laser Altimeter & Lidar

Project MARS 92, Russia

NASA Mars Polar Lander 98

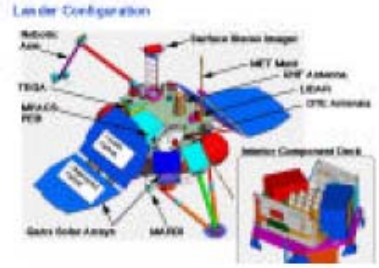

S.P.Pershin et all, IKI Russia

• Laser	diode 100nJ / 2kHz	
Optics	30 x 50 mm	
• Receiver	Si SPAD 40 um	
Optics	20 mm diameter	
• altimetry	0 - 5 km	
• visibility	0 - 50 km	
• clouds	heights, density	
• mass	400+400+100	900 g
• power average		< 30 mW
peak		< 4 W (LD heat)

LAPE Technology Demonstrator LASER
TRANSMITTER

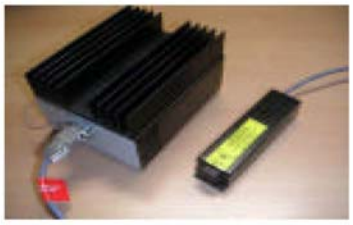

- diode pumped microlaser
- frequency doubled NdYAG
- 10 mW @ 532nm , 10 kHz
  = > 1 uJ / shot

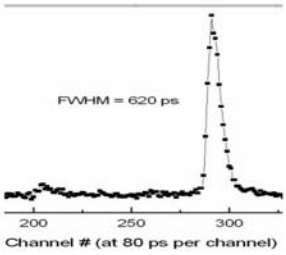

FWHM = 620 psec

TEM_{00} mode
divergence 4 mrad

LAPE Technology Demonstrator
Detector, Timing and Control

- DETECTOR PACKAGE
- # 1 SPAD on Silicon K14
- 25 um diameter, uncooled
  space qualified
- cw / gated, active quenching
- # 2 APD @ 1064 nm, cooled
  made by Silicon Sensors

- TIMING & CONTROL
- program. gate arrays 100MHz
- interval & epoch timing
- range gating
- µP controller

LAPE Technology Demonstrator

Energy Budget Link and S / N Scaling

- PHASE A indoor / static
  energy budget reduced 2.3 * 10^{10}
  = > range reduced 1.5 * 10^{5} 1-10 m indoor corresponds to 150-1500 km in orbit
  background increased 1 * 10^{1} Earth daylight corresponds to Mercury daylight

- PHASE B outdoor / air-born / dynamic
  energy budget reduced 2.3 * 10^{6}
  = > range reduced 1.5 * 10^{3} 100-1000 m ground corresponds to 150-1500 km in space
  background increased 1 * 10^{1} Earth daylight corresponds to Mercury daylight

LAPE Technology Demonstrator

Energy Budget Link and S / N Test Results

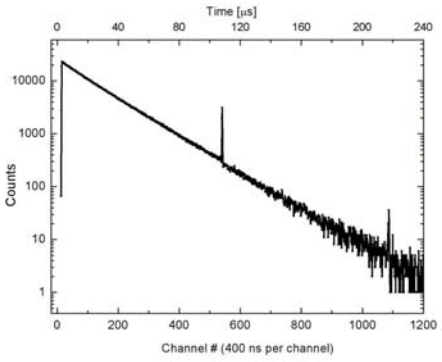

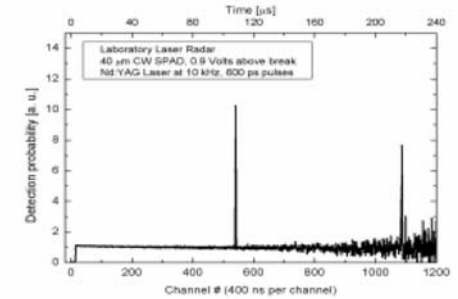

- INDOOR RANGING, Phase A
- 1.5 m distance < = > 225 km
- 10 kHz @ 532 nm laser
- high noon background
- raw data histogram, log scale
- echo data rate 100 / s
- window 240 us ~ 36 km

- the same data set converted to detection probabilities

- demonstrates the feasibility of 30 km wide range gates in daylight on a low altitudes

LAPE Technology Demonstrator
Planet Topography Contribution to S/N Ration Degradation

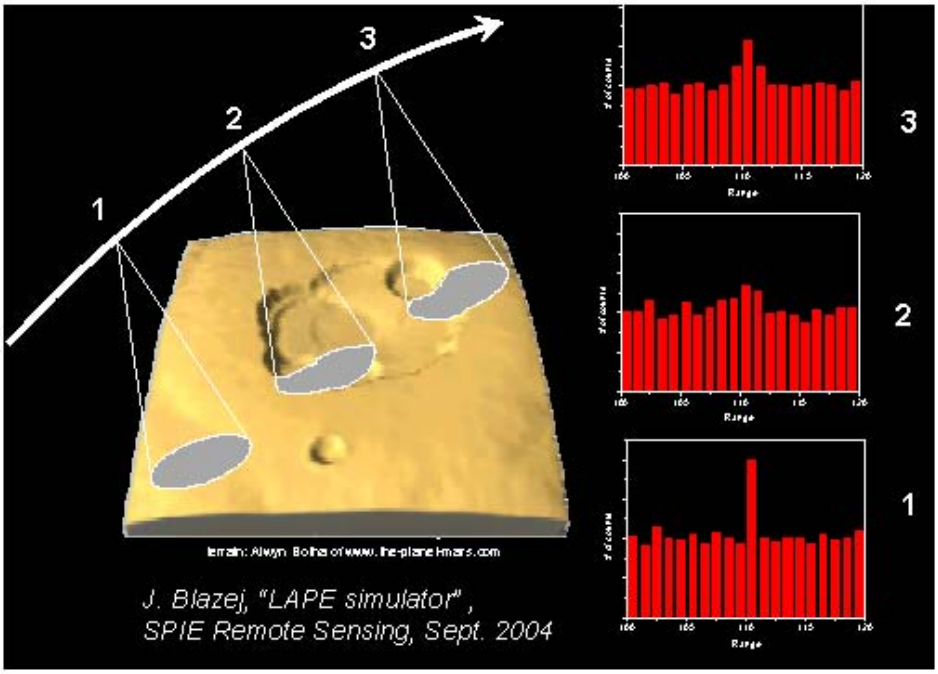

LAPE Technology Demonstrator

Conclusion

- The Technology Demonstrator of the photon counting Laser Altimeter for Planetary Exploration LAPE is under development
- PHASE A indoor / static tests
  - the Demonstrator version A -operational
    - 10kHz / 1uJ @ 532 nm / SPAD
      - -energy budget link
      - -S/N ratio for daylight
  - the planet topography contribution simulator under construction
- PHASE B outdoor / air-born / moving objects tests
  - 2 kHz/ 10 uJ @ 1064 / APD
  - project funding dependent

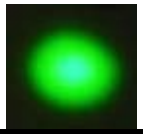

SCIENTIFIC APPLICATIONS OF PLANETARY LASER ALTIMETER RADIOMETRY

Maria T. Zuber (1,2), David E. Smith (2)
(1) Dept of Earth, Atmospheric and Planetary Science, MIT.
(2) Laboratory for Terrestrial Physics, NASA Goddard Space Flight Center.
zuber@tharsis.gsfc.nasa.gov Fax: 301 614-6015

Abstract

Laser altimeters in addition to providing topographic data of planetary bodies are sometimes able to provide a measurement of the radiance of the object at the wavelength of the laser/detector. At Mars the laser altimeter on the Mars Global Surveyor spacecraft had an adjustable threshold for the detector so that return signals would be kept within a specified dynamic range. The threshold was adjusted according to the strength of the previous return and thus the variation in threshold became an approximate measure of the reflectance of Mars at 1064 nm over the illuminated laser spot on the surface of Mars, approximately 165 meters in diameter. This method we refer to as the active radiometry mode. After the laser ceased to operate in June 2001, and in between laser firings when the laser was operating, the detector measured the radiance of the solar illuminated surface at 1064 nm over the detector field of view of approximately 385 meters. This mode is referred to as the passive radiometry mode. In the active mode the instrument acquired radiometry at 1 Hz, with a S/N of about 10; in the passive mode the instrument acquired radiometry at 8 Hz with a S/N of about 100. We now have nearly 3 Mars-years (over 5 Earth-years) of high resolution passive radiometry of Mars at 1064 ±1 nm for spatial footprints of under 400 meters. These observations are being used to study the intrinsic brightness of Mars and to monitor the changes in the polar icecaps due to the seasonal exchange of CO_2 between the atmosphere and the surface. Fig 1 shows the two polar regions of Mars at the same time of year (Ls =260) when the sun is just below the equator and moving northwards. Note the difference in radiance of the two regions and the lack of symmetry of the south polar icecap.

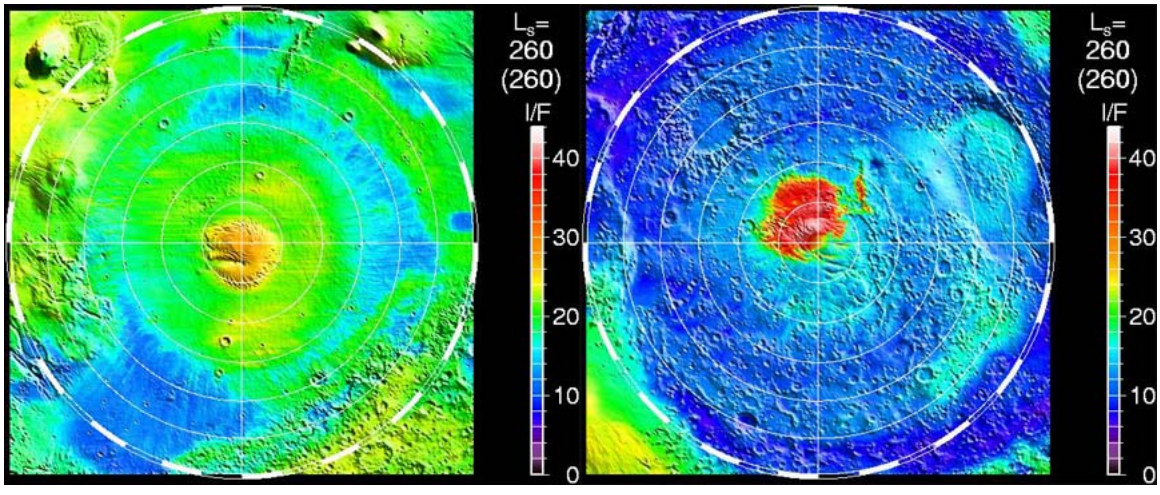

Fig 1. Radiometry at 1064 nm obtained by the laser altimeter at Mars during late Fall in the northern hemisphere (left chart) and late Spring in the southern hemisphere (right chart).

THE TWO-WAVELENGTH SATELLITE LASER RANGING EXPERIMENT AT SHANGHAI STATION

Zhang Zhongping, Yang Fumin, Hu Jingfu,Li Rendong, Chen Wanzhen, Chen Juping
Shanghai Observatory, CHINA
zzp@shao.ac.cn

Abstract

The paper presents multi-color ranging activities in Shanghai Observatory. An experimental two-wavelength SLR system with dual receiving channel is established at Shanghai station. Some LEO satellites have been observed successfully with a pair of 532nm/683nm.

Introduce

Several years ago, we were pleased to get an advance Raman cell from Dr. Gaignebet with which we began to work for multi-color ranging research. Two years ago, we cooperated well with Czech Technical University in researching the conversion efficiency of the Raman laser. We obtained fruitful results with Raman cell through an amount of the experiment: small wobbling of three wavelength beams and not low energy for Red/Blue color.
Last year, we got the support from national natural science foundation in China to research on two-wavelength SLR. During past year, we did a lot of improvements for routine system, including establishing two-SPAD receiver system, two counters recorded system, recoating all mirrors in the coude path etc. in order to work on multi-color satellite laser ranging.
An experimental two-wavelength SLR system with dual receiving channel and two-color transmitting simultaneously are established at Shanghai station. Some LEO satellites have been tracked with a pair of 532nm/683nm and over 20 passes were observed successfully.

Raman laser and optical system

Routine laser at Shanghai station is self-filtering unstable resonator (SFUR) with output energy of 35mj and pulse width of 30-40ps at 8Hz repetitive rate. We adopt the laser output to pump Raman laser. Raman laser with the length of 1 meter is focused on the middle of cell and AR-coat on the both end of the cell. 18bar pressurized with hydrogen is optimum for our laser system according to Hamel, Hu conversion efficiency experiment result (fig.1). Under the pressure, red/green /blue energy is 4mj, 10mj, 0.4mj respectively.

Fig.2 is the two/three wavelength optical scheme. The upper right block is SFUR laser. M1 and M2 are high reflection mirrors for 0.532. The green beam is forced into the Raman cell. M3 to M8 mirrors are used to separate three beams. Three expander telescopes are put on optical pass to allow divergence adjusted. M9, M10, M11 are used to recombine the three beams to enter coude system. Due to low energy for blue color, in first stage, we select 532/683 pair wavelengths in the experiment. By blocking one out of three beams, two other colors are transmitted simultaneously to satellite target. Switching between routine ranging and two-color ranging is easily by moving M14 and M15 mirrors. We found output energy of

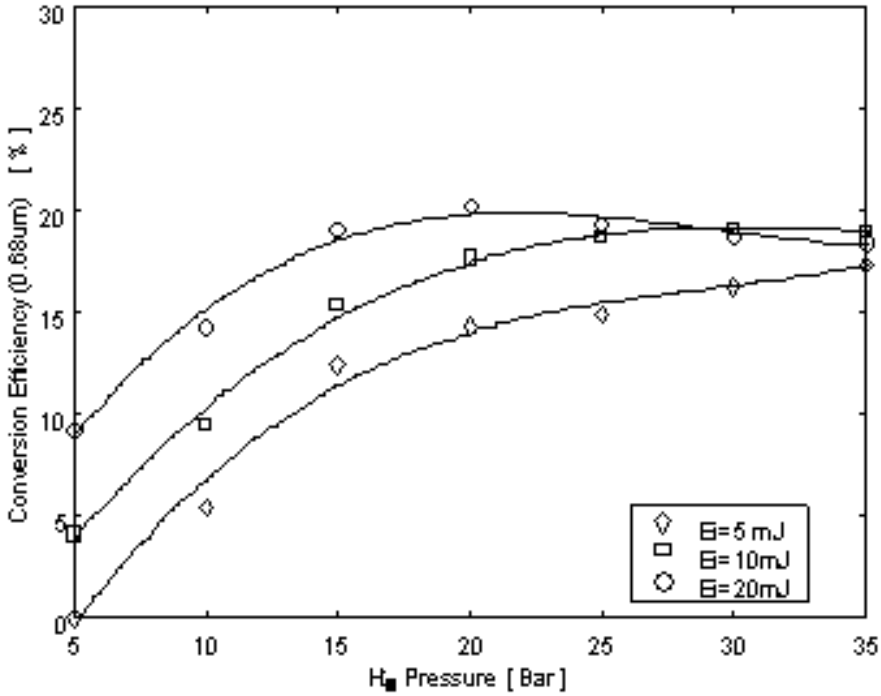

Fig.1 Conversion efficiency vs. pressure

Raman laser and ranging precision depended on the direction of laser on the both end of cell. It is necessary to adjust laser carefully before the experiment. Fig.3 is a laboratory for two-wavelength measurement.

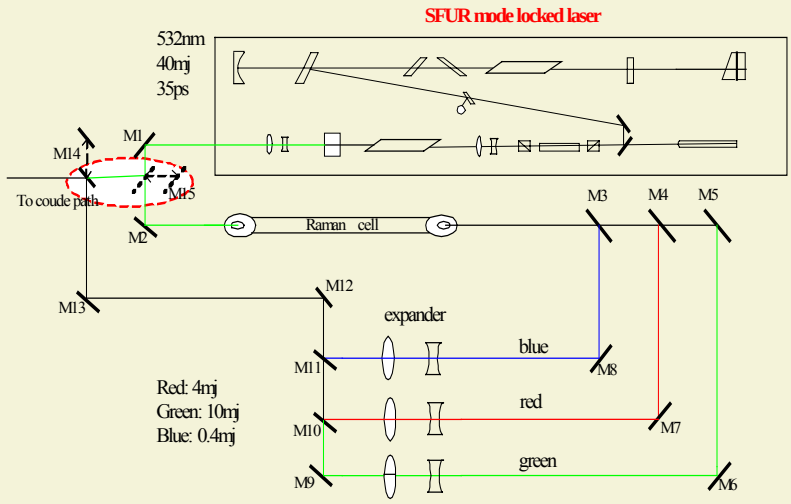

Fig.2 Two/three wavelengths optical scheme

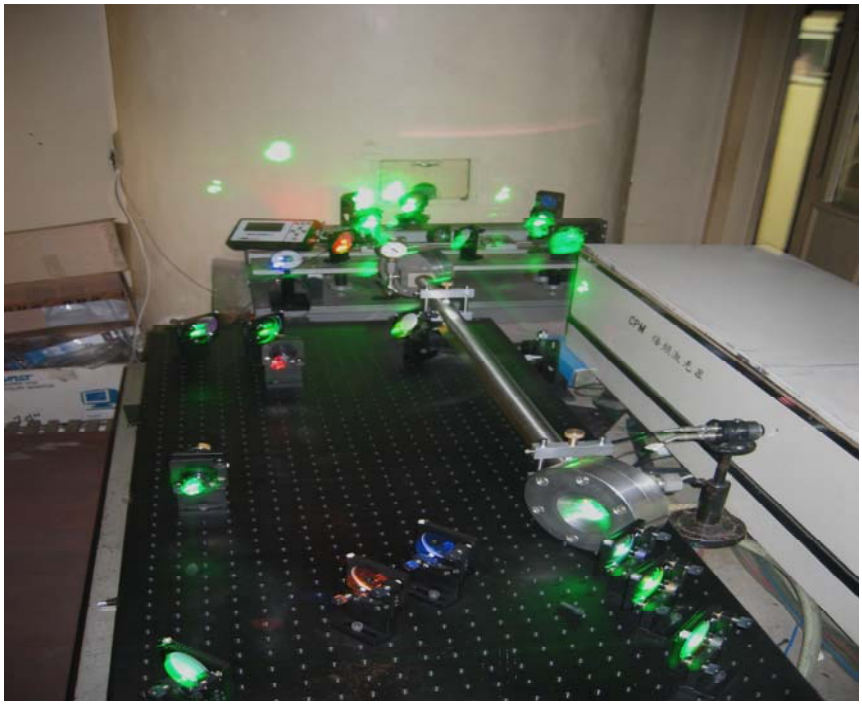

Fig.3 Two-wavelength system setup

In receiving system, two SPADs are used to receive signal of red/green color simultaneously. Two counters (SR620, HP5370) are adopted to record the two-wavelength return respectively. Independent calibration for two color /two SPADs is done at different receiving channel.

Tracking surface

Range residual (O-C) from both colors displays on same display interface of tracking, a fixed range bias is added on the ranges of red color return for identifying two returns easily

Ranging experiment and preliminary result

Only low earth orbit satellites are tracked due to low energy of 4mj at 683nm. It is important to adjust two beams to get better alignment before the experiment. After test to the near ground target, we started to range LEO satellites on July 27, 2003. More than 20 passes (including ERS-2, STARLETTE, TOPEX, JASON, AJISAI) were obtained for over two-month experiment Ranging precision is 0.8-1.2 cm for green color, 1.2-1.5cm for red color for most passes.

Conclusion

1. An experimental two-wavelength SLR system with dual receiving channel was established at Shanghai station. Some LEO satellites have been tracked with a pair of 532nm/683nm.

2. But the present system has some drawbacks:

   - The data from green color mixes with data from red one, it is difficulty for data preprocessing and degrades the ranging precision.
   - Low energy at 683nm and 432nm.

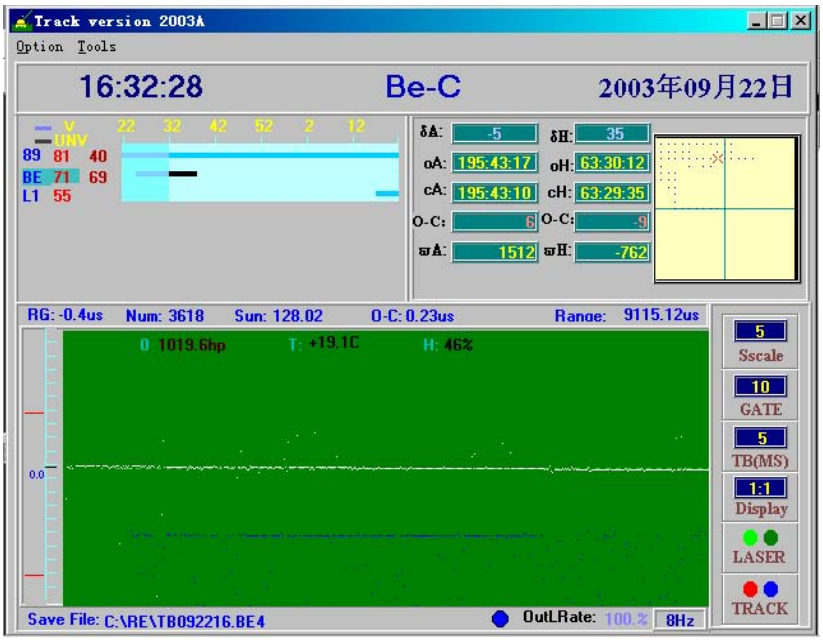

Fig.4 Real-time track interface on BEC

(An upper line in the figure is return signal from green beam, a down line from red beam)

Acknowledge:

We wish to thank Prof. Hamal and Prochazka for fruitful cooperation at the field of two-color SLR.

We wish to thank Dr.Gaignebet, for presenting the Raman cell to us.

The support provided by the National Natural Science foundation of China (Grant Nos.10373022) is greatly appreciated.

References:

1. Karel Hamal,etc. *Lasers for multiwavelength satellite laser ranging*, The 13th International workshop on Laser Ranging, Washington D.C,October 2002.
2. Kirchner, F.Koidl, *Multiple wavelengths ranging in Graz*, The 9th International workshop on Laser Ranging, vol.3,p609,1994.

REAL TIME SEPARATION ATMOSPHERIC TIP-TILT SIGNAL FROM LUNAR SURFACE

Xiong Yaoheng, Guo Rui Yunnan Observatory,
National Astronomical Observatories, Chinese Academy of Sciences Kunming
650011, Yunnan, P.R.China

Abstract

Considering atmospheric turbulence effects and returned photoelectron numbers on LLR, we think it's time to compensate turbulence effects in realtime on the LLR, especially for the effects of atmospheric tiptilt. In this paper, we present the computation method of atmospheric tiptilt from the lunar surface, and the experiment results at Yunnan Observatory 1.2m telescope that use a small area near the retroreflector array on the lunar surface as an expanded source to detect and compute the atmospheric tiptilt signal in real time.

Keywords: *LLR, returned photoelectron numbers, realtime tip-tilt sensing and compensation*

Introduction

Lunar laser ranging (LLR) represents the height of the single photon detection in which the received laser photoelectrons for one laser pulse emission by a 1m telescope on the ground are less than one. If we consider the atmospheric turbulence effects, especially for the short term beam wander, the returned photoelectron numbers of Kunming station 1.2m laser ranging system for one laser pulse emission using Apollo 15 retroreflector array are[1]:

$$Nr = 0.17 \times (1/40 \sim 1/6) \qquad (1)$$

The term in brackets represents the effect of the short term beam wander for the laser beam on the LLR.

We may say it is subsingle photon detection. When a laser beam propagates through the atmosphere, because of a random movement of the atmospheric turbulence, the index of refraction of the Earth's atmosphere has a fluctuation. That results in a series of effects on the laser beam propagation. All these atmospheric turbulence effects have a time scale: several ms, and relate to the Fried's coherence length r_o.

Fig.1 shows the relations of some atmospheric turbulence terms for the laser beam propagation

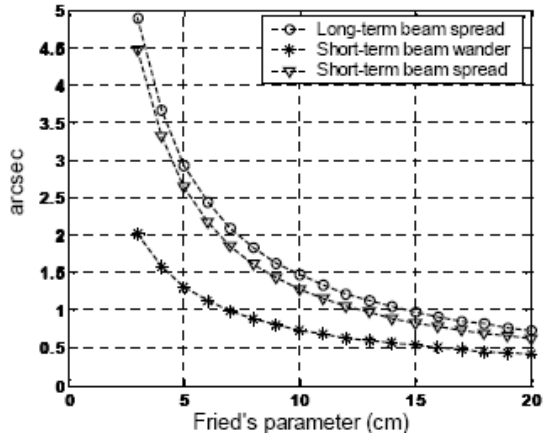

Fig. 1. Atmospheric effects for the laser beam at different r_o

Atmospheric turbulence also affect laser ranging accuracy with several mm to cm scale[1]. When returned laser photons are much less than 1 for one laser pulse firing, we need to consider a method to increase the returned photons. For current laser ranging, many aspects for increasing the returned photoelectron numbers have been considered. Using adaptive optics technique in the laser ranging is a way and proposed [2], especially for the LLR. Its purpose is to compensate atmospheric turbulence effects in real time, and to increase the returned photoelectron numbers on the lunar laser ranging. For simple and effective, we choose to compensate the shortterm wander that is caused by the atmospheric tiptilt as the first step on the LLR, and near 87% wavefront distortion is caused by the tiptilt[3]. That is to use the low order correction for the laser ranging, and to compensate the brackets factor in formula (1). The purpose is to increase the returned photoelectron numbers on the LLR.

Atmospheric Tip-Tilt Sensing From Moon Surface

When a ground station performs the LLR, its telescope will point and track the retroreflector array on the moon surface. So the atmospheric tiptilt information can only be obtained from a small area of the geomorphologic structure that is near the moon retroreflector. We use the absolute difference algorithm to track geomorphologic structure of the moon surface through the motion of the successive images.

First, a $N \times N$ pixels reference image $I_R(x, y)$ that is within the isoplanatic angle is sampled and stored in memory, and a time series $I_1(x, y)$; $I_2(x, y)$;…… $I_L(x, y)$ of two dimensionally resolved images of the same small area are sampled as live images. Then the absolute difference algorithm is used to determine the displacement between the reference image and the live images by computing the sum of the absolute values of the difference of them, for different relative shifts. For each $N \times N$ pixels live image $I_L(x, y)$, a $M \times M$ pixels window is extracted. This window of the live image is compared with the reference image at same positions. The absolute difference values $D(\delta x, \delta y)$ between them are given through the expression:

$$D(\delta x,\delta y)=\sum_{x=0}^{M-1}\sum_{y=0}^{M-1}\left|I_R(x+\delta x,y+\delta y)-I_L(x,y)\right| \tag{2}$$

The position $(\delta x_{min}, \delta y_{min})$ are obtained where $D(\delta x, \delta y)$ is minimum.

The tilt (Tx , Ty) can be determined using a parabolic interpolation. The Newton parabolic interpolation is used with a set of points $D(\delta x_{min} - 1, \delta y_{min}), D(\delta x_{min}, \delta y_{min}), D(\delta x_{min} + 1 , \delta y_{min})$ for the x-axis:

$$D(\delta x) = \alpha + \beta [\delta x -(\delta x_{min}- 1)] + \gamma [\delta x -(\delta x_{min}- 1)][\delta x - \delta x_{min}] \tag{3}$$

Using three point values to determine the parameters α ,β ,γ , when $D(\delta x)$ is maximum, $dD(\delta x) / d\delta x = 0$, this δx is the x component of the tilt, Tx:

$$T_x=\delta x_{\min}+\frac{1}{2}\cdot\frac{D(\delta x_{\min}-1,\delta y_{\min})-D(\delta x_{\min}+1,\delta y_{\min})}{D(\delta x_{\min}-1,\delta y_{\min})+D(\delta x_{\min}+1,\delta y_{\min})-2D(\delta x_{\min},\delta y_{\min})} \tag{4}$$

Same as xaxis, the y component of the tilt, Ty is:

$$T_y=\delta y_{\min}+\frac{1}{2}\cdot\frac{D(\delta x_{\min},\delta y_{\min}-1)-D(\delta x_{\min},\delta y_{\min}+1)}{D(\delta x_{\min},\delta y_{\min}-1)+D(\delta x_{\min},\delta y_{\min}+1)-2D(\delta x_{\min},\delta y_{\min})} \tag{5}$$

Tip-Tilt Sensing Experiment

Using Kunming SLR station 1.2m telescope, f = 6m, this experiment was done in 2003 with following device: 128×128 CCD, Frame rate: 419, 16μm×16μm for one pixel, 0.″55 /pixel Sampling area: near moon retroreflector array Apollo11, Apollo14, Apollo15 and Lunakhod2. Fig.2 show each one image around above arrays.

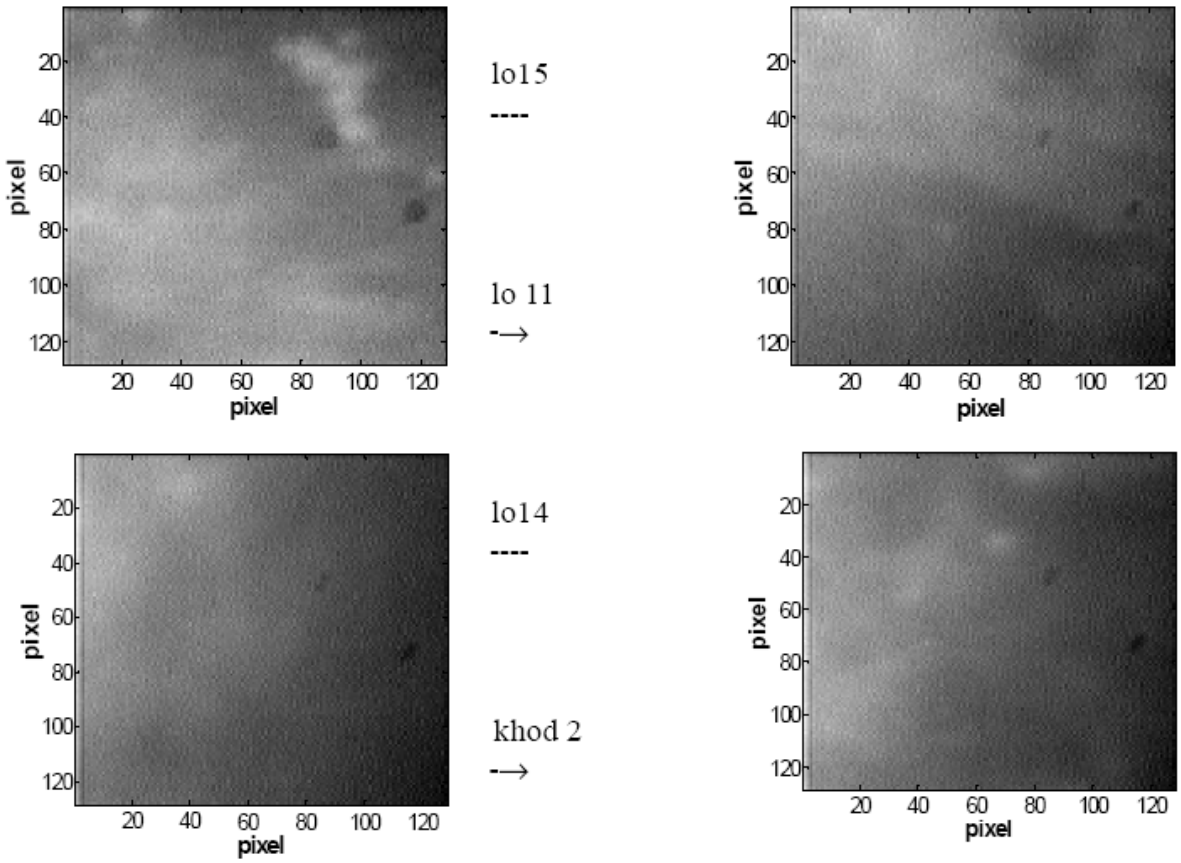

Fig.2. Lunar surface images near retroreflector array

Fig.3 and Fig.4 are computed atmospheric tip-tilt components using the absolute difference algorithm from the near Apollo15 array.

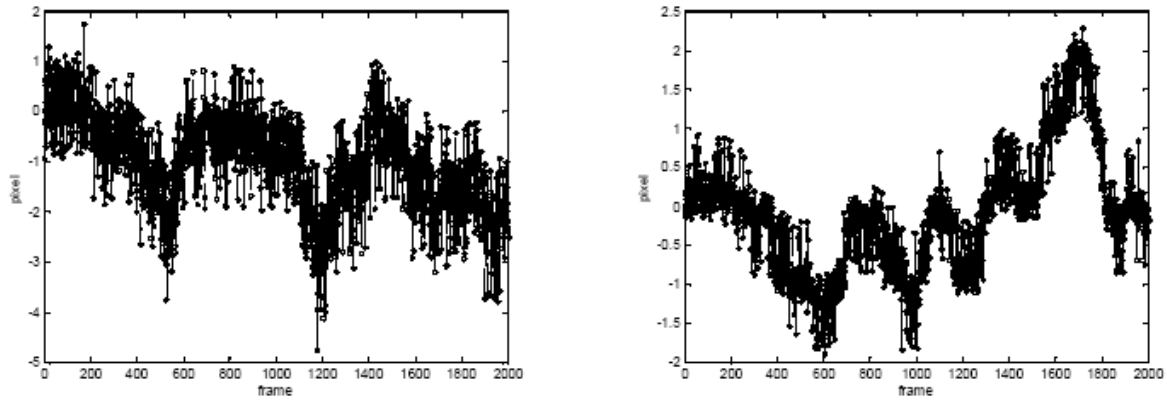

Fig.3 x and y component of tip-tilt with 16x16 pixels for Apollo15

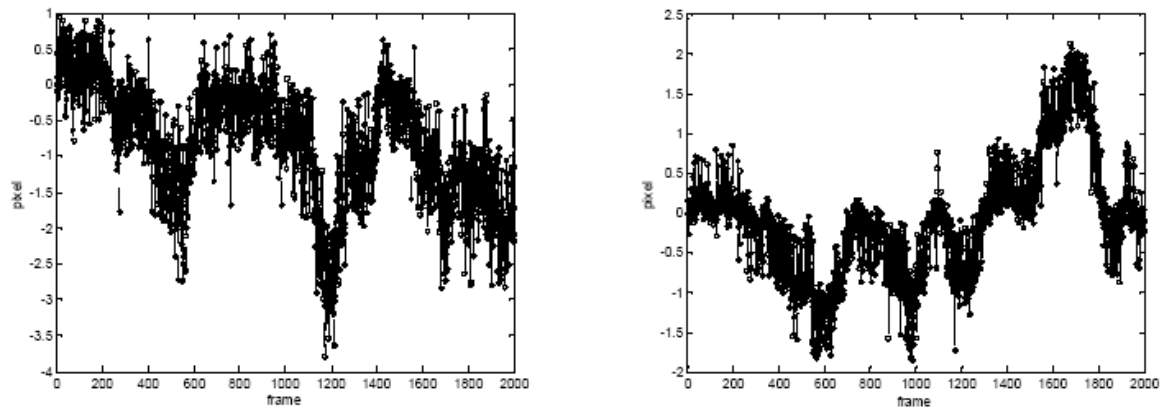

Fig.4 x and y component of tip-tilt with 32x32 pixels for Apollo15

For above proposal, the real-time property is a key factor for using. We also get following results:

When using a 32x32 pixel window to compute, it takes 25 seconds to compute 2000 images, i.e. 12.5 ms/one image.
When using a 16x16 pixel window to compute, it takes 6 seconds to compute 2000 images, i.e. 3ms/one image, within atmospheric turbulence time scale.

Technical Plan of Compensation tip-tilt on the LLR

For the LLR, using a wavefront sensor and the absolute difference algorithm, the wavefront tiptilt signal can be detected from the moon surface. That is to calculate the absolute difference values between a live image and a reference image those are taken from a same small area near the moon retroreflector in time sequence. Next is to separate and compute the atmospheric tiptilt from these values, then using them to drive a fast tiptilt mirror realtime (~ms) to compensate atmospheric tiptilt for the laser beam that will be emitted soon on the LLR.

For Kunming 1.2m laser ranging system, a tiptilt detection part and a tiptilt mirror have been built along optical path. It will perform the realtime tip-tilt compensation for the uplink and the downlink laser beam on the LLR.

Fig.5 is its optical layout for this technical plan.

When the system performs the LLR, according to the ephemeris of the moon retroreflector array, the retroreflector will be tracked by the telescope. Before starting a laser beam, the tip-tilt sensor is used to detect a series of images of the interested area near the moon retroreflector within the isoplanatic angle. M4 is a dichroic mirror that reflects laser wavelength and passes other lights. When the tiptilt signal is separated, it will be used to drive the tiptilt mirror to perform a realtime tiptilt compensation for a pulse laser beam that is emitted simultaneously.

The goal is to let the Gaussian laser beam hit the moon retroreflector accurately and centrally and let more laser photons return from it. It will compensate part of atmospheric turbulence effects on laser beam propagation, that is the brackets factor in formula (1). For about two second flying time, just before this pulse laser photon will be returned to the telescope, above process can be repeated. That will let the returned laser photons enter the receiver totally. There are other key techniques for a ground LLR station: the pointing accuracy of the telescope (±1″), the divergence of 1″ for the uplink laser beam, and the compensation of the returned laser aberration[4].

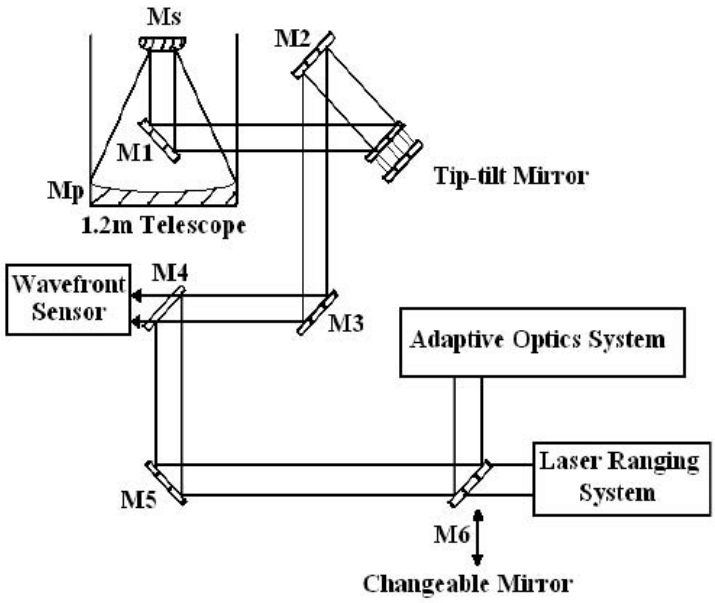

Fig.5. Optical scheme of Kunming 1.2m LR system for tiptilt correction

Acknowledgments

Special thanks are to McDonald LLR group for offering ephemeris of lunar retroreflector array, and to the Chinese HiTech project for support to establish the tiptilt detection part and the tiptilt mirror at Kunming station 1.2m telescope.

References

[1] Y.H. Xiong, H.S. Feng, "*Modification of Laser Ranging Equation*" Proc. of 13th International Workshop on Laser Ranging, 2002

[2] H.S. Feng, Y.H. Xiong, "*Compensation of Laser Beam Propagation for the LLR*" Proc. of 10th International Workshop on Laser Ranging Instrumentation pp. 196199, 1996.

[3] R Q. Fugate, "*Laser Beacon Adaptive Optics – Boom or Bust?*" Current Trends in Optics. Academic Press, Chapt. 21, pp. 289-304, 1994.

[4] Y.H. Xiong, H.S. Feng, "*Status and Possible Improvement of Lunar Laser Ranging*" Publication of the Yunnan Observatory, pp. 117-122, No.3, 2002

EFFECTS OF THE ATMOSPHERE ON THE SLR PRECISION

Jana Mulacova (1), Karel Hamal (1), Georg Kirchner (2), Franz Koidl (2)
(1) Czech Technical University in Prague. Brehova str. 7, 115 19 Prague 1, Czech Republic
prochazk@mbox.cesnet.cz phone +420 723 920 786, fax +420 224 922 822
(2) Satellite Laser Station Graz Lustbuehel, Graz, Austria

Abstract

The influence of the atmosphere has been examined at the Graz SLR station using several targets: 6 km ground, retro on balloon and others. The precision of 6km ranging is 6 psec rms. The experimental results are compared with the Greenwood-Tarzano atmospheric fluctuations spectral model.

INTRODUCTION

- **Goals**:
  - precise measurement of range by using a laser beam and a retro-reflector
  - prediction of the influence of atmospheric effects on the precision of the measurement
  - using an atmospheric model for correction of the measurement results
- **My task**:
  - study of known atmospheric effects and theoretical back-ground of laser ranging
  - writing a computer model of the atmosphere and checking its results experimentally

GARDNER GREENWOOD-TARAZANO MODEL

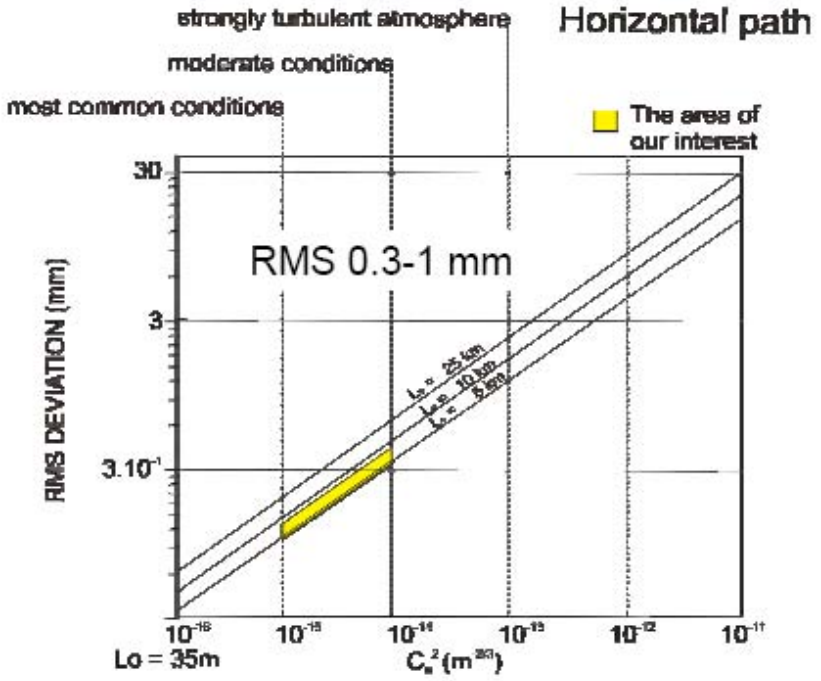

GARDNER GREENWOOD-TARAZANO MODEL

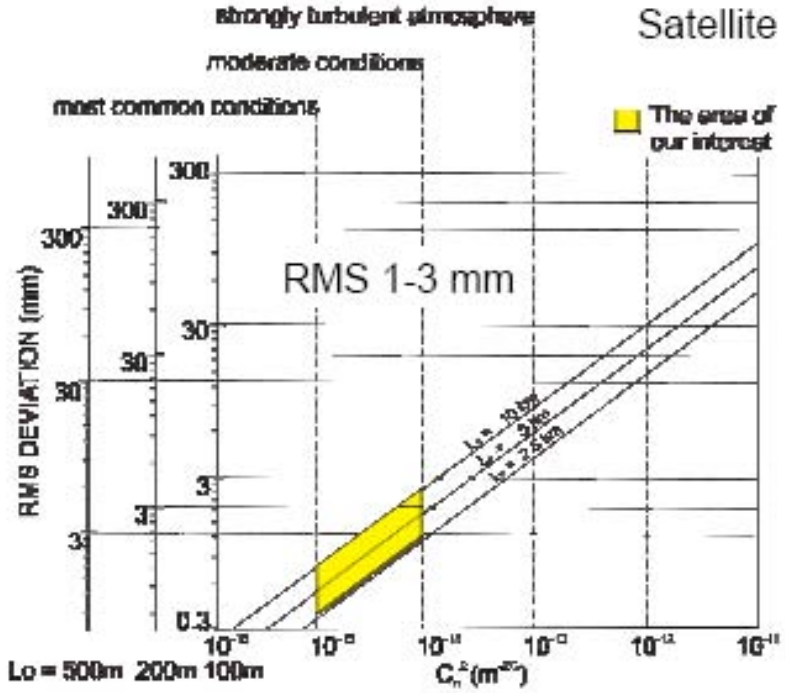

CLEAR AIR TURBULENCE
Prague Indoor Tests, June 2004

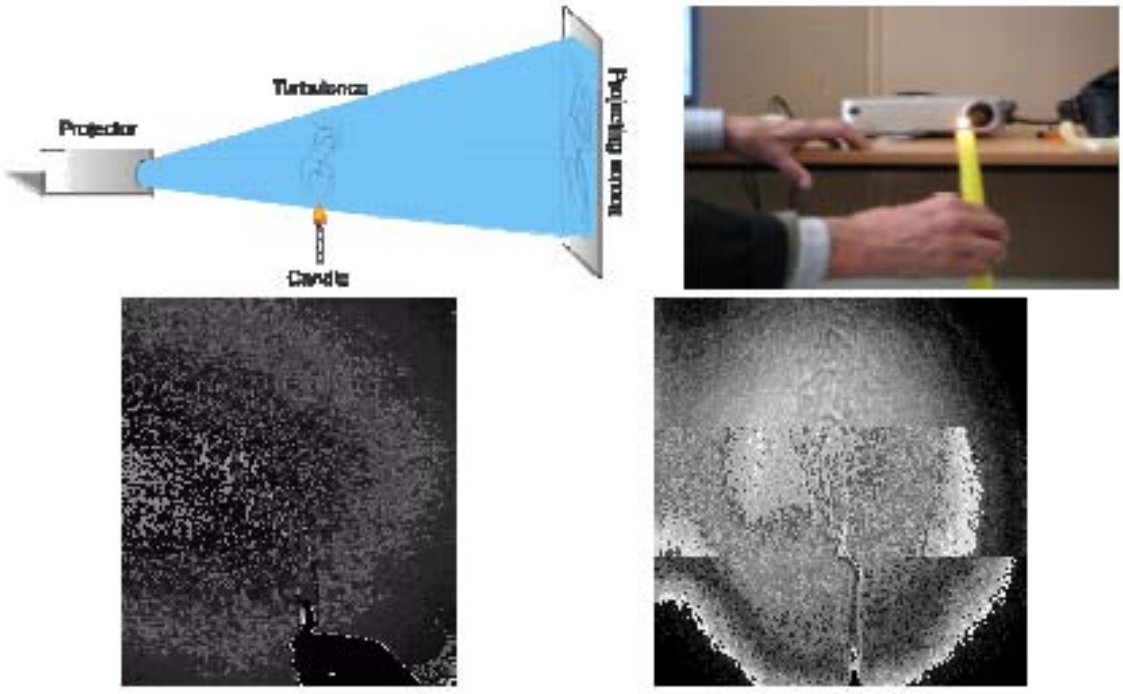

RETROREFLECTOR

- Spherical retro
- cross-section ~ 10^4-10^5 m^2

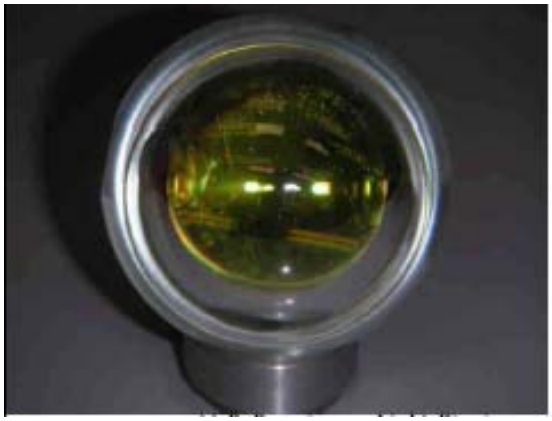

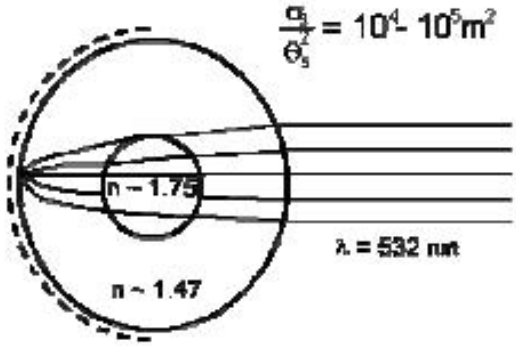

V. B. Burmistrov, N. N. Pharkomenko, V. D. Shargorodsky, V. P. Vasiljev

INTRODUCTION TO THE EXPERIMENTS

measured on the Graz observatory, using all the retros

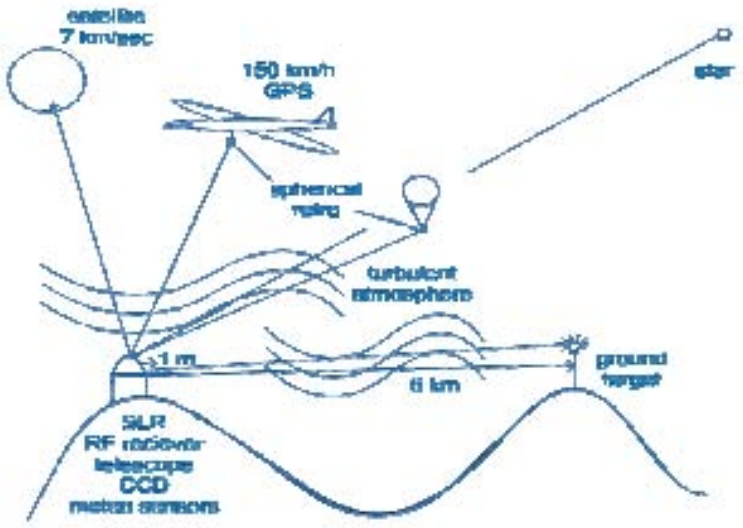

6 KM TARGET RESULTS
GRAZ, 30. 9. – 2. 10. 2003

for the horizontal path the RMS was predicted and measured 1 mm (6.6 picoseconds)

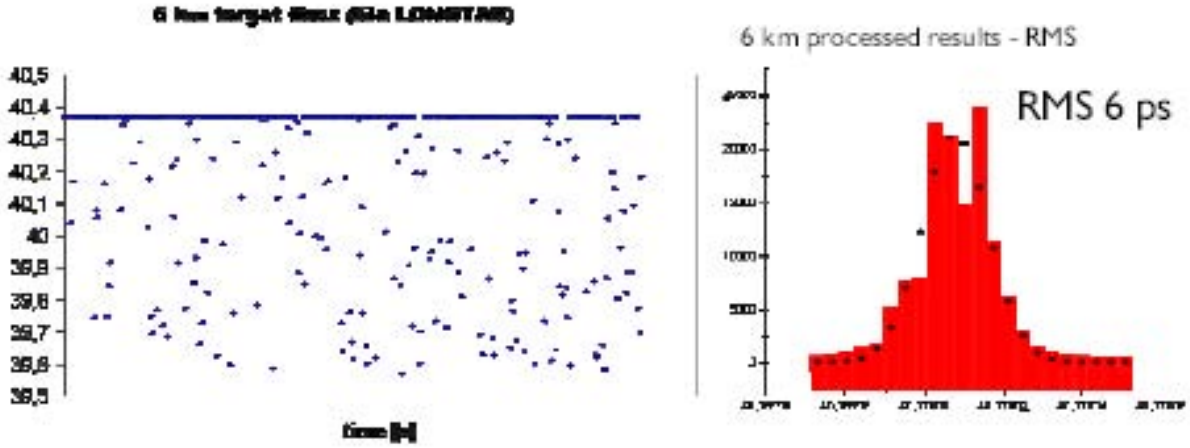

MOTOGLIDER 1
GRAZ, 30. 9. – 2. 10. 2003

- to check the theoretical prediction of RMS for non-horizontal path also not to space
- first attempt:a corner retro on the wing of a motoglider

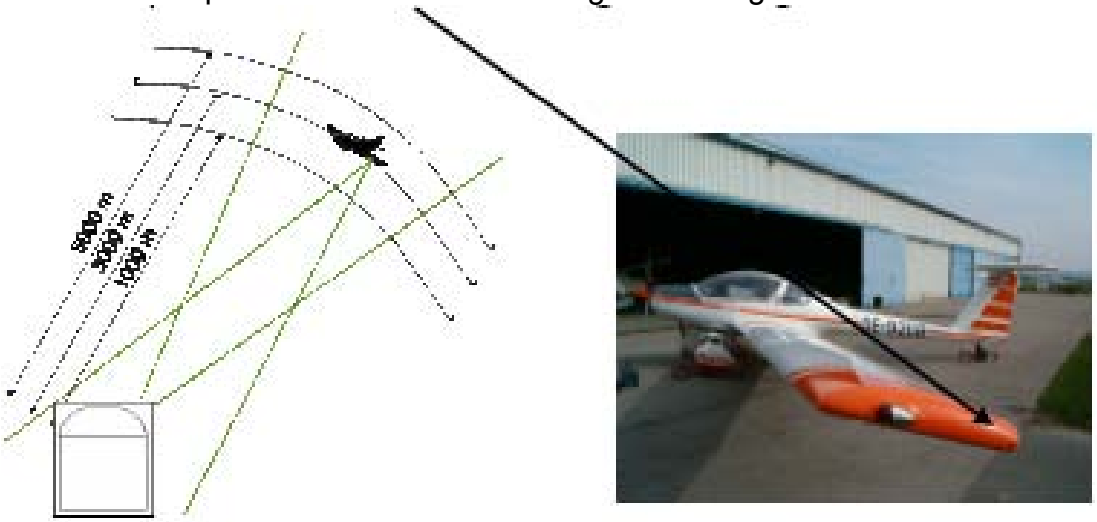

BALLOONS CARRYING "SHINY BALL"
GRAZ, 25. 10. -27. 10. 2003

- the next experiment was based on the same purpose - to check the predicted value of pathlength deviation on the slant path to closer target experimentally
- the balloons were bound on thread, equipped also by a searchlight for easier targeting
- the whole set was light and cheap, which allowed us to launch more of them
- the shiny ball = silver coated sphere for Christmas trees
- range 0 – 300 m

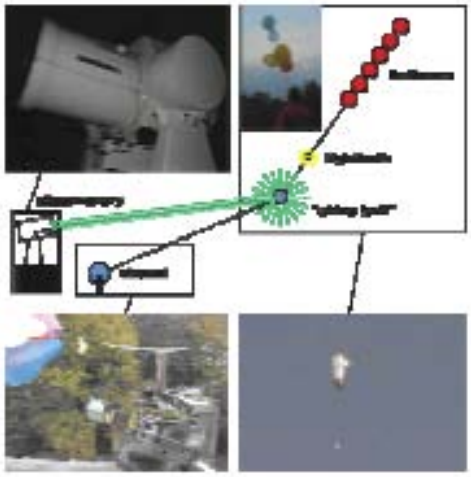

MOTOGLIDER 2
RESULTS

- Reflections from the sphere, corner cube and even the body of the glider were recognized
- Depicted the reflection from the corner cube retro result

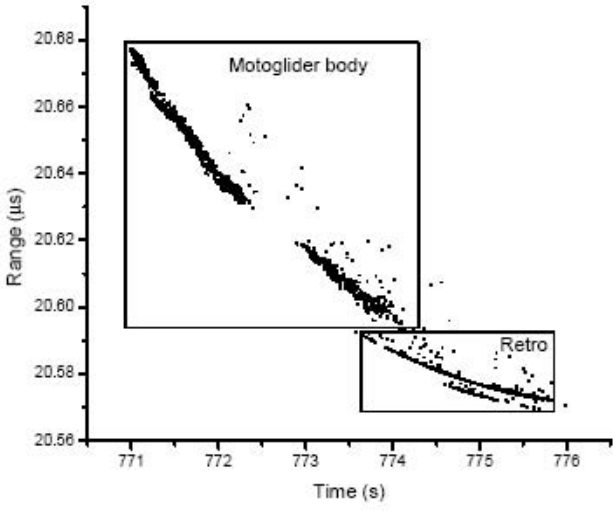

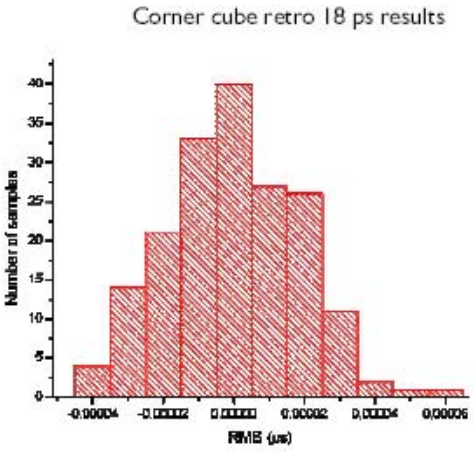

CONCLUSION

- Long term Graz and perhaps the other millimeter ranging stations show a discrepancy between the ground target RMS 1 mm and SLR 3 mm.
- Clear Air Turbulence CAT modeled by Gardner and Greenwoon-Tarazano might explain contribution to the overall SLR RMS.
- Our experiments (2 kHz laser) using several retros: “Shiny ball” equipped balloons, the Roof Prism and Spherical Retro equipped motorglider, show 2-4 mm RMS consistent with the Gardner and T-G model.
- 6 km – 4 km horizontal path shows routinely 1 mm RMS consistent with the Gardner and G-T model close to the machine RMS.
- Due to the signal strength RMS dependence more info might be expected from the Signal Strength Monitor build in Pico Event Timer 2k.

ATMOSPHERIC CONTRIBUTION TO THE LASER RANGING JITTER

Lukas Kral (1), Karel Hamal (1), Georg Kirchner (2), Franz Koidl (2)
(1) Czech Technical University in Prague. Brehova str. 7, 115 19 Prague 1, Czech Republic
prochazk@mbox.cesnet.cz phone +420 723 920 786, fax +420 224 922 822
(2) Satellite Laser Station Graz Lustbuehel, Graz, Austria

Abstract

We are reporting on the theory and experiments related to theatmospheric fluctuations and their contribution to the laser ranging jitter. The millimeter precision ground target laser ranging at the 2 kHz repetition rate enabled us to reveal the short period atmospheric fluctuations contribution to the laser ranging error budget. The amplitude and the time spectrum have been investigated for the first time on the picosecond resolution level. The relation of this effect to the seeing conditions has been investigated.

GOALS

- Investigate contribution of rapid atmospheric fluctuations (turbulence) to the laser ranging error budget
- Correlate the measured turbulence contribution with instantaneous atmospheric conditions (seeing)
- Investigate the time spectrum of the observed fluctuations
- Prove the existing theory by the first direct experiment

PHILOSOPHY

- Enjoy the high repetition rate, millimeter precision laser ranging station Graz, Austria
- Determine the turbulence contribution to the overall ranging jitter by numerical analysis of the raw ranging data
- Parallel measurement of astronomical seeing to determine the turbulence strength along the beam path
- Compare the results to theoretical predictions - correlation

THEORETICAL BACKGROUND

- Turbulent mixing of air of different temperatures à random fluctuation of refractive index along the beam path à random changes of the measured range
- Gardner (1976) derived analytical formula for prediction of the turbulence-induced ranging jitter:

$$RMS = 5.1\, L_0^{5/6} \sqrt{\int_0^L C_n^2(\xi)\, d\xi}$$

(Greenwood-Tarazano spectral model used)

L_o ..... outer scale of turbulence
$C_n^2(\xi)$ ... turbulence strength along the beam path
L ..... target distance

GARDNER, C. S. *Effects of random path fluctuations on the accuracy of laser ranging systems*. Applied Optics, 1976, vol. 15, no. 10, p. 2539–2545.

OBTAINING THE MODEL'S PARAMETER

- L_o ..... size of the largest turbulent eddies
  - horizontal path: *L*0 is between *h*/2 and *h*, where *h* is the beam height above the surface*
  - Ø slant path to space: *L*0 generally unknown, existing estimates from 5 up to 300 meters, varies with height
- C_n^2..... turbulence strengt
  - its integral along the beam path can be determined from the seeing measurement on the same path

**Handbook of Optics*, McGraw-Hill, 1992. Vol. 1, Chapter 44, Atmospheric Optics.

LASER RANGING EXPERIMENT SETUP I

- Satellite laser station Graz, altitude 500 m above sea
- Laser 2 kHz @ 532 nm, 8 ps
- Detector: C-SPAD, ET timing, precision 1 mm RMS

The laser telescope in Graz

Mask for ground target ranging

LASER RANGING EXPERIMENT SETUP II

- Targets:
  - ground-based retroreflector installed 4.3 km from the observatory; average beam height ~ 50 m above ground
  - satellites with low signature and high return energy (ERS-2, Envisat, pass segments selected)

4.3 km distant retroreflector illuminated by the laser

GROUND TARGET RANGING

GRAZ, 2004-05-10, 09:30 UTC, 1.2 KHZ RETURN RATE

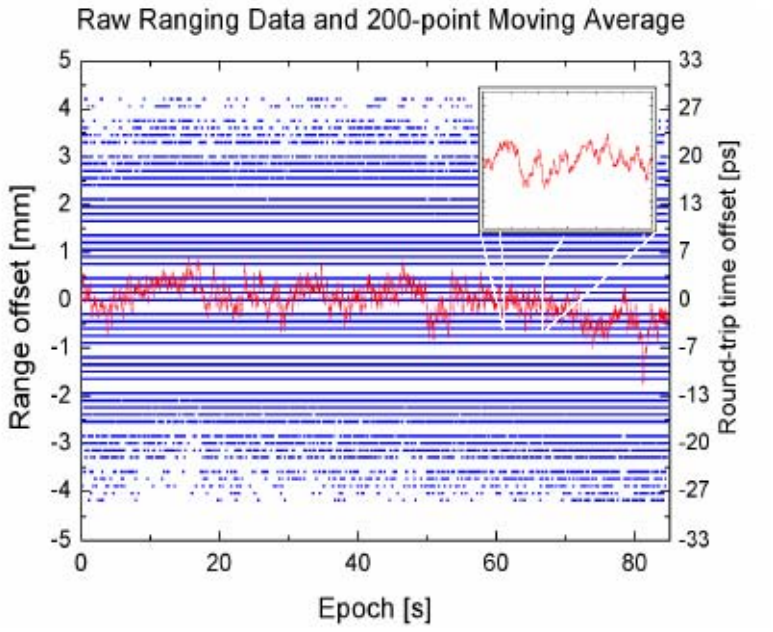

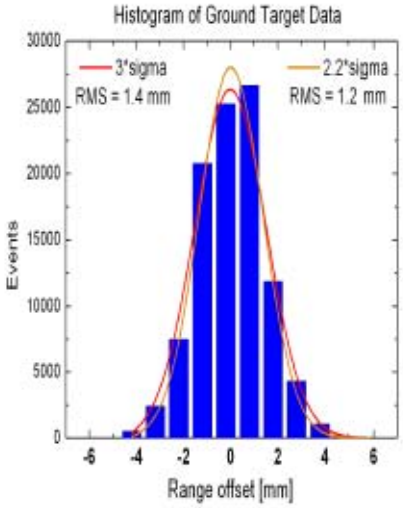

GROUND TARGET RANGING

GRAZ, 2004-05-10, 09:30 UTC, 1.2 KHZ RETURN RATE

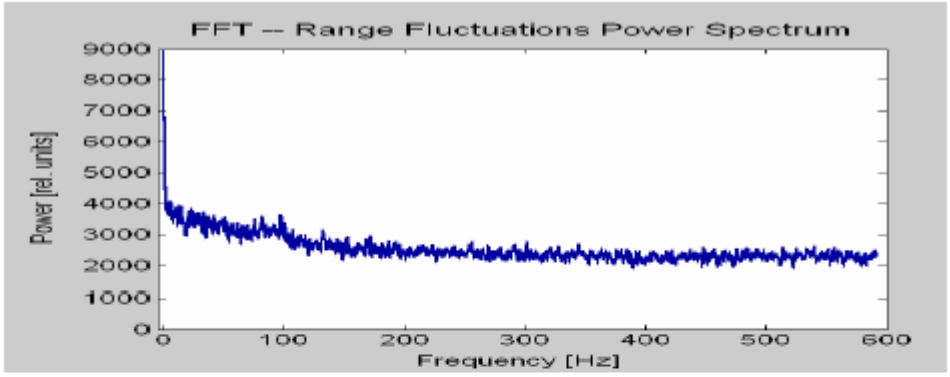

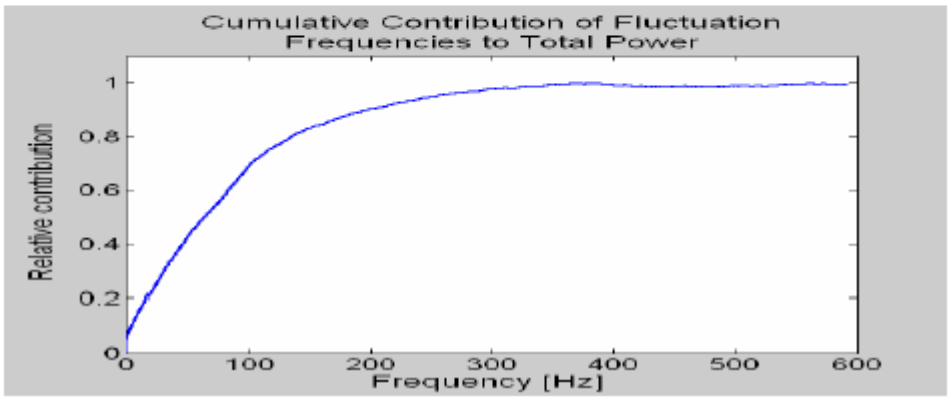

GROUND TARGET RANGING - RESULTS

GRAZ, 2004-05-10, 09:30 UTC, 1.2 KHZ RETURN RATE

Results of numerical analysis:
Overall jitter
1.4 mm RMS
=
Instrumental noise + **Turbulence-induced jitter**
1.2 mm RMS **0.6 mm RMS**

Extraction of turbulence contribution from the raw data:

- Much higher sampling rate (>1 kHz) than maximum frequencies of turbulent fluctuations (<200 Hz)
- Instrumental noise is random shot-to-shot ***/*** *turbulent fluctuations are correlated within several shots ("waves")*
  ➔ moving averaging

SEEING MEASUREMENT

- DIMM (Differential Image Motion Monitor)
  - standard astronomical site-testing technique
- Statistics of mutual movement of 2 images of a distant source
- Short exposure times 5 ms
- Hartmann mask + slightly defocused telescope (MEADE 16'')
- Targets 1) 2.8 km distant red bulb (day + night)
  2) bright star (night only)

Bulb, FOV 2 arcmin,
1 arcsec/pixel,
seeing 4.6 arcsec

SEEING MEASUREMENT - RESULTS

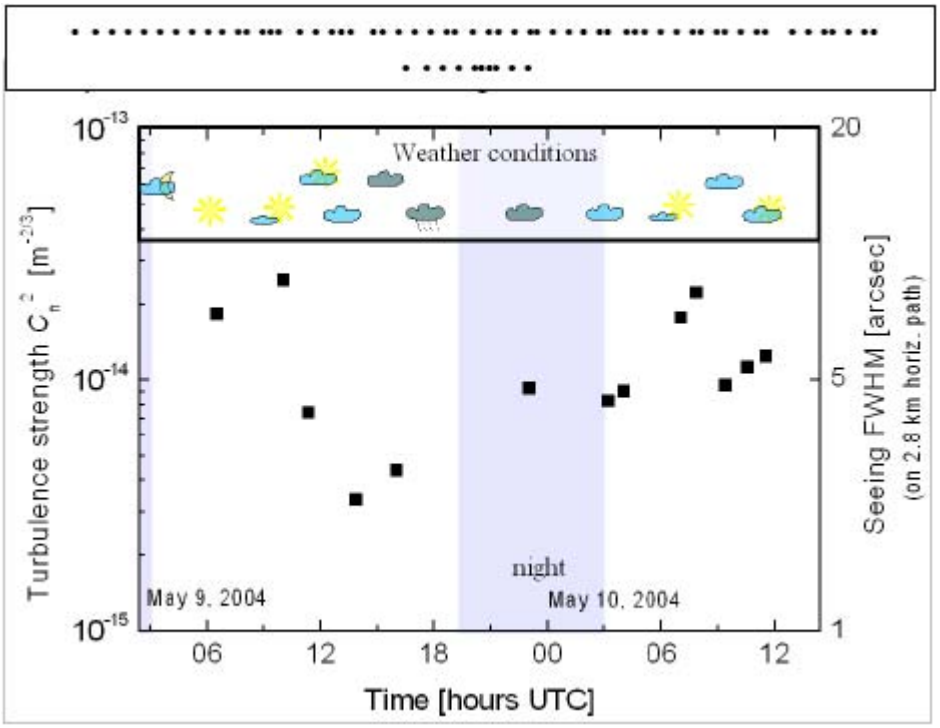

COMPARISON OF THEORY AND EXPERIMENT HORIZONTAL PATH

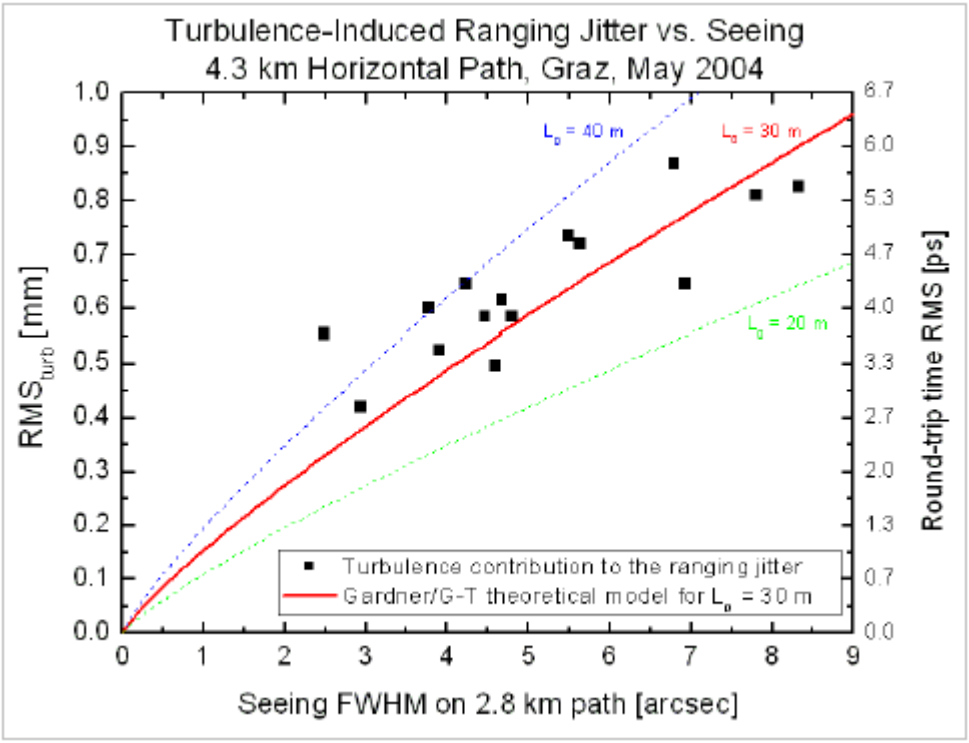

SATELLITE LASER RANGING RESULTS

- Typical seeing measured on a star: 2 arcsec → Gardner's theory ~ 0.3 mm RMS for $L0$ = 100 m
- Measurement → turbulence contribution 2 arcsec seeing ~ 0.3 mm RMS (good agreement)
- The major observed range fluctuations are completely random shot-to-shot → not caused by turbulence

CONCLUSION

- Atmospheric turbulence contribution to the laser ranging jitter has been proved and directly measured
- Observed contribution: RMS 0.4–0.9 mm 4.3 km horiz. Path ~ 0.3 mm for satellites
- Maximum frequencies of atmospheric fluctuations: ~200 Hz
- Correlation between atmospheric conditions and turbulenceinduced ranging jitter was found (good agreement with Gardner)
- Further measurements under various atmospheric conditions are planned to improve the statistics

MULTIWAVELENGTH REFRACTION MODELING IMPROVEMENTS FOR SLR OBSERVATIONS

G. Hulley(1), E. C. Pavlis(1), V. B. Mendes(2), D. E. Pavlis(3)
(1) Joint Center for Earth Systems Technology (JCET), UMBC, Baltimore, MD, USA; ghulley1@umbc.edu /Fax:+1 410 455 5868
(2) Faculdade de Ciencias da Universidade de Lisboa , Portugal
(3) SGT Inc. and NASA Goddard, Greenbelt, MD, USA

Abstract

Atmospheric refraction is an important accuracy-limiting factor in the use of satellite laser ranging (SLR) for high-accuracy science applications. In most of these applications, and particularly for the establishment and monitoring of the TRF, of great interest is the stability of its scale and its implied height system. The modeling of atmospheric refraction in the analysis of SLR data comprises the determination of the delay in the zenith direction and subsequent projection to a given elevation angle, using a mapping function. Standard data analyses practices use the 1973 Marini-Murray model for both zenith delay determination and mapping. This model was tailored for a particular wavelength and is not suitable for all the wavelengths used in modern SLR systems. Improved refraction modeling is essential in reducing errors in SLR measurements that study variations in the Earth's gravity field and crustal motion (especially for the vertical component), as well as monitoring sea-level rise, post-glacial rebound and other geophysical phenomena. Current models of atmospheric delay only take into account the elevation angle of the transmitted ray and assume a spherically symmetric atmosphere. In order to improve models of atmospheric delay, azimuthal asymmetries (gradients) in the atmospheric refractive index still need to be modeled and researched. In the past, VLBI and GPS groups used NCEP fields to estimate gradients in the atmosphere and to improve their analysis products. We are now entering a new era where global snapshots can be available from satellite-borne instruments on a daily basis. We will be using atmospheric profiles from an instrument aboard the AQUA satellite called the Atmospheric InfraRed Sounder (AIRS) in order to compute the gradients in the North-South and East-West directions as well as the atmospheric delay resulting from these gradients. Comparisons will be made between the delay calculated using a direct AIRS ray-tracing method, and the best available model [Mendes and Pavlis, 2004]. A new method to calculate the delay, called Two-Color laser ranging will be compared to the Marini-Murray model with data taken from the Matera SLR station in 2003.

New and Improved Zenith Delay Model

For reasons explained in detail in [Mendes and Pavlis, 2004], the standard atmospheric correction model in SLR, the Marini-Murray model of 1973, was deemed inadequate to meet the current and upcoming challenges facing space geodesy, and the SLR community in particular. This deficiency motivated the development of two new components that together contribute in the precise modeling of the atmospheric delay in SLR: a new mapping function [Mendes at al., 2002] and a new zenith delay model [Mendes and Pavlis, 2004]. The two together assure a uniformly precise performance from elevations as low as 3° and for all wavelengths used in SLR, from 355 nm to 1064 nm (Figure 1). The two formulations were developed on the basis of radiosonde data and had so far been also validated with radisonde data (independent from those used in their development), and a limited analysis of SLR data to the two LAGEOS'. With the availability of real and global observations of the atmosphere

from AIRS, we have the option and ability to further and more independently validate these models with the new data.

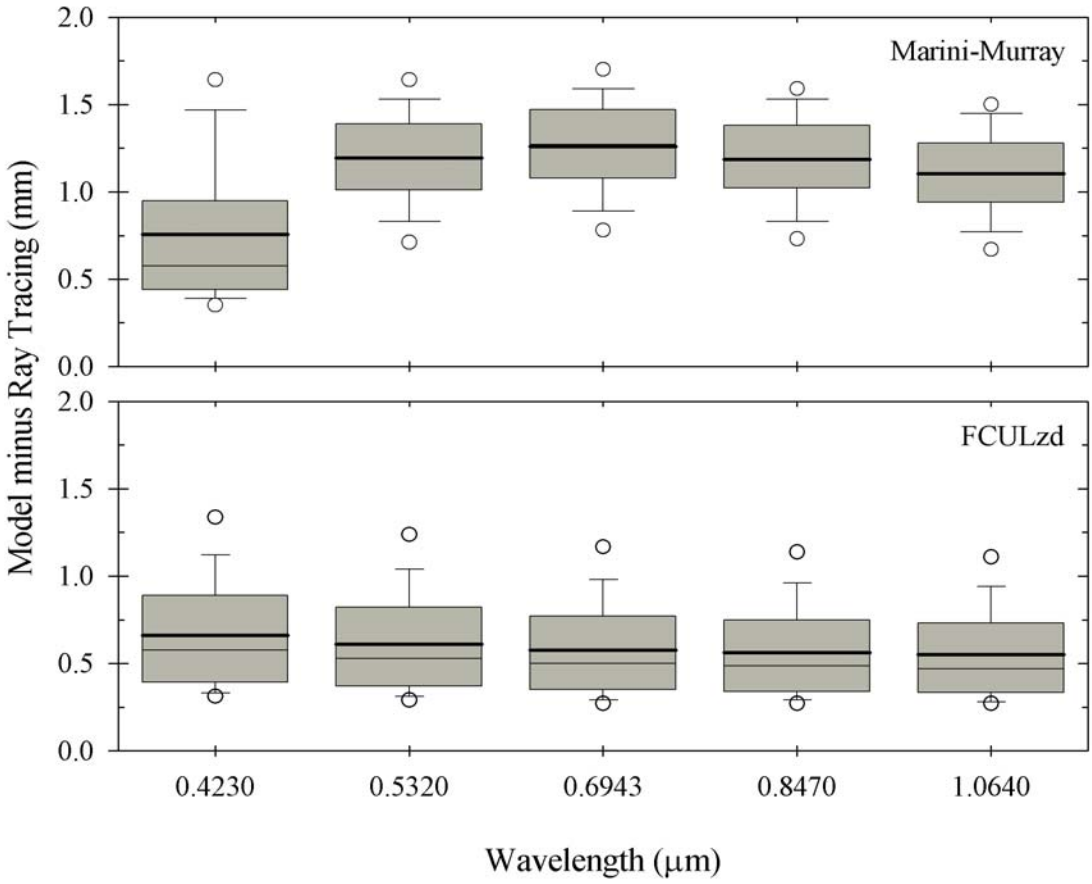

Figure 1. Box-and-whisker plots for the Mendes-Pavlis and Marini-Murray zenith delay models using radiosonde data as groundtruth, [Mendes and Pavlis, 2004].

This effort is part of the broader investigation into the possibility of using AIRS data (along with possibly other global data sets), for the computation of the atmospheric delay through either direct ray-tracing or from the new models amended with corrections for the effect of horizontal gradients. In our efforts to develop the alternative approaches, we follow closely the formulae that were used in the derivation of the new models, so that on one hand we can benefit from these, and stay within the bounds of the currently approved standards on the other.

AIRS data

We will be using meteorological data sets from NASA's Atmospheric Infrared Sounder (AIRS) in order to improve and develop new models that compute variations in horizontal refractive indices. The AIRS Level-2 data gives profiles of temperature, pressure, water-vapor mixing ratio and saturation water-vapor mixing ratio up to 28 standard pressure levels. The pressure levels extend from 1100 mb up to 0.1 mb. The AIRS data is retrieved in the

form of a "granule". One granule contains 6 minutes of data and is approximately 1600 (E-W) x 2300 (N-S) km in spatial extent with a 50 km resolution within the granule. One day of data yields 240 granules. We will be using granules corresponding to the locations of SLR tracking station sites around the globe.

AIRS Ray-Tracing (ART)

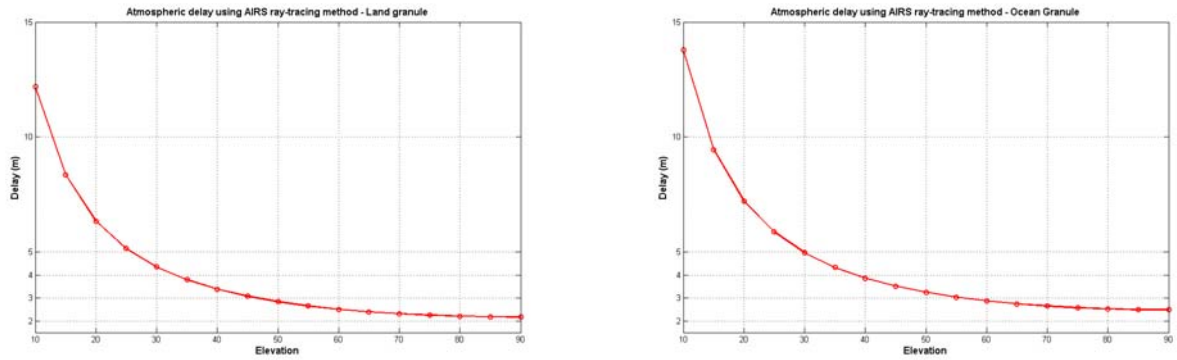

(a) **(b)**

Figure 2. Total atmospheric delay calculated using AIRS ray-tracing **(a)** over a land and **(b)** over an ocean granule.

We have developed an algorithm, that when given the initial position of the station within the granule as well as the azimuth and elevation of the pulse's path, it will pick out the refractivity gradient values (for horizontal gradient delay) or the total refractivity (for total atmospheric delay) values at each level along the ray path until the ray exits the granule. In this way the delay can be evaluated directly by integrating all the values through which the ray traverses. This method eliminates the need for a mapping function that could introduce errors at low elevation angles. We will be using a new formulation for the group refractivity based on formulas by Ciddor [1996].

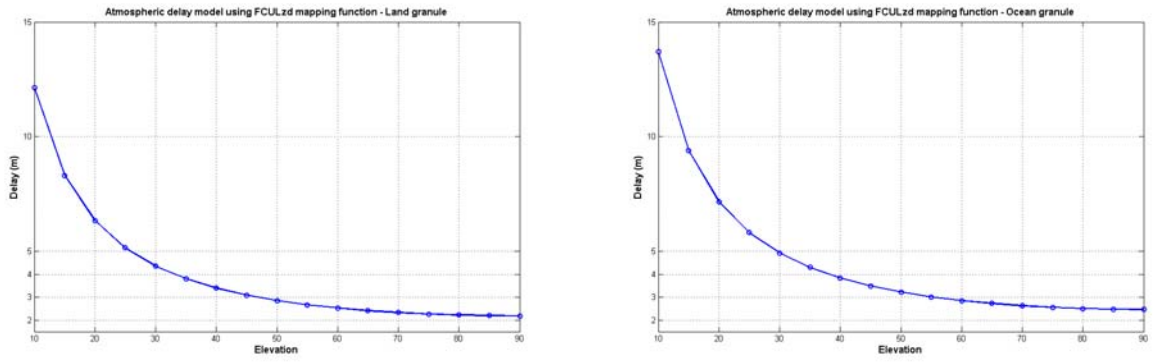

(a) **(b)**

Figure 3. Total atmospheric delay calculated using the Mendes-Pavlis model, **(a)** over a land and **(b)** over an ocean granule.

The new formulation includes both hydrostatic and non-hydrostatic components of the group refractivity. In order to perform the ray tracing, we will be using a 20° x 20° latitude/longitude grid up to 0.1 mb in order to build 3-D atmospheric profiles around each of the core SLR tracking stations. Figure 2 shows the total atmospheric delay over a land granule calculated by ray-tracing through AIRS data to the top of the atmosphere. Figure 3 shows the corresponding delay calculated using the newest model, [Mendes and Pavlis, 2004]. A comparison of the two pairs of figures indicates the very good agreement between the analytical model and the results from ray-tracing.

Azimuthal Asymmetries

Including the atmospheric delay due to azimuthal asymmetries in the total atmospheric delay is essential in minimizing errors in SLR measurements. This is important since a ray propagating through the atmosphere at one azimuth angle should realistically experience a different atmospheric delay traveling through a different azimuth angle given the fact that atmospheric circulation is prominent at all scales. It has been found that azimuthal asymmetries (gradients) in the atmosphere averaged out over one day can cause delays as large as 50 mm at an elevation of 10° [MacMillan et al., 1997]. A gradient produced with this magnitude is not unusual but probably would not stay constant for a full 24 hours at a particular site, due to a front moving in for instance. Chen and Herring [1997] have developed a parametric form for the gradient delay that can be used to analyze space geodetic data. The gradient coefficients in the N-S and E-W directions, equations (1) and (2), are calculated by integrating the refractivity gradients from the surface to the top of the atmosphere (TOA). The total delay (3) is then calculated by multiplying the coefficients by a mapping function (4) that models the elevation dependency of the delay.

$$L_{NS} = 10^{-6} \int_0^H \nabla N_{NS} \cdot h \cdot dh \qquad (1)$$

$$L_{EW} = 10^{-6} \int_0^H \nabla N_{EW} \cdot h \cdot dh \qquad (2)$$

$$L_{az} = L_{NS} \cdot m_{az}(\varepsilon) \cdot \cos(\varphi) + L_{EW} \cdot m_{az}(\varepsilon) \cdot \sin(\varphi) \qquad (3)$$

$$m_{az}(\varepsilon) = \frac{1}{\sin(\varepsilon) \cdot \tan(\varepsilon) + 0.0032} \qquad (4)$$

Figure 4 shows gradient profiles of the ray path through different azimuth angles. As expected the refractivity gradients are greatest nearer the Earth's surface, where fluctuations in temperature, humidity and density are stronger and have a larger effect. However above the tropopause (~11 km), where the atmosphere is stably stratified, the gradients diminish rapidly towards zero. The four vertical profiles of the N-S and E-W gradients were computed from AIRS data at four different azimuths and an elevation angle of 80°. We observe that there is a general agreement in the behavior of the gradients independent of the azimuth. We also note that the N-S gradient is far larger in magnitude compared to the E-W for the first 1-2 km of height. Above that height, both gradients are of comparable magnitude. This will probably not be the case for low elevation angles, since in that case the two rays will traverse

markedly different atmospheric strata. It is also evident, that there is no reason to include any of the strata above the tropopause.

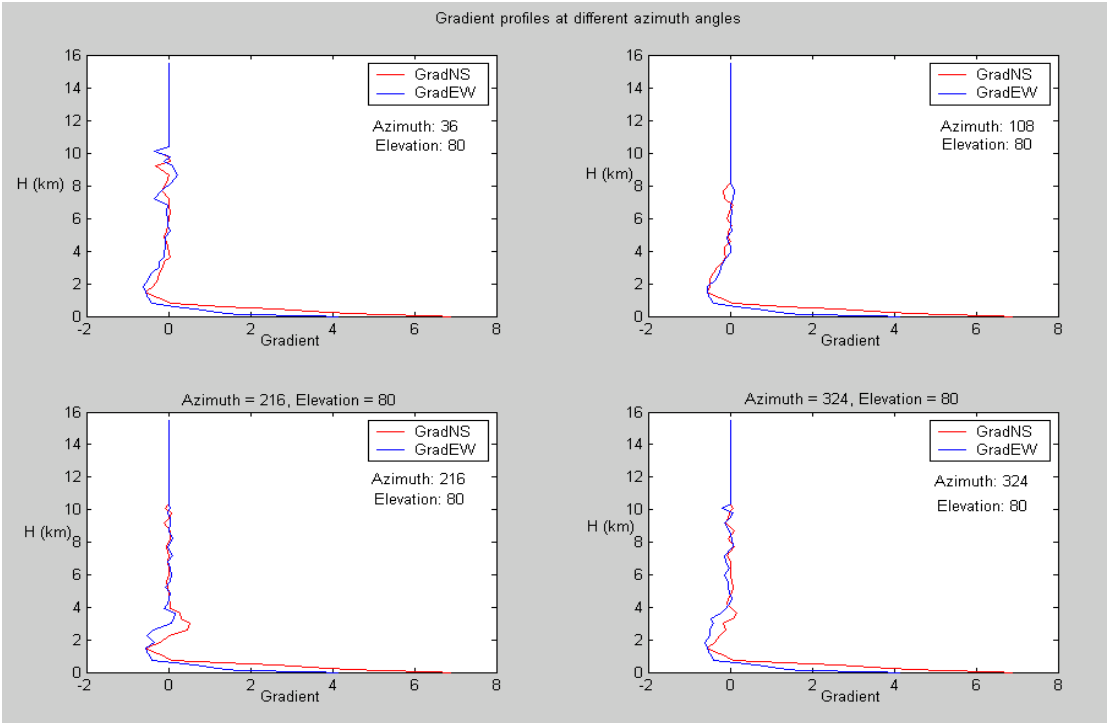

Figure 4. Gradient profiles at four different azimuths and 80° elevation.

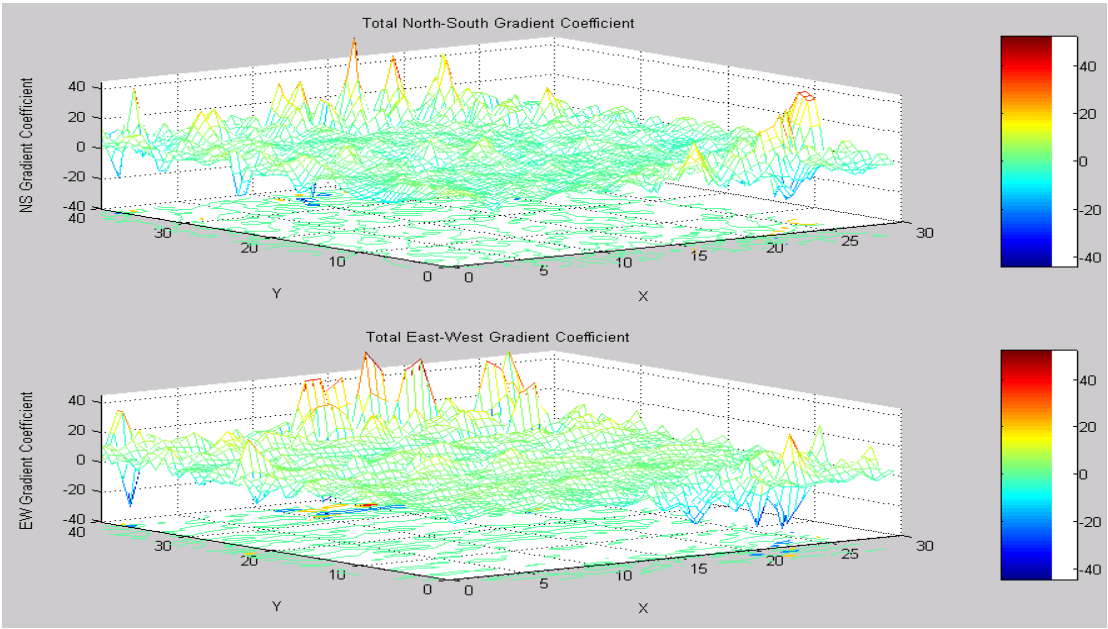

Figure 5. Total E-W and N-S gradient coefficients (eq. 1 & 2) integrated till TOA.

The total gradients for an entire AIRS granule are shown in Figure 5, integrated vertically, i.e. for a vertically propagating ray. Note the signal increase at the edges of the granule, which is not real, but a result of AIRS quality variations as we move further away from the center of the granule. This is a problem that has to be dealt with if we want to make serious use of these data, either through limiting the range of AIRS data used from each granule or by smoothing and editing the data prior to using them.

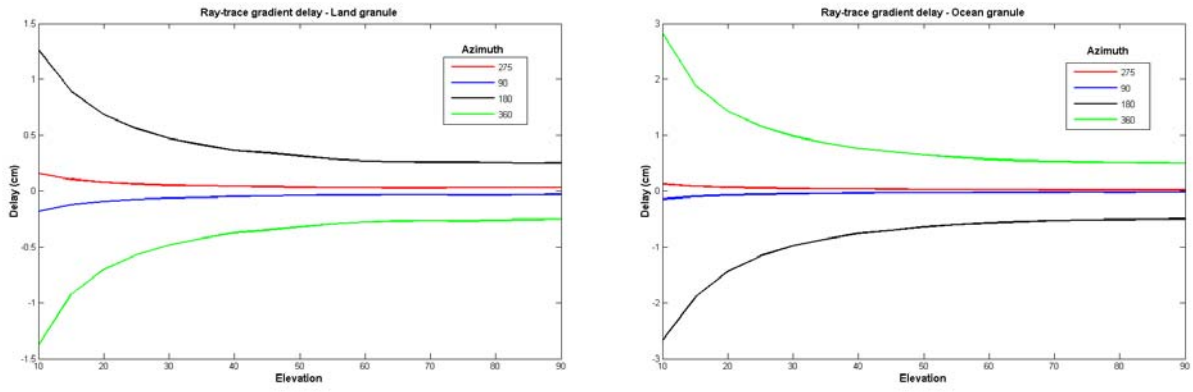

(a) **(b)**

Figure 6. Delay due to horizontal gradients **(a)** over a land granule and **(b)** over an ocean granule using the AIRS ray-tracing method (ART).

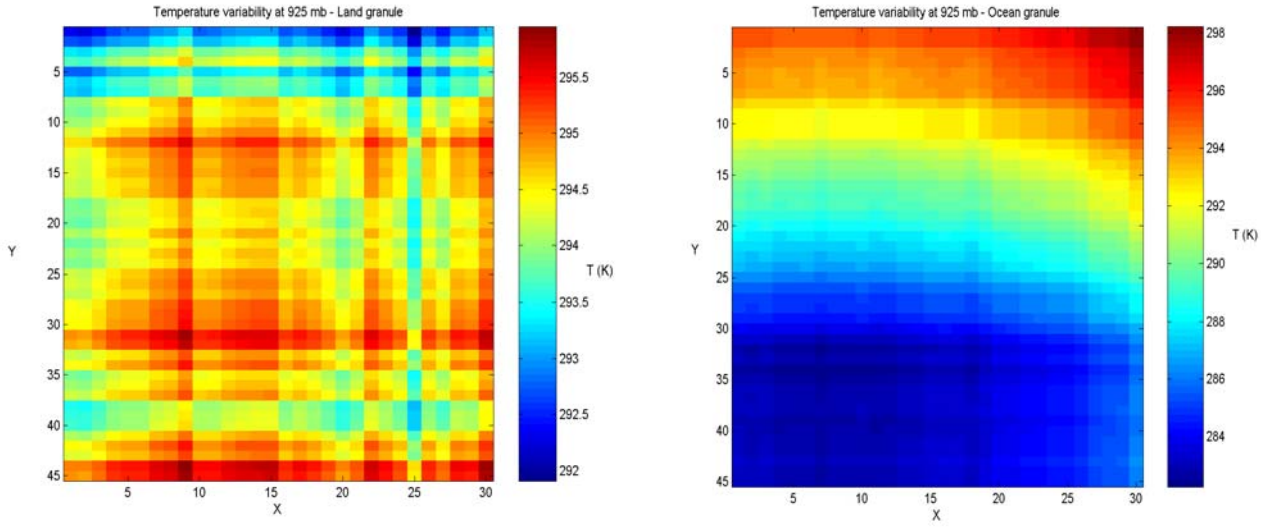

(a) **(b)**

Figure 7. Temperature variability **(a)** over a land granule and **(b)** over an ocean granule at 925 mb, Y-axis runs N-S and X-axis runs E-W.

Two-color Refraction Correction

The atmospheric delay can also be found by measuring the difference in time-of-flight for two pulses at different two colors, and multiplying the result by the speed of light, c. This approach has been advocated for sometime, and recently, a number of SLR stations have initiated two color operations. The atmospheric refraction correction is then given by [Degnan, 1993]:

$$AC = \gamma \cdot c(\tau_1 - \tau_2) \qquad (5)$$

where τ_1 and τ_2 are the measured one-way times of flight at the two wavelengths and,

$$\gamma = \frac{N_1}{N_2 - N_1} \qquad (6)$$

where N_1 and N_2 are the refractivities at the two different wavelengths.

γ can be approximated by:

$$\gamma = \frac{f(\lambda_1)}{f(\lambda_2) - f(\lambda_1)} \qquad (7)$$

where $f(\lambda_1)$ and $f(\lambda_2)$ are the laser frequency parameters at the two wavelengths.

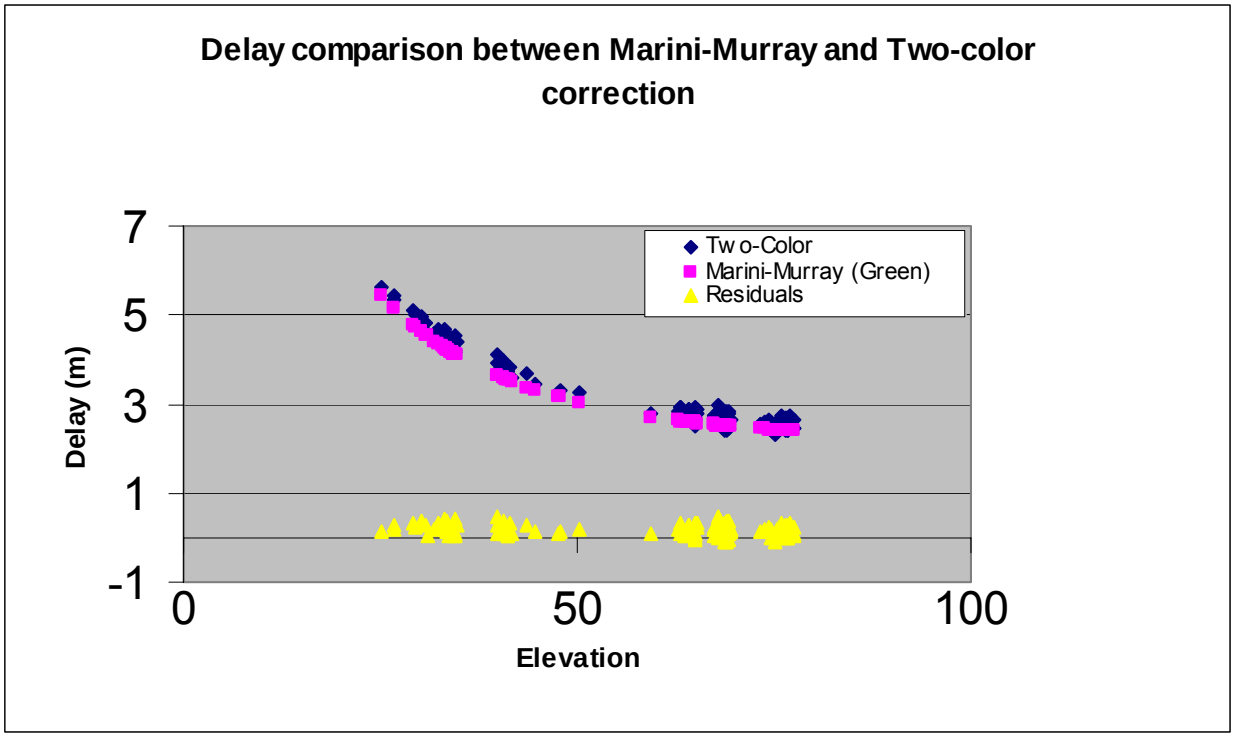

Figure 8. Data taken from Matera SLR station [2002, day-44, time-00:47]

Using this formulation, we have compared the atmospheric delay derived from two-color ranging at MLRO, Matera, Italy [V. Luceri, private communication], with the predicted delay from the Marini-Murray model and local met data. The results for two passes on different dates are shown in Figures 8 and 9. Qualitatively the corrections seem to always agree, albeit in some cases there is a significant offset bias (Fig. 9), quantitatively though, there are significant and impossible to accept differences, noticeably in the noise characteristics of the two series. Although it is natural to expect a noisier result from observations compared to an analytical model, we never expected to see the behavior indicated in the two figures. At the

moment there is no clear and definitive explanation for this, and since there are no more data available to examine, we will refrain from pursuing this analysis any further. An added complication with these data is that their preprocessing is performed by software that is not available for examination, so it is possible that errors at this step, or limitations in the precision with which the differential time delay between the two arriving pulses is recorded, are the cause of this excessive noise.

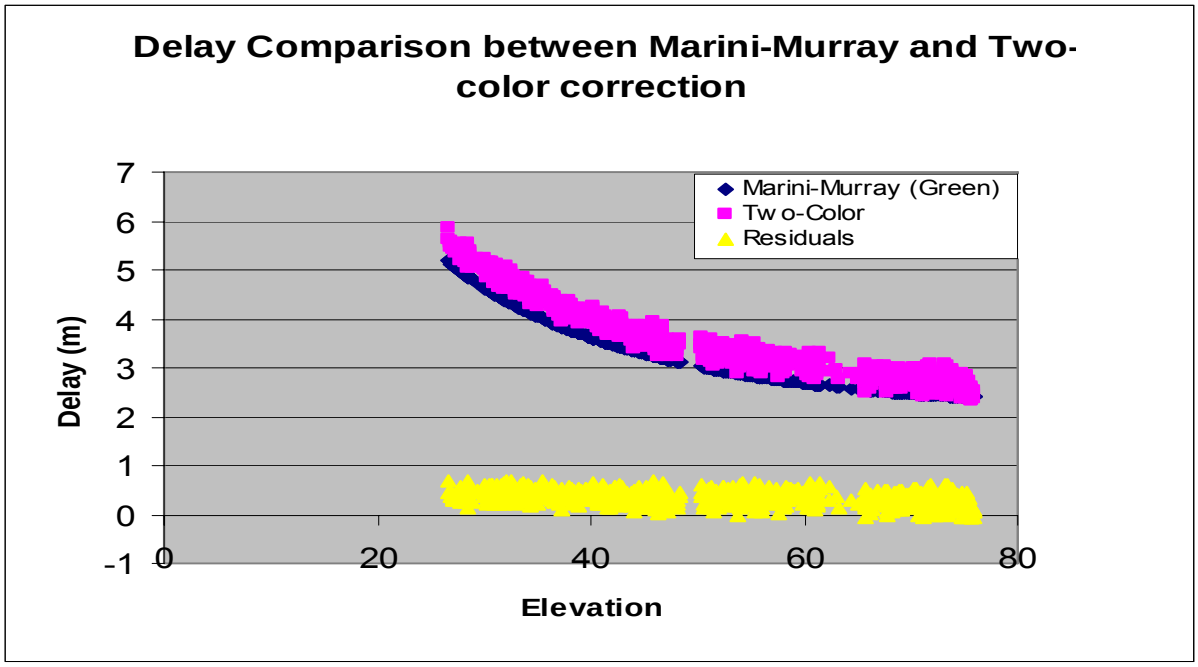

Figure 9. Data taken from Matera SLR station [2002, day-71, time-22:50]

Summary

We have presented the latest in validating the new zenith delay models and mapping functions for atmospheric delay computations in SLR, using globally available atmospheric observations from NASA's AIRS instrument. We also presented first results from the use of these fields in conjunction with analytical models and ray tracing techniques to account for horizontal gradients' effects in the propagation of optical signals. The validation tests for the new models indicate that they perform indeed within the error margins prescribed with them on the basis of radisonde tests. The use of two color ranging data has so far led to inconclusive results, mainly due to problems with the two color data or possibly with their preprocessing. The first results form our horizontal gradient modeling are encouraging and it seems that very soon, we should be able to account for these delays on the basis of either analytical models driven by surface meteorology at the sites, or globally observed fields, or a combination of the two. What is already certain is that the current science requirements dictate that the old models are inadequate and incomplete when it comes to meeting these requirements today, and certainly even more so in the near future.

References

Ciddor, P.E. "Refractive index of air: New equations for the visible and near infrared." Applied Optics, 35, (9), pp. 1566-1573, 1996.

Chen, G.E. and T.A. Herring, “Effects of atmospheric azimuthal asymmetry on the analysis of space geodetic data.”, *J. Geophys. Res.*, 102, B9, pp. 20,489-20,502, 1997.

Degnan, J. “Millimeter Accuracy Satellite Laser Ranging: A Review”, in Contributions of Space Geodesy to Geodynamics: Earth Dynamics, *Geodynamics 25*, D. E. Smith and D. L. Turcotte (eds.), pp. 133-162, American Geophysical Union, 1993.

MacMillan, D.S. and C. Ma, “Atmospheric gradients and the VLBI terrestrial and celestial reference frames”, *J. Geophys. Res.*, 24, (4), pp. 453-456, 1997.

Marini, J. W., and C. W. Murray, “Correction of laser range tracking data for atmospheric refraction at elevations above 10 degrees”, NASA Tech. Memo., NASA-TM-X-70555, 60 pp., 1973.

Mendes, V. and E. C. Pavlis "High-Accuracy Zenith Delay Prediction at Optical Wavelengths", *Geophys. Res. Lett.*, 31, L14602, doi:10.1029/2004GL020308, 2004.

Mendes, V. B., G. Prates, E. C. Pavlis, D. E. Pavlis, and R. B. Langley, “Improved mapping functions for atmospheric refraction correction in SLR”, *Geophys. Res. Lett.*, 29(10), 1414, doi:10.1029/2001GL014394, 2002.

Pavlis, E. C., V. Mendes, D. E. Pavlis and G. Hulley, “Atmospheric Refraction Modeling Improvements in Satellite Laser Ranging”, 2004 EGU, 26-30 April 2004, Nice, France, *Geophysical Res. Abs.*, (6), 04206, 2004.

FIVE-TARGET SYSTEM CALIBRATION

J.McK. Luck EOS Space Systems Pty.Ltd.
jmckluck@optusnet.com.au, Fax +61 2 6299-6575

"The man who has one ground target KNOWS what his system delay is. The man who has two is never quite sure."

Abstract

Stromlo SLR systems have five terrestrial calibration targets which are used in the MINICO method for verifying the assumptions made in calibrating the system delay. Four of the targets are mounted externally on pillars surrounding the System Reference Point (SRP) which is the telescope's intersection of axes. The fifth, which can act as a real-time internal target during satellite laser ranging, is the "Spider Retro" mounted on one of the vanes holding the secondary mirror. The full MINICO method involves ranging to all of these targets and estimating the horizontal coordinates (East & North) of the SRP, the distance between SRP and the Spider Retro, and the current system delay.
From data kindly supplied by Geoscience Australia, the stability of the solutions over the 3½ year period from July 1999 to January 2003 will be presented, and application of the method in the new Stromlo-III system will be discussed.

Figure 1: View of the EOS Space Research Centre on Mount Stromlo, taken from the North-East calibration pillar. The 1.0-metre SLR telescope is inside the Typhoon-III dome atop the main building. The large Icestorm dome houses a prototype 1.8-metre research telescope. The slender tower to the right contains a Differential Image Motion Monitor. The Fiducial Monument is to the left, with a GPS/GLONASS antenna on it.

Introduction

The EOS Space Research Centre including the new Stromlo-III SLR system is shown in Figure 1. One of the calibration targets can be seen in Figure 2. Their layout is depicted in Figure 3, and their positions derived from a comprehensive collocation survey performed in

December 2003 by Geoscience Australia *(Dawson et.al, 2004*) are summarized in Table 1. The pillars on which the ground targets are mounted are the same as those used for Stromlo-I

Figure 2: View from the DIMM Tower over the SLR building's roof to the North-East calibration pillar, to the left of the burnt-out Oddie building (centre).

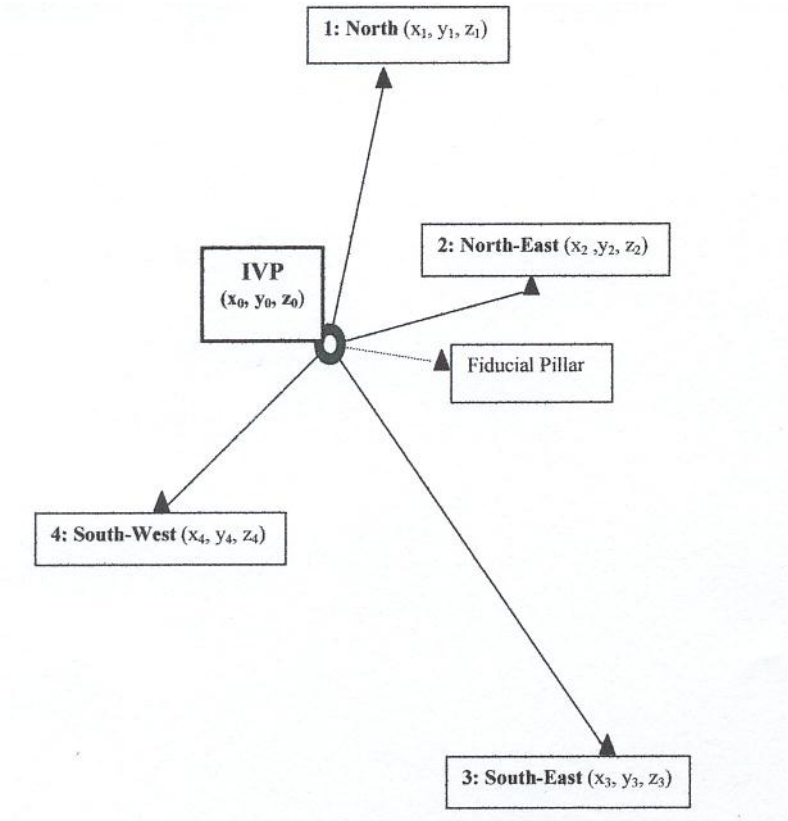

Figure 3: Planimetric layout of the external calibration targets relative to the intersection of axes of the SLR 1.0-metre telescope.

from 1998 to 2003 - they survived the firestorm. Of particular interest is the arrangement on top of the North pillar, shown in Figure 4, which holds the IGS GPS antenna as well as the target routinely used for pre-/post-calibration.

Table 1: Coordinates of the calibration targets relative to the System Reference Point (SRP). They refer to the targets' optical zeros (Effective Reflection Points).

Target	**East** (m)	**North** (m)	**Up** (m)	**Range** (m)	**Azimuth** (deg)	**Elevat'n** (deg)	**Notes**
North	15.6582	67.6123	-5.1257	69.5908	13.019	-4.225	Official survey results, 28/5/04
North-East	50.6242	19.8455	2.2953	54.4235	68.574	2.416	
South-East	74.2873	-90.6180	-3.3310	117.2234	140.637	-1.629	
South-West	-42.4571	-32.0138	-10.3644	54.1748	232.965	-11.029	
Spider				1.4562			1st guess

Figure 4: Example of very close collocation, between calibration target retroreflector, GPS antenna and survey monument plate on top of the North pillar.

A feature of laser ranging from Canberra stations since 1987 has been the use of internal calibrations from "Spider Retros", viz. retroreflectors mounted on the secondary mirrors' spider vanes *(Luck, 1992; Degnan, 1985; Luck & Johnston, 2000*). Given the right timing unit such as epoch timers and congenial detector gating characteristics, they can be performed simultaneously with satellite range measurements, hence constitute "real-time internal calibrations".

Using 3 or more ground targets to position the telescope is essentially a resection process, and was proposed in (*Greene, 1986*). The Keystone Network in Japan established a ground network of four calibration targets surrounding the SRP at each station, more-or-less equally spaced in azimuth (*Katsuo et al, 1999*). This concept was adopted at Stromlo, augmented by the Spider Retro.

The North Pier target is the standard used for routine pre/post system calibration during normal operations. The Spider Retro is an alternate standard for real-time system calibration. The primary purpose of weekly MINICO measurements to all 4 or 5 targets is to verify that the ranges to the North Pier and Spider Retro targets are correct, and hence that the inferred values of system delay are accurate. The solutions also reveal whether the horizontal coordinates of the SRP are constant with respect to the adopted coordinates of the targets, which can yield useful information about the system and its immediate environment. Finally, use of four targets provides the priceless commodity of redundancy in the determination of the system delay.

ESTIMATION OF SYSTEM DELAY

With 5 calibration targets available, there are several ways of estimating, applying or even eliminating the system delay, which represents all the optical and electronic delays on the laser/receiver side of the SRP. The system delay may legitimately be changed at any time (although preferably not while ranging!) and may fluctuate during ranging, so it must be calibrated against universal constants (or at least against local constants), at or very close to the time of ranging. These constants are, in practice, the surveyed distances from the SRP to the calibration targets. But they could themselves vary, so they need to be monitored.

Notation

Let: (x_0, y_0, z_0) be the local (East, North, Up) coordinates of the SRP;

$(x_{i,} y_i, z_i), i = 1,..,4$ be the local coordinates of the four ground targets;

$r_i, i = 1,..,4$ be the distances from SRP to the four ground targets;

g be the distance from SRP to Spider Retro optical zero projected parallel to the optical axis of the telescope;

$T_i, i = 1,..,4$ be the raw measurements of the ranges to the four ground targets;

$Q_i, i = 1,..,4$ be the system delay while ranging to the four ground targets;

$S_i, i = 1,..,4$ be the raw range measurements to Spider Retro during ranging to the four ground targets;

$\delta T_i, i = 1,..,4$ be known corrections to the ranges, such as atmospheric corrections and the additional delay when ranging through the dome's glass window;

$\delta S_i, i = 1,..,4$ be known corrections to the Spider Retro measurements, such as the additional delay through the prism and through any ND filters;

c be the speed of light in vacuum;

D be the reduced two-way range to a satellite, and $d = (c/2)D$.

The System Delay in Satellite Ranging

The raw measurement T to a satellite is given by:

$$T = D + Q + \delta T + \varepsilon \quad (1)$$

where δT is the sum of the known corrections such as extra delay through the dome window glass, and ε is random measurement error (which will be suppressed hereinafter). The system delay is Q. The reduced measurement D used to construct normal points is thus:

$$D = T - \delta T - Q \quad (2)$$

The problem is to determine Q (equivalently $q = (c/2)Q$) as near to the time of the satellite range measurement as possible.

General Solution for Five-Target Calibration Ranging

The full set of observation equations during ground target ranging including internal target is:

$$\begin{aligned} T_i - \delta T_i &= (2/c) r_i + Q_i, \quad i = 1,..,4 \\ &= (2/c)\sqrt{(x_i - x_0)^2 + (y_i - y_0)^2 + (z_i - z_0)^2} + Q_i \\ S_i - \delta S_i &= (2/c) g + Q_i, \quad i = 1,..,4 \end{aligned} \tag{3}$$

where it is assumed that each observation is subject to zero-mean random measurement errors. It is customary to assume that the system delays are the same during one MINICO session, i.e. $Q_i = Q$ for all i - any variations will be included in the measurement random errors. If we convert to linear measurements where necessary by putting:

$$t_i = (c/2)[T_i - \delta T_i], \quad s_i = (c/2)[S_i - \delta S_i], \quad q_i = (c/2) Q_i = q, \quad i = 1,..,4$$

then the observation equations become simply:

$$t_i = \sqrt{(x_i - x_0)^2 + (y_i - y_0)^2 + (z_i - z_0)^2} + q \tag{4}$$

$$s_i = g + q, \quad i = 1,..,4\,. \tag{5}$$

They can then be solved by least squares for the 5 parameters x_0, y_0, z_0, g, q. (They can also be solved if there are only 3 ground targets.) In practice, the elevation angle range is completely inadequate for determining the height z_0 so its survey value is adopted. Hence there are 8 observations in 4 unknowns, and a solution is possible. In particular, the solution includes both the Spider Retro distance *g* and the system delay *q*. The Keystone systems (*Katsuo et al, 1999*) used upwards-facing retroreflectors at ground level to enable height determination as well.

SRP and Spider Retro Stability

For geodetic monitoring of the stability of the SRP, as opposed to measuring the system delay, it is convenient to eliminate the system delay by subtracting equation (5) from equation (4). Thus:

$$\Delta t_i \equiv t_i - s_i = \sqrt{(x_i - x_0)^2 + (y_i - y_0)^2 + (z_i - z_0)^2} - g \tag{6}$$

leaving 4 observations in the 3 unknowns $x_0, y_{0,} g$ which include a good determination of the Spider Retro distance g, which can be a beast to measure directly by survey or engineering methods. But it does not yield a value for the system delay *q*.

Single Ground Target Pre/Post System Delay Calibration

Normal pre/post system calibration in the absence of Spider Retro is routinely accomplished from just equation (4) expressed as:

$$t_1 = r_1 + q + \varepsilon \tag{7}$$

using just one target $i = 1$.This can only be solved for *q* if the survey value for r_1 is adopted. This procedure, which is standard at most stations, does not have the advantage of observational redundancy.

Only Real-Time Spider Retro Calibration

With no ground target, only equation (5) is available which can only be solved for *q* if *g* is adopted. The value of *g* can be obtained either from survey (which as mentioned above is difficult) or from equation (6). In this case the reduced satellite measurement from equation (2) becomes:

$$D = (T - \delta T) - (S - \delta S) + (2/c)\,g \qquad (8)$$

in which the system delay *Q* has been eliminated in favour of real-time measurements *S*. In the "feedback calibration" pioneered in TLRS (*Silverberg, 1982*) the measurement of *g* had to include all the optical delays in the Coude path.

Internal Target and One Ground Target

The single ground target $(i = 1)$ can be used to calibrate the real-time internal target (*Kunimori et al, 1996; Nicolas et al, 1999*) by adopting the surveyed range r_1 and using it rather than its de-composition into coordinates in equation (6). The solution is immediately:

$$g = r_1 - (t_1 - s_1) \qquad (9)$$

This equation applies even if the internal target is on the laser/receiver table rather than near the secondary mirror. NRL@SOR uses 2 internal targets, on the optical bench and a Spider Retro "Headring" plus an external target (*Davis et al, 1999*). At Orroral (*Luck, 1992*) we adopted *g* from the survey results and only used equation (9) to monitor its stability.

RESULTS FROM STROMLO-I (7849)

The history of the Stromlo-I MINICO determinations, from data courtesy Geoscience Australia, is summarized in Figures 5-8, in which the legends are:

DX, DY: Solutions for (x_0, y_0) from equation (6), compared with survey values;

DG: Solutions for *g* from equation (6), compared with survey values;

DR = $\sqrt{DX^2 + DY^2 + DG^2}$.

Towards the end of the period, Spider Retro was not available so equation (4) was used.

Over the entire period, the single-session RMS in each coordinate including *g* was typically 1.5 mm, and the RMS of the quadratically combined coordinates was 2.8 mm which thus represents the accuracy with which the system delay *q* was determined. A good example from 2001 August 15 is given in Table 2, showing how the solutions vary slightly depending upon whether the Spider Retro values are not used (equation (4)), the system delay is eliminated (equation (6)), or Spider Retro measurements are included in the solution for *g* (equations (4) and (5) together). The RMS $(\hat{\sigma}_0)$ column gives the scatter of the input data about the solutions, whose estimated RMSs are also shown.

Table 2: Solutions from a typical MINICO session, 2001.

Sol'n Equ'n	Error w.r.t. Survey				RMS	RMS of Solutions			
	DX (mm)	DY (mm)	DG (mm)	Dq (ps)	$(\hat{\sigma}_0)$ (mm)	x_0 (mm)	y_0 (mm)	g (mm)	q (ps)
(4)	1.2	-1.9	-	442	1.9	1.5	1.4	-	6.9
(6)	0.0	-1.5	1.9	-	1.2	1.0	0.9	0.7	-
(4),(5)	1.2	-1.9	1.6	442	1.3	1.0	0.9	0.9	4.6

The correlation coefficients between the adjusted parameters are shown in Table 3. They do not vary from session to session. The correlation between *g* and *q* is quite high, because they are both treated as constants for all targets, bur they are partially de-correlated because the ground target measurements do not involve the Spider Retro explicitly.

Figures 5 and 6 are time-series graphs of DX,DY and DG,DR respectively (DR>0 always). None of the little patterns seen are considered significant. Figure 7 shows the distribution of the results with time-of-day, the only notable feature being clustering of observations when crews began or finished shifts! Figure 8 plots the planimetric positions of the SRP with respect to its nominal position. Their means, viz DX=0.4 mm, DY=-1.0 mm, therefore represent the inaccuracies in the ground surveys (or unmodelled systematic errors in the ranging system . . .).

Table 3: Correlation coefficients between parameters adjusted in the solution.

	SRP Coordinates		Spider Retro
	x_0	y_0	g
y_0	-.29	1.00	
g	-.28	.09	1.00
$\boldsymbol{q}$	.38	-.12	-.73

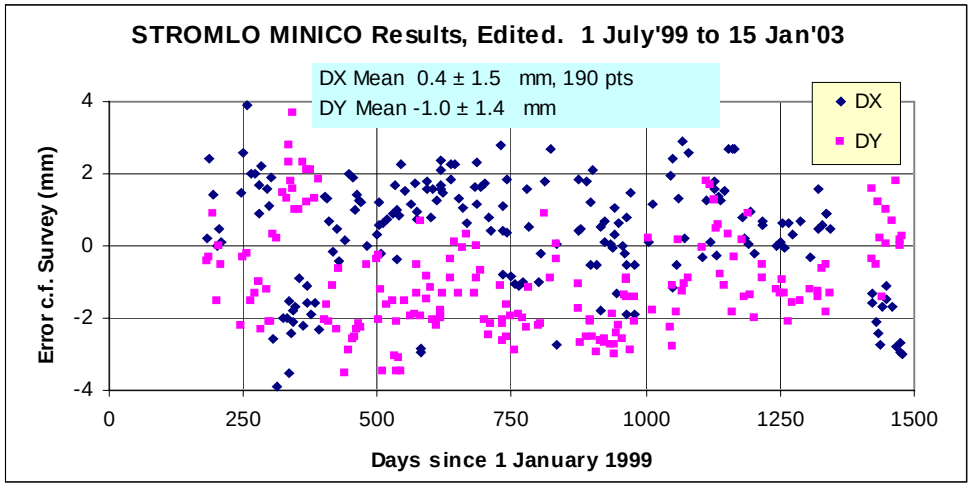

Figure 5: Time-series of MINICO determinations of the East (DX) and North (DY) components of the System Reference Point with respect to their adopted survey values.

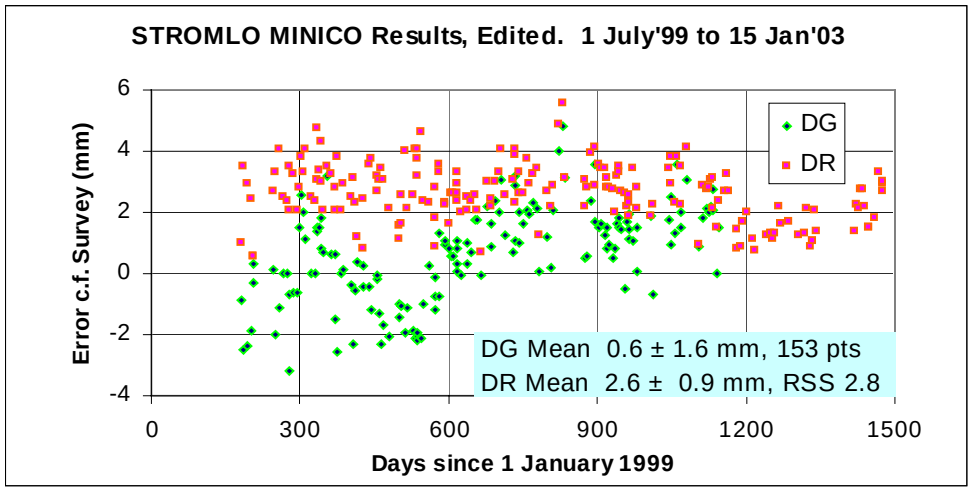

Figure 6: Time-series of MINICO determinations of the Spider Retro distance residuals (DG) with respect to its nominal value, and of the quadratically-combined errors of DX, DY and DG.

Comparison with Standard Single-Target System Calibration

I had planned to present graphs showing how these multi-target system delay determinations improved upon the usual single-target routine calibrations (or degraded them), but of course there is nothing to compare them against, because the value of q resulting from equation (7) depends entirely upon the assumption that the surveyed distance r_1 is absolutely accurate. The only way to check the accuracy of the single r_1 is to repeat the survey (which is recommended by ILRS to be done every two years).

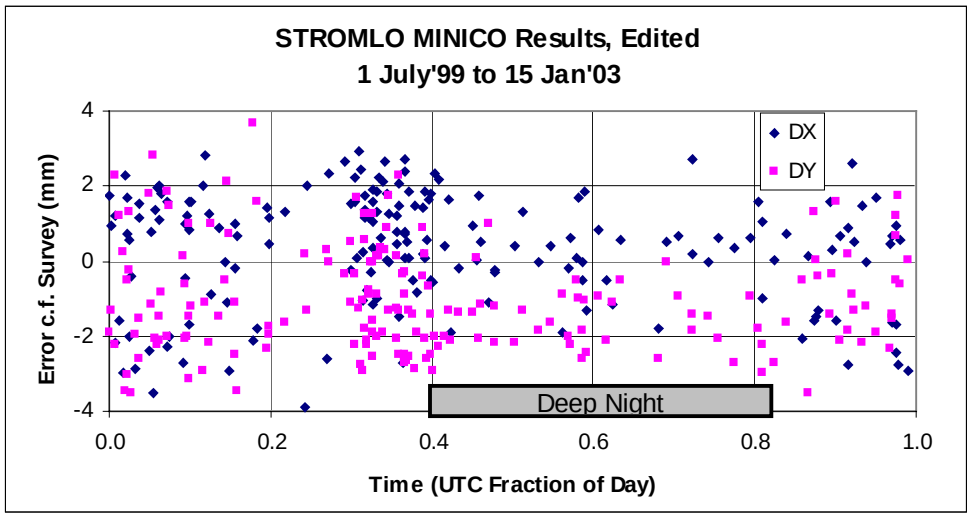

Figure 7: East and North MINICO determinations plotted against time of day (UTC).

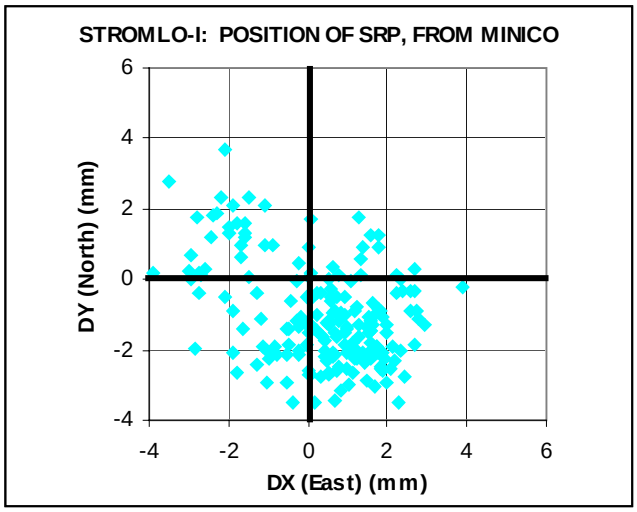

Figure 8: Map of the MINICO-determined positions of the System Reference Point, with respect to nominal.

PROCEDURE AT THE NEW STROMLO STATION (7825)

The four ground targets are available, so equation (4) can certainly be used to get improved values of (x_0, y_0) and hence a revised value of r_1 for use in subsequent single-target calibration. A Spider Retro retained from Orroral has been installed (see Figure 9) and tested in a limited way while ground target ranging at low laser power, but it is currently uncertain whether it can be safely integrated during satellite ranging.

The distance from the Spider Retro will be measured using the methods in this paper, not by scrambling around the telescope with tape measures and other apparatus in a very tight space close to its mirror surfaces. Its position will, however, be measured next time the geodetic collocation survey is performed.

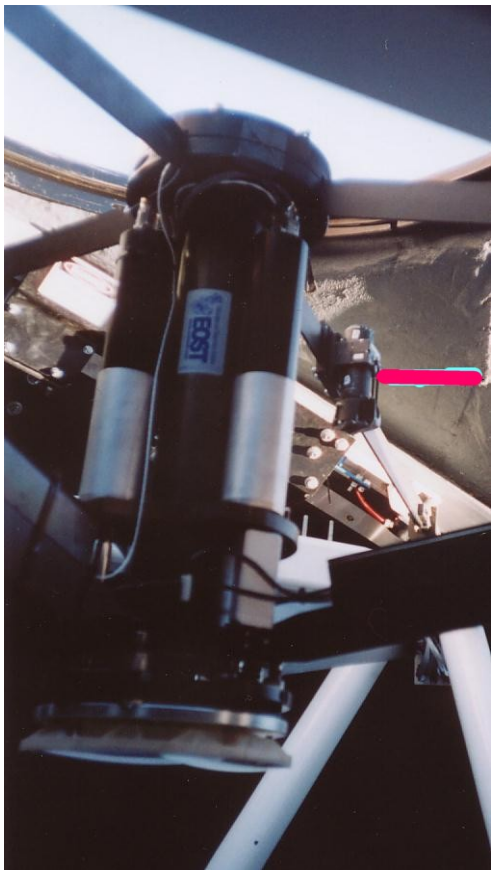

No decision has yet been made on whether the MINICO determinations of the SRP position - and hence of the "survey" values of the ranges to the targets - will be implemented, nor on how often they would be updated. Initially, the MINICO values obtained during Final Acceptance Testing will be checked for any significant differences from the GA 2003 survey values, and either theirs or ours will be adopted. There will follow a period when MINICO will be used to assess the stability of the adopted values, which will decide whether or not to implement a regime of frequent (weekly/monthly) updates.

The first successful MINICO with this system took place on 31 May 2004, yielding survey agreements of $x_0 : -1.0\text{mm} \pm 1.6$, $y_0 : -0.1\text{mm} \pm 1.5\text{mm}$ RMS, with g & q RMSs 1.5 mm and 7.2 ps respectively.

Figure 9: Red line points to the Spider Retro to the right of the secondary mirror focusing assembly. The secondary mirror is at the bottom left of the photo.

RESULTS FROM STROMLO-III

The range timing system was substantially revised in mid-September 2004. Results since then have been consistent to better than 0.5 mm (RMS) as shown in Figure 10. The typical RMS yielded by a single MINICO is 0.4 mm in DX and DY, and 1.7 ps in system delay. These are

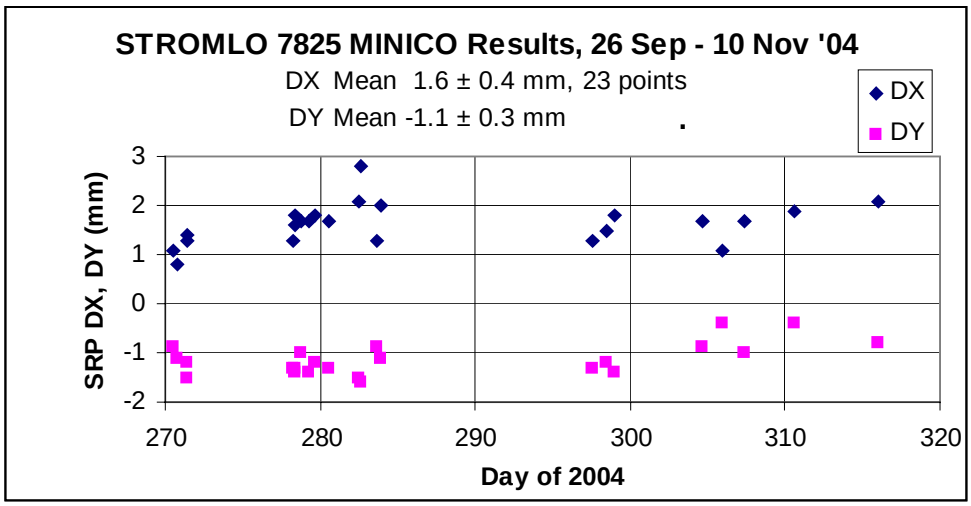

Figure 10: Time-series of MINICO determinations of the East (DX) and North (DY) components of the new System Reference Point with respect to their 2003 survey values.

considerable improvements over the corresponding values from the old system, given in Table 2, solution (4). To date it has not been possible to gather sufficient statistics on Spider Retro.

The 95% confidence interval of the DX mean is (roughly) $\pm 2x0.4/\sqrt{23} = \pm 0.17\text{mm}$, so its difference of 1.6 mm from the survey value is statistically very significant, and similarly for the DY mean of -1.1 mm. It is uncertain whether these are due to survey inaccuracies, to the behaviour of the range timing system over small time intervals (cf. *Benham, Gibbs & Smith, 2004*), or something else. But they are not really large enough to worry about yet.

CONCLUSIONS

This paper addressed the geometric aspects of system delay estimation. Other aspects as well as the geometric, directed towards the accuracy of measurements as they are affected by such things as detector processes and timing system vagaries, were discussed at the ILRS Colloquium on SLR-System Calibration Issues (*Schreiber, 2001*) but are not treated here, nor are historically interesting aspects such as a mysterious background effect from behind the calibration board at Herstmonceux (*Appleby and Matthews, 1990*).

The MINICO method effectively provides a convenient, on-site method for determining the accuracy of the system delay so vital for satellite laser ranging. Such an assessment is not possible by one-target systems except through repeated, costly re-surveys. For Stromlo-1, an upper-bound (1-σ) was 2.8mm. It also provides monitoring of the stability of the horizontal coordinates of the SRP, or looked at the other way, of the actual distances from the SRP to each of the ground targets.

The ground target configuration at Stromlo is not conducive to monitoring the height differences - targets at extremely high and low elevations would be needed - so height variations must be measured by other means, such as laser ranging to satellites . . . (no, it's not a circular argument).

Use of a Spider Retroreflector enables real-time measurement of the system delay, provided that detector and timing system responses do not introduce their own biases. In fact, the system delay is eliminated from the calculations. The MINICO method provides much the best way of estimating the range from the SRP to the Spider Retro.

Results emerging in the final stages of commissioning the new Stromlo SLR, using this method with four ground targets, indicate that the SRP coordinates can be determined with a precision of 0.4 mm RMS, and the system delay with an accuracy of 1.8 ps (0.3 mm).

"The man who has just one ground target only thinks that he knows the system delay. The man who has five can be very confident."

ACKNOWLEDGEMENTS

The staff of Orroral Observatory persevered with use of Spider Retro and proved its usefulness.

Jim Steed and Geoscience Australia kindly provided the Stromlo-1 data from their archives (much of which I had compiled anyway), and performed the local surveys with unprecedented precision and highly verifiable accuracy.

REFERENCES

Appleby, G.M. and Matthews, W.E.: "*An Analysis of Range Calibration Values from the UK SLR System, 1985-1989*", Proc. 7th International Workshop on Laser Ranging Instrumentation, Matera, Italy, 2-8 Oct.1989, OCA/CERGA (1990)

Benham, D., Gibbs, P and Smith, V.: "*New Internal Calibration Target at SGF Herstmonceux: Design and Results*", these Proceedings (2004)

Davis, M.A., Gilbreath, G.C., Snyder, G., Rolsma, P., Georges, J., and Eichinger, R.: "*NRL@SOR SLR Observation Verification Techniques using Lageos*", Proc. 11th International Workshop on Laser Ranging, Deggendorf, Germany, 20-25 Sept. 1998, Verlag des BKG, Vol. 1, pp. 232-244 (1999)

Dawson, J., Johnston, G., Naebkhil, S., Govind, R. and Luck, J.: "*The Mount Stromlo Satellite Laser Ranging (SLR) System Local Tie Connections Before and After the 2003 Destructive Canberra Fires*", these Proceedings (2004)

Degnan, J.J.: "*Satellite Laser Ranging: Current Status and Future Prospects*", IEEE Trans on Geoscience and Remote Sensing, Vol. GE-23, No. 4, pp. 398-413 (July 1985)

Greene, B.A.: "*Calibration of Sub-millimetre Precision Satellite Laser Ranging Systems"*, Proc. 6th International Workshop on Laser Ranging Instrumentation 22-26 Sept. 1986, Ed. J. Gaignebet and F. Baumont, CRGS-CERGA, Vol. II (1986)

Katsuo, F., Otsubo, T., Amagai, J., Nojiri, H.: "*A Concept of Measuring the Telescope Reference Point by Using Multiple Ground Targets*", J. Communications Research Laboratory, Tokyo, Japan, Vol. 46, No. 1, pp. 135-140 (March 1999)

Kunimori, H., Otsubo, T. and Gotoh, T.: "*Range Bias Correction of the Tokyo SLR Station (1990-1995)*", J. Communications Research Laboratory, Tokyo, Japan, Vol. 43, No. 1, pp. 13-22 (March 1996)

Luck, J.McK.: "*Performance of the Upgraded Orroral Laser Ranging System*", Proc. 8th Int. Workshop on Laser Ranging Instrumentation (Annapolis, MD, 18-22 May 1992), pp. 11-6ff, NASA Conference Publ. 3124 (1992)

Luck, J.McK. and Johnston, G.: "*Local Ties and Verification of Calibrations*", presented to 12th Int.Workshop on Laser Ranging (Matera, Italy, 13-17 November 2000), unpublished (2000)

Nicolas, J., Exertier, P., Bonnefond, P., Pierron, F., Boudon, Y., Mangin, J-F., Barlier, F., Kasser, M., and Haase, J.: "*Stability Control of Range Biases on the French Laser Ranging Stations*", in Laser Radar Ranging and Atmospheric Lidar Techniques II, Ulrich Schreiber, Christian Werner, Editors, Proceedings of SPIE, Vol. 3865, pp. 27-32 (Sept. 1999)

Schreiber, U.: "*Documentation - Colloquium on SLR-System Calibration Issues*", Florence, Italy, 1999, Fundamentalstation Wettzell (2001)

Silverberg, E.C.: "*The Feedback Calibration of the TLRS Ranging System*", Proc.4th Int. Workshop on Laser Ranging Instrumentation (University of Texas at Austin, 12-16 Oct. 1981), pp. 331-337, Bonn Geodetic Institute (1982)

NEW INTERNAL CALIBRATION TARGET AT SGF HERSTMONCEUX; DESIGN AND RESULTS

David Benham, Philip Gibbs, **Victoria Smith**
NERC Space Geodesy Facility, Herstmonceux Castle, Hailsham BN27 1RN, E.Sussex, UK
dben@nerc.ac.uk, pgib@nerc.ac.uk, vism@nerc.ac.uk

Abstract

Calibration is of course fundamental to realising the full potential accuracy of the satellite laser ranging technique. For several years, the SGF laser ranging system has used parallax-free targets at 100 and 400m distances for routine calibration and additionally for investigations into subtle distance-dependent effects in the Stanford counter cluster. However, the advantages of a close target include accurate environmental control, ease of access and, not least, availability during periods of poor weather. At SGF Herstmonceux we have designed and built a new calibration target fixed inside the laser telescope dome. This paper describes the mechanical features of the target, the difficulties encountered in arming the C-SPAD for such a close target and current investigations into observed small calibration differences between this new target and our existing long-range targets. We will attempt to show from experiments carried out on our additional moveable calibration target that this uncertainty in our measured calibration is caused by the behaviour at short range of the SR620 timers.

Existing Targets

We have 5 targets at Herstmonceux. Two stainless steel retro reflectors to the west at a distance of ~120 metres, two stainless steel retro reflectors to the East at a distance of ~600 metres and one flat board target at ~600 metres – this was our original target. When we changed our detector from a PMT to SPAD system we had to change to one of our retro reflector targets, as we could not get enough data back through our telescope system onto the very small diode of the SPAD.
The flat board target, one of the east targets and our current calibration target in the west were all included in the original site survey. A recent survey in 2003, which included all targets, gave agreement in the distances to the targets at the 3mm level.
We try to take calibration measurements to all our targets at least once a week and monitor the differences obtained when compared to our standard target. This is more to ensure that the targets/telescope are not drifting than to get a definitive value for calibration. We have been aware for some time that the SR620 can give us different results for these comparisons depending on what configurations we use.

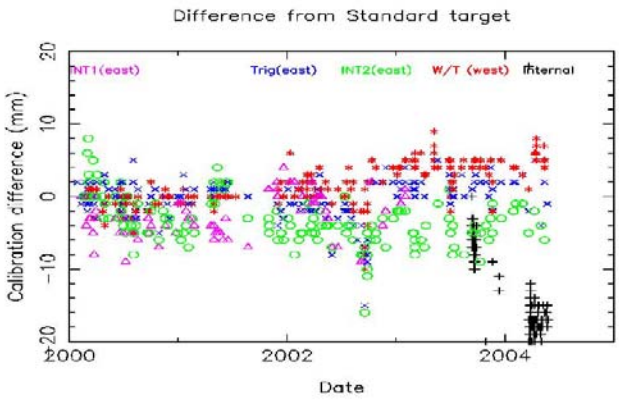

Shown here are the differences for all our targets compared with our current calibratio n target. The difference for the internal target for 2004 clearly stands off. The pre-2004 internal target data used an unmeasured estimate of the distance from telescope to target.

New Internal Target

Shown here is the new Internal target. The “retros” are two mirrors with the reflective coating facing the telescope. A grating is situated in front of the mirrors to reduce the return rate.

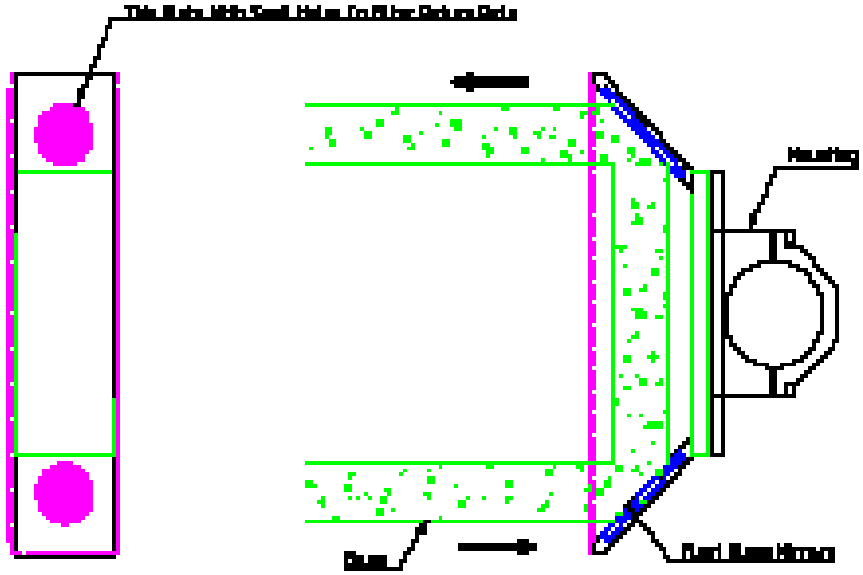

Arming the C-SPAD

Because we have a C-SPAD detector we need to arm the device in time for the returning laser. The round trip time for the laser is ~110 ns. The minimum time for our arming route is ~400ns. This means we cannot arm the C-SPAD in the normal way. We measured the time taken from issuing a fire command and the actual time of firing and found an uncertainty of 10microseconds. Therefore we tried to detect the build up of laser energy by placing a diode i) behind the dye cell mirror ii) near the wedge in laser cavity The uncertainty in detection at both these points was large (>10microseconds). Given that the uncertainty in detecting the laser early is as great as the variations in time delay when the request is sent from the PC we abandoned any attempt to detect the laser and just bypassed our normal arming system. This

of course means the C-SPAD may be armed well before the true return from the target and the C-SPAD may easily be triggered by internal noise. This has to be taken into account when determining the return rate to keep the system at single photon.

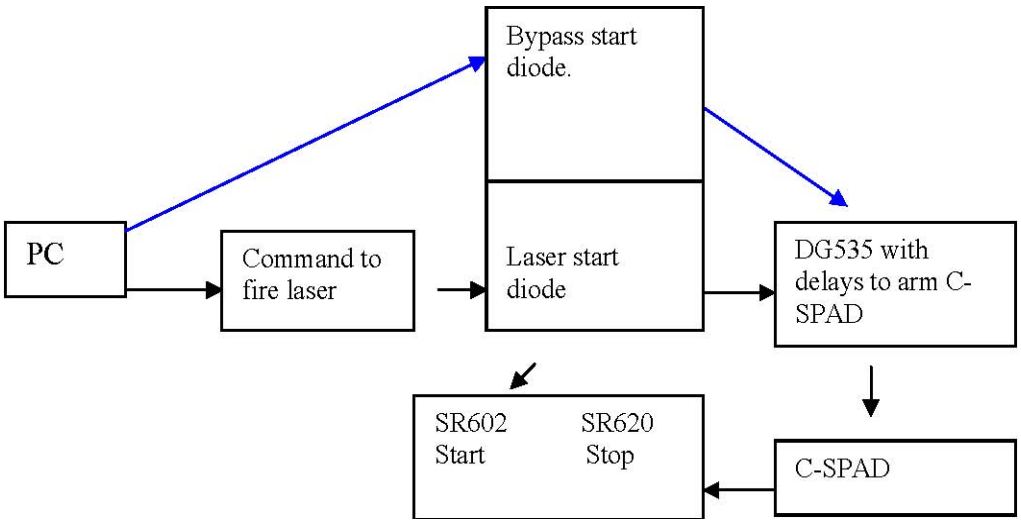

First Results

Now we can measure the distance from the target to the telescope axis, control C-SPAD arming and control return rate. We would therefore expect to get good agreement between our new target and existing targets at the few mm level. This turned out not to be the case.

Shown below are the results for our system, which has four SR620 timers, 2 connected to the uncompensated channel of the C-SPAD, 2 connected to the compensated channel. The results for the four timer/detector systems are made simultaneously and in theory should at least all agree.

Standard set-up Main Target – Internal Target

– Uncomp A 16mm D 17mm

– Comp B 9mm C 10mm

Given there seems to be a difference between the compensated and uncompensated systems we tried a couple of non-standard setups and connected all our SR620s firstly to the uncompensated channel of the CSPAD and then to the compensated channel.

Non-standard setup

– Uncomp A 17mm B 15mm C 14mm D 18mm

– Comp A 16mm B 12mm C 12mm D 15mm

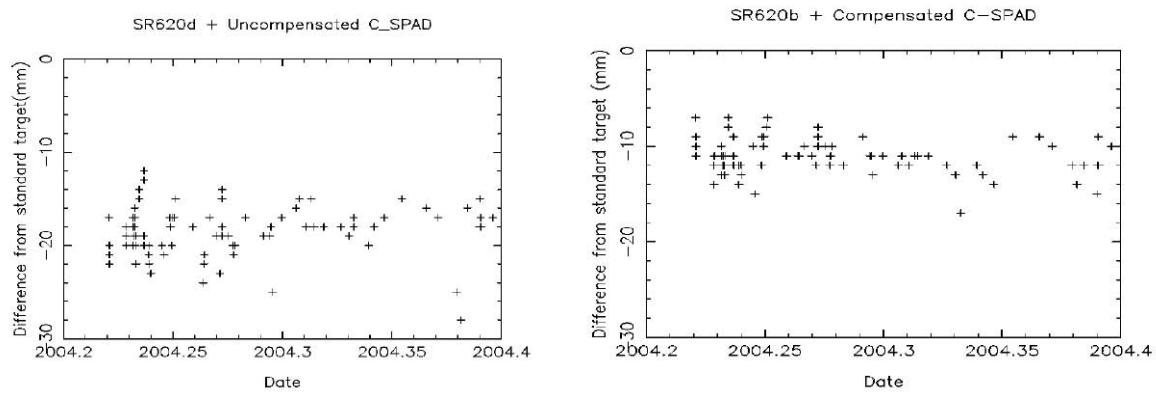

Shown above are the time series for both the SR620/Uncompensated and SR620/Compensated systems.

So whatever set-up we use we would appear to have a difference between our internal target and our standard target of 10-18mm.

Possible sources of these differences

There are four possible sources of error that we can think of: - there may of course be others we haven't thought of

i) Survey measurements or measurement to Internal target wrong – this we do not believe is the case due to the site survey of 2003
ii) Uncontrolled single photon rate
iii) Decay in C-SPAD due to early arming
iv) Timer non-linearity.

i) Survey measurement

The survey of 2003 would seem to confirm to distances to the external targets and we are convinced we have measured the distance to the internal target correctly

ii) Uncontrolled Single Photon Rate

The shown previously above were taken at very close to 0% return rate. If it was a return rate problem it should only show in the uncompensated channel. Even if there is a variable rate problem, the compensated data would indicate there is still a discrepancy of order 10-12mm

iii) Decay in C-SPAD due to early arming

We know there are errors if you do not arm the C-SPAD adequately in advance. The requirements are

– Uncompensated 50ns - if not errors can be up to 15mm
– Compensated 100ns - if not errors can be up to 40mm.

For the internal target we arm the C-SPAD very early (up to 10microseconds).

–Can this cause a problem?

To check this we ranged to our 600 Metre target and armed C-SPAD between 100ns to 4000ns early. The calibration values varied only at the 1mm level. We are therefore happy that it is not an arming problem with the C-SPAD.

iv) SR620 timer non-linearity

The SR620 manual describes two differential non-linearities with plots shown below.

Specification Guide

Graph 1: Differential Non-linearity for time differences of 0 to 11 ns. This shows the residual non linearity of the time-to-amplitude converters.

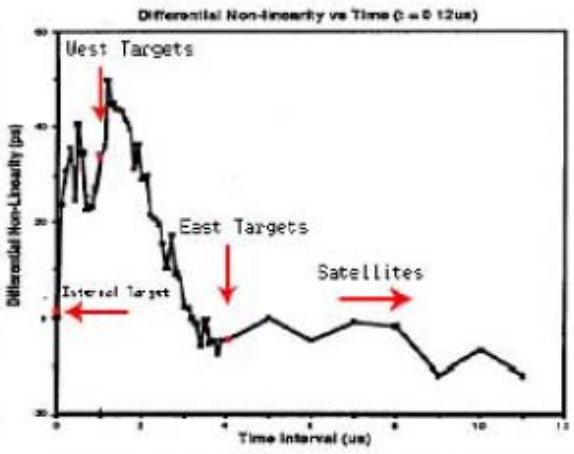

Graph 2: Differential Non-linearity for time differences of 0 to 11 μs.

To try and investigate the first of these non-linearities over the 11ns (90KHz) range we constructed a moveable target. The target was mounted on a rail to be moved known distances. The rail allows movement of 2 metres (4 metres round trip, >11ns).

Calibration measurements were taken at given distances along the rail. Using the semi-train enables data sets of some 40ns for our tests. Adding cables to the start/stop train can also shorten or lengthen the measured range. For a truly linear system we would expect a change in calibration equivalent to the movement of the target.

In the graphs shown below a 'run' is determined as one set of measurements across the 2m rail, successive runs indicate the addition of cable lengths. Due to these cable lengths the start point for each run can be said to be arbitrary.

Shown below are the results for each of our Stanford Timers, labelled A-D, D is taken first as it is currently used for our ranging measurements.

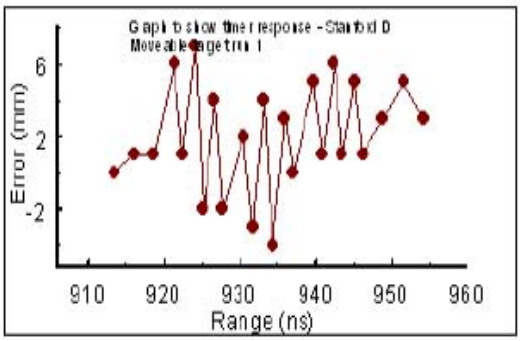

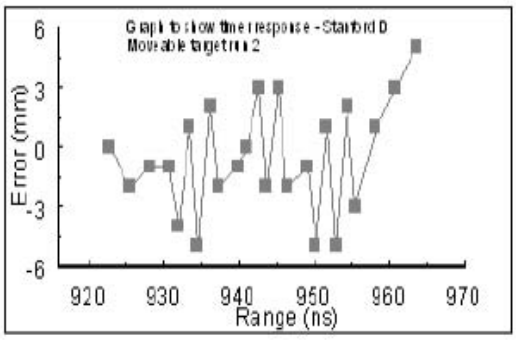

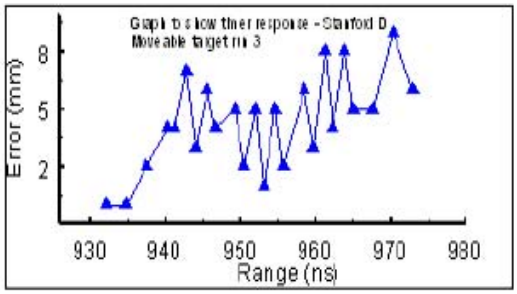

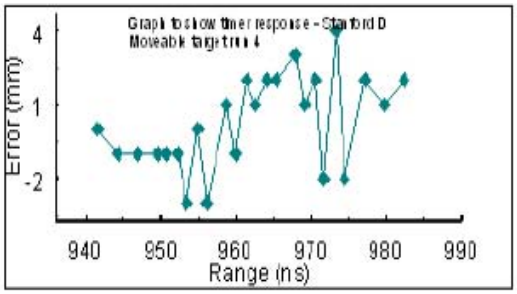

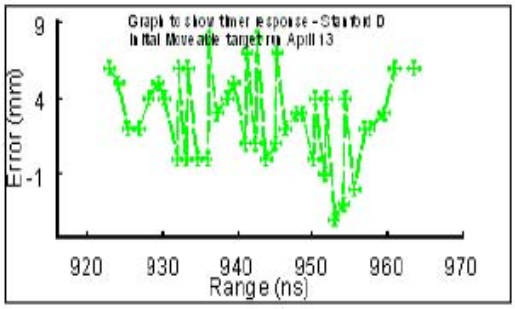

The above show a possible deviation of ± 6mm from the ideal of zero.

To better understand any trends which may appear on the above, the graph data was overlaid to produce one graph. This is somewhat messy however but we believe behaviour trends are shown. This can be more clearly seen by the second graph shown below.
Throughout the distance range shown on the graph on the right behavioural trends can be seen. At nearly every point where data has been obtained for the same range, the behaviour of the two data sets agree.

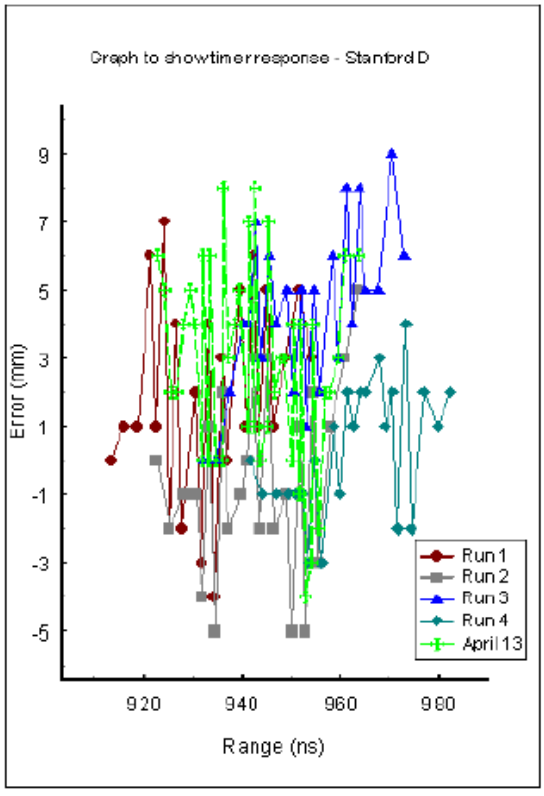

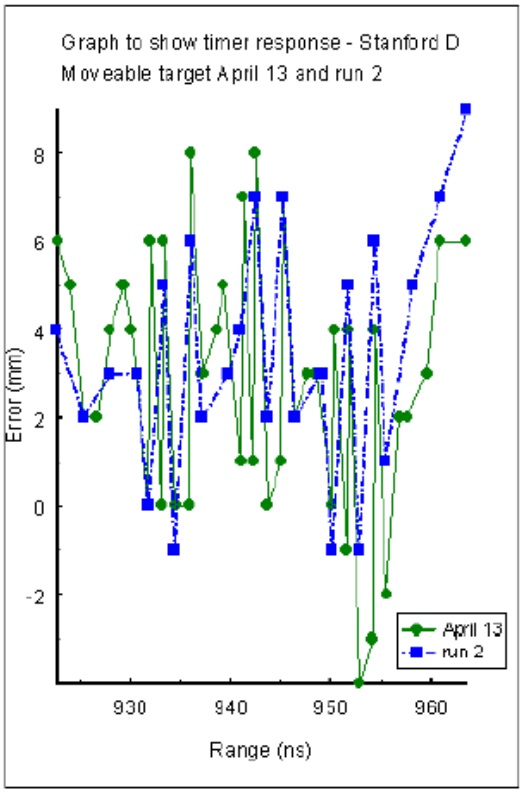

Similar results were obtained for timers A,B and C. All timers exhibited similar behaviours. A copy of this paper including the results, and new results as they are obtained, for all the timers is available on our website http://nercslr.nmt.ac.uk

Conclusion

It has been seen that each timer displays a different characteristic response but this response is repeatable if the same ranges are used. It would appear each Stanford timer displays an inherent characteristic and surmised that due to the nature of the electronics the behaviour would not be identical for each device.
However we do not believe the 11ns characteristic as given in the Stanford manual is apparent for any of the four Stanford Timers. In fact we see a much greater scatter on any 11ns period shown.
These tests are in an early stage and will probably only be concluded with the advent of future comparisons at Herstmonceux with an Event Timer.

MLRO PERFORMANCE CHARACTERIZATION

G. Bianco (1), R. Sala (2), V. Luceri (2)
(1) Agenzia Spaziale Italiana, Centro di Geodesia Spaziale, Matera, Italy
(2) Telespazio S.p.A., Matera, Italy
giuseppe.bianco@asi.it

Abstract

The Matera Laser Ranging Observatory (MLRO) has recently completed its warranty period and is now fully available for observational activities and further developments. This presentation describes the system performances after three years of operations, including substantial debugging and fine tuning efforts, giving an estimate of the system ranging precision and efficiency, calibration stability, estimated biases, accuracy of estimated position, etcetera. Examples are given of the system behaviour on different geodetic satellites as well as on moon targets, along with a thorough description of the calibration procedures, options and capabilities.

PORTABLE PICO EVENT TIMER 2 kHz

Karel Hamal, Ivan Prochazka
Czech Technical University in Prague. Brehova str. 7, 115 19
Prague 1, Czech Republic
prochazk@mbox.cesnet.cz phone +420 723 920 786, fax +420 224 922 822

Abstract

To make happy the "VIP SLR 2k Club" founded in Koetzting,October 2003 we have been developing the Pico Event Timer PET2k. The Portable version P-PET2k proofs the features when operating stand-by at the SLR station. The timing resolution is 1.2 psec, timing interval jitter below 3 psec, linearity better than 2.5 psec, the repetition rate up to 2 kHz. The P-PET2k is interfaced via a standard parallel communication port to a notebook. The P-PET2k contains the range gate generator, and the Signal Strength Monitor SSM for a C-SPAD based receiver.

PORTABLE PICO EVENT TIMER 2k

GOALS

- Portable Pico Event Timer 2kHz
- Signal Strength Monitor Built in
- Dedicated for Portable Calibration Standard 2k

PORTABLE PICO EVENT TIMER 2k

PORTABLE CALIBRATION STANDARD

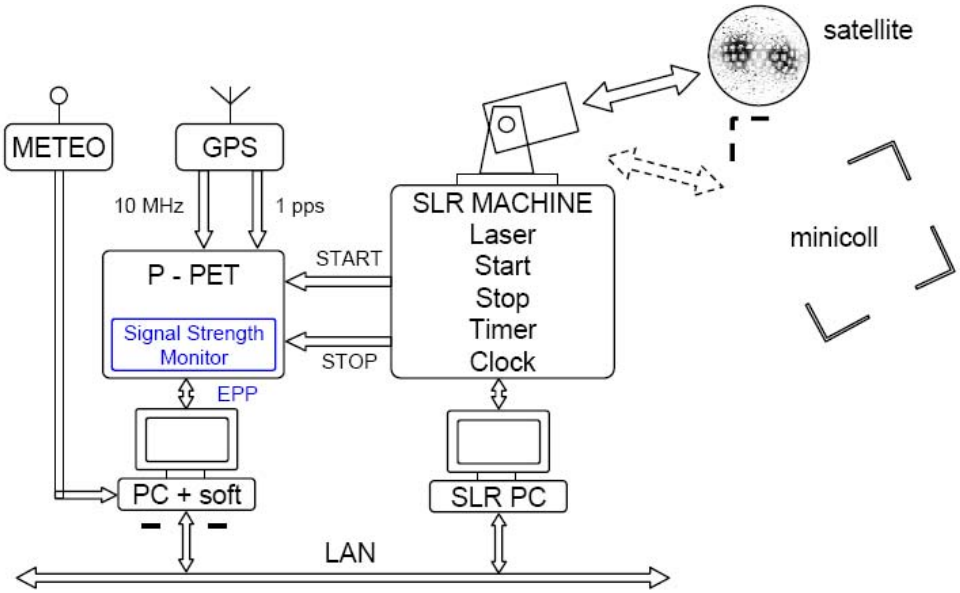

K. Hamal et al, EGS-AGU-EUG Joint Assembly, Nice, April 2003

PORTABLE PICO EVENT TIMER 2k

PRAGUE INDOOR TESTS, JUNE 2004

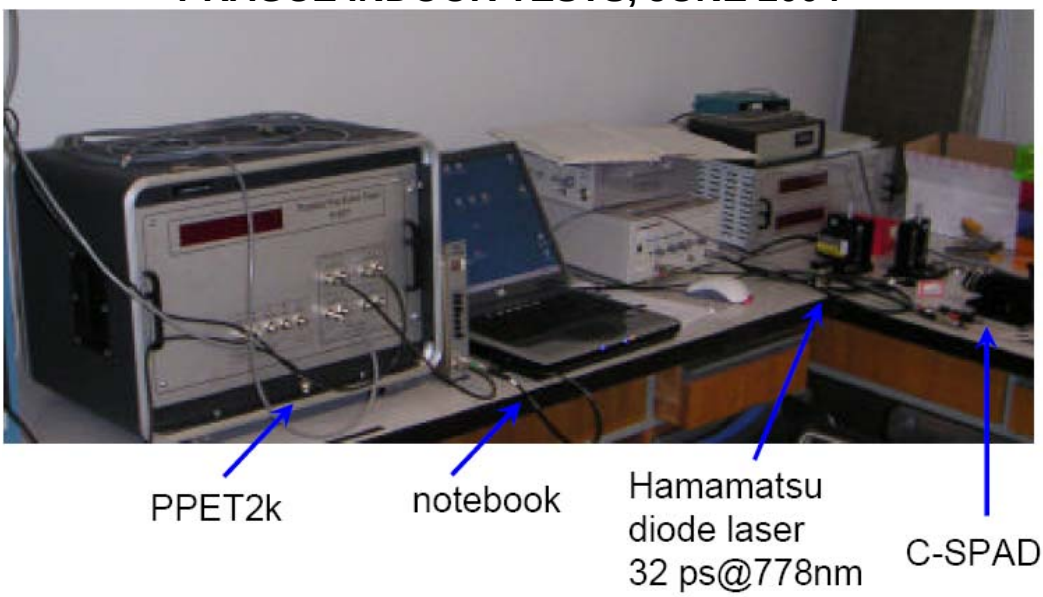

PORTABLE PICO EVENT TIMER 2k

P-PET PARAMETERS

Upgrade Summary

London '97 => Wash 2002 => **San Fernando**

• timing resolution	1.2 ps		
• timing jitter / channel	5 ps	2.5 ps	
• non-linearity / channel	< 5 ps (spec)	< 2.5 ps (meas)	
• temperature drift	< 0.7 ps/K	< 0.53 ps/K	
• adjustment	NO		
• temporal stability	± 1.0 ps/hr	± 0.45 ps/hr	
• max. repetition rate	30 Hz	100 Hz	**2 kHz**
• no. of channels	2(4)		
• interface	RS232		**EPP**
• mass transport	32 kg		
• Signal Strength Monitor			**built-in**

K. Hamal et al, EGS-AGU-EUG Joint Assembly, Nice, April 2003

PORTABLE PICO EVENT TIMER 2k

ILRS NETWORK TIME OF FLIGHT DEVICES

Van Husson, Loyal Stuart, 13th WLR, Washington, Nov. 2002

Manufacturer	Curent Model	Year	Approach	Resolution (ps)	Jitter (ps)	Linearity (ps)	Stability [ps/K]	Stability [ps/hour]	Max. repitition rate	Max. TOF (Secs)
SR	620	1988	Interval	4	22	50	5		100	1000
HP	5370B	1982	Interval	20	35	20			10	10
Latvian Univ.	A013a	2002	Interval	10	20	2		2	80	0.209
Ortec	TD811	<1980	Event	100			40			N.A.
PESO Cons.	PET4/TIGO	1999	Event	1.2	3.5	3	<0.3	<0.5	>100	N.A.
EOS	MRCS V.4	1998	Event	2	10	1		1	1000	N.A.
HTSI	MLRO	1998	Event	0.5	<2			0.5	2000	N.A.
PESO Cons.	**P-PET 2k**	**2004**	**Event**	**1.2**	**2.5**	**3**	**< 0.3**	**< 0.5**	**2000**	**N.A.**

K. Hamal et al, EGS-AGU-EUG Joint Assembly, Nice, April 2003

PORTABLE PICO EVENT TIMER 2k

CONCLUSION

- Portable Pico Event Timer
- Signal Strength Monitor
  next paper
- Dedicated for Portable Calibration Standard 2k

1997	20 Hz
1998	100 Hz
2004	2000 Hz

TESTS OF STABILITY AND LINEARITY OF THE A031-ET EVENT TIMER AT GRAZ STATION

C. Selke(1), F. Koidl(2), G. Kirchner(2), and L.Grundwalt(1)
(1) GeoForschungZentrum Potsdam
(2) Institut für Weltraumforschung Graz.
grun@gfz.potsdam.de /Fax +49-331-1732

Abstract

The event timer A031-ET (made bythe Institutof Electronics and Computer Science, University of Latvia, Riga) offers an interestig alternativeto the widely used SR620 time-of-flight counters. In order to chek for the linearity and the stability of this instrument, a series of intercomparisons of the A031 and the "E.T." at Graz SLR station (consisiting of top-level Dassault modules) was performed. The obtained data covers the full range of time intervals which is of interest for SLR measurements (70 ns - 200 ms) and shows both excellent linearity and stability of the Riga Instrument. The different test methods and the results of the intercomparisons between both event timers are discussed and some hints for the optimum operation of the A031 are given.

Introduction

It is well known that the widely used SR620 time interval counters display a simple - and range-dependent non-linearity of the measured time intervals within the range of intervals used for Satellite Laser Ranging [Gibbs,2002]. Those non-linearities can amount up to several 10ps and have to be taken into account in order to avoid time-dependent range biases (cf. Fig.1)

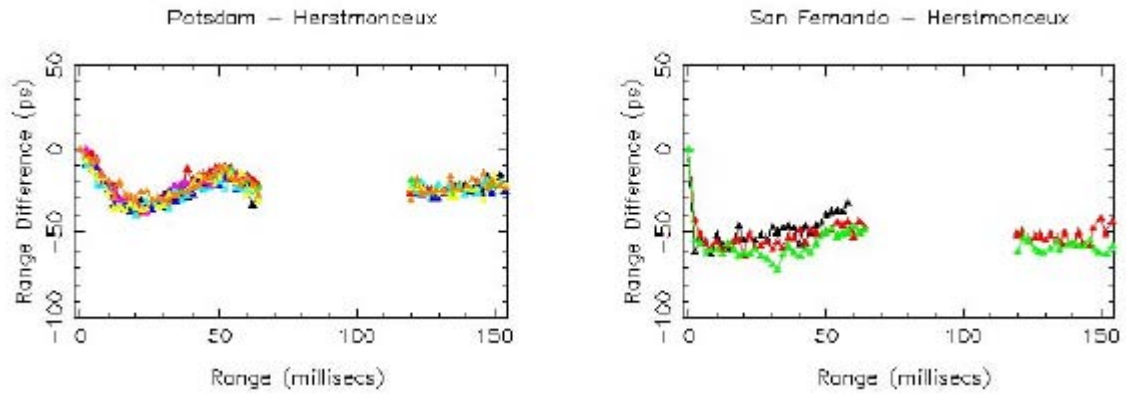

Figure 1. Examples of non-linearities for two different samplesof SR620 counters(adapted from [Gibbs,2002])

While this range-dependent non-linearity appears to be fairly stable within 10-20ps and can thus be corrected for in post-processing, it would be desirable to use timing devices which are virtually free of such effects. Event timers based on the commercially available Dassault modules are claimed to display non-linearities of $\leq$ 2.5ps but are rather expensive. The newly developed event timer A031-ET (University of Riga, Latvia) is far less expensive and might offer an interesting alternative to the SR620 in case the non-linearity was far below the values found for the Stanford counters. The intention of our experiments was to investigate the stability and linearity of the A031-ET as compared to an event timerbased on Dassault modules.

The A031-ET Instrument

The A031-ET is the most recent development within the family of timing instrumentation from the Institute of Electronics, University of Riga [Artyukh et al., 2002]. It is a rather compact unit with the NIM inputs for start/stop events and an optional electronic gate, and requires a 10 Mhz external timebase and a 1 pps timing signal (both TTL level) for means of epoch synchronization. The application software is running under Windows® on a PC interfaced via EPP to the event timer. This PC is to be connected to a local network via TCP/IP for fast data exchange.

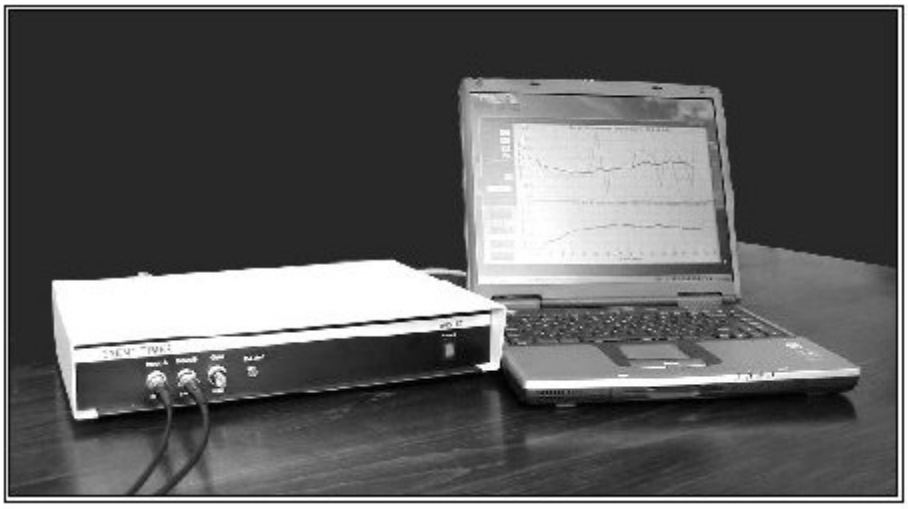

Figure 2. The A031-ET instrument with the interfaced PC for the application software

The single-shot RMS is tipically in the order of 10-12 ps, the dead time is about 70 ns. Up to 6550 time tags per operating cycle may be registered before the internal buffer has to be dumped to the host PC via the parallel port. The A031-ET can be operated both the AT (event timing on both inputs A and B) and TI mode (advanced time inteval measurement with A arming B, but B with capableof registering multiple stops, taking into account the dead time). Triggering can be performed both externally or internally.

Test setup at Graz SLR station

Test of linearity and stability were performed in February 2004 at the SLR station 7839 Graz (Austria) against the "E.T." [Kirchner and Koidl, 2000] which is made from Dassault modules and exhibits a non-linearity of < 2.5 ps. The A031ET was supplied with the clock- and time-reference of the SLR station and registered data from calibrations, satellite tracking and simulations in parallel. Because target and satellite data yield only a limited range of time intervals between 1....200 ms. For this purpose the tracking software was modified in a way that the delay of the range gate was increased in ms-steps every 2 seconds, and the first noise pulse after opening the gate was taken as stop pulse. For checking the range of 100ns...1ms, a pulse generator with manual stepping of delay time was used because the range gate could not be set to values of less than 1 ms. This range is important because the typical SLR calibration time interval is in the order of 100ns for short-way links and several μs for remote targets. A certain constrain was caused by the above-mentioned fact that the A031-ET in its present hardware configuration can only record max. 6550 events/cycle in full speed AT mode (this correspond to a registration time of about 1.6 s at 2kHz laser repetition rate at the Graz

station) followed by a gap for data transfer of about 1s. Therefore only 60% of events could be recorded in parallel between the "E.T." and the A031, but this was sufficient for this test. The data processing was performed by LabVIEW-programs created in situ. They were written for searching such data that both event timers had registered. For a detailed analysis of nonlinearity the difference values of simulation measurements were processed as follows:

- 2.2 sigma filtering
- computing the mean values for each ms-step (red curve in Figure 3)
- low pass filtering with f_u = 0.02Hz (the scan rate of stepping was about 0.5 Hz) (blue curve in Figure 3)

This way the noise of the individual samples was much reduced, and possible trends could be visualized in a more simple way.

Test results

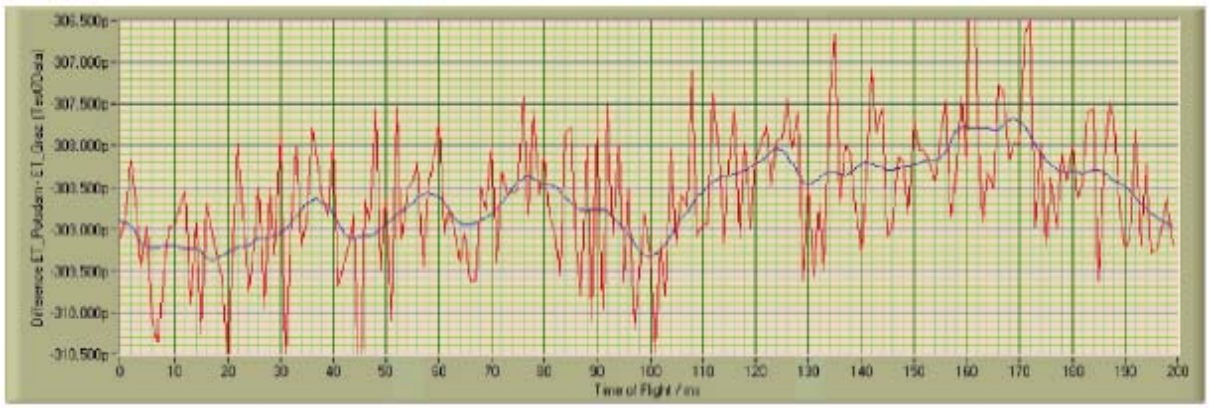

Figure 3. Results of a simulation measurement (obtained at 500 Hz, 11 February 2004)

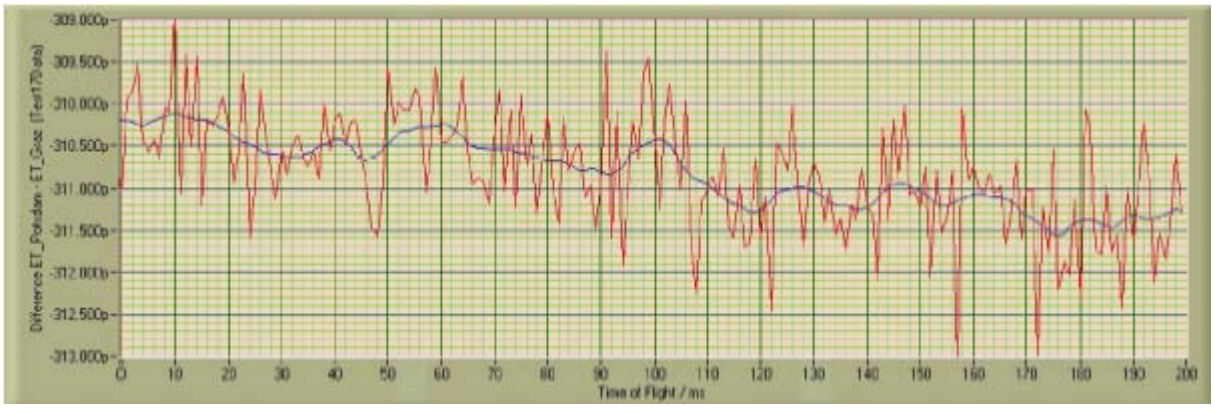

Figure 4. Results of a simulation measurement (obtained at 2000 Hz, 12 February 2004)

In Figures 3 and 4 the results of simulation measurements within the range of 1...200 ms are shown. The full vertical scale is 4 ps. The scatter of the mean values (red curve) is sightly higher in the data obtained on 11 February due to the lower number per point at a reduced rate of data taking (500Hz vs 2000Hz), but there is neither nonlinearity nor drift observable. The variation of the low-pass filtered data (blue curve) is less than 3 ps in both diagrams.

Figure 5 shows a summary of all measurements in a logarithmic scale. This way the range between 100ns...1ms is much better resolved. The linearity is excellent over the full scale. The data from simulation measurements are filtered (blue curves in Figures 3, and 4) tha data from satellite trackings are plotted without any additional filtering and thus show a certain scatter as expected. The RMS of target data is 10...11 ps, that of satellite data about 9 ps.

Because the RMS of the Graz "E.T." is about 4 ps the main part of measured RMS is caused by the A031ET which is an excellent agreement with the RMS data as specified by the manufacturer.

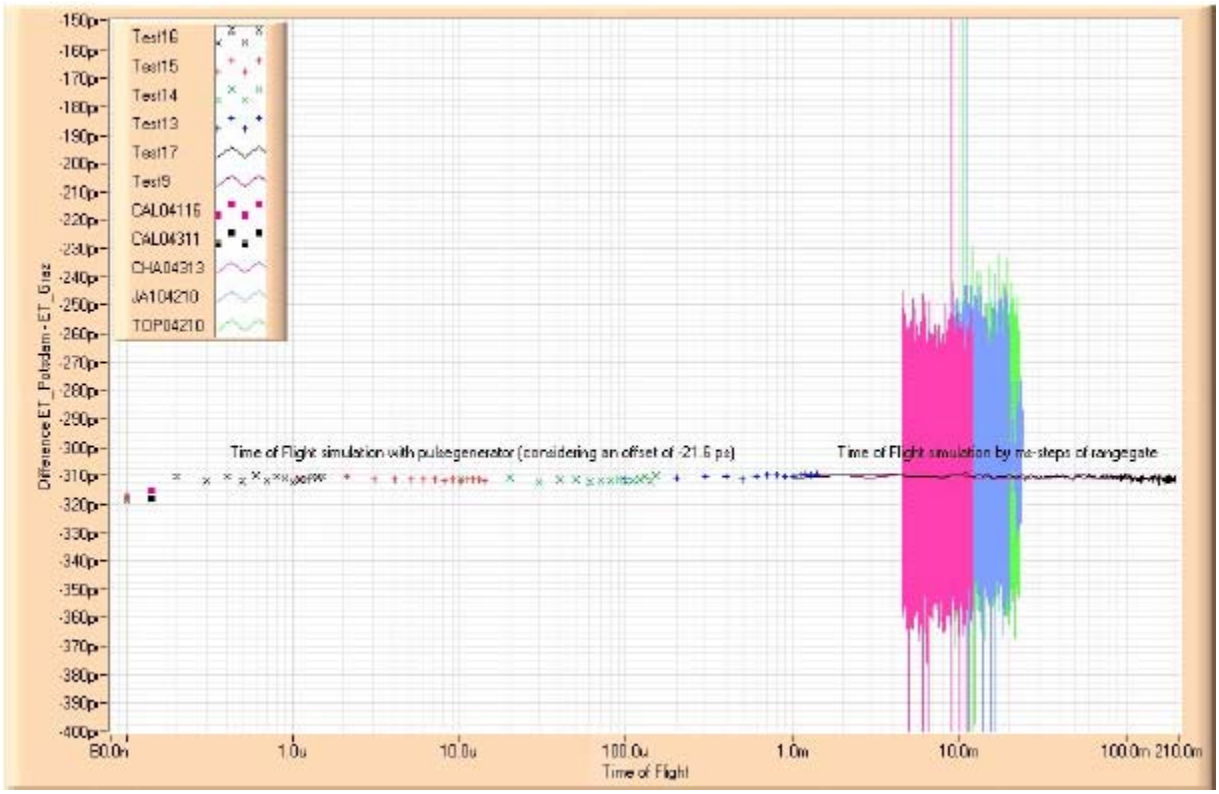

Figure 5. Combined results from all types of linearity measurements.

Assuming that the event timer of the Graz station was well within its linearity specification (<2.5 ps) during the tests, it can be stated that both the temporal stability and non-linearity of the A031-ET are excellent over the full range of SLR ranging intervals. A small offset (in the order of 5 ps) may be present for very short time intervals just exceding the dead time of the event timer. Already for intervals of > 150 ps there is no more sign of such an effect.

This high performance makes the A031-ET an interesting alternative to the SR620 at a comparable price but with much better stability and linearity than the Stanford instrument.

A031-ET Settings for Routine Operation

As already mentioned above, the present hardware layout of the A031-ET with the need of data dumping via EPP poses a certain problem for the use at systems with very high repetition rates which have to operate the A031-ET in the AT (event timer) mode. This was realized by the manufacturer meanwhile, and upcoming versions of the event timer will take into account the special needs of such stations, e.g. bu the use of a cyclic internal buffer and a faster PC interface as USB [Lapuschka, 2004].

For the present 10 Hz SLR systems the Riga instrument can readily be adapted without such modifications already now. The operation software allows for settings of the data taking which satisfy all needs of a 10 Hz system. As a simple way to implement the A031-ET into an existing system we suggest to use the advanced TI mode with a number of events/cycle set of a value of 2 and the number of cycles as high as 100.000. These settings allow the data to be dumped from the internal buffer after the pass, and this way even very long passes of satellites as Lageos, Glonass or Etalon can be observed without overwriting the memory of the A031-ET. The data are internally recorded in binary format which results in relatively small files. Start and stop channels can easily be distinguished within the raw data by the opposite signs which are assigned to A (negative) and B (positive).

References

Artyukh, Yu., Bespal'ko, V., Boole,E. and Lapushka, K. *A010 Family of Time Interval Counters Adapted toSLR Applications*, 13th Intern. Workshop on Laser Ranging, Washington D.C., 2002

Gibbs, Ph. *Range Comparisons Results for Various Eurolas SR Timers*, 13th Intern. Workshop on Laser Ranging, Washington D.C., 2002

Kirchner, G., and Koidl, F., *Graz Event Timing System: E.T.* 12nd Intern. Workshop on Laser Ranging, Matera, 2000

Lapushka, K., private communication 2004

MOUNT MODEL STABILITY

J.McK. Luck
EOS Space Systems Pty.Ltd.
jluck@eos-aus.com, jmckluck@optusnet.com.au, Fax +61 2 6299-6575

The most important factor in mount model stability is to have a stable mount.

Abstract

The ability to acquire an invisible satellite target with minimum delay is vital in autonomous SLR systems as well as those manually operated. It is a particularly stringent requirement in LLR. Yet we don't want to waste hours doing star calibrations too often, so a Mount Model which yields 1 second of arc absolute accuracy for many months is needed.

Since the coefficients of the usual analytically-based Mount Model can yield useful diagnostic engineering information, it is important that they truly represent the errors being modeled, un-corrupted by aliasing from the other errors. There is a great deal of correlation between terms of the usual model, resulting in absurdly high condition numbers in the solution algorithm. For example, terms in secE and tanE are necessarily almost perfectly correlated.

The stability of the model is assessed firstly by the smallness of the pre-fit residuals of subsequent star calibrations, secondly by the variability of the solution coefficients over long periods of time, and thirdly by the condition numbers of the solutions. Some methods for reducing these are given.

The possibility of adding (not replacing) an orthogonal polynomial solution to the usual model is briefly discussed, using even-only or odd-only Legendre Polynomials. If anyone knows of a set of polynomials which are orthogonal over a hemisphere, please let me know!

Preliminary results from the new Mount Stromlo 1-metre telescope suggest that 1 second of arc stability is likely, which is probably due more to its excellent mechanical construction than to any algorithm improvements.

Introduction

Computer control of astronomical telescopes large and small, optical and radio blossomed in the 1970s when computer speeds and interfacing capabilities made it feasible. Before then, pointing and tracking were done by such means as, in 1964: "The telescope for the GODLAS system . . was pointed by a modified Nike-Ajax missile tracking mount controlled by two operators guiding on a sunlit satellite under joystick control. One operator controlled azimuth and the other controlled elevation." (*Degnan, 1996*). See also (*Mueller 1964*). The need for rapid acquisition of faint objects and for perfect tracking in astronomy using ever more automated instrumentation, and for tracking invisible objects day and night in space geodesy, made absolute pointing to a few seconds of arc essential. Pioneering work was done in Australia at Mount Stromlo Observatory (*Hovey, 1974*) and the Anglo-Australian Observatory (*Wallace, 1976; Straede and Wallace, 1976)*) in which both surface-fitting methods and the now-commonplace model-fitting methods were developed (although not necessarily invented) and published. Parallel investigations included use of spherical harmonic functions *(Powell, 1977*) and application to X-Y mounts (*Matzke, 1976*). The first published work in SLR I could find was by Randy Ricklefs (*Ricklefs, 1982*) who applied the model-fitting method to arbitrary mount configurations - some of his old Fortran code survives to this very day.

More recently, the explosion in automated small telescopes has produced popular works on the subject (*Trueblood and Genet, 1997; Wallace, 2004*). And last year Bob Meeks of EOS

Technologies in Tucson completed a detailed critique of model fitting (*Meeks, 2003*) aimed at 1 second-of-arc absolute pointing accuracy.

From very limited data under testing conditions, the precision of absolute pointing on both new telescopes at the EOS Space Research Centre on Mount Stromlo is better than 1.5 seconds of arc, assessed from star calibrations and a 23-coefficient model. Anecdotally (*Moore, 2004*), the accuracy is comparable because tracking biases seldom need to be applied while tracking satellites on the SLR 1.0 metre system.

In this paper, the numerical stability of solutions to the standard model plus variants and competitors is discussed, and various tricks to improve confidence in the coefficient values are studied.

THE MOUNT MODEL

The alignment errors commonly modeled to describe errors observed during star calibrations, whatever the mount configuration, are:

- Encoder zero-point displacements;
- Encoder scales;
- Tilt of the major axis, e.g. the azimuth axis;
- Non-orthogonality of the secondary axis (e.g. the elevation axis) to the major axis;
- Collimation error, i.e. non-perpendicularity of the optical axis to the secondary axis;
- Bending (flexure) in the telescope tube;
- Bending or torsion of the mount, where applicable (e.g. X-axis in alt/alt mount).

Subject to taste, to these are added "empirical terms" describing repeatable patterns of unidentified or speculated physical origin. It is not common to include electronic effects such as servo, following error which should be physically adjusted during installation, or misalignments of the mirrors in the Coude path because they are not mathematically describable in a solvable way. Great care must be exercised when including empirical terms - they must be repeatable night after night, and even so can easily degrade the final solution.

Rigorously, the model is developed by applying a series of rotation matrices to the incoming beam from a star, that is, to the actual direction that the telescope sees after refraction has been applied to the direction in vacuum. Each rotation matrix describes the effect of a particular misalignment. The outputs are the actual encoder readings for the directions seen at the eyepiece or camera when the star is centered by some means. In practice, the mathematics are made more tractable by linearizing, i.e. by assuming that $sin\theta = \theta, \cos\theta = 1$ where θ is the misalignment under consideration. Of course, this implies that the optical and mechanical alignments are sufficiently good that the products of terms neglected in the approximations really are negligible. This always seems to be assumed, and will be here, too. Thus, the model is algebraically linear in its coefficients, and solution by least squares is simple and un-iterated.

The result is a set of Model Equations (Observation Equations if the random error terms were included) in the form suitable for azimuth/elevation mounts:

$$\delta A_i = \sum_{j=1}^{m} c_j F_j(A_i, E_i), \quad i = 1, \ldots, n$$
$$\delta E_i = \sum_{j=1}^{m} c_j G_j(A_i, E_i), \quad i = 1, \ldots, n \qquad (1)$$

where:

δA_i = [encoder reading - refracted position] is the observation residual in azimuth for star *i*, and similarly for the observation residual in elevation δE_i;

c_j, $j = 1, \ldots, m$ are the model coefficients for the *m* terms (in our case, $m = 23$);

$F_j(A_i, E_i)$ is the function in azimuth residual describing the j^{th} misalignment, depending upon the azimuth A_i and elevation E_i of star $i, i = 1, \ldots, n$; and similarly for the function in elevation residual $G_j(A_i, E_i)$. The full model used at Stromlo is given in Table 1.

Table 1: The Stromlo Mount Model.

Term	Description	Azimuth Function (F)	Elevation Function (G)
1	Azimuth encoder offset	1	-
2	Elevation encoder offset	-	1
3	Azimuth axis tilt about North	$-\cos A \tan E$	$\sin A$
4	Azimuth axis tilt about East	$-\sin A \tan E$	$-\cos A$
5	Collimation (optical axis misalign)	$\sec E$	-
6	Non-orthogonality of Az & El axes	$-\tan E$	-
7	Azimuth bearing ellipticity (sin)	$\sin A$	-
8	Azimuth bearing ellipticity (cos)	$\cos A$	-
9	Elevation bearing ellipticity (sin)	-	$\sin E$
10	Elevation bearing ellipticity (cos)	-	$\cos E$
11	Telescope tube flexure	-	$\cot E$
12	Azimuth encoder scale error	$A / 2\pi$	-
13	Elevation encoder scale error	-	$E / 2\pi$
14	Bi-periodic in azimuth (empirical)	$\sin 2A$	-
15	Bi-periodic in azimuth (empirical)	$\cos 2A$	-
16	Elevation encoder stiction (sin)	-	$\sin A$
17	Elevation encoder stiction (cos)	-	$\cos A$
18	Elevation bearing stiction (sin)	-	$E \sin A$
19	Elevation bearing stiction (cos)	-	$E \cos A$
20	Scaled bi-periodic in azimuth (sin)	$\sin 2A \sec E$	-
21	Scaled bi-periodic in azimuth (cos)	$\cos 2A \sec E$	-
22	Bi-periodic in elevation (sin)	-	$\sin 2A$
23	Bi-periodic in elevation (cos)	-	$\cos 2A$
(24)	Observing clock error (not used)	$\sin\phi \cos E - \cos\phi \sin E \cos A$	$\cos\phi \sin A$

Note that the azimuth and elevation residuals are coupled through the coefficients which have effect in both equations, such as the azimuth axis tilt terms. An alternative formulation would describe different coefficients in each of the two residual sets, so that each of the

ModelEquations is completely independent of the other. This was done for the X-Y mount at Orroral (*Luck, 1993*) and worked better there for some unknown reason.

STATISTICS

The statistics of interest are:

$N = 2n$: Number of observations from *n* stars successfully observed;

$\hat{\sigma}_0$: Standard error of unit weight = post-fit RMS of residuals if observations are unweighted;

σ_j: Standard error of coefficient *j*;

ρ_{jk}: Correlation coefficient between coefficients j and k, from the variance-covariance matrix of solved coefficients;

κ : Condition number of the Normal Matrix $\mathbf{N}$. κ is defined (*Dahlquist and Bjorck, 1974*) by:

$$\kappa(\mathbf{N}) = \|\mathbf{N}\|\|\mathbf{N}^{-1}\| \tag{2}$$

where $\|\mathbf{N}\|$ is a given norm of $\mathbf{N}$ in the solution for coefficients $\underset{\sim}{\mathbf{c}}$ in linear equations $\mathbf{N}\underset{\sim}{\mathbf{c}} = \underset{\sim}{\mathbf{u}}$. Then the perturbations $\delta\underset{\sim}{\mathbf{c}}$ arising from input perturbations $\delta\underset{\sim}{\mathbf{u}}$ are characterized by:

$$\frac{\|\delta\underset{\sim}{\mathbf{c}}\|}{\|\underset{\sim}{\mathbf{c}}\|} \le \kappa(\mathbf{N})\frac{\|\delta\underset{\sim}{\mathbf{u}}\|}{\|\underset{\sim}{\mathbf{u}}\|} \tag{3}$$

so κ is a measure of the instability of the solution. A perfectly stable solution gives $\kappa = 1$. Large correlations will give large condition numbers, as the Normal Matrix then tends to singularity.

Table 2: Mount Model solution from 29 star Star Calibration of 23 March 2004.

Number 29. **Sigma-Hat 1.29 arcsec** **Condition Number 0.6577D+06**

Term	Description		δ_Parameter (arcsec)	Sigma (arcsec)
1	(Az) Az encoder offset:	1	4686.38	2.31
2	(El) El encoder offset:	1	-507.56	**194.71**
3	(Both) Az tilt about N:	cosA.tanE	15.17	0.29
4	(Both) Az tilt about E:	sinA.tanE	32.98	0.45
5	(Az) Collimation error:	secE	-125.20	3.09
6	(Az) Non-orthogonality:	tanE	-1.11	2.37
7	(Az) Az bearing ellipt:	sinA	-26.59	0.56
8	(Az) Az bearing ellipt:	cosA	-15.24	0.46
9	(El) El bearing ellipt:	sinE	116.61	**79.27**
10	(El) El bearing ellipt:	cosE	-216.26	**147.41**
11	(El) Tube flexure:	cotE	-18.36	8.94
12	(Az) Az encoder scale:	A/twopi	0.87	0.74
13	(El) El encoder scale:	E/twopi	-1924.44	**1088.51**
14	(Az) Az encoder double-cycl:	sin2A	-0.28	0.65
15	(Az) Az encoder double-cycl:	cos2A	2.01	1.80
16	(El) El encoder stiction:	sinA	-6.56	0.98
17	(El) El encoder stiction:	cosA	-45.57	0.92
18	(El) El bearing stiction:	E.sinA	10.64	1.34
19	(El) El bearing stiction:	E.cosA	29.84	1.02
20	(Az) Double periodic :	sin2A/cosE	-0.51	0.35
21	(Az) Double periodic :	cos2A/cosE	-1.48	1.37
22	(El) Double periodic :	sin2A	-0.34	0.36
23	(El) Double periodic :	cos2A	-0.99	0.39

RESULTS

From a single 29-star calibration on the Stromlo 1.0-metre SLR telescope, the simple solution is given in Table 2:

Note the raw post-fit RMS of residuals, 1.3 arcseconds, which is far better than anything I have ever seen before. However, the condition number of $6.6*10^5$ is huge, as are the highlighted standard errors of coefficients 2, 9, 10 and 13, so big correlations between some of the coefficients are indicated. Accordingly, some of the correlation matrix is shown in Table 3.

Table 3: Correlation coefficients between parameters (coefficients) in Table 2. Extremely high correlations are highlighted.

CORRELATION MATRIX
========== Condition Number : 0.658D+06

Term	1	2	3	4	5	6	7	8	9	10	11	12
2	0.00											
3	0.40	0.00										
4	-0.68	0.00	-0.40									
5	**-0.97**	0.00	-0.28	0.64								
6	**-0.90**	0.00	-0.10	0.57	**0.97**							
7	-0.41	0.00	-0.26	0.68	0.38	0.33						
8	0.16	0.00	0.61	-0.27	-0.08	0.00	-0.15					
9	0.00	**0.94**	0.00	0.00	0.00	0.00	0.00	0.00				
10	0.00	**-1.00**	0.00	0.00	0.00	0.00	0.00	0.00	**-0.96**			
11	0.00	**-0.92**	0.00	0.00	0.00	0.00	0.00	0.00	-0.72	**0.88**		
12	0.00	0.00	0.05	0.14	0.02	0.02	-0.14	-0.03	0.00	0.00	0.00	
13	0.00	**-0.99**	0.00	0.00	0.00	0.00	0.00	0.00	**-0.97**	**1.00**	**0.87**	0.00

There are some correlations with effectively $|\rho_{jk}| = 1.00$, hence the Normal Matrix is singular so should not be inverted as it stands. This has got nothing whatsoever to do with floating point precision; it shows true intrinsic instability.

STABILITY IMPROVEMENT

Four ways have been tested to improve the stability of mount model solutions.

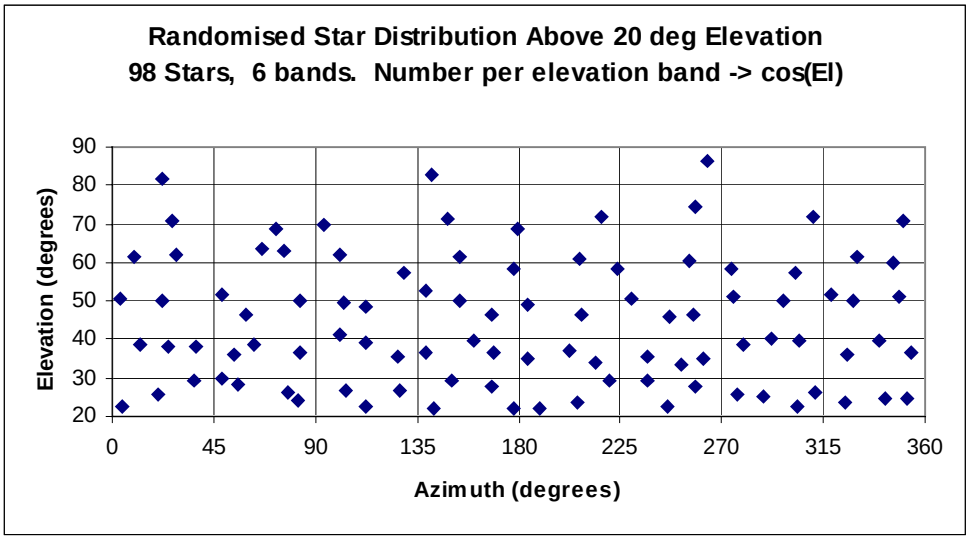

Figure 1: Proposed centres of search regions for equal-sky-area star distribution.

1. Star Distribution

Obviously, it is necessary in the star calibration to sample the entire region of the sky over which satellites are going to be tracked. It is particularly important in alt-az systems to observe stars as close to the zenith as possible because of the "keyhole" there, leading to terms like $\tan E$, and for all mounting systems close to the horizon because of $\cot E$ terms as with tube flexure. The implications of observing in azimuth outside the range $0 \le A \le 2\pi$ must be carefully considered, too, for this is generally done to cope with cable wrap-around strategies and could introduce discontinuities in the azimuth scale - especially if there is a gap in the encoder tape. (There were no such problems with the Orroral X-Y mount: the "keyholes" were on the un-reachable horizon, both axes were restricted to only half a revolution, and cable wrap-around was non-existent. Perfect, really.)

An algorithm has been devised to produce star distributions covering equal areas of sky for any selected number of stars between nominated elevation limits. The results for 98 stars between 20^o and 90^o elevation are illustrated in Fig. 1, and could be used to choose the centres of little regions from which real stars are selected from the catalogue. Details may be obtainable from the author.

It hardly needs saying that as many stars as possible should be observed, the only constraint being the observing time available. Centering on the "cross-hairs" must be free of parallax, which is not always possible even when using a camera and display screen; and the cross-hair or fiducial spot must be bore-sighted with the transmitted laser beam. (Once again, at Orroral the fiducial spot was the small fraction of the laser beam reflected from the Spider Retroreflectors (*Luck, 2004a*) through the dichroic tertiary mirror into an eyepiece at the Cassegrain focus.)

2. Parameter Deletion

One of the perils of using least-squares is over-fitting in an attempt to reduce the overall RMS. Terms 5 and 6 are collimation error and axes non-orthogonality whose respective functions in azimuth are $\sec E$ and $\tan E$. Their correlation coefficient in Table 3 is 0.97. Now:

$$\sec E = \pm\sqrt{\left[1+\tan^2 E\right]},\ \text{i.e. } \sec E \approx \tan E \text{ as } E \to \pi/2 \qquad (4)$$

so they are virtually indistinguishable at high elevation angles, hence really cannot be separated. Another example is terms 2 (elevation encoder offset) and 11 (tube flexure) in elevation, whose functions are 1 and $\cot E$, respectively, and whose correlation coefficient is -0.92. *Prima facie* they should be well separable, but both are influenced jointly by other correlations.

Some of these coefficients can be deleted from the solution - but great care is needed. Incorrect choices can lead to considerable blow-out in the RMS of residuals with consequent degradation in the predictive power of the solution, i.e. the model will then be under-fitting the observations. One way around this is to delete first the coefficient which has the largest number of large correlations. In Table 3, parameters 2 and 13 each have 4 huge correlations. We would choose to delete 13 (elevation encoder scale) first because parameter 2, the elevation encoder offset, is physically a much more fundamental item. The choice is actually made easier by the methods of the next section.

3. Normalizing to the Means

As a simple introduction, suppose a set of observations $(t_i, y_i), i = 1,\ldots,n$ are related by the straight line $y_i = a + bt_i$. Imagine that the times t_i are expressed in full Julian Dates, but the data only span this year. Then the intercept *a* gives the value at Jan 0.5, 4713BC which is of no interest to anyone. Further, there is a great correlation between *a* and *b* because a small change in the slope *b* will produce a huge change in *a* so far back in history. The correlation coefficient is numerically real but totally misleading (except perhaps to archaeologists . . .). However, if the model is expressed as $y_i = a + b(t_i - \bar{t})$ where $\bar{t}$ is the mean of this particular data set then there is zero correlation between the solution values of *a* and *b*. On the other hand, if the observations are repeated in some other time span, the new value of *a* will be different, so this trick is a mixed blessing.

This trick can be applied to star calibrations, with the advantage that the data span is always (nominally) the same because the same region of sky is sampled every time. In analogy to $\bar{t}$ above, define for each F_j about its mean $\bar{F}_j$ over the observable cap of sky:

$$\bar{F}_j = \int_{A=0}^{2\pi}\int_{E=E_0}^{\pi} F_j(A,E)\cos E\,dE\,dA \Big/ \int_{A=0}^{2\pi}\int_{E=E_0}^{\pi} \cos E\,dE\,dA \tag{5}$$

and similarly with each $\bar{G}_j, \quad j = 3,\ldots,m$ (the constant term in each series is not modified). Each of these means is a number, not a function. The model equations (1) then become:

$$\begin{aligned} \delta A_i &= \sum_{j=1}^{m} c_j' \left[F_j(A_i,E_i) - \bar{F}_j \right], \quad i = 1,\ldots,n \\ \delta E_i &= \sum_{j=1}^{m} c_j' \left[G_j(A_i,E_i) - \bar{G}_j \right], \quad i = 1,\ldots,n \end{aligned} \tag{6}$$

It turns out that $c_j' = c_j,\ j = 3,\ldots,m; \quad c_1' = c_1 + \sum_{j=3}^{m} c_j \bar{F}_j; \quad c_2' = c_2 + \sum_{j=3}^{m} c_j \bar{G}_j$. All the variation due to differing star distributions from star cal to star cal are then absorbed into the constant terms 1 and 2 which thus become the prime criteria for the numerical stability of successive solutions.

This concept was tested by simulations, including some with perturbations in the "true" star positions arising from interpolation errors as found in (*Luck, 2004b*). As will be seen in Table 4, it reduces the condition number by a factor of about 10, i.e. from huge to large. It also reduces the number of large correlation coefficients substantially, making it much easier to select terms for deletion. On the basis of the simulations and of this "normalization to the means", a good selection of terms to delete is 6, 9, 11, 13 and 15 which results in a negligible increase in residual RMS from 1.29 to 1.32 seconds of arc for the real data. Deletion of these terms also yields a dramatic decrease in condition number from 658,000 to 37 and removal of even more terms from the list of large correlation coefficients.

4. Use of Prior Information

The local tie surveys give results *inter alia* for the non-orthogonality between axes and for the components of azimuth axis tilt away from vertical, and their variances (*Dawson et al, 2004*). They can be used as weighted constraints upon these parameters which is a simple application of Bayesian inference using prior information. In this case the weights must be proportional to the inverse variances both in the constraints and in the original observations,

Table 4: Comparison of solutions with and without normalization and deletions.

Item	**23-Term Solutions**		
Solution Type	*Raw*	*Normalized*	
Terms Deleted	0	0	6,9,11,13,15
Az Post-fit RMS	0.8	0.8	0.8
El Post-fit RMS	1.2	1.2	1.3
Total Post-fit **RSS**	1.3	1.3	1.5
Residuals RMS	1.29	1.29	1.32
Condition Number	6.60E+05	6.80E+04	32.4
Solution Values			
1 Az Encoder	4686.38	4459.23	4458.75
2 El Encoder	-507.56	-837.63	-838.01
3 Az Axis Tilt @ N	15.17	15.17	15.50
4 Az Axis Tilt @ E	32.98	32.98	32.92
5 Collimation	-125.20	-125.20	-124.82
6 Non-Orthogonality	-1.11	-1.11	-
7 Az Bearing sinA	-26.59	-26.59	-26.64
8 Az Bearing cosA	-15.24	-15.24	-15.03
9 El Bearing sinE	116.61	116.61	-
10 El Bearing cosE	-216.26	-216.26	45.76
11 Tube Flexure	-18.36	-18.36	-
12 Az Encoder Scale	0.87	0.87	0.92
13 El Encoder Scale	-1924.44	-1924.44	-
14 Az Enc.Bi-periodic	-0.28	-0.28	0.20
15 Az Enc.Bi-periodic	2.01	2.01	-
16 El Encoder Periodic	-6.56	-6.56	-6.68
17 El Encoder Periodic	-45.57	-45.57	-44.95
18 El Bearing Stiction	10.64	10.64	10.19
19 El Bearing Stiction	29.84	29.84	28.91
20 Az Enc.Bi-modified	-0.51	-0.51	-0.88
21 Az Enc Bi-modified	-1.48	-1.48	-0.04
22 El Enc.Bi-Periodic	-0.34	-0.34	-0.33
23 El Enc.Bi-periodic	-0.99	-0.99	-1.14

and the standard error of unit weight ($\hat{\sigma}_0$) becomes a measure of how well the weights have been assigned, the goal being 1.0.

Table 5 summarizes the inputs and statistical results of applying prior information in several ways, as well as the effects of "normalizing to the means" and of deleting the five parameters from the solution. In all cases the initial guesses of the solution values are all zero, so deleted coefficients remain zero. The software can handle incremental updating wherein previously determined values are held fixed, but that feature might give too optimistic a picture here. The results in Table 5 show that the changes in parameter values caused by the available constraints are not especially severe even when the constraints are "tight", i.e. have relatively large weights. All that this really shows is that the constraints chosen are consistent with the observations.

SPHERICAL HARMONIC MODEL

An alternative approach to equation (1), which uses physically identifiable models, is to fit a surface model which is completely empirical. This might satisfy the primary purpose of

Table 5: Solutions with prior information. Results for constrained parameters are highlighted. The columns labeled "Prev Sol'n" use values and standard errors from an un-constrained solution, as a sanity check. Units are seconds of arc.

	Full Sol'n	**Constrained Solutions of 23-Term Model**						
Solution Type	*Raw*	*Normalized*						
Terms Deleted	Nil	Nil			6, 9, 11, 13, 15			
Constraints	Nil	Nil	GA Survey	Prev. Sol'n	Nil	GA Survey		Prev .Sol'n
			Loose	Tight	Tight		Loose	Tight	Tight
Prior Information Input									
S.E. of star obs			1.5	1.32	1.32		1.5	1.32	1.32
(3) Tilt @ N			21.0	21.0	15.5		21.0	21.0	15.5
s.e.			30.0	1.5	1.3		30.0	1.5	1.3
(4) Tilt @ E			42.4	42.4	32.9		42.4	42.4	32.9
s.e.			30.0	1.5	1.3		30.0	1.5	1.3
(6)Non-orthogonality			26.1	26.1	-1.1		26.1	26.1	-1.1
s.e.			10.0	1.5	1.3		10.0	1.5	1.3
Statistics Output									
Az post-fit RMS	0.8	0.8	2.1	5.2	1.0	0.8	2.1	10.1	1.7
AzcosE post-fit RMS	0.6	0.6	0.6	1.8	0.6	0.7	0.6	1.1	0.6
El post-fit RMS	1.2	1.2	1.2	1.2	1.2	1.3	1.3	1.3	1.3
Total post-fit **RSS**	1.3	1.3	1.4	2.1	1.3	1.5	1.5	1.7	1.5
Sigma Unit Weight $(\hat{\sigma}_0)$	1.29	1.29	0.88	1.63	0.89	1.32	0.89	2.96	0.92
Condition Number (κ)	658000	68300	68300	68300	68300	32.4	18.0	13.3	12.5
Num.Correlations>0.8	15	9	10	8	8	2	3	1	1
Solution Values									
1 Az encoder offset	4686.38	4459.	4459.	4461.	4459.	4458.	4458.	4459.	4458.7
2 El encoder offset	-507.56	-837.6	-837.6	-837.6	-837.6	-838.0	-838.0	-838.0	-838.0
3 Az axis tilt about N	**15.17**	**15.17**	**15.17**	**17.11**	**15.15**	**15.50**	**15.37**	**16.77**	**15.4**
4 Az axis tilt about E	**32.98**	**32.98**	**32.79**	**37.59**	**32.70**	**32.92**	**32.50**	**36.82**	**32.67**
5 Collimation error	-125.20	-125.2	-118.8	-92.27	-125.1	-124.8	-124.7	-124.4	-124.7
6 Non-orthogonality	**-1.11**	**-1.11**	**3.68**	**23.64**	**-1.04**	-	-	-	-
7 Az bearing (sin A)	-26.59	-26.59	-26.78	-23.73	-26.84	-26.64	-26.96	-24.20	-26.85
8 Az bearing (cos A)	-15.24	-15.24	-15.24	-13.93	-15.28	-15.03	-16.17	-14.31	-15.16
9 El bearing (sin E)	116.61	116.6	116.6	116.6	116.6	-	-	-	-
10 El bearing (cos E)	-216.3	-216.3	-216.3	-216.3	-216.3	45.76	45.76	45.76	45.76
11 Tube flexure	-18.36	-18.36	-18.36	-18.36	-18.36	-	-	-	-
12 Az encoder scale	0.87	0.87	0.81	1.15	0.77	0.92	0.81	0.98	0.82
13 El encoder scale	-1924.4	-1924.	-1924.	-1924.	-1924.	-	-	-	-
14 Az encoder (sin 2A)	-0.28	-0.28	0.10	1.32	0.16	0.20	0.56	1.80	0.61
15 Az encoder (cos 2A)	2.01	2.01	3.57	8.35	2.14	-	-	-	-
16 Az bearing in El (sinA)	-6.56	-6.56	-6.56	-8.50	-6.54	-6.88	-6.55	-7.95	-6.58
17 Az bearing in El (cos A)	-45.57	-45.57	-45.76	-40.97	-45.86	-44.95	-45.37	-41.05	-45.20
18 El stiction (Esin A)	10.64	10.64	10.64	10.64	10.64	10.19	10.19	10.19	10.19
19 El stiction (Ecos A)	29.84	29.84	29.84	29.84	29.84	28.91	28.91	28.91	28.91
20 Az mod.bi-period (sin)	-0.51	-0.51	-0.71	-1.65	-0.78	-0.88	-1.11	-2.12	-1.15
21 Az mod.bi-period (cos)	-1.48	-1.48	-2.77	-6.88	-1.57	-0.04	0.10	0.10	0.10
22 Az bearing in El (sin2A)	-0.34	-0.34	-0.34	-0.34	-0.34	-0.33	-0.33	-0.33	-0.33
23 Az bearing in El (cos2A)	-0.99	-0.99	-0.99	-0.99	-0.99	-1.14	-1.14	-1.14	-1.14

Mount Modelling, which is to provide the best possible pointing predictions for satellite tracking. The natural functions to use over a sphere such as the whole sky are the Legendre Polynomials $P_{nm}(A,E)$, which are orthogonal over the whole sphere given a uniformly dense set of observations (*Heiskanen and Moritz, 1972*). However, there are at least four problems:

1) I am not sure how well they cope with the zenith "keyhole".
2) The available sky is rather less than a hemisphere, so not all the polynomials will be orthogonal hence there will necessarily be correlations between some of the

coefficients. If only odd-degree terms are used, they are orthogonal over a hemisphere but the risk of under-fitting is severe.

3) The number of terms increases rapidly with the maximum degree chosen, so one could easily run out of degrees of freedom.
4) There can be no cross-coupling between the azimuth and elevation residuals such as occurs through the tilt terms in the physical model, so completely independent solutions are required on each axis, which halves the number of observations available for each solution.

Nevertheless, some study was made of this approach on the same realistically simulated data sets as used for testing the physical model approach. A more extensive report will be prepared later, but the preliminary results suggest that the spherical harmonic approach is considerably inferior. A possibility is to fit spherical harmonics to the post-fit residuals after a physical-model solution - provided that the coefficients thereby produced are repeatable over many data sets. It is emphasized that such coefficient repeatability is also required for the empirical and exotic terms included in the physical model approach.

REPEATABILITY OF SOLUTIONS

The acid test is to compare the coefficient values obtained from one night to the next, and month after month. Regretfully, only one data set has become available in usable form (computer crashes have spoilt May's data), so this assessment must wait until another day. (Subsequent star cals indicate the need for even deeper investigations.)

CONCLUSIONS

This study in effect has been a search for the perfect (matrix) inversion which will give a mount model solution which can be used with absolute confidence to predict celestial positions at all azimuths and at all elevations from the horizon right up to the zenith, year after year, from limited numbers of stars observed in each calibration session.

One of the real practical difficulties is finding and observing stars close to the zenith. The model is therefore often required to extrapolate towards zenith. This aspect alone, in my opinion, justifies the effort required in this study. Otherwise, surface-fitting techniques such as fitting Legendre Polynomials might be considered purely as an interpolation strategy, but they have some conceptual problems and simulations suggest that they are less than satisfactory.

By far the largest problem with the physical model approach is trying to fit too many terms. The process of "normalizing to the means" greatly facilitates identification of superfluous terms which, when deleted, hugely improves the Normal Matrix condition for inversion, i.e. takes it well away from being singular, with consequent massive increase in confidence in the solution values. The correct choice of terms will barely affect the residual RMS, which is only one of the criteria upon which the accuracy of the model should be judged.

Despite the aids mentioned above, the selection of terms for deletion was still somewhat arbitrary. The experience gained when more data become available will guide a maybe even better selection.

A pointing precision of 1.5 seconds of arc can certainly be claimed for the Stromlo SLR 1.0 metre telescope. There is high confidence that accuracy and stability will be at the same level, and that all will produce sub-arcsecond absolute pointing in the very near future.

None of which would be possible without the extraordinary mechanical stability of the telescope.

ACKNOWLEDGEMENTS

Prof. Urho A. Uotila, Department of Geodetic Science, The Ohio State University, for his inspired, stimulating, exhaustive and exhausting courses in Least Squares Adjustments.

Chris Moore, EOS Space Systems Pty.Ltd., for acquiring and re-formatting the real data used.

Adrian Loeff, EOS Technologies Inc. (EOST), for developing many of the empirical terms, and Bob Meeks of EOST for many fruitful discussions.

REFERENCES

Dahlquist, G. and Bjorck, A.: "*Numerical Methods*", Prentice-Hall, Inc. (1974)

Dawson, J., Johnston, G., Naebkhil, S., Govind, R. and Luck, J.: "*The Mount Stromlo Satellite Laser Ranging (SLR) System Local Tie Connections Before and After the 2003 Destructive Canberra Fires*", these Proceedings (2004)

Degnan, J.J.: "*Thirty Years of Satellite Laser Ranging*", Proc. 9th International Workshop on Laser Ranging Instrumentation, Canberra, Australia, 7-11 November 1994, Ed. J.McK. Luck, Vol. 1, pp. 8-20, AGPS (1996)

Hovey, G.R.: "*Software Corrections of Astronomical Telescope Pointing Errors*", Ph.D thesis, Dept. Engineering Physics report EP-T18, Australian National University (Jan. 1974).

Luck, J.McK.: "*Performance of the Upgraded Orroral Laser Ranging System*", Proc. 8th International Workshop on Laser Ranging Instrumentation, Annapolis, MD, 18-22 May 1992, Ed. J.J. Degnan, NASA Conf. Publ. 3214, p. 11-6ff (1993)

Luck, J.McK.: "*Five Target System Calibration*", these Proceedings (2004a)

Luck, J.McK.: "*Is Your Performance being Ruined by Interpolation Errors?*", these Proceedings (2004b)

Matzke, D.E.: "*An Error Model for an X-Y Antenna*", DBA Systems, Inc. internal report (April 1976)

Meeks, R.L.: "*Improving Telescope Mechanical Error Estimates Using Pointing Data*", Ph.D dissertation, Dept. Mechanical Engineering, Colorado State University (Spring 2003)

Moore, C.: Private communication (1 June 2004)

Mueller, I.I.: "*Introduction to Satellite Geodesy*", Frederick Ungar Publishing Co. (1964)

Powell, M.E.: "*Computer Correction of Absolute Telescope Pointing Errors by Use of Spherical Harmonic Functions*", M.S.Eng. thesis, The University of Texas at Austin (Dec. 1977)

Ricklefs, R.L.: "*Orienting a Transportable Alt-Azimuth Telescope*", Proc. 4th International Workshop on Laser Ranging Instrumentation, Software Sessions, Ed. P.J. Shelus, University of Texas Publications in Astronomy, No. 19, pp. 289-295 (Aug. 1982)

Straede, J.O. and Wallace, P.T.: "The Anglo-Australian 3.9 metre Telescope: Software Controlled Slewing, Setting, and Tracking", Publ. Astronomical Society of the Pacific, Vol. 88, No. 525, pp. 792-802 (Oct. 1976)

Trueblood, M. and Genet, R.M.: "*Telescope Control*", 2nd ed., Willman-Bell Inc. (1997)

Wallace, P.T.: "*AAT Pointing: Analysis and Models*", Anglo-Australian Observatory internal report (Oct. 1976)

Wallace, P.T.: "Telescope Pointing", Tpoint Software, www.tpsoft.demon.co.uk/pointing.htm (Feb. 2004)

SIGNAL STRENGTH MONITOR FOR C-SPAD RECEIVER

Ivan Prochazka, Karel Hamal
Czech Technical University in Prague. Brehova str. 7, 115 19
Prague 1, Czech Republic
prochazk@mbox.cesnet.cz phone +420 723 920 786, fax +420 224 922 822

Abstract

We are reporting on the possibility of echo signal strength monitoring in the C-SPAD based laser ranging systems. Theoperating principle and the experimental results will be presented. The Signal Strength Monitor SSM has been incorporated into the Portable Pico Event Timer 2k. The standalone electronics device has been designed, it determines the photon number estimate in a receiver chain based on C-SPAD detector package. The device is interfaced to a station computer via conventional serial link.

GOALS

- to estimate the echo signal strength in laser ranging based on C-SPAD detector
- the SPAD chip current pulse risetime depends on photon number *(Kirchner, Koidl, 1995)*
- C-SPAD circuit provides two output timing pulses, their interval corresponds to the detected signal energy
- to construct the Time to Digital Converter to record the interval and hence the echo signal energy

C-SPAD Detector Package # 0406

Measured: Delay (Comp-Uncomp Output) with PPET

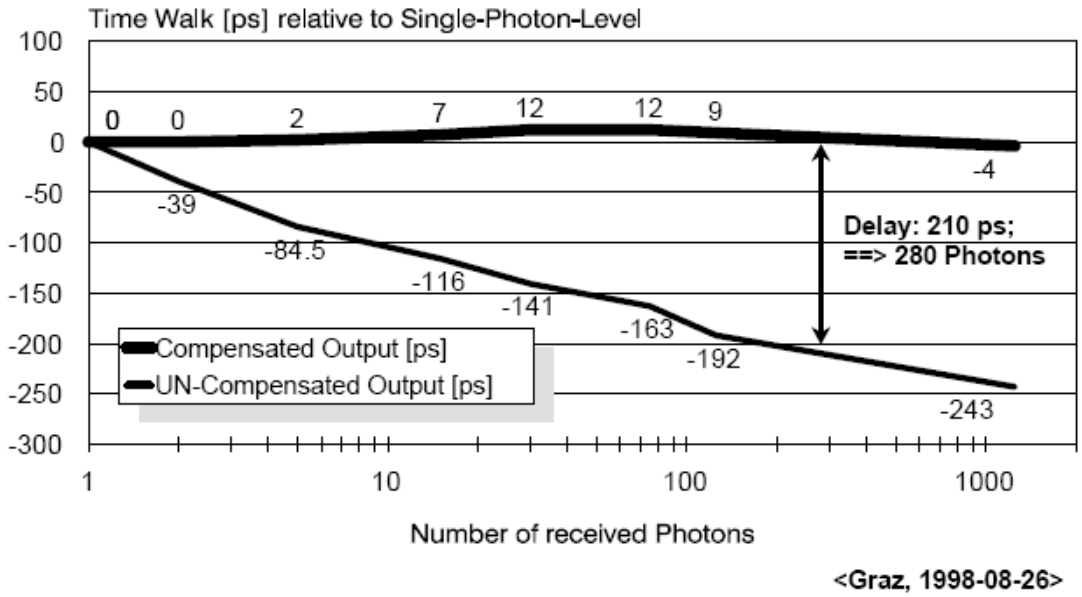

<Graz, 1998-08-26>

- avalanche build up time effect expanded by built-in circuit *(G.Kirchner, F.Koidl)*
- large data sets averaging

SLR with Photon Number Estimate

RMS vs. Received # of Photons

Rec. Energy: Meas. by PPET (Compens.Delay)

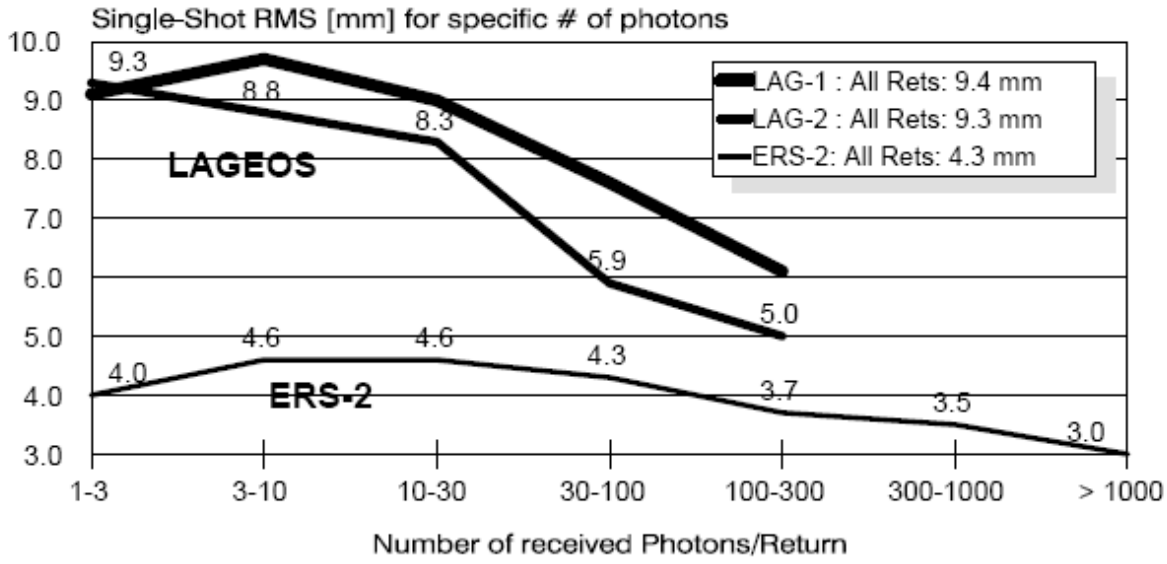

<Graz, 1998-09-11>

G. KIRCHNER1), F. KOIDL1), I. PROCHAZKA2), K. HAMAL2,,11th WLRI, Deggendorf, 1998

Photo Number Estimate Indoor Calibration Tests

- compensated versus un-compensated output
- shot by shot data processing
- PET4 timing, NdYAG 32 ps @ 532 nm, indoor

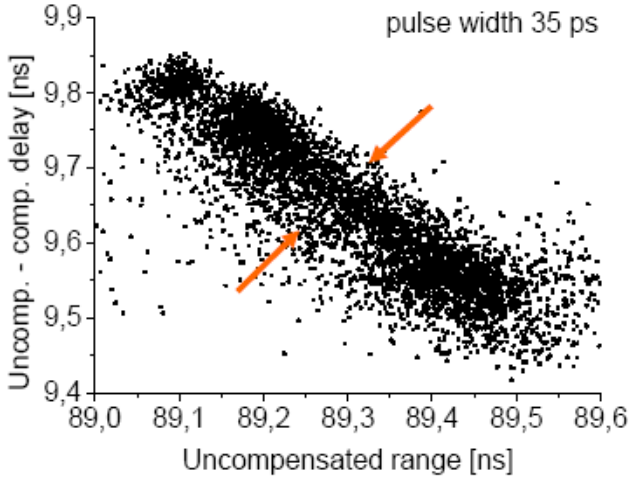

1 PE 10 PE 100 PE 1000 PE

- data spread ~ 50 ps rms
- = > **ultimate photon number resolution 3 x**

J. Blazej et al, NIST-ARDA Workshop on Single Photon Detectors,NIST, Washington DC, 2003

Time to Digital Converter for C-SPAD Based Energy Monitor

REQUIREMENTS:

- resolution 20 ps
- range 8 bits / ~ 1.6 ns
- dead time < 400 us

DESIGNED CIRCUIT

- time expander, capacitor charge / discharge
- expansion factor ~ 2ooo x
- digital counter 30 / 15 ns on Programmable Gate Array

Time to Digital Converter Calibration

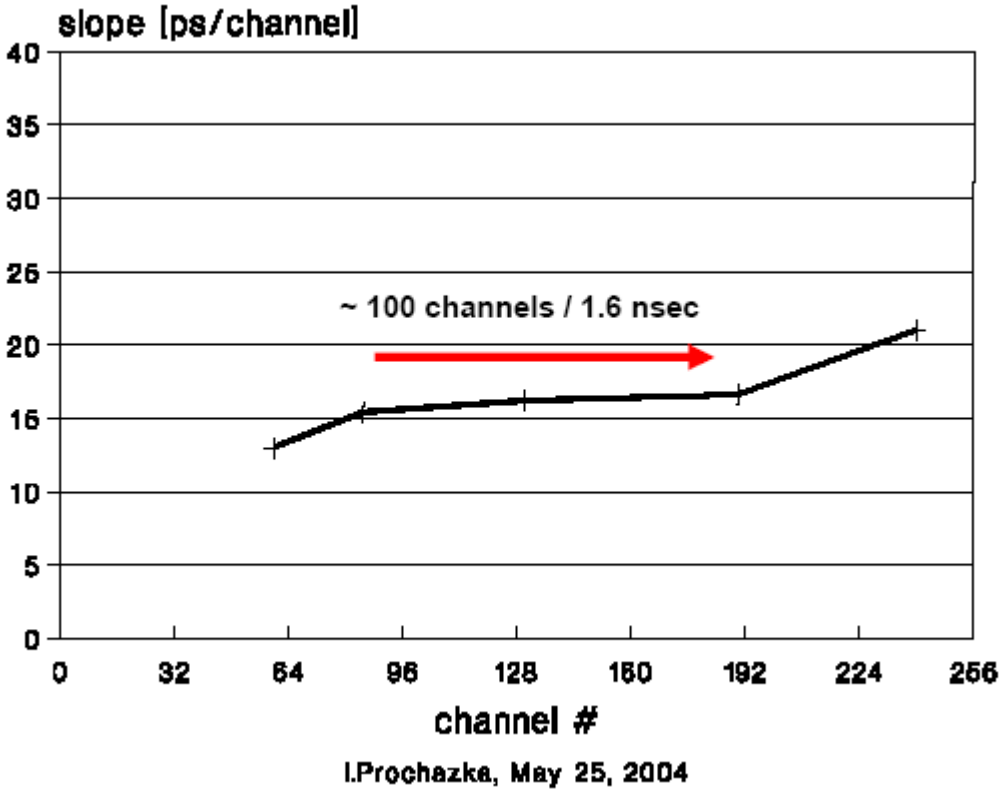

Indoor Laser RangingTest

Prague, June 2, 2004, 2 kHz, 32 ps laser diode, C-SPAD, PET2k

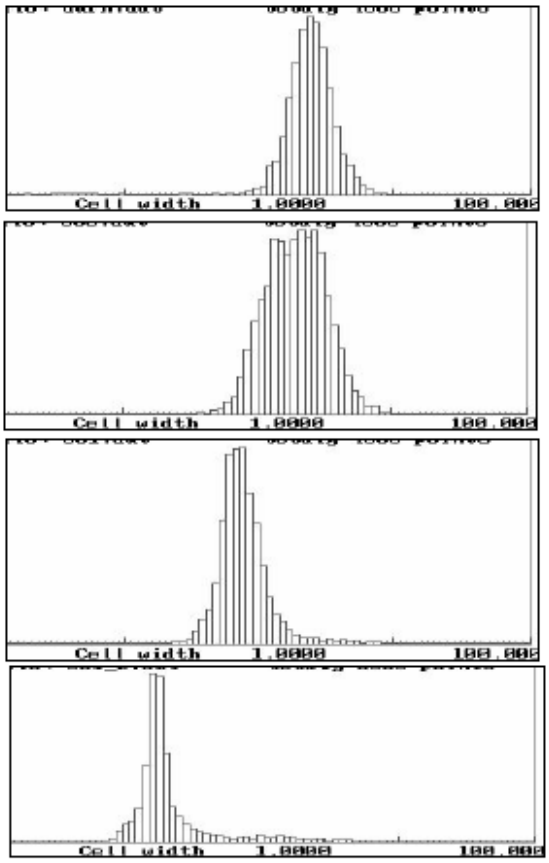

- 1 PE dark count — 23 ps rms
- 1 ~ 10 PE — 23 ps
- ~ 100 PE — 12 ps
- ~ 1000 PE — 8 ps

Ground Target Laser Ranging Energy Spectrum

Graz, May 5, 2004, 2 kHz, 8 ps laser, C-SPAD, PET2k

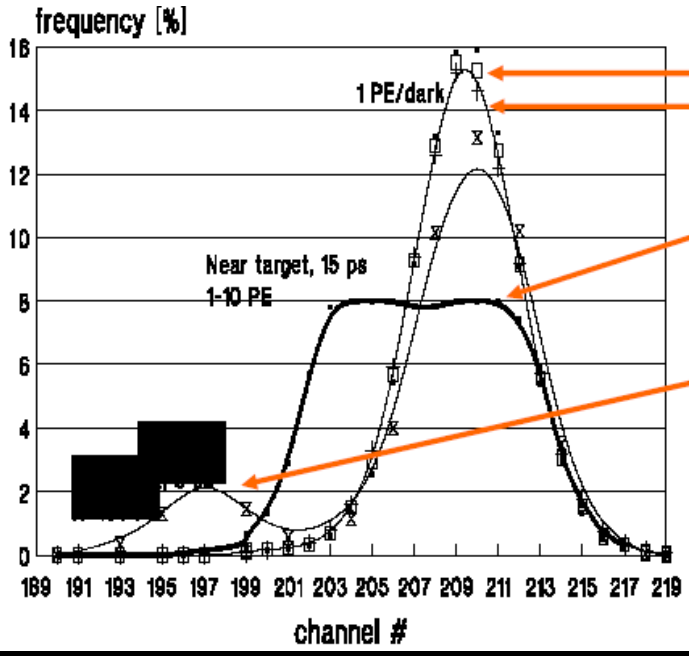

dark counts / stability
2 series, 24 hours apart

1 m ground target ranging
1 - 10 PE, 15 ps rms

4 km ground target ranging
~ 1000 PE, 6 ps rms

CONCLUSION

- the C-SPAD based receiver package energy monitor has been constructed and tested
- FEATURES:
- built in the PET2k
- 7 energy levels resolution / shot - by – shot 1-3, 3-10, 10-30, 30-100, 100-300,300-1000, > 1000
- self - calibrating /via dark counts on 1 PE/
- temperature & temporal stability < 0.1 ch / day
- STAND BY device of the C-SPAD energy monitor has been constructed and is available for SLR stations operating C-SPAD

NUMERICAL NOISE IN SATELLITE LASER RANGING DATA PROCESSING

Ivan Prochazka (1), Georg Kirchner (2)
(1) Czech Technical University in Prague. Brehova str. 7, 115 19 Prague 1, Czech Republic
prochazk@mbox.cesnet.cz phone +420 723 920 786, fax +420 224 922 822
(2) Satellite Laser Station Graz Lustbuehel, Graz, Austria

Abstract

The SLR station Graz is producing millimeter precision ranging data at a return rate of 2 kHz. Ranging to terrestrial targets, the ranging precision below 1 mm is achieved, ranging to low pulse spreading satellite, the precision of 2-3 mm is achieved. These ranging data sets have been analyzed / smoothed using two different algorithms and working groups. The first solution has been based on the polynomial fitting, the second one on the orbital fitting approach. The computed o-c residuals have been compared for both solutions on a shot by shot basis. These differences are on single picosecond level, just indicating the order of magnitude of a numerical noise within the SLR data processing algorithms.

GOALS

- WHAT CAN WE GET FROM 2kHz / mm large volumes data averaging ?
- To optimise the procedure for 2kHz millimeter ranging data processing
- To estimate the performance of the SLR data processing software:
  - fitting algorithms (orbit, residuals) accuracy
  - numerical noise of the computation

PHILOSOPHY

- numerical experiments based on Graz SLR data Oct.2003 -Jan 2004 2 kHz / C-SPAD, rms < 3mm
- satellite signature eliminated by single CCR echoes / data selection
- inter-comparison of two completely independent data processing / fitting algorithms on a echo-by-echo basis: Graz SLR X Portable Calib. Standard PET2k
- MERIT2 data format : 1 psec granularity

SLR DATA FITTING PROCEDURES COMPARED

- Graz SLR data fit

- orbit IRVINT integrator, 1 minutes x,y,z
- 8-pt Lagrange interp., topocentric conversion
- optional manual RB / TB tuning
- Polynomial fitting, standard scheme, deg. 5-10 (20)
- data screening / editing

- Portable Calibration Standard 2k

- orbit RGO integration, 1 minutes x,y,z
- 8-pt Lagrange interp., topocentric conversion
- automated RB / TB / DUT tuning
- Iterative polynomial fitting & automated data editing

SLR DATA SAMPLE USED FOR TESTS

2 ns

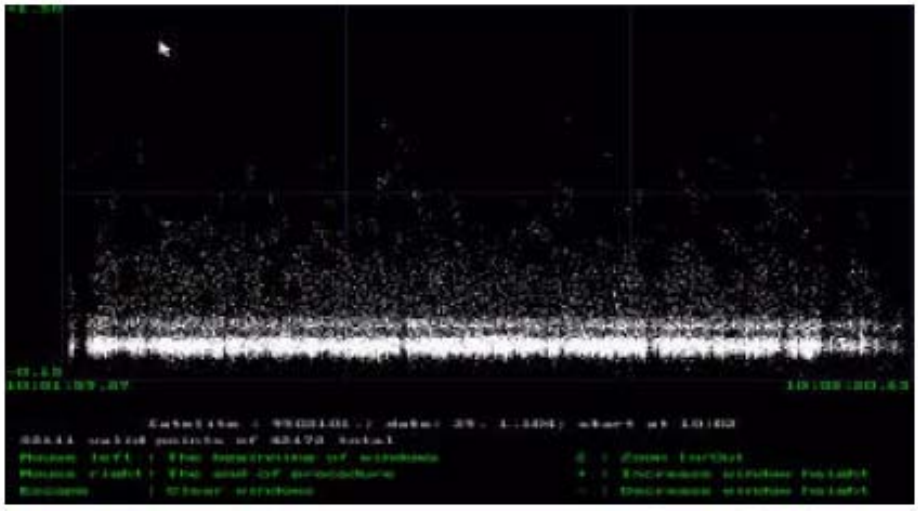

- ERS-2 Jan 29, 2004, 10 h UT, 86 deg. max. elevation,
- first 80 seconds of tracking selected, 32 000 echoes
- note two retro response, the first one used, only

SAMPLE SLR DATA FITTING

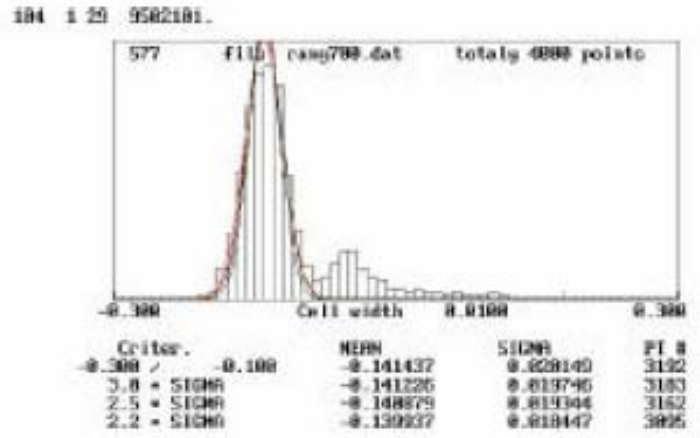

- ERS-2 Jan 29, 2004, 10 h UT, 86 deg. max. elevation,
- first 80 seconds of tracking selected, 32 000 echoes
- PCS data fit,
  - the first retro => 18 ps RMS (1-10 PE)
  - the second retro => 22 ps RMS (1 PE)

SLR DATA RESIDUALS COMPARISON

Graz - PCS2k residuals differences

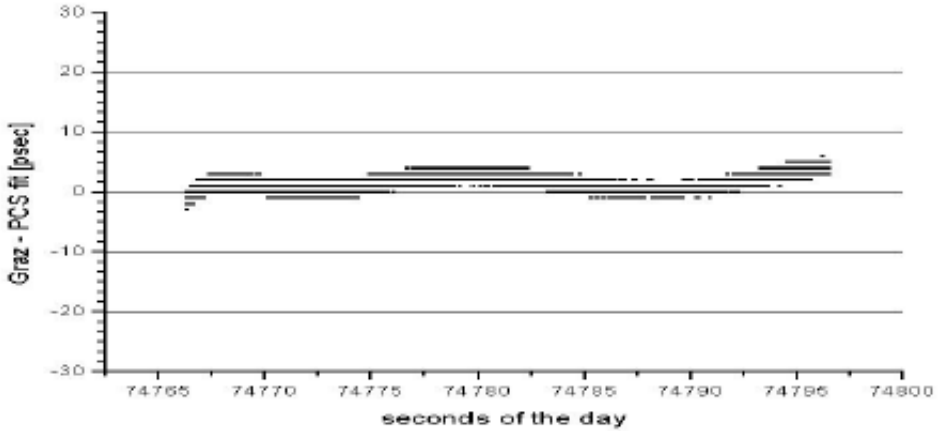

- random / numerical noise / format < 1 ps RMS
  < 2 ps half p-p
- slowly varying +/- 3 ps half p-p

NORMAL POINT CONSTRUCTION

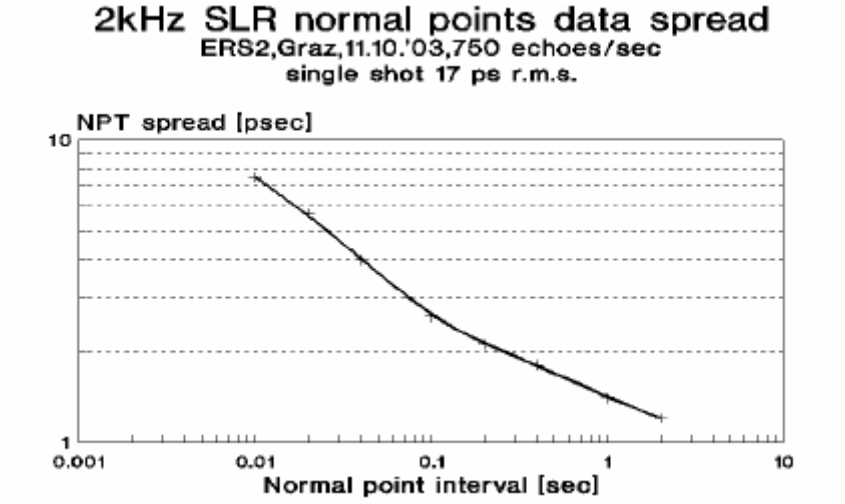

- deviation from ideal : > 100 echoes / NPT 2.5 psec
- saturation : > 2000 echos / NPT 1.0 psec

CONCLUSION

- The limits of averaging of the 2kHz / mm data have been characterised
- The SLR data processing numerical noise is of the order of 1 psec (random numerical, interpolation)
- The normal point precision saturates at 1 psec level compressing > 2000 echoes
- These limit values are negligible in comparison to satellite signatures (!)

IS YOUR PERFORMANCE BEING RUINED BY INTERPOLATION ERRORS?

J.McK. Luck
EOS Space Systems Pty.Ltd.
jluck@eos-aus.com, jmckluck@optusnet.com.au, Fax +61 2 6299-6575

Introduction

Improper interpolation methods can have devastating effects on Normal Point (NP) accuracy, telescope pointing accuracy, and indeed any other performance measure.

The issue was raised by Werner Gurtner at the 13th Workshop (Gurtner, 2002), was subsequently discussed by the ILRS Prediction Format Study Group on 9 April 2003 in Nice, France (*Seemueller 2003*), and presented at the Koetzting Workshop (*Luck 2003*). This study quantifies the effects of interpolation errors on the accuracy of SLR NPs, and also looks at LLR and at telescope pointing errors.

The crux of the issue is the tabular interval used for interpolating the predictions used in generating the NPs. The type of interpolating function (cubic spline or Lagrange) and its degree are also important. For example, the Orroral predictions were integrated in steps equal to the NP bin sizes recommended by ILRS, which thus formed the tabular points on which subsequent interpolations were based. The tabular intervals between these points are much too large for successful low-order interpolation, and can produce many **nanoseconds** of error in the shot-by-shot predictions and **minutes of arc** in the pointing. It is shown that the effects on NP generation can amount to errors of several centimeters, in the worst case being 1/3 of the interpolation error.

It is recommended to tighten the ILRS Normal Point Algorithm. Several addenda address interpolation errors in pointing angles which can be large and oscillatory; the best order of Lagrange interpolation to use, and a computationally convenient version of Lagrange's formula.

INTERPOLATION ERRORS

Test data

The satellite data used in this study were kindly supplied by Chris Moore of EOSSS. They consist of the predictions in range, azimuth and elevation integrated from real IRVs in steps of 1 second. These 1-second points are taken to be "truth", i.e. perfect. The tabular points for the interpolation tests were then simply chosen as every *k*-th point from that set, where the tabular interval is *k* seconds. They are equally spaced.

The tests consisted of interpolating using cubic splines, which have desirable continuity properties, and Lagrange's formula based on 4 points (order 4), i.e. a cubic to match the splines, and on 6 (order 6) or more points, then subtracting the "true" values from the outcomes. See for example (*Dahlquist & Bjorck 1974*).

For LAGEOS predictions, tabular intervals of 60 seconds were used rather than the ILRS bin size of 120 seconds. For Apollo-15, either the old value of 900 seconds, or 120 seconds, was used, generated by a revision of the classical program EULER.

Test results

The results are summarized in Table 1. The following graphs are a selection of those generated. They cover a variety of maximum elevations. The maximum interpolation errors are often several nanoseconds, or at best several hundred picoseconds. The improvements caused by increasing the Lagrange order (Fig. 1), and by reducing the tabular interval (Fig. 3), are evident by comparing the 'Range Error' scales of the graphs. Fig. 2 illustrates the typical periodicity in the error, while Fig. 4 shows how bad a perfectly ordinary pass can be. Fig. 2 reveals that spline interpolation errors are smooth, whereas Fig. 1(a) shows the spikiness of Lagrange interpolation errors at the tabular points. Fig. 5 illustrates that lunar ranging is not exempt from these errors.

Table 1: MAXIMUM INTERPOLATION ERROR MAGNITUDES, Cubic Splines, and Lagrangians of given order

PASS	Max. El (deg)	Num Pts	Tab. Int (sec)	Lagr. order	Az. Error (arcsec)		El. Error (arcsec)		Range Error (nanosec)	
					Spln	Lagr	Spln	Lagr	Spln	Lagr
AJISAI-1	87.7	1468	15	4	Huge	huge	420	340	1.0	9.5
			15	6	Huge	huge	415	410	3.2	0.5
AJISAI-2	72.8	1451	5	10	-	-	-	-	.011	tiny
LGEOS1-1	84.5	4183	60	4	Huge	huge	huge	huge	1.5	11.8
			60	6	600	950	55	75	1.3	0.04
			60	10	-	400	-	160	-	tiny
LGEOS1-2	31.0	3483	60	4	-	-	-	-	2.3	6.0
			60	6	-	-	-	-	2.3	tiny
ETLON1	62.8	25363	200	4	-	-	-	-	0.75	1.45
			200	6	-	-	-	-	0.75	tiny
STELLA	37.8	887	15	6	0.5	0.2	0.12	0.08	3.6	0.8
CHAMP-1	25.4	582	10	4	0.3	2.2	0.2	1.6	2.7	24.0
			10	6	0.3	0.1	0.2	0.03	2.7	0.6
			5	6	-	-	-	-	0.15	0.01
CHAMP-2	51.7	615	5	4	0.55	4.5	0.3	2.5	0.7	6.5
			5	6	0.55	0.3	0.3	tiny	0.7	0.1
APO-15	82.1	917	900	4	70.	390	5	20	11.5	2.3
			900	10	-	38	-	2	-	0.09
		5533	120	4	0.02	0.17	0.02	0.02	0.7	0.73
			120	10	0.02	0.08	0.02	0.02	0.7	0.07

Note that Cubic Splines (order 4) outperform Lagrange Interpolation of order 4.However, Lagrange Interpolations of order 6 outperform Cubic Splines substantially, and even higher order Lagranges do vastly better.

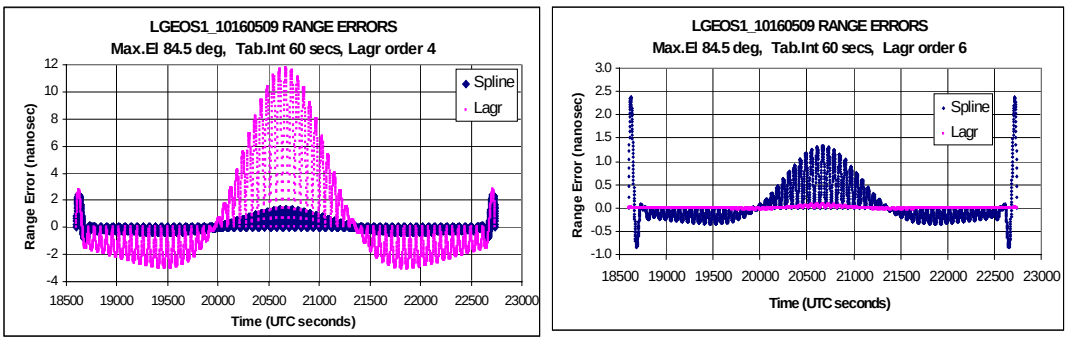

Figure 1: High LAGEOS-1 pass. Note poor behaviour of both at start and end. (a) Lagrange order 4 to match cubic splines. (b) Lagrange order 6.

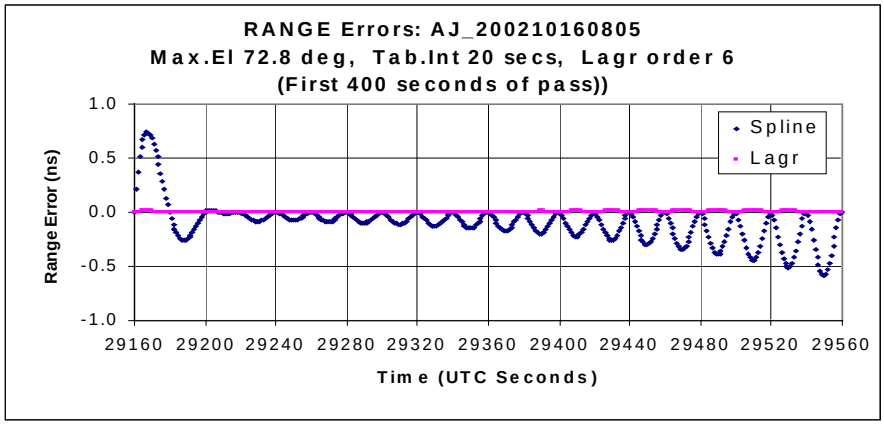

Figure 2: The start of a fairly high AJISAI pass, clearly showing the error periodicity.

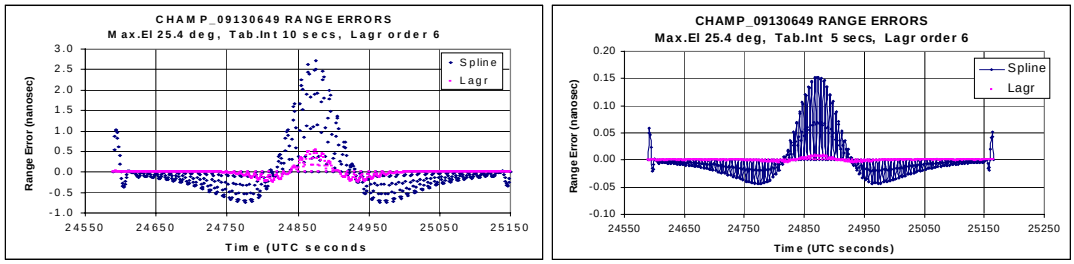

Figure 3: Range interpolation errors for a low CHAMP pass, Lagrange order 6.
(a) at 10-second tabular interval. (b) at 5 second tabular interval.
Note the 'Range Error' scales!

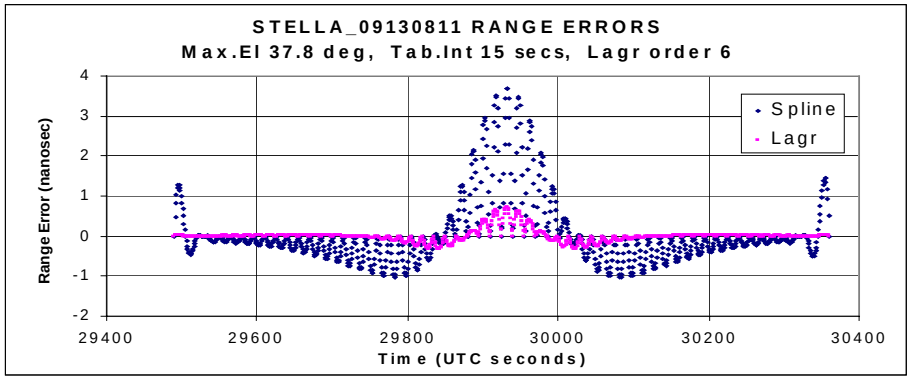

Figure 4: A moderate-elevation STELLA pass. Lagrange errors are significant even at order 6.

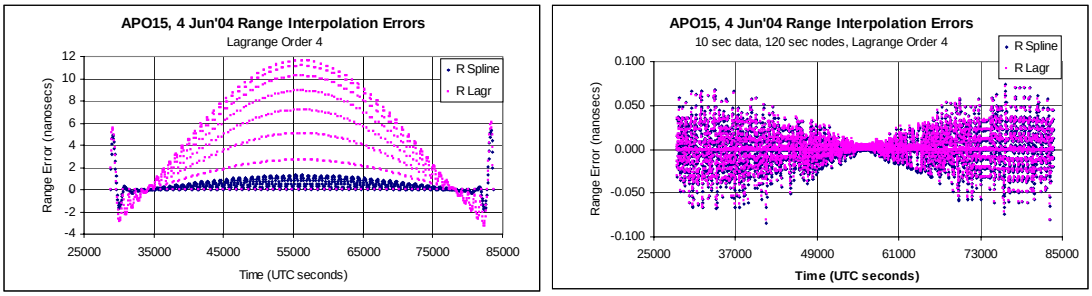

Figure 5: Apollo-15 Range interpolation errors for Lagrange order 4.
(a) 900 second, and (b) 120 second tabular intervals.

NORMAL POINT GENERATION

ILRS Algorithm

The 1997 ILRS Normal Point Algorithm is given in the website:
http://ilrs.gsfc.nasa.gov/products_formats_procedures/normal_point/np_algo.html .
It is summarized here and in Fig. 6, with some expansion of notation.

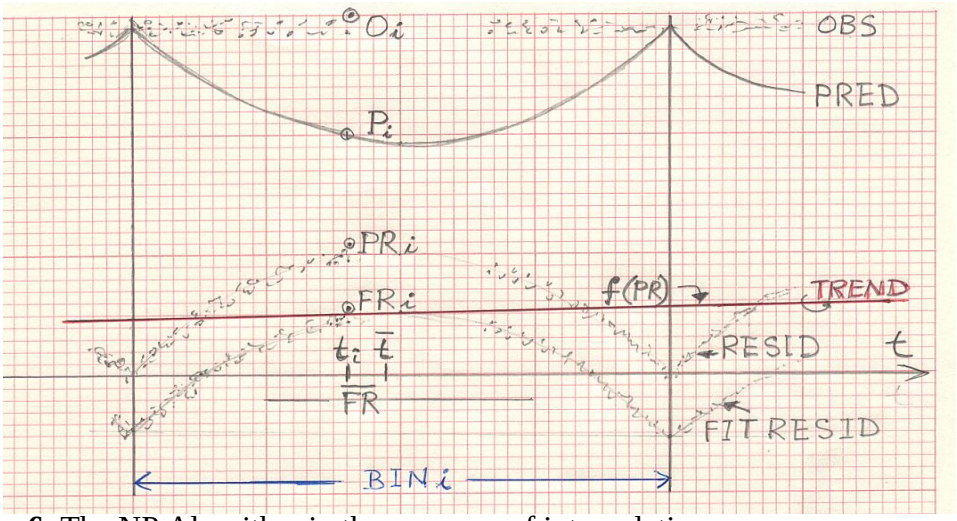

Figure 6: The NP Algorithm in the presence of interpolation error.

(1) Use high precision predictions to generate **prediction residuals** $PR_j = O_j - P_j$ where j indexes all returns in the pass.
(2) Use a suitable range window to remove large outliers.
(3) Solve for a set of parameters . . . to remove the systematic **trends** of the prediction residuals, giving the **trend function** $f(PR)$.
(4) Compute **fit residuals** $FR_j = PR_j - f(PR_j)$ and omit outliers.
(5) Iterate steps (3) and (4) until the process converges.
(6) Subdivide the accepted fit residuals FR_j into bins at fixed intervals.
(7) Compute the **mean value** $\overline{FR_i}$, the **mean epoch** $\bar{t}$ and the **number** n_i within a bin i.
(8) Locate the **particular observation** O_i with its fit residual FR_i and epoch t_i such that $|t_i - \bar{t}|$ is minimum.
(9) The **NP** is computed as $NP_i = O_i - FR_i + \overline{FR_i}$.
(10) Compute the RMS_i for bin *i*.
(11) Report t_i, NP_i, n_i, RMS_i.

Simple Case

To clarify the argument without (I believe) compromising its general validity, suppose that, in a single bin *i*, the observed ranges happen to be approximately constant with values:

$$O_j = O_0 + \delta O_j \text{ where } \sum_{j \in bin(i)} \delta O_j = 0$$

as shown in Fig. 6. In particular, the observed value of the point selected in step (8) above is:

$$O_i = O_0 + \delta O_i ,$$

and the value of the NP should be simply O_0. The prediction residual PR_i for this point is then, from step (1):

$$PR_i = O_0 + \delta O_i - P_i .$$

The trend function is fitted through all the PR_j in the pass after filtering (steps (3) and (4)). It therefore smoothes out the short-period interpolation errors illustrated in Figs. 1-5. Suppose that it happens to be very well-behaved in bin *i*, in fact constant:

$$f(PR_j) = f .$$

Then the fit residual (step (4)) for the selected observation is:

$$FR_i = PR_i - f$$
$$= O_0 + \delta O_i - P_i - f$$

while the average fit residual within the bin (step (7)) is:

$$\overline{FR} = O_0 - \overline{P} - f \quad \text{since} \quad \sum \delta O_j = 0.$$

Step (9) then yields after some simple manipulation:

$$NP_i = O_0 + (P_i - \overline{P}).$$

<u>The true result is therefore perturbed by the prediction error</u> $(P_i - \overline{P})$.

Magnitude of the Prediction Error

From the graphs, it seems reasonable to model as a first step the interpolation errors by a quadratic function between the tabular points at t_0, t_1 bounding bin *i*. (It is more likely a quartic, especially for cubic splines.) Let the prediction interpolation error be denoted by ΔP_i so that at the representative point:

$$P_i = P_i(true) + \Delta P_i, \text{ and similarly}$$
$$\overline{P} = \overline{P}(true) + \overline{\Delta P}, \text{ averaged over } j \in bin(i)$$

Since *i* is selected close to the mean point, we have:

$$P_i(true) \approx \overline{P}(true)$$
$$\therefore P_i - \overline{P} \approx \Delta P_i - \overline{\Delta P}$$

The interpolation error model will thus be:

$$\Delta P_j = 4\beta \left(t - t_0\right)\left(t_1 - t\right)$$

which is zero at $t = t_0$ and $t = t_1$, and its maximum value is:

$$\Delta P_j(\max) = \beta \left(t_1 - t_0\right)^2 \text{ at } t = (t_0 + t_1)/2.$$

Its mean value is:

$$\overline{\Delta P} = \int_{t_0}^{t_1} \Delta P_j dt \Big/ \int_{t_0}^{t_1} dt \text{ if considered uniformly dense}$$
$$= \tfrac{2}{3} \beta (t_1 - t_0)^2$$

Hence the Normal Point Error can be as large as:

$$\Delta NP_i(\max) \equiv \Delta P_i(\max) - \overline{\Delta P} = \tfrac{1}{3} \beta \left(t_1 - t_0\right)^2 \qquad (1)$$

and β is read from the relevant graphs above. From the examples shown, the errors can be many centimeters.

Because the distribution of observations within bins is usually non-uniform, and because the NP error reduces to zero at the tabular points (net points, nodes, knots), it will behave something like a random variable with unknown properties but no greater than this maximum. The effects on NP accuracy, and on the ILRS metric "Normal Point Precision", could be disastrous.

SOLUTIONS

There are many possible solutions, based on the well-known properties of the errors in polynomial interpolation. If the formula uses *n* points (degree *n*-1), the tabular interval is *h*, the n^{th} derivative at some point ξ in (t_0, t_1) is $f^{(n)}(\xi)$ and the underlying interpolating polynomial is $p_n(t)$, the error $\varepsilon(t)$ is:

$$\varepsilon(t) = h^n p_n(t) f^{(n)}(\xi) / n! \qquad (2)$$

The solutions include:

More Appropriate Interpolation Formulae

1. Increase the order *n*. This can be done easily with Lagrange-based formulae such as Newton, Bessel, Everett, etc., but is not available with cubic splines.
2. Reduce the tabular interval *h*. In the context of this study, it implies that the step size of the orbit integration must be no greater than *h*. Since the NP bin sizes are set by ILRS, it also implies that any one NP bin will generally contain several tabular points. It is NOT RECOMMENDED to retain a larger integration step-size and reduce the tabular interval by interpolation! Decreasing the integration step-size does not add significant rounding error (Chris Moore, private communication, 2003).

Different Trend Function Regime

3. We note that step (3) of the ILRS Procedure - iteratively fit a trend function - is designed mainly for filtering, but it is also used for calculating the mean fit residual within a bin in step (7). If a new trend function, e.g. a quadratic, is calculated from only the prediction residuals within each bin, it automatically removes (much of) the interpolation error.

Interpolate on Cartesian Coordinates

4. The 1-second files available for this study only contained range, azimuth and elevation. It was found that, by converting them back to topocentric Cartesian coordinates (East, North, Up) for the interpolations, the errors reduced dramatically. This can be readily understood by noting that the conversion equations:

$$\begin{aligned} range &= \sqrt{X^2 + Y^2 + Z^2} \\ azimuth &= \tan^{-1}(X / Y) \\ elevation &= \sin^{-1}(Z / range) \end{aligned} \qquad (3)$$

   are not at all well represented by polynomials of any reasonable degree. See Addendum 2.
5. Werner Gurtner and Chris Moore have found that interpolating on Geocentric Cartesian coordinates, then converting to range, azimuth and elevation on every shot, also produces dramatic improvements. This is studied in more detail in Addendum 3.

CONCLUSIONS

The accuracy and precision of NPs may be corrupted badly by inappropriate interpolation of the predictions. The magnitude of the resulting NP error in any bin may be as much as 1/3 of the magnitude of the interpolation error (see equation (1)) and amount to very many centimeters. They behave as unmodeled random errors so may be quite difficult to detect.

It is crucial to use tabular intervals as small as possible, consistent with memory size and speed limitations; and to take great care in choosing an interpolation formula which is appropriate to the function tabular interval being interpolated. The degree of the interpolating polynomial must not be too low nor too high.

Interpolation into tables of range, azimuth and elevations should be avoided. Rather, interpolate on Cartesian X,Y,Z coordinates.

The ILRS NP Procedure requires "high precision predictions" but is otherwise not specific and does not, as written, cope adequately with the problem.

RECOMMENDATIONS

1. It is recommended that this issue be considered by the Data Formats and Procedures Working Group, and that appropriate warnings be included in the ILRS Normal Point Algorithm document.
2. Interpolation should be performed on Cartesian coordinates, NOT on azimuth, elevation and range, using a Lagrange (or equivalent) interpolator of order 8.

ACKNOWLEDGEMENTS

Werner Gurtner's work alerted me to the potential of problems with algorithms used both in SLR operations and in post-processing, including on-site NP generation and star calibrations for telescope pointing accuracy. This report confirms his findings.

Chris Moore extracted the data needed.

REFERENCES

Dahlquist, G. and Bjorck, A.: "*Numerical Methods*", Prentice-Hall, Inc. (1974)

Gurtner, W.: "*Interpolation of Ephemerides*", 13th International Workshop on Laser Ranging, Washington D.C., 7-11 October 2002

Luck, J.McK.: "*Interpolation Errors in Normal Point Generation*", EUROLAS Workshop, Koetzting, October 2003

Ricklefs, R.L.: "*Consolidated Laser Ranging Prediction Format*", prepared for the ILRS Prediction Format Study Group of the ILRS Data Formats and Procedures Working Group, San Fernando, June 2004 *et seq*.

ADDENDUM 1: INTERPOLATION ERRORS IN POINTING ANGLES

The same problem affects pointing. Extreme examples are shown in Figs. 7-9.

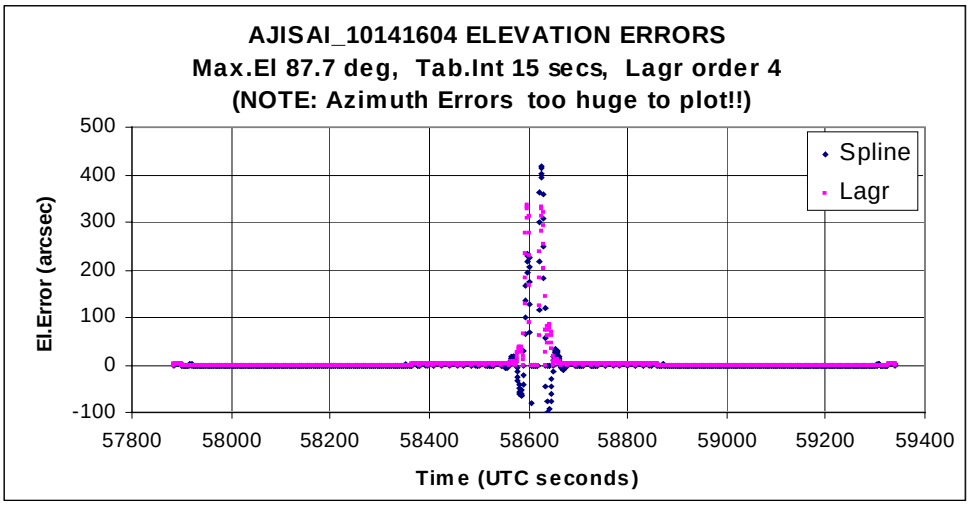

Figure 7: Elevation errors from interpolation errors near TCA on a high AJISAI pass.

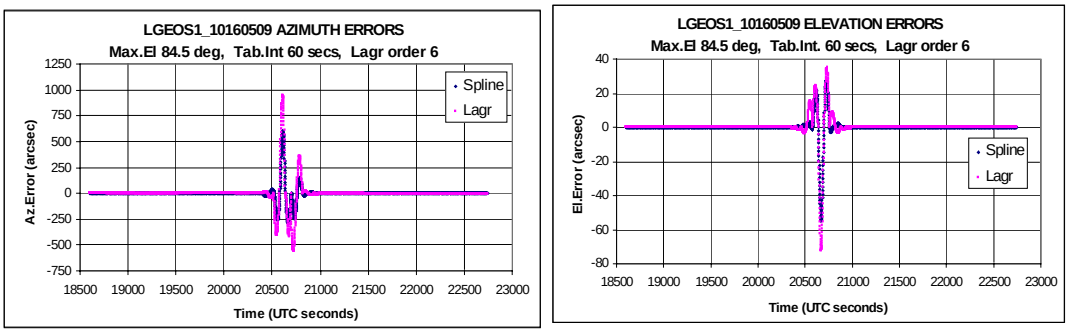

Figure 8: Interpolation-induced errors on a high LAGEOS pass.
(a) Azimuth. (b) Elevation.

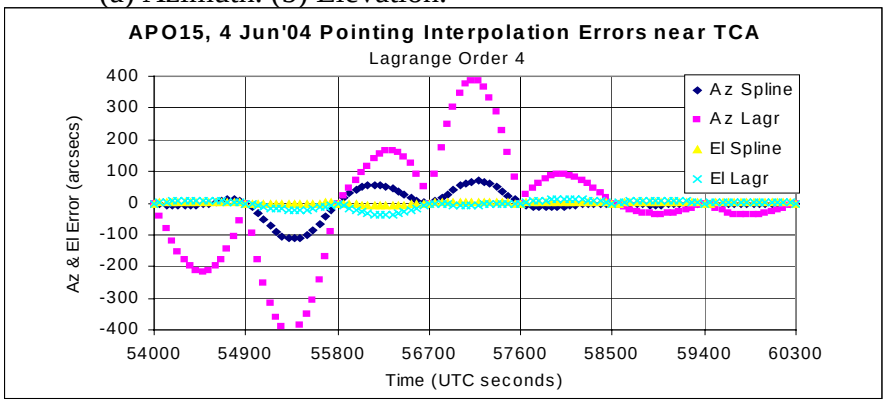

Figure 9: The worst of interpolation errors in azimuth and elevation angles during an Apollo-15 “pass”, selected around time of maximum elevation.

ADDENDUM 2: GENERAL NOTE ON INTERPOLATION DEGREE

In Step (3) of the NP Algorithm description, it is noted: ". . while not introducing spurious high-frequency signals (as can occur by fitting a high-order polynomial)." As part of a wider study on interpolation techniques and limitations, I fitted polynomials of degree up to 19 to the 1-second predictions (NOT the Prediction Residuals!) in azimuth, elevation and range, and in topocentric X,Y,Z (East, North, Up), over entire passes using Least Squares. The results are summarized in Table 2 in terms of the RMS of the (Raw - Fitted) differences. Consistent with the remarks in SOLUTIONS 4. above, it was found that such fits converged in X,Y,Z at degrees 8 to 12, while azimuth, elevation and range did not converge even up to degree 19, although the (truncated) ETALON pass came close and actually converged in range at degree 9.

TABLE 2: Least Squares Polynomial Fits to Pass Predictions.

PASS	El @ TCA (deg)	Degree at which RMS reaches 5 ps			RMS of Degree 19 Fit		
		X (E)	Y (N)	Z (U)	Az (arcsec)	El (arcsec)	Range (nanosec)
AJISAI-A	87.7	10	9	10	32589	3373	374.4
AJISAI-B	72.8	12	12	11	3573	865	299.0
LGEOS1-A	84.5	10	10	11	12165	1255	922.3
LGEOS1-B	53.7	10	10	10	19	7	119.6
LGEOS1-C	31.0	10	8	10	6	1	136.6
ETALON1	62.8	6	6	7	(0 at degr 6)	(0 at degr 6)	(0.034 at degr 9)
STELLA-A	37.8	9	9	9	44	30	238.5
STELLA-B	73.5	9	10	10	6598	1835	> 1000
CHAMP-A	25.4	8	8	8	16	13	105.6
CHAMP-B	51.7	8	8	8	1386	776	> 1000

There is a clear correlation between badness-of-fit and maximum elevation when fitting to azimuth and elevation.

To illustrate the spurious signals appearing after convergence, Fig. 10 shows plots of (Raw - Fitted) differences in X for pass STELLA-A in which the RMSs were 0 ps for degrees 9-12. It is interesting to note that the divergence comes from the beginning and end of the pass rather than from periodicities within.

As a side comment, the condition number (κ) of the Normal Matrix inversion process increases vastly with increasing fit degree, and is unacceptably large at d = 2 anyway. This indicates that the coefficients of any of the fitted polynomials are absurdly highly correlated. Fitting Chebyshev polynomials gave condition numbers $\kappa \approx 1.0$ right up to degree 19, as expected from the theory of orthogonal polynomials, which is the ideal and indicates that the coefficients are completely uncorrelated. However, they did not change the RMSs one little bit.

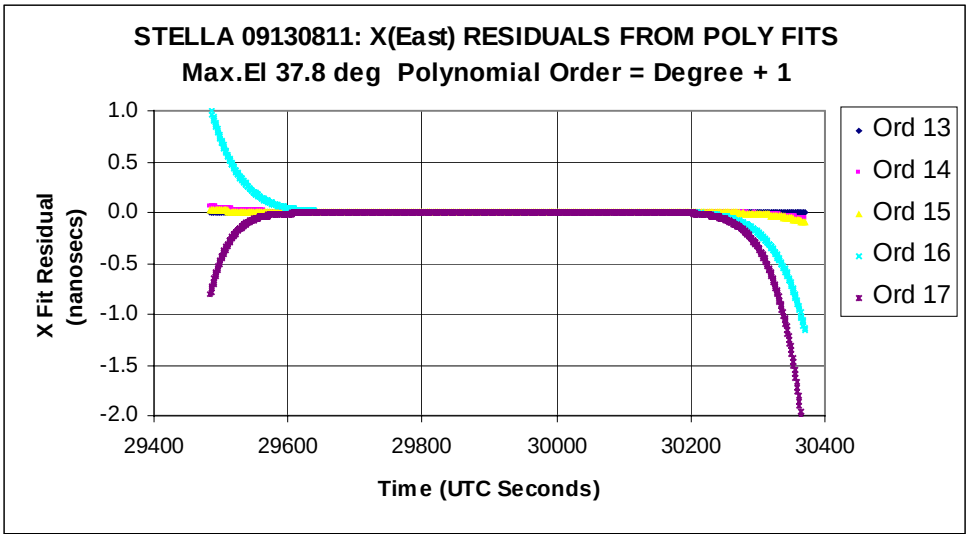

Figure 10: Residuals of predictions in X (Raw - Fitted) for increasing orders of fit after convergence which occurs at degree 9 (order 10).

ADDENDUM 3: MAXIMUM TABULAR INTERVALS

The proposed ILRS Consolidated Predictions Format (CPF) (*Ricklefs, 2004*) advocates the dissemination of predictions in body-fixed X,Y,Z coordinates, at nominated tabular intervals per satellite, to replace IRVs. The magnitudes of interpolation errors as functions of tabular interval and of order were studied, ignoring all other error sources, in 4 coordinate systems:
I: Celestial True-of-Date X,Y,Z, using data at 1-second intervals, again kindly supplied by Chris Moore. These constituted (quasi-) inertial coordinates.
G: Body-fixed in Greenwich X,Y,Z, emulating the CPF scheme. They were generated from "I" by rotating through sidereal time. UT1-UTC and polar motion were ignored.
T: Topocentric East-North-Up. They were generated from "G" by the usual transformations involving geodetic latitude, longitude and ellipsoid height for the new Stromlo station 7825.
P: Polar, i.e. range, azimuth and elevation at the station, generated from "T" by equations (3).

The interpolation errors were characterized by what I loosely call their RSS values (actually, RMS about zero mean), for this purpose defined by:

$$RSS(range) = \sqrt{\sum_{i=1}^{n} \left(\text{Interpolated range - True range}\right)^2 / n}$$

where the sum is over all 1-second points in about a day; and similarly for azimuth and elevation. The results for LAGEOS are shown in Fig. 11 as log-log graphs against tabular intervals of 15, 30, 60, 120, 240, 480 and 960 seconds using the equal-spaced Lagrange formulae for orders 4, 6, 8, 10 and 12. Similar graphs were obtained for CHAMP, STARLETTE, AJISAI and GPS35. The "floors" in the graphs are due to rounding errors when subtracting large numbers, and are very negligible. Otherwise, the curves for Cartesian frames are linear, consistent with equation (2). For any given order, the graphs when interpolating into the three Cartesian systems I, G and T are indistinguishable, and are all far better than for the Polar system P.

Table 3 gives the tabular intervals read from the graphs required to keep the interpolation errors (RSS) below 1 ns (just for target acquisition) and 10 ps (for NP generation) in range, and 1 second of arc in azimuth and elevation. It is evident that the CPF Recommendations are satisfactory, provided that order 8 is used on the body-fixed Cartesian predictions to be supplied.

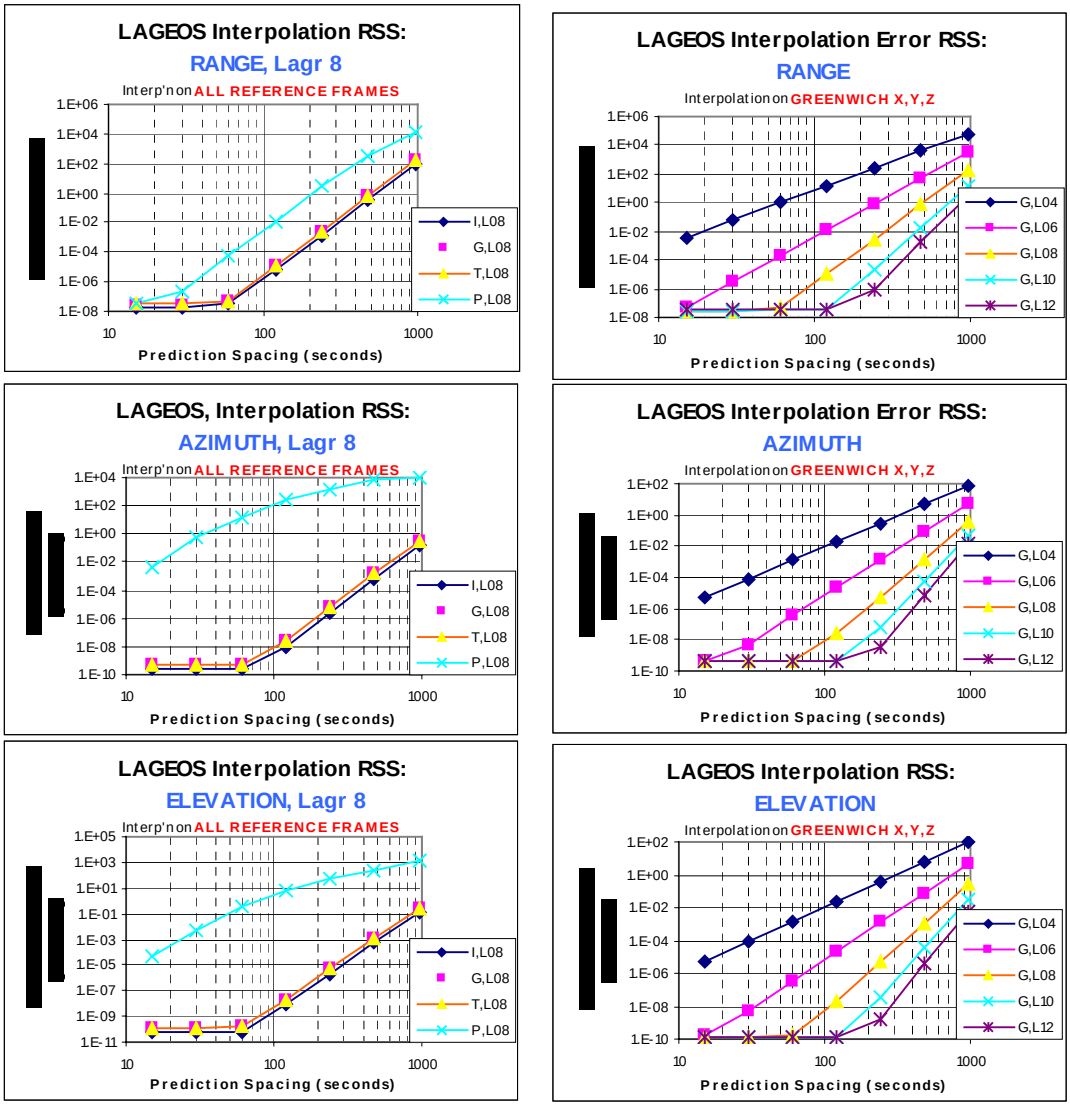

Figure 11: Typical errors due only to interpolation, for LAGEOS over approx. 1 day.

Table 3: Tabular intervals to yield required error specifications

Satellite	Maximum Grid Spacings (seconds) when using 8th-order Lagrange Interpolation				CPF Rec.	
	RANGE		AZIMUTH	ELEVATION	Deg 7	Deg 9
	1 ns	10 ps	1 arcsec	1 arcsec		
Champ	234	127	441	456	120	180
Starlette	240	127	466	519	180	240
Ajisai	310	170	617	628	240	300
Lageos	501	280	1097	1118	300	600
GPS35	1360	763	2970	3160	900	1800

ADDENDUM 4: NEWTON'S FORWARD DIFFERENCE FORMULA

As is well known, the Lagrange formulation reduces to (*inter alia*) Newton's Forward Difference Formula when the tabular points are equally spaced. Let $f_i \equiv f(t_i)$ be the given values at the tabular points surrounding the interpolation point *t*, let *h* be the tabular interval, let $\Delta^n f_k$ be the n^{th} forward difference at the first tabular point t_k used, and let $x = (t - t_k)/h$, so $0 \le x < k - 1$. Then the interpolated value $y(t)$ is given by:

$$y(t) = f_k + x.\Delta f_k + \frac{x(x-1)}{2!}\Delta^2 f_k + \frac{x(x-1)(x-2)}{3!}\Delta^3 f_k + \cdots + \frac{x(x-1)\cdots(x-n+2)}{(n-1)!}\Delta^{n-1} f_k$$

t_k should be chosen so that *t* falls in the middle interval used, so for example *x* will lie between 2.0 and 3.0 for a 6-point formula ($n = 6$). The beauty of this is that a matrix of coefficients can be pre-computed to enable rapid calculation in real-time by Horner's Rule. Thus, at each tabular point *k* pre-compute $c_{k,i}$ as:

$$c_{k,i} = \Delta^{i-1} f_k / (i-1)!, \quad i = 1, \cdots, n, \quad k = 1, \cdots, \text{num.tab.pts}$$

Then in real-time at time *t* choose the best *k*, calculate *x* and obtain $y(t)$:

$$y(t) = c_{k,1} + x[c_{k,2} + (x-1)[c_{k,3} + \cdots + (x-n+2)c_{k,n}]\cdots].$$

This pre-computation/Horner rapid-evaluation technique has been claimed as an advantage for cubic splines, but it can be applied to any equally-spaced method.

ENGINEERING DATA FILE PROCESSING AND DISTRIBUTION

K.Salminsh
Institute of Astronomy, University of Latvia
kalvis@lanet.lv /Fax: +371 7034582

Abstract

Engineering data files (EDF) were proposed by the ILRS working group "Networks and Engineering" as an additional tool to the orbital analysis to deal with the SLR station long term stability issues by maintaining the history of local station parameters like calibration related values, meteorological data, ranging system data and checking out for the anomalies, comparing data among the SLR stations and exchange these data within SLR community.

This paper discusses different ways how to work with EDF files at the station and eventual data distribution procedures within the SLR community and implementation details as well.

Introduction

Original idea for the EDF was developed within the Networks and Engineering Working Group (NEWG) during the meeting in Nice (1) and refined further in the ILRS technical workshop (2). EDF are intended to help orbital analysis to detect station range biases and hardware anomalies by maintaining history of its vital parameters and comparing similar equipments' performance across the tracking network. XML based EDF format was developed to handle requirements for the data exchange and flexibility, including possible future extensions and additional station custom information (3). The main goals for the EDF are following:

- Inter-comparison among parameters of different SLR stations
- Rapid identification of system drifts or degradation effects
- Correlation of system data with bias reports based on orbital analysis
- Easy implementation
- Flexibility

EDF are supposed to be created for each station calibration run and contain information about calibration, meteorological data, hardware description and optional parameters, including station specific parameters. Using EDF data the time series for the station hardware parameters like calibration values, RMS etc. can be built and compared with the other stations, checked for the anomalies (jumps, drifts).

EDF Generation

EDF creation should be treated as an additional station data product like normal points, time biases etc. Each time when the station calibration is done, the corresponding EDF should be created. Information saved in the EDF can be divided in the three groups: mandatory, optional parameters and station custom data. The currently defined EDF content overview is summarized in Table 1, for more details, including formal EDF definition with the XML schema and implementation examples, see (3). Actual EDF example from the Graz station is shown in the Appendix A. EDF can be generated either by using native XML support, available now in the most of the modern operating systems and compilers or just as a text files without using any specific XML techniques. The experience of the existing EDF implementations at the SLR stations Graz and Potsdam shows that the EDF generation shouldn't create large problems at the station, but in some cases there may be a necessity to improve or adjust the internal data handling when required data for the EDF are scattered across different files and computers.

Table 1. EDF elements

Item	Required data	Optional data
EDF epoch	Calibration epoch	
Station data	Name, SOD, System change indicator (SCH), System Configuration Index (SCI), calibration method, timescale used (Name is just a name of the station, all other parameter values are defined by the ILRS)	
Laser	Wavelength (nm), pulse width (ps) , energy (mJ)	Repetition rate (Hz), number of semi train tracks, divergence (mrad)
Signal detector	Detector model, type	Device ID (here and further: unique number/name like serial number to distinguish devices in cases when multiple same model items are available)
Filter	Filter model, bandwidth (nm)	Device ID, filter transmission (%)
Timer	Timer model	Device ID
Meteo data	Temperature (Celsius), pressure (mbar=hPa), humidity (%)	Temperature (Celsius), pressure (mbar=hPa), humidity (%) from alternative (backup) source
Calibration	2-way value (ps) , RMS (ps), 1-way target distance (m)	Skew, kurtosis, sigma criteria used, peak minus mean, recorded points, accepted points, return rate
Custom data	Each station can add their own data here	

EDF distribution and processing

EDF can be exchanged directly among the SLR stations or uploaded to the data centers, wherethey and results of its processing are available to all community. While the flexibility of XML format allows to write software which can be shared and used at the stations across the SLR network, there are still problems with the different operating systems and the program update management to name a few. To avoid these issues the preferred approach at the beginning would be to perform common analysis and checks at the server, where the results will be immediately available online. The benefit for the server based approach is that any change, introduced in the processing software, will be immediately available to all users.

Stations can write additional programs to perform their own or alternative checks with their data when appropriate either before formatting EDF or using EDF as a basis of the station parameter database. Server based processing will allow to build a used equipment database using EDF as an information source, to overview the system parameter history over the time, see (Figure 1) or as numerical data and to compare the performance of similar devices and systems. To achieve it some kind of hardware registry with the commonly used equipment like event timers, discriminators etc. is needed.Users will be able to access the system through

the WWW. There is also a possibility to build a web services for the EDF database which will allow to use EDF data in other applications which may require access to the station data.

Conclusions

The first experience with the EDF shows that while there may be a necessity in some cases to rearrange station internal data handling and to modify existing programs, the EDF generation and upload implementation at the station shouldn't create large problems and can be done within 1-2 days. The EDF data will be collected and made accessible to the SLR community at the data center. The preferred way to process EDF at the beginning will be a server based processing, which will allow to acess the results online using WWW, but stations can do their own data checks either based on the EDF usage or not.

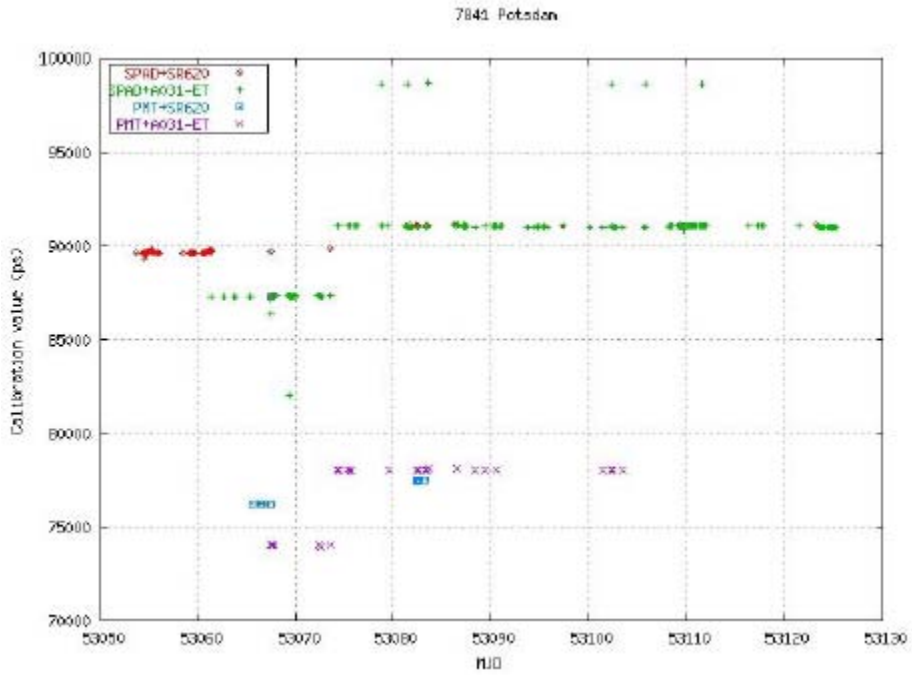

Figure 1 7841 calibration history

References

1. Agenda Items for NEWG Meeting, http://cddisa.gsfc.nasa.gov/ilrs/working_groups/networks_and_engineering/networks_activities/nice_2003_agenda.html , 2003.
2. ILRS Technical Workshop, Koetzing, Germany, http://ilrs.gsfc.nasa.gov/reports/ilrs_reports/oct_2003_technical_workshop.html , 2003.
3. SLR Engineering Data Files, http://www.astr.lu.lv/EDF , 2004.

Appendix A.

```
<EDF Version="1.0" MJD="53275.7083796296" Epoch="2004-09-27T17:00:04"
     xmlns:Graz="http://www.astr.lu.lv/Graz">
  <Station SOD="78393402"
    SCH="0" SCI="1" CalibMethod="0" TimeScale="3" Name="Graz" />
  <Hardware>
    <Laser Wavelength="532.0" Energy="0.0004"
     PulseWidth="10" Divergence="0.000050" RepRate="2000" />
    <Receiver>
     <Detector Model="C-SPAD" DeviceID="1"
```

```
    DetectorType="SPAD" TWCompensation="Yes" />
   <Filter Model="Andover 003FC10-25"
    DeviceID="20010705" BandWidth="0.3" />
  </Receiver>
   <Timer Model="Graz_ET" DeviceID="Module 1+2" CorrectionID="0" />
  </Hardware>
  <Meteo Temperature=" 13.2" Pressure="962.8" Humidity="58.8"
   Graz:InternalTemperature="24.4" Graz:InternalHumidity="33.8"/>
  <Calibration TargetDistance="1.742" CalValue="129700" PeakMinusMean=" 0"
   RecordedPoints="10000" AcceptedPoints=" 8741" SigmaUsed="2.2" RMS=" 15"
   Skew=" 0.000" Kurtosis="2.343"
   Graz:ReturnQuote=" 55.0" Graz:RawCalValue="141326"/>
  <CustomData></CustomData>
</EDF>
```

Text 1 EDF example. Data items with the prefix "Graz:" marks station specific data.

Herstmonceux time bias system as a possible real-time QC tool

Ingrid Bayer (1), Philip Gibbs (2), Matthew Wilkinson (2)
(1) Fachhochschule Deggendorf, Edlmairstr. 6 + 8, 94469 Deggendorf, Germany
(2) NERC Space Geodesy Facility, Herstmonceux Castle, Hailsham BN27 1RN, E.Sussex, UK pgib@nerc.ac.uk, matwi@nerc.ac.uk

Abstract

For some years the NERC Space Geodesy Facility has been operating a daily QC service based on long and short-arc analysis of most of the satellites tracked by the ILRS network. The results continue to be presented each day on the Facility website. In addition, every hour the system at Herstmonceux downloads the latest hourly file of Normal Points from CDDIS. These observations are then used in an orbital solution to form a time bias (TB) relative to all available prediction sets for each individual pass. These individual TBs are then added to the global set and a function fitted through them to produce the time bias functions that are made available to the ILRS network via a server at Zimmerwald, Switzerland. However, generation of these functions is sometimes complicated by the existence of poor data from one or more tracking stations. Much of the effort going into improving this TB service is currently centred on the development of an automatic system to detect and remove from the fit the poor data. As a bye-product and on a somewhat ad-hoc basis we pass the details of any poor data to HTSI who then report back to the station. We believe this system has the potential to send out a report automatically and directly to the station in near real-time and although not perfect would enable stations to detect gross problems quickly and complement our other QC tools.

Long-Arc

The long-arc solutions (six day orbits) are run once per day. Although we run the long-arc solutions for all satellites, we currently only place the solutions for the Lageos and Etalon satellites on the web. We do have plans to expand this to all satellites in the future. It is down to the station to look at the long-arc solutions for problems. Errors can be seen at the 10-20cm level. We could make an automatic system which would inform the station when any NPs have residuals above the 20cm level. Before we can do this we would need to devise a method of logging to avoid sending our message every day for the 6-day orbit. We also have to overcome the problem of poor orbits for satellites with sparse data sets.

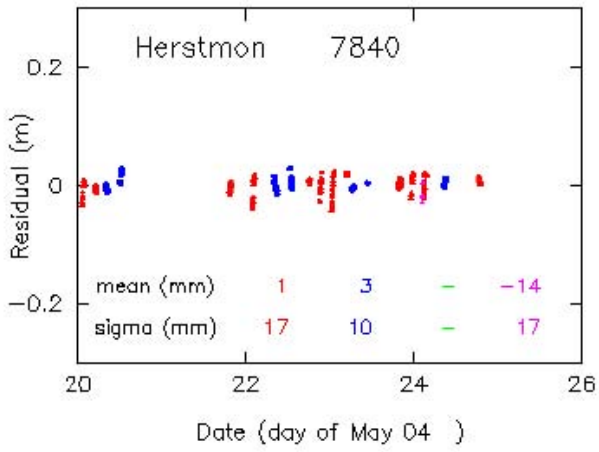

Shown here is a typical longarc plot for Lageos 1&2 and Etalon 1&2.

Short-arc

The short-arc solutions are run once a day and require the long-arc orbit and simultaneous observing from at least two core stations. Currently there is no feedback – it is up to each station to check the short-arc on a daily basis. Errors can be seen at the 5-10cm level. We could make an automatic system which would inform the station when any NPs have residuals above the 10cm level. Before we can do this we would need to devise a method of logging to avoid sending our message every day for the 6-day orbit. We also have to overcome the problem of poor orbits for satellites with sparse data set As simultaneous data is required the amount of passes checked is limited, particularly for stations that have no other station near enough to get simultaneous tracking for all satellites

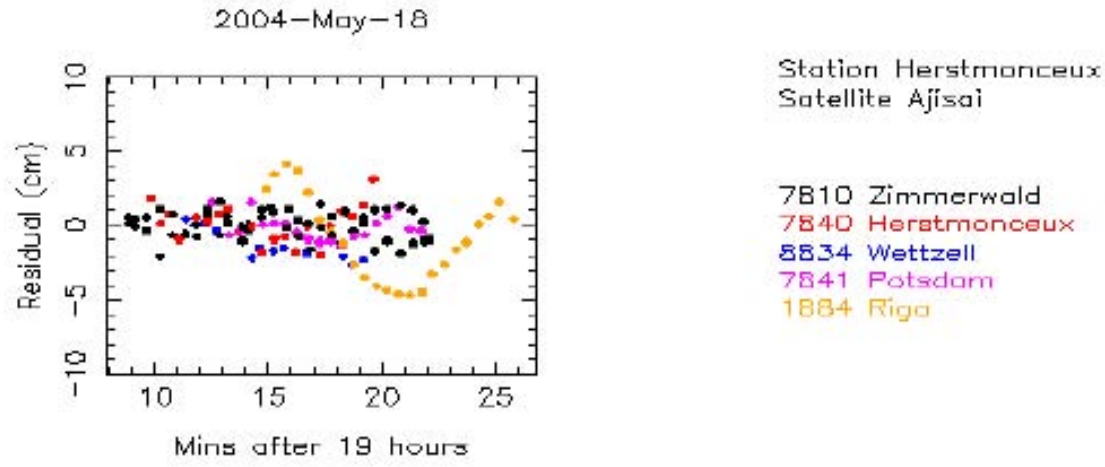

Shown above is a typical short-arc plot for Ajisai. The scatter in their data would indicate that they are all near single photon level. The above plot would indicate that there may be a problem with the data for 1884 for this pass.

Herstmonceux Time Bias Service.

To maintain an up-to-date time bias function for predictions, the automatic system at Herstmonceux generates an individual time bias, using a cut down version of the orbit fitting program SOLVE, for every observation as soon as it becomes available. Data becomes available in the following ways

–Herstmonceux data is available immediately after a reduction.
–Through E-mail – many stations send us data directly to speed up the TB process.
–Hourly downloads from CDDIS

Once new NP data is available a time bias is generated and a new function is calculated. These functions are made available through the Berne ftp system every 15 minutes. A poor time bias can easily corrupt the time bias function (as can a poor IRV set). To try to get the best time bias function we need to be able to detect and remove outliers. It is this process of detecting the “bad” passes that we are proposing to use as a general QC tool.

Pros	Cons
-Once an hour all new data is downloaded from CDDIS. This means stations can be informed in near real-time of potential problems. -Being near real-time, it allows us to correct the data (remembering to increment version number) or withdraw it quickly (we really should be able to do this), hopefully before the users have downloaded the data they require, as users rarely go back and recollect data. -Well-tuned monthly IRVs allow us to see many potential errors clearly in the time bias data.	-As the system only solves for two orbital parameters (along, across track) it can have trouble separating the two, thus giving spurious tb values. This is particularly true when a pass contains only a few NPs or has very little change in Az/El. -The system has problems around manoeuvres. -There are some satellites which the system has problems getting time biases for – Glonass, Etalon, Champ, Grace. -We have to generate monthly IRVs - this is only a very minor problem

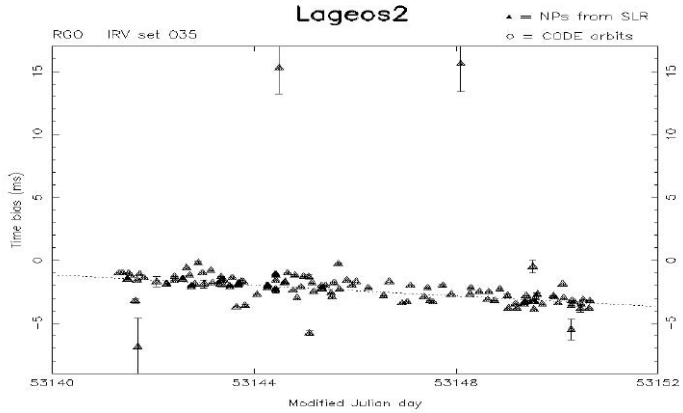

A typical time bias plot. There would appear to be 2 clear outliers at 15ms (both in value and RMS- each point has error bars plotted but they are generally <0.1). There are also a few difficult to define points.

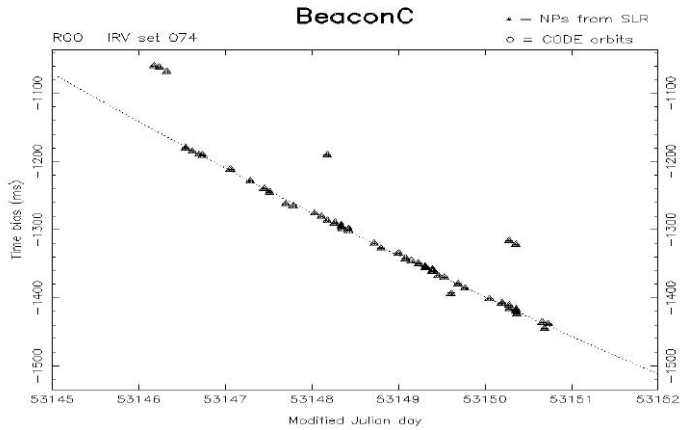

The plot shown for BeaconC shows a number of clear outliers. Note the large value of the time biases - although this IRV set is a month old we can still clearly see the outliers.

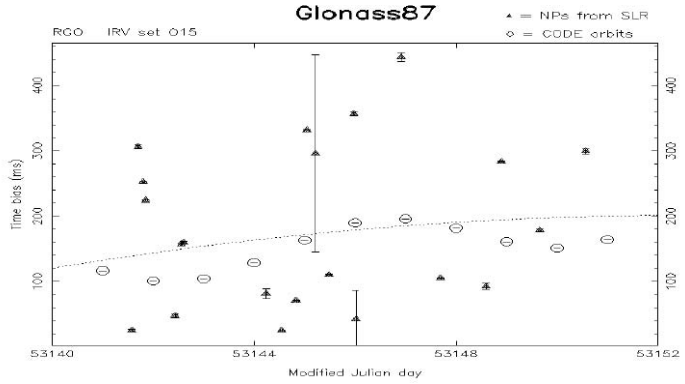

Shown here is a typical Glonass set of data. The range of time biases (some 500ms) is due in the main to stations only getting a few normal points when the satellite is at its closest approach. Detecting bad data is almost impossible

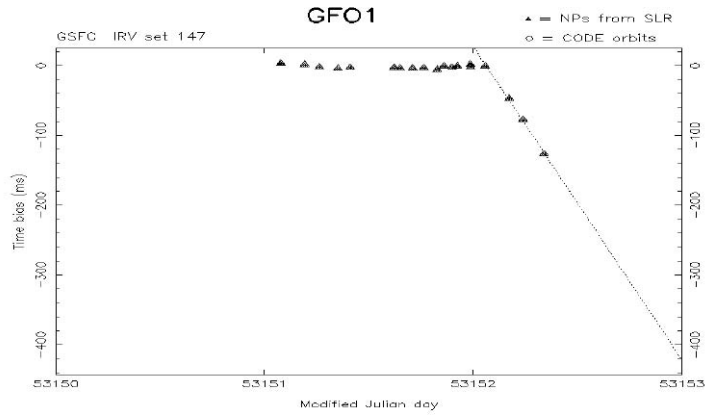

Shown here is a data set around a manoeuvre. When not informed in advance of a manoeuvre the system will probably send out all post-manoeuvre passes out as errors.

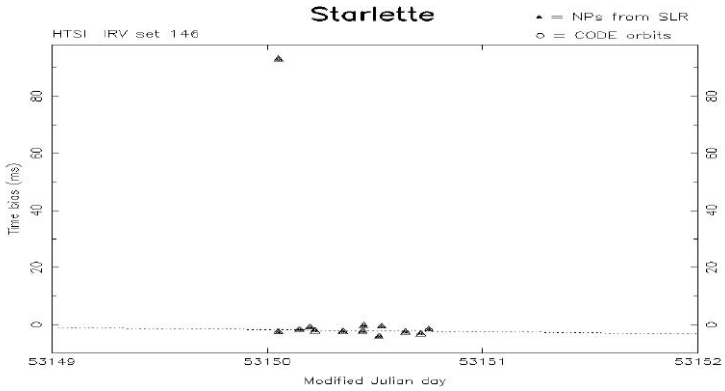

Why do we use monthly IRV sets instead of daily IRV sets? When collected in chronological order this data set would have one good and one bad pass on which to make a judgement. With a monthly set it knows which is wrong

Summary

We can detect outliers and advise the stations, for satellites up to Lageos (apart from Champ & Grace) at about the 10ms level with some certainty, although we may have problems if we are not advised of manoeuvres.

We can advise stations when the orbit fit gives a poor (large) RMS.

We will expand the long-arc to include all of the satellites.

Conclusion

We can implement reporting bad data directly to the station to give near real-time QC

If we implement any of these systems as QC checks we would like feedback – hopefully we will be able to improve the detection criteria from the feedback.

Stations should make every effort to stop bad data from being released – not rely on QC to detect problems.

To implement any of these systems we need an e-mail address for each station to send the information to – we would also inform EDC/CDDIS

We are happy to offer this service (for TBs) to any station even if it is not used as an official ILRS QC check – just let us know the e-mail address to send the feedback to.

Implementation

After running offline tests to look at the flagged errors to resolve any false alarms we started the system in August 2004. At this point some fifteen stations have taken up the offer to receive an e-mail if a potential problem is detected within their data. It may well be coincidence but shortly after the system was introduced the number of bad data points dropped off markedly.

DETERMINATION OF THE STATION COORDINATES FOR QUALITY CONTROL OF THE SATELLITE LASER RANGING DATA

S. Schillak
Space Research Centre of the Polish Academy of
Sciences. Astrogeodynamic Observatory, Borowiec
sch@cbk.poznan.pl / Fax: +48-61-8170-219

Abstract

The paper presents the method of quality control of the SLR data on the base of the station topocentric coordinates. The coordinates were determined from monthly orbital arcs of satellites LAGEOS-1 and LAGEOS-2. The orbital arcs were calculated on the basis of results of 15-17 fixed stations with very good quality of coordinates in ITRF2000 system. The orbital arc RMS was on a level of 1.8 cm. The differences between topocentric coordinates obtained from orbital results and local geodetic tie were presented for three sites: Grasse (7835-7845) from 4.5-year period, Potsdam (7836-7841) from year 2003 and Maidanak (1864-1863) for the period from May 2002 to the end 2003. The differences between coordinates determination for two colors for stations Zimmerwald (7810, 6810) and Concepcion (7405, 6405) were also presented. The coordinates and velocities of Riyadh station (7832) in ITRF2000 system has been corrected and Arabian tectonic plate motion were determined. The coordinates determination and control of their stability for the new points were presented for FTLRS system: Ajaccio (7848) and Chania (7830). The example of continuous coordinates determination in the long period is Borowiec SLR station (7811). The stability of coordinates and the movement of Eurasian tectonic plate for this station were determined for the 10-year period from 1993.5 to 2003.5.

Introduction

The continuous determination of the coordinates of the satellite laser ranging stations is one of the methods for quality control of the laser ranging data. This method reflects the quality of SLR data in the form of the station position stability, especially systematic effects (range bias) in vertical component and also quantity of normal points, which decided about standard deviation of coordinates determination. The possibility of immediate comparison with results of GPS are also very important in this method. The description of the method and results of the coordinates determination of Borowiec SLR in 1999 and all SLR stations in the period 1999-2001 were presented in the previous papers of the author (*Schillak, 2000, Schillak and Wnuk, 2002), Wnuk et al., 2002*). The method needs stable terrestrial reference frame, which assures the best stations position for the same epoch. One of the best terrestrial coordinates frame is ITRF2000, which includes four space techniques, for the most SLR stations SLR+GPS. The difference between determined coordinates and ITRF2000 is result of several effects:

- real station displacement (for example Arequipa, Tateyama),
- systematic errors of the measurements (from SLR system and environment) – main source of difference,
- orbital effects from not correct or not included some perturbations of the satellite and station positions,
- systematic differences of the real position with ITRF2000 (not correct position and velocity in ITRF2000).

The advantage of this method is presentation on one graph full picture of all station errors as the effect of quality and quantity of measurements of the given station. The method includes also all hitherto parameters for estimation of station quality like orbital RMS and Range Bias. The stations coordinates were determined by using orbital program GEODYN-II. The most important parameters are presented below:

• Earth gravity field: EGM96 20x20
• polar motion: IERS C04 (every one day) • one month arcs,
• LAGEOS-1 and LAGEOS-2 as one solution,
• 15-17 fixed stations for orbit determination: coordinates and velocities in ITRF2000,
• no weights,
• no range bias determination (range bias will be see in vertical component).

Estimated parameters:
• satellite state vector, • one station geocentric coordinates,
• acceleration parameters along-track, cross-track and radial at 5 days intervals.

Results

The paper presents results of coordinates determination for some choice stations, especially for comparison of two SLR systems in the same site and the coordinates determination for new stations or upgrading of not correct ITRF2000 coordinates. The control of coordinates determination were performed by comparison of orbital results with local geodetic tie between two stations in Grasse; SLR (7835) and LLR (7845) from the 4.5 years of common LAGEOS1 and LAGEOS-2 observations of both stations (Fig. 1). The determined geocentric coordinates of the LLR station 7845 were transferred to the point 7835 on the base of local geodetic tie from log file of Grasse SLR station. The differences of the coordinates between stations for common months in all components are present in figure 1. The differences are not significant and show very good agreement between orbital and ground surveying data. The similar method was used for the two SLR stations in Potsdam (7836 and 7841) (Fig. 2). In this case the differences in East-West and vertical component are significant. It was caused by systematic errors of the local geodetic tie. The third example of the two SLR stations in one site is Maidanak (1864, 1863) (Fig. 3). The geocentric coordinates for station 1863 were determined form observations performed in the period May, 2002 – May, 2003 and on the base of the difference with Maidanak 1864 ITRF2000, the coordinates were transferred to common point 1864. The results for the station 1863 are significantly better in comparison with 1864. The significant and variable differences between these stations in vertical component are result of systematic errors of the station 1864, probably from frequency standard walk. The next example is comparison of the determination of coordinates from measurements of one station in two colors; blue (423 nm) and infrared (846 nm) for stations Zimmerwald (Fig. 4) and Concepcion (Fig. 5). The differences of the station coordinates determined independently for both colors are not significant. The new station coordinates in ITRF2000 system were determined for three points; Concepcion (7405), and two FTLRS sites: Ajaccio (7848) and Chania (7830) (Fig. 6). The stability of these coordinates for three components was equal to 11.4 mm, 13.3 mm and 8.3 mm for Concepcion, Ajaccio and Chania respectively. The final values of geocentric coordinates of these points for epoch 1997.0 are present in figures 5 and 6.

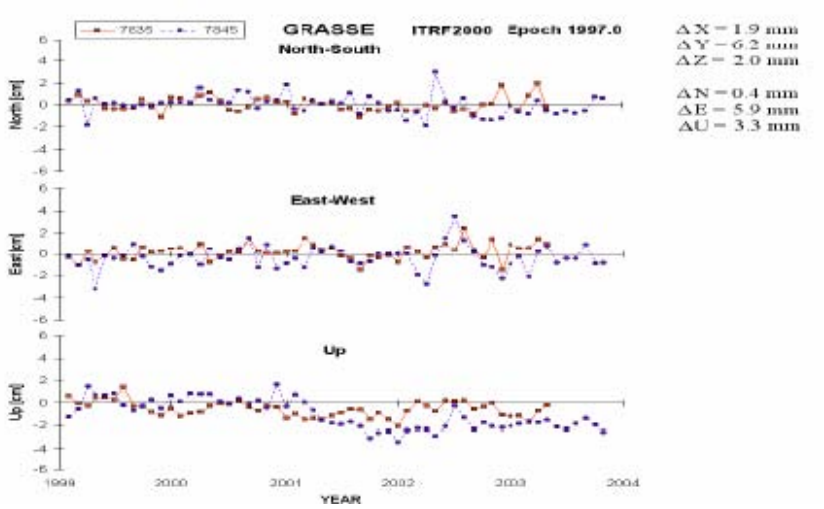

Figure 1. Topocentric coordinates of the Grasse SLR stations 7835 and 7845 in the period 1999.0-2004.0 in comparison to ITRF2000 for epoch 1997.0. The geocentric coordinates of the station 7845 were transformed to the point 7835 on the base of the local geodetic tie (Grasse log file).

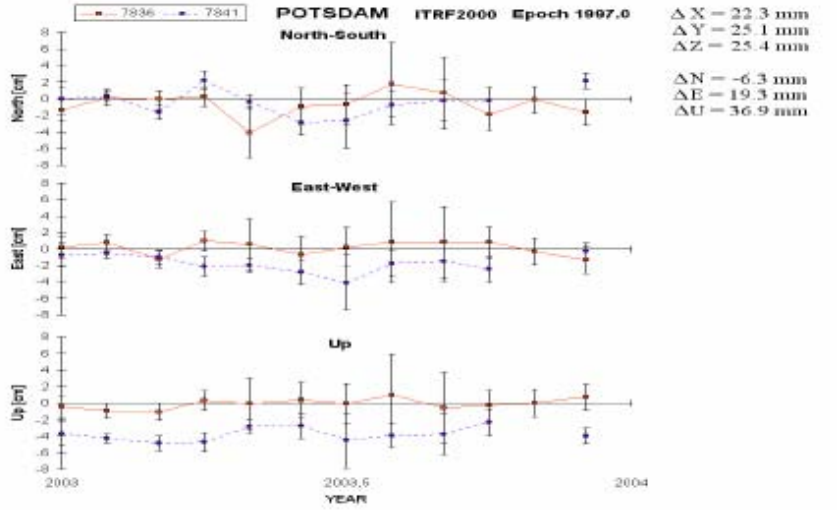

Figure 2. Topocentric coordinates of the Potsdam SLR stations 7836 and 7841 in the period 2003.0-2004.0 in comparison to ITRF2000 for epoch 1997.0. The geocentric coordinates of the station 7841 were transformed to the point 7836 on the base of the local geodetic tie (Potsdam log file).

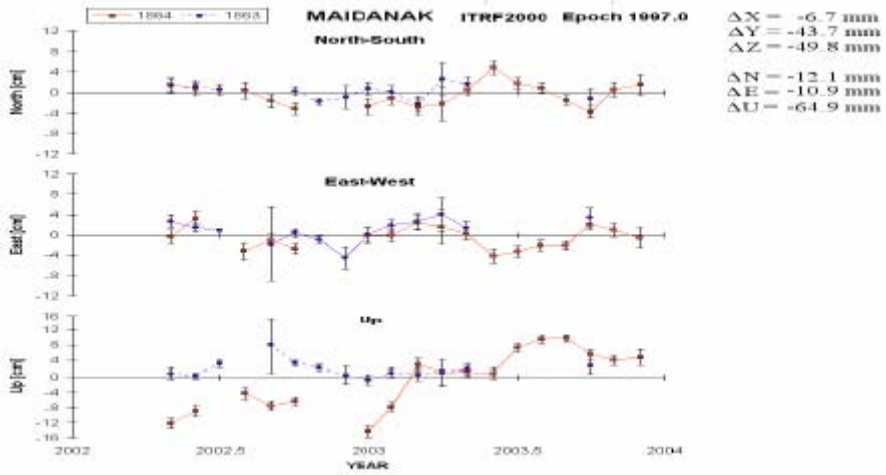

Figure 3. Topocentric coordinates of the Maidanak SLR stations 1864 and 1863 in the period 2002.0-2004.0 in comparison to ITRF2000 for epoch 1997.0. The geocentric coordinates of the station 1863 were transformed to the point 1864 on the base of the difference between geocentric coordinates of both stations.

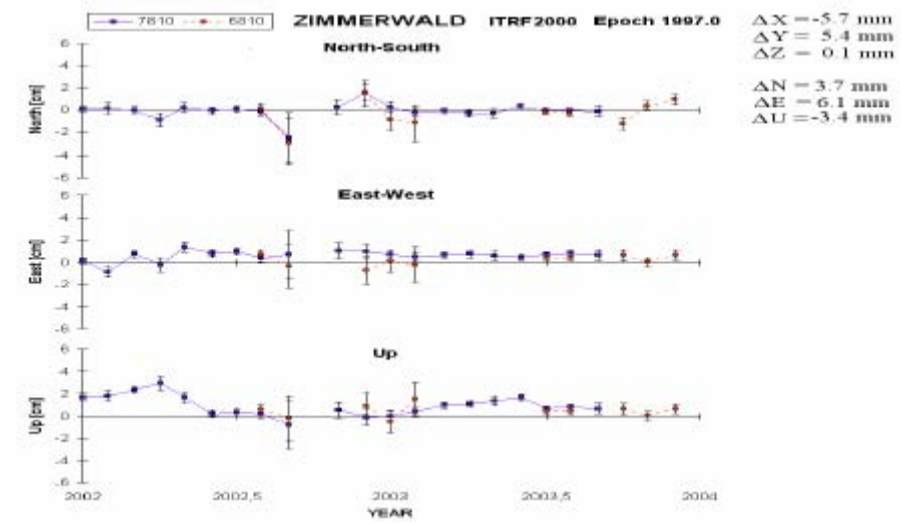

Figure 4. Topocentric coordinates of the Zimmerwald SLR station for two colors: blue (7810) and infrared (6810) in the period 2002.0-2004.0 in comparison to ITRF2000 for epoch 1997.0.

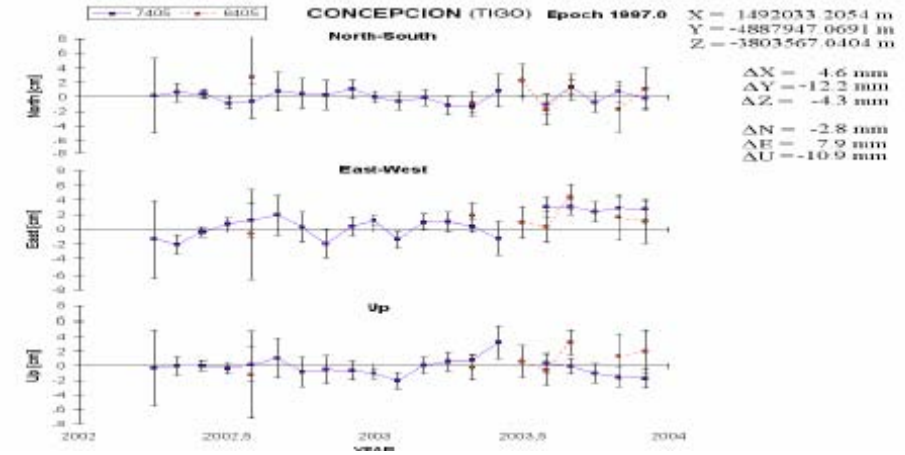

Figure 5. Topocentric coordinates of the Concepcion SLR station (TIGO) for two colors: blue (7405) and infrared (6405) in the period 2002.0-2004.0 in comparison to the new determined coordinates for epoch 1997.0.

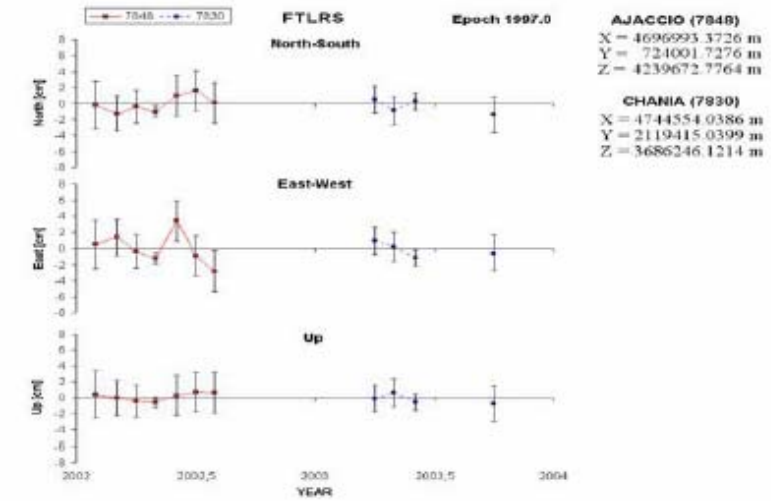

Figure 6. Topocentric coordinates of the FTLRS for two points: Ajaccio (7848) – left side, and Chania (7830) – right side, in the period 2002.0-2004.0 in comparison to the new determined coordinates for epoch 1997.0.

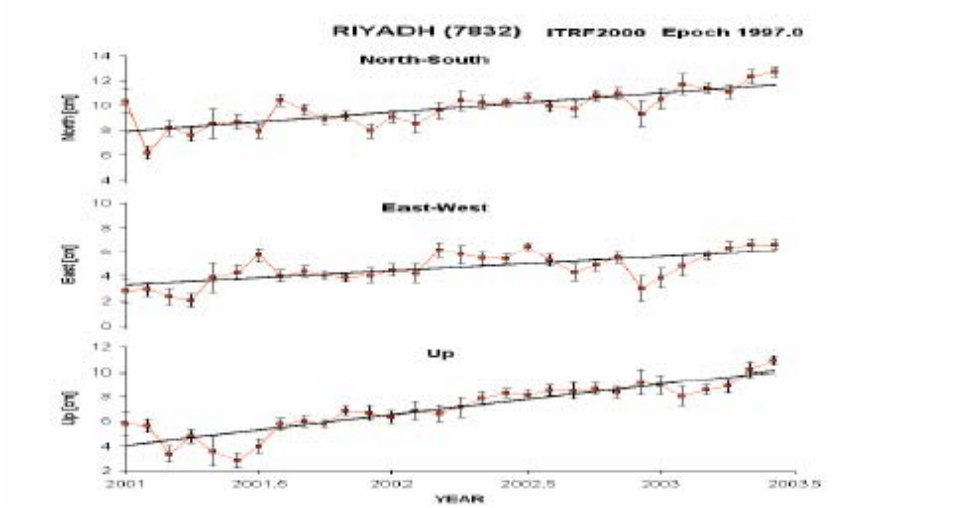

Figure 7. Topocentric coordinates of the Riyadh SLR station 7832 in the period 2001.0-2003.5 in comparison to ITRF2000 for epoch 1997.0. Non correct velocities in ITRF2000 are clearly visible.

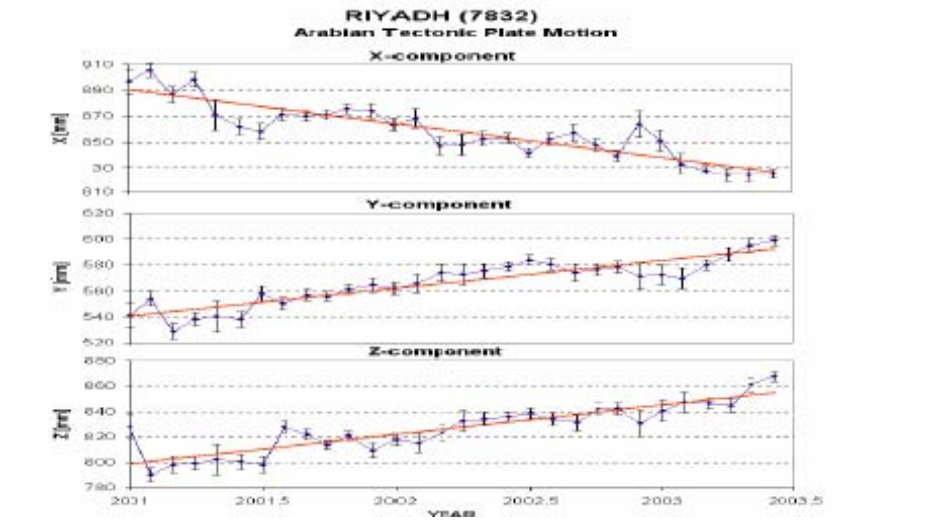

Figure 8. Geocentric coordinates of the Riyadh SLR station 7832 in the period 2001.0-2003.5 for first day of every monthly arc. Inclination of the coordinates shows Arabian tectonic plate motion.

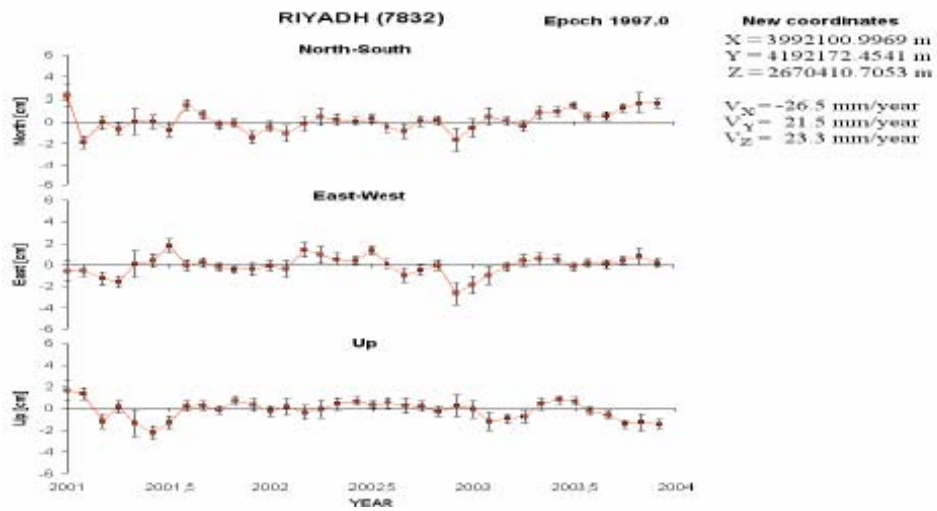

Figure 9. Topocentric coordinates of the Riyadh SLR station 7832 in the period 2001.0-2004.0 in comparison to the new determined coordinates and station velocities for epoch 1997.0.

The non correct station coordinates and velocities in ITRF2000 were detect for SLR station in Riyadh (7832)(Fig. 7). The correct coordinates and velocities for this station are very important due to its localization and high quality and quantity of results. The new coordinates and velocities of this station were determined by linear regression method from geocentric coordinates (X, Y, Z) determined for reference epoch of the every month arc (first day of the month) (Fig. 8). The new coordinates in ITRF2000 system for epoch 1997.0 attached in figure 9 are significantly better.

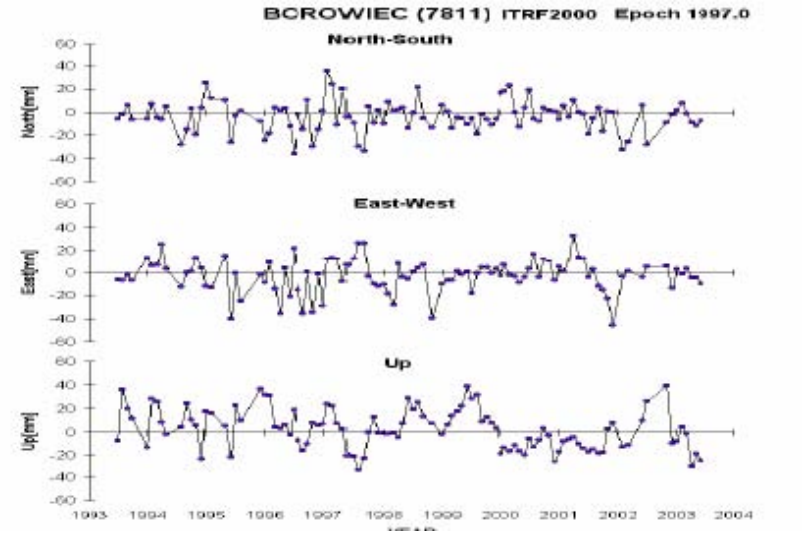

Figure 10. Topocentric coordinates of the Borowiec SLR station 7811 in the period 1993.5 – 2003.5 in comparison to ITRF2000 for epoch 1997.0

The long term stability of the station coordinates are present for Borowiec SLR station (7811) (Fig. 10). Stability of coordinates in ten years period was equal to 15.4 mm. The vertical component shows some systematic effects which reflect station Range Bias. The mean value of differences with Borowiec ITRF2000 coordinates for epoch 1997.0 for North-South, EastWest and vertical components are equal to –3.9 mm, -3.4 mm and 2.3 mm respectively. These results show very good agreement with coordinates of the Borowiec GPS station (BOR1) (the coordinates of Borowiec in ITRF2000 were mainly determined from GPS results).

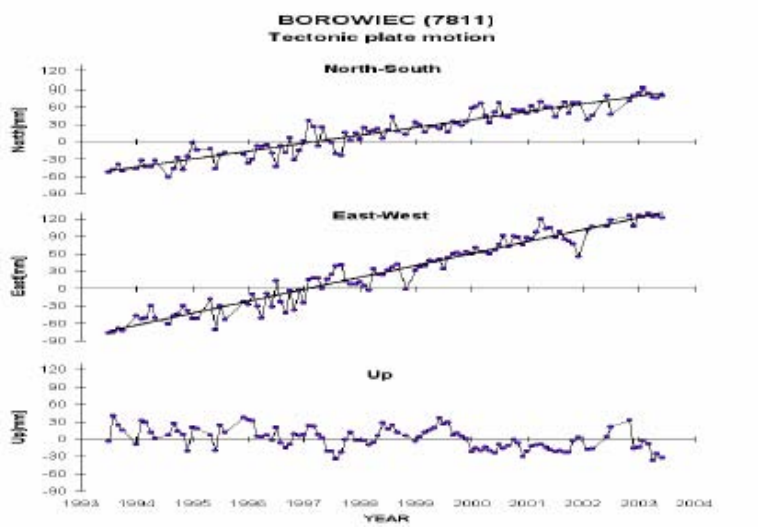

Figure 11. Topocentric coordinates of the Borowiec SLR station 7811 for first day of every monthly arc. Inclination shows Eurasian tectonic plate motion,the vertical component is free from this movement.

The coordinates determined for arc reference epoch (first day of every month) show the effect of Eurasian tectonic plate motion (Fig. 11). This effect is visible only for horizontal components. The vertical component is free from this movement (monthly coordinates are the same as in figure 10). The plate velocity is in very good agreement with tectonic plate motion model NNR-NUVEL1A and ITRF2000 velocities.

Conclusions and future plans

-Conclusions:

- good agreement between orbital results and local geodetic tie for 4.5 years period of GRASSE SLR stations confirm properly parameters and options of orbital program,
- the observatories which have two SLR stations (GRASSE, POTSDAM, MAIDANAK...) are asked for parallel observations of LAGEOS satellites as long as possible – good standard for control of the orbital method,
- accurate (1 mm) geodetic tie for these observatories and its periodical control is very important for verification of orbital analysis,
- important is the number of normal points per station – 50 NP/month is critical for coordinates determination,
- determination of the station velocities in ITRF2000 for new stations is possible with sufficient accuracy only for periods longer than two years,
- the presented method of QC of the SLR data illustrate variation of the quality (range bias, RMS) and quantity of results on one graph,
- very good agreement between orbital RMS and range biases for LAGEOS-1 and LAGEOS-2 for the most stations was detect (for example for stations 7835: 15.3, 15.3; 3.3, 4.7 mm, 7845: 18.5, 18.3; 5.9, 7.1 mm).

-Future plans:

- the all SLR stations coordinates for the period 5 years (1999.0 – 2004.0) are available (sch@cbk.poznan.pl),
- the station coordinates and the tectonic plate motions for the 10-year period (1993.5 – 2003.5) for the more than ten SLR stations will be prepared in the near future – this method is the good control of the long term or periodical positions changes,
- near-real time monitoring of the station coordinates is necessary for quick detection of station systematic errors or real position changes,
- the orbital program need upgrading for minimize the effects from orbital analysis
  - new or improved models of satellite and station position perturbations (atmosphere, loading effects, model of Earth gravity field…)
  - new precession-nutation model (IAU2000),
  - new celestial and terrestrial reference system (IAU2000).

Acknowledgements

The author wishes to thank the NASA geodesy group from the Goddard Space Flight Center for the consent to use GEODYN-II orbital program.

References

Schillak S. (2000). *Determination of the Borowiec SLR Coordinates*, Proc. 12th International Workshop on Laser Ranging, Matera, 13-17.11.2000, ed. G.Bianco, V.Luceri, Matera, Italy.

Schillak S., Wnuk E. (2002). *The Stability of the SLR Stations Coordinates Determined from Monthly Arcs of LAGEOS-1 and LAGEOS-2 Laser Ranging in 1999-2001*, Proc. 13th International Workshop on Laser Ranging, Washington, 7-11.10.2002.

Wnuk E., Schillak S., Kuźmicz-Cieślak M. (2002). *Stability of Cooridnates of the Borowiec SLR Station (7811) on the Basis of Satellite Laser Ranging*, Adv. in Space Res., 30, No. 2, pp. 413-418.

THE SLR TRACKING DATA QUALITY CONTROL DURING THE OPERATIONAL PROCESSING

H. Mueller
Deutsches Geodaetisches Forschungsinstitut (DGFI), Muenchen.
mueller@dgfi.badw.de FAX :+49-89-230311240

Abstract

Since June 2003 DGFI participates in the test phase of the operational production of station coordinates and earth orientation parameters of the ILRS Analysis Working Group. On a weekly basis we process tracking data to LAGEOS-1 and LAGEOS-2 and since March 2004 additionally to ETALON-1 and ETALON-2. During this processing we accomplish a number of quality checks, mainly detection of outliers and biases. The final biases and statistics are based on precise orbits. We will reveal the processing scheme and show some of the actual results.

Introduction

The ILRS analysis centre at DGFI processes on a weekly basis SLR tracking data to LAGEOS-1/2 and ETALON-1/2 to process combined solution containing earth orientation parameters (X-, Y-pole and LOD) and station coordinates. These solutions will be combined at the ILRS combination centres (ASI, DGFI) to compute weekly combined solutions. During this processing a number of checks were performed to guarantee a good reliable product. The quality control covers the incoming data sets, the single satellite arcs and the history of the generated products. It also includes the generation of a bias report for all four satellites, which can be accessed from our home page at **http://ilrsac.dgfi.badw.de/.**.

Processing Scheme

Every Tuesday all tracking data from the previous week, Sunday to Saturday, were collected from the Eurolas Data Center at DGFI. In a first step we perform formal checks on the incoming data sets, like double passes or wrong fields, and report problems back to EDC. For the next steps we use the DGFI developed s/w package DOGS (DGFI orbit and geodetic parameter estimation software). First we compute weekly single satellite arcs, solving for range and time biases to detect possible time biases. In a second run we solve for range biases only. For the actual processing those

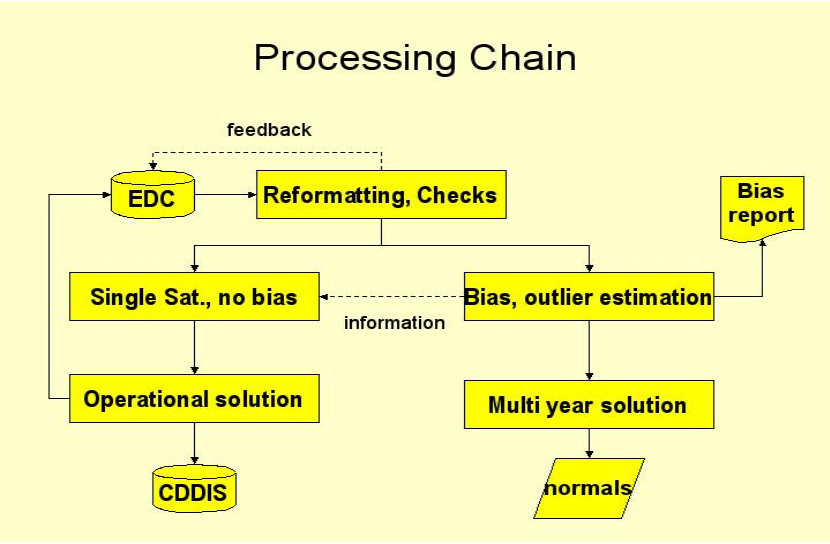

Figure 1: Processing chain of operational weekly processing

passes with range biases greater than 10 cm and time biases greater than 0.2 milliseconds were eliminated. The result of this check is listed in bias reports which contain the bias information for all stations, there are two reports per satellite and week, one with range and time bias and one with range bias only. In future there will only be one report with all range biases and only the significant time biases (see Figure 2). After that we compute four single satellite arcs and generate free normal equations. For a better analysis we visualise trends of biases and station coordinates.

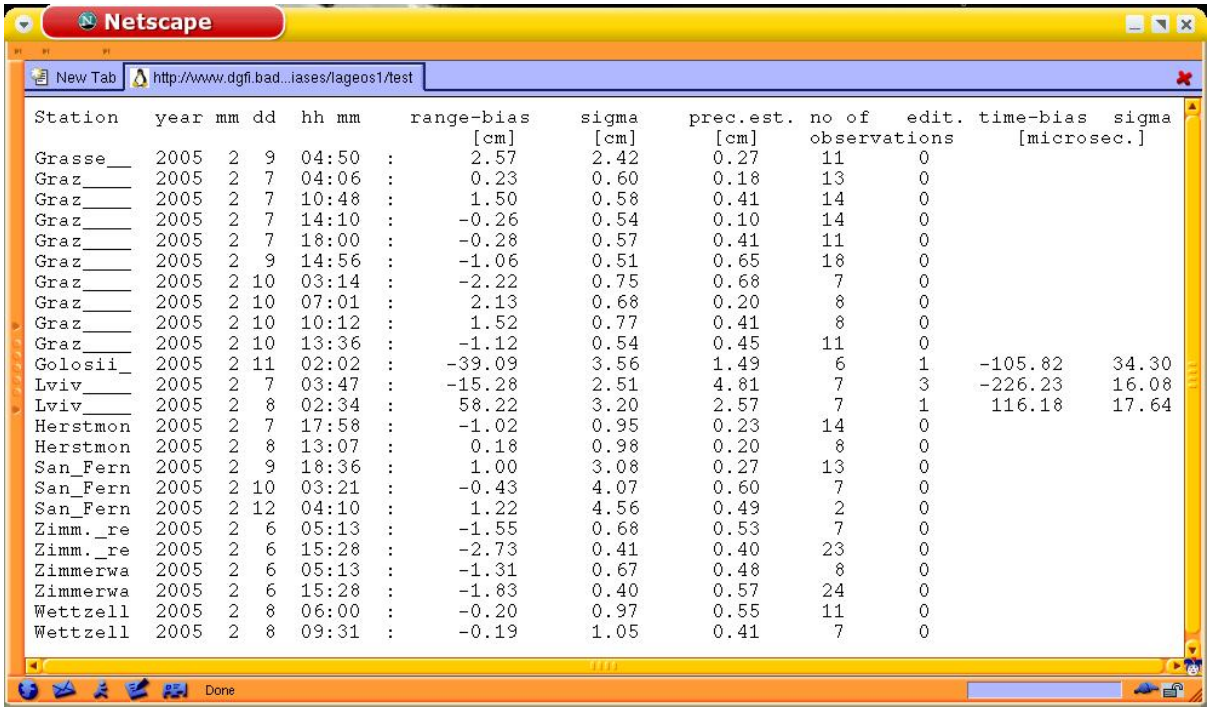

Station	year	mm	dd	hh mm		range-bias [cm]	sigma [cm]	prec.est. [cm]	no of observations	edit.	time-bias [microsec.]	sigma
Grasse__	2005	2	9	04:50	:	2.57	2.42	0.27	11	0		
Graz____	2005	2	7	04:06	:	0.23	0.60	0.18	13	0		
Graz____	2005	2	7	10:48	:	1.50	0.58	0.41	14	0		
Graz____	2005	2	7	14:10	:	-0.26	0.54	0.10	14	0		
Graz____	2005	2	7	18:00	:	-0.28	0.57	0.41	11	0		
Graz____	2005	2	9	14:56	:	-1.06	0.51	0.65	18	0		
Graz____	2005	2	10	03:14	:	-2.22	0.75	0.68	7	0		
Graz____	2005	2	10	07:01	:	2.13	0.68	0.20	8	0		
Graz____	2005	2	10	10:12	:	1.52	0.77	0.41	8	0		
Graz____	2005	2	10	13:36	:	-1.12	0.54	0.45	11	0		
Golosii_	2005	2	11	02:02	:	-39.09	3.56	1.49	6	1	-105.82	34.30
Lviv____	2005	2	7	03:47	:	-15.28	2.51	4.81	7	3	-226.23	16.08
Lviv____	2005	2	8	02:34	:	58.22	3.20	2.57	7	1	116.18	17.64
Herstmon	2005	2	7	17:58	:	-1.02	0.95	0.23	14	0		
Herstmon	2005	2	8	13:07	:	0.18	0.98	0.20	8	0		
San_Fern	2005	2	9	18:36	:	1.00	3.08	0.27	13	0		
San_Fern	2005	2	10	03:21	:	-0.43	4.07	0.60	7	0		
San_Fern	2005	2	12	04:10	:	1.22	4.56	0.49	2	0		
Zimm._re	2005	2	6	05:13	:	-1.55	0.68	0.53	7	0		
Zimm._re	2005	2	6	15:28	:	-2.73	0.41	0.40	23	0		
Zimmerwa	2005	2	6	05:13	:	-1.31	0.67	0.48	8	0		
Zimmerwa	2005	2	6	15:28	:	-1.83	0.40	0.57	24	0		
Wettzell	2005	2	8	06:00	:	-0.20	0.97	0.55	11	0		
Wettzell	2005	2	8	09:31	:	-0.19	1.05	0.41	7	0		

Figure 2: Example of the new bias report at DGFI.

As a following step we combine these normal equations and solve for station coordinates and earth orientation parameters. The results are compared with USNO Bulletin A values, ITRF2000 coordinates and produce time series of transformation parameters respectively station positions and generate plots with time series of these results. Finally we generate sinex files which will be uploaded at CDDIS and EDC. The normal equations for all satellites will be used to update the multi year solution for station coordinates and velocities.

Results

Following only an excerpt of the plots and statistics which will be generated during the weekly processing will be presented. Figure 3 shows the series of similarity transformation parameters to ITRF2000. These series will be updated weekly and are generated from the weekly transformations, see table 1. We produce bias statistics and plots for all stations. Figure 4 is an example for the tracking station Yarragadee in Australia which has a good tracking history. The biases plot shows all range biases to

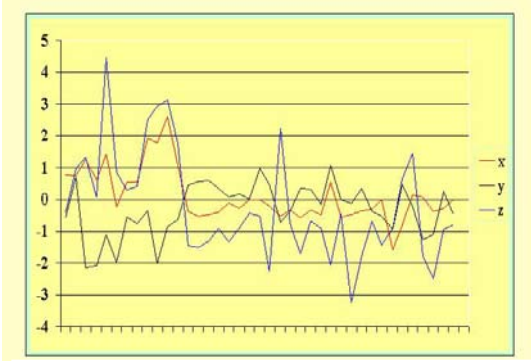

Figure 3: Similarity transformation parameters, x,y,z in centimetre of the weekly solution to ITRF2000

```
tx  [cm]:       -0.27    +-     0.50
ty  [cm]:       -0.48    +-     0.48
tz  [cm]:        0.88    +-     0.46
rx [µrad]:       0.07545 +-     0.00090   [cm]:        48.12
ry [µrad]:       0.01844 +-     0.00094   [cm]:        11.76
rz [µrad]:       0.02222 +-     0.00084   [cm]:        14.17
sc [ppm]:        0.00124 +-     0.00072   [cm]:         0.79
residuals
parametername, Phi-  Lamda-, Height- coordinate in [cm]
7839 A1  11001S002 Graz, fixed                0.20    -0.19     0.94
7811 A1  12205S001 Borowiec, fixed           -2.10     0.20    -0.31
1884 A1* 12302S002 Riga, Latvia              -0.17    -0.18     0.10
7840 A1  13212S001 Herstmonceux , fix.       -0.87    -0.96    -0.05
8834 A1  14201S018 Wettzell, Germany          0.62    -0.36     1.33
7832 A1* 20101S001 Riyad, Saudi Arabia       17.60     6.56    13.55
7837 A1  21605S001 Shanghai, China            0.31     1.57     0.03
7237 A1* 21611S001 Changchun, China          -2.39     5.77    -0.79
7838 A1  21726S001 Simosato, Japan           -1.83    -0.29    -2.93
7501 A1  30302M003 Hartebeesthoek mobil      -0.29    -1.04    -0.31
7080 A1  40442M006 Fort Davis CDP7080         0.65     1.64    -0.58
7105 A1  40451M105 Washington, Moblas-7       2.82    -0.41    -0.94
7110 A1  40497M001 Monument Peak, CA         -1.87    -1.34     0.49
7090 A1  50107M001 Yarragadee, Moblas-5       2.43     1.24     1.65
7124 A1* 92201M007 Tahiti, French Polyn      -2.48    -3.49    -1.00
7941 A1  12734S008 Matera New system          0.71    -0.47     0.67
estimated  standard deviation [cm]:    1.37277
```

Table 1: Example of the weekly similarity transformation to ITRF2000, * indicates that the station was not used for the transformation.

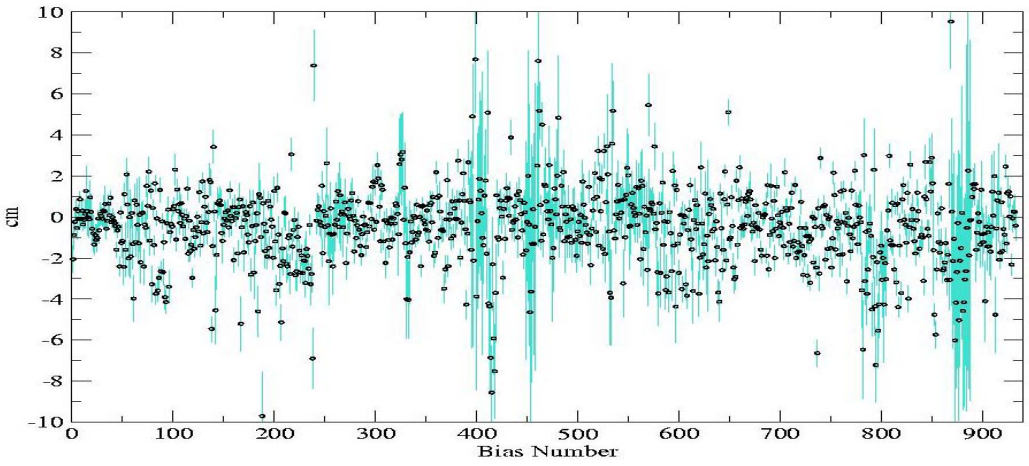

Figure 4: LAGEOS-1 **b**ias history for Yarragadee with error bars (blue)

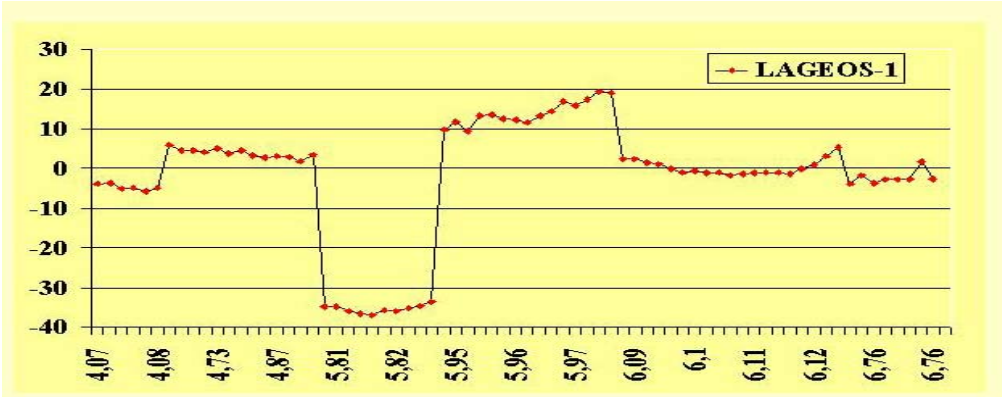

Figure 5: Residuals during one week for SLR station Riga

LAGEOS-1 from November 2003 till March 2005 with formal error bars. There are only a few biases above 5 cm which shows the stability of the station. Because of the free solution do not use produce plots of station positions. The residuals after the similarity transformation (see table 1) are available. Figure 6 shows the history for Yarragadee from June 2004 to March 2005.

In

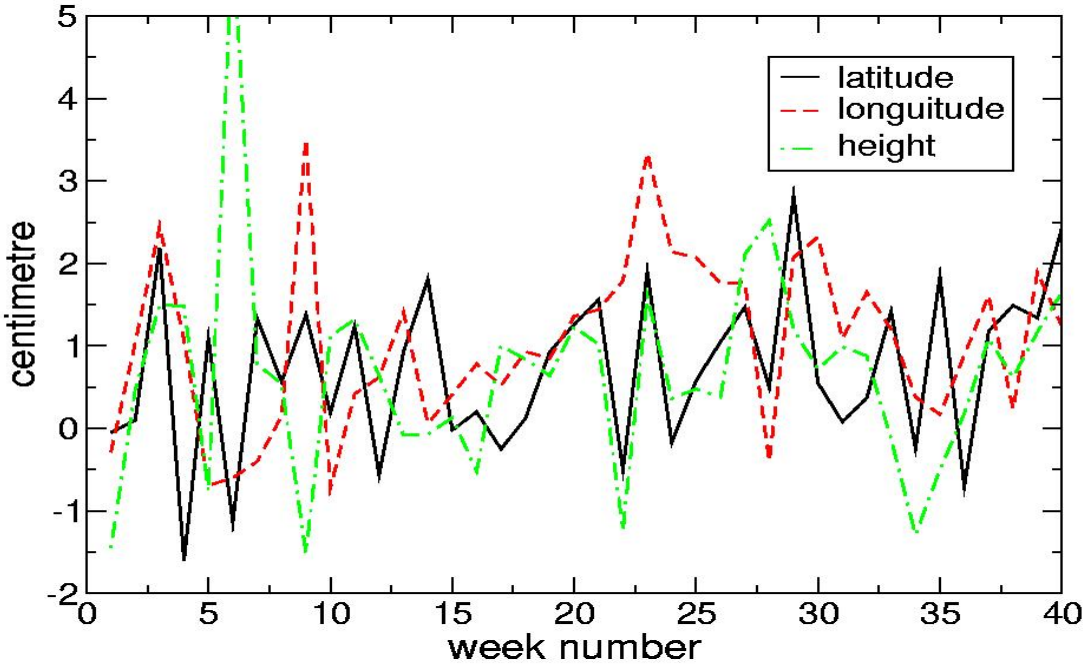

Figure 6: History of Yarragadee coordinates relative to ITRF2000

figure 5 the residuals of all observations during one week from the Riga tracking station. We use these graphics for a quick overview on the weekly arcs. In this example the bias of the third pass can identified whereas pass number four remained in the processing.

Conclusion and Outlook

Our results, as well as the results from the combination centres show the quality of the generated solutions. The plots help to detect outliers and problems. For the ETALON satellites a realistic estimation of biases is not possible because of the small number of observations and we have to develop new methods to get a realistic bias information.
Because of the ongoing work at the analysis centre we will continue to generate the bias reports, with the modification that only one bias report per satellite and week with range biases for all stations, and only significant time biases will be generated (see figure 2). A MYSQL based data bank will be installed to allow access to all plots of the station performance and transformation parameters. For a quicker overview on the station performance and the quality of the DGFI weekly solution we will add tables and plots in near future.

MCC ANALYSIS PROCEDURE OF THE SLR DATA QUALITY AND STATIONS PERFORMANCE.

V.Glotov, N.Abylchatova, V.Mitrikas, M. Zinkovsky
Russian Mission Control Center, Central Research Institute of Machine Building, Russian Space Agency
vladimir.glotov@mcc.rsa.ru; cnss@mcc.rsa.ru

Abstract

There are different independent estimations for the LAGEOSes passes quality that are calculated in the Analysis Centers. Sometimes there are the considerable differences between these results, especially for the new or not too very stable SLR stations. It is necessary to find the fruitful procedure of the complex analysis of the different Analysis Centers results for the SLR station staff support, especially in the questionable situations. In the paper are given some proposals and recommendations for this problem solving.

Introduction

Below in Figure 1 are showing the Riga station LAGEOS 1&2 range biases that given in comparison between three data Analysis Centers (CSR, MCC and DUT). The graph in the Figure 1 is taken from Kazimirs Lapushka message to ILRS and AC's. The graph is showing the problem very clear. "The differences into range biases from different Analysis Centers don't be shipped to the stations as the measuring errors" wrote K. Lapushka. For example, the pass number 175 (in Figure 1with arrowed line) showing that, where CSR and DUT are giving huge opposite RB and MCC close to zero. "Is that a Station error?" asked K. Lapushka.

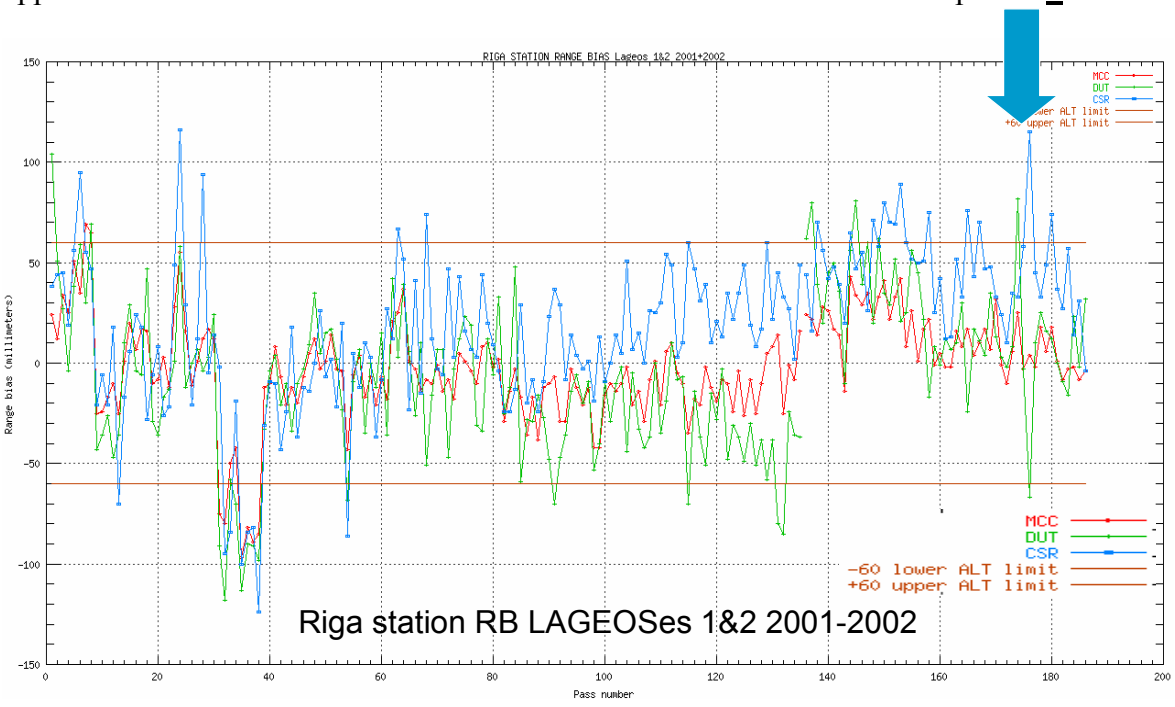

Figure 1. The estimations of the Riga station range biases in comparison between three Analysis Centers.

MCC analysis procedure of the stations performance

MCC analysis procedure of the SLR LAGEOSes data quality and stations performance is based on the following standard steps:

- SLR data analysis and "bad" points rejection using automatic or/and manual procedure
- Precise orbits determination with the its real accuracy (rms) estimation
- The measurements residuals calculation for the separate passes
- The different statistic values calculation (ME, RMS, ORMS etc.)
- The attempt to interpret the measurement residuals as function of the Range Bias and Time Bias (depending on the both ascending and descending branches tracking during estimated pass)
- The forming of "MCC Residual Analysis Report" for ILRS stations

Once more it is necessary to emphasize that really MCC Service (and other Analysis Centers) calculate the SLR data residuals based on the precise satellite orbits and station co-ordinates (see in Figure 2 the values ME – "Mathematical Expectation", RMS – "Root Mean Square for ME" and ORMS – "Root MEAN Square for the Orbit" from the MCC Weekly Residual Analysis Report). ME, RMS and ORMS are very important objective characteristics for the SLR data quality control.
Only for the next step MCC Service (and other Analysis Centers) tries to interpret the calculated SLR data residuals as Range and Time Biases based on the different mathematical procedures (see in Figure 2 the values TB – "Time Bias", RB – "Range Bias" and PRMS – "Precise Root MEAN Square for the Polynomial").
The main reasons of the different Range Bias and Time Bias results for the different Analysis Centers are following:

- Differences in the satellite precise orbits that used for the SLR data analysis
- Different co-ordinate sets of the SLR stations that used in the Centers by SLR data analysis (really it's very difficult to find the correct and precise co-ordinates for the unstable and "often modernized" stations)
- Incorrect attempts to interpret the measurement residuals as function of the Range Bias and Time Bias (Especially it's very difficult or practically impossible for the short passes)
- Differences in the "bad" points rejection procedures for Analysis Centers

Russian Mission Control Center
Residual Analysis Report

Maidanak (1864 NP)

	TTL	INC	ME	RMS	ORMS		TB	RB	PRMS	SCI
			mm	mm	mm		us	mm	mm	
1864 …	06	05	8	16	17	…	17	22	4	0
1864 …	10	07	8	17	20	…	18	6	5	0
1864 …	10	07	-28	10	32	…	8	-28	7	0

From orbits
From polynomial

Figure 2. The fragment from the MCC Weekly Residual Analysis Report.

Figure 3 shows the problems by the interpretation of the SLR data residuals as function of the Range Bias and Time Bias for the short and long passes. As you can see from the graph in Figure 3 it is impossible to find without ambiguity the RB and TB for the short passes (left graph). The

short pass data residuals can be interpret as function RB only (TB=0) or as function TB only (RB=0) or as any combination of the RB and TB. There is perfectly other situation with the long passes (the right graph in the Figure 3). There is one version in this case only for the interpretation of the SLR data residuals as function of the RB and TB. The RB and TB errors for the long passes are the consequence of the satellite orbit and station co-ordinates precision only.

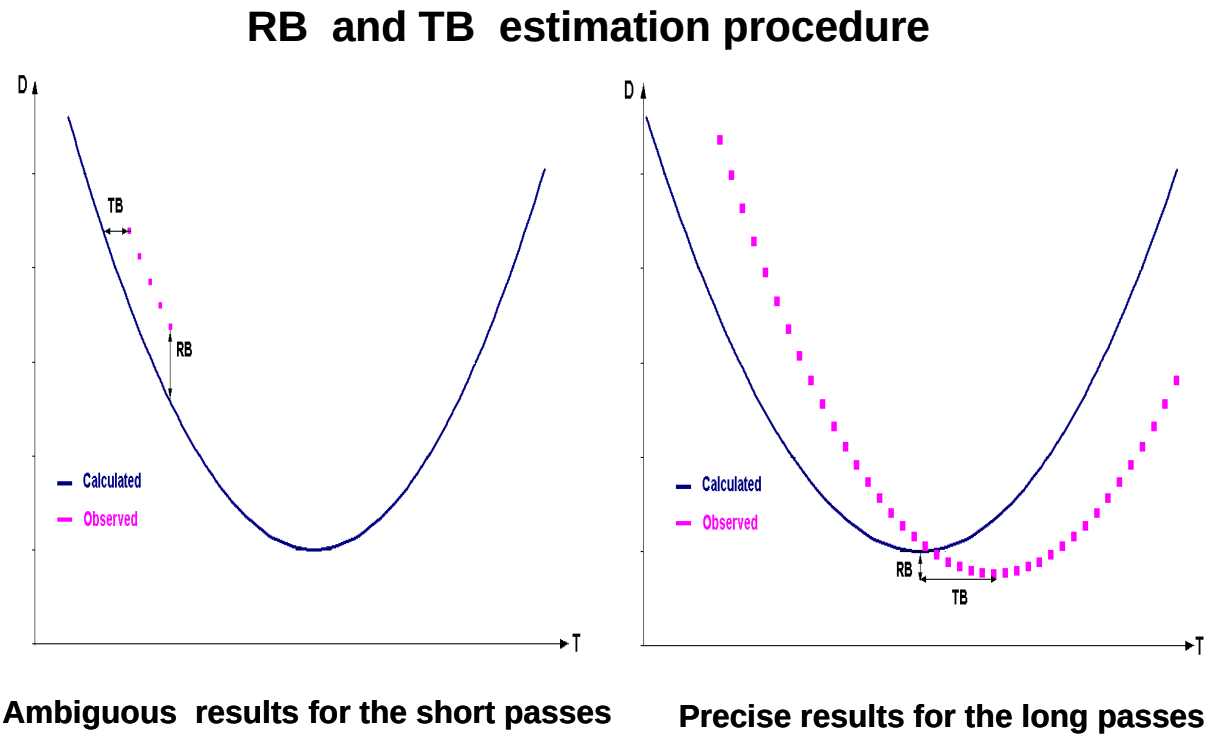

Figure 3. The estimations of the Riga station range biases in comparison between three Analysis Centers.

It is possible to propose some recommendations for the SLR stations and Analysis Centers on the base of this paper matters.

The tracking recommendations for the stations:

- Both ascending and descending branches tracking (especially for the station calibration);
- Min 10-minutes pass duration for Lageoses and 5-minutes for low orbiters;
- Min 6 QLNP per one pass;
- Min 20 deg elevation (especially for the station calibration);
- As much passes duration as possible (especially for calibration and precise TB and RB estimation).

The recommendations for the Analysis Centers:

- The coordination in the main methodology questions by the SLR data analysis;
- The agreement of the stations coordinates sets;
- The coordination in the RB&TB understanding for the both (long and short) passes;
- The separation of the short and long (calibrating) passes estimation;
- The timely and quickly contacts with other Analysis Centers in the case of necessity based on the concrete ILRS solution and recommendations

18 YEARS OF QC ANALYSIS AT DELFT UNIVERSITY OF TECHNOLOGY

R. Noomen
Department of Earth Observation and Space Technology, Delft University of Technology, Delft, The Netherlands.
ron.noomen@deos.tudelft.nl

Abstract

In this paper the development and performance of the Quick-Look Data Analysis Center of Delft University of Technology over almost two complete decades is evaluated. Based on orbit computation of the LAGEOS satellites, this analysis has been used for a variety of purposes: (i) support of the WEGENER/MEDLAS project, (ii) rapid-turnaround EOP determination, and (iii) quality control of the global network of SLR stations. The threshold for reliably assessing possible data problems has been reduced by a factor of about 10 over this time-frame, to a level of a few cm at this moment. In addition to illustrating this development and highlighting current performance, recent developments are also addressed.

Introduction

The Quick-Look Data Analysis Center (QLDAC) of Delft University of Technology was initiated in the mid-1980s, as one of the Delft contributions to the WEGENER/MEDLAS project [*Reinhart 1985*]. This project was aimed at the determination of crustal deformations in the central and eastern Mediterranean area, by deploying transportable SLR systems on specific locations for relatively short periods of time, and doing repeat observations in successive years. QLDAC started its operations officially in January 1986. With the exception of the first few months of 1987, the analysis system has operated continuously, and still does so to this very day. In essence, three different (partly overlapping) time-periods can be distinguished, which are more-or-less governed by the specific targets of the weekly analyses.

Initially, the analysis activities were fully devoted to support the observational campaigns. Here, the specific goal of the analysis was twofold: (*i*) perform a semi real-time quality assessment of the observations taken by the mobile SLR systems, and (*ii*) keep track of the number of high-quality passes taken on LAGEOS-1 (LAGEOS-2 was launched in October 1992). As for the first requirement, it was crucial to spend as little time as possible at any location. Possible data problems needed to be identified as soon as possible, which prompted this QC service. At the time, a turnaround period of between 3 days and 10 days was considered acceptable: the analyses were performed every Tuesday, and basically covered the full week from Sunday to Saturday prior to that. As for the second requirement, it was deemed necessary to acquire 50 good passes on LAGEOS-1 to fulfil the science objective, and once that was achieved, to move to the next location. QLDAC operated in this campaign-oriented style in the years in which WEGENER/MEDLAS organized campaigns in the Mediterranean area: 1986, 1987, 1989 and 1992.

A second characteristic element was initiated in the middle of 1987. Initially considered as a by-product, QLDAC was ”forced” to solve for Earth Orientation Parameters (EOPs) on a regular basis to maximize the quality of the geometric component of the weekly analyses. Since the semi real-time monitoring of polar motion was an activity done by few analysis

centers only at the time, QLDAC was approached by the BIH to submit these parameters for inclusion in their weekly reports. This started in the middle of 1987, and continues to this very day (as contributions to the IERS Bulletin A reports).

Finally, the QC service was expanded to the entire network of SLR stations: it was soon realized that the QC activities were equally well applicable to the other SLR stations, and could be used for their benefit was well. This more global target came to fruition in the years after 1992 for obvious reasons.

Measurement statistics

It is worth while to take a look at the input material first. A direct issue here is statistics on the number of stations and passes that have been processed by QLDAC. Figure 1 shows the yearly number of stations that have been active, as well as the yearly number of passes obtained on each of the satellites LAGEOS-1 and –2 (table complete until May 2004).

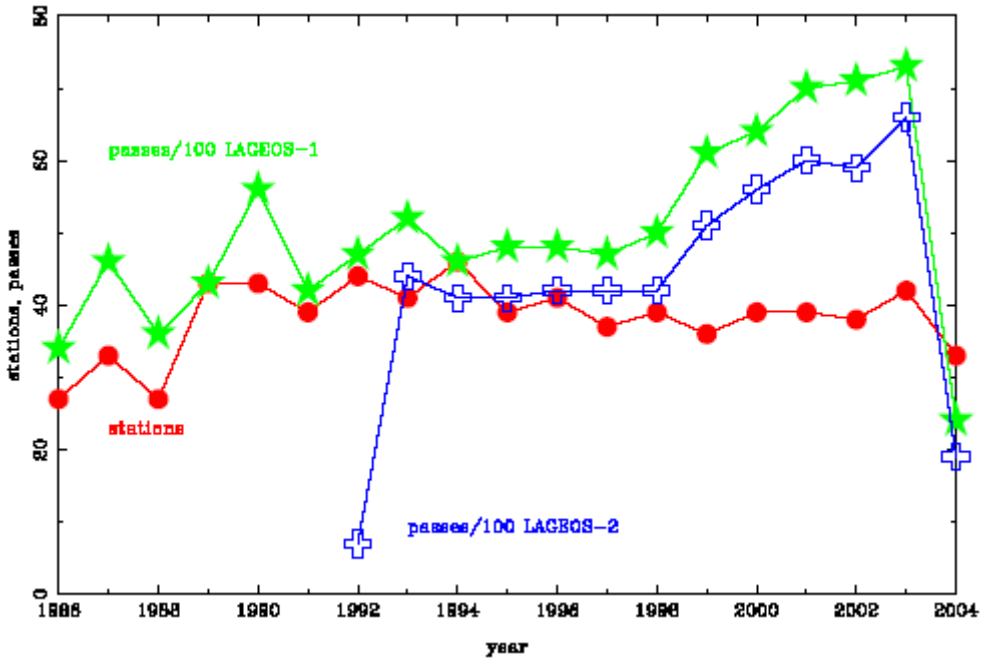

Figure1: Overview of the yearly number of stations that have tracked LAGEOS-1 and/or LAGEOS-2, plus the yearly number of passes on each of those satellites.

It is clearly visible that the number of stations was modest in the late 1980s, but rapidly increased to about 40 since then. The yearly number of satellite passes shows a steady value in the years until 1998, and a linear rise in the years after that, to about 7500 for LAGEOS-1 and about 6500 for LAGEOS-2. Since the number of stations remains stable, this increased productivity must be ascribed to better efficiencies: more shifts, interleaving, automation, less hardware failures, etc. The data yield on LAGEOS-1 exceeds that of LAGEOS-2 because of more favorable orbital characteristics of the former.

Quality

A crucial element of the QLDAC analyses is of course the overall quality of the computation results; this holds in particular for the QC aspect. This is basically driven by three issues: (*i*) the quality of SLR observations themshelves, (*ii*) the quality of the computation model and (*iii*) the analysis strategy, including the parameters that are solved for and related issues.

Observations

Clearly, the first issue is beyond the control of any analysis center. However the claimed

precision or consistency is known to have improved considerably with time. To illustrate this, Figure 2 shows the single-shot RMS values for a number of stations in thier configuration of 1997 and 2002. It is obvious tha these stations (representative for the entire network) have shown considerable progress on this aspect. Clearly, they (and effectively the far majority of the global network) are below 20 mm level for single-shot precision, with obvious consequences for the precision of their normal points. The absolute accuracy can be expected to have made similar progress, and this will be the subject of the next section.

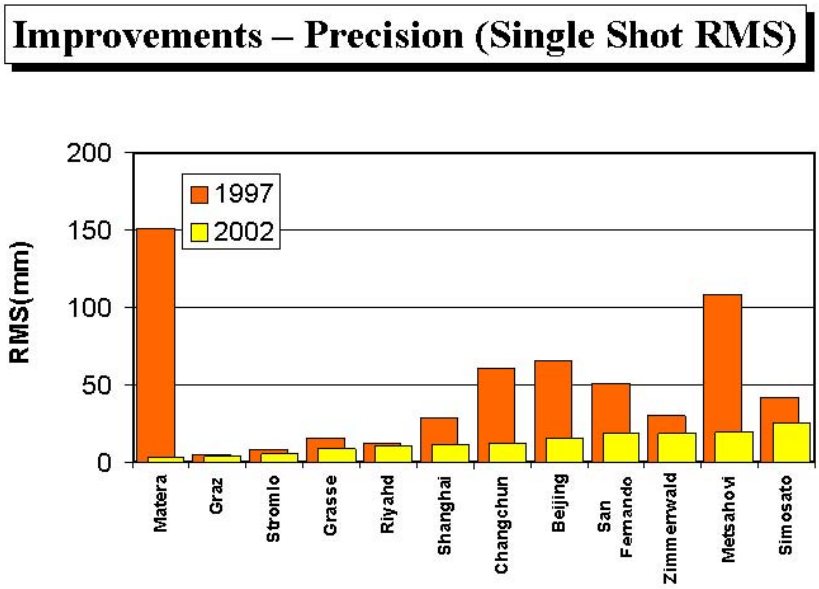

Figure 2: The single-shot precision of a number of SLR stations, for their technical configurations of 1997 and 2002 (courtesy Van Husson).

Models

The quality of the computation model and the analysis strategy are crucial for the level of significance of the QC service. The most important developments are summarized in Table 1. This table clearly shows that the improvements have taken place continuously throughout this 18-year period, albeit that new elements have been introduced ”block-wise” at specific dates. Because of the high altitude of the satellites, the LAGEOS pair is relatively insensitive to the (details of the) dynamic forces acting on it; it is reasonable to expect that the changes in the geometric component of the problem (earth reference system, measurement modeling) have played a dominant role here.

Although not of direct influence on the overall technical performance of the analysis system, it is worthwhile to mention here that QLDAC has gone through various stages of practical implementation of the QC activities. Initially, in the WEGENER/MEDLAS years, the analysis system relied on human interference: manual starting of the various conversion and analysis steps, a detailed checking of results, etc. In the 1990s, the system was basically operated in a menu-driven configuration, with interactive means to perform a large variety of QC activities, but always in need of a human operator. Reflecting the decrease of human capacity, the absence of dedicated observational campaigns and benefitting from the improved quality and reliability of the SLR observations and the means of communication, the QLDAC analysis options were trimmed down to the basic elements and the overall system was converted into a fully automatic mode of operation around the turn of the year 2002/2003; in essence, checking of the results is not done until several hours after they have been distributed to the community (or, in case of holidays or meetings abroad, weeks after the event).

Results

The core of the analysis activities is the fitting of a mathematical model of the satellite orbit(s) through the observations taken by the global SLR network, currently in data arcs of 8 days length. This is done with the NASA program for data reduction and geodetic parameter estimation GEODYN-II [*Eddy 1990*]. Here, the root-mean-square of the weighted residuals (the difference between the actual

date	model element	strategy
January 1986	*initial setting*	*initial settings*
May 1987	DUT/SOM 87.1 station coordinates	
	Wahr solid earth tides	
	Schwiderski ocean tides	
April 1989	GEM-T1 gravity and tides	
	DUT/SOM 89.3 station coordinates	
July 1991	GEM-T2 gravity and tides	data weight rss 50 mm + station noise
	DUT/SOM ERS90 station coordinates	
October 1992	LAGEOS-2	1-cpr radial accelerations estimated
	251 mm c.o.m. offset	
January 1994	JGM-2 gravity and tides	3-day EOPs estimated
	DUT/SOM 93L05 station coordinates	data weight rss 30 mm + station noise
January 2003	EGM96 gravity and tides	1-cpr cross-track accelerations estimated
	ITRF2000 station coordinates	data weight rss 15 mm + station noise
	zero degree elevation cut-off	
July 2003	ocean loading	1-day EOPs estimated
	atmospheric pressure loading	degree-1 gravity field terms estimated
		estimation of 1-cpr terms twice per arc

Table 1: Overview of the major developments in the QLDAC processing.

observations and the model equivalents) is minimized. Therefore, this rms-of-fit is a good first indicator of the quality of the solution. The time-history of this rms-of-fit is depicted in Figure 3, which covers the full period from 1986 to May 1, 2004. The thin line shows the values for the individual analyses, whereas the red line indicates the running average taken over 15 weekly computations.

It is clearly visible that this fit, and thus the quality of the orbital solutions and that of other parameters, has made significant progress through time: from about 10-12 cm in the WEGENER/MEDLAS days to a consistent 10-15 mm in 2004. As expected, this trend shows a large correlation with the development of the analysis model and the modifications in the analysis strategy, as reported in Table 1. It will be obvious that the capabilities for the monitoring of the performance of the individual SLR stations, including the detection of possible data anomalies, are proportional to this overall rms-of-fit. In essence, it means that the current threshold for detecting potential data problems (in particular possible range biases) can be put at about 2-3 cm, or equivalent to two times the level of significance as represented by the weighted rms-of-fit.

As an illustration of the current capabilities, Figure 4 shows just one example of the estimated values for the apparent range biases of the station Yarragadee (Australia, site id 7090). This example is representative for the results obtained weekly for the entire network of SLR stations. These biases are not necessarily to be considered as real (systematic) errors in the SLR observations; as long as they remain below the 2σ level (*i.e.* about 2-3 cm), they may

equally well reflect the radial uncertainty of the (satellite orbit) solution and/or the model (station coordinates). Only when these range bias values exceed this value, the result is to be interpreted as an actual systematic error of the observations, albeit with an inherent uncertainty of a few centimeter again. Figure 4 also shows the values derived by the Center for Space Research (CSR) in Austin, Texas. It is clearly visible that the CSR solutions, too, show a similar inherent bias uncertainty of 1-2 cm for this station. It can be shown that real range biases are picked up by QLDAC and CSR with a consistency of a single cm or better. Equivalently, the analysis system provides estimates for the so-called timing

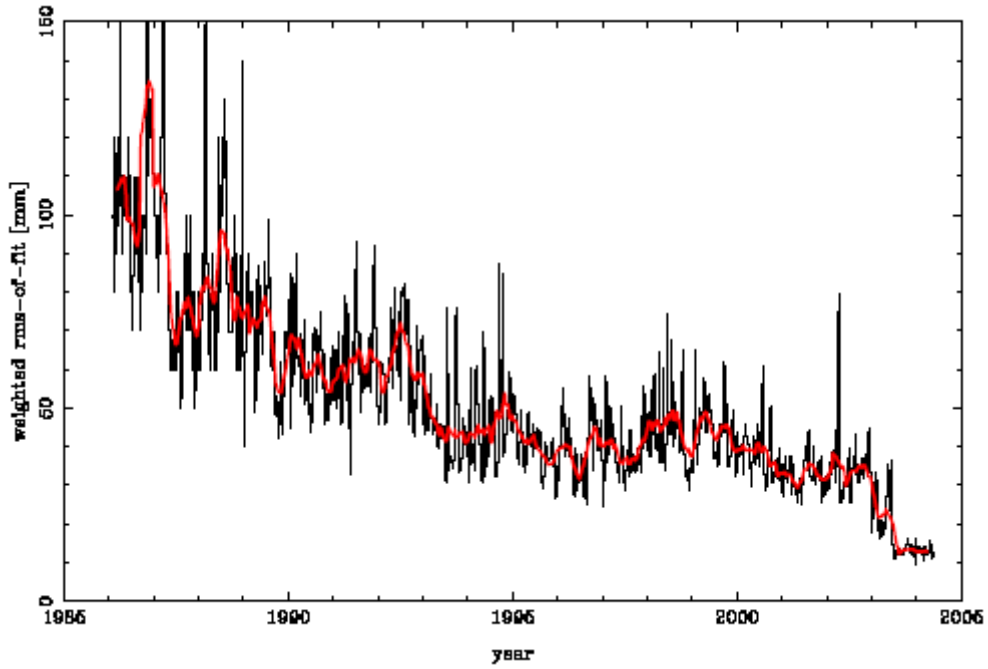

Figure 3: The weighted rms-of-fit of the weekly data analysis, covering the 18-year period over which QLDAC has been operational.

biases. However, since the SLR stations are synchronize dat the level of a single nanosecond by virtue of GPS timingt echniques, it is unrealistic to interpret these timing biases as real errors of the (time-tagging of the) SLR observations, unless they are very large. Instead, they represent either uncertainties of the orbital solutions, or errors in the model for this particular station position. These timing biases typically have an rms value of about 12 μsec, which corresponds with an uncertainty in the along-track component of the orbital solutions of about 5 cm [*Bock2004*].

As mentioned before, one of the spin-offs of the weekly QC analyses is the solution of EOPs. Because of the 100% correlation with the ascending node of the satellite(s), estimation of the UT1-UTC component cannot be considered as a realistic contribution, and is to be ignored by definition. The time-interval for which EOPs have been estimated has changed throughout the years from 5 days to 3 days to 1day (cf. Table 1). The rms scatter of the daily pole position solutions is about 0.4-0.5 marcsec. A similar rms value was representative for the quality of the EOP solutions in the late 1980s and 1990s, albeit for 5-day and 3-day estimation intervals, so progress is visible here too.

Recent developments

At this moment (June2004), the QLDAC analyses are performed on a weekly basis: the QC assessments are performed every Tuesday, and relate to the observations taken in the previous week running from Sunday to Saturday. It is recognized that this analysis frequency and delay

w.r.t. the actual epoch of data-taking is far from ideal according to modern standards. Therefore, QLDAC has been testing a daily analysis of the observations. This analysis is performed around noon every day, and covers the 8 full days directly prior to the day on which the analysis is done. Intechnical details and procedures, this daily analysis is identical to the current standard product. Clearly, the major benefit from this high-frequency evaluation is the rapid QC feedback to the stations. These can be expected to benefit from the rapid turn-around of these new high-frequency analyses (which, on average, reduces the time-delay from 0.5 x 8 + 2 = 6 days to 0.5 + 0.5 = 1 day). This new daily service will replace the current weekly service in the Summer of 2004.

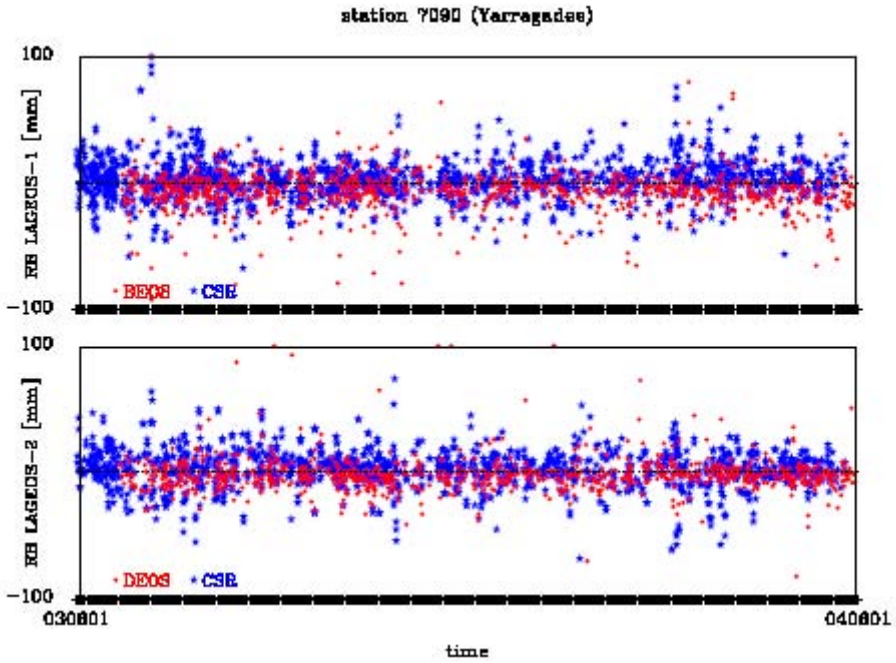

Figure 4: Time-history of the apparent range biases of station Yarragadee (Australia, 7090), as determined by QLDAC (red circles) and CSR (blue stars), during the period June 2003 - June 2004, for LAGEOS-1 (top) and LAGEOS-2 (bottom), respectively.

Conclusions

In conclusion, the performance of QLDAC has shown a considerable development over the course of almost two decades as described here, and with it the capability to detect possible data problems: initially this was at the level of several dm, whereas nowadays this has been reduced by a factor of about 10. QLDAC is expected to shift from a weekly, fully automated operational scheme to a daily scheme, in order to better satisfy modern turn-around requirements for data quality evaluations.

Acknowledgements

The following persons are creditted for their valuable contributions to the (development of the) Quick-Look Data Analysis Center throughout the 18-year period described here: Boudewijn Ambrosius, Dagmar Bock, Wim van Gaalen, Ernst Hesper, Hans Leenman, Robert de Muynck, Gert-Jan Ourensma, Wim Simons, Karel Wakker. We thank the SLR community and its representative organisation, the ILRS, for providing the measurements without which this activity never would have been initiated. Richard Eanes (CSR) is courteously acknowledged for providing input to this paper through his weekly analysis reports. Van Husson (HTSI) is credited for providing the picture with the single-shot precision.

References

Bock, D., R. Noomen and H.-G. Scherneck, *Atmospheric pressure loading deformation at SLR stations*, J. Geodynamics, 2004 (submitted).
Eddy, W.F., J.J. McCarthy, D.E. Pavlis, J.A. Marshall, S.B. Luthke, L.S. Tsaoussi, G. Leung and D.A. Williams, *GEODYN-II Systems Operations Manual* Vol. 1-5, contractor report, ST System Corp., Lanham MD, USA, 1990.
Reinhart, E., P. Wilson, L. Aardoom and E. Vermaat, *The WEGENER Mediterranean laser tracking project: WEGENER-MEDLAS*, CSTG Bulletin, Vol. 8, p. 145-162, 1985.

RAY MATRIX APPROACH FOR THE REAL TIME CONTROL OF SLR2000 OPTICAL ELEMENTS

John J. Degnan
Sigma Space Corporation, Lanham, MD 20706 USA
John.Degnan@sigmaspace.com, FAX: +01-301-552-9300

Abstract

NASA's SLR2000 is an autonomous, eye-safe, photon-counting satellite laser ranging (SLR) system. As such, it requires some unique real-time control elements that are not generally found in conventional, high powered, manned systems. These include autonomous mechanisms and associated software for: (1) maintaining telescope focus over wide ambient temperature excursions; (2) conducting automated star calibrations and updating mathematical mount models; (3) centering the optical receiver field of view (FOV) on the satellite return based on single photon returns; (4) varying transmitter beam divergence and point ahead; and
(5) controlling the receiver spectral bandwidths and spatial Field-of-View (FOV). Most of these real-time functions can be accomplished mathematically by utilizing a ray matrix approach. As an additional benefit, the ray matrix model can be used as a diagnostic tool to track the geometric size and orientation of beams and/or images anywhere in the system. Recent optical analyses of SLR2000 using the ray matrix model and experiences gained in satellite field experiments have led to some proposed modifications and simplifications to the optical transceiver, which will also be discussed.

INTRODUCTION

Paraxial ray matrices are a convenient and simple way to model ray propagation in optical systems [Kogelnik and Li, 1966]. In complex 3-dimensional systems, reflections off mirrors cause the propagation path to change direction several times, and one must go through a series of coordinate transformations where the precise form of the matrix depends on whether we are dealing with the p-component (in the mirror plane of incidence) or s-component (orthogonal to the plane of incidence) of the ray. In SLR2000, the ray changes direction 9 times before encountering the exit window of the telescope. If we consider a segment where propagation is along the local d-axis, any ray can be represented by the vector $r = (p\ \alpha p\ s\ \alpha s)$ where (p,s) is the transverse position of the ray at the optical element and (αp, αs) is the angle the ray makes with the d-axis when projected into the p-d and s-d planes respectively. Each optical element or propagation path between elements is represented by a 4x4 matrix, which operates on the position and direction of the ray. The SLR2000 optical train consists of three major subsystems: (1) optical transceiver; (2) the Coude mount; and (3) the main telescope. Each major subsystem can be represented by a single 4x4 matrix equal to the product of the element matrices making up that subsystem. From Figure 1, we see there are three parallel branches within the optical transceiver: (a) the transmitter/Risley prism path;
(b) quadrant detector range receiver (two equal but orthogonally polarized paths) and (c) CCD star camera. In what follows, the initial propagation path for each branch (d-axis) runs vertically (down to up) in the figure, the positive p-axis on the transceiver bench points to the right of the figure (as if we were looking from behind the various elements toward the telescope), and the s-axis is directed out of the page toward the reader.

In this paper, we provide a summary of the analytical results. A detailed mathematical analysis of the SLR2000 system [Degnan, 2004] yields the following 4x4 matrices for rays

propagating from the transceiver bench to the telescope exit window. The matrices describing outward propagation through the three branches of the transceiver have the general form

$$M_{1x} = \begin{vmatrix} a_x \Lambda & b_x \Lambda \\ c_x \Lambda & d_x \Lambda \end{vmatrix} \qquad \Lambda = \begin{vmatrix} 1 & -1 \\ 1 & 0 \end{vmatrix}$$

a = transmitter
x = b = quadrant detector
c = star camera

*a*nd the specific forms

$$M_{1a} = \begin{vmatrix} 3\Lambda & 2.267\Lambda \\ 0\Lambda & 0.333\Lambda \end{vmatrix} \quad M_{1b} = \begin{vmatrix} 0.079\Lambda & 2.57\Lambda \\ -0.0392\Lambda & -0.101\Lambda \end{vmatrix} \quad M_{1c} = \begin{vmatrix} -35.559\Lambda & 0.405\Lambda \\ -2.469\Lambda & 0\Lambda \end{vmatrix}$$

All of the mount motion is contained in the matrix for the Coude mount given by

$$M_2(\gamma) = \begin{vmatrix} \Gamma & d_c\Gamma \\ 0 & \Gamma \end{vmatrix} \qquad \Gamma = \begin{vmatrix} -\cos\gamma & -\sin\gamma \\ \sin\gamma & -\cos\gamma \end{vmatrix} \qquad \gamma = \alpha - \alpha_0 - \varepsilon$$

where d_c = 1.742 m is the total Coude path length, a is the azimuth angle, e is the elevation angle, and a_o = 67.4º (defined in Figure 1 where North corresponds to 0º azimuth). Finally the telescope matrix is

$$M_3 = \begin{vmatrix} m_t I & d_t I \\ 0 & 1/m_t I \end{vmatrix} \qquad I = \begin{vmatrix} 1 & 0 \\ 0 & 1 \end{vmatrix}$$

and m_t = 10.16 is the main telescope magnification and d_t = 5.758 m.

For outgoing rays, one now multiplies the three matrices together to transfer a ray emanating from one of the branches of the transceiver, $\vec{r}_x$, to the output window of the telescope, i.e

$$\vec{r}_{out} = M_{tot}\,\vec{r}_{in} = M_3\,M_2(\gamma)\,M_3^{-1}\vec{r}_{in} = \begin{vmatrix} A_x\Gamma' & B_x\Gamma' \\ C_x\Gamma' & D_x\Gamma' \end{vmatrix} \vec{r}_{in} \qquad \Gamma' = \begin{vmatrix} -\sin\gamma & \cos\gamma \\ -\cos\gamma & -\sin\gamma \end{vmatrix}$$

The transfer of incoming rays, $\vec{r}_{in}$, from the telescope exit window to one of the three transceiver branches is given by the inverse of the matrix, i.e.

$$\vec{r}_x = M_{tot}^{-1}\,\vec{r}_{in} = M_{1x}^{-1}\,M_2^{-1}(\gamma)\,M_3^{-1}\vec{r}_{in} = \begin{vmatrix} D_x\Gamma'^{\mathrm{T}} & -B_x\Gamma^{\mathrm{T}} \\ -C_x\Gamma'^{\mathrm{T}} & A_x\Gamma'^{\,\mathrm{T}} \end{vmatrix} \vec{r}_{in} \qquad \Gamma'^{\mathrm{T}} = \begin{vmatrix} -\sin\gamma & -\cos\gamma \\ \cos\gamma & -\sin\gamma \end{vmatrix}$$

STAR CALIBRATIONS

Overall system focus is maintained over a wide ambient temperature range by a computer-controlled three-power beam expander located in the common transmit/receive path. The quality of the system focus is determined and controlled by the sharpness of star images in the

CCD camera used for star calibrations. Periodic image checks ensure not only the sharpnessof the star image for calibration but also the collimation of incoming and outgoing beams in other legs of the transceiver and the stability of the system focus at the variable aperture field stop (spatial filter).

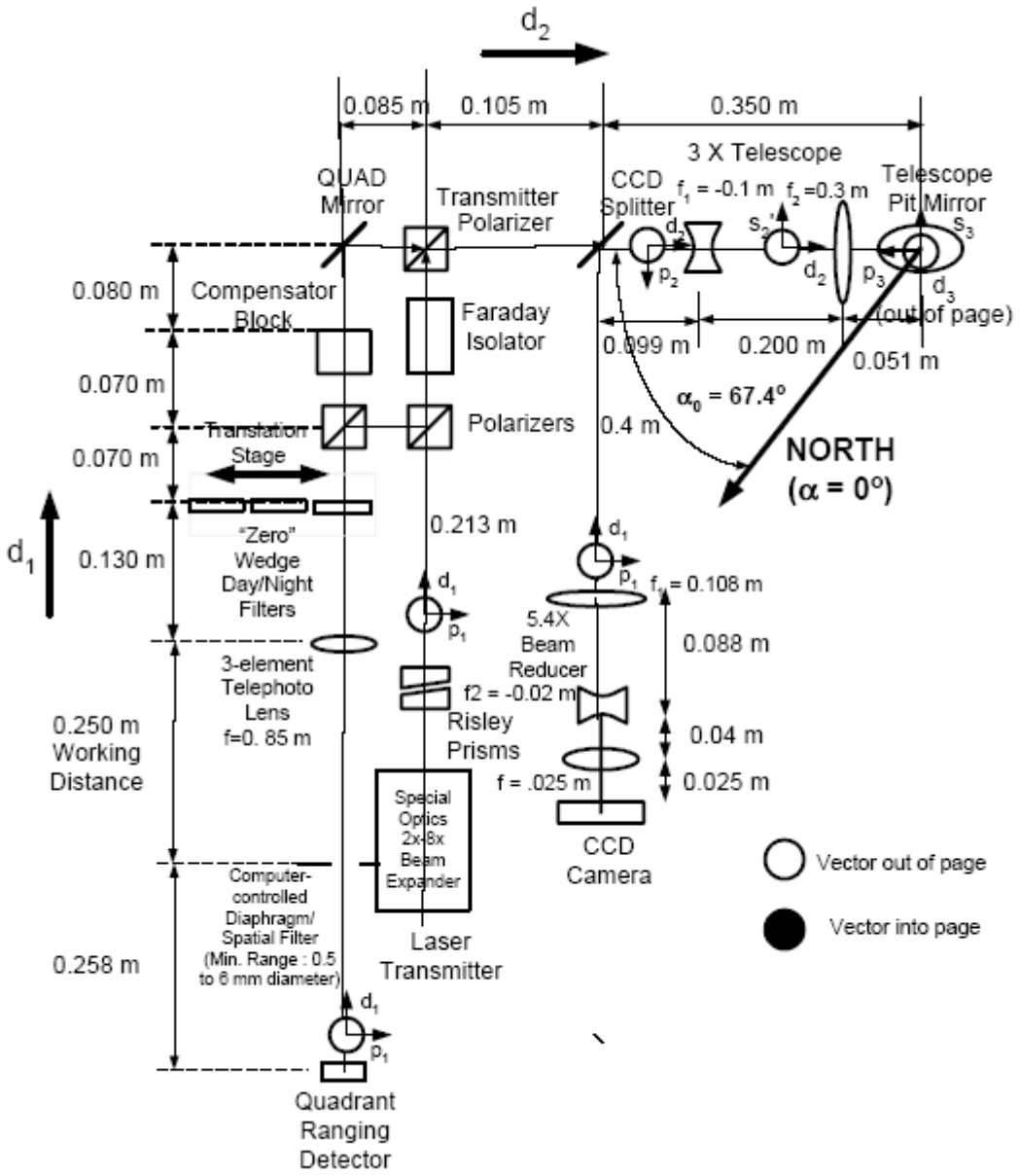

Figure 1: Block diagram of the upgraded SLR2000 optical transceiver.

For star calibrations, the ray model provides the information needed to automatically drive an off-axis star to the telescope optical axis. If n_p and n_s respectively denote the column and row number of the pixel containing the star image in the CCD array as viewed from behind the detector, the offset of the star image in azimuth and elevation space is given by the matrix equation

$$\begin{vmatrix} \Delta\alpha \\ \Delta\varepsilon \end{vmatrix} = \frac{0.5 arc\sec}{pixel} \begin{vmatrix} \sec\varepsilon \sin\gamma & -\sec\varepsilon \cos\gamma \\ \cos\gamma & \sin\gamma \end{vmatrix} \begin{vmatrix} n_p \\ n_s \end{vmatrix}$$

In particular, it provides the scale factor (0.5 arcsec/pixel) relating the magnitude of the position offset of the star image in the CCD camera to the magnitude of the angular offset in azimuth-elevation space. The dependence on *g* and *e* provides the star (or satellite) image orientation in the CCD camera as a function of the instantaneous mount azimuth-elevation angle.

RECEIVER POINTING ERROR CORRECTION

In high power manned systems, the operator can manually make two-axis corrections in the pointing angle in an attempt to peak the signal strengths off the satellite. This is not possible in a photon-counting system where the mean signal per pulse is normally much less than one photoelectron. Thus, SLR2000 uses a quadrant ranging detector, which, in addition to providing precise timing on single photoelectron returns, informs the system computer of the quadrant that detected it. This information is accumulated over many laser fires (e.g. a frame interval) by a Correlation Range Receiver (CRR), which extracts the signal counts and discards the vast majority of background noise counts. The remaining counts (mostly signal) are then tallied by quadrant of occurrence, and the differences between quadrant counts are then used to compute a centroid for the count distribution during that frame [Degnan and McGarry, 1997]. The ray model provides the following equation

$$\begin{vmatrix} \Delta\alpha \\ \Delta\varepsilon \end{vmatrix} = \frac{10.5 arc\sec}{mm} \begin{vmatrix} \sec\varepsilon \sin\gamma & -\sec\varepsilon\cos\gamma \\ \cos\gamma & \sin\gamma \end{vmatrix} \begin{vmatrix} p_c \\ s_c \end{vmatrix}$$

for converting the centroid position (p_c,s_c) on the quadrant detector into azimuth and elevation pointing corrections, *Da* and *De*. From the equation, we also see that a 1 mm displacement of the centroid from the optic axis corresponds to a 10.5 arcsec pointing error and the orientation is again determined by the dependence on *g* and *e*.

TRANSMITTER POINT AHEAD

Balancing the count distribution among the detector quadrants orients the receiver/telescope optical axis toward the “apparent” position of the satellite, i.e. where it was located one light transit time earlier when photons from the previous pulse were reflected from the satellite retroreflector array. However, for the tighter transmitter divergences, the point-ahead can sometimes exceed the beam divergence so that the future position of the satellite may fall outside the transmitted laser beam if left uncorrected for point-ahead. Thus, to achieve maximum illumination of the satellite and the highest count rate on subsequent pulses, we must offset the transmitter axis from the “apparent” receiver axis by the angular travel accumulated by the satellite during the time it takes a light pulse to travel to and from the satellite. In SLR2000, the point-ahead correction is accomplished via two Risley prisms in the transmit leg of the transceiver (see Fig. 1). The ray model allows us to compute the proper orientation of the two Risleys in real time to produce the appropriate point-ahead as a function of the instantaneous azimuth and elevation rates, $\dot{\alpha}$ and $\dot{\varepsilon}$.

Let us denote the magnitudes of the angular deflections of the first and second wedges by δ_1 and δ_2 and the orientations of the individual prism deflections by the angles ξ_1 and ξ_2, as measured from the positive p-axis as defined previously. Ideally, $\delta_1 = \delta_2 = \delta$ permits total cancellation of the deflections when the wedges are oppositely aligned, but we are allowing for some manufacturing error in the prisms. The beam deflection is in the direction of the thickest part of the prism and has a magnitude $\delta = (n-1)\theta$ where n is the glass index of refraction and θ is the wedge angle. The ray matrix formulation provides the following relationship between the ray angle out of the Risley prisms (left-most vector) and the

transmitter point ahead in azimuth and elevation space (right-most vector)

$$\begin{vmatrix} \alpha p_{rp} \\ \alpha s_{rp} \end{vmatrix} \equiv \begin{vmatrix} \delta_1 \cos\xi_1 + \delta_2 \cos\xi_2 \\ \delta_1 \sin\xi_1 + \delta_2 \sin\xi_2 \end{vmatrix} = m_T \begin{vmatrix} -\sin\gamma\cos\varepsilon & -\cos\gamma \\ \cos\gamma\cos\varepsilon & -\sin\gamma \end{vmatrix} \begin{vmatrix} \dot{\alpha}\tau_r \\ \dot{\varepsilon}\tau_r \end{vmatrix}$$

where m_T = 30.48 is the total post-Risley magnification of the transmitter beam and τ_r is the roundtrip time of flight to the satellite. The latter provides two equations for the two unknowns, ξ_1 and ξ_2 from which we can obtain the following sequential solution

$$\Delta\xi \equiv \xi_2 - \xi_1 = \cos^{-1}\left\{ \frac{m_T{}^2\left[(\dot{\alpha}\bar{\tau}_r\cos\varepsilon)^2 + (\dot{\varepsilon}\bar{\tau}_r)^2\right] - \left(\delta_1^2 + \delta_2^2\right)}{2\delta_1\delta_2} \right\}$$

$$\cos(\xi_1) = \frac{-m_T\left[(\dot{\alpha}\tau_r\cos\varepsilon)(\delta_1\sin\gamma + \delta_2\sin(\gamma-\Delta\xi)) + (\dot{\varepsilon}\tau_r)(\delta_1\cos\gamma + \delta_2\cos(\gamma-\Delta\xi))\right]}{\delta_1^2 + \delta_2^2 + 2\delta_1\delta_2\cos(\Delta\xi)}$$

$$\sin(\xi_1) = \frac{m_T\left[(\dot{\alpha}\tau_r\cos\varepsilon)(\delta_1\cos\gamma + \delta_2\cos(\gamma-\Delta\xi)) - (\dot{\varepsilon}\tau_r)(\delta_1\sin\gamma + \delta_2\sin(\gamma-\Delta\xi))\right]}{\delta_1^2 + \delta_2^2 + 2\delta_1\delta_2\cos(\Delta\xi)}$$

$$\xi_2 = \xi_1 + \Delta\xi$$

where the second and third equations unambiguously define the orientation of the first prism.

CONTROLLING TRANSMITTER BEAM DIVERGENCE

Signal count rates and orbital time bias estimates vary widely over the range of satellite altitudes. In order to obtain an acceptable photon count rate for the higher satellites (e.g. LAGEOS, ETALON, GPS) while still meeting eye safety requirements at the telescope exit aperture, we must tightly control the SLR2000 transmit beam diameter (ω = 36 cm) and divergence half angle (θ = 4.3 arcsec). For lower satellites, the angular uncertainty of the satellite position and the signal count rates are both relatively high. Therefore, although it may be helpful to relax the beam divergence half angle to as much as 17 arcsec, the transmitter spot radius must be kept relatively constant at about $\omega = a$ /1.12 = 18 cm where a = 20 cm is the telescope primary radius [Klein and Degnan, TBD] to maintain eye safety and control vignetting losses. Transmitter beam size and divergence at the telescope exit window are controlled in SLR2000 by a commercial Special Optics beam expander in the transmitter path as in Fig. 1.

For real time beam control, the ray model relates the desired quasi-Gaussian transmitter beam parameters at the telescope exit aperture to the corresponding parameters at the output lens of the beam expander. We can represent the Gaussian beam at any point z in the propagation path by the complex "q-parameter" defined by

$$\frac{1}{q(z)} = \frac{1}{R(z)} - j\frac{\lambda}{\pi\omega^2(z)}$$

where λ = 532 nm is the laser wavelength and *R(z)* and *w(z)* are the phasefront radius of curvature and the Gaussian beam radius respectively. At any subsequent point in the path, the q-parameter is given by

$$\frac{1}{q(z)} = \frac{C + \dfrac{D}{q(z_0)}}{A + \dfrac{B}{q(z_0)}} \qquad M(z, z_0) = \begin{vmatrix} A & B \\ C & D \end{vmatrix}$$

where $M(z, z_0)$ is the ray matrix which propagates the rays between the two points in the propagation path. The ray model provides the following two expressions for the beam diameter in the telescope window

$$\omega = m_T \omega_0 \sqrt{1 + \frac{2d_T}{m_T R_0} + \left(\frac{d_T}{m_T R_0}\right)^2 \left[1 + \left(\frac{\lambda R_0}{\pi \omega_0^2}\right)^2\right]} \cong m_T \omega_0 \left(1 + \frac{d_T}{m_T R_0}\right)$$

and the far-field beam divergence half angle

$$\theta_t = \frac{\lambda}{\pi m_T \omega_0} \sqrt{1 + \left(\frac{\pi \omega_0^2}{\lambda R_0}\right)^2} = \theta_{\min} \sqrt{1 + \left(\frac{\pi \omega_0^2}{\lambda R_0}\right)^2} \cong \frac{\omega_0}{m_T R_0}$$

where $m_T = 48.30$ is again the total post-Risley magnification of the transmitter beam, d_T = 0.033 m, and $R_0 = R(z_0)$ and $\omega_0 = \omega(z_0)$ are the phase front curvature and beam radius at the output of the transmitter beam expander. The approximations hold for $\pi\omega_0^2 / \lambda R >> 1$ where the beam divergence is purposefully set well beyond the diffraction limit of the large exit beam, i.e. θ_{min} = 0.2 arcsec. The latter two approximate equations can be solved for the required Gaussian beam properties out of the transmitter magnifier, i.e

$$\omega_0 = \frac{\omega - m_T d_T \theta_t}{m_T} \cong \frac{\omega}{m_T} = 5.9mm$$

and

$$R_0 = \frac{\omega - m_T d_T \theta_t}{m_T^2 \theta_t} \cong \frac{\omega}{m_T^2 \theta_t} = \frac{1.92 \times 10^{-4} m}{\theta_t}$$

where, for a divergence half-angle range of 20 μrad $< \theta_t <$ 80 μrad, 2.4 m $< R_0 <$ 9.6 m. The latter values for ω_0 and R_0 are produced by manipulating two lens positions in the magnifier.

RECEIVER SPATIAL FIELD OF VIEW

A changing beam divergence must be accompanied by a corresponding change in the receiver FOV to avoid missing possible satellite returns. The ray model allows us to compute the diameter of the spatial filter pinhole as a function of the full receiver FOV. The aperture diameter, D_a, is adjusted by means of a computer-controlled stepper motor to match or slightly exceed the transmitter beam divergence discussed previously according to the equation

$$D_a \geq \frac{0.25mm}{arc\,\sec} \theta_t$$

SPECTRAL BANDWIDTH

The spectral bandwidth is controlled by a translation stage perpendicular to the optical path, which presently inserts one of the following into the receiver path: an open aperture (night), a 1 nm filter (twilight), or a 0.2 nm (daylight) filter. The wedge in these filters must be compensated at the arcsecond level to avoid introducing angular biases and severe vignetting at the spatial field stop.

SUMMARY

To summarize, the 2-D ray matrix approach provides us with the mathematical tools to calculate in real time:

- The scale factor and angular rotation for converting star image offsets from the CCD camera center to azimuth and elevation biases
- The scale factor and angular rotation for converting quadrant centroid position to satellite pointing correction in azimuth-elevation space
- Transmitter point ahead as a function of round trip time-of-flight and the instantaneous azimuthal and elevation angular rates
- Iris diameter (spatial filter) setting for a given receiver FOV
- Transmitter beam size and divergence at the telescope exit aperture as a function of transmit telescope lens spacings

REFERENCES

Degnan, J. J., “Ray Matrix Analysis of the SLR2000 Optical System”, Internal Report, Sigma Space Corporation, to be published, 2004.

Degnan, J.J. and J. F. McGarry, “SLR2000: Eyesafe and autonomous single photoelectron satellite laser ranging at kilohertz rates”, in *Laser Radar Ranging and Atmospheric Lidar Techniques*, *SPIE Vol. 3218*, pp. 63-77, 1997.

Klein, B. J. and J.J. Degnan, "Optical Antenna Gain. I. Transmitting Antennas", *Applied Optics,* 13, pp. 2134-2141, 1974.

Kogelnik, H. and T. Li, "Laser beams and resonators", *Applied Optics* , Vol. *5*, pp.1550-1569, 1966.

REMOTE OPERATION OF GUTS-SLR

Takashi Uchimura, Mikio Sawabe (1) Shigeru Murata(2) ,Yoichi Matsuoka(3), Thomas Oldham(4), Jeff Maloney(5)
(1)Japan Aerospace Exploration Agency.(2) NEC Corporation. (3) NEC TOSHIBA Space Corporation (4)Honeywell Technology Solutions, Inc. (5)Brashear LP
uchimura.takashi@jaxa.jp /Fax:+81-29-868-2990

Abstract

The GUTS-SLR is operated by remote control from the Tsukuba Space Center (TKSC).The approximate distance between TKSC and SLR station is 1100km. In this paper, we present the overview of the remote control and the function of system for supporting remote operation.

System overview

Japan Aerospace Exploration Agency's (JAXA) Satellite Laser Ranging system, which iscalled "GUTS-SLR" (GMSL, Tanegashima), has been completed in the spring of 2004. We are now in the training phase. The GUTS-SLR is located in Tanegashima Island,where the Japanese launch site is also located.

The GUTS-SLR is operated by remote control from the Tsukuba Space Center (TKSC). The approximate distance between TKSC and the SLR station is an approximate1100km. A 512-kbps communication line between the SLR station and TKSC is used for transmission of data such as system status data, operational parameters and observation data. For the transmission of surveillance monitor image, a 256-kbps line is used. JAXA will contribute to the ILRS in daylight and night using this system. The configuration of GUTS-SLR is shown in Fig.1-1.

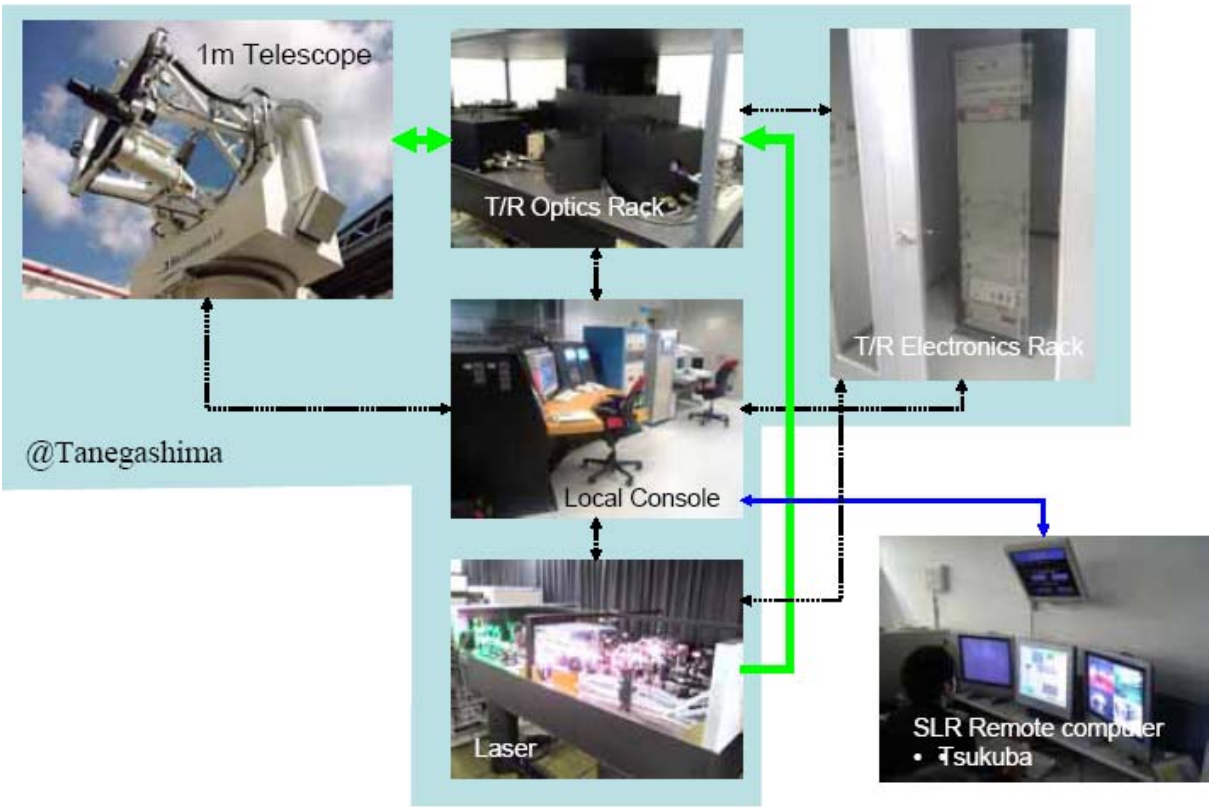

Fig.1-1 GUTS-SLR system configuration

Functions for remote control

The GUTS-SLR system has the following functions for remote control.

(1) Weather monitoring system

In order to monitor the weather condition of SLR station, the weather monitoring system has a wind direction/anemometer and the raindrop sensor, but the weather in Tanegashima can't be grasped precisely at TKSC at this present. We use the weather information such as the conditions of the present sky and weather forecast on the Internet at present. We will develop the all sky monitoring system with infrared camera in near future to solve this problem.

Fig.1 Weather Monitoring system

(2) Station Monitoring System

The ITV camera is installed in order that a safe surveillance system can always monitor the SLR observation building and its surroundings from the TKSC. There are two monitor screens at TKSC. One is a four-split screen to monitor the station environment. The other is used to monitor optical tracking and the laser beam profile.

Moreover, the door sensor is attached to detect an intrusion into the SLR building, etc., and the signal of the sensor is interfaced to the Laser interlock equipment directly. Fig.2-2 shows the appearance of operation console at TKSC.

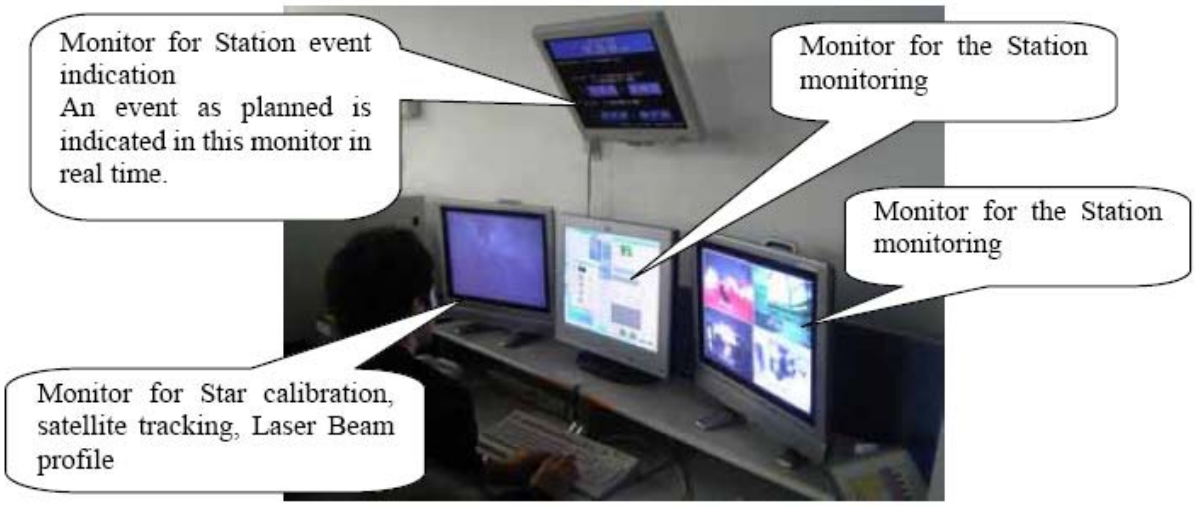

Fig.2 Station control system in Tsukuba

(3) Aircraft Surveillance Radar

In order to avoid laser hazard to aircraft such as airplanes, hang gliders and paragliders,we installed the aircraft surveillance radar, which follows the telescope, and also installed the wide-view camera as the backup. The appearance of Radar and wide-view camera is shown in Fig.2-3 (a) and (b)

(4) Sun Exposure Avoidance

In order to protect the mirror from being damaged by the direct sunlight in SLR daylight operation, the telescope system automatically avoid the sun exposure using software and hardware such as the sunlight sensor. The computer of telescope system calculates the sunlight direction and automatically closes and opens the mirror cover. The operator can be applied without being conscious of interference with the sun. The photograph of sun sensor is shown in Fig.2-3(c).

(a) Aircraft Surveillance Radar (b) Wide-view Camera (c) Sun Sensor

Fig.3 Appearance of Safety System

(5) Communication Outage

In case of anomalies such as a communication outage between TKSC and SLR station,SLR station's computer detects the communication outage and stops laser radiation, stows a teles-

Fig.4 Video Tracker monitor

cope, closes the dome shutter, then sets the whole subsystem to the standby mode until the restoration of communication line.

(6) Star Calibration and Satellite Tracking

This system has a video tracker function. This function is to assist an operator in the star calibration operation. It also facilitates the acquisition of flashing satellites. The Fig.2-4 is a screen shot of the video tracker image. The video tracker captures the flashing target and aims the telescope at the target automatically.

(7) Operation planning

The tracking schedule of SLR is automatically generated considering sunlight direction, satellite priority and satellite elevation angle (>20deg).

If these functions work properly, the operator checks the weather conditions, confirms the daily schedule, the dome open/close, the primary mirror cover open/close and Laserfiring. Fig.2-5 shows an example of a tracking schedule at Tanegashima. We plan a tracking schedule over 20 degrees elevation. The figure shows the visibility information for each satellite with AOS/LOS time, Maximum elevation angle, information about the sunlight, and daylight or night. The planning software can automatically create a tracking schedule for 2 weeks period (Maximum) according to a predetermined priority list.

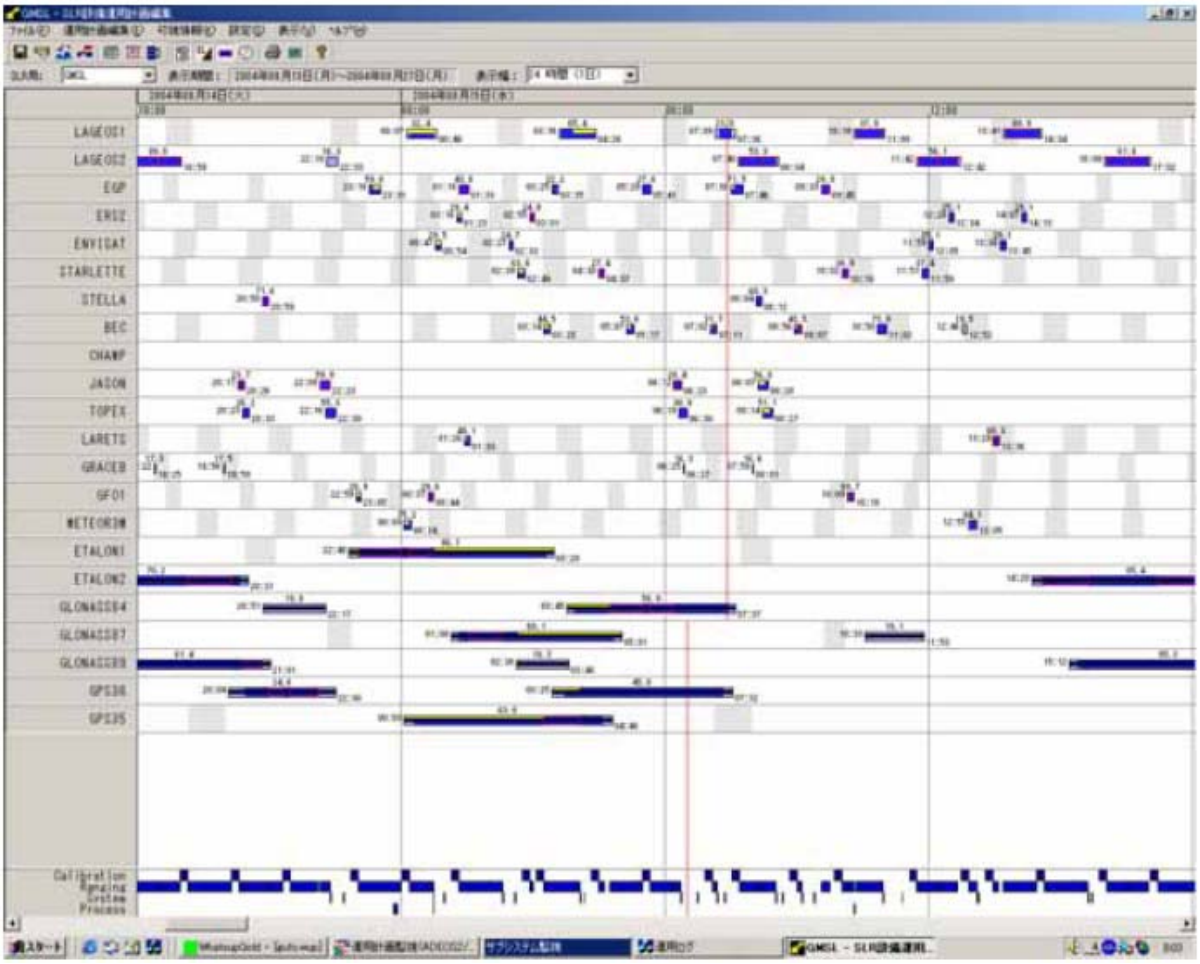

Fig.5 Example of tracking schedule

Conclusions

This would be the first experience ever in the world with such a long distance for routine SLR remote operation.

CONSOLIDATED LASER RANGING PREDICTION FORMAT: FIELD TESTS

R. RicklefsCenter for Space Research, The University of Texas at Austin
ricklefs@csr.utexas.edu /Fax: 1-512-471-3570

Abstract

The new International Laser Ranging Service (ILRS) consolidated ranging target prediction format has been developed by the ILRS Prediction Formats Study Group to provide a single format to encompass traditional artificial satellite and lunar ranging targets as well as proposed transponder targets on or around the moon and other planets. The primary benefit will be to allow any ranging station convenient access to ranging any of these target categories. In addition, the new format is designed so that predictions will not be subject to the inaccuracies inherent in tuning to a specific gravitational or drag model as found in the current IRV format.

While details of a few extensions to the format remain to be worked out, the core lunar and satellite components of the format are stable and have been subjected to a pilot study at the McDonald Laser Ranging Stations (MLRS). A discussion of the sources for the new predictions is presented, as is an analysis of the results of the ranging tests. Plans for future tests and implementation are also discussed.

Introduction

The Consolidated Prediction Format (CPF) provides a method of ranging to disparate targets using one format. [1] This allows cross-technique ranging attempts. A lunaronly station can then easily try to range a satellite or transponders target. An SLRonly station can perform feasibility tests on the moon. When a new deep-space satellite is launched, there are 40 stations around the world that should be able to track and possibly range to it.

Some additional advantages of the new format are that it does not rely on on-site gravity model, tuning, or separate drag and time bias functions. It is a tabular format containing un-tuned state vectors at time intervals appropriate to the target. The state vectors are typically in true body fixed system of date.

Purpose of Field Tests

Field tests have begun for the purpose of demonstrating the new format. The tests are necessary to verify that nothing has been forgotten, either in the data fields or in the overall concepts. The tests also give an opportunity to assess the performance of the predictions in some of the various configurations – low and high earth satellites as well as lunar reflectors, and, eventually, transponders.

There will inevitably be some bottlenecks, confusion, and mis-steps in producing and handling the predictions. Tests with a small number of stations will allow these to be identified and corrected before the entire network is involved.

A side-effect of the tests will be the building of infrastructure for network implementation. As various prediction centers and stations come into the tests, the distribution network will be put into place and shaken out.

MLRS Field Tests

To begin field testing, MLRS has taken a multi-faceted approach. To track satellite targets, HTSI Tuned Inter-range Vectors (TIVs) [2] are numerically integrated to produce one-minute state vectors which are then converted into the new format. This provides an easy way to start testing, using existing data products and provides a way to check out real-time point angles and ranges against existing software and predictions. The NERC Space Geodetic Facility (NSGF) tabular predictions are also being evaluated for use in the tests. For lunar ranging, the JPL DE-403 ephemeris is used as a basis for predictions produced in the new format.

Changes to the MLRS data acquisition software permit both old and new formats to be used, for quick switching during tests. This also minimizes maintaining nearlyduplicate versions of the code during the period prior to full switch-over to the new format.

Satellite and lunar normalpoint software does not currently use the new tabular format, due to development time constraints. The plan is to find time within the next few months to modify the normalpoint code so that it can use either the new or old format.

There have been no transponder tests, although Mars Global Surveyor predictions have been produced in the new format and verified to reproduce the original ephemeris to about 10 meters with the sample interpolation code. Hopefully, when Mercury Messenger returns in mid-2005, a number of stations will be able to track it using the new format.

Results

Preliminary code modifications are in place at MLRS, and predictions are available for internal tests. Data has been acquired on 4 satellite passes using the HTSI-derived predictions described above. At this time, the NSGF predicts are being evaluated. A couple of problems are delaying lunar tests, but those do not constitute major difficulties.

Conclusion

The fields tests are just starting at MLRS, and the results are encouraging, with passes being successfully tracked with the new format. LLR tracking with the new format should be tested soon. As time progresses, we expect more sources of predictions and more stations taking part in the tests.

Acknowledgements

Members of the ILRS Prediction Format Study Group have been involved in various phases of the field tests. To name 2, David Rowlands of Goddard Space Flight Center has provided Mars Global Surveyor predictions, and Graham Appleby of NSGF has provided satellite predictions in the CPF. We also wish to acknowledge funding for this project from NASA Contract NAS5-01096, NASA Grant NAG5-11464, and NSF Grant AST-0204127.

References

[1]. R. Ricklefs, “Consolidated Laser Ranging Prediction Format”, Proceedings of theThirteenth International Workshop On Laser Ranging, Washington, D.C., October 2002.

[2] “SLR IRV Format”,
http://ilrs.gsfc.nasa.gov/products_formats_procedures/predictions/tirv_format.html.

ZIMMERWALD REMOTE CONTROL BY INTERNET AND CELLULAR PHONE

Werner Gurtner Astronomical Institute, University of Berne

Abstract

The Zimmerwald Laser Station can be operated from a remote system using telnet and Xwindow clients, supervised using any web browser, and controlled to a certain extent by cellular phone. The paper describes the control possibilities available on the different media. The presentation includes online demonstrations depending on the actual communication conditions during the workshop session.

Introduction

At the 14th International Workshop on Laser Ranging in San Fernando the author of this paper presented a live demonstration of the remote control of the Zimmerwald SLR station during the session "Automation and Remote Control". This paper is a written illustration of the demonstration.

A detailed description of most components necessary for a successful remote control and/or automated operation of the Zimmerwald SLR station has already been presented at earlier Workshops on Laser Ranging by the author (Gurtner et al.1999, Gurtner et al. 2002).

1.Remote Control Architecture

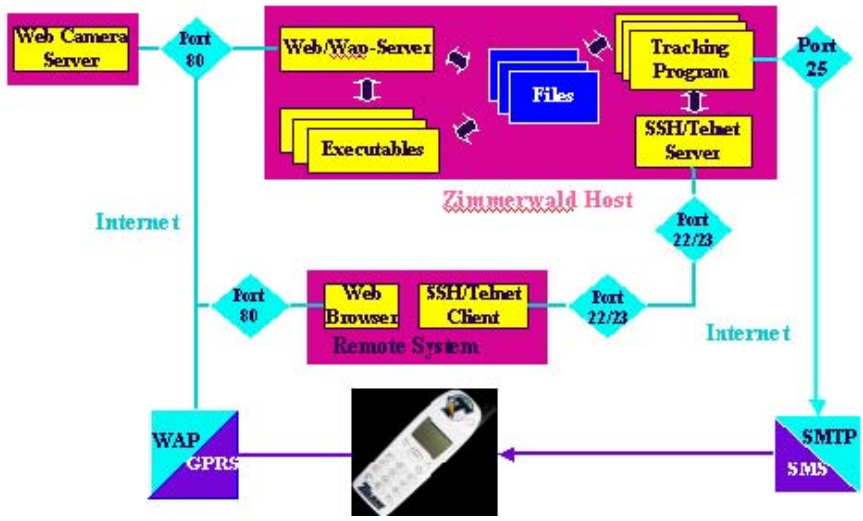

Figure 1: Remote Control Architecture

Fig. 1 shows the main components used for remote control of the SLR station. The station computer, an Alpha server running under the VMS operating system, hosts the programs used for the SLR operation (prediction management, satellite tracking, data acquisition, post-processing, and data submission) as well as a telnet and SSH (secure shell) server for remote login, and a web server. The latter also deals with Wireless Application Protocol (WAP) requests for Wireless Markup Language (WML) web pages to be sent to cellular phones. By means of an Email-to-SMS converter utility the programs running on the station computer can also generate short messages to be sent to any cellular phone (e.g., completion or error messages).

2.Web Access

The web server running on the main computer can, on request of the user, execute a number of programs to prepare web pages with system/station information in real-time:

2.1 System Status

Current use of the system, status of various components:

```
The Telescope / CAMAC are currently used by:

Account            : LASER
Terminal           : FTA15
Remote port        :
Mode               : INTERACTIVE
Program            : ZIMLAS
Observer           : EP
Start time         : 07:41 UT
Stop  time         : 08:42 UT
Remote ctrl        : No
Auto mode          : No

Laser              : ON
LS air temperature: 19.9
LS osc.temperature: 21.6
Dome               : Open
ZIMLAT PC          : ON
CAMAC PC           : ON
CAMAC Crate        : ON
Rain               : NO
```

Figure 2: Current System Status

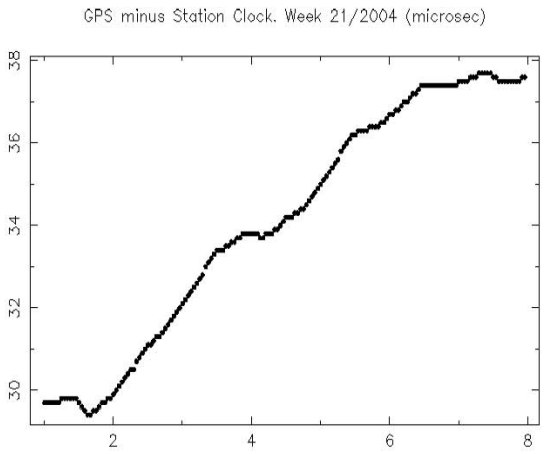

Figure 3: Station Clock Behavior

2.2 Station meteorology

Current met sensor readings, maximum/minimum values, time series, RINEX met files.

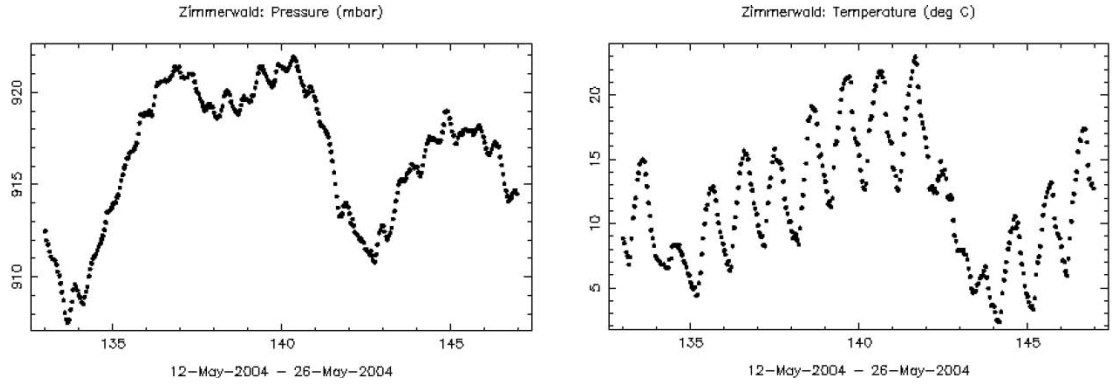

Figure 4: Surface Met Values (Pressure, Temperature)

```
2                    METEOROLOGICAL DATA                     RINEX VERSION / TYPE
MET_STORE                 AIUB                  17-MAY-04 00:02     PGM / RUN BY / DATE
ZIMMERWALD                                                          MARKER NAME
     3    PR    TD    HR                                           # / TYPES OF OBSERV
PAROSCIENTIFIC          740-16B                          0.2    PR SENSOR MOD/TYPE/ACC
ROTRONIC PT100          MP409A                           0.3    TD SENSOR MOD/TYPE/ACC
HYGROMER C94            MP409A                           2.0    HR SENSOR MOD/TYPE/ACC
        0.0               0.0              0.0         950.0    PR SENSOR POS XYZ/H
                                                                 END OF HEADER

 04  5 17  0  2  3  918.9    9.4   64.0
 04  5 17  0 25  2  918.8    9.2   65.0
 04  5 17  0 55  2  918.7    8.9   66.0
 04  5 17  1 25  2  918.7    8.8   65.0
 04  5 17  1 55  2  918.6    9.2   63.0
 04  5 17  2 25  2  918.6    9.3   62.0
 04  5 17  2 55  2  918.7    9.1   61.0
 04  5 17  3 25  2  918.7    9.0   62.0
 04  5 17  3 55  2  918.7    8.8   61.0
 04  5 17  4 25  2  918.8    8.2   70.0
 04  5 17  4 55  2  919.0    8.3   65.0
 04  5 17  5 25  2  919.1    8.9   73.0
 04  5 17  5 55  2  919.2    9.5   71.0
 ..  .  .  . ..  .  .....    ...   ....
```

Figure 5: RINEX Met File

2.3 Web cameras

Two cameras on the roof are connected to a camera web server. They show the current weather conditions. One camera also gives an external view of the SLR telescope.

The pictures are available as individual frames (jpeg files) or (password protected) as continuous streams ("server push" mode).

Figure 6: Roof North

Figure 7: Roof South

2.4 List of possible passes

Pass lists can be generated and displayed for any interval within the next seven days.

Observable Satellite Passes From 09-Jun-04 13:00 To 09-Jun-04 17:05 MESZ

No.	Satellite	UTC	MESZ	Filename	Sun	Day	Ele
267	GLONASS-87	11:00 - 13:07	13:00 - 15:07	R709JN04I	Y	Y	67
281	GFO-1	11:00 - 11:05	13:00 - 13:05	GF09JN04K	Y	Y	86
282	AJISAI	11:27 - 11:42	13:27 - 13:42	AJ09JN04L	Y	Y	58
283	GRACE-A	11:28 - 11:31	13:28 - 13:31	GA09JN04L	Y	Y	21
284	GRACE-B	11:29 - 11:31	13:29 - 13:31	GB09JN04L	Y	Y	21
285	JASON	12:09 - 12:21	14:09 - 14:21	JA09JN04M	Y	Y	39
286	TOPEX	12:16 - 12:28	14:16 - 14:28	TP09JN04M	Y	Y	37
	--- Break ---	13:07 - 13:30	15:07 - 15:30	23 min			
287	AJISAI	13:30 - 13:44	15:30 - 15:44	AJ09JN04N	Y	Y	80
	--- Break ---	13:44 - 14:14	15:44 - 16:14	30 min			
288	LAGEOS	14:14 - 15:01	16:14 - 17:01	L109JN04O	Y	Y	62
289	LAGEOS-2	14:20 - 15:05	16:20 - 17:05	L209JN04O	Y	Y	44

Figure 8: Pass List

2.5 Observers' schedule

The table shows the scheduled observers for the two daily shifts for the current month. It can be modified over the web by the observers (password-protected, if not on site).

Beobachterliste für den Monat JUNI 2004

Datum	Tag	Betreuung	Nacht	Abwesend WG	JU	EP
Di/Mi 1 Jun	JU		RM			
Mi/Do 2 Jun	A+R		MP			
Do/Fr 3 Jun	WG		CM			
Fr/Sa 4 Jun	EP		PF	*		
Sa/So 5 Jun	MP		U+M / (TF)	*	*	
				*	*	

Figure 9: Observers' schedule

The following items are only available during the actual satellite tracking!

2.6 Operator screen

The web copy of the real-time operator screen is updated every 30 seconds.

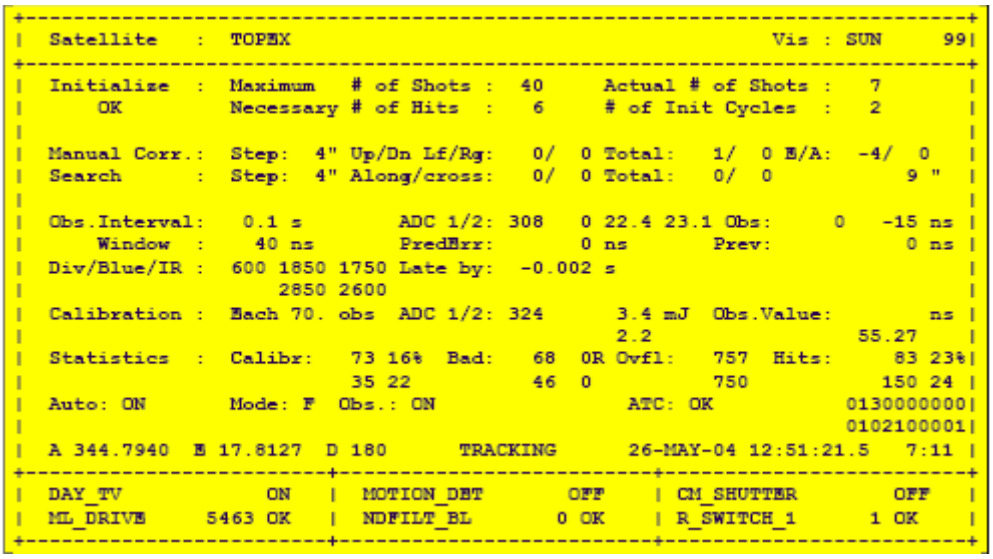

Figure 10: Operator screen

The password-protected login (telnet or SSH) allows the user to display this screen with continuous update on the remote terminal in a separate window.

2.7 Pass scheduler

The tracking program automatically generates a pass schedule taking into account the priorities of the various satellites. This schedule can be overruled by the observer anytime during the tracking. The web copy shows the actual schedule (updated every 30 seconds).

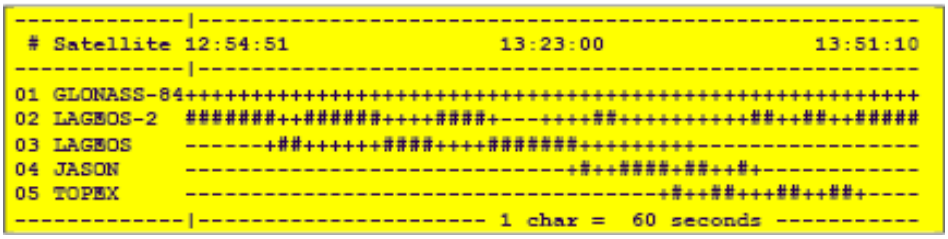

Figure 11: Pass schedule

2.8 Sky plot

The sky plot shows the ground tracks of all selected satellites and their current position, the position of the sun and moon and the pointing direction of the telescope. It is continuously displayed on the operator's console and (updated every 30 seconds) as a copy on the web.

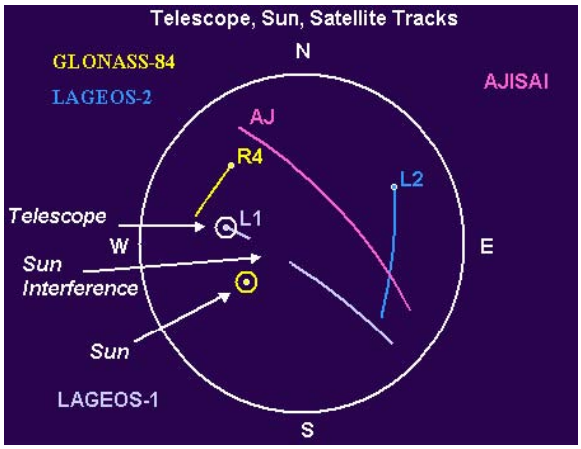

Figure 12: Sky Plot

2.9 Telescope cameras

The two telescope cameras show the sky in the pointing direction (there are two separate cameras for day and night). Their images are continuously displayed on a separate screen at the observer's working place. Their output signal is also branched to the above mentioned web camera server, which provides frames or continuous updates to any remote web browser.

Figure 13: Tracking (day)

Figure 14: Tracking (night)

2.10 Observed passes (lists, graphics)

Fig. 15 shows a list of all observed passes within a certain time period. The first two characters of the file names are a code for the satellite names. Other items are: Number of returns accepted in real time, the actual time bias (sec), a wavelength code, the number of accepted returns during post-processing, the rms of the observations, number, rms, and average value of the real-time calibrations, pass duration in minutes. The second line in each pass contains the data from the second receiver chain (infrared) and the average difference between the observations of the two receiver chains (calibrations and refraction corrections applied).

CONTENT OF LOG FILE "SATLOG.D30" FOR THE FOLLOWING TIME INTERVAL:

FROM: 2004-05-23 12:00 TO: 2004-05-24 12:00

FILE NAME	START	NHIT	DT0	WL	O-SCR	O-RMS	C-SCR	C-RMS	C-CST	O 1-2	Q	DUR
L123MY04M	12:51:36	334	-.001	1	342	.156	217	.111	31.21		Y	20
		899		2	843	.173	224	.172	54.91	0.05	Y	
JA23MY04N	13:27:35	523	0.003	1	517	.094	402	.104	31.21		Y	9
		378		2	315	.145	359	.176	54.91	-0.02	Y	
TP23MY04N	13:34:36	691	0.001	1	594	.204	615	.102	31.21		Y	12
		690		2	511	.236	567	.177	54.91	-0.06	Y	
L223MY04O	14:23:13	993	-.001	1	966	.131	851	.097	31.22		Y	53
		2147		2	2004	.167	858	.196	54.90	0.03	Y	
AJ23MY04O	14:39:24	301	-.002	1	286	.259	432	.096	31.22		Y	8
		326		2	292	.271	422	.194	54.91	-0.04	Y	
JA23MY04P	15:24:30	125	0.003	1	111	.120	583	.107	31.21		Y	11
		299		2	232	.155	604	.192	54.88	-0.03	Y	
TP23MY04P	15:32:13	276	0.002	1	240	.190	564	.107	31.21		Y	9
		310		2	222	.224	585	.190	54.88	-0.07	Y	

Figure 15: Observed Pass

2.11 Documents

Operator manuals, documents, protocols, etc. can be accessed over the web (password-protected for remote users).

3. Access by Mobile Phone

The web server at Zimmerwald also accepts requests for wireless markup language (WML) pages using the wireless application protocol (WAP). As the functionality of WML documents is smaller than the one of HTML-based web pages and the display possibilities on cellular phone screens are rather limited, only part of the web-based access and control has been prepared for cellular phones.

Figure 16: Zimmerwald (part of the) Main Access Menu

The following samples have been generated using a PC-based WAP emulator (and not an actual cellular phone).

Figure 17: Station Status

Figure 18: Roof Camera

Depending on the cellular phone capabilities images from the four cameras can also be downloaded (Fig. 18).

There are interactive WAP pages allowing to remotely switch on/off the laser or to even start

a fully automated observation session in batch mode.

By entering a start time and a time interval the system generates a list of possible passes within this interval (satellite, start time, pass duration): Fig. 21.

Fig. 22 shows a list of recently observed passes: Satellite, day of the month, hour of the day (A = 00 h, B = 01 h, etc.), number of observations, number of accepted observations after post-processing).

Figure 19: Switch Laser On/off

Figure 20: Start a Session

Figure 21: Future Passed

Figure 22: Observed Passed

4. Full Remote Control

Using Telnet (within the University's Local Area Network) or an SSH Secure Shell client the authorized user can remotely connect to the main station computer. All the functionalities of the onsite operation is available at the remote site.

Graphics as e.g. the sky plot or a real-time display of the returns are transferred to the remote location as x-window applications.

The images of the cameras (external cameras, cameras on the telescope) can be transferred to the remote web browser as a continuous stream of frames (depending on the available band width of the internet connection).

During onsite operation it is also possible to remotely connect to the running tracking program to enter commands in parallel to the onsite control. This possibility is used in three situations: Remote support for new observers, remote trouble shooting, and occasional interaction with a fully automated program run.

5. Conclusions

Thanks to the remote control of the Zimmerwald SLR system by Telnet and SSH it is possible to quickly support onsite observers in case of problems and to occasionally control or intervene during fully automated operation.

Web-based information about the station can be used for public relations, tutoring, and remote status checks with simple web browsers.

The interaction with the station by mobile phone is another means to easily and quickly check the system status under fully automated operation or to launch (or abort) an observing session during unexpected weather changes. The station is not manned by default, the observers usually depend their presence on the actual weather conditions, and they may extend their shift or bridge gaps between the two daily shifts by unmanned, fully automated operation.

References:

Gurtner W., E. Pop, J. Utzinger (1999). „Automation and Remote Control of the Zimmerwald SLR Station“. Proceedings of the 11th International Workshop on Laser Ranging, Deggendorf, September 20-25, 1998. Mitteilungen des Bundesamtes für Kartographie und Geodäsie, Band 11, Frankfurt am Main, 1999.

Gurtner, W., E. Pop, J. Utzinger (2002): "Improvements in the Automation of the Zimmerwald SLR Station". Proceedings of the 13 th International Workshop on Laser Ranging, October 7-11, 2002, Washington D.C.

LASER RETROREFLECTOR ARRAY OF GEOSTATIONARY SATELLITE, ETS-VIII

Takashi Uchimura, Mikio Sawabe, Akinobu Suzuki, Hiroyuki Noda
Japan Aerospace Exploration Agency
uchimura.takashi@jaxa.jp /Fax:+81-29-868-2990

Abstract

JAXA' Engineering Test Satellite-VIII (ETS-VIII) will conduct positioning experiments, combining the clock signals with GPS data, to study basic satellite positioning systems. It will be launched in 2006-2007 and located into the geostationary orbit at 146 degrees east. ETS-VIII will carry a high precise clock system, and also Laser Retroreflector Array (LRRA) that will be used for the evaluation of experiment results such as precise orbit determination and onboard clock estimation. The LRRA consists of 36 corner-cubes which are contained within an envelope of 26cm x 30cm x 5cm. Its approximate weight is three kilograms. SLR stations in the Asia-Pacific region will be able to Laser-track to the ETS-VIII. We will present an overview of ETS-VIII, LRRA and result of link budget analysis.

1.ETS-VIII Mission Description

1.1 Outline

The ETS-VIII is an advanced satellite being developed primarily to establish and verify the world's largest-class geostationary satellite bus technology, which is necessary for space missions of the 21st century. The ETS-VIII will conduct orbital experiments on the Largescale

Deployable Reflector (for S-band), which is widely applicable to largescale space structures, as well as the High-Power Transponder, and the On-Board Processor, which are all required to realize mobile satellite communications with hand-held terminals, similar to popular cellular phones.

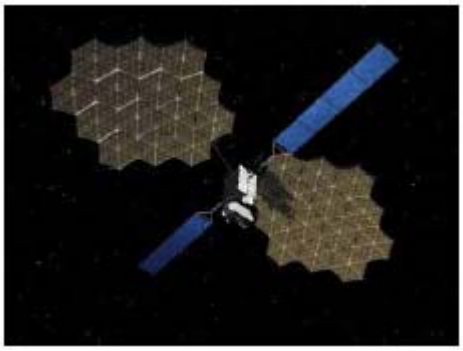

Overview of ETS-VIII

Moreover, the ETS-VIII will carry the High Accuracy Clock (HAC) system and a Time Compare Equipment (TCE) system for the study of satellite positioning system. The SLR tracking data will be utilized in this study. The ETS-VIII mission will carry out on the Geostationary Orbit (GEO) (Longitude 146degE (tentative)). Mission life is designed for 3 years. (The satellite bus is designed to have 10-year life.)

The orbit will be maintained within 0.1 degree range respectively toward the north, south, east and west direction.

1.2 Mission Objectives

The ETS-VIII is being developed to establish and verify the following technologies:

(1) An advanced 3-ton-class spacecraft bus
(2) Large-Scale Deployable Reflector

(3) Mobile satellite communication system technology that will enable audio/data communications with hand-held terminals

(4) Mobile satellite multimedia broadcasting system technology for CD-level sound and image transmission

(5) Satellite positioning using the High Accuracy Clock

1.3 Experiments plan using HAC system

JAXA will conduct the following positioning experiments, combining the clock signals with GPS data and SLR, to study basic satellite positioning systems using HAC system.

(1) AF (Atomic Frequency mode): Positioning signal is generated by on-board CFS (Cesium Frequency Standards).

(2) BP (Bent Pipe mode): Positioning signal in S-band (779fc/3) and pilot signal in S-band (260fc) are generated by HTS (HAC Transmission Station) and transmitted to ETS-VIII as left handed circular wave. Then, the carrier frequency of positioning signal is converted to L-band (156fc) and S-band (487fc/2) by using pilot signal. Pilot signal used in frequency conversion is selected by taking account of phase coherency of pilot signal and positioning signal. (i.e. The same Doppler effects and phase delay due to the common ionosphere.)

(3) TCE (Time comparing mode): NICT (National Institute of Information and Communications technology) will carry out experiments for comparing the on-orbit CFS time and UTC(NICT) using bidirectional communication of navigation signal.

(4) SLR (Satellite Laser Ranging): ETS-VIII has also carries LRRA (Laser Retro-Reflector Array, $\sigma>1x10^9$ m^2) and the SLR operation is planned. SLR operation can be performed without conflict for other operations. JAXA will conduct the precise orbit determination of ETS-VIII using SLR and its result will be used for the evaluation of other experiment results such as precise orbit determination using navigation signal and onboard clock estimation.

(5) USR (User positioning experiment) Effectiveness of overlaying ETS-VIII data and GPS data will be evaluated from the user's standpoint. USR mode is not ETS-VIII operation mode but just observation mode in ground. USR is a portable station, and will be placed at some location during mission period. Observed data by USR will be processed in 2 ways as follows:

- Applying user positioning algorithm to evaluate the usefulness of ETS-VIII overlay for users. The effect ETS-VIII overlay will be analyzed in off-line analysis for the case of adding ETS-VIII positioning signal, or introducing system state estimation.
- Using USR observed data for estimating system status as the data of 5 SMS in off-line analysis.

2. Overview of LRRA

2.1 General

The Laser RetroReflector Array (LRRA) is made of aluminum alloy and consists of 36 corner cubes mounted in a panel, which are 4.1 cm in diameter. The corner cubes are constrained to allow for differential thermal expansion of the structure and the quartz corner cubes. The

array assembly weighs less than 3100 g. The array is 26 cm length, 30 cm width and 5.5 cm height.

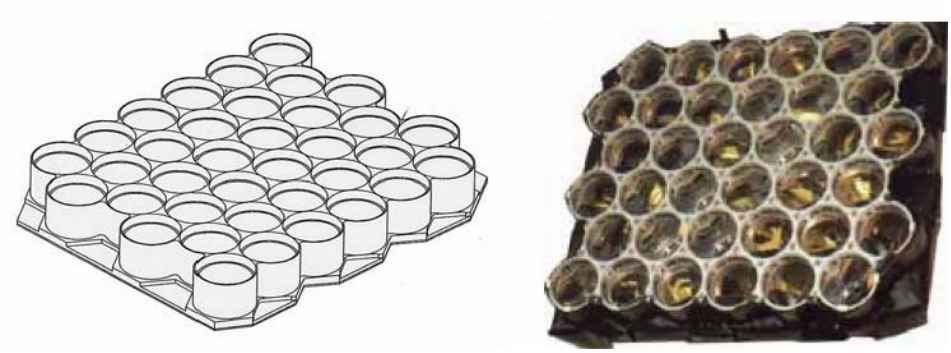

Fig.2-1 ETS-VIII Retro-Reflector Array

2.2 Corner Cube Description

The 36 corner cubes are made of highly homogeneous fused silica, Suprasil-1(quartz). The individual corner cubes are 4.1 cm diameter and optimized for the velocity aberration of the satellite as well as for a wavelength of 5320 Angstroms. The surface flatness is 1/10 wavelength at 5320 Angstroms. The reflective coating external reflection is specified to exceed 75% at 5320 Angstroms. The net optical efficiency of the prism is specified to exceed over 95% at 5320 Angstroms.

2.3 LRRA Specification Summary

Table 2-1 summarizes the LRRA specification.

Table 2-1 LRRA Specification Summary

Type	Reflector array
Wavelength	optimized for 532 nm
FOV (half angle)	10 deg
Optical Cross Section	1.63×108 m2
Shape	Flat array
Size of Array	26×30×5.5 cm
Mass	< 3.1 kg
Reflector Number	36 corner cubes
Cube diameter	4.06 cm
Reflectivity	>75%
Beam divergence	20 μrad

2.4 LRRA Position

LRRA is installed on the top of ETS-VIII's antenna-tower. (See Fig.2-2) The attitude of ETS-VIII affects the position and the direction of LRRA. The performance of ETS-VIII attitude orbit control subsystem is as follows:

Attitude control error (3σ),

Roll	Pitch	Yaw
<±0.05	<±0.05	<±0.15

(deg)

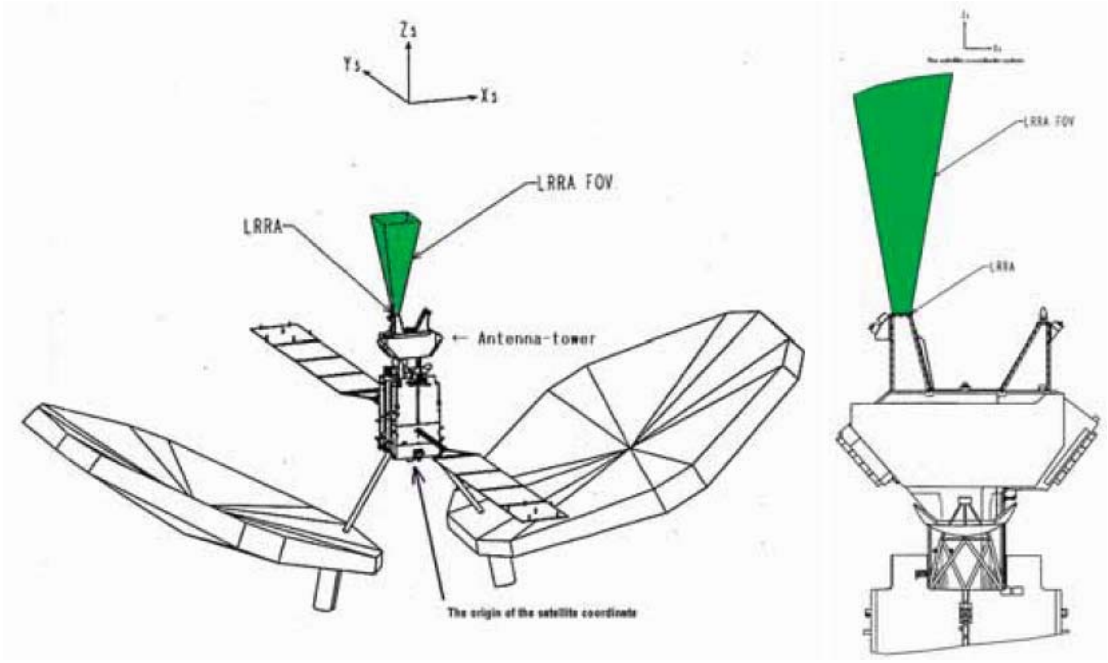

Fig.2-2 The satellite coordinate system of the ETS-VIII / LRRA installation position

3. Candidate SLR Station and Link Budget Analysis

3.1 Candidate SLR Station

The ETS-VIII will be carried into geostationary transfer orbit (Longitude 146 degrees East) by H-IIA launch vehicle from Tanegashima Space Center in Japan. Figure 3.1 shows the FOV (Field Of View) of the ETS-VIII LRRA and candidate SLR stations. Thus, SLR stations in the Asia-Pacific region will be able to track ETS-VIII.

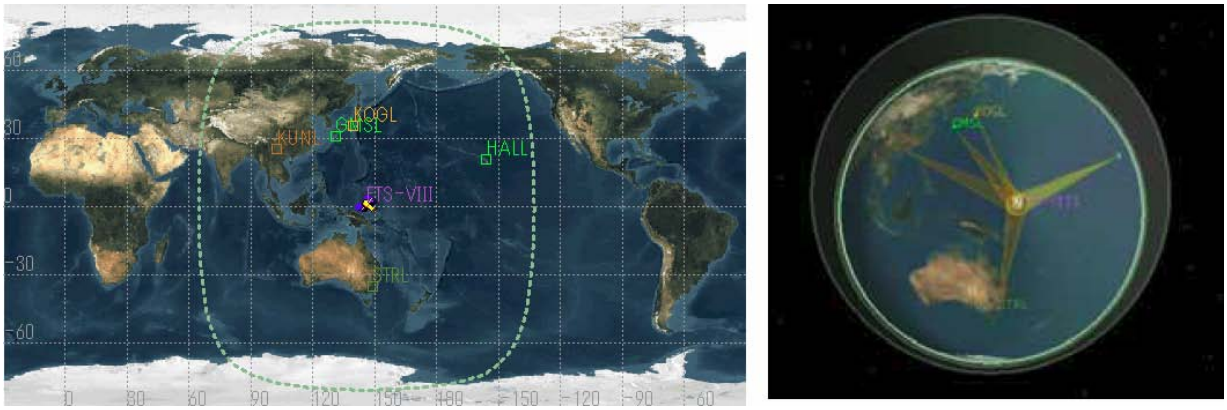

Fig 3-1 FOV of the ETS-VIII LRRA and candidate SLR stations

3.2 SLR Link Budget Calculation

The example of link budget calculation result for each candidate station is shown in Table 3-1. We calculated link budget for each station based on the station site log on the ILRS web site. We confirmed the return energy from ETS-VIII for individual station by link budget calculation. The Lageos normalized signal level is approximate 0.01. According to this result, most candidate stations are possible to get return signals from ETS-VIII, but we need to re-calculate link budget using more detailed parameters and also to examine other parameters

such as range gate, detecting method, etc.

Table 3-1 Link budget calculation result for each candidate station

	GMSL	KOGL	STRL	KUNL	YARL
Cirrus Cloud Transmission	1	1	1	1	1
Atmospheric Transmission	0.2	0.2	0.2	0.2	0.2
Longterm Beam Spread [1×10-6 rad]	5	5	5	5	5
Shortterm Beam Spread [1×10-6 rad]	20	20	20	20	20
Receive Efficiency	0.5	0.1	0.41	0.5	0.76
Satellite Backscattering Cross Section [1×106 m2]	168	168	168	168	168
Quantum Efficiency [%]	10.4	15	20	20	15.5
Receive Aperture [m2]	0.78	1.76	0.44	0.88	0.4536
Satellite Height [km]	37000	37100	37100	38300	37100
Wavelength [1×10-6 m]	0.532	0.532	0.532	0.532	0.532
Transmit Efficiency	0.5	0.3	0.41	0.5	0.95
Pulse Energy [mJ]	300	50	50	120	100
Average signal level [p.e.]	6.551428	1.687381	0.787913	4.965641	5.407543
Lageos normalized signal level	0.016596	0.016418	0.016418	0.014455	0.016418

4. SLR Tracking Plan and Orbit Analysis

4.1 SLR Tracking Plan

HAC Experiment Ground System will conduct real-time orbit determination of ETS-VIII using navigation signal of ETS-VIII, 24 consecutive hours every 2 weeks. SLR data must be acquired at the same time. The example of SLR data acquisition pattern is shown in Fig.4-1.

Time(UT)	0	1	2	3	4	5	6	7	8	9	10	11	12	13	14	15	16	17	18	19	20	22	22	23
Case 1																								
Case 2																								
Case 3																								

Fig. 4-1. SLR data acquisition pattern (sample)

Fig. 4-1 describes the SLR data acquisition cases of ETS-VIII. In Case 1, data are collected every pass of the satellite - every five minutes of every one hour - for 24 consecutive hours at each station at the same time. Case 2 and Case 3 are additional cases, in which acquisition times of data are shorter than Case 1, in order to reduce the workload of the stations. In principle, even if a data acquisition timing at one station is later than that of other stations due

to the weather etc., data acquisition will be performed. Actual operation plan will be determined by the adjustment result with station and the analysis result.

4.2 Orbit Analysis Result

We carried out the analysis of orbital determination accuracy based on the operation case shown in the Section 4.1. Table4-2 shows the example case of orbit analysis. We analyzed the influence of orbit determination accuracy by changing the number of stations and data acquisition period. In Table4-2, (1) is an analysis case about the combination of station and (2) is an analysis case of observation conditions. Actually, we executed more cases by combining (1) with (2).

Table 4-2 Orbit Analysis Case

(1) Combination of Station

	GMSL	KOGL	STRL	KUNL
Case-1	○			
Case-2	○	○		
Case-3	○		○	
Case-4	○			○
Case-5	○	○	○	
Case-6	○	○		○
Case-7	○	○	○	○

(2) Observation condition

	Orbit Arc (Hour)	Ranging Period
Case-A	24	5min/hour
Case-B	12	5min/hour
Case-C	6	5min/hour

As the result, we verified that we could achieve target accuracy (~10m) by the combination of Mt. Stromlo station (STRL) and Tanegashima station (GMSL), but we need the support of NICT station (KOGL) and KUNMING station (KUNL) when considering weather conditions.

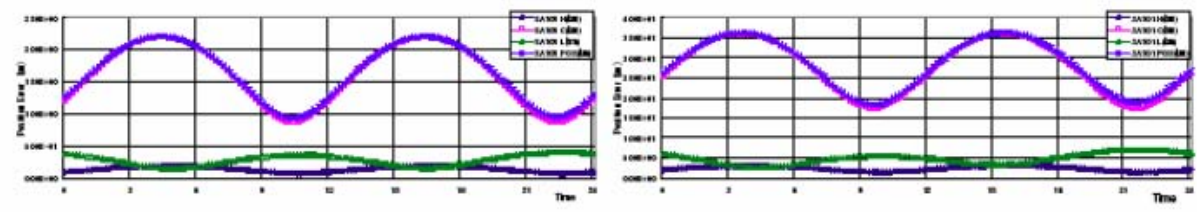

(a) Case 1 + Case A(only GMSL, 24 hours) (b) Case 1 + Case B(only GMSL, 12 hours)

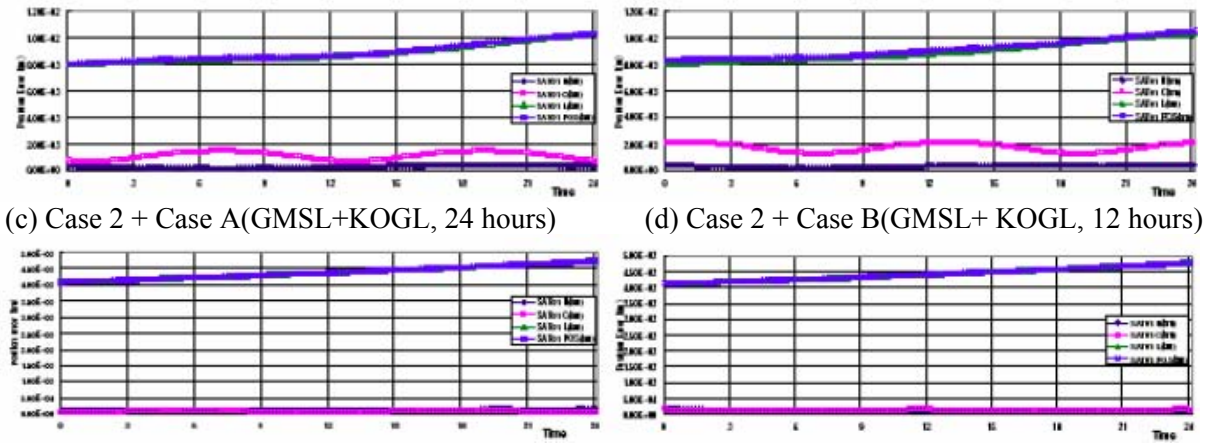

(c) Case 2 + Case A(GMSL+KOGL, 24 hours) (d) Case 2 + Case B(GMSL+ KOGL, 12 hours)

(e) Case 3 + Case A(GMSL+STRL, 24 hours) (f) Case 3 + Case B(GMSL+STRL, 12 hours)

Fig.4-2 Example of orbit determination analysis result

5. References

Tomoichi Sato and Hiroyuki Noda, *Introduction to fundamental experiment on satellite positioning system in ETS-VIII project*, ISTS-2000-d-04 (2) Akinobu Suzuki, ETS-VIII SLR tracking Standards, QNX-030008.

DESIGN OF LASER RETRO-REFLECTOR ARRAY AND LASER RANGING EXPERIMENT FOR SHENZHOU-4 SATELLITE

Yang Fumin, Chen Wanzhen, Zhang Zhongping, Chen Juping, Wang Yuanming
Shanghai Astronomical Observatory, Chinese Academy of Sciences; yangfm@shao.ac.cn

1. Introduction

The China's fourth unmanned spacecraft "Shenzhou IV" was launched on December 30, 2002. One module of the spacecraft so called the manned module was returned to the Earth on January 6, 2003. The other part, the orbital module, was remained in the orbit and carried on some scientific experiment. The orbital altitude of the module was 350 km. One of the instruments on board was a microwave altimeter for sea level measurement. There were a laser retro-reflector array (LRA) and a GPS receiver onboard for precise orbit determination. The LRA was designed and manufactured by the Shanghai Observatory. The laser ranging experiment for the Shenzhou-4 satellite among the Chinese SLR stations was carried out during Jan. 7- March 27, 2003.

2. Design of the LRA for Shenzhou-4

The photo and the mechanical drawing of the LRA are shown in Figure 1 and 2. The angle between the normals of the central reflector and the side ones is 50 degrees. The diameter of the single corner-cube is 30mm. The diameter of the LRA is 200mm, and the height is 67mm. The divergence of the corner-cube is about 12-16 arcsec.

Diameter: 20cm
Corner-cubes: 9
Material: Fused quartz
Weight: 850g

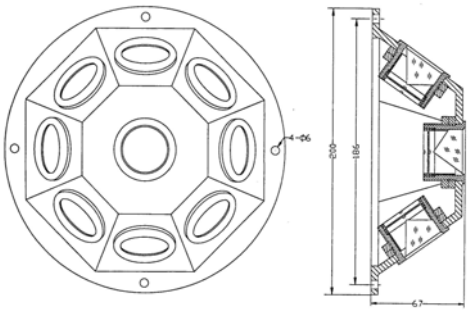

Fig. 1. Configuration of LRA

Fig.2.Mechanical drawing of LRA

3. Calculation of Effective Reflection Area of Shenzhou-4

3.1. Calculation for the incidence angle of laser beam with respect to the retro-reflector that has an inclination angle with the direction of the satellite-earth's center

The relation between the incidence angle and the relative effective area is given by:

$$\eta = \frac{2}{\pi}\cdot\left(\sin^{-1}\mu - \sqrt{2}\cdot\mu\cdot tgi_r\right)\cdot\cos i_0$$

Where, $\mu = \left(1-2tg^2 i_r\right)^{1/2}$, $i_r = \sin^{-1}\left(\frac{\sin i_0}{n}\right)$

η is relative effective geometric area,

i_0 is incidence angle of laser beam,

i_r is refraction angle of laser beam,

n is index of refraction for retro-reflector, usually the retro-reflector is made of fused quartz (n=1.445).

While $i_0 = 0$, then $\eta = 1$

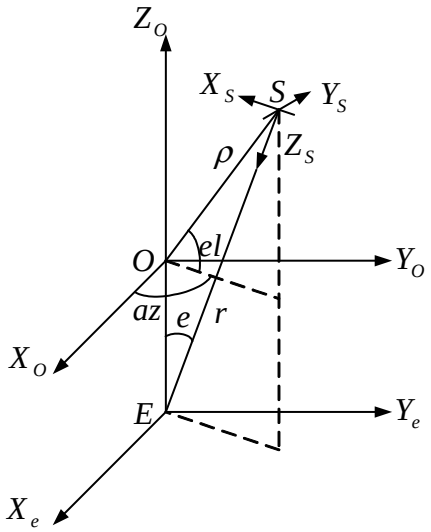

Fig.3. Three coordinate systems

If the normal of the retro-reflector deviates from the direction of the earth's center with a special angle, it is necessary to find out a reference plane to measure the orientation angle of the normal. The orbital plane of the satellite is adopted as the reference plane, and the normal direction is defined as follows: the normal of the reflector deviates from the satellite-the earth's center direction both in the orbital plane with an angle of α, and in the perpendicular plane to the orbital one with an angle of β. We suppose the deviation angle is invariable as the satellite moves. There are three coordinate systems as follows (Fig. 3):

(1) Satellite coordinate system ($S - X_S Y_S Z_S$): the satellites (S) as the origin, the satellite's instantaneous motion direction as the X_S axis, forward is positive. The direction from the satellite to the earth's center as the Z_S axis, to the earth is positive. Y_S axis determined by right-hand rule.

(2) Station coordinate system ($O - X_O Y_O Z_O$): The station (O) as the origin, the $X_O O Y_O$ is a tangent plane of the earth's surface. Y_O axis directs to the projection of the highest point of satellite apparent orbit for the satellite apparent orbit for the station on the plane $X_O O Y_O$. Z_O axis point to the zenith of the station.

(3) Geocentric coordinate system($E - X_e Y_e Z_e$): Move only the origin of the station coordinate

system to the geocentric, and keep X_e, Y_e and Z_e axes parallel to X_O, Y_O and Z_O axes respectively.

Suppose a satellite is located at an arbitrary position of space, and the incidence angle of laser beam to the retro-reflector is the angle between the laser beam vector and the normal of retro-reflector. Choosing geocentric coordinate system for calculation, we can convert both the laser beam vector from the station coordinate system and the normal of retro-reflector from the satellite system to the geocentric system. Then we can obtain the incidence angle easily.

Azimuth (*az*) is the angle between X_O axis and the projection of the laser beam on the plane $X_O OY_O$. It should be noted that the azimuth here is different from the one defined in astronomy.

The elevation is the angle between the laser beam and its projection on the plane $X_O OY_O$, as shown in Fig. 3.

The unity length vector of the laser beam both in station coordinate system and in geocentric coordinate system is the same:

$$L = \begin{bmatrix} \cos(el)\cos(az) \\ \cos(el)\sin(az) \\ \sin(el) \end{bmatrix},$$

In geocentric system, the unity length vector of the satellite position is

$$S = \begin{bmatrix} \sin(e)\cos(az) \\ \sin(e)\sin(az) \\ \cos(e) \end{bmatrix}.$$

Here, e is the geocentric angle of satellite $\angle SEO$. It can be gotten by

$$e = \arcsin\left(\frac{\rho}{r_s} * \cos(el)\right),$$

Where ρ is the slant distance from the station to the satellite, and r_s is geocentric distance of the satellite.

In the satellite coordinate system, the normal vector of retro-reflector is

$$\vec{n} = \begin{bmatrix} n_x \\ n_y \\ n_z \end{bmatrix} = \begin{bmatrix} \cos\beta\sin\alpha \\ \sin\beta \\ \cos\beta\cos\alpha \end{bmatrix}$$

The transformation from satellite coordinate system to geocentric coordinate system is as follows:

$$\begin{bmatrix} x_e \\ y_e \\ z_e \end{bmatrix} = \begin{bmatrix} 1 & 0 & 0 \\ 0 & \cos\theta_1 & \sin\theta_1 \\ 0 & -\sin\theta_1 & \cos\theta_1 \end{bmatrix} \begin{bmatrix} \cos\theta_2 & 0 & -\sin\theta_2 \\ 0 & 1 & 0 \\ \sin\theta_2 & 0 & \cos\theta_2 \end{bmatrix} \begin{bmatrix} x_S \\ y_S \\ z_S \end{bmatrix}$$

Where

$$\theta_1 = \cos^{-1}\left(\cos(e)/\cos(c)\right),\ \ \theta_2 = \pi - c,\ \ c = \sin^{-1}\left(\sin(e) * \cos(az)\right)$$

In geocentric coordinate system, the unity length vector of the normal of the retro-reflector N is

$$\begin{bmatrix} N_x \\ N_y \\ N_z \end{bmatrix} = \begin{bmatrix} 1 & 0 & 0 \\ 0 & \cos\theta_1 & \sin\theta_1 \\ 0 & -\sin\theta_1 & \cos\theta_1 \end{bmatrix} \begin{bmatrix} \cos\theta_2 & 0 & -\sin\theta_2 \\ 0 & 1 & 0 \\ \sin\theta_2 & 0 & \cos\theta_2 \end{bmatrix} \begin{bmatrix} n_x \\ n_y \\ n_z \end{bmatrix}$$

The incident angle of laser beam to the reflector i is given by

$$i = \arccos\left(\vec{L} \cdot \vec{N}\right)$$

Obviously, the incidence angle is the function of the azimuth, elevation of satellite, and the deflection angle of the normal of retro-reflector α and β. So, the effective reflection area of retro-reflector is also the function of these factors. The total effective reflection area for the LRA can be obtained by summing up the contributions of all retro-reflectors with different deflection angles on the array.

3.2 Calculation result of distribution of effective reflection area for Shenzhou-4 LRA

According to the formula above, we calculated the distribution of the effective reflection area for the Shenzhou-4 LRA. Fig. 4 shows the distribution of the satellite's effective reflection area, supposing θ=50° and the orbital altitude (h_s) is 330km. The value of contour line is the relative effective reflection area, and suppose the reflection area of single retro-reflector as 100. The outermost large circle stands for the horizon circle, and dashed circles for the contour lines with different elevations. From the outermost to the center, the elevation of dashed circles is 10°, 30°, 50° and 70° respectively, and the center stands for the zenith of station. The total effective reflection area is about 123 when the satellite is located at the zenith and the maximum area is

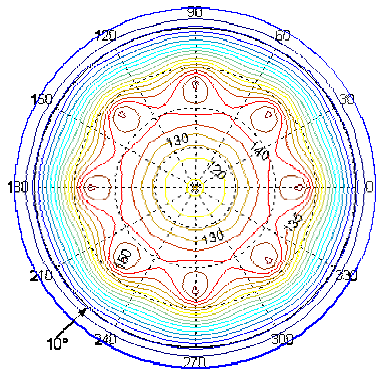

Fig.4
Calculation result of distribution of effective reflection area on Shenzhou-4 LRA

about 150 at the elevation of 32.8°. The effective reflection area is greater than 70 at the elevation of 10°. It should be noted that the retro-reflectors of the Shenzhou-4 are without high reflectivity coating. For this kind of fused quartz retro-reflector, they do not always meet the specification of

the total reflection at the incidence angle bigger than 16.6°. It depends on the azimuth of the incident beam. Because the satellite motion is too complicated to calculate the azimuth of the incident beam accurately, the actual total effective reflection area will be less than the calculation result.

4. Optical tests of LRA

4.1 Test of the surface flatness and divergence

The surface flatness and divergence of LRA are measured with a ZYGO Interferometer. The divergence of reflectors are 12-16 arcsec.

4.2 Optical reflectivity measurement

See Fig. 5, the average reflectivity of a single corner-cube is about 92.5%.

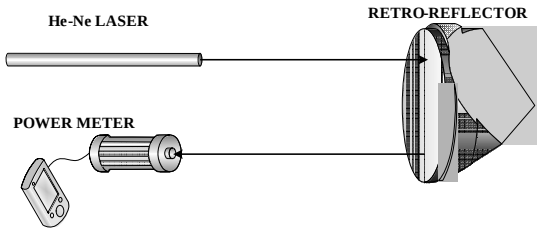

Fig.5 Optical reflectivity measurement

4.3 Relative reflection area measurement

The relative reflection area of a corner-cube was measured as Fig. 6. As the corner-cube had no coating on the back surfaces, the relative reflection area depends on the azimuth angle φ of the incident beam (see Fig. 7). The measurement results shows in Fig. 8.

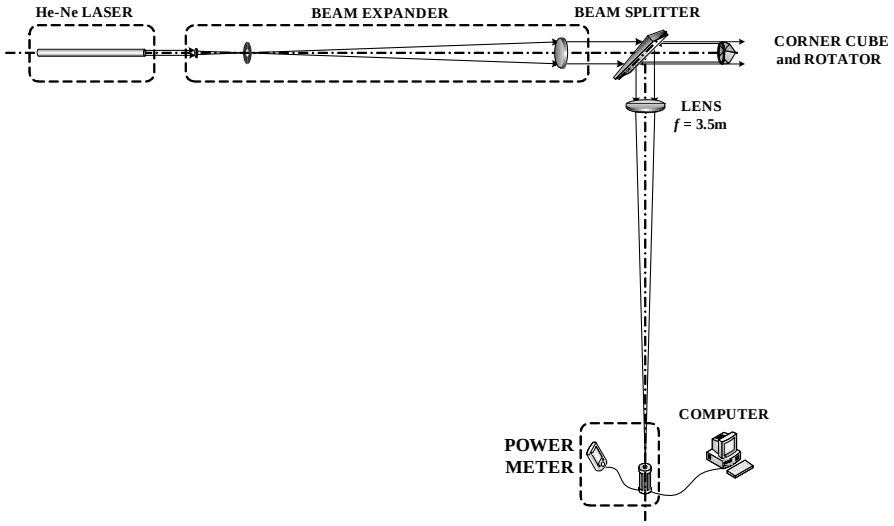

Fig. 6 Relative reflection area measurement

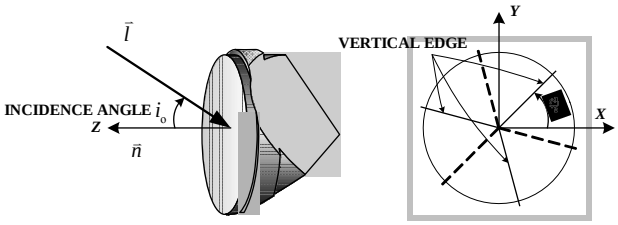

Fig. 7 Azimuth angle of corner cube

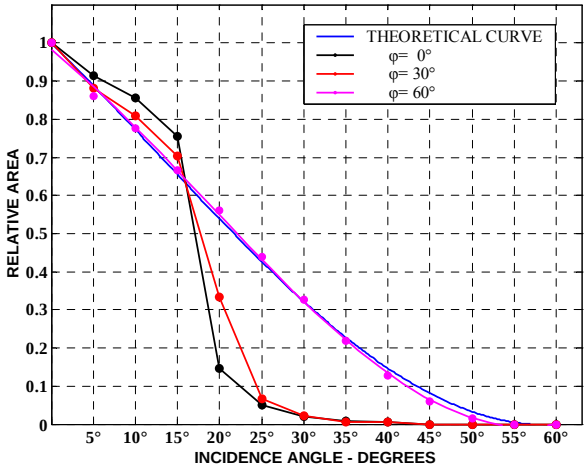

Fig. 8 Measurement result of the relative reflective area via incidence angle of corner cube with different azimuth angles

4.4 Far Field Diffraction Pattern Measurement

The set up of the measurement is shown in Fig. 9 and the results are shown in Fig. 10.

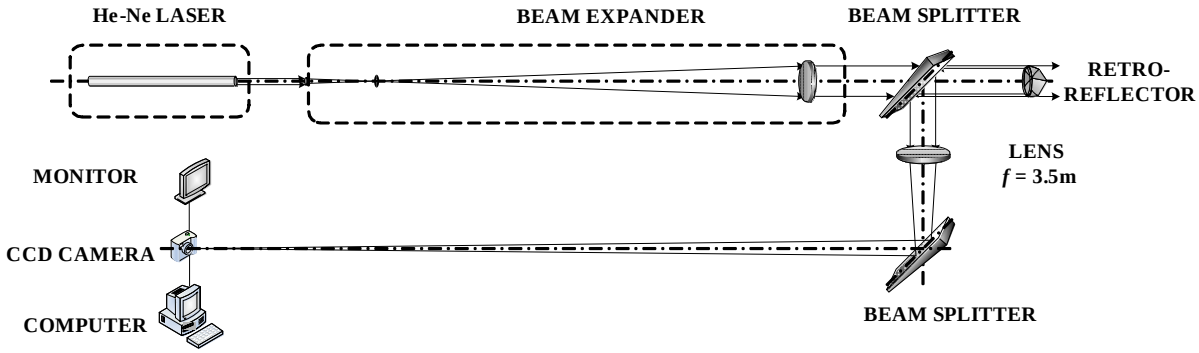

Fig. 9 Far field diffraction pattern measurement

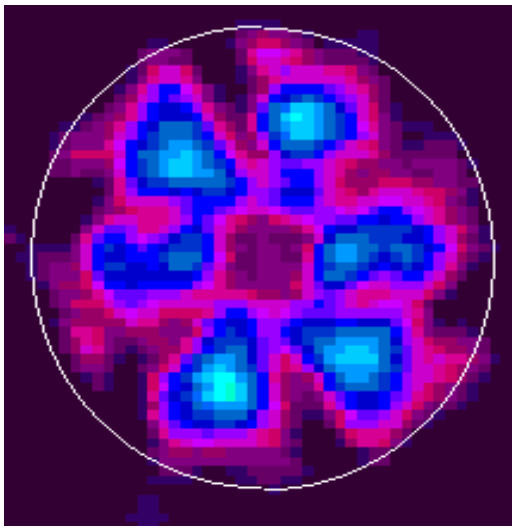

Fig.10. Far field diffraction patterns

5. Laser ranging campaign of Shenzhou-4 in China

Since January 7, 2003, the Beijing, Shanghai, Changchun, Wuhan and BeijingA (Argentina) stations started to track the orbital module at an altitude of 350 KM. The predictions were provided by the Xi'an Mission Control Center, with the USB (United S-Band Ranging and Range Rate) system and pass by pass precise orbit prediction. So, the 5 stations can track the module even in the earth shadow. In total, 82 passes experimental ranging data were obtained from the 5 stations during January-March, 2003. The module fell down in August 2003.

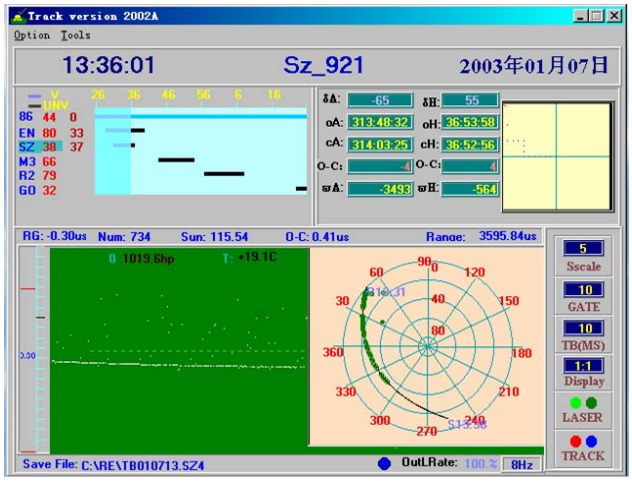

Fig.11 Real time display of Shenzhou-4 tracking at Shanghai

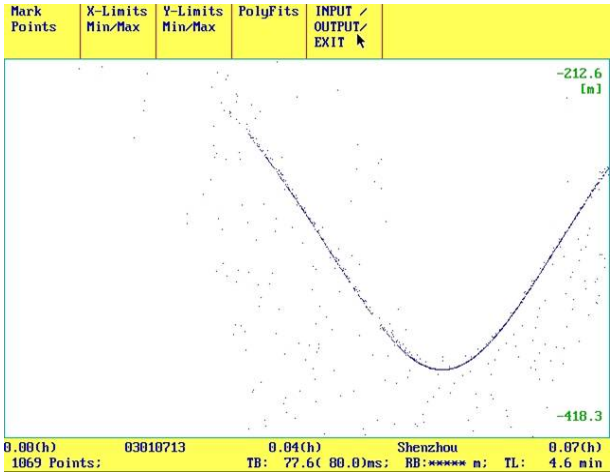

Fig. 12 One pass from Shanghai station on Jan.7, 2003

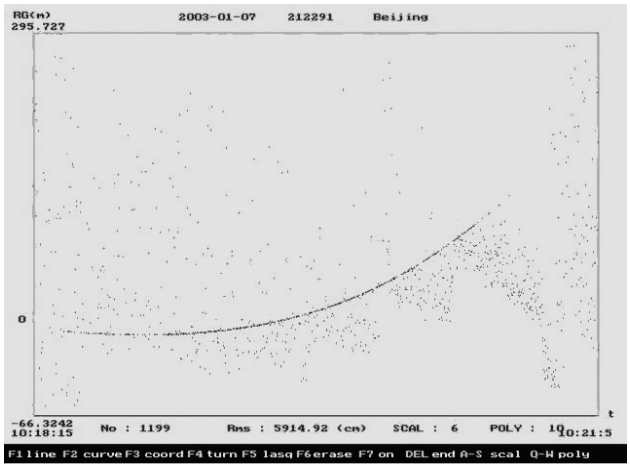

Fig.13 The first pass from Beijing station on Jan.7, 2003

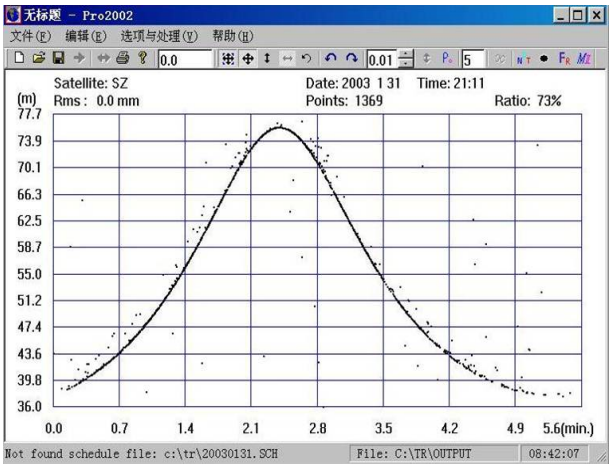

Fig.14 One pass from Changchun station on Jan.31, 2003

Acknowledgement

We would like to thank the Center fro Space Research and Application and Xi'an Mission Control Center for their support and suggestions during the design and test of LRA experiment.

REFLECTOR, LARETS and METEOR-3M(1) what did we learn from tracking campaign results

V.B. Burmistrov, N.N. Parkhomenko, V.D. Shargorodsky, V.P. Vasiliev
IPIE, Russia

Abstract

Brief description is presented of main observation results, as well as conclusions and recommendations drawn from the campaign results.

REFLECTOR

The REFLECTOR microsatellite detailed description was presented at the 12-th Laser Ranging Workshop in Matera (Italy), and later some observation results were presented in Washington, DC (USA) during the 13-th Laser Ranging Workshop. The specialty satellite (Fig. 1), designed exclusively for calibration of large active optical observation systems, has been successfully tracked during a period from 21.12.2001 to 07.03.2003.

Figure 1 Reflector microsatellite outlook

The REFLECTOR satellite has the following orbit parameters:

Major semiaxis of the orbit	7391 km
Inclination	99.64 deg
Eccentricity	0.0008
Orbit height	1018.63 ±10.71 km
Orbiting period	105.34 min

The tracking campaign results demonstrated the operability of its passive attitude control system, while the oscillation damping (with help of magnetic hysteresis rods) was slower than anticipated prior to launch (Fig 2).

The SLR observations also demonstrated that, using adequately arranged retroreflectors (or RR groups) on board of a spacecraft (SC), it is possible to determine the SC attitude from distance measurements at any moment with an accuracy sufficient for practical purposes

(Figures 3 and 4; the data were kindly provided by the Herstmonceux SLR station staff).

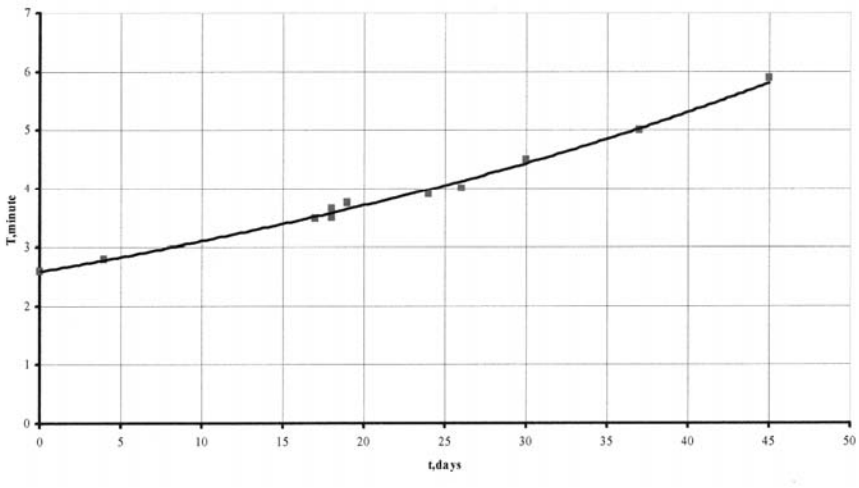

Figure 2. Variation of the period of fluctuation (rotation) REFLECTOR satellite (from the results of observations 23.12.2001 to 06.02.2002)

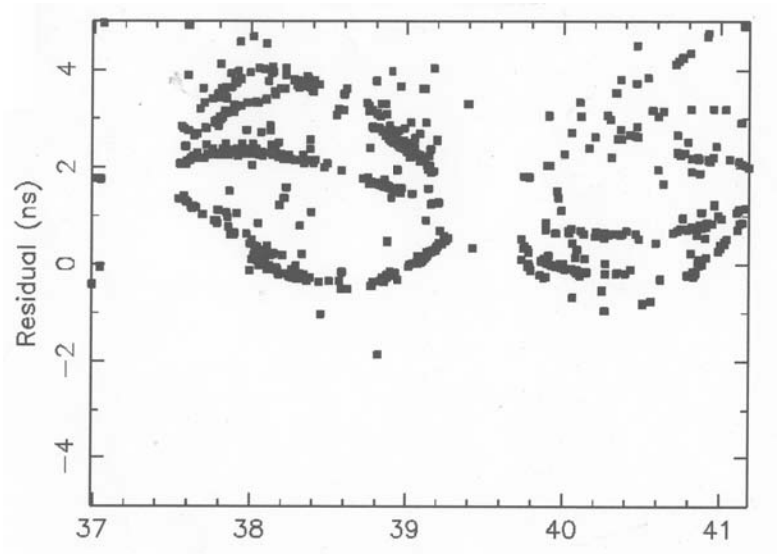

Figure 3. Pass 637 REFLECTOR. 19.01.2004, 21 hrst+

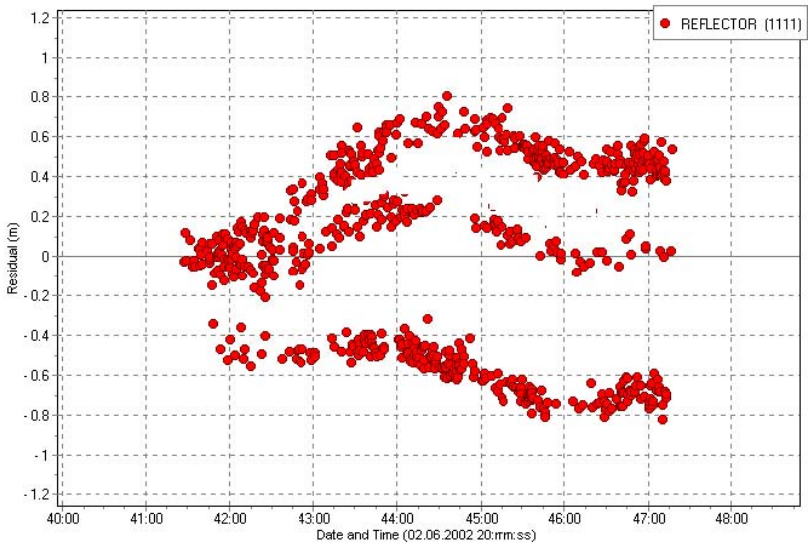

Figure 4.

After termination of the ILRS tracking campaign, the REFLECTOR microsatellite is open for observations in accordance with its basic purpose

LARETS

The satellite (Fig. 5) is a modified version of the formerly launched GFZ-1 and WESTPAC (a spherical brass body 21.5 cm in diameter, 23.9 kg mass, carrying 60 cube corner retroreflectors). The CCRs are recessed in the brass body to limit the single CCR field of view (instead of using external baffles, like on WESTPAC). Thus, we increased the target cross-section, and eliminated the dead time intervals between the bursts of return signals, typical for WESTPAC. LARETS has also a much higher rotation rate than WESTPAC.The RMS target error of LARETS (about 1.5 mm) is only slightly more than with WESTPAC, while the cross-section, according to preliminary estimations, is approximately one fourth of that one of STELLA and STARLETTE, but much higher than that one of WESTPAC.

Figure 5. LARETS. Orbit height 690 km.
Used for scientific and applied tasks in geodesy and geodynamics

The LARETS satellite appears to be a reasonably successful design. Observation results demonstrate that actually a single cube corner reflector is active at any moment of ranging. We are very interested in the SLR community opinion on preferable orbit heights where the application of such a satellite will be most efficient.

Currently, an investigation program is conducted to estimate the LARETS characteristics, as well as effort to use it for calibration of high-accuracy optical and microwave measurement systems. Therefore, we ask to extend the LARETS observation campaign for one year more.

METEOR-3M(1)

The operational principle and design of the retrereflector based on the optical Luneberg lens idea has been reported at three previous Laser Ranging Workshop (Deggendorf, Germany, 1998; Matera, Italy, 2000; Washington DC, USA, 2002).

The first experimental spherical retroreflector, 6 cm in diameter, mounted on board the METEOR-3M(1) spacecraft, has been successfully tracked during 2.5 years. The initial part of tracking campaign demonstrated a good agreement with pre-launch predictions based on theoretical calculations and lab measurements (Figure 6).A preliminary analysis of the campaign results shows that the initial cross-section value has gradually decreased; this is possibly due to the non-radiation-resistant glass used in the experimental retroreflector (the initially planned observation period was only 6 weeks — just to verify the design parameters).

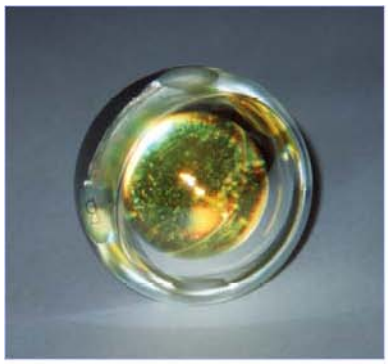

RR outlook

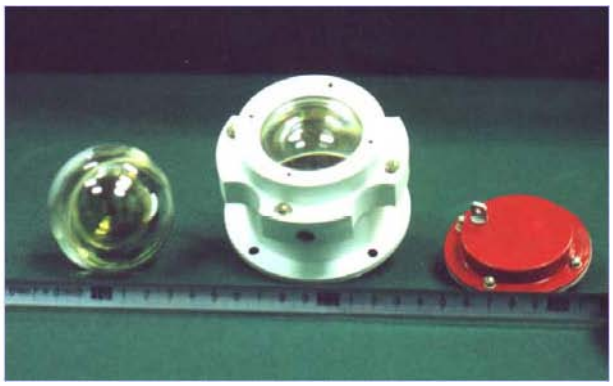

RR and holder

Figure 6. First spherical retroreflector

Currently we have completed the manufacturing of two larger spherical retroreflectors (17 cm in diameter, and about 7,5 kg mass) (Fig. 7); after a period of parameter investigation, we will be ready for launching of at last one of them as an autonomous SLR satellite with a practically zero target error.Such a target satellite may be used for extreme accuracy measurements in geophysics, geodynamics, etc., and may stimulate further SLR hardware development to obtain better precision. The ILRS Government Board has addressed the Federal Space Agency of Russia to support an appropriate launching; IPIE will now take responsibility for organizing and preparation of a corresponding launching.

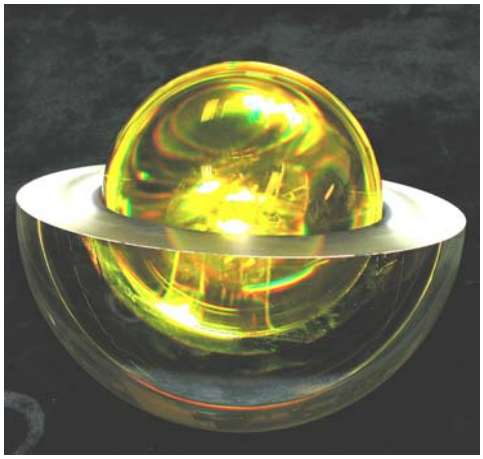

Figure 7. 17 cm-diameter spherical retroreflector (dissembled)

A NEW APPROACH FOR MISSION DESIGNING OF GEODETIC SATELLITES

Martin Lara (1), Itziar Barat (2)
(1) Real Observatorio de la Armada, 11110 San Fernando, Spain.
(2) European Space Research & Technology Center, 2200 AG Noordwijk, The Netherlands
mlara@roa.es ,Itziar.Barat@esa.int

Abstract

Repeat ground track orbits are frequently used in the geodetic applications of an artificial satellite. The usual procedure for designing a mission requiring repetition of the ground track is based on trial and error interactive corrections. We propose a different approach that can be completely automated, and has been implemented as a software tool dubbed SADSaM. In just a few seconds, SADSaM provides the initial conditions of an exactly periodic orbit with the requested repeat ground track cycle, and also provides the orbit stability character, as well as the averaged orbital elements.

Introduction

In the geodetic applications of an artificial satellite, associated measurements are frequently sampled along the ground track of the satellite's nadir point. The points where the ground track of a satellite intersects itself on the surface of the earth are called crossover points. Crossover points provide relevant measures in satellite geodesy, for instance in the calibration of a gravity field model [1]. Techniques for the determination of crossover locations have been introduced in several studies. The relevant bibliography can be found in [2].

The ideal situation occurs when the satellite repeat its ground track on the surface of the Earth, and repeat ground track (RGT) configurations are therefore preferred. The procedure of mission design starts from the experiment requirements, which constrain the orbital parameters to a subset of limited values. Then a first order of J_2 design is done as a rough estimate of the nominal solution. Further refinements of the orbital elements —usually in the presence of a medium degree zonal model, but sometimes including drag— will provide the nominal orbit.

The refinement procedure aerospace engineers normally use is based on trial and error interactive corrections that converge to a good nominal set of orbital elements; "good" meaning that the satellite does not drift substantially from the RGT. A fine "tuning" of the eccentricity in a manual iterative sequence does this refinement.

On the contrary, it has been recently shown that periodic solutions exist for a zonal model of the artificial satellite when the problem is formulated in a synodic frame, i.e. a rotating frame attached to the planet [3]. These periodic orbits repeat exactly their ground track on the surface of the planet and, hence, are ideal candidates as nominal orbits for RGT missions. In this communication we describe SADSaM, a software tool for computing RGT orbits. It is based on the continuation of families of periodic orbits, and is totally automated. By simply introducing the RGT cycle between the nodal periods and nodal days as input, SADSaM provides the initial conditions of an exactly RGT orbit either sun synchronous or at the required inclination in just a few seconds —even for a high degree (zonal) gravitational model. Besides SADSaM provides the stability character of the RGT orbit and its averaged orbital elements.

We illustrate the usefulness of this tool computing a nominal orbit for ENVISAT, a satellite that is actually tracked by the laser station of ROA. We find that the orbital parameters provided by SADSaM are very close to the real mission parameters.

Frozen orbits

The experiment constrains of an earth observation mission –normally related to technical limitations of the sensors and geographic or geodesic aspects related to the experiment– limit on the acceptable range of the orbit elements as well as the repeat ground track cycle. For these kinds of satellite tasks, mission designers try to minimize the altitude variation of the satellite over the surface of the Earth searching for orbits with a small constant value of the eccentricity and with a frozen argument of perigee. When one only considers the J_2 effect, the Lagrange equations for the secular motion of the orbital elements show that there are no secular variations in semimajor axis, inclination and eccentricity. But there is a constant regression of the line of nodes, and, except at the critical inclination sin i =2/√5 a constant motion of the perigee given by:

$$\frac{\mathrm{d}\omega}{\mathrm{d}t} = \frac{3n\left(4-5\sin^2 i\right)}{4\left(1-e^2\right)^2} J_2 \left(\frac{\alpha}{a}\right)^2$$

where a is the semimajor axis, e the eccentricity, i the inclination, ω the argument of the perigee, n the mean motion, α the equatorial radius of the Earth, and t is the time. But when considering also the J_3 effect, one finds

$$\frac{\mathrm{d}\omega}{\mathrm{d}t} = \frac{3n\left(4-5\sin^2 i\right)}{4\left(1-e^2\right)^2}\left[J_2\left(\frac{\alpha}{a}\right)^2 + \frac{1}{2} J_3\left(\frac{\alpha}{a}\right)^3 \sin\omega \; \frac{\sin^2 i - e\left(1-\sin^2 i\right)}{e\left(1-e^2\right)^2 \sin i} \right]$$

$$\frac{\mathrm{d}e}{\mathrm{d}t} = -\frac{3n\left(4-5\sin^2 i\right)}{4\left(1-e^2\right)^2} \frac{1}{2} J_3\left(\frac{\alpha}{a}\right)^3 \cos\omega \sin i$$

The equilibrium solutions (de/dt) = (dω/dt) = 0 of the reduced system above are usually called “frozen orbits”, and, besides the critical inclination case mentioned above, one can find frozen orbits whit low eccentricity and argument of the perigee ±π/2 at any inclination. As appreciated in Fig. 1, one important property of frozen orbits is that close to the values e_0,ω_0,that “freeze” the orbit, the orbit perigee oscillates.

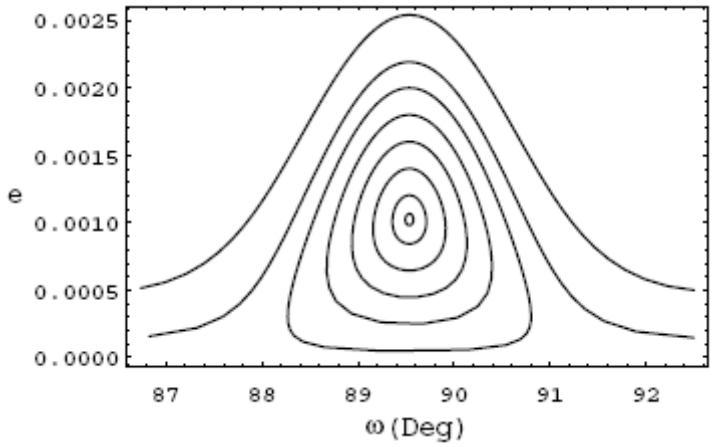

Figure 1. Oscillation of the perigee in the vicinity of a Spot-type frozen orbit (a = 7200.548 km, i = 98.723°)

Periodic Orbits

A more general definition of frozen orbits is that they are relative equilibriums of an averaged form of the zonal problem. With this definition, and regardless of the motion of the node, one can map frozen orbits onto periodic solutions of the (two dimensional) non-averaged zonal problem. When using cylindrical coordinates, the zonal problem is decoupled into the motion in the (ρ, *z*)-plane and the motion of this plane: the rotating meridian plane of the satellite. Frozen orbits are periodic solutions of the two degrees of freedom problem that represents the motion in the (ρ, *z*)-plane [4]. Figure 2 shows an example of a frozen orbit in cylindrical coordinates, with averaged orbital elements: a = 10559.26 km, e = 0.34633, i = 116.556°, ω= 270°.

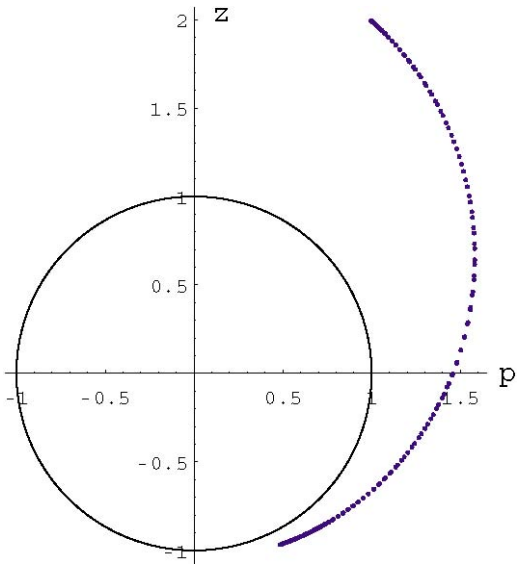

Figure 2. Ellipso™ Borealis-type frozen orbit in the (ρ, z)-plane

In some cases the nodes rate of precession is commensurate with the rotation rate of the Earth and the frozen/periodic orbits are exactly periodic solutions in a rotating frame attached to the Earth. That is: orbits that exactly repeat the ground track on the surface of the Earth. As appreciated in Fig. 3 (after Lara, 1999), there exist almost circular, repeat ground track, periodic orbits for all inclinations, and elliptic, repeat ground track, periodic orbits at the critical inclination.

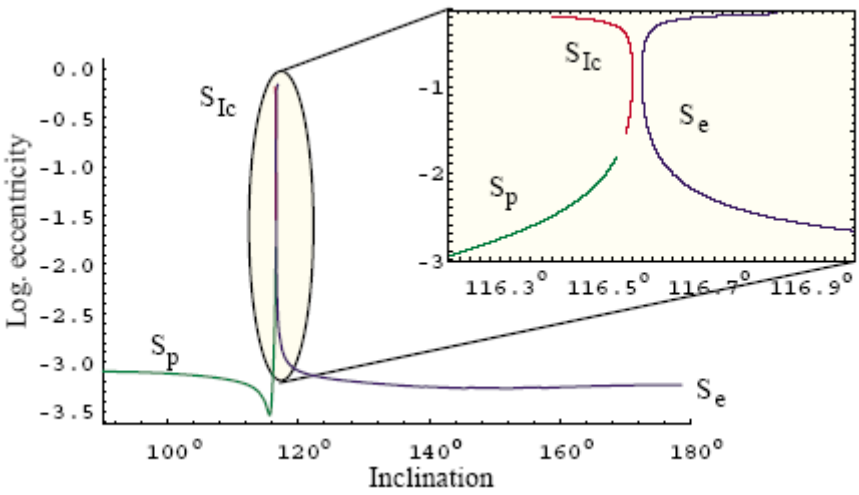

Figure 3. Families of orbits with a repeat ground track cycle of 8 nodal periods (retrograde inclination orbits only)

Therefore, the computation of three-dimensional periodic orbits in a rotating frame attached to the Earth is a new approach for designing satellite missions that require a repeat ground track orbit condition. As described below, this can be done in a totally automated way.

Practical approach: SADSaM

SADSaM, an acronym for a **S**oftware **A**ssistant for **D**esigning **Sa**tellite **M**issions, is a computer application intended for helping mission designers for artificial satellites in their search for repeat ground-track, frozen orbits. Briefly, SADSaM assumes a zonal model for the Earth gravitational potential. Thus, when formulated in the inertial frame the problem is bi-parametric: while the energy E determines the size (and period) of the orbit, the polar component Λ of the angular momentum vector is related to its inclination –except for the critical inclination, where variations of Λ imply variations in the eccentricity for fixed inclination. Therefore, the exploration of the (Λ, E)-plane allows finding either a sun synchronous solution or an orbit at the selected inclination, fulfilling the desired repeat ground-track condition.

The flowchart of Fig. 4 presents the main sequence of computations done by SADSaM. After launching the application, SADSaM asks the user for the number of nodal days and periods after which the ground track of the satellite repeats over itself, and also for the kind of solution desired, either sun synchronous or at fixed inclination or eccentricity. A first approximation to the solution is then computed from a first order of J_2 analytic approximation. It follows the inner loop, where the initial conditions are iteratively refined until finding a frozen orbit. If this frozen orbit does not repeat its ground track, the second loop improves the initial conditions of the orbit that, after differential corrections, will correspond to a repeat ground track orbit. Then, after computing average values of the orbital elements, SADSaM verifies that the orbit parameter –either inclination i, or eccentricity e, or nodes precession rate– corresponds to the value (i_0, e_0, or sun synchronism) specified by the user. If the solution is obtained, then it is written to a file and SADSaM ends. Otherwise, the polar component Λ of the angular momentum of the orbit is varied in the outer loop.

Additional information accepted by the program is the name of the file with the potential model, and the order of the higher zonal harmonic coefficient to take into consideration. By default, SADSaM uses coefficients J_2–J_9 of the WGS84 gravity field.

Application to ENVISAT

In order to show the efficiency of SADSaM, we compare the long term propagation of the actual orbital elements of ENVISAT (a = 7159.49 km, e = 0.00115, i = 98.5425°, ω = 91.9°) with those provided by SADSaM for the same mission requirements (sun synchronous; repeat cycle 35 days; length 501 orbits), namely, a = 7159.49 km, e = 0.00114, i = 98.5446°, ω= 90°. Figure 5 present the long-term propagation (2500 days) in each case. A full perturbation model was considered, including the Sun and Moon perturbations, and the GEMT-1 36 ×36 gravity model. Since the eccentricity of the ENVISAT orbit is very small, the frozen condition is better perceived using the elements $x = e \cos \omega$, $y = e \sin \omega$. As appreciated in the figure, the results are very similar in both cases but with clear advantage to SADSaM.

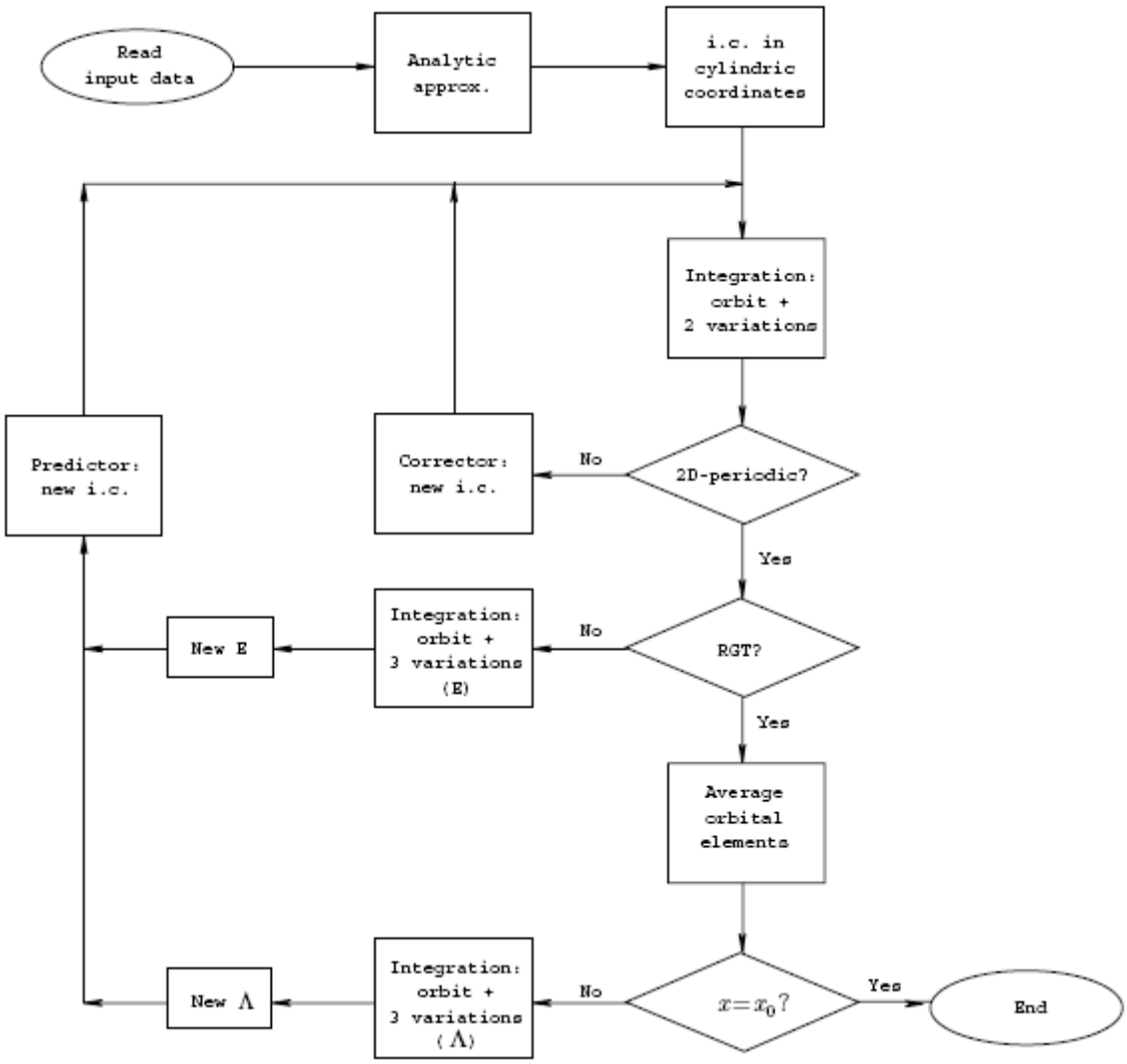

Figure 4. Flowchart of SADSaM

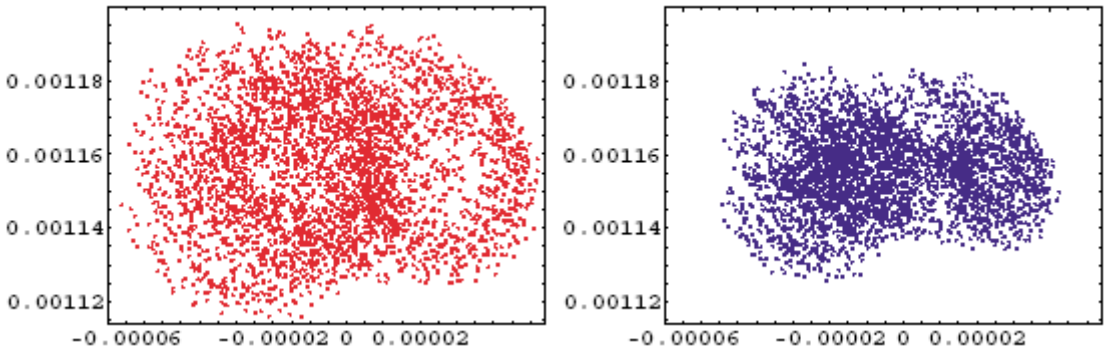

Figure 5. ENVISAT long-term evolution(e cos ω, e sin ω). Left actual. Right SaDSaM

Conclusions

Repeat ground track orbit configurations are highly desirable for missions of geodetic satellites. But, when only considering the Earth gravitational force, repeat ground track orbits

are found to be three-dimensional periodic orbits in a rotating frame attached tothe Earth. The classical approach for mission designing of repeat ground track orbits is based on trial and error manual iterative corrections. On the contrary, the software application described here is a totally automated tool for computing initial conditions of repeat ground track solutions. Our tool has two clear advantages with respect to other software programs: on one side it is not restricted to sun-synchronous solutions; on the other side it automatically determines an accurate value of the eccentricity without need of "a priori" assumptions. Application of this tool to simulate a real mission shows the reliability of the new method proposed.

Acknowledgements

M. Lara thanks partial support from the Spanish Ministry of Technology and Science(Grant # ESP2002–02329).

References

[1] Klokocnick, J, Wagner, CA (1994), Bull. Geod. 68: 100-108

[2] Kim, MC (1997), J. of Geodesy 71: 749-767

[3] Lara, M (1999) J. of the Astronautical Sciences 47: 177-188

[4] Lara, M, A. Deprit, A. Elipe (1995) Celest. Mech. and Dyn. Astron. 62: 167-181

ASYMMETRIC RADIATION PRESSURE ON LAGEOS

David A. Arnold (1), Graham Appleby (2)
(1) 94 Pierce Rd, Watertown, MA 02472, 6179243811.
(2) NERC Space Geodesy Facility, Herstmonceux, Hailsham, E. Sussex, UK

Introduction

This is a abbreviated version of the original paper. For the complete paper see the SPWG website 'http://nercslr.nmt.ac.uk/sig/signature.html'.

Analysis of the orbits of the LAGEOS satellites indicates that the radiation pressure on the satellites is not perfectly symmetrical. There is an unexplained force component along the spin axis. I was asked to review paper entitled "LAGEOS Satellites Germanium CubeCorner-Retroreflectors and the Asymmetric Reflectivity Effect", David M. Lucchesi, Celestial Mechanics and Dynamical Astronomy 88: 269291, 2004. This paper attempts to explain the asymmetry as due to the germanium cube corners. I feel that the physical model used in the Lucchesi paper is incorrect. I recommended rejecting the paper. This paper discusses my objections to the physical model and outlines a different modeling approach.

The physical problem.

The LAGEOS satellite is subjected to perturbing forces from incident radiation and thermal radiation emitted by the satellite. The incident radiation is primarily solar radiation (1412.5 w / m^2), but there are also forces due to solar radiation reflected from the earth (earth albedo 38.1 w / m^2), and thermal radiation from the earth (66.5 w / m^2). The incident radiation is partially reflected from the satellite and partially absorbed.

The satellite has an aluminum surface (bare, machined 6061T6 aluminum) and brass core. The absorptivity of the aluminum is .15 and the emissivity is (.05). The average core temperature is 55 deg C. For a nonspinning satellite the hot side and cold side temperatures are 60 deg C and 52 deg C. The corresponding maximum and minimum retroreflector face temperatures are 16 and 8 deg C.

Thermal vacuum tests run on two of the infrared cube corners gave temperatures of 104.4 and 106.7 deg C with full solar illumination. The cube corners would be opaque at this temperature. With the solar illumination reduced by the factor $1/\pi$, the temperatures fell to 55.5 and 52.8 deg C for the two cubes. This illumination corresponds to an incidence angle of 71.4 deg. With no solar illumination, the temperatures were 12.2 and 26.6 deg C.

The optical cube corners are colder than the core because they have a high emissivity (.90) and low volumetric solar absorptivity (.05). The mounting cavity is designed to minimize both radiative and conductive heat transfer between the core and the cube corners to minimize thermal gradients which would distort the diffraction pattern of the cube corners.

The energy absorbed by the satellite must be emitted as thermal radiation. The force due to the incident radiation is instantaneous. As long as the reflecting properties of the satellite are uniform there is no asymmetry. However, because of the time constants involved in the thermal behavior, the thermal radiation will be in a different direction from the incident radiation. Since the spin rates of LAGEOS-1 and LAGEOS-2 are different, the thermal behavior will be different for the two satellites. Since the optical and thermal parameters of the germanium cubes are different from the parameters of the optical cubes, they run at different temperatures and the pressure of the thermal radiation is different. This results in an asymmetric thermal radiation pressure.

Asymmetry due to the germanium cube corners.

The author assumes that the optical cubes cover the LAGEOS satellite uniformly and that there would be no asymmetry in the radiation pressure on the satellite with only optical cubes. The premise of the paper is that replacing 4 of the optical cubes with 4 germanium cubes results in an asymmetry in the radiation pressure on the satellite because the reflectivity of the germanium cubes with respect to solar radiation is different from the reflectivity of the optical cubes. The asymmetry is illustrated by a simple example below.

In the diagram below, there are two mirrors on a spherical satellite which are at a 45 degree angle with respect to the incident solar radiation which is in the vertical direction. The mirrors have a reflectivity of 100 percent. The light hitting the left mirror is reflected to the left and the light hitting the right mirror is reflected to the right. The momentum transfer is perpendicular to the mirror in the direction of the center of the satellite for both mirrors. The force on each mirror can be resolved into horizontal and vertical components. The horizontal components cancel and the net force on the satellite is in the vertical direction, parallel to the incident solar radiation. There are no torques or unbalanced horizontal forces. This is the definition of a symmetrical radiation pressure on the satellite.

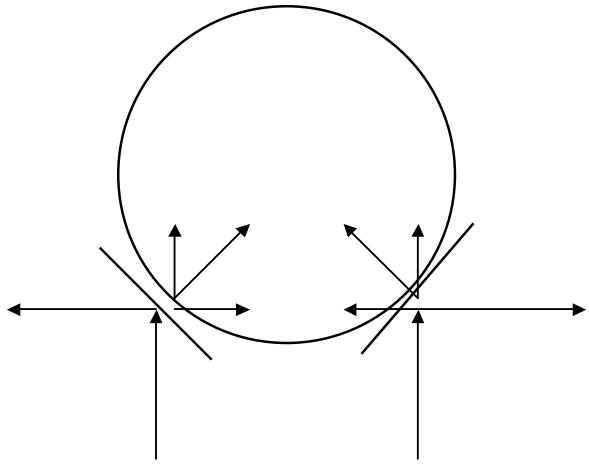

If the mirror on the right is replaced by a black body, the radiation is totally absorbed and the pressure on the black body is in the vertical direction. This creates an asymmetry . There is a net force to the right because the pressure on the black body has no component to the left to balance the horizontal component of the force on the left mirror.

Suppose the reflectivity of the right mirror is 50 percent. The force due to the absorbed component is in the vertical direction. The force due to the reflected component is as shown in the diagram except that the magnitudes of the components are half as great. The force on the satellite is asymmetrical since the horizontal components do not balance.

Suppose the reflectivity of the right mirror is 99 percent. The radiation pressure on the satellite would be nearly symmetrical but there would be a small asymmetrical component.

If one replaces an optical cube corner on LAGEOS with a germanium cube corner, the effect is to subtract the force on the optical cube and add the force on the germanium cube.

Perturbation to the orbit.

A. First approach

One approach to determining the orbital perturbation caused by the germanium cube corners which I think gives a good physical understanding of the problem is the following:

1. Do an orbital simulation with only optical cubes on the satellite computing all the forces on the satellite due to incident radiation on the cube corners and the core, and the force due to thermal radiation from the core and the cube corners.

2. Replace 4 optical cubes with germanium cubes. Do a second orbital simulation computing all the forces on the germanium cubes, the optical cubes, and the core from incident radiation, and the forces due to thermal radiation by the germanium cubes, optical cubes, and the core.

3. Compute the difference between the state vectors or orbital elements from the two simulations. This is the perturbation due to the germanium cube corners. Step 2 will give a different answer from step 1 because the force on the germanium cubes is different from the force on the optical cubes they replace.

B. Second approach

Since the only thing that matters in computing the perturbation is the difference between the force on a germanium cube and the force on the optical cube it replaces there is a simpler approach to computing the perturbation as follows:

1. Do an orbital simulation with only a central force and no perturbations. The orbital elements are constant for this case.

2. Compute the difference between the force on a germanium cube and the force on an optical cube. Do a second simulation using only the central force and the difference in force on the two types of cube corners.

3. Compute the difference between the state vectors or orbital elements from the two simulations. This is the perturbation due to the germanium cube corners.

The Lucchesi model

In the paper by Dr. Lucchesi, the perturbing force is computed as the difference between the force on a germanium cube and the force on a black body. This implies that the optical cube is a black body. A black body has zero reflectivity. It absorbed all the incident light.

In principle, one could use a black body as a reference in the following way. Suppose we assume that there is no asymmetry with only quartz cubes on the satellite. Let us call the force on a quartz cube $\vec{Q}$, the force on a black body with the same area $\vec{B}$, and the force on a germanium cube $\vec{G}$. Suppose one removes a quartz cube and replaces it with a black body. The imbalance created is $(\vec{B} - \vec{Q})$. Suppose the black body is then replaced by a germanium cube. This introduces an additional imbalance given by $(\vec{G} - \vec{B})$. The total imbalance due to the two substitutions is $[(\vec{B} - \vec{Q}) + (\vec{G} - \vec{B})] = (\vec{G} - \vec{Q})$. Introducing the intermediate step of a black body is unnecessary and using only $(\vec{G} - \vec{B})$ is incorrect.

Numerical comparison of the two models.

There is no available model for computing the radiation pressure on an optical cube corner as a function of incidence angle. However, the case of normal incidence is simple to compute. Let us assume that momentum p is incident on a cube corner at normal incidence and compute the momentum transfer for various different cases.

Case 1. Normal incidence on an optical cube corner.

In this case, the reflectivity of an uncoated cube corner is nearly 100 percent due to total internal reflection. The momentum of the radiation before reflection is $+p$ and the momentum after reflection is $-p$. The difference $2p$ is the momentum transferred to the cube corner.

Case 2. Normal incidence on a germanium cube corner with a reflectivity of 100 percent.

The answer in this case is $2p$ the same as Case 1. This was the assumption in the author's original calculation and the computations were never revised.

Case 3. Normal incidence on a black body.

The momentum of the radiation before absorption is $+p$. The momentum of the radiation after absorption is zero. The difference $+p$ is the momentum transferred to the black body.

Case 4. Normal incidence on a germanium cube with reflectivity 50 percent.

The momentum of the radiation before striking the cube is $+p$. The momentum of the 50 percent that is reflected is $-p/2$. The difference is $3p/2$ which is the momentum transferred to the cube corner. Half of the energy is absorbed by the cube and must be emitted as heat.

Case 5. Asymmetry using the Lucchesi model

In the model used by the author the perturbation is computed as the difference between the momentum transferred to a germanium cube and the momentum transferred to a black body. This is given by the difference between Case 2 and Case 3. We have

$2p - p = p.$

Case 6. Asymmetry using my model

In the model I have proposed, the perturbation is computed as the difference between the momentum transfer to a germanium cube with reflectivity 50 percent and the momentum transfer to an optical cube. This is given by the difference between Case 4 and Case 1. We have

$3p/2 - 2p = -p/2.$

Discussion of the differences between the two models.

The method used by the author over-estimates the magnitude of the perturbation due to the difference in reflectivity between a germanium cube and an optical cube as shown by comparing Case 5 and Case 6. However, the author's model neglects thermal radiation. The absorbed radiation has to be emitted as heat. If all the absorbed radiation were emitted instantly perpendicular to the front face, this would add another force proportional to $p/2$ so that the total momentum transfer in Case 4 would be $2p$ the same as for an optical cube. Case 6 would then give zero instead of a negative number.

Asymmetry of the radiation pressure on an optical retroreflector.

The figure below shows a two-dimension hollow cube corner. Light entering the cube corner at F is reflected from the right side at B, the left side at D, and exits in the direction of point H. Light entering at G is reflected near the vertex at C and exits in the direction G. Light entering at H is reflected at points D and B and exits in the direction of point F. The

light that enters between points H and F is retroreflected and the radiation pressure is in the direction of the incident radiation.

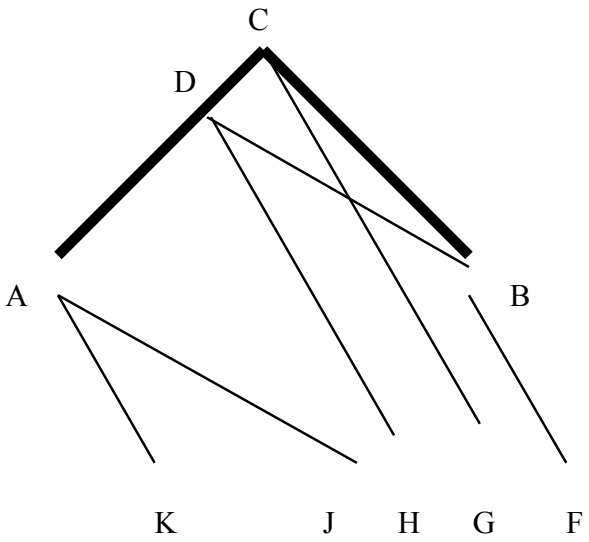

Light that enters the cube corner at K is reflected from the left side, misses the right side, and exits in the direction J. All light that enters between K and H is reflected only from the left side. The radiation pressure for this part of the radiation is perpendicular to the surface AC. This part of the radiation pressure is asymmetric. Appendix B gives a numerical calculation of the radiation pressure as a function of incidence angle. At normal incidence all radiation is retroreflected. Past about 27 degrees, the asymmetric component of the radiation pressure is larger than the retroreflected component. Beyond 45 degrees, which is the cutoff angle for retroreflection, all the radiation pressure is asymmetric.

A real cube corner has three reflecting faces. In addition to radiation that is reflected from only one face there may be radiation reflected from only two faces. The direction of these beams can be easily calculated. The more difficult part is calculating the amount of energy in each beam which depends on complicated geometric calculations of the reflecting area of each beam. This radiation pressure from this component is also asymmetric.

Each back face reflects one component of the incident momentum. Except at normal incidence on the cube corner, the momentum transferred to the cube corner is not normal to the front face. It is the sum of momentum transfers normal to the back reflecting faces.

The direction of the normal to each of the three faces depends on how the cube corner is installed in its holder. The cube corner can be rotated at any angle about its symmetry axis. In order to reduce systematic effects due to the angle at which the cubes are installed, the orientations of the cube corners have been randomized. As a result the direction of the asymmetric component of the radiation pressure on the optical cubes is random. The net radiation pressure on all the optical cube corners depends on the method used to randomize the orientations.

If the cube corner is solid, some of the radiation is reflected from the front face by dielectric reflection. The radiation pressure of this component is perpendicular to the front face. Since the optical cube corners cover the satellite in a reasonably uniform manner, the radiation pressure of this component is probably reasonably symmetric except for the presence of the germanium cubes.

Since there can be loss of total internal reflection in an uncoated cube, some radiation may be transmitted into the cavity and undergo further reflections or absorption by the core. Also, the light my strike unpolished surfaces of the cube where it has been cut into a spherical shape. Both these components are asymmetric.

There is no way at present to calculate the asymmetry due to the optical cubes because there is no existing model for the radiation pressure on the optical cubes. The only part of the reflection from an optical cube that has been modeled is the retroreflected part.

The radiation pressure on a germanium cube is easy to calculate. However, the equations used in the Lucchesi paper are incorrect. The correct equations are given in Appendix A.

Summary.

1. The asymmetry is the force on a germanium cube minus the force on the optical cube it replaces. Calculating the deviation from a black body is unphysical and over-estimates the asymmetry due to the germanium cubes.

2. The author's model neglects the force on the cube corners due to thermal radiation. There is an asymmetry because the germanium cubes are warmer than the optical cubes.

3. The equations used to compute the radiation pressure on the germanium cubes are incorrect by a factor of 2 even if one accepts the validity of the black body model.

4. The author neglects the asymmetry in the radiation pressure on an optical cube corner.

Conclusions and recommendations.

The apparent partial agreement between the calculations and the observed orbital perturbations should be considered accidental because the physical model and equations are not correct. The satellite can be considered to consist of 4 parts:

A. The optical cubes
B. The germanium cubes
C. The retaining rings
D. The surface of the core

The information needed to do a proper calculation of the asymmetry is the solar radiation pressure on each of the parts and the temperature of each part. The temperature is then used to calculate the pressure of the thermal radiation.

Appendix A. Radiation pressure on a germanium cube (see SPWG website)
Appendix B. Radiation pressure on a two-dimensional cube corner (see SPWG website)

CENTRE-OF-MASS CORRECTION ISSUES: TOWARD MM-RANGING ACCURACY

Toshimichi Otsubo (1) and Graham M Appleby (2)
(1) Kashima Space Research Center, National Institute of Information and Communications Technology 8931 Hirai, Kashima 3148501 Japan otsubo@nict.go.jp
(2) NERC Space Geodesy Facility, Monks Wood, Abbots Ripton, Huntingdon PE28 2LS United Kingdom gapp@nerc.ac.uk

Abstract

Target signature effect is currently one of the major error sources in satellite laser ranging (SLR) observations. We need to handle stationdependent centreofmass corrections, and, more importantly, eliminate the intensity dependence of range measurements which have been detected for most multiphoton CSPAD systems. Otherwise, the station height solutions may be significantly biased, which results in a degradation of SLRbased terrestrial reference frame.

Introduction

Along with the system noise and potential errors in the current tropospheric delay models, the spread of retroreflection due to multiple reflectors on the satellites is now recognized as a key error factor and is called "satellite signature effect" [Appleby, 1992]. As reported in past workshops ([Neubert, 1994; Otsubo and Appleby, 2002]; also published in [Otsubo and Appleby, 2003]), the centre-of-mass correction for spherical satellites cannot be treated as a constant.

It depends on the optical detectors and also on the observation policy. For single photon systems like the Herstmonceux station, the correction is likely to be smaller than the widely used standard values; for instance 242 mm instead of 251 mm for LAGEOS. Also, for multiphoton systems, the correction depends upon the optical strength of each return pulse. We calculated the effect for LAGEOS, AJISAI and ETALON based on the actual characteristics and location of each reflector, and found that the centre-of-mass correction varies by about 1 cm for LAGEOS and by between 4 and 5 cm for AJISAI and ETALON. The variation range is illustrated in Figure 1. Note that, except for the Herstmonceux values (marked as "Hx"), these correction values are based not on the actual systems but on the simplified, simulated system responses.

The centre-of-mass correction is not only station-dependent but can be intensitydependent as seen in "C-SPAD" measures in Figure 1. The station dependency can be removed by solving for a range bias in the orbit determination process, as long as it is a constant offset. However, the intensity dependency is more troublesome.

Existence of intensity-dependent bias

A special data analysis reveals the existence of such intensity-dependent range bias. We looked into the dependence of post-fit SLR residual data on the average intensity of return in each normal point. Following the previous studies [Otsubo, 2000; Otsubo and Genba, 2002], we used the number of single-shot returns per normal point bin width (i.e. column 44-47 of data record) as a measure of return intensity.

We analysed LAGEOS (two satellites) and AJISAI data observed from July 2003 to May 2004 (300 days). One set of station coordinates and range bias was adjusted per site and per satellite. The orbits were solved for every 4 days for LAGEOS and every day for AJISAI. The post-fit RMS was about 1.3 cm for LAGEOS and 2.5 cm for AJISAI.

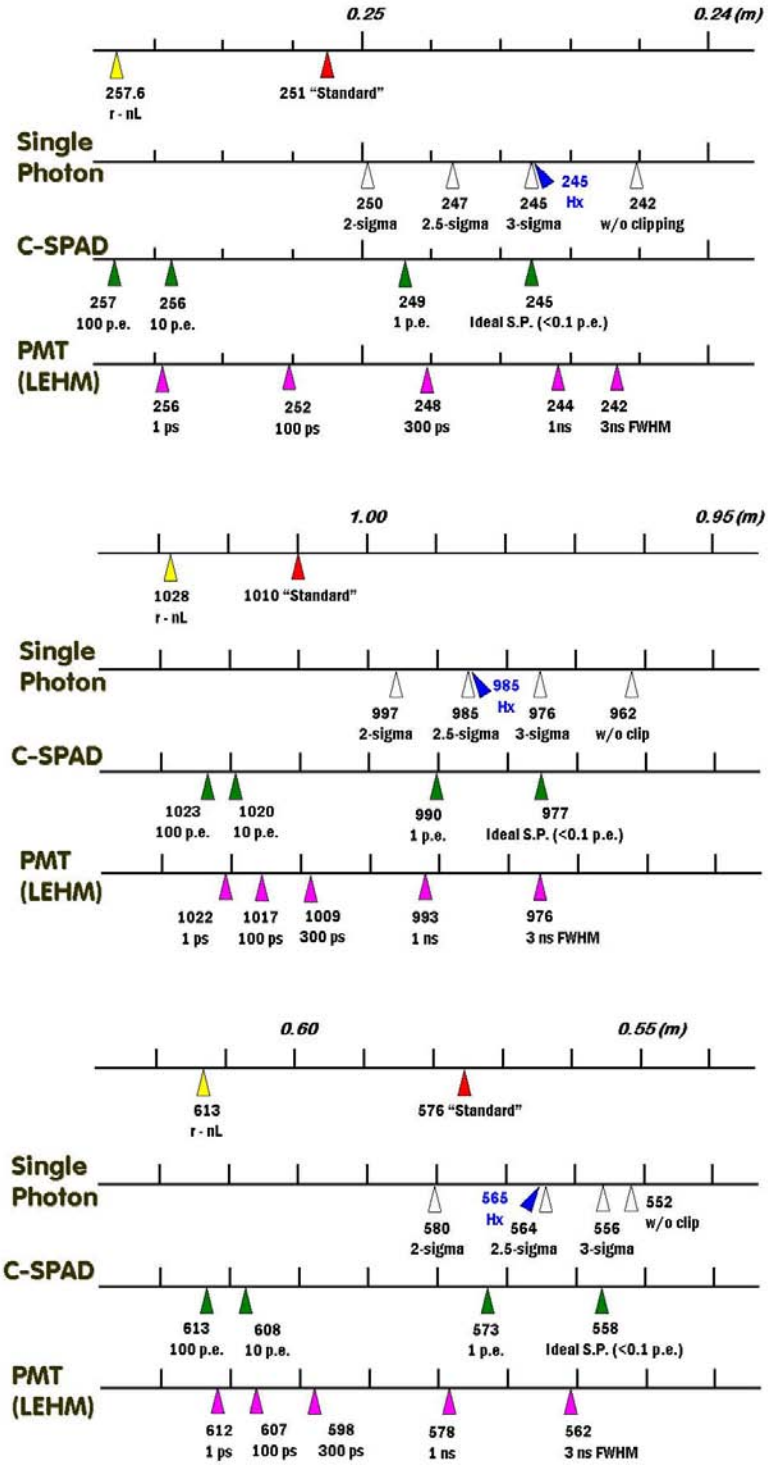

Figure 1. Centre-of-mass correction for geodetic satellites (top: LAGEOS, centre: AJISAI, bottom: ETALON). See Otsubo and Appleby [2003].

The residual profile with respect to the number of single-shot returns per bin was generated for each of the ILRS laser ranging stations. Figure 2 shows three typical results, for an MCP systems, a C-SPAD system and a single photon system. The graphs for all 24 systems analysed are available at:

http://www.nict.go.jp/ka/control/pod/bias-intensity2.pdf

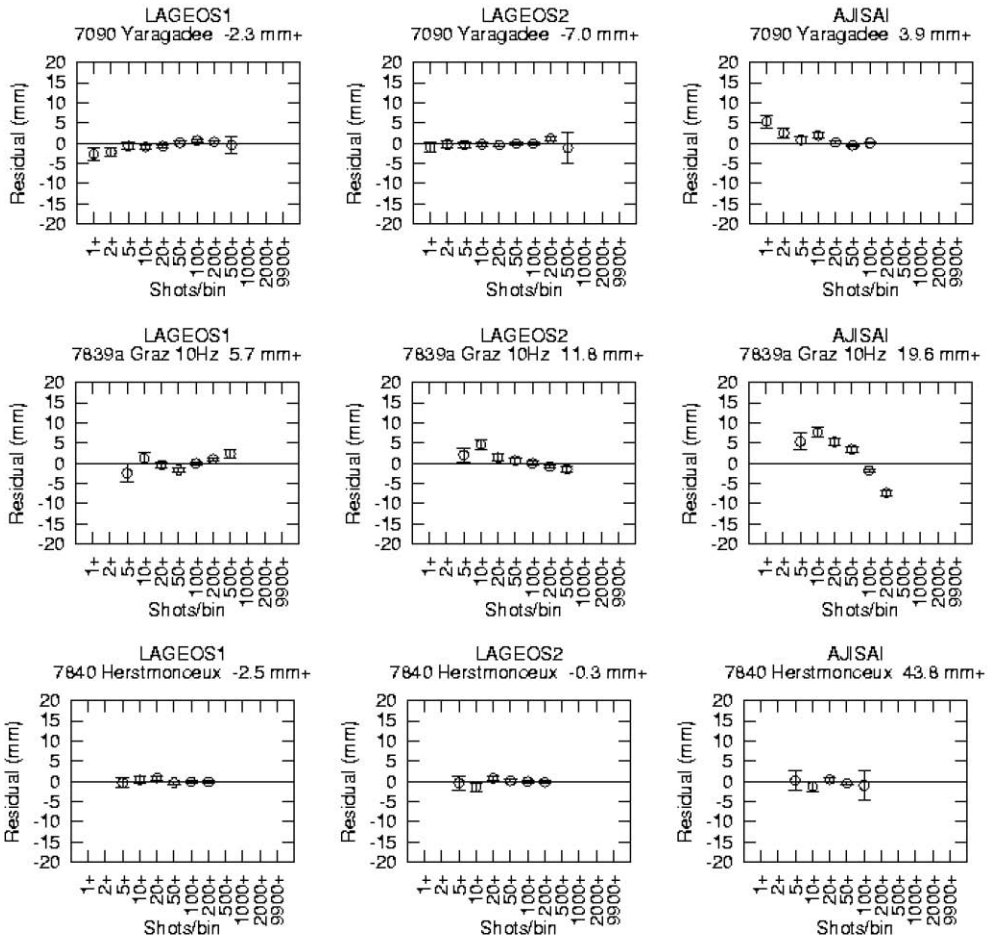

Figure 2. Range residuals sorted by number of returns per bin for an MCP-CFD system Yarragadee (top), a multi-photon C-SPAD system Graz (centre) and a single-photon system Herstmonceux (bottom).

This result indicates that the C-SPAD range has a significant intensity dependence of up to 5cm peak-to-peak for AJISAI and sub-cm for LAGEOS. Smaller trends are also seen in some MCP stations. On the other hand, the single photon systems (Herstmonceux and Zimmerwald) are the most robust with a nicely flat trend.

This analysis method used postfit residuals, but, during the parameter estimation process, such a systematic error will be partly absorbed, and therefore any intensity dependence will tend to be underestimated. It should be further noted that this analysis is special — the SLR data analysts do not apply this kind of approach on a regular basis, which means these biases have been routinely contaminating the geodetic products.

Intensity-dependent bias corrupting the geodetic results

Due to varying station-satellite distance and atmospheric attenuation, the intensity variation is related to the elevation angle. That is, a strong signal is expected from a high elevation and a weak signal from a low elevation. Such a systematic effect might be expected to corrupt the geometry in the observation equation.

To assess the extent of this effect, we artificially added a systematic bias to a set of actual SLR data. For a 50-day LAGEOS-1 and LAGEOS-2 data set (April to June 2003), we added ±5 mm systematic bias to the normal points of three most productive stations in the 50-day span (Yarragadee, Hartebeesthoek and Graz (10 Hz)) based on the following rule:

-Using the number of single shot returns per bin, categorise all normal point data as [a] dense points (highest 25%), [b] medium points (middle 50%) and [c] sparse points (lowest 25%).

(The [a]-[b] boundary was 223 shots/NP bin for Yarragadee, 322 for Hartebeesthoek, and 234 for Graz. The [b]-[c] boundary was 48, 109 and 65, respectively.)

-Add -5 mm range bias to the group [a] and +5 mm range bias to the group [c], which makes laser range shorter for strong returns and longer for weak returns.

We then solved for station coordinates and range bias before and after adding this artificial bias, and determined the effect by comparing the results:

	Height change	Range bias change
Yarragadee	+7.4 mm	+4.2 mm
Hartebeesthoek	+8.4 mm	+4.8 mm
Graz	+6.0 mm	+4.9 mm

The horizontal components did not change by more than 1 mm. This result shows that the applied intensity-dependent bias quite directly degrades the solutions for station height that are used to define the scale of a terrestrial reference frame. It also suggests that such bias is possibly routinely being absorbed in the parameter estimation solutions.

Conclusions

The intensity-dependent range bias induced by the satellite signature effect is actually seen in a number of stations. It amounts to 4 to 5 cm in AJISAI. For LAGEOS, it is theoretically expected to be about 20% of AJISAI (= 1 cm) although it is not quite seen at that level in our analysis. Through a test analysis where we added an artificial, but realistic, intensity-dependent range bias, derived station heights are found to be sensitive to such biases.

Stations should strive to keep such biases constant by avoiding variable intensity in their laser returns, which inevitably leads to a variable bias that is almost impossible to remove. Otherwise, SLR-advantageous geodetic products such as a terrestrial reference frame [Altamimi, 2002] are sure to be contaminated.

References

Altamimi, Z., P. Sillard, and C. Boucher, ITRF2000: A new release of the International Terrestrial Reference Frame for earth science applications, J. Geophys. Res., 107(B10), 2214, doi:10.1029/2001JB000561, 2002.

Appleby, G. M., Satellite signatures in SLR observations, Proc. 8th International Workshop on Laser Ranging Instrumentation, 2.1-2.14, Annapolis, 1992.

Neubert, R., An analytical model of satellite signature effects, Proc. 9th International Workshop on Laser Ranging Instrumentation, 8291, Canberra, 1994 (some minor corrections available at http://www.gfz-potsdam.de/pb1/SLR/tiger/signat.htm).

Otsubo, T., New approach to quality check: multiple satellite and intensity dependence, Proc. 12th International Workshop on Laser Ranging, Matera, 2000.

Otsubo, T. and G. M. Appleby, Recovery of Target Response Function for Centre-of-mass Corrections of Spherical Satellites, Proc. 13th International Workshop on Laser Ranging, Washington DC, 2002.

Otsubo, T. and T. Genba, A New Approach to Quality Check (2) -Range Bias vs Applied System Delay, Proc. 13th International Workshop on Laser Ranging, Washington DC, 2002. Otsubo, T., and G. M. Appleby, System-dependent center-of-mass correction for spherical geodetic satellites, J. Geophys. Res., 108(B4), 2201, doi:10.1029/2002JB002209, 2003.

RETURN ENERGY ESTIMATES DERIVED FROM NORMAL POINT AND FULL-RATE LASER DATA

Matthew Wilkinson Phillip Gibbs and Graham Appleby NERC Space Geodesy Facility, Herstmonceux Castle, Hailsham BN27 1RN, E.Sussex, UK
matwi@nerc.ac.uk, pgib@nerc.ac.uk, gapp@nerc.ac.uk

Abstract

To fully understand and model Centre-of-Mass corrections for individual stations one needs to have an understanding of the levels and degree of variation of return energy for each station. The potential range measurement inaccuracy due to such a variation is demonstrated by observations of a number of satellites at high and low levels of return rate. Using full rate data and knowledge of the laser repetition rates for each station we are able to estimate the return rates for different satellites for the major ILRS stations. These values are investigated for repeatability and elevation dependence and some inferences made on relative CoM corrections appropriate for each station.

Introduction

During the routine operation of satellite laser ranging, the strength of the return signal from the observed satellite may not be constant. A stronger return signal is observed for low Earth orbiting satellites, for higher elevations, or as a result of better atmospheric conditions. A weaker signal is observed for higher orbiting satellites, lower elevations or poor sky conditions. Stations may also experience characteristic levels of return energy due to their location and laser pulse energy.

Such variations in return energy may have implications on the range measurements made. For spherical satellites, such as the geodetic Lageos satellites, measurements made at high return rates are made close to the front of the satellite. Range measurements made a low return energy, however, are from across the satellite surface and the effective reflection point is consequently deeper into the satellite. These two different states of observation require two different Centre-of-Mass corrections to refer the range measurement to the centre of mass of the satellite.

In addition, an uncompensated single photon avalanche diode (SPAD) channel experiences a ‘time walk’ error in range measurement, which varies with return energy strength. This could produce cm order errors in the range measurement. A compensated SPAD reduces this time walk error to less than a few millimetres.

High and low return energy experiments

At Herstmonceux, the return energy is maintained at a low, single-photon level using a neutral density wheel. Software detects satellite track, estimates the return energy level and increases or decreases the neutral density filtering accordingly. By removing the neutral density filtering during a satellite observation, the system can be forced to operate at a high level of return energy.

To determine whether return signal strength effects can be seen in range measurements, the satellites Ajisai, Envisat and Lageos 1 were observed at both low and high levels of return energy. Each pass was predominantly observed at low return signal strength and also included periods of high return energy. All measurements taken over the full pass were used to generate an orbit solution from which Observation-Calculation residuals were plotted.

Figure 1 contains the residuals from an observed pass for each satellite using both the uncompensated and compensated C-SPAD channels. The black squares are minute binned residual points and the red stars are an estimation of the return energy. Each plot contains a region that was observed at high return energy.

Ajisai is a large spherical target and for both C-SPAD channels an offset can be seen for the high return energy measurements. There is a difference of about 8cm in the range measurements between the two states for the uncompensated channel. The compensated channel removes the effects from the laser pulse width and detector to leave only the satellite effects. The offset for this channel is about 6cm and is due entirely to the shape of the satellite.

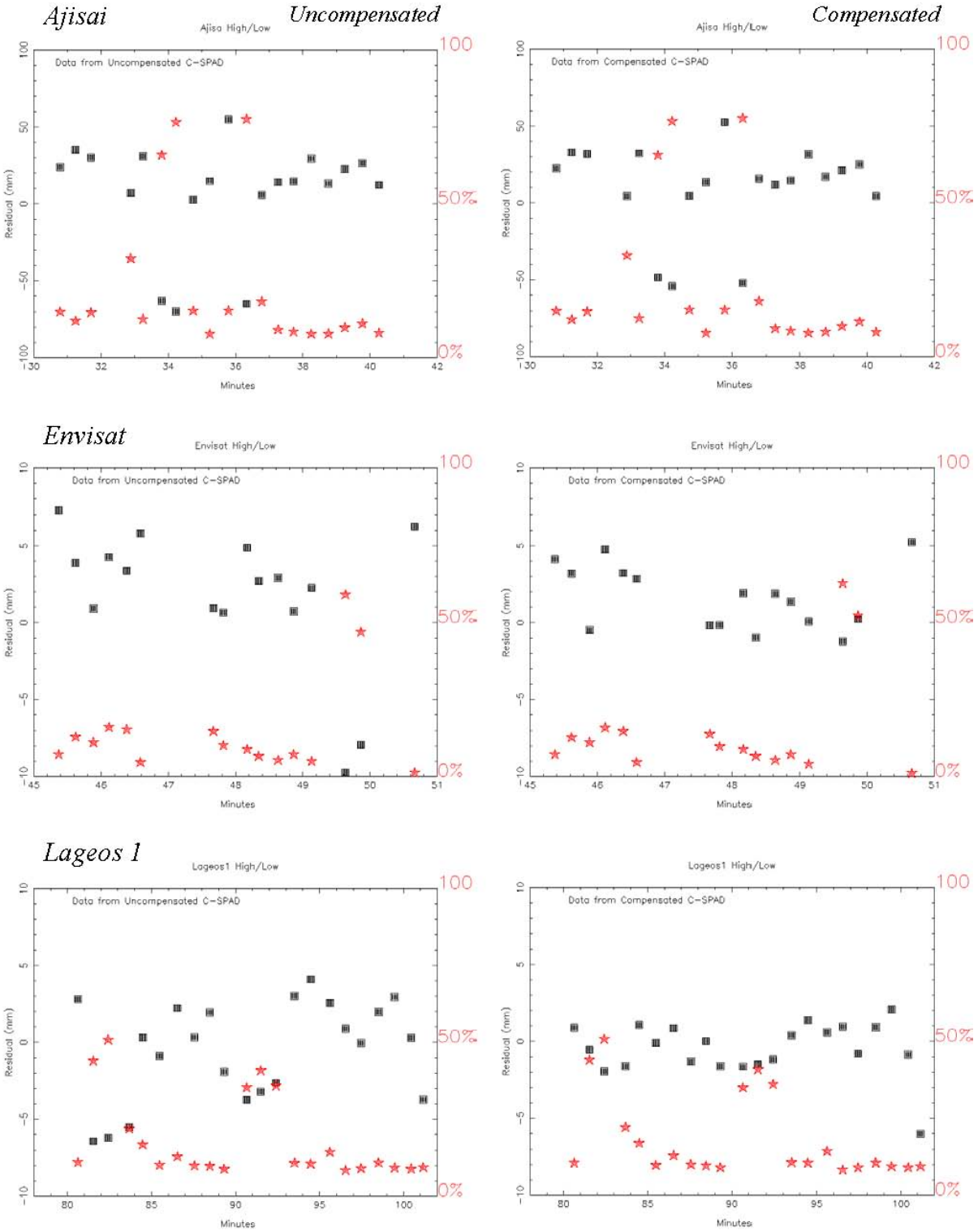

Figure 1. Residual plots for the satellites Ajisai, Etalon and Lageos 1 for both the uncompensated and compensate C-SPAD channels. The black squares on the plots are binned residuals points and the red stars are an estimation of the return energy.

Envisat is a small target and an offset in range measurement can only be seen for the uncompensated channel. The magnitude of the offset if on a much smaller scale than that of the Ajisai offset. The absence of an offset for the compensated channel suggests that there is no satellite effect due to the size of the target.

Lageos is spherical target, yet an offset in the range measurement can only be seen for the uncompensated channel. The return signal only reaches an estimation of about 40% and at this level of return energy the satellite is behaving as a small target. Table 1 summarises these results and includes attempts to quantify the offset from the plots in figure 1.

Table 1. Estimations of the offsets in range measurement at high return energy for three satellite passes.

Satellite	Uncompensated offset	Compensated offset
Ajisai	80+ mm	60+ mm
Envisat	10+ mm	~ 0 mm
Lageos	~ 5 mm	~ 0 mm

Variable return energy

The residuals in figure 1 show that there is potentially a difference in range measurements observed at high and low return energy. These plots were produced by forcing the system at Herstmonceux to stop observing at the single photon level and instead observe at high energy. The following investigation is concerned with whether there are variations in the return energy in the routine operation of ILRS systems.

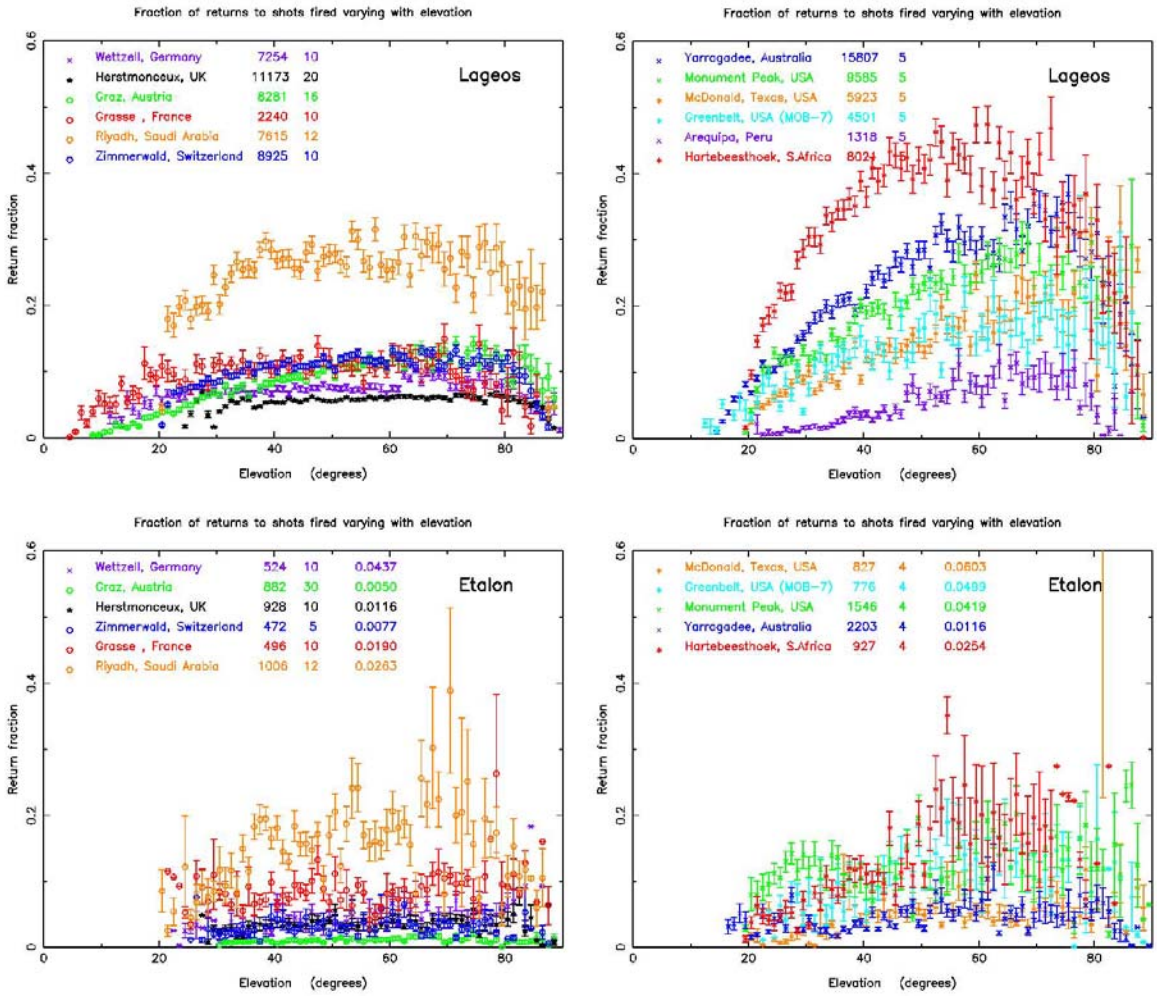

Figure 2. Return rate estimation from 2003 full rate data volume against elevation for combined Lageos and Etalon satellites for CSPAD and NASA MCP systems. Each plot contains standard error bars

It was assumed that an estimation of the return rate can be made from the ratio of the number of range measurements to the number of shots fired. The effective number of shots fired depends on the station firing rate, the use of the semi train and the use of an event or interval timer. The return rate estimation was made using the complete 2003 full rate data volume.

Figure 2 contains plots of estimated return rate against elevation. The top left plot contains the combined Lageos 1 and 2 data from stations using C-SPAD systems. Each colour represents an ILRS station and the plot shows most stations operating at a consistent low return rate with increasing elevation. Riyadh in Saudi Arabia operates at a higher rate of return. All stations observe at a lower return rate at low and high elevations, where the satellite may be lost due to the atmosphere or zenith tracking respectively.

The top right plot is the combined Lageos observations for the NASA MCP stations. Each station can be seen to operate at a characteristic level of return rate at any particular elevation. Also, each station produces a characteristic return rate variation with elevation. The degree of this variation is different between stations, all have reduced return rate at low and high elevations.

The bottom left plot in figure 2 contains combined Etalon 1 and 2 return rate data. Each station operates at a low level of return rate and is more consistent with increasing elevation. This is due to the greater height of the Etalon satellites and the consequent difficultly to observe at a high level of return rate. The bottom right plot in figure 2 is the combined Etalon NASA MCP data and shows a reduced return signal and, consequently, a reduced variation of return signal with elevation.

Receive Amplitude

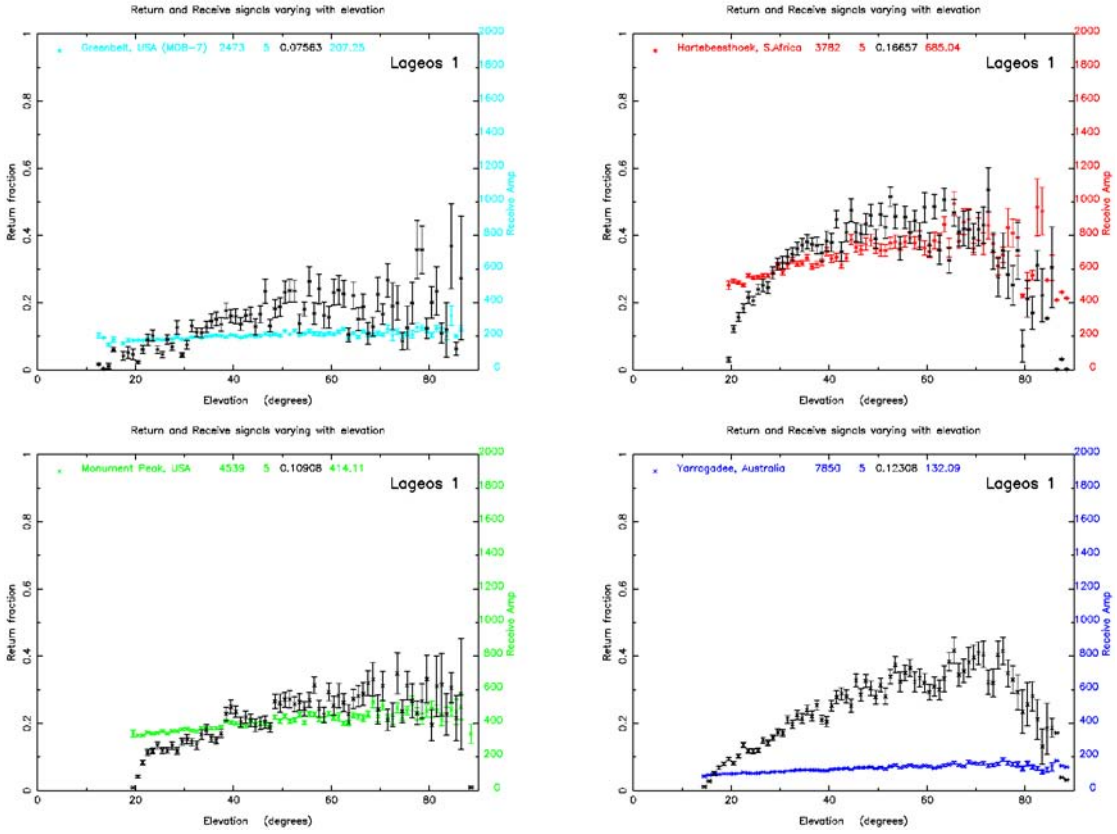

Figure 3a). A comparison between the receive amplitude entry in the full rate data volume and an estimation of the return rate for the Lageos 1 satellite.

The full rate data contains an entry named ‘receive amplitude’ and is used by some NASA systems in their operation. It is a linear scale from 0 to 2000 relating to the return energy and could be used as a substitute in analyses. However, the information is supplied by only a few stations and we believe it is incorrectly scaled for Yarragadee, Australia. Figure 3 contains plots of the two values on a scaled y axis for Lageos 1 and Etalon 1. Al plots exhibit reasonable agreement, except for Yarragadee for Lageos 1.

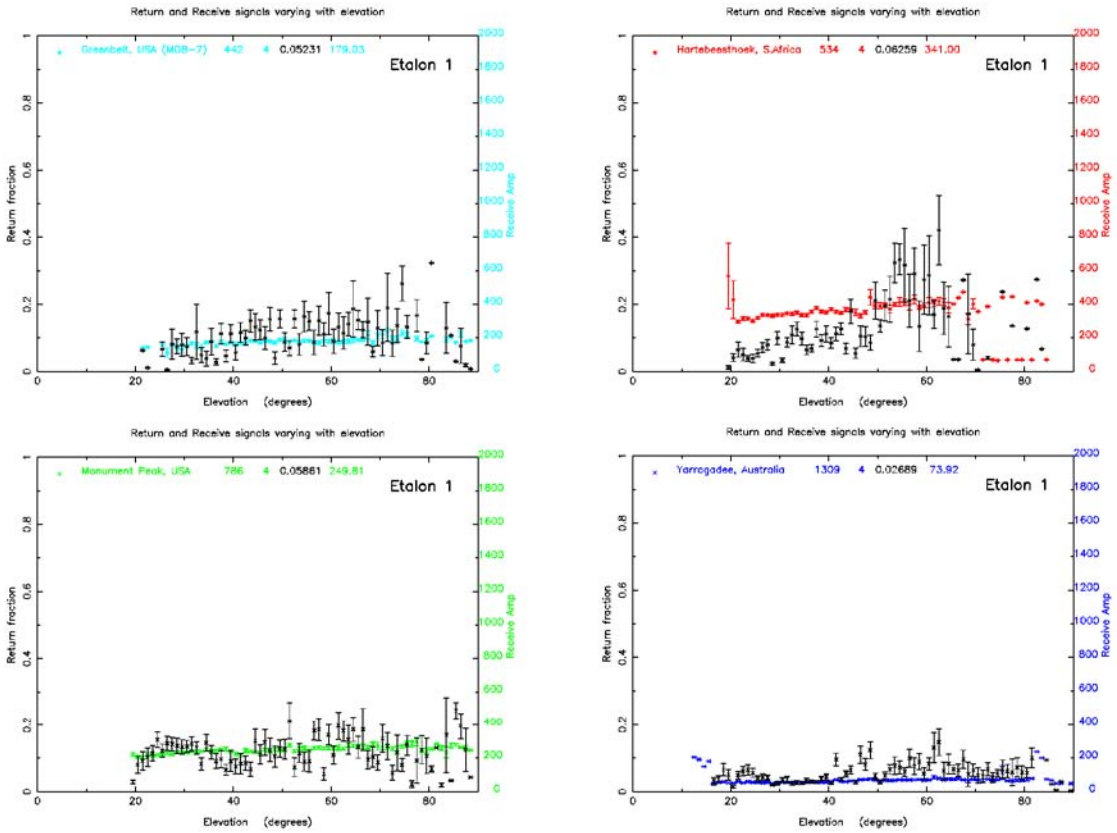

Figure 3b). A comparison between the receive amplitude entry in the full rate data volume and an estimation of the return rate for the Etalon 1 satellite.

Conclusions

The strength of the return signal from a satellite can affect the accuracy of the resulting range measurement. A range difference is present in O-C residuals when a satellite is observed at both high and low levels of return. This difference depends upon the shape and size of the satellite and can be quantified for large targets using the residual plots.

All stations experience a variation in return signal strength when observing between different satellites and at different elevations. These variations are individual to the station. Maintaining a consistent return rate during all observations will provide more consistent measurements.

CENTRE-OF-MASS CORRECTION ISSUES: DETERMINING INTENSITY DEPENDENCY AT A MULTI-PHOTON (MOBLAS-5) STATION.

R. Carman and V. Noyes (1) and T. Otsubo (2)
(1)Moblas-5 SLR Station – Yarragadee moblas@midwest.com.au / Fax: +61-899-29-1060
(2)National Institute of Information and Communications Technology, Japan Otsubo@nict.go.jp /Fax: +81-299-84-7160

Introduction

As reported by T. Otsubo and G. Appleby at the workshop in Koetzting, in the drive towards mm ranging accuracy, the effects of signal intensity on centre-of-mass correction values needs to be evaluated. While some work has been done on data sets from single photon (Herstmonceux) and other C-SPAD stations, evaluation of the effect on multi-photon MCP systems still needed to be undertaken.

Background

To determine the effect that varying return energy has on residuals, passes need to be taken using a special tracking regime. It involves varying the return energy via ND wheel, so that the level alternates between high and low throughout the pass. This was not as simple as we had assumed and took some practice to perfect.

So far three test passes have been taken, Ajisai, Lageos-2 and Envisat. Getting a significant dynamic separation on the strong/weak returns for Ajisai and Envisat was relatively simple due to the normally strong receive energies associated with these satellites. However we had to wait for good conditions (post summer dust), to get a good separation on Lageos-2.

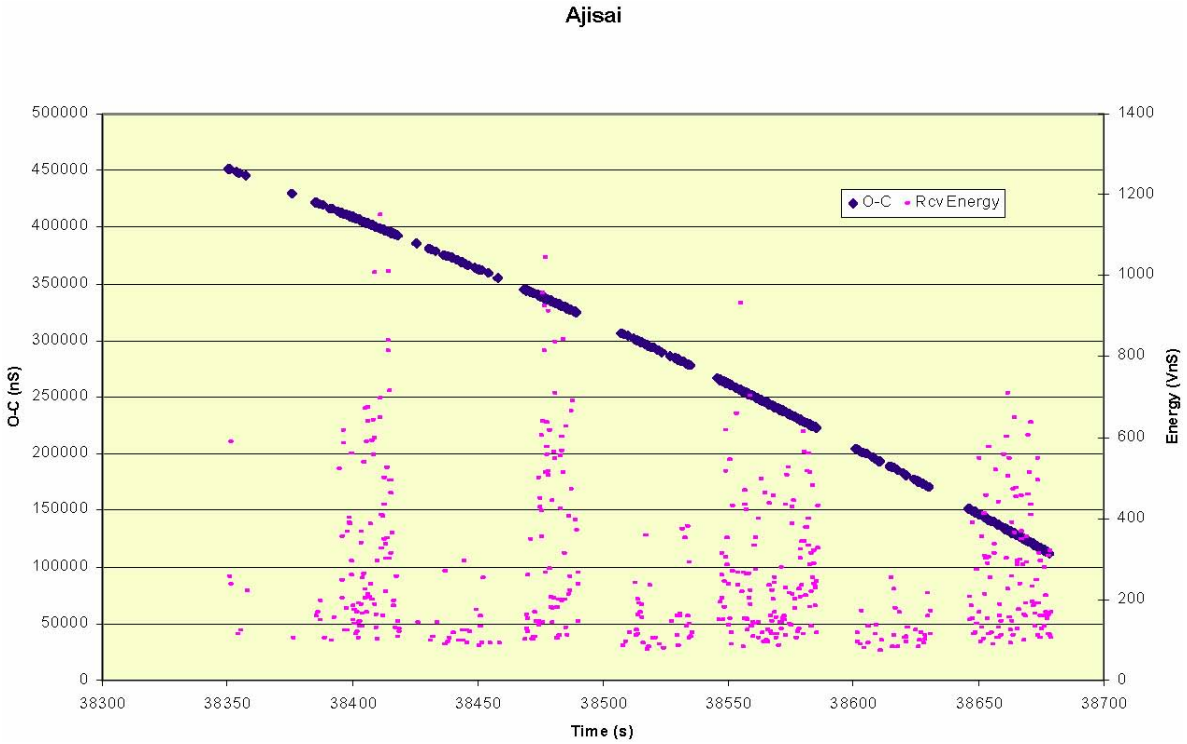

Figure 1. O-C and Received Energy plots for Ajisai

Initial Results

The passes were processed in three ways. Firstly the passes were processed normally and the Quick Look (ql) data submitted. Secondly the raw data was delogged to give O-C vs time for all returns. Thirdly, each pass had its strong and weak segments separated and each part was

processed separately. Initial analysis of the passes shows good separation between strong and weak returns. See Figures 1 to 3 for this separation with Blue diamonds for O-C and Pink Rectangles for received energy.

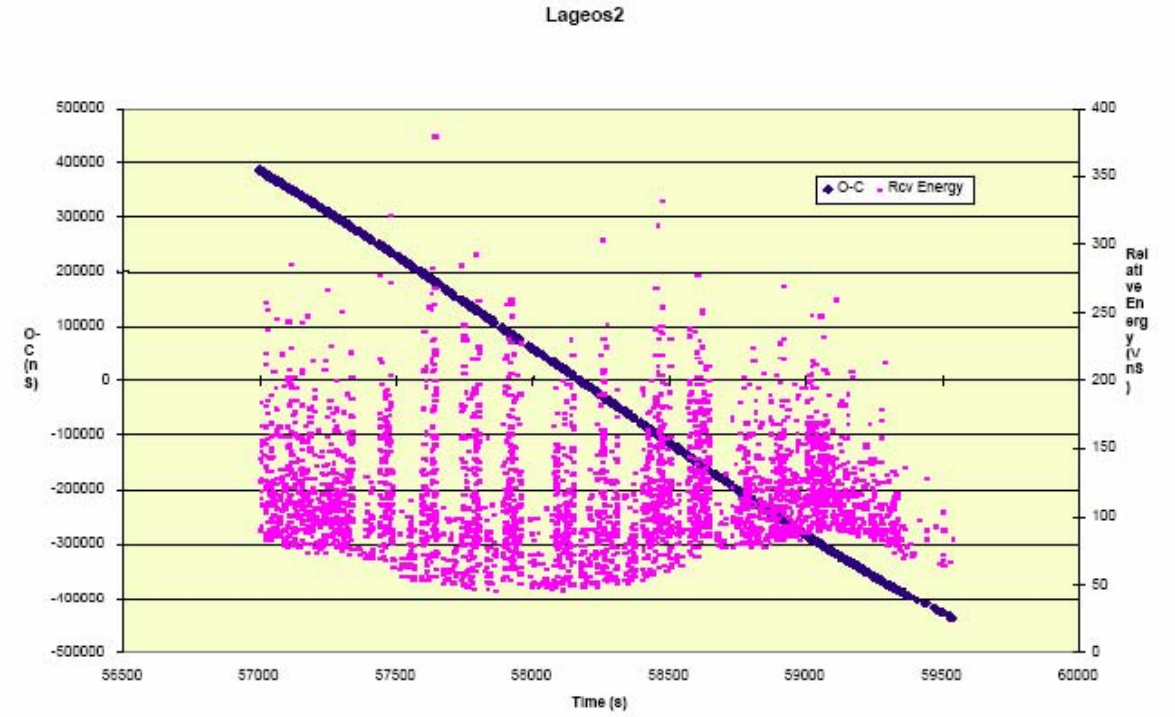

Figure 2. O-C and Received Energy plots for Lageos-2

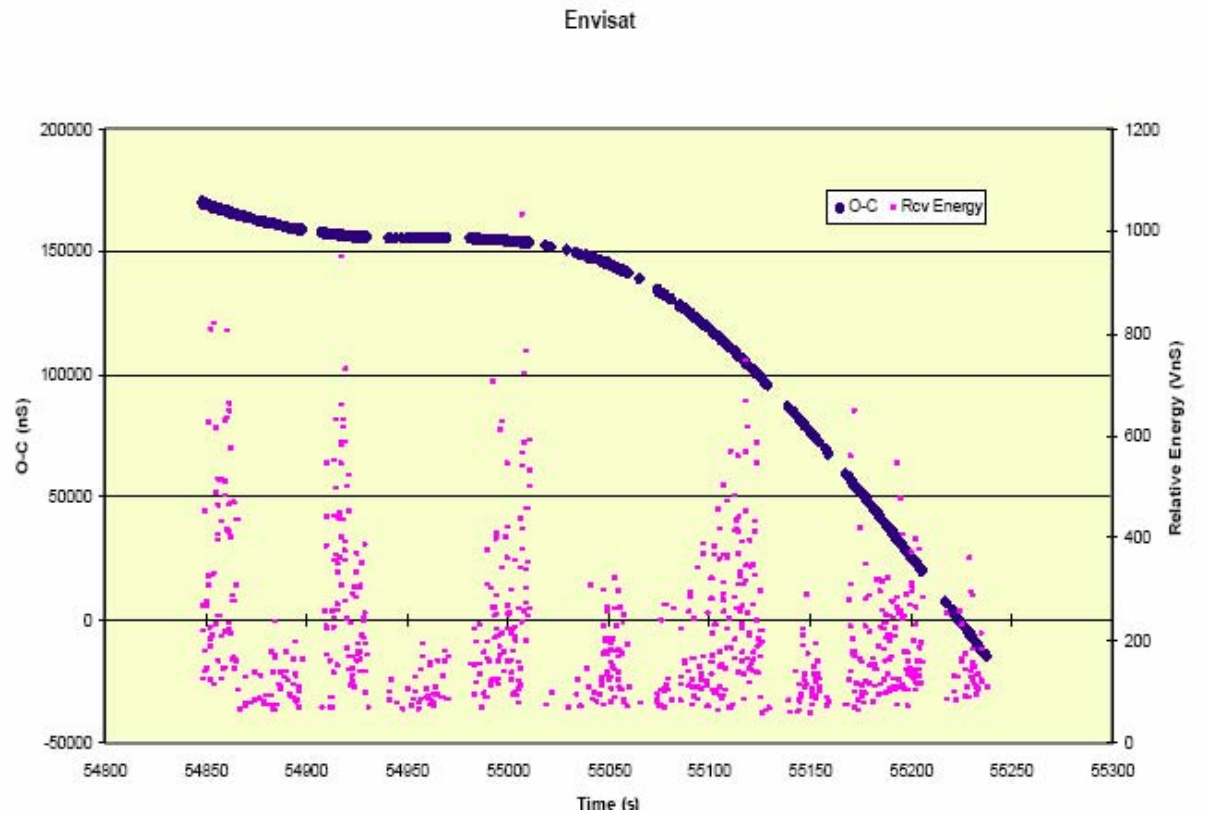

Figure 3. O-C and Received Energy plots for Envisat

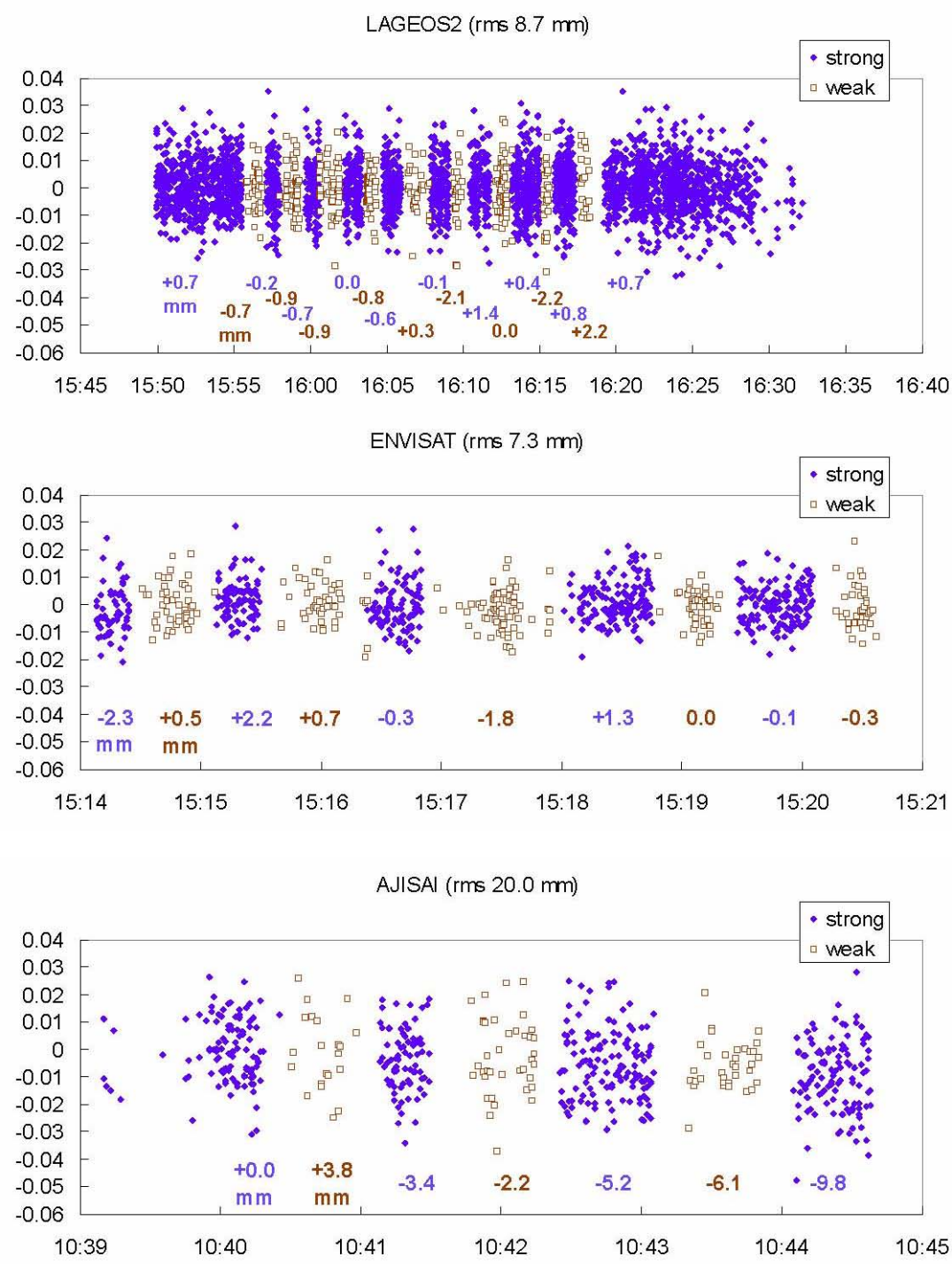

Figure 4. Flattened shot-by-shot returns.

Data Flattening Procedure and Results

Now we need to see whether there is a range offset between the strong returns and the weak returns. To do so, we flattened the full-rate data of the three passes (LAGEOS-2, ENVISAT and AJISAI). Using NICT analysis software 'concerto', orbital parameters (six elements, along-track constant acceleration and along-track once-per-revolution acceleration) were fitted to the full-rate pass and several normal-point passes before and after the pass. The shot-by-shot post-fit residuals are plotted in Figure 4 above. The scatter rms of the full-rate points was 8.7 mm for LAGEOS, 7.3 mm for ENVISAT, and 20.0 mm for AJISAI.

According to the target signature studies [*Otsubo and Appleby*, 2003] for multi-photon

CSPAD systems, a strong return makes the laser range shorter than a weak return, and the difference is dependent on the target's depth—AJISAI the largest with up to 5 cm and LAGEOS-2 the second with 1 cm.

In Figure 4 above, strong returns are plotted as solid blue points and weak returns are plotted as hollow red points. There seems to be a small difference for AJISAI but no clear intensity dependence for LAGEOS-2 and ENVISAT. The average 'strong minus weak' differences are:

LAGEOS-2	-0.6 mm
ENVISAT	-0.3 mm
AJISAI	+3.1 mm

Comments

Although this is still a preliminary result, we find the MCP+CFD system at Yarragadee more robust over the intensity variation than multi-photon C-SPAD systems. More strong/weak signal returns from dedicated satellites need to be taken before any conclusions could be drawn.

References:

Otsubo, T., and G. M. Appleby, *System-dependent center-of-mass correction for spherical geodetic satellites*, J. Geophys. Res., 108(B4), 2201, doi:10.1029/2002JB002209, 2003.

IDENTIFYING SINGLE RETRO TRACKS WITH A 2KHZ SLR SYSTEM-SIMULATIONS AND ACTUAL RESULTS

David Arnold (1), Georg Kirchner (2), Franz Koidl (3)
(1) 94 Pierce Rd, Watertown, MA, 6179246812.
(2) Austrian Academy of Sciences, Institute for Space Research
kirchner@flubpc04.tugraz.ac.at / Fax: +433168734641.
(3) Austrian Academy of Sciences, Institute for Space Research.

Introduction.

This is a abbreviated version of the original paper. For the complete paper see the SPWG website 'http://nercslr.nmt.ac.uk/sig/signature.html'.

The new 2kHz SLR system at Graz can generate single photoelectron histograms in a short period of time. Plots of the range residuals vs time show how the return pulse shape varies during a pass. Many satellites, including Lageos, appear to show single retro tracks. Computer simulations have been used to calculate return pulse shapes as the viewing angle on the array changes. Plots of the simulated data look very similar to plots of the actual data. The simulations indicate that the tracks can be single retros for small arrays, or groups of closely spaced retros for large arrays.

Data collection and processing.

The 2kHz SLR system at Graz uses a CSPAD detector. The system can operate in either a multiphotoelectron mode or a single photoelectron mode. If the system is operating in a multi-photoelectron mode, the range measured is basically the leading edge of the pulse.

For high satellites like LAGEOS, the system operates in a single photoelectron mode because of the low signal strength. The return pulse shape is the probability function for obtaining a photoelectron. The return pulse shape can be plotted by making a histogram of the range residuals using a large number of returns. The Graz system takes data so rapidly that it is possible to plot single photoelectron histograms in a very short period of time. Plotting the range residuals vs time shows a plot of the pulse shape vs time.

For low satellites with strong signal strength one would not expect a plot of the data to show the pulse shape since the system is measuring only the leading edge. In fact, there are large variations in signal strength for low satellites so that there is a significant fraction of single photoelectron data even for low satellites. The result is that the data often shows the pulse shape even though the average signal strength is fairly strong.

Computer simulations.

The return pulse shape from an array can be computed using program RETURN which is described in Appendix A and Appendix C of Reference 1. This program has been used to compute return pulse shapes for various satellites as the viewing angle on the array changes. Successive pulse shapes are plotted using a gray scale plotter. This give a visual representation that is very similar to the plots of the range residuals vs time.

LAGEOS1

a.-Plot of the actual data

Figure 1 shows a plot of data from a LAGEOS1 pass. There are tracks clearly visible in the data. Since LAGEOS1 is spinning very slowly, it is not possible to use the photometry of the solar reflections from the front face of the cube corners to determine the orientation of the satellite. Since the orientation is unknown it is not possible to do a computer simulation for the actual conditions of the data.

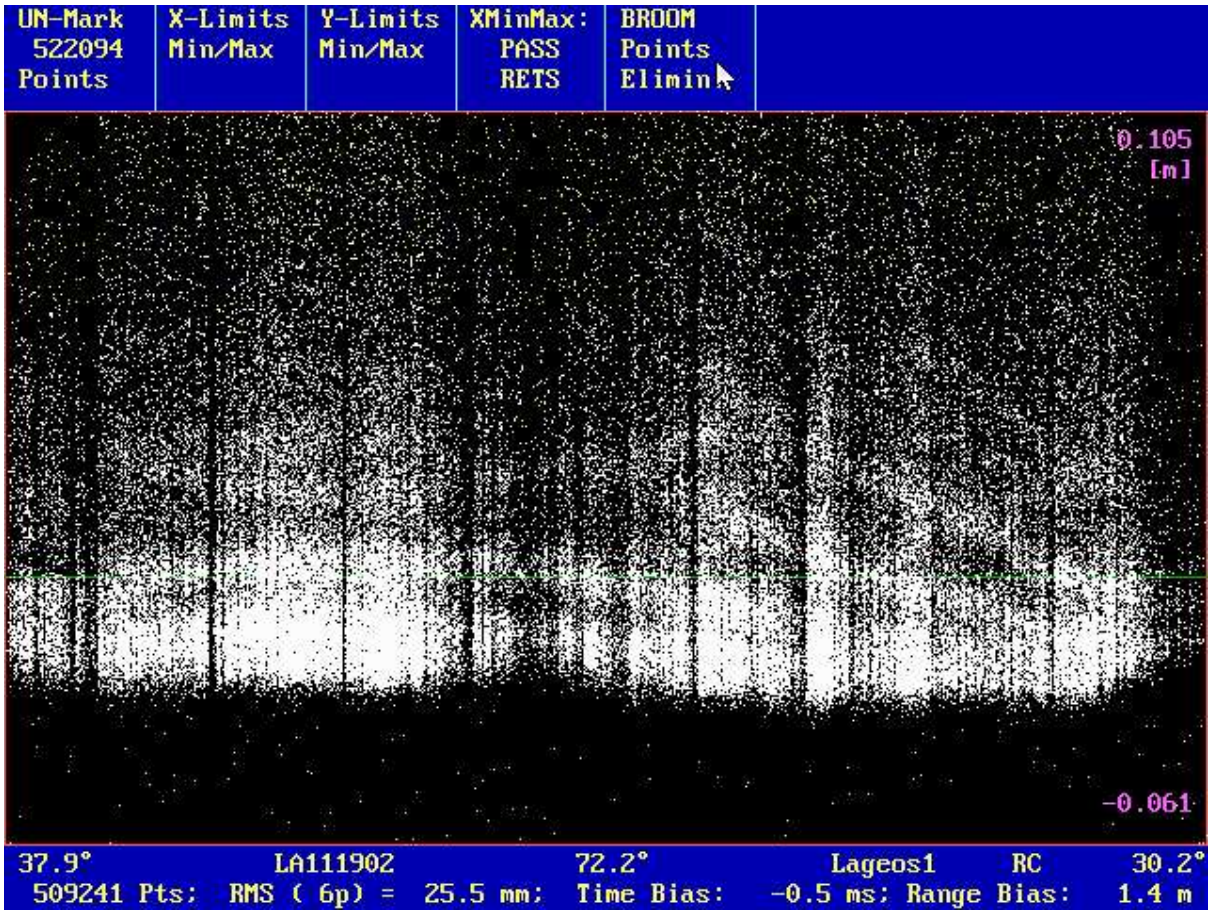

Figure 1. Plot of data from a night time pass of LAGEOS1 with about 500 k returns.

b.-Simulated LAGEOS data.

Figure 2a. 90 deg angle with the spin axis (equatorial)

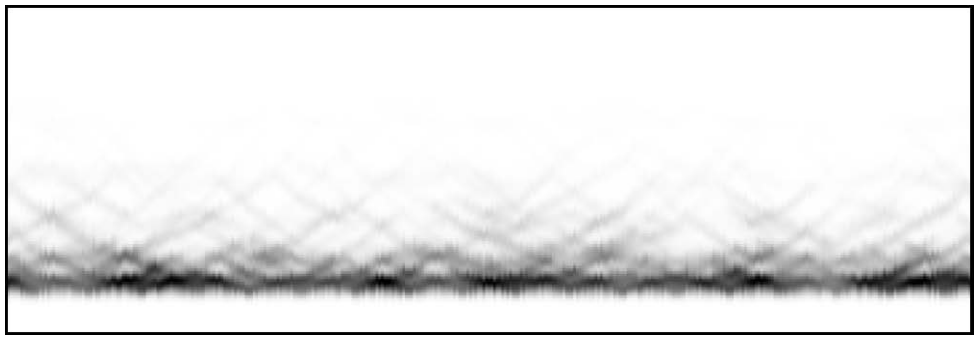

Figure 2b. 30 deg angle with the spin axis.

Figure 2c. 0 deg angle with the spin axis (polar). (See SPWG website)

Figure 2 shows inverted gray scale plots of the simulated data for three different angles with respect to the spin axis. The horizontal axis of the plot is one complete revolution (360 deg). The vertical axis is .28 to .55 meters (twoway).

There are 32 cube corners in each of the equatorial rows and this is reflected in the structure of Figure 2a. At 30 degrees incidence angle there is no well defined periodicity because the signal is the sum of rows having different numbers of cube corners.

The transmitted pulse width is 10 ps for the Graz laser. However, the rms noise in actual laser ranging is about 20 ps, probably due to atmospheric effects. This is roughly equivalent to having a 40 ps transmitted pulse in terms of pulse spreading. In Figure 2, the input pulse is 40ps FWHM to simulate the rms system noise of about 20ps.

The simulation in Figure 2b looks similar to the plot of the actual data in Figure 1. There is no way to do a plot for the actual conditions since the orientation of the satellite is unknown.

c.-Simulated pulse shape.

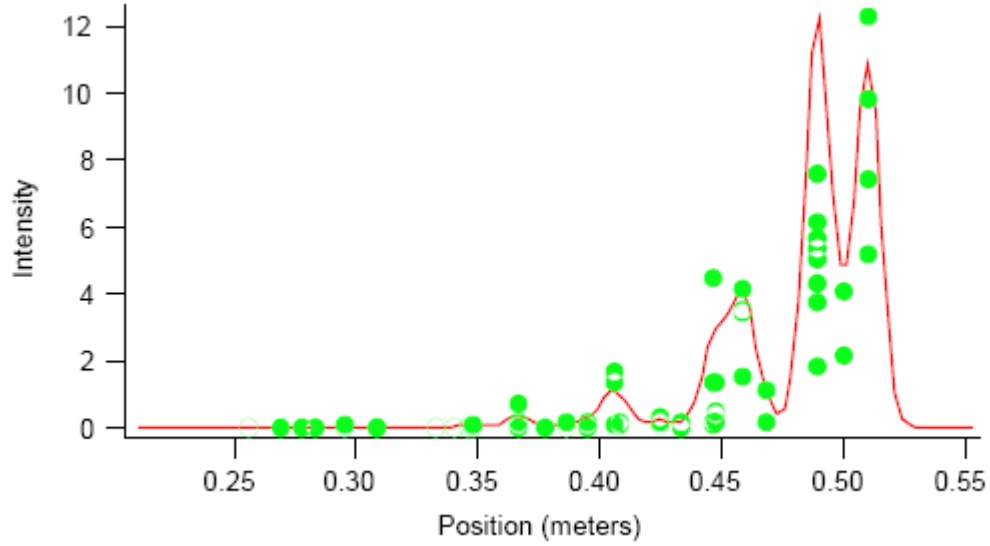

Figure 3. Plot of pulse shape at a single orientation with a 40 ps transmitted pulse. The red curve is the incoherent pulse shape and the green dots are the reflectivity of individual cubes at their position in the pulse. The positions of the individual retros and the plot scale of the pulse are multiplied by a factor of two because of the two way travel time. The range correction would be half the mean position of the pulse.

The pulse shape in Figure 3 gives the appearance of showing individual retroreflectors. However, the green dots showing the positions of the active retroreflectors shows that the peaks are actually the result of looking at groups of retroreflectors. There are 4 peaks in Figure 3. This is roughly consistent with the number of peaks evident in Figure 1 showing the actual ranging data.

TOPEX.

a.-Actual TOPEX data

There are a number of tracks evident in Figure 4. Since TOPEX gives a very strong signal it is somewhat surprising that the tracks from retros far from the leading edge are clearly visible in the plot. The explanation is that there is always a certain percentage of single photoelectron returns which can be from anywhere in the pulse.

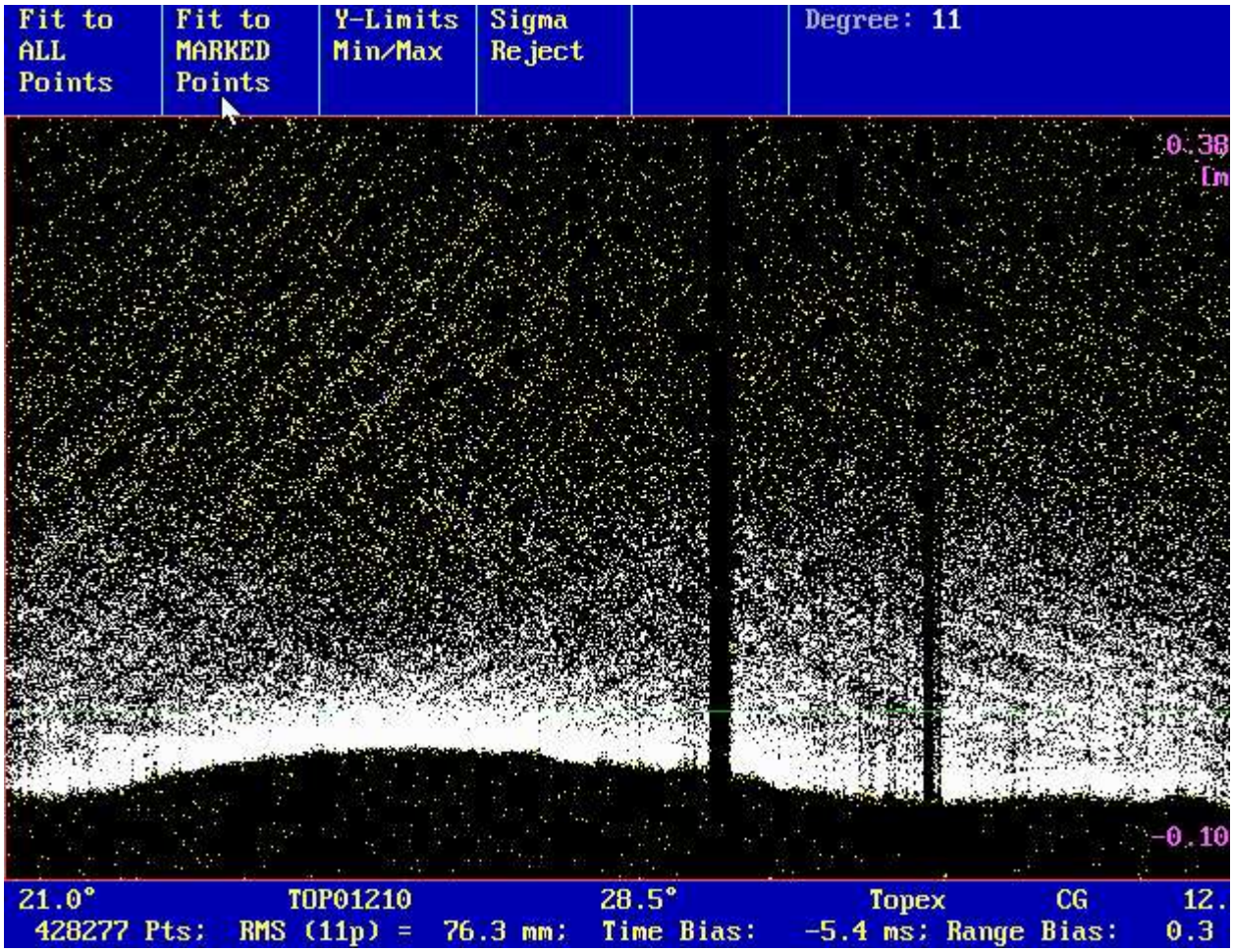

Figure 4. Plot showing about 400 k returns from TOPEX.

b.-Simulated TOPEX data.

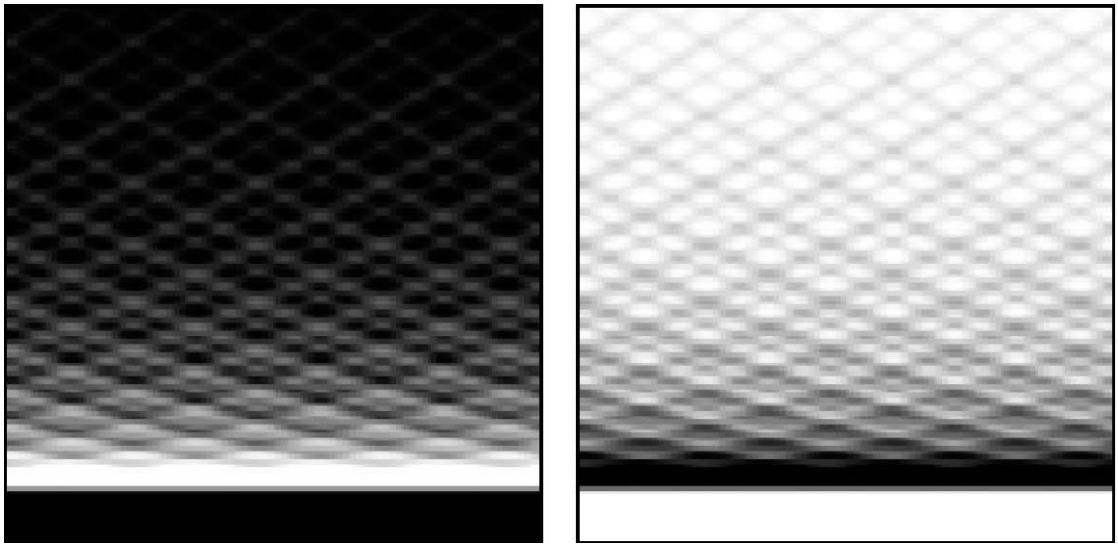

Figure 5. Simulated data for a 24 degree rotation of the satellite about the symmetry axis. The angle from the symmetry axis is 40 deg. The vertical axis is .55 to 1.188 meters (twoway) and the horizontal axis is 0 to 24 degrees rotation about the symmetry axis.

The simulation shows the structure in much more detail than the actual data. If the TOPEX data were all single photoelectron it should show the structure in more detail.

c.-Simulated TOPEX pulse shape.

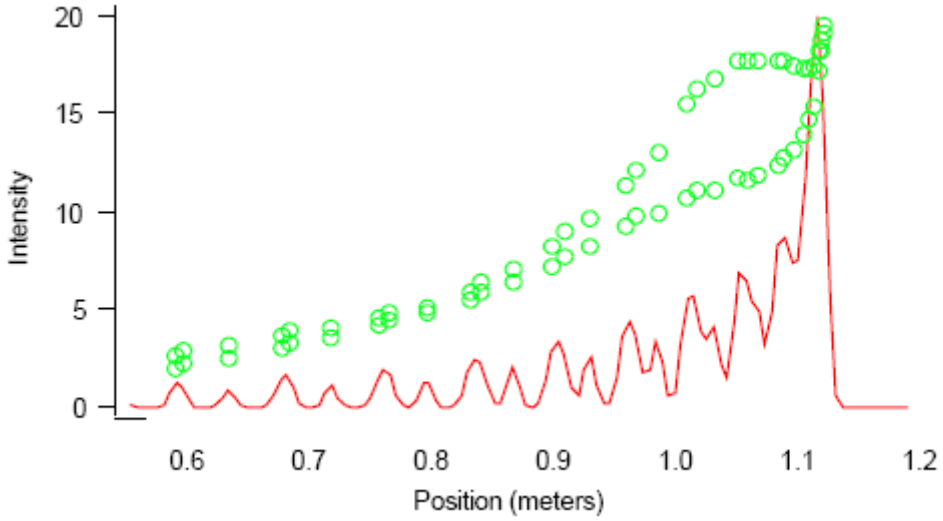

Figure 6. Pulse shape and distribution of retoreflectors for TOPEX. The incidence angle on the array is 40 degrees. The horizontal axis is twoway meters. The pulse has been truncated below .55 meters to preserve resolution in the plot. The pulse actually starts below 0. meters. The input pulse is 40ps HMFW to simulate the 20ps rms noise in the receiver.

There is more than one retroreflector contributing to each peak. The part of the pulse between .6 and .9 meters shows that the peaks correspond alternately to 2 and 4 retroreflectors.

ERS, ENVISAT

a.-Simulated data

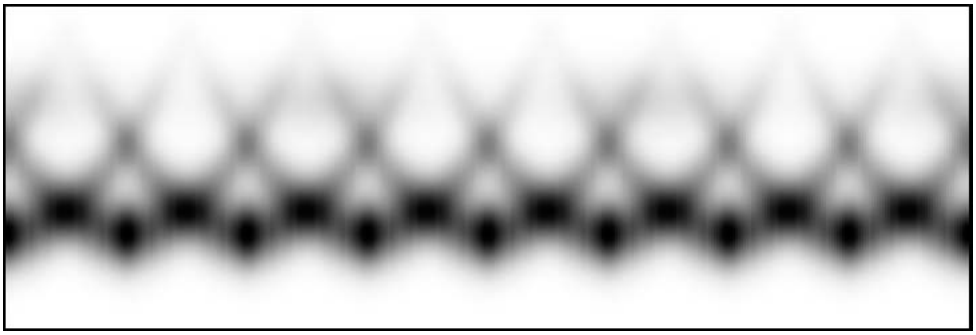

Figure 7. Simulation of pulse shape from ERS and ENVISAT which are identical arrays. The horizontal axis is from 0 to 360 deg (one revolution). The vertical axis is from .046 to .119 meters. Polarization is irrelevant since the cube corners are coated. The velocity aberration is (0,35) microradians. The input pulse width is 40ps FWHM to simulate the 20ps rms noise. The ERS type arrays have a pole cube and 8 cubes tilted at a 50 degree angle with respect to the symmetry axis. The incidence angle on the array is 40 degrees. The figure shows 8 similar segments as the array rotates through one complete revolution. The first 1/8 of the simulated data looks similar to the actual data in Figure 8.

b.-Actual ranging data.

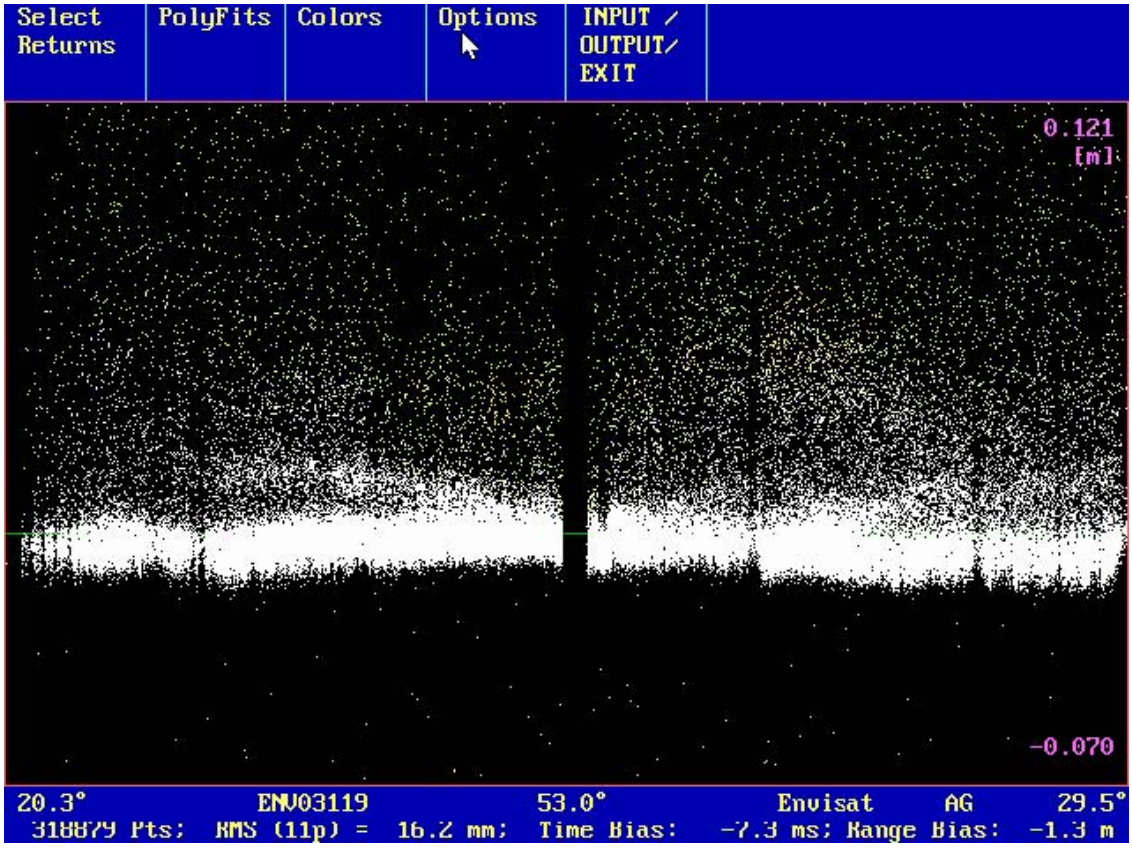

Figure 8. Plot of about 300 k data points from ENVISAT. The data shows evidence of a second track in parts of the plot.

c.-Simulated return pulse shape.

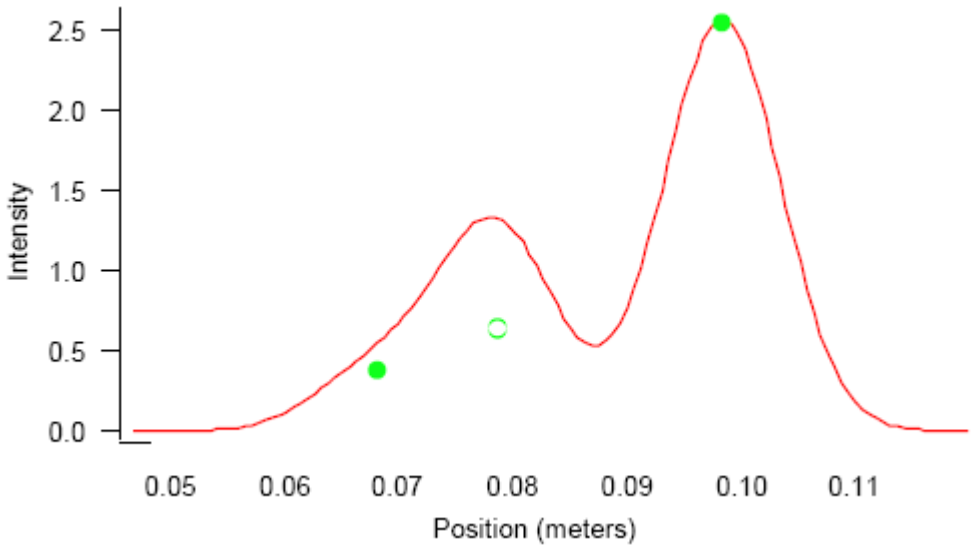

Figure 9. Pulse shape (red curve) and position of cube corners (green dots). The middle dot is actually two cube corners at the same distance. The first retro in the table is the closest one in the ring of 8. The next two are the adjacent cubes in the ring. The last retro is the pole cube.

JASON 1 (see SPWG website)

LAGEOS2

Plots of tracking data from LAGEOS2 do not show the kind of tracks shown in Figure 1 for LAGEOS1. This is an unexpected result since the arrays are identical except for the placement of the infrared cube corners. The explanation has to do with the rotation rate. The rotation rate of both LAGEOS satellites decreases with time. The rate for LAGEOS1 is very low since it has been in orbit since 1976. On the other hand, the rotation period of LAGEOS-2 is a few minutes.

For LAGEOS1 the incidence angle on the satellite will change as a result of the orbital motion even if the satellite is not rotating. However, it is possible to accumulate a lot of data before the incidence angle changes significantly. For this reason the plots of the data show the variations in the pulse shape. For LAGEOS2 the incidence angle changes too rapidly to allow the accumulation of enough data to form a good single photoelectron histogram at each orientation.

Figure 11. (see SPWG website)

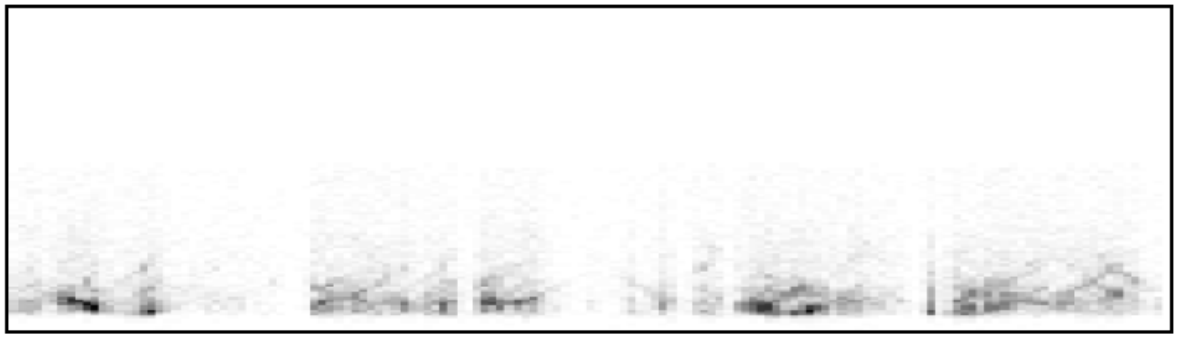

Figure 12. Plot of measured LAGEOS2 data from 60730 to 60873 sec (143 sec interval).

Figure 13. (See SPWG website)

Being able to see tracks in LAGEOS2 data is basically a question of signal to noise. In order to improve the signal to noise ratio, some LAGEOS2 data has been averaged by creating bins that are one second long and 20 picoseconds in range. The results are displayed as gray scale plots in Figures 11, 12, and 13. There are gaps in the data and the structure is still not as clear as one would like. However, there are places in each of the plots that appear to show the same kind of structure seen in the simulated data of Figure 2b.

A new method of applying range corrections.

The fact that the Graz data is capable of taking enough data to create a histogram of the pulse shape in a reasonably short period of time suggests an alternative way of correcting the range for the geometry of the retroreflector array. If the orientation of the array is know, it is possible to compute the positions of the individual retroreflectors along the line of sight and calculate the return pulse shape using the intensity of the reflection from each cube corner. This can then be compared to the measured pulse shape to determine the range correction to the center of mass. This is discussed in detail in the appendix.

Reference

"Retroreflector Array Transfer Functions" by David A. Arnold, 94 Pierce Road, MA 02472-3035 617-924-6812, Proceedings of the 13th International Workshop on Laser Ranging, October, 2002, Washington, DC. Also available on the website of the Signal Processing Working Group of the ILRS at http://nercslr.nmt.ac.uk/sig/signature.html

Appendix (See SPWG website)

THE NEW MOUNT STROMLO SLR SYSTEM

B. Greene, C. Smith, Y. Gao, J. Cotter, C. Moore, R. Brunswick, C. Burman
EOS Space Systems Pty Limited
bengreene@compuserve.com, Ph +61 2 6298 8010, Fx +61 2 6299 6575

Abstract

The Mount Stromlo SLR system was totally destroyed by fire on 19 January 2003. Construction of a new facility commenced on 4 July 2003. This system is now operational and undergoing final data testing before being re-integrated to the ILRS network.
The system includes new technology in the laser, telescope, and receiver systems that allow it to initially imitate the performance of the old system, and then progressively move forward to higher performance limits.

OVERVIEW OF GUTS SLR STATION

Mikio SAWABE, Takashi UCHIMURA, Akinobu SUZUKI (1), Shigeru MURATA(2), Yoichi MATSUOKA(3), Thomas Oldham(4), Jeff Maloney(5)
(1) Japan Aerospace Exploration Agency.
(2) NEC Corporation.
(3) NEC TOSHIBA Space Corporation
(4) Honeywell Technology Solutions, Inc.
(5) Brashear LP
sawabe.mikio@jaxa.jp /Fax:+81-29-868-2990

Abstract

Japan Aerospace Exploration Agency's (JAXA) Satellite Laser Ranging system (GUTS-SLR) has been completed in the spring of 2004. Its SLR station is located in Tanegashima Island,southern part of Kyushu.GUTS-SLR has capability of ranging to various satellites from low earth orbit to geostationary orbit. The 1-meter Cassegrain telescope, with its associated 5 meters diameter Dome assembly will be used to precisely point the outgoing Laser beam and to acquisition the reflected signals from various targets with Az: 25 degrees/sec and El: 10 degrees/sec maximum slew rate. The Laser subsystem generates both 50mJ/pulse (for LEO) and 300mJ/pulse (for GEO) with wavelength of 532nm. The pulse width of Laser is designed to be 60 psec (for LEO) and 300 psec (for GEO) respectively in order to avoid the damage on the optical components. The ranging subsystem provides the optical interfacing hardware, range measurement electronics, standard frequency sources and system control signals needed for the SLR application. The GUTS-SLR system will be able to range to LAGEOS satellites with a single-shot RMS of less than 10 mm RMS, less than 30 mm RMS for ETS-VIII (JAXA geostationary satellite). The GUTS-SLR is operated by remote control from the Tsukuba Space Center (TKSC). An approximate distance between TKSC and SLR station is 1100km. 512-kbps communication lineis used for transmission of system status, operational parameters and observation data, 256kbps for the transmission of surveillance monitor image (ITV camera). The operation of GUTS-SLR station will be kept almost autonomous manner according to the automatic sequence. Operator only intervenes in the initial power supply on/off, manipulate for the initial acquisition when the orbit prediction has an error and regular maintenance of system. An operational plan of the whole GUTS system is unitary planned by master control and operation planning subsystem, which is called COPs, and COPs also monitors operational conditions of each subsystem.

Exterior of GUTS-SLR facility Exterior of 1m Telescope

EARLY SATELLITE TRACKING RESULTS FROM SLR2000

J. McGarry (1), T. Zagwodzki (1), J. Degnan (2), P. Dunn (3), J. Cheek (3), D. Patterson (4), H. Donovan (4), A. Mann (4), A. Mallama (3), R. Ricklefs (5).
(1) NASA Goddard Space Flight Center.
(2) Sigma Space Corporation.
(3) Raytheon Information Technology and Scientific Services.
(4) Honeywell Technology Solutions Incorporated,
(5) University of Texas at Austin.
Jan.McGarry@nasa.gov

Abstract

NASA's SLR2000 was conceived as a totally autonomous, eye-safe, photon-counting, twokilohertz satellite laser ranging (SLR) system. Prototype development of SLR2000 has been underway for the past several years at the Goddard Space Flight Center. These efforts recently culminated in successful satellite tracking. The authors now have an integrated semi-automated prototype system that can range to satellites and can perform many of its functions without operator intervention. Results from recent satellite and ground ranging experiments will be presented along with the current system status and plans for further development.

Introduction

SLR2000 was conceived in the mid-1990s to be NASA's next generation Satellite Laser Ranging System, capable of operating completely autonomously and continuously for months without any manned intervention [Degnan 1994]. The system was envisioned to be completely free of optical, electrical and chemical hazards and would use the internet for two-way communications with a central facility. The system performance was expected to be similar to current NASA MOBLAS capabilities: ~1 cm RMS single shot (or better) with 1 mm precision Normal Points for LAGEOS.

Today the prototype SLR2000 system (Figure 1) is a reality, currently going through system testing and debug. The system still has a few technical challenges to resolve, and it is not yet completely automated, but the system is getting returns from satellites. Star calibrations are now performed routinely, appear to be very stable, and generate mount models with RMS values around 2 arcseconds. Ground calibrations have been performed on many occasions and system delays are being calculated for all four detector quadrants. Satellite returns have been obtained for segments of STARLETTE, BEC, AJISAI and TOPEX passes.

The SLR2000 system characteristics are given in Table 1 below. Details of the various subsystems can be found in previous Laser Workshop papers [Degnan 1996], [Titterton 1996], [Degnan 2002], [McGarry 2002], [Patterson 2002].

The purpose of this paper is to describe the current performance of the prototype system, and to show the plans for its completion.

Table 1: Current SLR2000 prototype system characteristics

Laser:	Nd:YAG Diode pumped Osc/Amp
Fire rate:	2 kHz
Pulse Energy:	~60 microJoules/pulse at exit aperture
Beamwidth:	10 to 40 arcseconds (FWHM)
Point ahead:	Risley prism pair (0-30 arcseconds)
Detector:	Photek quadrant MCP PMT
Gain:	3.E+6

QE:	13% at 532 nm
Image area:	6mm diameter quadrant centered
Receiver:	4 independent channels
Field of View:	10 to 40 arcseconds
Discriminator:	Phillips Scientific 708
TIU:	Honeywell Technology Solutions, Inc.
	1.5 psec resolution Event Timer
T/R switch:	Passive (Polarization insensitive)
Tracking mount:	Xybion Corp Az/El gimbal
Tracking error:	~1 arcsecond RMS
Telescope:	Orbital Sciences Corporation 40 cm off-axis

Figure 1: SLR2000 Prototype at NASA's Geophysical and Astronomical Observatory

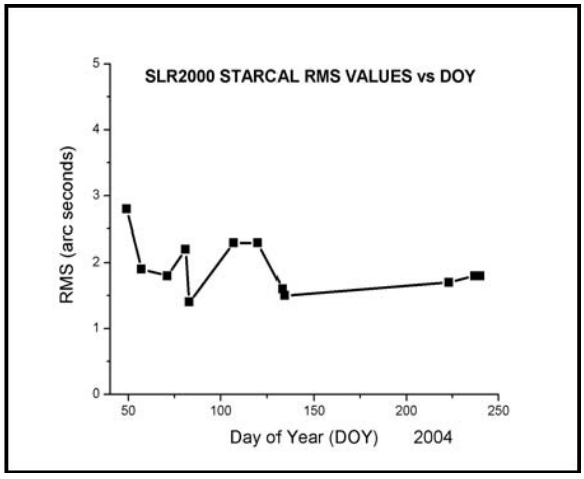

Figure 2: Star calibration RMS model fit versus day of year.

Star Calibrations

Star calibrations are performed routinely. The system pointing is at the arcsecond level and the mount model appears good for several days after the data has been taken. The current 22 term mount model provides a good fit (~ 2 arcsec) for elevations between 10 degrees and 90 degrees. Once the dome is open the star calibration executes completely autonomously and takes approximately 30 minutes to accumulate information for 66 stars. The solution is calculated from a least squares fit to the 22 term trigonometric model. Figure 2 shows the RMS values of all star calibrations for the current version of the mount model.

The mount model corrections can reach a sizeable fraction of a degree. Figure 3 shows model corrections for the star calibration on May 13, 2004, which are typical for SLR2000.

Ground Calibrations

Successful real-time signal processing of ground target range data is now routine. The automated search and acquire also works well. Currently the range returns are manually centered on the quadrant detector, but implementation of closed loop tracking using the quadrant detector information will soon make the ground calibrations semi-autonomous. System setup for ground ranging, including adding required ND filters and setting appropriate gating for the PMT, is still manually performed.

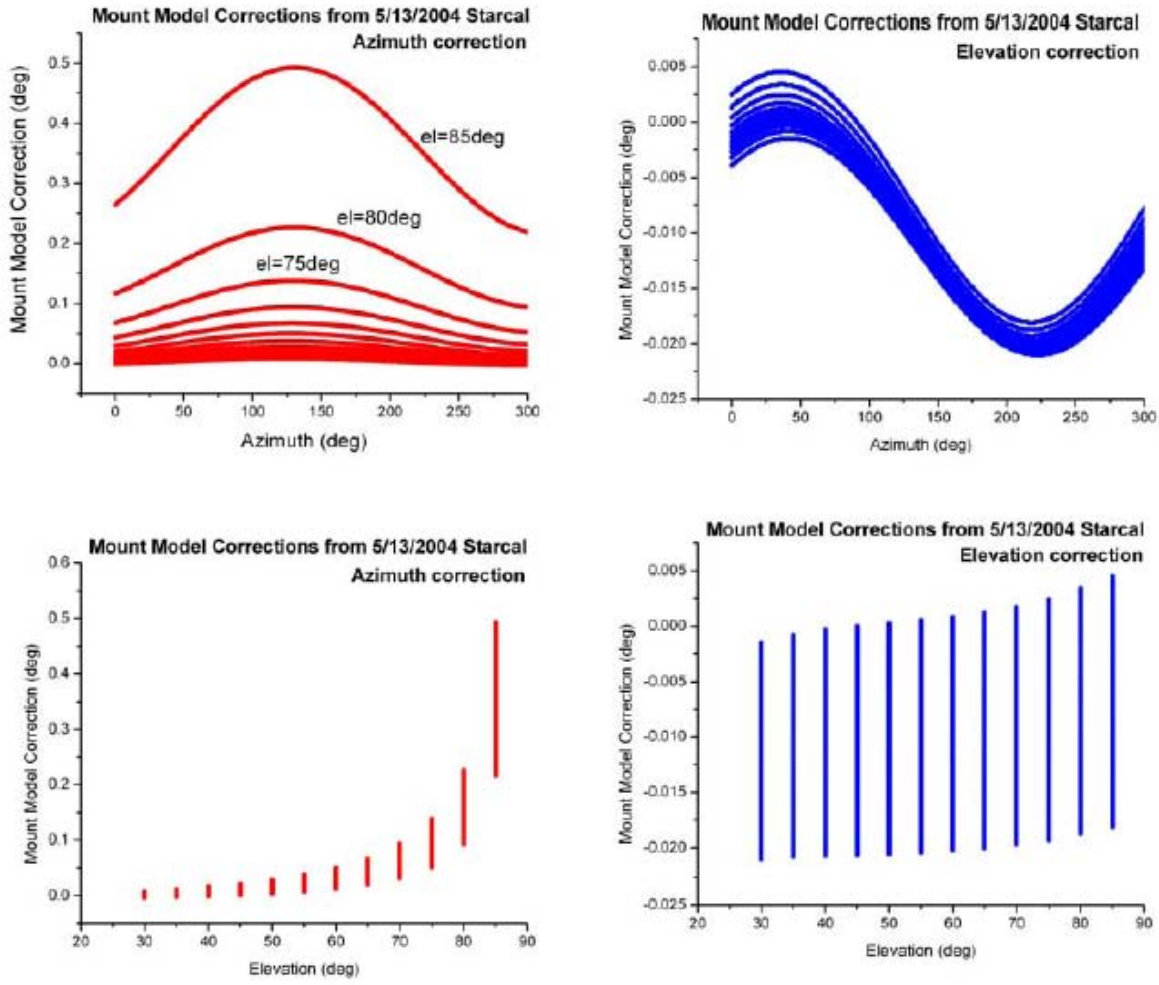

Figure 3: Mount model corrections calculated from May 13, 2004 star calibration. BottomTop plots give azimuth and elevation corrections versus mount azimuth. plots show same corrections as a function of mount elevation

A system delay is calculated for each of the four quadrants independently. The nominal system delay for quadrant 1 is 45 nanoseconds. To overcome the 100 nanoseconds deadtime in the Event Timer, each quadrant's return is delayed 100 nanoseconds relative to the previous one using a fixed delay line. Thus quadrant 2's system delay is ~145 nsec, quadrant 3 is ~245 nsec, and quadrant 4 is ~345 nsec. In photon-counting mode, the range data RMS should mimic the convolution of the transmitter pulsewidth and the receiver impulse response, and the observed high values are consistent with the 300 psec pulsewidth of the current laser. The plots in Figure 4 show the measured return ranges minus a fixed relative range for all four quadrants. In this plot each of the quadrants has been corrected with its corresponding system delay. For those viewing this document in color, quadrant 1 is black, 2 is red, 3 is green, and 4 is blue. As viewed from behind the detector on the transceiver bench, quadrant 1 is upper right, quadrant 2 is lower right, 3 is lower left, and 4 is upper left.

Satellite Laser Ranging

SLR2000 has tracked segments of about a dozen Low Earth Orbiting (LEO) satellite passes, including AJISAI, TOPEX, STARLETTE, and BEC. The current laser on SLR2000 is the preliminary version and outputs only about 120 microJoules of green energy (60 microJoules out of the telescope), which is 40% of the required laser transmit energy. Satellite ranging is,

unfortunately, not routine yet, and our ability to get returns appears to be related to the orientation of the pass. Some problems in the receive optics have been identified, and will be corrected during the fall of 2004. This combined with a higher power laser and the addition of closed loop tracking should make satellite ranging much easier.

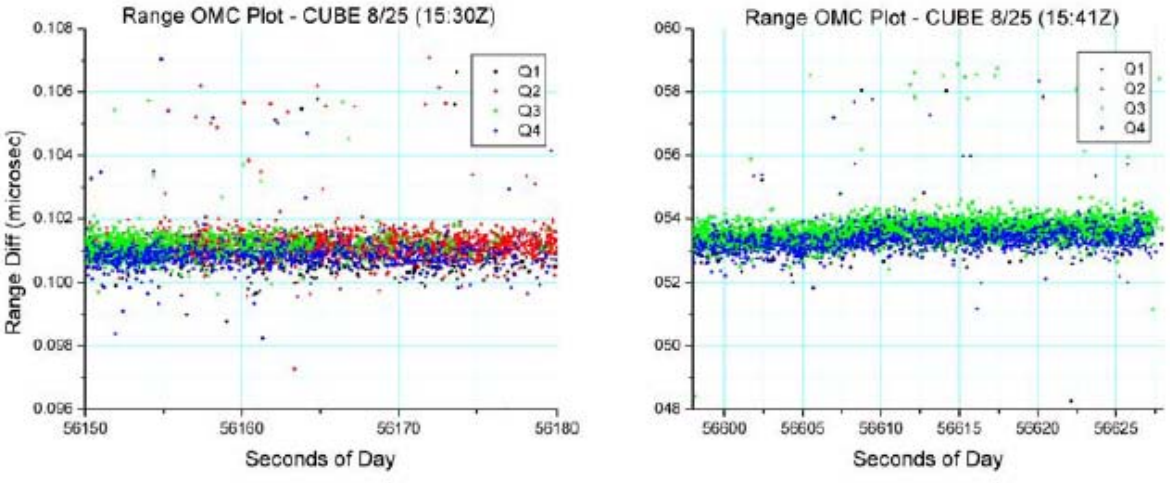

Figure 4: Measured minus fixed relative ranges to the ground target versus seconds of day. All data has been corrected using system delays for the relevant quadrants.

Figure 5 shows the measured range minus the predicted range (OMC) plotted versus seconds of day for various SLR2000 satellite tracks. The upper left plot (AJISAI 5/13/2004) is from a daylight track taken around 11:00 am local time. The rest of the plots are from nighttime tracks. All of the satellite, as well as ground target data, shows an as yet unidentified noise signature which seems to be proportional to the signal strength. It can be clearly seen in the upper right hand plot (AJISAI 5/13/2004) as the bloom in the noise near the start of the plot when the signal strength is high. It disappears as the signal strength decreases. The envelope of this noise is several hundred nanoseconds. We currently believe this problem resides in the detector but more testing is needed to determine this conclusively.

Summary and Future Work

The SLR2000 system has finally become a reality. The system open loop pointing appears to be very good and very stable, the realtime signal processing works as expected, and segments of approximately a dozen satellite passes have been tracked. There is still much work to be done. The current goal for the SLR2000 prototype is to complete the major technical challenges within the next year and arrive at a semi-automated satellite laser ranging system that can track all of the current SLR targets. To accomplish this the following activities must be completed:

1) Operational laser must be completed by Q-Peak or developed in-house.
2) Receiver optics must be upgraded to include:appropriate daylight / twilight bandpass filters, adjustable iris field of view stop, and more angularly sensitive focusing to support quadant detector closed loop tracking.
3) High noise signature problem must be resolved and corrected.
4) Transmitter point-ahead must be implemented. The telescope will be pointed behind and the transmitter will be offset pointed using a Risley Prism pair to steer the beam ahead to where the satellite will be when the light reaches it.
5) Closed loop tracking using information from the quadrant detector must be added.

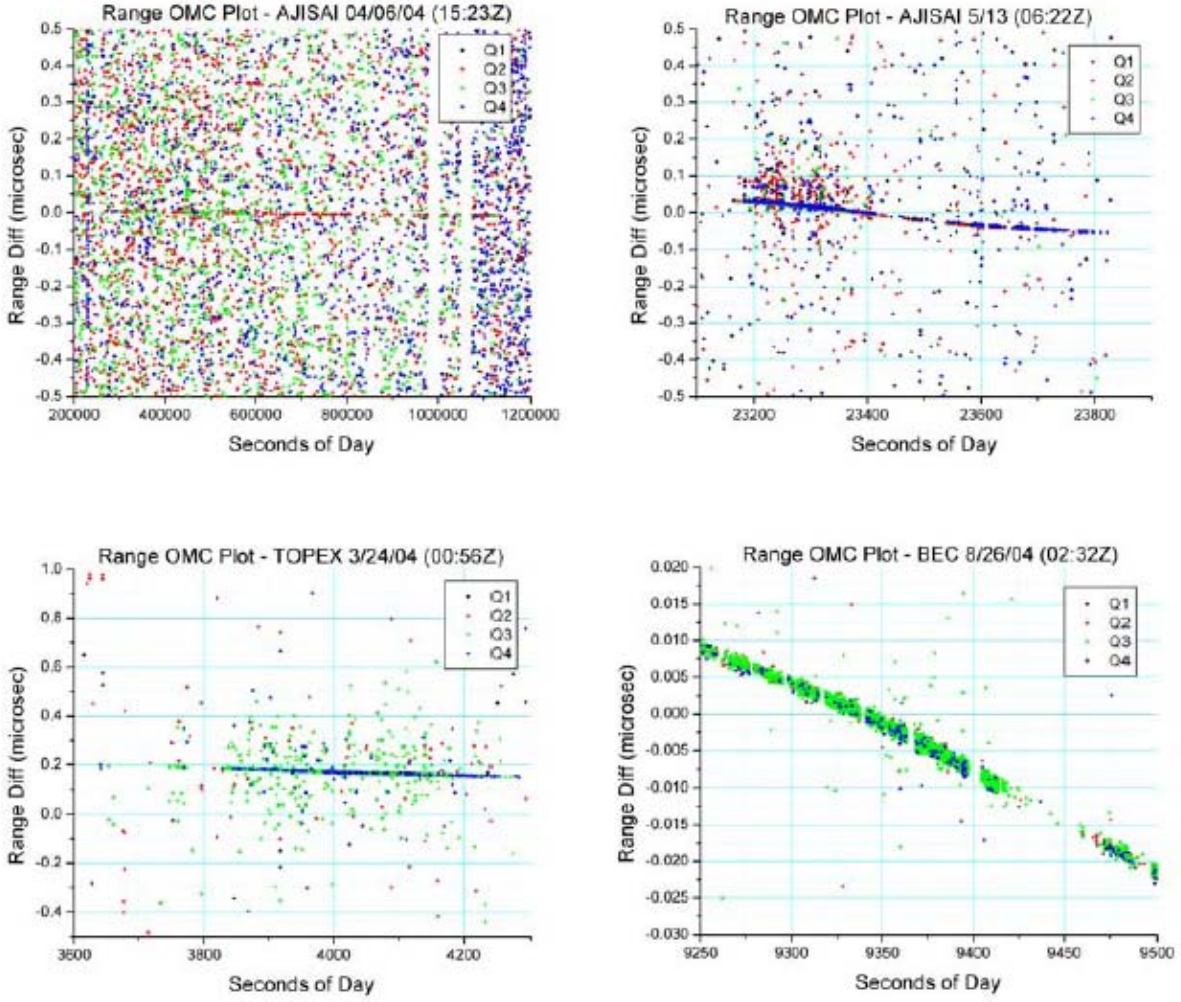

Figure 5: Observed minus calculated (OMC) ranges versus time for various SLR2000 satellite tracks. Measured ranges have been corrected for corresponding quadrant system delay.

6) Automated realtime scheduling and realtime signal processing parameter update must be completed, making use of the system knowledge of the sky conditions and background noise.
7) Normal point generation from SLR2000 data needs to be analyzed.

We plan to complete the first six of these items within the next year. The system will then be collocated with MOBLAS-7 and used to collect data for Normal Point algorithm analysis.

References

Degnan, J., " SLR2000: An Autonomous and Eyesafe Satellite Laser Ranging System," Proceedings of Ninth International Workshop on Laser Ranging Instrumentation, Australian Government Publication Services, John McK Luck (ed.), pp 312-325, Canberra, 1994.

Degnan, J., J. McGarry, and T. Zagwodzki, "SLR2000: An Inexpensive, Fully Automated, Eyesafe Satellite Laser Ranging System," Proceedings of 10th International Laser Workshop on Laser Ranging Instrumentation, Chinese Academy of Sciences, Yang Fumin (ed.),. 367-377, Shanghai, 1996.

Degnan, J., "SLR2000: Progress and Future Applications," Electronic Proceedings of 13th International Workshop on Laser Ranging, Ron Noomen (ed.), Advanced Systems and Techniques Session, Washington, DC, 2002.

McGarry, J., T. Zagwodzki and J. Degnan, "SLR2000 Closed Loop Tracking with a Photon-Counting Quadrant Detector," Electronic Proceedings of 13 th International Workshop on Laser Ranging, Ron Noomen (ed.), Automation and Control Session, Washington, DC, 2002.

Patterson, D. and J. McGarry, "Overview of the Data for SLR2000 Tracking Mount and Performance Testing," Electronic Proceedings of 13th International Workshop on Laser Ranging, Ron Noomen (ed.), Automation and Control Session, Washington, DC, 2002.

Titterton, P. and H. Sweeney, "Correlation Processing Approach for Eyesafe SLR2000, Proceedings of 10th International Laser Workshop on Laser Ranging Instrumentation, Chinese Academy of Sciences, Yang Fumin (ed.),. 378-384, Shanghai, 1996.

GRAZ KHZ SLR SYSTEM: DESIGN, EXPERIENCES AND RESULTS

G. Kirchner, F. Koidl
Austrian Academy of Sciences. Institute for Space Research
Lustbuehelstrasse 46. A8042 GRAZ, AUSTRIA
kirchner@flubpc04.tugraz.ac.at

Abstract

Within the last years, we have prepared our Graz SLR system for kHz operation; since October 2003, this 2 kHz SLR system is operational.

Our previous 10 Hz laser (35 mJ @ 532 nm, 35 ps pulse width) has been replaced by a 2 kHz, DPSS Nd:Van laser system, using a SESAM seed laser with a Regenerative amplifier and a post amplifier; this laser delivers 400 µJ @ 532 nm per shot, with a pulse width of 10 ps FWHM; due to the low energy per shot, we receive mainly single photons from higher orbiting satellites, like LAGEOS or higher; from Low Earth Orbiters (LEOs) we still get multi – photon returns, resulting in close to 100% return rates.

As single photon detector we use a standard CSPAD (Single Photon Avalanche Diode, Peltier cooled) with Time Walk Compensation; the Range Gate Generator with 500 ps resolution was implemented with an FPGA chip in Graz. Time of flight is measured with our Graz E.T. (based on Dassault Event Timer modules) with 1.2 ps resolution; the system is capable of handling up to 500 shots in flight simultaneously.

The system single shot RMS now is 2.5 mm for satellites with low signature; due to high data density of Normal Points – up to 100.000 returns per NP – this system offers in principal accuracies far below the 1 mm level.

Due to the high data density and the high single shot accuracy, the Graz kHz SLR system now can detect single retroreflector tracks from many satellites; this allows to select only echoes from the nearest retroreflectors, resulting in a much better defined mean point of reflection, improving again the accuracy. In addition, it is also possible to derive the rotation of passive sphere satellites.

The Laser

The laser starts with a SESAM oscillator (SEmiconductor Saturable Absorber Mirror), which is very stable, more or less maintenance free, and produces short pulses with excellent stability. This is followed by a Regenerative Amplifier, which is controlled by an external Pockels Cell to switch in/out the pulses; the amplified pulse is fed into a post amplifier, followed by an Second Harmonic Crystal to convert > 50% of the IR energy into green (532 nm). This last amplifier is pumped by pulsed diodes (with about 90 A in 60 µs), while the first two modules are pumped with CW diodes. The pump diode modules are user replaceable, without having to realign the system; lifetime of the pump diodes is specified with > 5000 h; by minimizing the current, and by fully automatic software control (e.g. automatic switching off at longer periods of inactivity) we expect about 3 years of operation before exchanging the pump diodes.

The Range Gate Generator

The CSPAD has to be gated about 65 ns before expected arrival of the return photon(s); on detection of a start pulse, the epoch time of this start pulse is determined, the epoch of the expected return photon calculated and stored in the Range Gate Generator (RGG). Because in our 2 kHz system up to 300 pulses are travelling at the same time to or from a satellite, the RGG uses FIFO registers to store and handle the individual gate epochs. The next expected RG epoch is compared to an actual time scale; if this time arrives, the RGG issues the Range Gate pulse.

This system is implemented within an FPGA (Field Programmable Gate Array) device, but would achieve only resolutions of 100 ns (10 MHz); to improve the resolution, a programmable, analogue delay generator covers an additional resolution of 0 – 100 ns, thus increasing the resolution to < 0.5 ns.

Receive – Transmit Pulse Overlaps

When ranging with kHz to satellites, there are repeatedly periods of overlaps between returning photons, and just fired laser shots; the backscatter of these shots – from the first few km travelling through the troposphere – would cause significant noise on the single photon - diode, reducing the detection probability for the return photon.

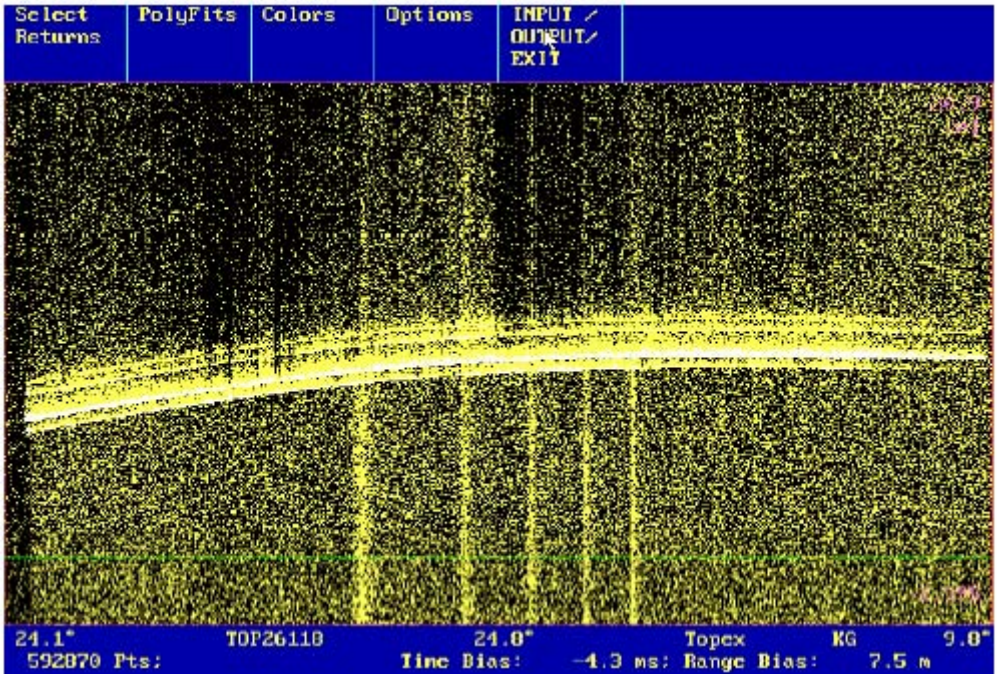

Figure 1: Receive Transmit Pulse Overlap scan increase the noise

To avoid these situations completely, we use the same RGG FPGA chip to produce all laser firing and laser control commands; if return photons are expected within 30 µs after laser firings, an extra delay of 50 µs is inserted before the following laser shot; because all necessary information – next expected Range Gates, AND time of next fire pulse – are already known within the FPGA chip, this processes can run fully automatically within the FPGA hardware, and without any further intervention from the control PC.

In Fig. 1 – an early test pass of TOPEX/POSEIDON satellite – this overlap avoiding feature has been switched OFF intentionally during the central part of the pass, but was switched ON during the first and during the last part, resulting in clearly visible, short periods with increasing noise points due to backscatter during the overlaps.

The Software

The RealTime Control of the SLR Station Graz is based on a 2.4 GHz PC, with 3 ISA Slots (96 Bit DIO, a Universal IOCard, and a IEEE488 Card); to get maximum speed and deterministic realtime response, the PC is running on MSDOS; all RT programs are written in Fortran. The ranging programs are designed to allow untrained observers to range successfully to satellites after a minimum training period of a few hours only; many automatic routines make even relatively tricky things – like daylight ranging with weak laser pulses and Single Photon Detection as close as 15° to the bright sun – even with only minimum experience simple and straightforward.

The software tries to identify possible returns within the 2 kHz stream of pulses; these identification routines have to be fast, and should deliver stable and informative results. The identification is based on a very simple scheme: For each detected stop event, we calculate the residual (observed minus calculated range), and compare it with the last 1000 residuals; if some minimum number of residuals (e.g. 3) are within a certain band (e.g. 100 ps), the new residual is flagged as "identified", plotted on the screen, and stored on disk. This minimum number can be set by observers to adjust sensitivity versus amount of false alarms; the acceptance band width is adjusted by other routines automatically, according to satellite, range gate width and other parameters. This simple procedure is fast, effective, and gives a very nice user interface for a variety of satellites: Low Earth Orbiters with close to 100% return rate result also in easy interpretable graphics as high orbiting satellites – like GPS, which can have return rates far below 1%.

Other routines are filling all identified returns into histogram bins; the bin with maximum identified returns is plotted on the screen –another useful and indicative feature for observers - and serves as a guide number for automatic control of range gate width, range gate shift etc. Thus, most noise points are eliminated, and usually neither displayed nor stored, which not only has advantages for the user interface, but also minimizes storage sizes, amount of data to be handled etc.; To keep the system at the highest possible accuracy, it is calibrated at least once per hour; during the calibration, the laser pulses are attenuated by dephasing the pump diodes of the last amplifier (the laser diodes are still pumped with the same pulses to keep the thermal equilibrium, but about 300 µs too late, so that the last amplifier does not contribute anymore); these attenuated pulses are directed into our near calibration target, about 1 m in front of the telescope [4]; in each calibration run, 10000 returns are measured – which takes only about 10 seconds at 2 kHz and 50% return quote – and averaged to give the calibration value plus statistical information (skew, kurtosis, peak minus mean etc.). The main emphasis is on closely watching any changes of the calibration values (usually stable within a few ps), and symmetric distribution of the returns, i.e. peak minus mean should be about ZERO; in 2004, the average was –0.4 ps (Fig. 2).

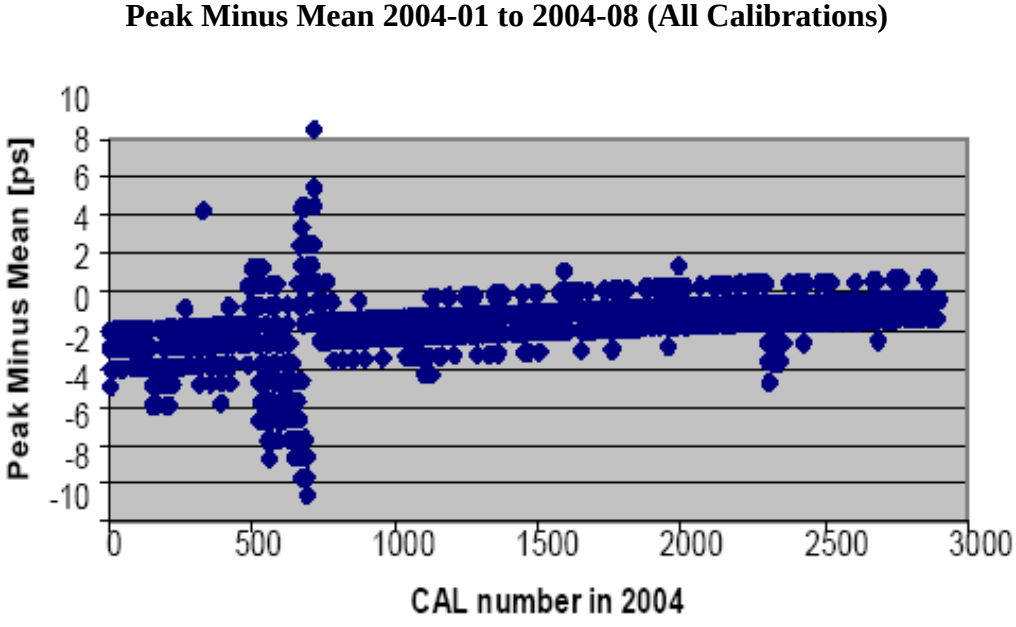

Figure 2: CAL: Peak Minus Mean; 0.4 ps

Results

The 2 kHz repetition rate, combined with return quotes not far from 100% for LEO satellites, results in corresponding huge return numbers (Table 1), as compared to conventional SLR stations with 5 or 10 Hz repetition rates; for example, we have measured passes of LAGEOS-1 and AJISAI with more than 1 million returns, and for many LEO satellites with more than half a million returns; when compressing these returns into Normal Points, these NPs contain up to > 100 k points / NP, with corresponding better definition, higher accuracy etc., than the previous NPs of our old 10 Hz system with few 100 points / NP maximum (Table 1).

Table 1: Returns per Pass, Returns per Normal Point

	Old Laser: 35 mJ	New Laser:400 μJ / Shot	New Laser:400 μJ / Shot
Satellite	Returns per Pass	Returns per Pass	Returns per NP
ENVISAT	5000	Up to 400.000	> 25.000
JASON1	5000	Up to 530.000	> 20.000
TOPEX	7000	Up to 750.000	> 20.000
AJISAI	8000	> 1.000.000	> 50.000
LAGEOS	14000	> 1.000.000	> 100.000
GPS 35/36	300	≈ 10.000 / hour	> 5.000

Detecting Single Retro Tracks

The huge amount of data, much more stable NPs etc. are not the only results; in addition, it turned out that we are now able to identify the single retroreflectors of most satellites within the data stream; typical ERS2 examples of a very low elevation pass (max. elevation <17°, Fig 3) and a very high elevation pass (max. elevation 82°, Fig.4) are given below; the low elevation pass shows a clear track of a second retroreflector, as it deviates around Closest Approach; both tracks than disappear due to clouds; the high elevation pass shows that around maximum elevation also a second retroreflector is involved; while these effects are now clearly visible with a kHz system with up to 500.000 returns per pass, they have not been seen in any of the 10 Hz systems (although the effect is there also !)

In general, all stabilized satellites (mostly earth observation satellites) and those satellites which already stopped their original rotation (e.g. LAGEOS1) allow in many passes identification of different retroreflectors (or retroreflector panels, as in case of the various GLONASS satellites); the exceptions are CHAMP and LaretC satellites, for Champ, theoretically such multitracks could be visible at elevations above 70°, but these passes are very rare (due to the low altitude of Champ) and difficult to track continuously due to the necessary high telescope azimuth speed.

References:

1. Kirchner, G., Koidl, F., Graz Event Timing System: E.T., Proceedings of 12th Int. Workshop on Laser Ranging, Matera, 11/2000; http://geodaf.mt.asi.it/html/news/iwlr/index.htm

2. Kirchner, G., Koidl, F., Short Distance Calibration; Proceedings of 10Int. Workshop on SLR Instrumentation, Shanghai 11/1996:, pp 431 435

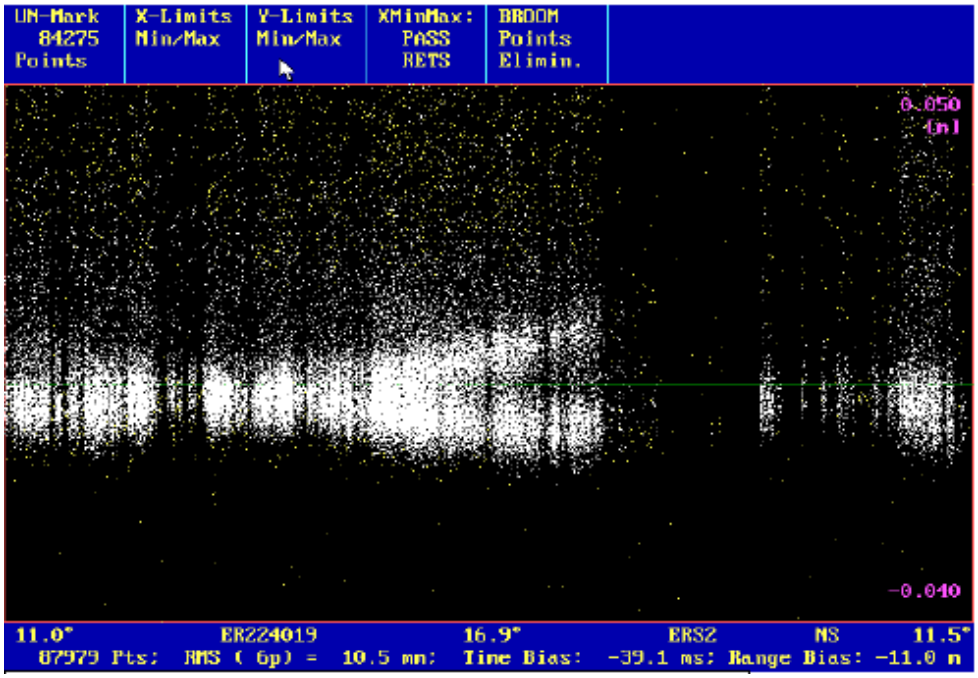

Figure 3: ERS-2, Elevation 17°: 2nd Retro

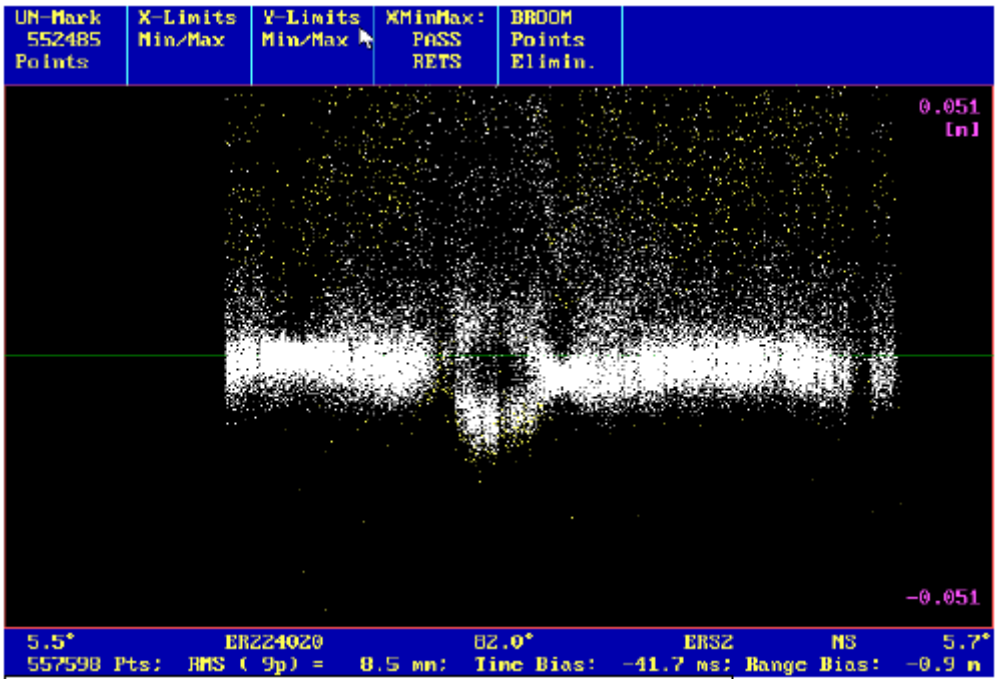

Figure 4: ERS-2, Elevation 82°: 2nd Retro

THE SOS-W -A TWO COLOUR KILOHERTZ SLR SYSTEM.

Stefan Riepl(1), Wolfgang Schlüter(1), Reiner Dassing(1), Karl-Heinz Haufe(1), Nikolaus Brandl(1), Pierre Lauber(2), Alexander Neidhardt(1)
(1) Bundesamt für Kartographie und Geodäsie. D-93444 Koetzting, Germany
(2) Technische Universität München. Fundamentalstation Wettzell. D-93444 Közting, Germany

Abstract

This paper presents the design of the newly envisaged SLR system termed Satellite Observing System Wettzell (SOSW). The key idea behind the project is to provide support especially for low earth orbiting satellites, a kilohertz laser transmitter and a detection package being capable to perform two colour laser ranging. On completion the new system is mentioned to decrease the workload and configuration diversity of the WLRS, which, in turn, will be optimized for high altitude satellites and lunar laser ranging only. The SOSW will be set up at the existing SLR facility building of the Fundamentalstation Wettzell, which already hosted the Satellite Ranging System (SRS) two decades ago. As the rough design of the transmit and receive optics is terminated, plans for modifying the building and dome installation are set up, which will allow a site installation and successive operation of the system during 2006.

Introduction

The design of the Satellite Observing System (SOSW) attempts to integrate to best knowledge the requirements for SLR systems at least for the current and upcoming decade, which in our view can be cast into the following items:

- Minimization of all systematic error sources at or even below the millimeter level.
- Permanent two colour operation during day and nighttime conditions to strive against the elimination of the most potential systematic error source remaining in the SLR data, the atmospheric refraction.
- Capability of monitoring local baselines to support intertechnique combined solutions.
- Support of LEO gravity _eld missions with an adequate data rate.
- Support of navigation satellite missions.
- Highly autonomous or even totally automatic system operation.

To realize these goals the design is driven in order to match the following constraints:

- Operation in single photoelectron mode introducing the least systematic biases, especially space segment induced biases.
- Utmost timing precision and reproducibility.
- Utmost spectral and spatial filtering improving the signal to noise ratio.
- External calibration with paralax compensation, which is indispensible for local baseline monitoring.

- Internal calibration at any pointing direction allowing for interleaved calibration e.g. whilst satellite switching.
- Beam pointing verification at any pointing direction to maximize data acquisition periods.
- Point ahead mode (aberration compensation) to enhance the maximum target distance and signal to noise ratio.
- Support of kilohertz repetition rates minimizing the random error which is especially required for low altitude satellites.
- Closed and pressurized optical chain to protect the coated surfaces.

Laser Specification

Within the last ten years, vast progress has been achieved in laser technology. Especially the mode locking techniques for picosecond pulse lasers have been revolutionized by Semiconducting Saturable Absorber Mirrors (SESAM), which are commercially available nowadays. In contrast to Kerr lens and acoustooptic mode locking the SESAM technique works as well with femtosecond and picosecond pulses, i.e. it offers a broad operating bandwidth ensuring fourier limited pulse generation. Moreover it is preferable to dye cell modelocking due to the lower service requirements arising from the solid state design. The laser output will be polarized circular at 850nm and 425nm, ensuring the least wavelength dependent systematic error in terms of center of mass correction (see [3]).

- 850nm/425nm Ti:SAP CW oscillator, passive modelocking by SESAM
- pulselength shorter than 50ps at 850nm, time band width product < 1
- pulse to pulse jitter < 1 ps
- active oscillator length control referenced by frequency standard down to +- 4Hz
- frequency stability < 4GHz
- regenerative and linear ampli_er generating 1W CW-power at 1kHz repetition rate
- contrast ratio < 1:1000
- variable SHG conversion rate
- M**2 < 1.5 at both harmonics
- output power < 2 percent rms
- circular polarization at both harmonics

Telescope and Mount Design

In contrast to the SLR2000 design [1] which is based on a monostatic telescope configuration, the SOS-W employs a separate transmit and receive telescope. Due to the fact that the chosen continuous wave mode locked oscillator pollutes the optical path with it's constant emission of the high repetition rate pulse train (typically 100 MHz), it is mandatory to provide the utmost optical isolation between the transmit and receive optical path, which can be met only by a bistatic configuration. Moreover the bistatic design isolates the high sensitive photon counting detectors from optical splashes caused by backreection from the optical surfaces which is a known problem in every monostatic SLR system. The remaining backscatter in the atmosphere in a bistatic system can be diminished

very effectively by proper spatial filtering. Figure 1 shows a preliminary design of the telescope mount and tube. The beamsplitter in the transmit path, realized by a highly reflective dichroic laser line mirror, enables for

- internal calibration to the flipable calibration reflector (CR),
- paralax compensated external target calibration through the transmit telescope,
- and star observations through the transmit telescope by guiding the backward light leakage through the subsequent mirror assembly S3, ST3 and S4 to a focusing lens L1 in the elevation axis. Passing through a second dichroic beamsplitter (coude mirror in the receive telescope), the two telescope optical paths are unified and propagated to the adjustable field stop.
- aperture (1 to 120 arcseconds) and recollimating optics (LA3) after which they are guided to the receiver box.

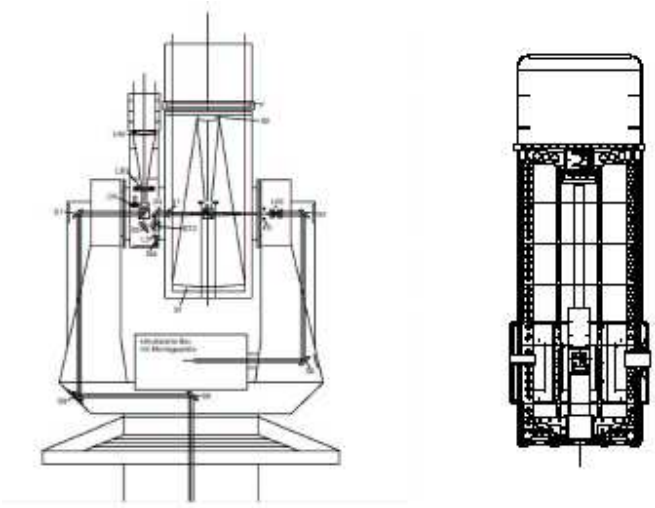

Figure 1: The SOS-W telescope according to a preliminary design by Baader-Planetarium

As the ordinary mount modeling procedure is assumed to be realized by pointing optimization of the receive telescope, residual deviations of the transmit telescope pointing direction as a function of elevation can be compensated by transversal adjustment of LA1 which is mounted on a piezo translation stage. Moreover mirror S7 is vernier controlled in two axes to realize the point ahead mode (aberration compensation) for the transmit optical path.

Detection Package

To fully exploit the lightweight telescope tube and main mirror construction, the detection package will be housed in a hermetically sealed and climatized receiver box located on the Nasmyth (Azimuth-) platform of the telescope. The housing is designed to host two standard and one auxiliary detection channel with individual spectral filtering and attenuation devices as illustrated by figure 2. Moreover a CCD camera with a special filter wheel is installed for mount modeling, beam pointing and beam quality analysis as well as

autoguiding with sunlit satellites during night time. Table 2 summarizes the design guidelines for the detection package.

50cm f/3 primary mirror, light weight construction, centric mount
f/11 secondary focus
lightweight telescope tube sealed sealed BK7 front window
16cm transmit achromat
pointing accuracy < 1 asec
pointing correction devices
direct drive
max. velocities 20deg/sec in azimuth, 10deg/sec in elevation
open cable wrap

Table 1: Specifications for the SOS-W telescope, which will be contructed by Baader-Planetarium.

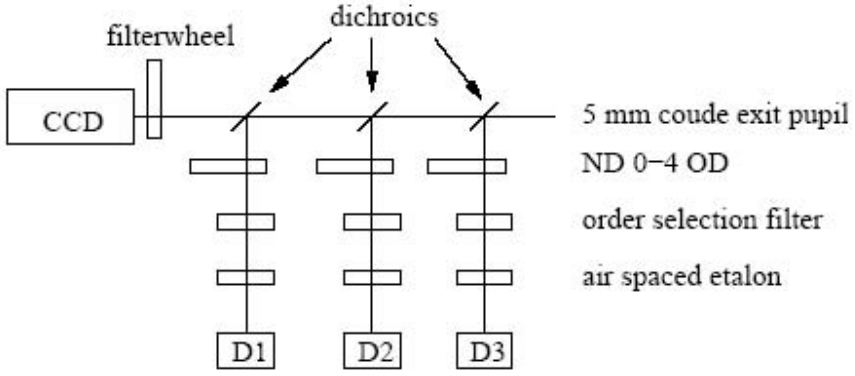

Figure 2: The schematic setup for the detection package

Narrow air-spaced FP Etalon (bandwidth < 0.05nm, transmission > 90%)
High transmission (approx. 80%) high blocking (5 OD) order selection filter
Return rate control by variable ND filter (0-4 OD)
MCP detectors at both wavelengths (Transit Time Spread < 30ps)
Housed in climate box on Nasmyth (Azimuth) platform
Custom discriminators at detectors
Realized with OEM components

Table 2: Specifications and guidelines for the detection package

Baader Planetarium guarantees 10 years serviceless operation
Turbulence/seeing limiting design
High quality surface finish
Up to 30 deg/sec Velocity
Sustains harsh environmental conditions
Hermetically sealed (when closed)
Ambient dry air system keeping outdoor temperature to avoid temperature gradients
Integrated heavy duty lifter (for Telescope)

Table 3: Features of the Baader-Planetarium Dome

Dome Features

The company Baader-Planetarium being in charge of the dome manufacturing for the SOS-W has gathered thorough experience in serviceless design and dome operation in harsh environmental conditions. This is proven by dome installations ranging from Spitzbergen to Teneriffa and even in stringent environments of high mountains, where the dome mechanics are frequently confronted with ice coverage. The features of the dome for the SOS-W are summarized in table 3.

Software Development

Within the in house control software development for the WLRS and the TIGO SLR system vast experience has been gained regarding this issue. Based on the achieved software efforts in these two systems, the existing control system software will be upgraded and improved in order to support kilohertz repetition rates as well as autonomous operation. To realize this goal it is planned to adapt the VLBI- field system software philosophy for this project, since it enables for e.g. support of diverse observation hardware, processing of system independent observation schedule and allows a manual intervention of an automatically processed observation schedule. It should be pointed out that the VLBI-field system as well as the TIGO SLR control system operate with Linux. The realtime extension for Linux RTAI offers even support for time critical software problems arising in SLR systems. The goal of the SOS-W software project is to realize a counterpart of the VLBI Field System, the SLR Field System which should be adaptable to any existing SLR systems.

Outlook

The SOS-W comprises a kilohertz capable two color laser ranging system designed at the utmost but achievable limits of nowadays technology. It represents an up to now unique approach to two wavelength ranging using single photon counting techniques. Moreover the project aims to operate the SLR system autonomous or remote. The expectations on normal point accuracy scaled by error budget, return rate and link budget considerations respectively are in the submillimeter range, i.e. internal accuracy excluding to date unmodeled error contributions.

In terms of refraction correction derived from the measurements in the two wavelength domains an evaluation of the two colour capability of the TIGO SLR system [0] scaled top the SOS-W system parameters leads to approximately 3mm obtained within a normal point interval of 120 seconds, if one assumes perfect modelling of the wavelength dependent center of mass correction. For quasi single reflector targets like STARLETTE the obtainable accuracy for the refraction correction within a normal point interval should be at the millimeter level. Due to the envisaged spatial filtering at the seeing limit, a minimum sun proximity of 20 degrees should be achieved. The control system software will support global coordinated experiments, e.g. time transfer and transponder missions for which a mandatory observation schedule has to be processed, similar to the VLBI-Field-System capabilities. The software will be developed using open source code standards which will facilitate the portability and application to other SLR systems. Throughout the development of the SOS-W control system we will approach solutions entirely based on software from the Free Software Directory, which is a joint project of the Free Software Foundation and the UNESCO. The system is expected to be operational in early 2007.

References

[1] John Degnan, *SLR2000: Progress and Future Applications*, Proceedings of the 13th International Laser Ranging Workshop, Washington D.C., 2001

[2] U. Keller, K. J. Weingarten, F. X. Kärtner, D. Kopf, B. Braun, I. D. Jung, R. Fluck, C. Hönninger, N. Matuschek, J. Aus der Au, Invited Paper, *Semiconductor saturable absorber mirrors (SESAMs) for femtosecond to nanosecond pulse generation in solid-state lasers*, IEEE J. Selected Topics in Quantum Electronics (JSTQE), vol. 2, pp. 435-453, 1996.

[3] D. Arnold, *Wavelength Dependence of Range Correction*, Proceedings of the 13th International Laser Ranging Workshop, Washington D.C., 2001.

[4] S.Riepl, D.Ramirez, C.Guaitiao, *Validation of Mapping Functions*, Proceedings of the 13th International Laser Ranging Workshop, Washington D.C., 2001

A COMPACT, TOTALLY PASSIVE, MULTI-PASS SLAB LASER AMPLIFIER BASED ON STABLE, DEGENERATE OPTICAL RESONATORS

John J. Degnan, Sigma Space Corporation, Lanham, MD 20706
USA John.Degnan@sigmaspace.com, FAX: +01-301-552-9300

Abstract

Low energy, picosecond pulse oscillators typically require several orders of magnitude amplification to be useful in kHz satellite laser ranging systems, altimetry, or other applications. The present paper describes a totally passive amplifier design, based on degenerate optical resonators, which permits high multipass amplification of ultrashort pulses in a compact package, requires no active switching components, and should be relatively simple to align.

INTRODUCTION

New kilohertz satellite laser ranging systems rely on either passively Q-switched microchip or SESAM (**SE**miconductor **S**aturable **A**bsorbing **M**irrors) laser oscillators for the generation of picosecond pulsewidths. Microchip lasers (e.g. SLR2000) typically generate several microjoule pulse energies at few kHz rates with pulsewidths on the order of a few hundred picoseconds. SESAM devices (e.g. Graz) can produce much shorter pulses between 10 and 25 psec but with significantly lower energies, typically sub-microjoule. Furthermore, if one operates at kHz fire rates, the amplifiers can be pumped with CW diode laser arrays for longer life and reliability, but the resulting gain per pass is relatively low compared to pulse-pumped systems. As a result, the pulse must pass through several stages of low-gain amplification in order to reach pulse energies of several hundred microjoules required for robust photon-counting of satellite returns. In the NASA SLR2000 system, the oscillator pulse is passed six times through a single amplifier head using three carefully aligned mirrors while, in the High-Q system used at Graz, the SESAM oscillator pulse is input to a relatively large regenerative amplifier with complex pulse switching electronics followed by a conventional amplifier. As an alternative, we propose a totally passive, multipass amplifier based on the concept of "stable degenerate optical resonators" [Ramsay and Degnan, 1970]. A comparison of the three multipass amplifier techniques is illustrated in Fig. 1.

STABLE DEGENERATE OPTICAL RESONATORS

The characteristics of any optical resonator are defined by the radii of curvature of two mirrors, b_1 and b_2, and the distance d between them. Paraxial rays will never walk out of the resonator,

$$0 \le \left(1-\frac{d}{b_1}\right)\left(1-\frac{d}{b_2}\right) \le 1 \qquad (1)$$

At certain mirror separations, the resonator becomes "degenerate" and can be characterized by an integer N. These discrete separations are defined by the equation

$$d_{\pm}(N,K) = \frac{b_1+b_2}{2} \pm \frac{1}{2}\sqrt{b_1^2+b_2^2+2b_1b_2\cos\left(\frac{2\pi K}{N}\right)} \qquad (2)$$

K=0 for N=1
1< K<N/2 for N > 1
provided K >1 is not
divisible into N

For each value of K and N, there are two distinct separations which produce the degeneracy. Table 1 illustrates the valid values for K up to N =8

N =	1	2	3	4	5	6	7	8
K=	0	1	1	1	1	1	1	1
					2		2	3
							3	

Table 1: Valid K-values as a function of the degeneracy factor, N.

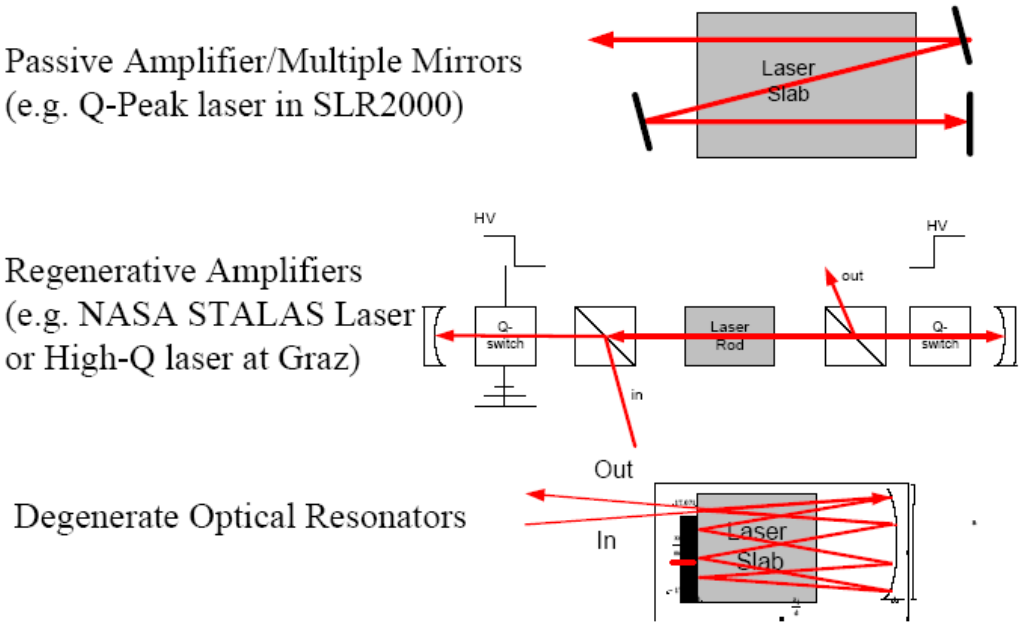

Figure 1: Some multipass amplifier approaches.

Degenerate resonators exhibit a number of interesting physical effects, among them:

- The Hermite-Gaussian (TEM_{mnq}) resonator modes divide into N discrete frequencies separated by c/2NL where L is the resonator length; thus, N=1 represents the highest degeneracy where all spatial modes oscillate at the same frequency.
- Hole-coupled lasers exhibit large power losses because the frequency-degenerate TEM modes can couple together to create a low loss composite mode with a null at the coupling hole
- Internal ray paths can be defined which repeat themselves after N round trips in the resonator.

It is this last feature which suggests their use in passive multipass amplifiers.

SPECIAL CASE #1: SYMMETRIC RESONATORS

If the two mirror radii of curvature are equal ($b_1 = b_2 = b$) , the degeneracy equation simplifies to:

$$d_{\pm}(N,K) = b\left[1 \pm \cos\left(\frac{\pi K}{N}\right)\right]$$

Figure 2 displays the resonance positions of a symmetric resonator for N = 1 to 6. The vertical scale indicates the level of degeneracy, N.

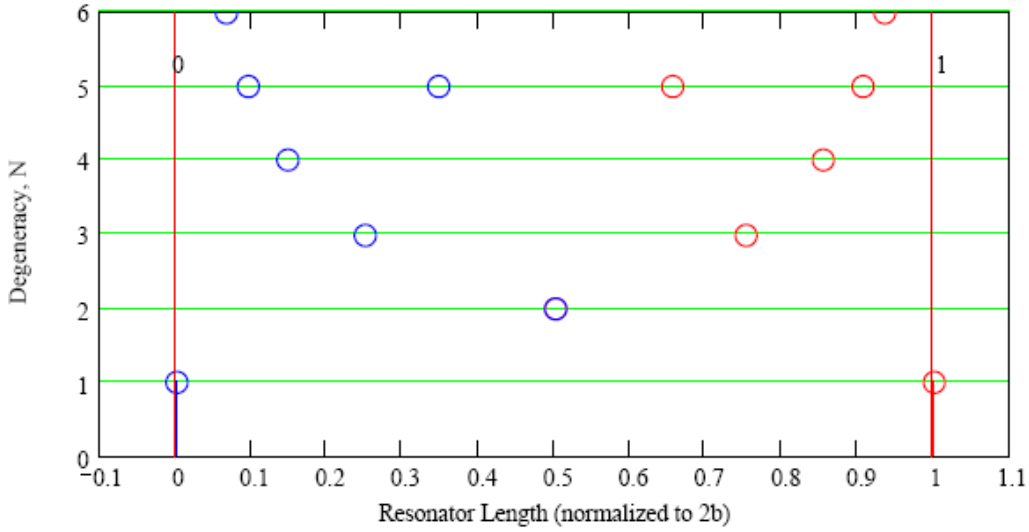

Figure 2: Degenerate mirror separations for a symmetric resonator for N = 1 to 6. The stable range is 0 < d < 2b. The d+ and d-positions are indicated by the red and blue lines respectively.

For each degenerate separation, there are two types of ray paths, “ecliptic” or “non-ecliptic”, as illustrated in Figure 3 for N = 4 and K =1. Ecliptic rays make N passes through the amplifier slab before retracing the same path in the opposite direction. Non-ecliptic rays, on the other hand, never retrace the same path and therefore have the following potential advantages over ecliptic rays:

1. The angularly separated input and output beams do not require additional optical isolation between the oscillator and amplifier
2. There is no need for an independent means (e.g. polarization rotation) of separating the input and output beams
3. The circulating beam samples more of the pumped amplifier volume for better energy extraction

Ecliptic ray paths, on the other hand, may offer advantages in terms of ease of alignment since the input and output beams are coaxial and normal to the reflecting surface of the input mirror. Furthermore, as we shall see later, ecliptic paths also lend themselves more easily to variable pass amplifier systems.

SPECIAL CASE #2: FLAT-CONCAVE RESONATORS ($b_2 = \infty$)

If one mirror radius of curvature is infinite ($b_2 = \infty$) , the degeneracy equation simplifies to:

$$d\ (N,K) = \frac{b_1}{2}\left[1 - \cos\left(\frac{2\pi K}{N}\right)\right]$$

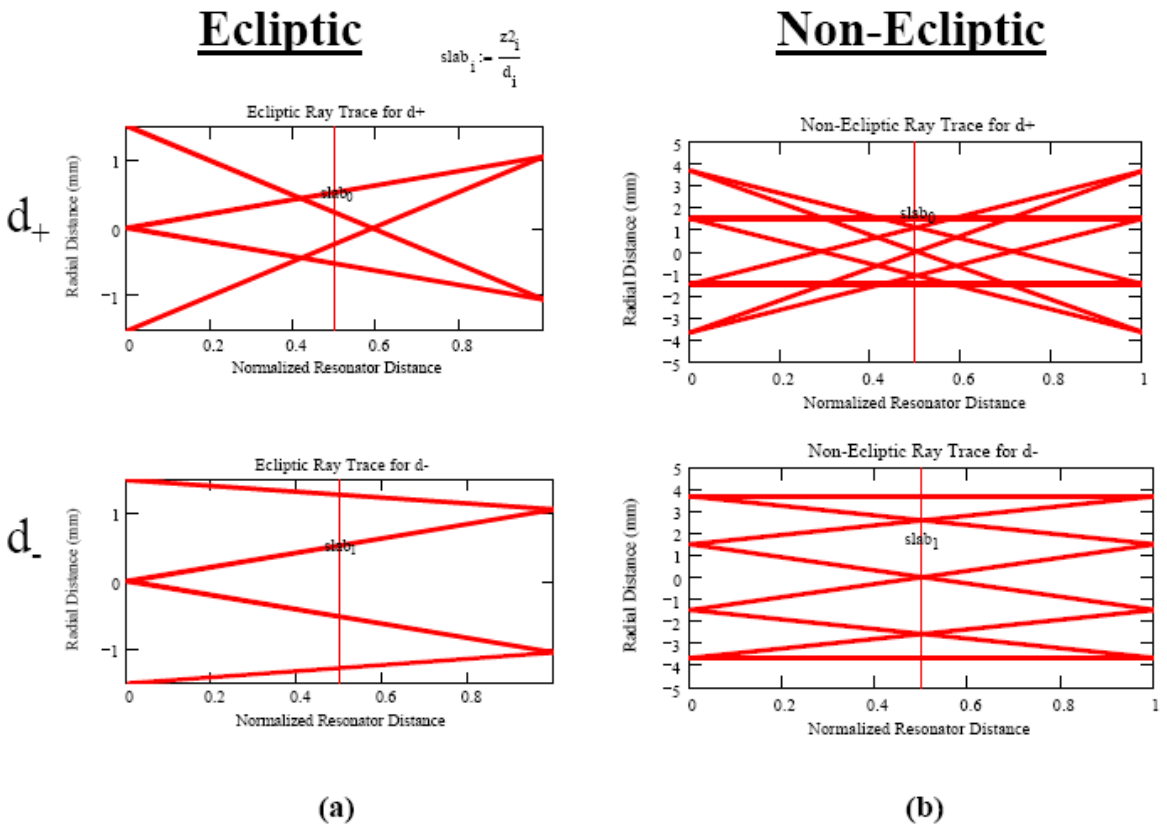

Figure 3: Ray traces for a symmetric resonator with degeneracy N =4 and K =1; (a) Ecliptic ray traces for d+ (top) and d- (bottom) ; (b) Non-ecliptic ray traces for same geometries.

Figure 4 displays the resonance positions of the flat-concave resonator for N = 1 to 6. The vertical scale again indicates the level of degeneracy, N. Unlike the general or symmetric resonator cases, there is now only one degenerate mirror separation for each value of N and K. For each degenerate position, one can again define ecliptic and non-ecliptic ray paths which repeat themselves after N round trips through the resonator.

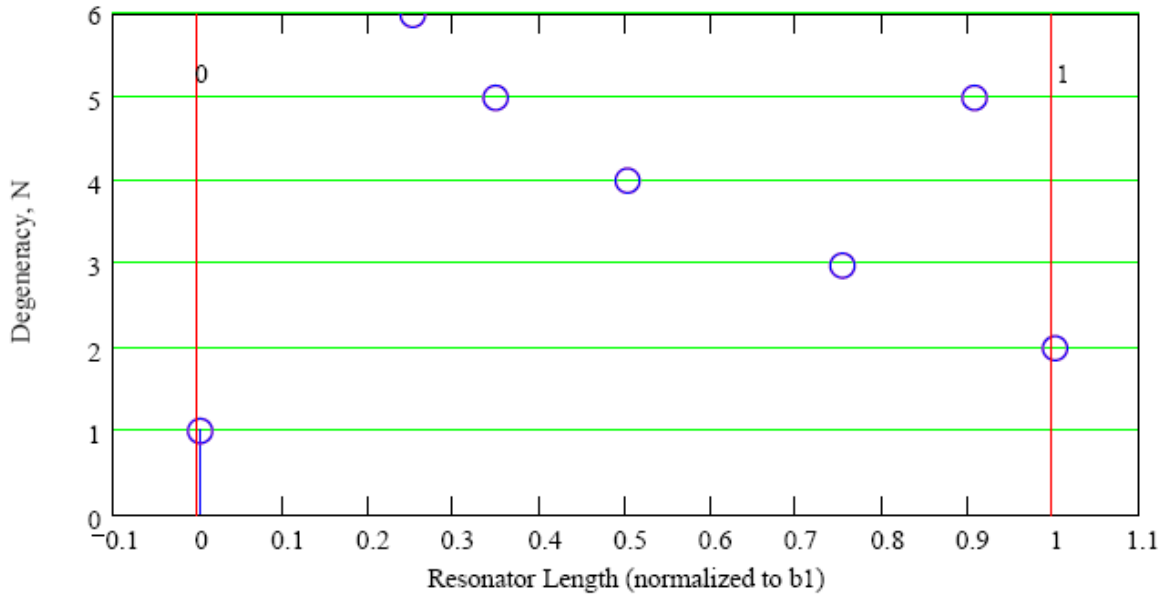

Figure 4: Degenerate mirror separations (normalized to the radius of curvature *b1* of the non-flat mirror) for the generalized flat-concave resonator for N = 1 to 6. The stable region is now defined by 0 < *d* < *b1*.

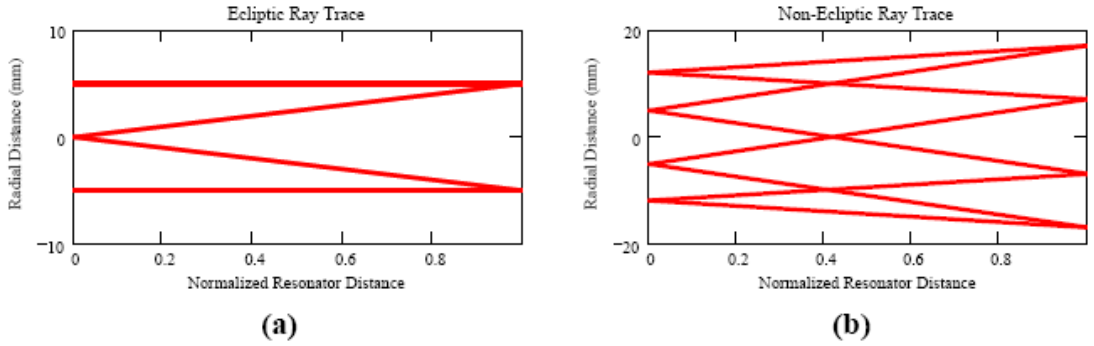

Figure 5: Ray traces for a Flat-Concave resonator with degeneracy N =4 and K =1; (a) Ecliptic ray trace; (b) Non-ecliptic ray trace. The flat mirror is assumed to be located to the left of each ray trace.

VARIABLE PASS AMPLIFIER DESIGN

Figure 5(a) suggests a design for a simple variable pass amplifier. As illustrated in Figure 6, the incoming collimated p-polarized beam from the oscillator passes through the polarizer and is rotated to circular polarization by a quarter-wave plate. Assume that the left edge of the slab is coated with a highly reflecting mirror at 1064 nm except for a small section at the top which is antireflection (AR) coated. The input beam is then inserted normal to the slab surface in the AR-coated region, makes an arbitrary number of passes (2N) through the amplifier dependent on the positioning of the single translatable mirror on the right, exits the multipass amplifier through the same AR-coated surface as the entry beam, is rotated to s-polarization by the second pass through the quarter-wave plate, and is reflected off the input polarizer. Diode pumping of the slab can be accomplished through the edges of the slab or through the top of the slab The amplifier design also transfers the Gaussian properties (radius, phasefront curvature) of the input beam to the exit beam at all degenerate mirror separations since the round trip ray matrix for the resonator taken to the Nth power always equals the identity matrix [Ramsay and Degnan,1970]. Thus, the exit beam will have the same spot size and divergence as the input beam [Degnan, 2004].

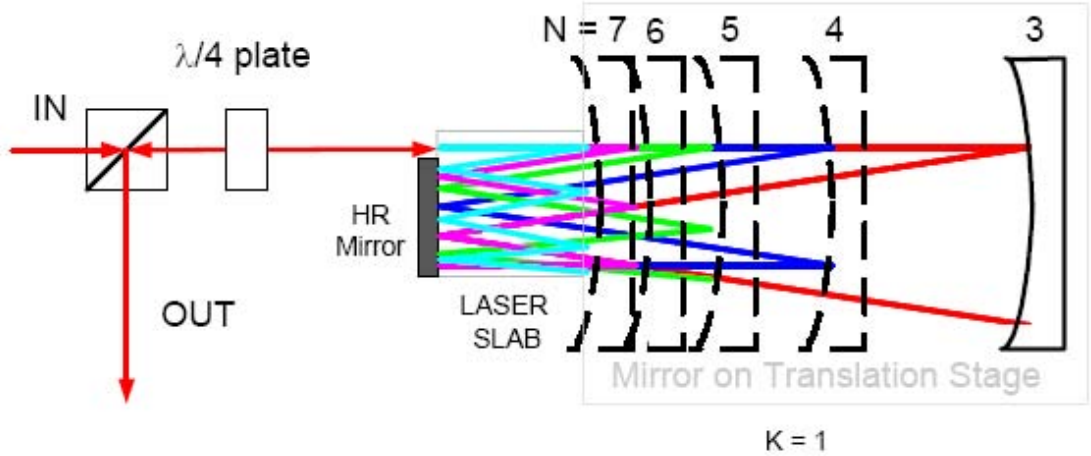

Figure 6: Concept for a compact, passive, multipass amplifier based on ecliptic rays in a flat-concave degenerate resonator. The degeneracy N, and the number of passes through the amplifier (2N), can be varied by moving the spherical mirror on a precision translation stage. Differently colored rays are associated with different values of N (red =3, blue = 4, green = 5, etc)

In order to suppress self-oscillations along or near the amplifier optic axis where the two mirror surfaces are approximately parallel, it may be necessary to introduce a region of low reflectivity in the center of the spherical mirror by either (1) leaving the center uncoated, (2) AR-coating the center, or (3) introducing a central hole. This has no effect on the amplification since the ecliptic rays entering from the flat side of the resonator never reflect off the center of the spherical mirror. However, the diameter of the low reflectivity area will impose an upper limit on the number of roundtrip passes that can be achieved without having the amplified beam attenuated by the low reflectivity spot.

SUMMARY

Microchip and SESAM oscillators can generate picosecond pulses at multi-KHz rates but only at low single pulse energies (several microjoules or less). Since many applications (SLR, 3D imaging lidar, etc.) require pulse energies ranging from several tens of microjoules to several millijoules, there is a general need for high amplifications in a compact, efficient, diode-pumped package. Furthermore, since CW-diode pumped amps typically have low single pass gains, many passes through the amplifier may be required to reach the required pulse energies and to extract the stored energy efficiently. Regenerative amplifiers can achieve this, but they are usually quite large and require high speed, high voltage electro-optic switches Totally passive degenerate resonator multipass amplifiers are an attractive alternative to multiple mirror systems as used in SLR2000 and can potentially provide :

- High multipass gain in a compact, easily aligned package
- A fair amount of isolation from the oscillator and reduced internal feedback for suppressing self-oscillations within the amplifier
- Variable number of passes with one translating mirror which can be set for optimum performance or compensate for a degradation in oscillator power
- Excellent beam control since it preserves the gaussian parameters of the input beam at the output due to periodic refocusing

REFERENCES

Ramsay, I. A. and J. J. Degnan, "A Ray Analysis of Optical Resonators Formed by Two Spherical Mirrors", *Applied Optics*, Vol. 9, pp. 385-398, February, 1970.

Degnan, J.J., “Ray Matrix Approach for the Real Time Control of SLR2000 Optical Elements”, these proceedings, 2004.

RECENT ACHIEVEMENTS IN DETECTORS FOR EYE SAFE LASER RANGING

Ivan Prochazka , Karel Hamal.
Czech Technical University in Prague. Brehova str. 7,
1150115 19 Prague 1, Czech Republic
phone +420 723 920 786, fax +420 224 922 822,
prochazk@mbox.cesnet.cz

Abstract

We are reporting on the latest results in the research and development of the solid state proton counters suitable for detecting individual photons in the near infrared wavelength region. The separate absorption and multiplication layer avalanche photodiode based on an InGaAs are one of the most promising candidates for the solid state photon counter for the eye safe laser ranging. Using the laboratory sample of InGaAs structure we have achieved the dark count rate as low as 30 kHz at modest temperature –60 C. The detector active area is 80 microns in diameter, its timing resolution of the detector is 1.8 nsec.

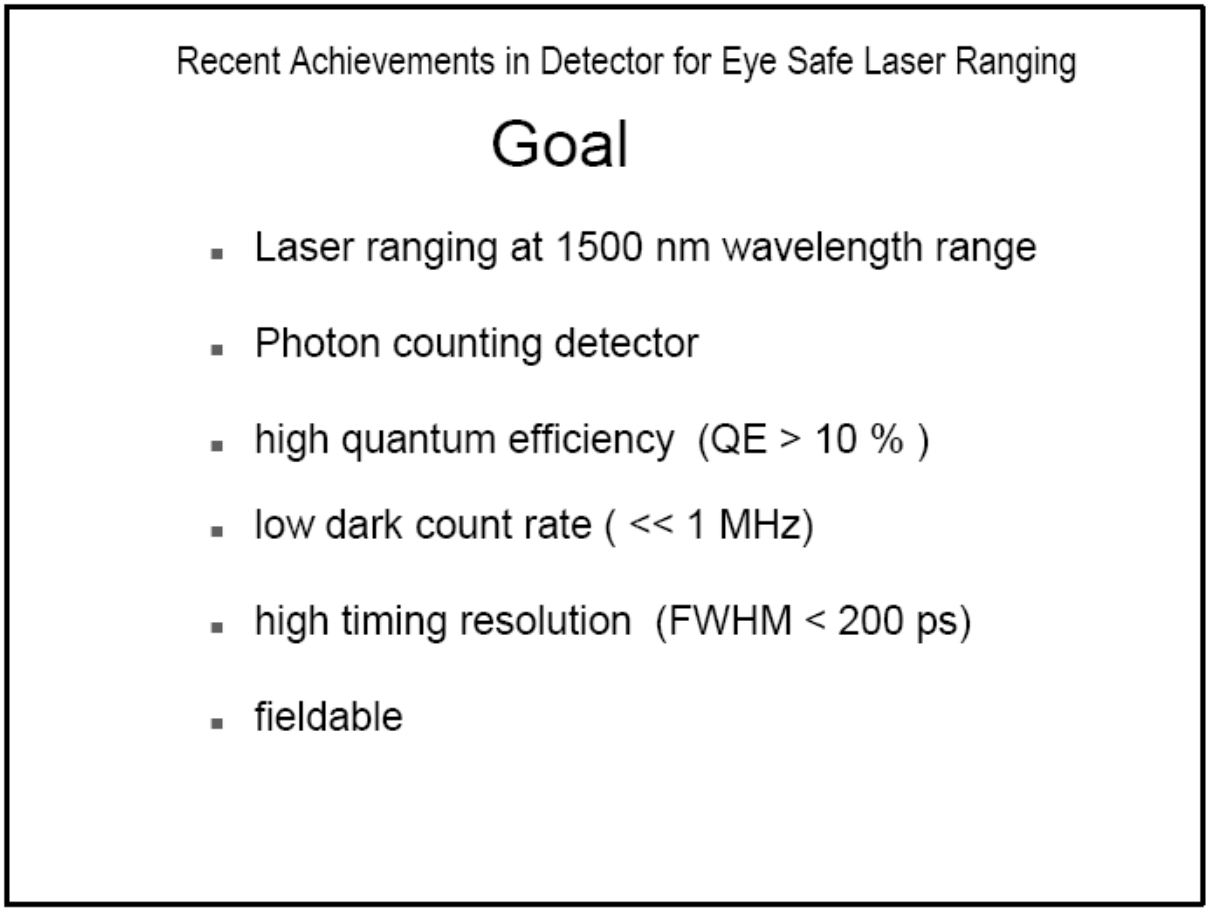

Single Photon Avalanche Diodes
Semiconductor materials

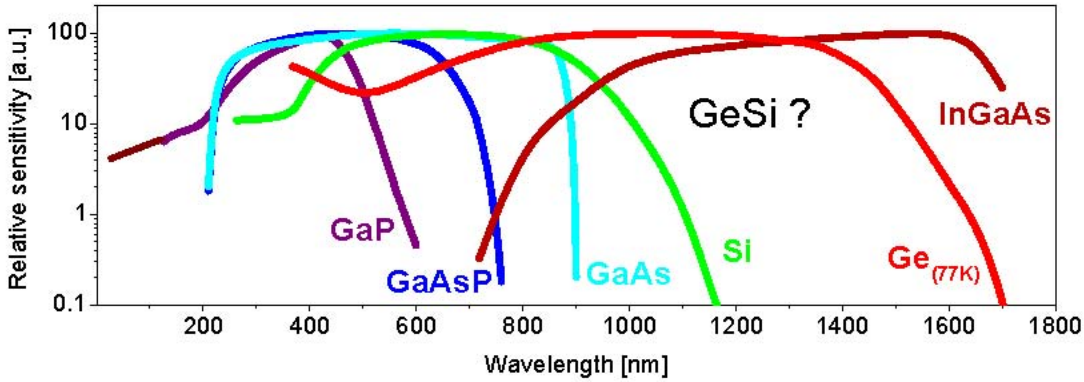

Laser wavelengths used for SLR / SPADs

Eye safe

Germanium SPAD Detector Package
The first eye safe SLR in Tokyo, CRL & PESO & EOS, 1996

Ge SPAD, 100 um
compact liquid N_2 cryostat, 77 K
the electronics built in
timing resolution 25 ps rms
QE 2-5% @ 1540 nm
dark count >= 1 MHz

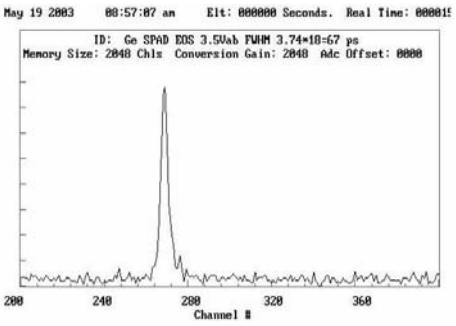

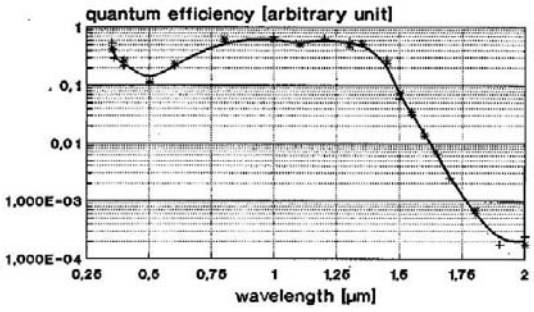

InGaAs Detectors for Photon Counting

- quantum efficiency > 10%
- operating temperatures 150-300 K

- high after pulsing effects
- high serial resistance => low avalanche currents (<< 1mA)

- structure is difficult to manufacture, limited chips availability

InGaAs SPAD Detector Package
New active quenching and gating circuit

GOALs - to minimize the charge flowing trough the APD to reduce after-pulsing and hence the dark counts
- to respond to APD small pulses

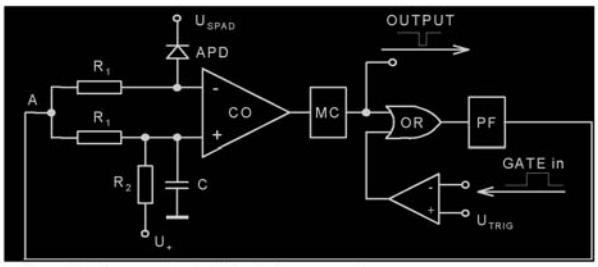

Figure 1: Active quenching circuit for the laser transponder

CO comparator
PF pulse forming
MC monostable
OR gate

responses to 10 mV / 1 ns pulses
loop delay 2.6 ns
ECL logic, SMD
=> 1 V above break max.

Low dark count rate InGaAs SPAD

Chip 80um in diameter, ECL active quenching, 1 kHz gate

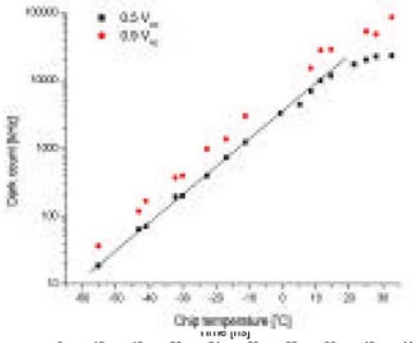

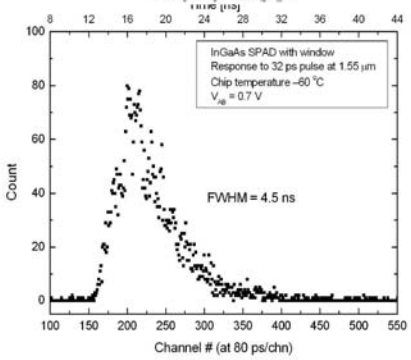

Dark count rate

25 kHz @ -60°C

Timing resolution

FWHM	4.5 ns
rms	1.8 ns

Fast response InGaAs SPAD

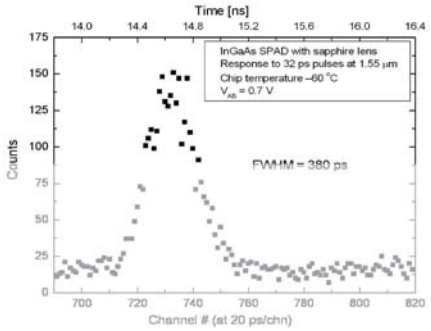

Timing resolution

FWHM	380 psec
rms	160 psec

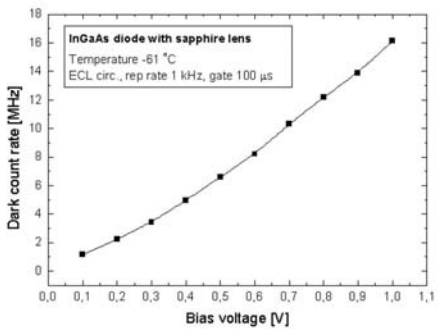

Dark count rate

small drop with temperature

12 MHz @ -60°C

SPAD on $Ge_{04}Si_{06}$

Development status quo

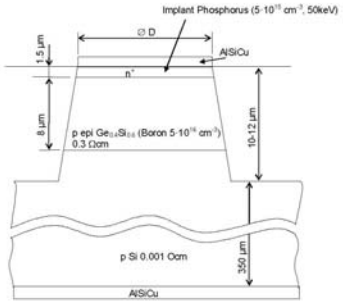

technology tests:
- GeSi layer 5 um on top of the Si
- diffusion, implantation, masking,..
- test purpose MESSA structure,

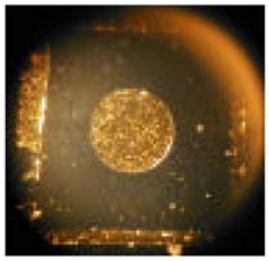

The first Geiger operation reported

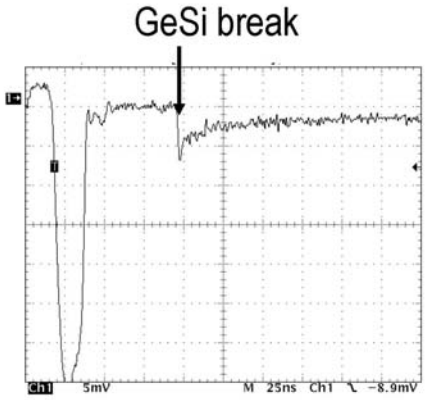

Conclusion

- PROGRESS
  in solid state photon counters for eye safe laser ranging
- new APD structures on InGaAs (30-80 um)
- new control circuits
- new cooling setups for 150 - 210 K
- ACHIEVED PARAMETERS (InGaAs @ 1550nm)
- quantum efficiency 13 %
- dark count 25 kHz @ -60 C
- timing resolution 160 psec
- however, the last two not at the same time
- „long way “ to operational GeSi detectors

Available Detectors Summary
Status Quo 2004

- Si
  - compact package, 0.25 - 1.1 um, ps timing,
  - gated, not-gated operation
  - 20 .. 200 um, TE cooling, low noise,
  - photon number estimate
  - space qualified

- GaP
  - room temperature, X .. 0.8 um
  - 300 um, ps timing

- Ge
  - 77 K , 0.25..1.6 um
  - 100 um, 1 MHz dark, gated, ps timing,

- InGaAs
  - 150..210 K, wavelength 1…1.8 um
  - 30 - 80 um diamater
    - ns timing, dark < 30 kHz
    - ps timing, dark ~ 10 MHz

ADVANCED TECHNIQUES AT THE EOS SPACE RESEARCH CENTRE

B. Greene, C. Smith, Y. Gao, J. Cotter, C. Moore, I. Ritchie, C. Burman
EOS Space Systems Pty Limited
bengreene@compuserve.com, Ph +61 2 6298 8010, Fx +61 2 6299 6575

Abstract

The EOS space Research Centre [SRC] at Mount Stromlo is committed to research and development of laser ranging and tracking, as well as related techniques in astronomy and optical communications.
The SRC has very substantial infrastructure and a super-set of tracking system characteristics. Current facilities include 100 cm and 180 cm telescopes, kW-class lasers, and AO systems. These capabilities allow the SRC to develop metrics for a wide range of operational trackingsystems, including systems specifically designed for the accurate tracking of space debris.
An outline of EOS programs in space debris tracking and harm mitigation will be presented.

DATA YIELD OF THE ILRS GLOBAL NETWORK OVER THE PAST DECADE

E. C. Pavlis
JCET/UMBC and NASA Goddard, Maryland, USA
epavlis@JCET.umbc.edu/Fax: +1-410-455-5868

Abstract

We present an analysis of the data yield history of the ILRS Global Network. Variations due to seasonal, weekly and anthropogenic effects will be evaluated and quantified. The data from only the two LAGEOS satellites are used in this study. This ensures that the results are independent of other reasons for which an increase or decrease in data yield could be observed (e.g. targeted campaigns, loss of scientific interest in a particular target, ranging restrictions due to mission constraints, etc.). We will attempt to quantify the effect of the recent NASA-network reduction in the overall yield of the GLTN.

Introduction

The Global Laser Tracking Network (GLTN) is now managed by the International Laser Ranging Service (ILRS) and its coordinating bodies. It is no secret that Satellite Laser Ranging (SLR) never managed to achieve a uniform global distribution of tracking sites, not even close to those of other space techniques like GPS and DORIS. The non-uniform landmass distribution on the globe is the primary reason, with the high cost of equipment and operations being a close second. In recent years the lack of southern hemisphere sites had been slowly addressed with the strategic transfer of older and new systems in targeted locations. Unfortunately this process not only came to a screeching halt, it was entirely reversed, with NASA's decision to resolve funding shortcomings with the closing of the Haleakala, Hawaii and the Arequipa, Peru sites in 2003, and curtailment of operations at the rest of the NASA-supported GLTN sites. With autonomously operating systems soon to become available, the fortunes of the GLTN may soon be reversed, however, it was felt that a closer look be taken of the data yield from GLTN over the past decade, in order to assess the trends in data collection and identify any systematic shortcomings due to the current schedule of routine operations. We decided to do this by looking at the data yield of the network when tracking the two geodetic satellite targets LAGEOS and LAGEOS 2. The reasons behind this are the fact that according to ILRS rules, an operational site must meet minimum tracking requirements for these two targets, which are the primary targets when it comes to the definition of the Terrestrial Reference Frame (TRF) and monitoring Earth Orientation Parameters (EOP) on a daily basis. Additionally, focusing on these two satellites, avoids confusing temporary data yield variations due to targeted campaigns, special target tracking requirements and changes in the scientific interest on some SLR targets over time. We will examine in detail the data yield for the first quarter of 2004, and then we will look at the statistics of the 1993-2003 data set collected by the GLTN. The analysis is done on the basis of the total daily data yield on both LAGEOS and LAGEOS 2 satellites for each of the active tracking sites.

First quarter 2004 results

The GLTN sites are shown in Figure 1. The highly non-uniform distribution of sites over the northern and southern hemispheres is obvious. It is also very clear that there is a very high density of stations over central Europe.

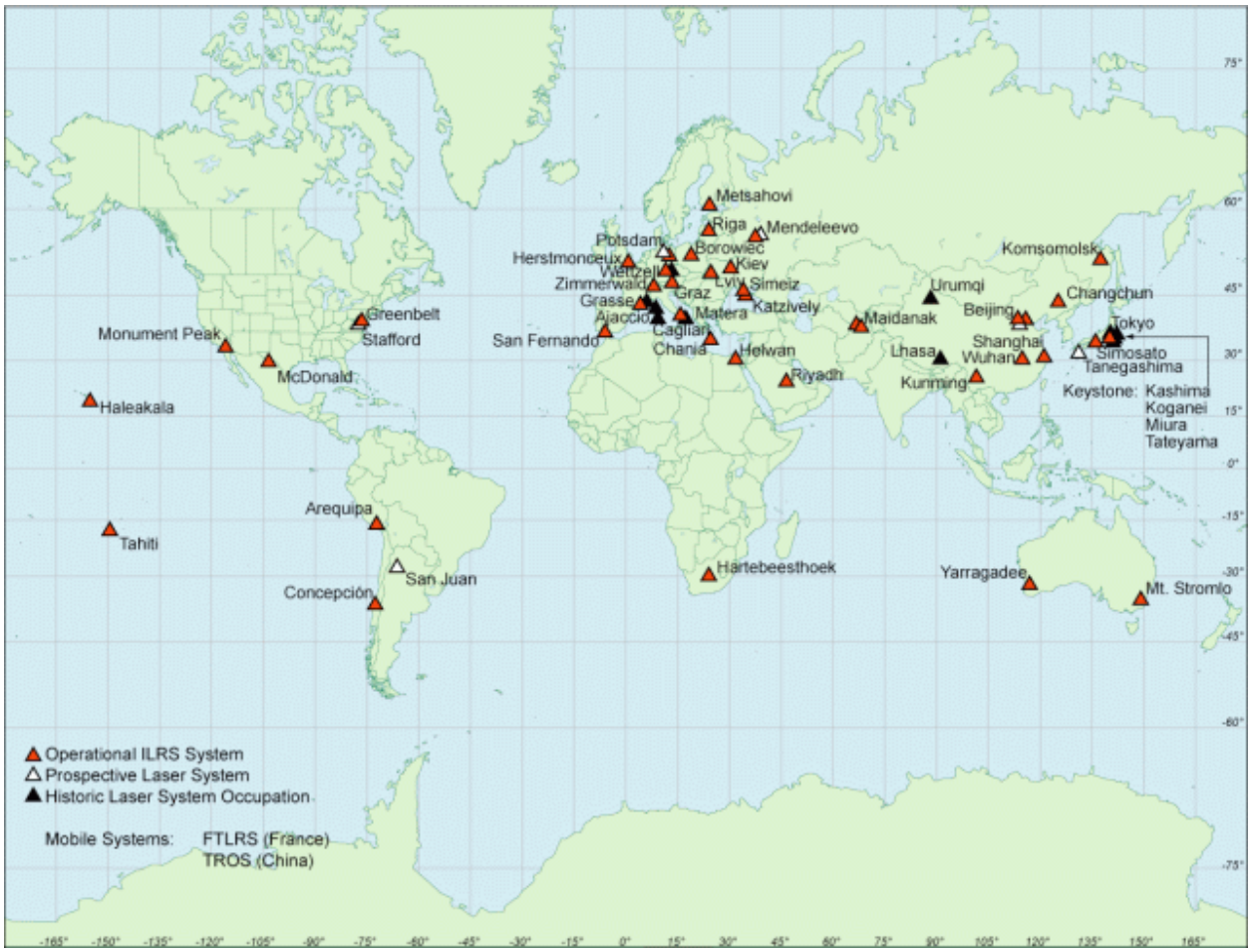

Figure 1. The ILRS Global Laser Tracking Network at present (ca. mid-2003).

The repercussions of this lopsided distribution are exacerbated by the fact that not all stations perform or operate in a similar way, and others despite their high quality equipment, are situated in areas affected by weather that prevents SLR operations over long time periods at a time. Examining the data yield from the recent first quarter period of 2004 (Figure 2), we notice that in its present configuration, the network fails to ensure a geometrically strong daily network, with a median number of tracking sites at eleven, but with a wide variation (a standard deviation of three sites), with a minimum of as little as five stations, and a maximum of nineteen sites, a number that can not even be considered acceptable for TRF maintenance and EOP monitoring purposes. In contrast for instance, the IGS GPS network uses a network of "core" sites in the order of sixty around the globe, with a similar situation for the other satellite technique, the DORIS network. In terms of data points, the daily median of about 350 normal points, with a large standard deviation of some 135 points, indicate that there is

severe lack of robustness in the network yield, with wild variations which are only worse due to the further burden of the unequal quality of data from various sub-groups of stations.

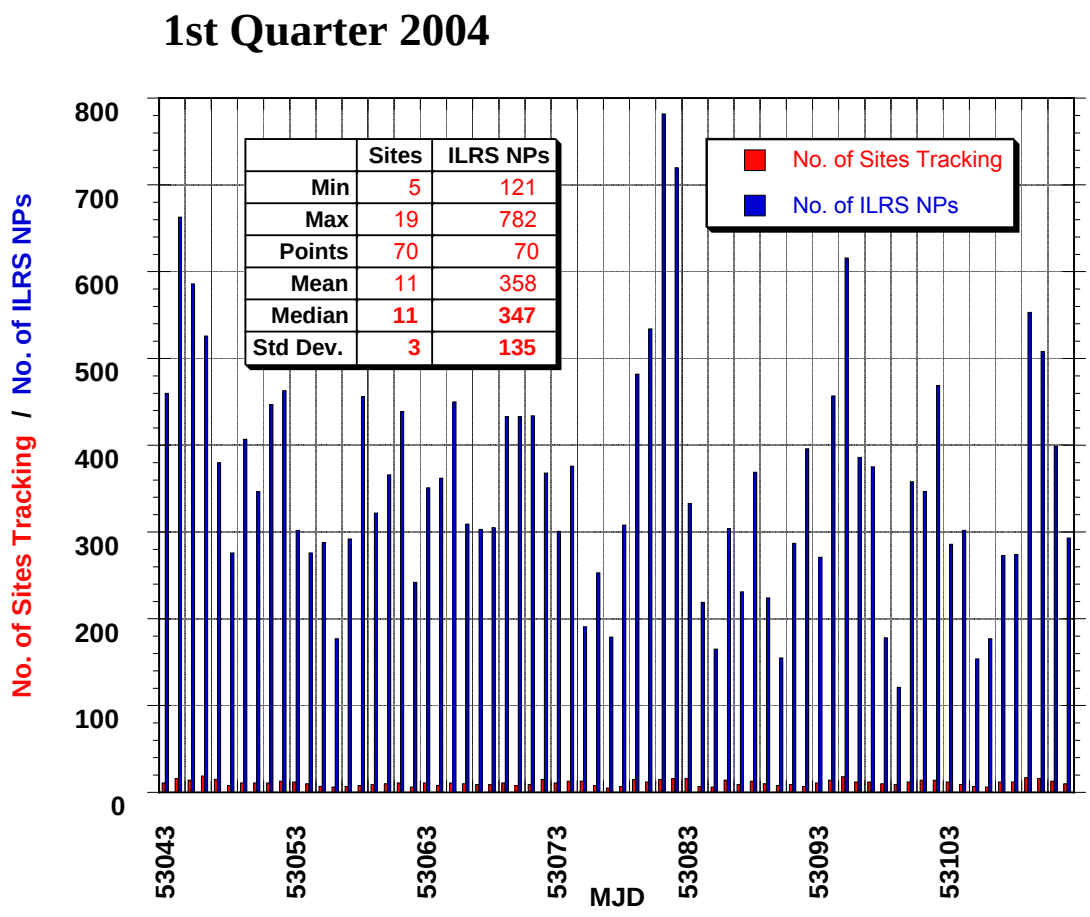

Figure 2. Daily normal point and tracking station distribution for the 1st quarter of 2004.

The latter has significant geographic correlation, and that generates even more problems in our contributions for the stable (in time) definition of the TRF, its origin (geocenter), scale, orientation, and other attributes [Pavlis, 2002; and in these proceedings].

The histogram of Figure 2 indicates some obvious periodicities in the data. In the past, it was observed that SLR data yield dropped significantly during the weekends, and the effect was termed naturally, the "weekend effect". We therefore decided to fit a model that included a bias, a slope and a 7-day periodic component. Given all other factors that affect data yield as we outlined above, it is really amazing how well this model fits the data during this time period. The results are displayed in Figure 3, along with the parameters and statistics of the fitted model. The –1.2±0.7 NP/d drop in data is much too insignificant to worry, but the fact that the weekend effect has an amplitude of some 81 NPs and it is significant at the 4-σ level, is something we need to address. The model explains about half of the variance in the data set (47%), considering though the previously estimated standard deviation of some 135 NPs in the data yield, we conclude that the weekend effect is largely responsible for most of this variability. The fact that this drop is concentrated over the weekend, a more appropriate model would be to look at the data variability over the weekdays separately from the weekends.

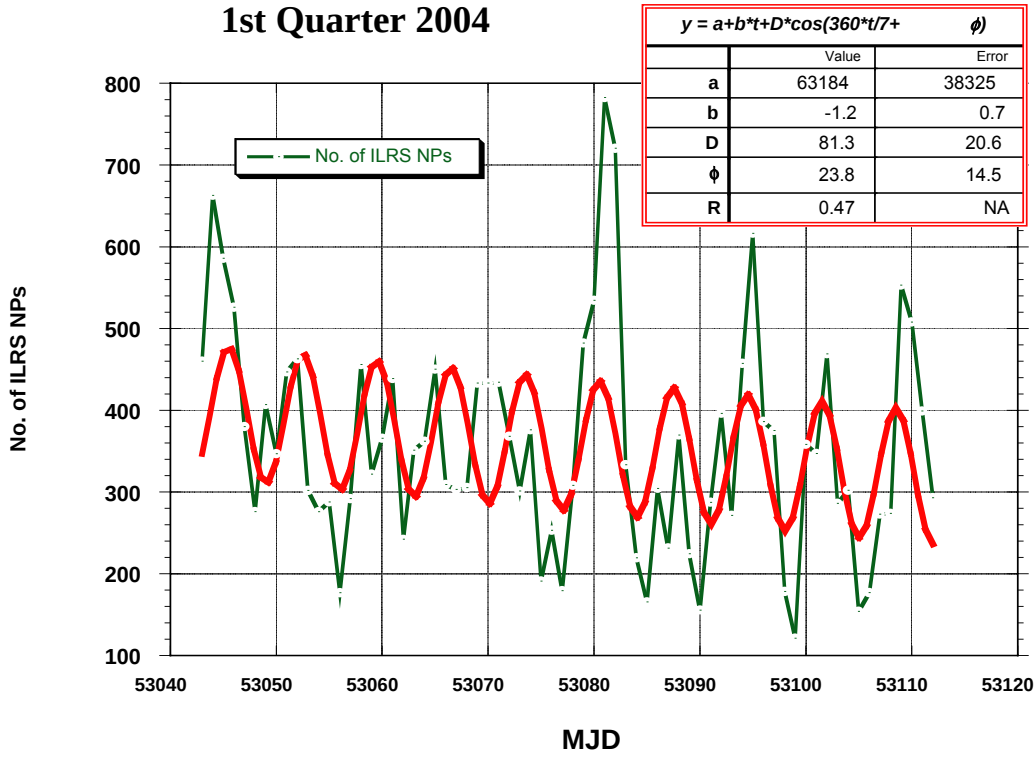

Figure 3. Model fit with a 7-day periodic component for the 1st quarter of 2004 data.

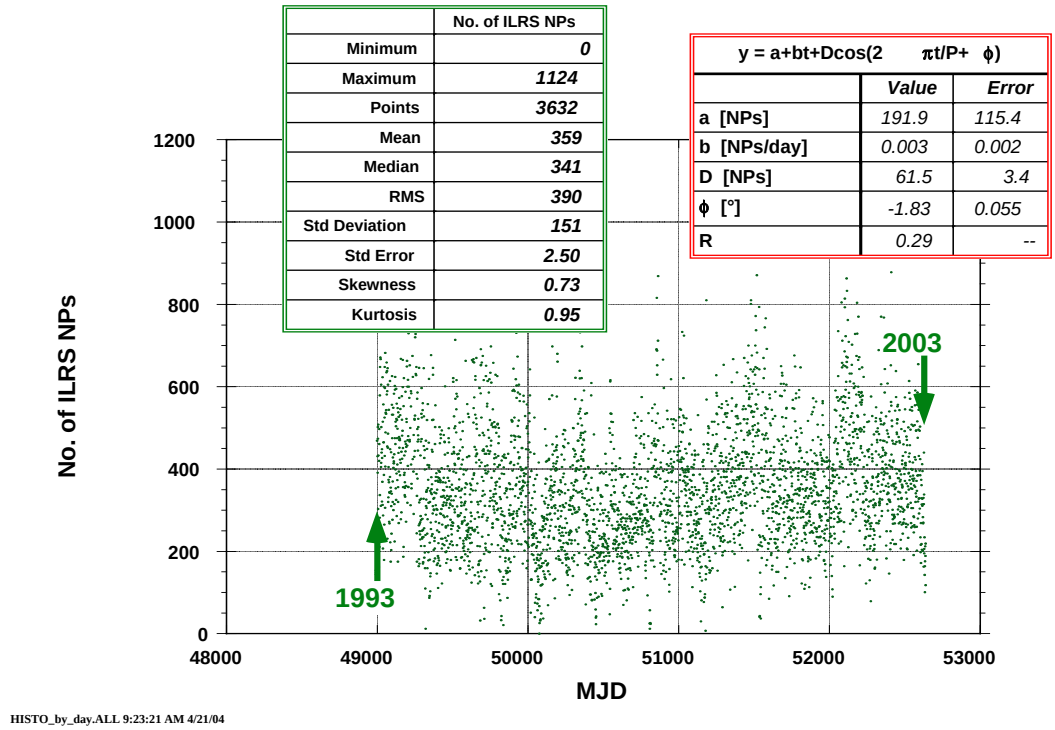

Figure 4. Model fit as in Figure 3 but on the entire 1993 – 2003 SLR LAGEOS data set.

Fitting the same model to the entire data set 1993 to 2003, we find similar if not identical results (Figure 4). It now explains only about 30% of the variance, but that is not surprising given the so many changes that the GLTN undergoes over periods of time due to operations

changes, change of tracking priorities, targeted campaigns, long-term weather patterns, addition or deletion of stations, etc. One parameter that seems to be even better determined from the longer record is the amplitude of the weekend effect. Although over the longer time the magnitude undergoes variations and the value drops to just over 61 NPs from 81 that we found during the 1st quarter of 2004, the standard deviation is now down to 3.4 NPs, indicating this is a real effect, and if want a GLTN that will deliver products with a uniform quality, it has to be addressed and resolved.

Despite significant changes and additions to the GLTN over the examined period, it is disappointing to see that the median daily yield and associated standard deviation over the longer period is practically the same with what we observed over the recent 1st quarter of 2004 analysis. Since it is impossible to see any details in a figure that covers a whole decade, we have generated individual plots corresponding to approximately one-year slices of Figure 4. These are illustrated in Figure 5 (a) through (j). The model that was fit to the entire data set is overlaid on each figure, centered at the median daily value. We did not consider any slope, since its value is statistically insignificant. A close examination of the actual data yield during each year, in comparison to the average indicated by the model, reveals some very interesting facts.

First of all, it seems that 1993 was our best year in data yield and it has been downhill ever since. Year 1996 had a low yield, while 1997 had an exceptionally low yield. For the rest of the years, except for an above average performance in 2001, they are all at about average. Looking at each year even more closely, we find that in 1994, the second half of the year shows enhanced yield, and a similar performance in 1999. In 1995 and 2000, we have a strong annual signal, and although not as pronounced due to the severe drop in yield, years 1996 and 1997 also show similar signals. In 1998 we notice a drop in the second half of the year, while in 2001, there is a very significant enhancement in the middle of the year. Finally, the end of 2002 shows a very strong decrease in yield over about the period of a month.

Summary

The analysis of the ten-year record of tracking data from the ILRS GLTN for LAGEOS and LAGEOS 2 indicates that there is a strong weekend effect present throughout the years. The large variability of station participation in the daily network, compounded by the non-uniform quality of the network sites, results in a degraded contribution for such research areas requiring high quality and stability, as the definition of the TRF and its origin, scale and orientation, and monitoring their changes over time. Planning of any system improvements or network expansions, one should consider these issues first, if the goals outlined in national and international programs under consideration are to be served by the SLR technique properly.

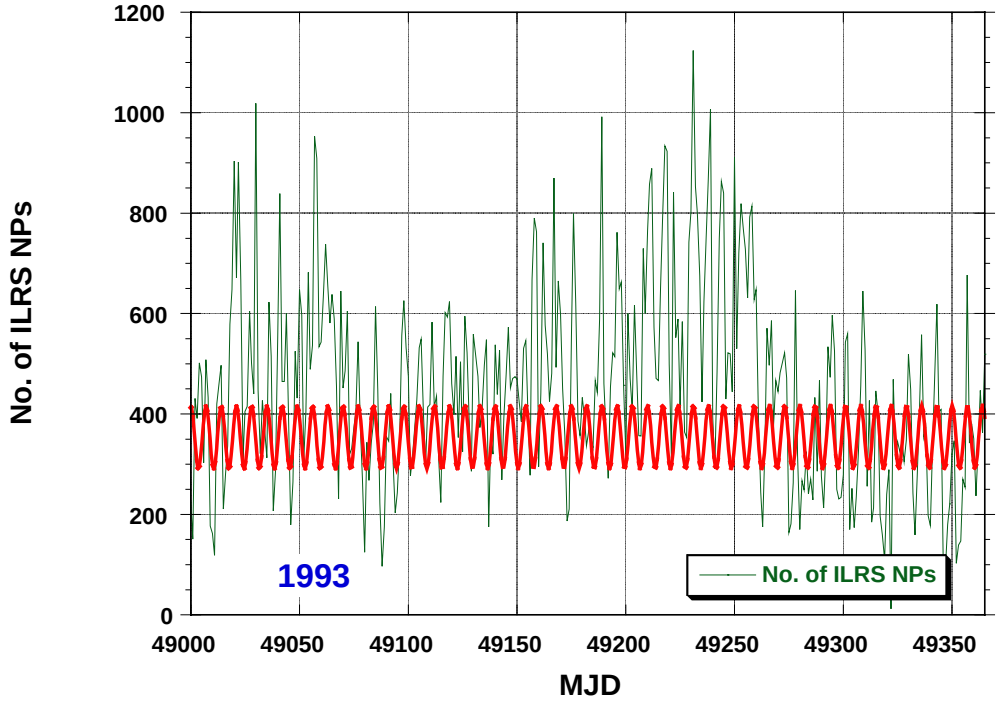

Figure 5. (a) Daily data distribution for 1993.

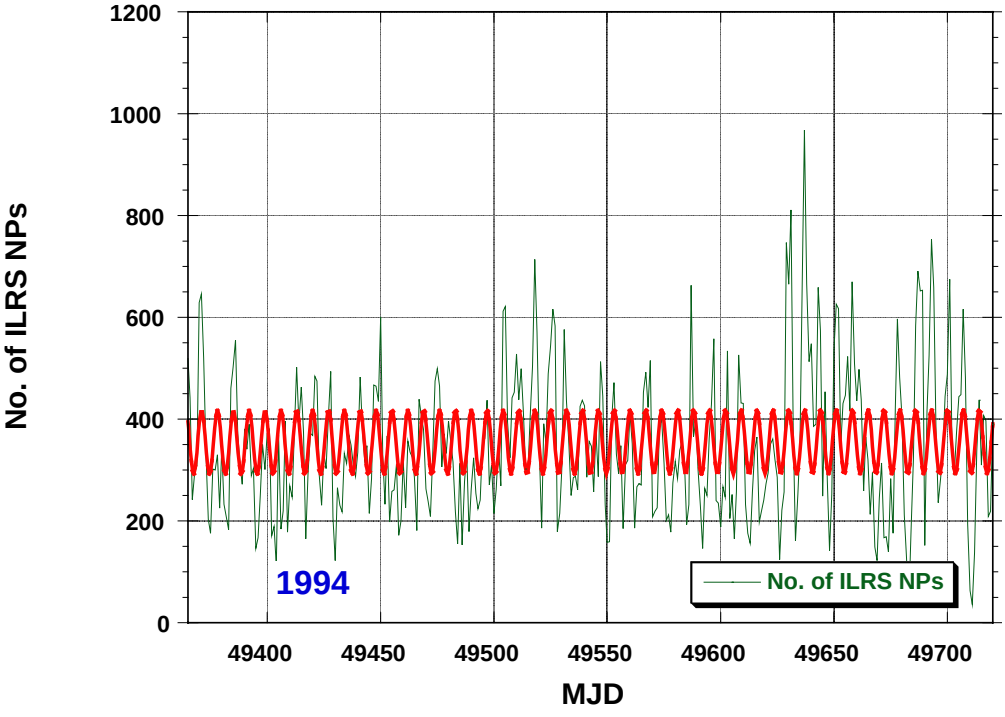

Figure 5. (b) Daily data distribution for 1994.

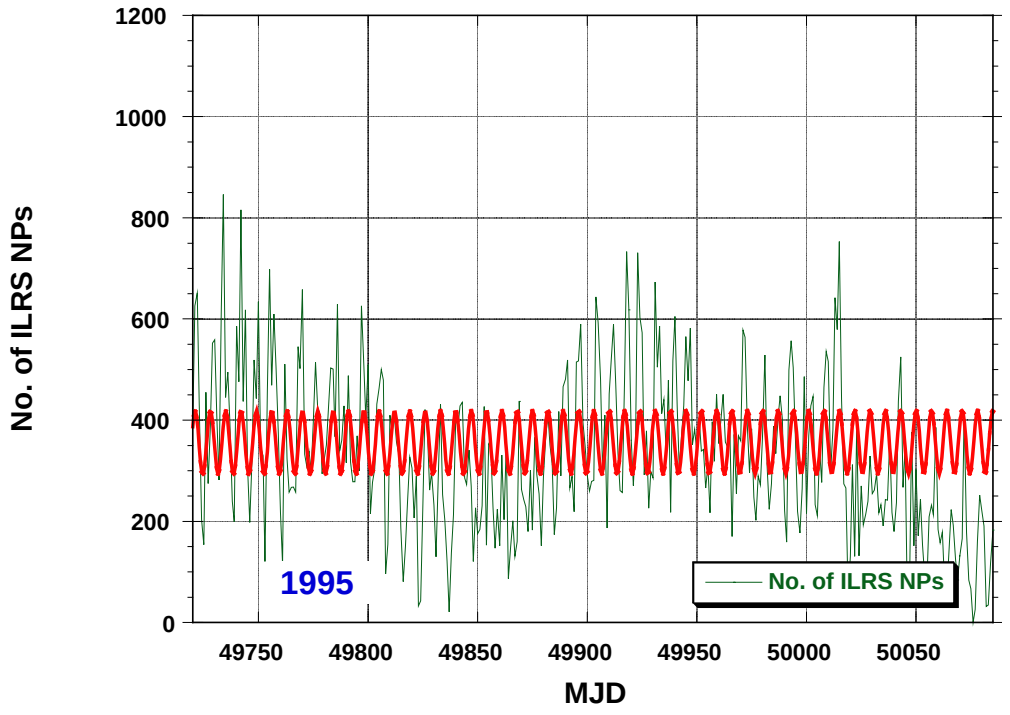

Figure 5. (c) Daily data distribution for 1995.

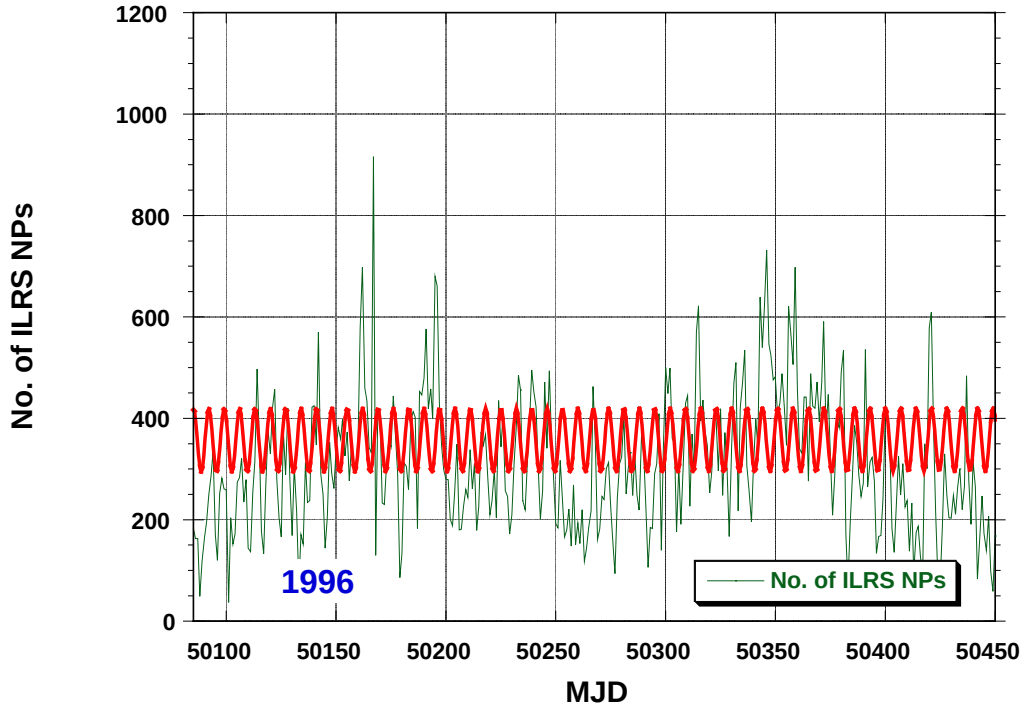

Figure 5. (d) Daily data distribution for 1996.

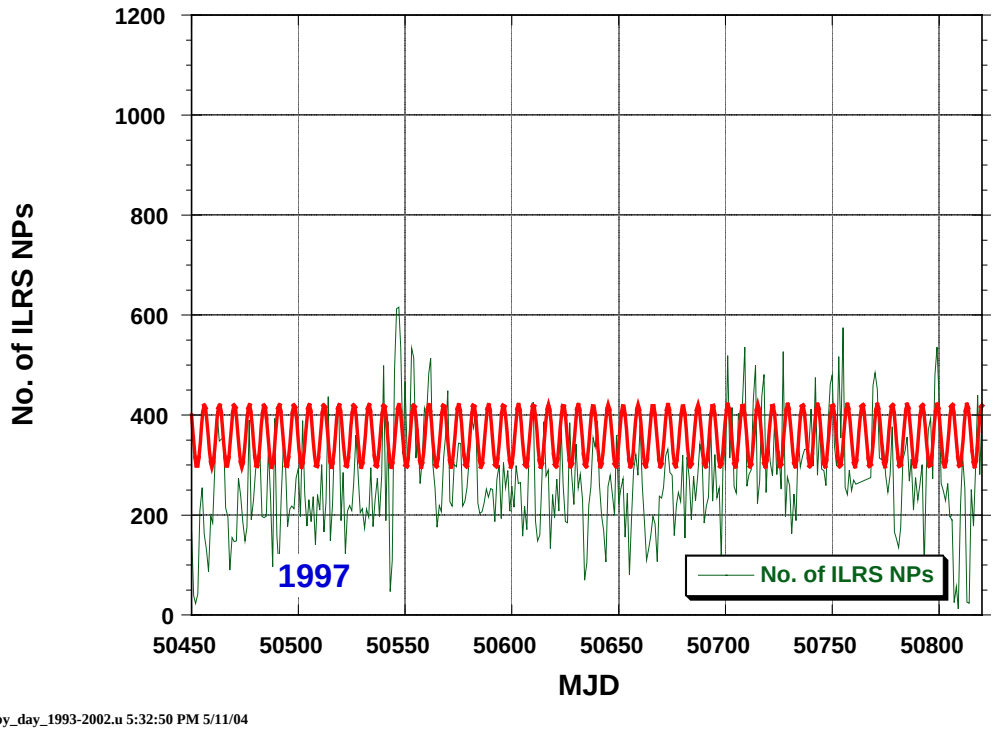

Figure 5. (e) Daily data distribution for 1997.

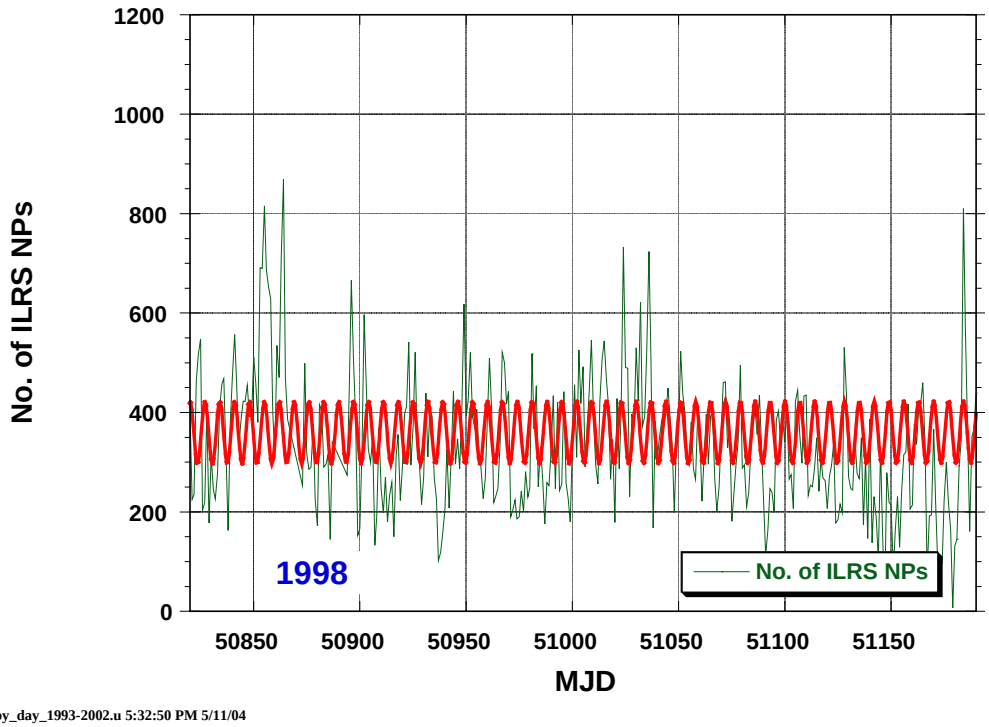

Figure 5. (f) Daily data distribution for 1998.

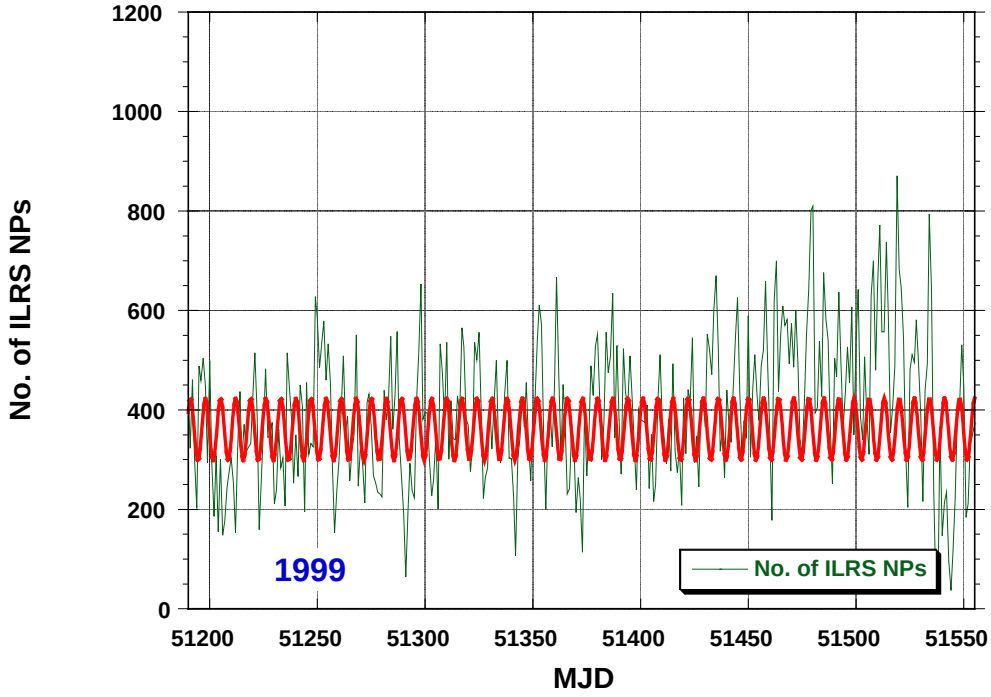

Figure 5. (g) Daily data distribution for 1999.

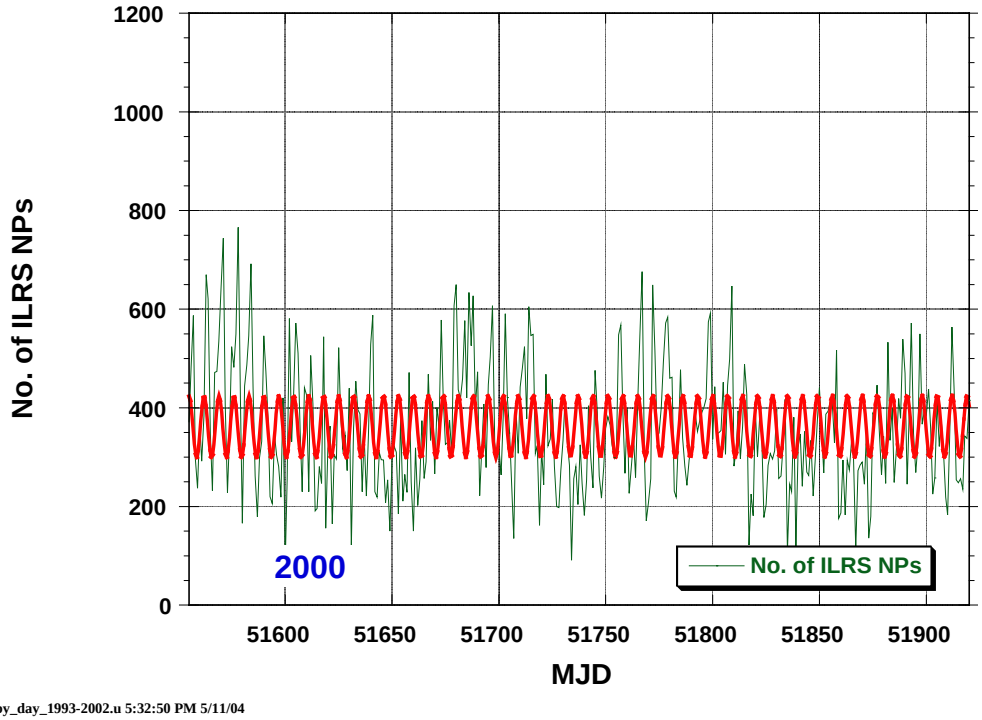

Figure 5. (h) Daily data distribution for 2000.

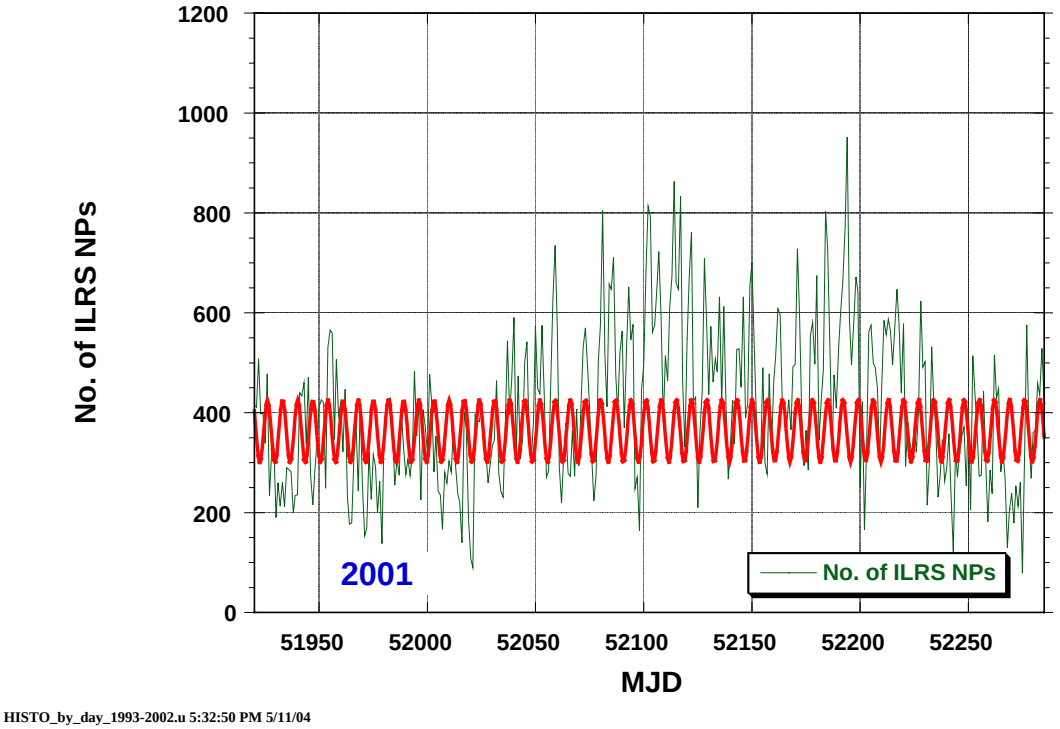

Figure 5. (i) Daily data distribution for 2001.

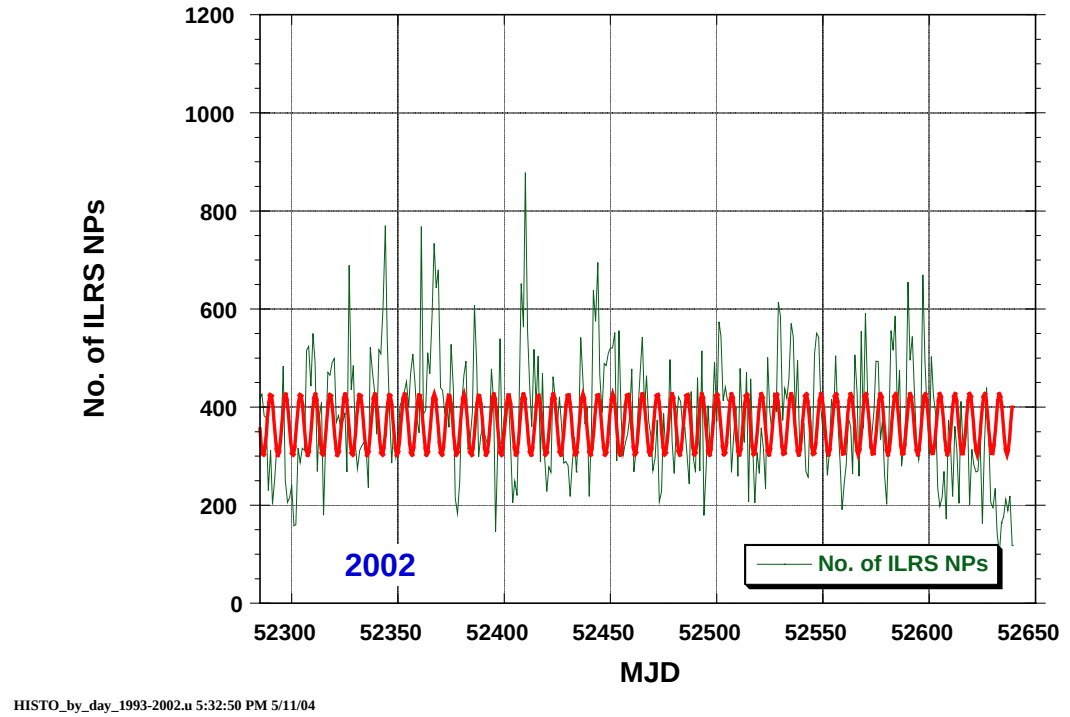

Figure 5. (j) Daily data distribution for 2002.

References

Pavlis, E. C. Dynamical Determination of Origin and Scale in the Earth System from Satellite Laser Ranging, in *Vistas for Geodesy in the New Millennium*, proceedings of the 2001

International Association of Geodesy Scientific Assembly, Budapest, Hungary, September 2-7, 2001, J. Adam and K.-P. Schwarz (eds.), Springer-Verlag, New York, pp. 36-41, 2002.

THE ILRS REPORT CARD AND PERFORMANCE CHARTS

M. Torrence (1), V. Husson (2)
(1) Raytheon Information Technology and Scientific Services
(2) Honeywell Technology Solutions Inc.
mtorrenc@terra.stx.com/Van.Husson@Honeywell-tsi.com

Abstract

The Central Bureau has worked to fill the gap left by the change in staffing. A revised Report Card and performance charts are now available at the ILRS web site. Examples of these charts will be presented.

KOREA'S FIRST SATELLITE FOR SATELLITE LASER RANGING

Jun Ho Lee(1), Seung Bum Kim(1), Kyung Hee Kim(1), Sang Hyung Lee(1), Yong Jo Im(1), Yang Fumin(2), Chen Wanzhen(2)
(1)Satellite Tech. Research Center, Korea Advanced Institute of Science & Tech. (KAIST),
373-1 Guseong-dong, Yusong-gu, Daejeon, 305-701, Republic of Korea,
(2)Shanghai Observatory, Chinese Academy of Sciences,
80 Nandan Rd., Shanghai 200030, China

Abstract

Science Technology Satellite-2 (STSAT-2) has been developed since Oct. 2002 as a sequel mission to KAISTSAT-4 (STSAT-1). STSAT-2 is schedule to be launched into an ellipsoidal orbit of 300km x 1500km in Dec. 2005, which seems to be delayed by two years, by the first Korea Satellite launch Vehicle KSLV-1. STSAT-2 has two payloads: a Lyman-alpha imaging solar telescope and a laser reflector array (LRA) for satellite laser ranging. The paper first presents a brief introduction to the STSAT-2 program. Then this paper presents the current status of the LRA development. In addition, we also introduce the beginning activities on SLR in Korea.

NEAR-REAL-TIME STATUS EXCHANGE

Werner Gurtner
Astronomical Institute, University of Berne, Switzerland

Abstract

For several years now up to about 10 mostly European laser stations have been exchanging their tracking status, especially the current time bias of successfully tracked satellites, in real-time. The use of this information can help stations to acquire satellites with poor orbit predictions more easily and more rapidly, and it can be the basis for a more sophisticated coordination of the satellite tracking The paper describes the communication protocol, the message format, and the utilities needed to participate in this program.

1. Introduction

The ILRS laser stations in Europe are located in a cluster relatively close together. A consequence of this geometry is the fact that very often part or all of the European stations will track the same satellite simultaneously or in rapid succession.

Occasionally the orbit predictions for some satellites can be fairly poor, and it might be rather difficult and time-consuming to get first successful range observations by searching the area in the sky around the predicted positions.

The largest component of the prediction error tends to be along the orbit. Therefore the station operators will mainly search for the satellite in the along-track direction. The along-track error is equal to a time error, i.e., the satellite is either early or late within the predicted orbit. Comparing the first successful range observations with the predicted ranges and taking into account the geometry between the satellite orbit and the tracking station it is easy to compute the apparent along track error in time, assuming that the observed difference is generated by an along-track error, only. Alternatively a station could apply a series of controlled time biases to its tracking procedure until it gets successful returns from the satellite and note the actual time bias.

This prediction error could be transmitted to all other stations nearby to be used for a faster acquisition of the respective satellite.

Simultaneously tracking the same satellite by many stations nearby might not be the optimum scenario if another satellite happens to pass the area in the same time. It might be more effective if some stations concentrated their tracking to this other satellite, especially if due to geometry or prediction quality acquisition was difficult and did not allow for rapid pass interleaving. If the information about the current tracking status were shared among the stations, real-time decisions about changes in the tracking priority could be easily taken by the operators.

Several years ago we proposed and successfully implemented a status exchange scheme and server program at the Zimmerwald station computer as described in the following sections.

2. Architecture of the Status Exchange

2.1 Client-Server Concept

A simple solution for an organized status exchange among an arbitrary number of stations is a client-server concept:

- Each station (the client) sends its status to a server
- The server collects the individual status messages and merges them into a simple table
- Each station receives in return the tabulated status information

2.2 Communication Protocol

Rather simple and easy to use for communication between computers is the Internet TCP/IP protocol: Information (e.g., character strings) can be sent to another computer by specifying

- the IP address (a number or a name, e.g., `130.92.25.24` or `aiuas3.unibe.ch`) and
- the so-called port number on which the receiving computer expects to get the data

to specific communication subroutines available for many programming languages and most operating systems (often assembled in the *socket library*).

On the other end of the communication line the target computer receives the messages on the specified port by means of the respective communication subroutines.

Usually the connection between two computers is established in a client-server mode:

- The server starts to listen on the specified server port for incoming connection requests
- As the need arises a client asks the server to establish a connection for data transmissions
- Request granted and connection established either one of the two partners can start sending data, depending on the rules previously specified and agreed upon.

After completion of the planned data transmission (one or more uni- or bilateral exchanges of data messages) the connection can be stopped either by the client or the server.

The communication rules for our implemented status exchange are as follows:

1. The communication between a client (an SLR station) and the server starts with the request by the client
2. The connection is established by the server
3. The server accepts status messages from the client anytime whenever the connection is open
4. The client (station) generates status messages periodically, e.g., every 15 seconds and sends them to the server
5. The server sends the compiled status message back to the client every 15 seconds as long as the connection remains open
6. The server can simultaneously establish connections to a number of different clients (currently 50).
7. Individual status messages consist of an ASCII character string delimited by a line-feed character (see below).

8. The compiled status message consists of a series of individual status messages plus a final record of a string of dashes, also delimited by a line-feed character.
9. The client may leave the connection open for as long as it likes or can close it after each successful transmission cycle.
10. Messages older than 30 minutes are discarded by the server.

As there is no need for a client to actually send any status messages to the server the connection can also be used by anybody to just receive the compiled status messages for monitoring purposes.

2.3 Format of the Status Messages

The status messages contain

- the station name (no pre-defined names)
- the current date and time (UTC)
- the satellite currently tracked (names according to the standard time bias file distributed through the same channels as the satellite orbit prediction, i.e., no hyphens, blank space or underscores, first letter uppercase, except names like ERS2, GFZ1)
- the station status:
    - NXT : Pass to come next, the system is waiting for this pass
    - CUR : Currently tracking
    - LST : Most recent pass, no new pass initiated
    - CAL : Calibration
    - OUT : Not operating
- the number of successful returns
- the used set of satellite predictions (label formed from an acronym for the prediction center and the sequence number of the current prediction set, see also in the standard time bias file)
- the current time bias in seconds (w/r to the distributed predictions) applied or determined in real-time from the observed ranges

```
Graz           2004-06-21 07:11:00  Topex       CUR  9786  HON172 -0.005
Zimmerwald     2004-06-21 07:11:07  Topex       CUR   384  HON172 -0.006
Potsdam        2004-06-21 07:11:01              OUT
Wettzell       2004-06-21 07:11:06  Topex       CUR   124  HON172 -0.004
MLRO-Matera    2004-06-21 07:11:07              OUT
Ftlrs_Sfdo     2004-06-21 07:05:00              OUT
Grasse_slr     2004-06-21 07:02:12              OUT
Herstmonceux   2004-06-21 07:10:50  Topex       CUR   391  HON172 -0.005
Yarragadee     2004-06-21 07:11:04              OUT
------------------------------------------------------------------------
```

Table 1: Example of a compiled status message

Table 2 contains the format of all data fields of a status message (in Fortran notation).

```
A13           I4   I2 I2 I2 I2 I2  A10         A3  I5     A6     F6.3
------------ ---- -- -- -- -- --  ---------- --- -----  ------ ------
station      date       time      satellite   stat obs    irvset t-bias
             yyyy-mm-dd hh:mm:ss                          cccnnn
```

Table 2: Format of a status message

2.4 Generation of the Status Message

The client has to generate periodically (e.g., every 15 seconds) the current status of the station and to prepare and send the status message as described in sections 2.3 and 2.5. Of course this is only possible if such a program has access to the respective system data automatically and in real time. Depending on the procedures used for the data transmission the program might store the message intermediately for later use, pipe it into the communication program or send it directly to the server.

The time bias should refer to the prediction set as declared in the status message, i.e., it should be the sum of any a priori time bias used and the additional time bias as determined from the range observations or as applied to the introduced range predictions.

2.5 Status Exchange

Messages are to be sent to port **`7810`** at the server **`aiuas3.unibe.ch`**.

There are several possibilities for a client how to actually send and/or receive messages:

Receive only:

`Telnet` to port **`7810`** can be interactively invoked. Messages will be received and displayed or sent to the standard output as long as the `telnet` connection is alive:

```
telnet aiuas3.unibe.ch 7810
telnet aiuas3.unibe.ch /port=7810
```

Send and receive:

- Write your own program (C language: Use the *socket* libraries)
- Use the program **`eurostat`**, see chapter 3, below.

2.6 Exchange of General Text Messages

Each station may also upload a text message line (< 70 characters) to the server containing a message to be appended to the station status lines. The first character of such a line has to be an exclamation mark.

Example:

```
!This is a general text message
```

More details can be found at ftp://ftp.unibe.ch/aiub/slr/slr_stat.txt.

3. The `eurostat` Program

In order to simplify the real-time status exchange between the laser stations we have prepared a C program to be run under UNIX or on a Windows PC. It directly connects to port **`7810`** on our system, sends a line of text and receives the current merged status messages.

The program is called as follows:

```
eurostat aiuas3.unibe.ch 7810 'n' [<textfile] [>statusfile]
```

The program reads from the standard input the locally generated status line and writes the received status to the standard output.

The standard input (i.e., the local status line) can of course be piped into the program, the received merged status on the standard output can be piped into some display program if necessary.

'**n**' is the number of receive cycles to be run, a zero means an infinite number. Usually '**n**' should be set to 1 and the program should be called in a loop every 15 to 30 seconds.

The program can also be used to just receive the compiled status file indefinitely by omitting any standard input and by setting 'n' to zero.

The source code, a DOS executable as well as a more detailed description can be found at ftp://ftp.unibe.ch/aiub/slr.

4. Conclusions

The real-time status exchange as described above and implemented at the Zimmerwald server `aiuas3.unibe.ch` and as clients at a number of (mostly European) laser stations has proven to be an easy to use tool for the rapid exchange of real-time satellite time bias and status information. Operators at the tracking stations also started to like the possibility to "see" what the other stations are currently tracking, it may improve the "corporate feeling" among the ILRS station operators and may even generate a friendly competition for successful tracking.

We encourage all ILRS stations currently not taking part in the status exchange program to join the group. For questions and support please contact the author.

Acknowledgment

I would like to thank Martin Ploner of our institute for the generation of the `eurostat` C program.

CDDIS ARCHIVE STRUCTURE SUPPORTING LASER RANGING DATA

C. Noll (1), M. Dube (2)
(1) NASA Goddard Space Flight Center
(2) Raytheon Information Technology and Scientific Services
Carey.Noll@nasa.gov /mdube@pop900.gsfc.nasa.gov

Abstract

The Crustal Dynamics Data Information System (CDDIS) has archived laser ranging data since 1982. These data consist of on-site normal points and full-rate. Products derived from the data are also archived in support of the ILRS. A new Linux-based server was recently procured for the CDDIS. During the transition to this new server, modifications to the on-line directory structure and filenames for the laser data archive will be made. This presentation will outline the new structure and filenames proposed for the CDDIS laser ranging archive.

Introduction

The CDDIS has archived laser ranging data for over twenty years. As the data products have changed over the years, it is now an appropriate time to revisit the structure of the archive and the naming of the data files.

Proposed Changes

The proposed structure for the CDDIS laser data archive provides a more logical and user-friendly format for both directories and filenames. This structure and naming convention also provides uniformity between the normal point and full-rate data types. Furthermore, the layout of the laser data archive will be more consistent with other types of space geodesy data available through the CDDIS.

The changes to the CDDIS laser data archive, as shown in Figure 1, are in the structure of the directories and the names of the files. The contents of the files will not change: daily normal point files contain data received in the previous 24-hour period, hourly normal point files contain data received in the previous onehour period, and monthly normal point and fullrate files contain data dated for the month reflected in the file name. The formats of normal point and fullrate data also remain unchanged.

These structure modifications will be implemented on the new CDDIS server, cddis.gsfc.nasa.gov, which will be operational in the fall of 2004. To allow users time to prepare their data retrieval scripts for the new directory structure and file naming convention, the existing CDDIS server, cddisa.gsfc.nasa.gov, will remain accessible for some months after the new server becomes operational. Through the first few months of 2005, the data and product archives of both cddis.gsfc.nasa.gov and cddisa.gsfc.nasa.gov will be updated and maintained. After a suitable transition period, updates to the older UNIX server, cddisa.gsfc.nasa.gov, will no longer occur and the system will be taken off-line.

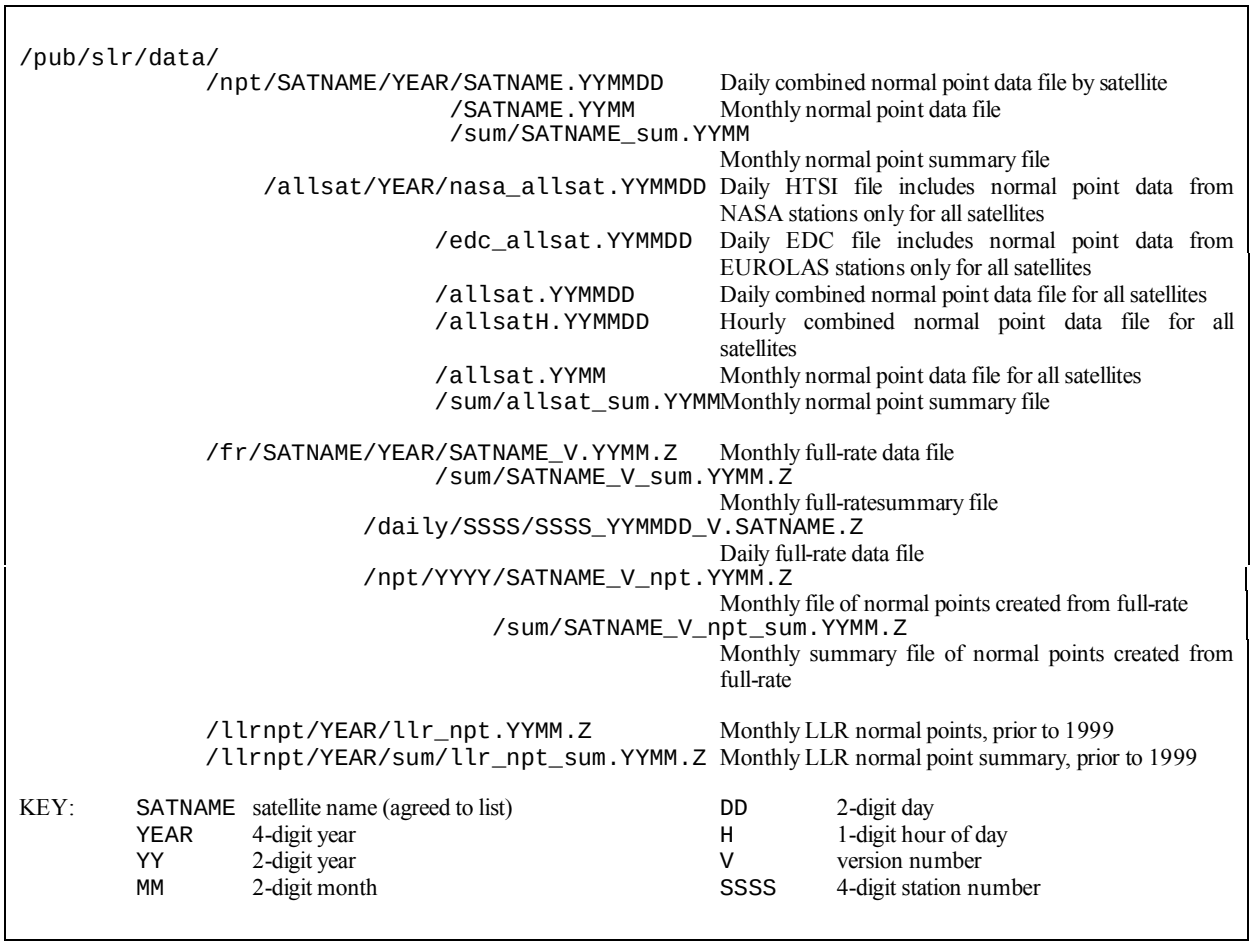

Figure 1. Proposed Structure for CDDIS Laser Data Archive

Further Information

Any questions concerning the proposed changes to the laser data archive of the CDDIS should be directed to the CDDIS Manager, Carey Noll (Carey.Noll@nasa.gov).

MINISTERIO
DE DEFENSA